PROBLEMS OF SOURCES
of deep magmatism and plumes

Проблемы источников глубинного магматизма и плюмы

PETROPAVLOVSK - KAMCHATSKY
IRKUTSK
2005

Russian Academy of Sciences
Vinogradov Institute of Geochemistry
Siberian Branch of RAS
Institute of Vulcanology and Seismology
Far East Branch of RAS
Russian Foundation of Basic Research

Problems of sources of deep magmatism and plumes

(Проблемы источников глубинного магматизма и плюмы)

PROCEEDING
of International Workshop
« Problems of sources of deep magmatism and plumes »
Edited by Dr. N.V. Vladykin

PETROPAVLOVSK-KAMCHATSKY

IRKUTSK

2005

UDK 552.33+ 552.32

Problems of sources of deep magmatism and plumes.

Proceedings of the 5 Interntional Conference. Petropavlovsk-Kamchatsky. Publishing House of the Institute of Geography SB RAS, 2005, 287 p., ISBN 5-94797-077-5. Vol. 1.

The given book presents invited reports of the 5th International Similar «Deep-seated magmatism, its sources and the association with plume processes», 2005, Petropavlovsk-Kamchatsky.

The invited reports discuss the features of alkaline, carbonatite and kimberlite magmatism.

These papers view the features of alkaline, carbonatite and kimberlite magmatism. They also disclose the influence of the fluid on the thermal regime of mantle plumes. The study of Sr and Nd isotopes of numerous carbonate sites in Siberia and Mongolia was dwelled upon when researching the relation of the type of their mantle sources with geodynamic regime of complex formation. The origins of carbonate complexes of folded areas and basalts of Altay, Sikhote-Alin and Kamchatka were considered. The investigations of mantle xenolith substance from kimberlites were looked upon, and the inhomogeneity of the mantle and evolution of mantle substance is verified. The paper describes non-kimberlite diamondiferous rocks. In addition, the study was presented on the evolution of loparite chemistry in the stratified Lovozersky complex and features of magmatism in the Mongolia - Zabaikalian Mesozoic rift zone.

The book is of great importance for petrologists, geochemists, and specialists studying deep alkaline and kimberlite magmatism, students and teaching staff of universities.

Published following the decision of the Scientific Council
of Vinogradov Institute of Geochemistry SB RAS

Editor: Prof. N.V. Vladykin

Reviewers: Prof. O.M. Glazunov and Prof. V.S. Antipin
Original-model: T.S. Torbeeva

ID№ 05215 от 28.06. 2001г.

Institute of Geography SB RAS
664033, Irkutsk, lanbatorskaja str. 1

Published in Glazkovskaya printing House
Irkutsk, Gogol str., 53.
Order №1120. Edition 150 copies.

ISBN 5-94797-077-5

The book cover depicts the sample of layered benstonite cabonatite from the Murun massif. The yellow color designates benstonite, grey is quartz, black is pyroxene, brown is tinaxite and green shows microcline.

TABLE OF CONTENTS

FOREWORD

The fact is well accepted that alkaline rocks represent unique formations on the Earth. They have been long attractive for research because large Nb, Ta, Zr, Y, TR, Cu and P deposits, gemstones of charoite, Cr-diopside, dianite are associated with them. For instance, in Australia diamonds are recovered in lamproites. The complicated processes of their formation provoked scientific disputes still going on. The newly developed analytical methods and techniques provided abundant information on the composition of alkaline rocks. The data on geochemistry of isotopes confirm the evidence on the mantle sources of the substance of alkaline rocks. The new concepts of plume tectonics are applied by scientists when studying alkaline rocks as the deep-seated geodynamics of the Earth is interpreted based on these data.

These problems were discussed at the international workshops held in 2001 at the Institute of Geochemistry in Irkutsk; in 2002 at the Far-East Geological Institute, Vladivostok; in 2003 at the Institute of Tectonics and Geophysics in Khabarovsk and 2004 at Geological Institute in Ulan-Ude, Siberian Branch of the Russian Academy of Sciences.

This book offers invited papers of the international workshop organized in 2005 in the city Petropavlovsk-Kamchatsky under the title “Sources of deep-seated magmatism and plumes”.

These papers view the features of alkaline, carbonatite and kimberlite magmatism. They also disclose the influence of the fluid on the thermal regime of mantle plumes. The study of Sr and Nd isotopes of numerous carbonate sites in Siberia and Mongolia was dwelled upon when researching the relation of the type of their mantle sources with geodynamic regime of complex formation. The origins of carbonate complexes of folded areas and basalts of Altay, Sikhote-Alin and Kamchatka were considered. The investigations of mantle xenolith substance from kimberlites were looked upon, and the inhomogeneity of the mantle and evolution of mantle substance is verified. The paper describes non-kimberlite diamondiferous rocks. In addition, the study was presented on the evolution of loparite chemistry in the stratified Lovozersky complex and features of magmatism in the Mongolia - Zabaikalian Mesozoic rift zone. All works assume the plume mechanism of fusion of primary alkaline magmas in the some areas of the Earth and in different age periods.

The book might present interest to specialists involved in petrological and geochemical investigations as well as those studying deep alkaline and kimberlite magmatism.

Chief Editor **Dr. N.V. Vladykin**

UDK 550.42

Fluid and thermal regime of mantle plumes

Ryabchikov I.D.

(IGEM, Russian Academy of Sciences)

Geochemistry of magmas related to plume environment bear hidden information concerning the composition and thermodynamic parameters of inner shells of the Earth, including the contents of volatile components. Recent geophysical and geochemical data suggest that the largest plumes may arise at the CMB. If this is true, the whole cross-section of the silicate Earth is available for our investigation, and this may help to reveal the main features of fluid regime of the deepest geospheres. This problem directly concerns the mechanism of plume formation.

The widely accepted point of view on the causes of ascent of deep seated material and its partial melting assumes mechanical instability of thermal boundary layers in lower mantle and partial melting of plume material when it reaches upper mantle due to the adiabatic decompression. This is because adiabatic gradient is steeper by comparison with the Clapeyron slope of solidus.

The alternative point of view supported by a number of investigators proposes the main reason of magma genesis in mantle plumes to be the uprising fluxes of reduced fluids from the Earth's core, which are oxidized due to the interaction with upper mantle and produce water, which reduces the melting temperature of silicate material. These investigators suggest that the model of hot spots should be replaced by the model of wet spots. Because of this the problem of fluid regime of mantle plumes acquires the principal importance.

PLUMES FROM THE CORE-MANTLE BOUNDARY

One interesting finding which suggested the involvement of core material (BRANDON et al., 1998)in the source of plume related magmas was the discovery of synchronous positive deviations from chondritic values of ^{186}Os/^{188}Os and ^{187}Os/^{188}Os ratios for Hawaiian picrites and Norilsk ores (Fig. 1). At the same time, the samples reflecting Os isotope composition in upper mantle (such as MORBs, chromites from ophiolitic complexes etc) have ^{186}Os/^{188}Os isotope ratios close to chondritic. ^{187}Os in rocks and ores increases at the expense of radioactive decay of ^{187}Re, whereas ^{186}Os is produced by the decay of ^{190}Pt. This implies that the sources of Hawaiian picrites and Siberian traps had long lived elevated values of Pt/Os and Re/Os ratios, exceedind chondritic values. It has been suggested that this is due to the entrainment of the small amount (ca 1%) of the material from metallic core by magma generating plumes. The overall core composition is certainly characterized by chondritic PGE ratios, but the crystallization of inner core could have resulted in the increase in Pt/Os и Re/Os ratios in the outer (molten) core, inasmuch as Pt and Re enter Fe-rich solid alloy in lower proportions by comparison with Os. This is confirmed by experimental data and by the behaviour of PGEs in iron meteorites. Norilsk ores correspond to higher $^{187}Os/^{188}Os$ and $^{186}Os/^{188}Os$ ratios on correlation plot by comparison with Hawaiian picrites. It permits to consider magmatic rocks of the Siberian trap province, which also include the ore-bearing intrusions of the Norilsk-Talnakh region, as the probable source of geochemical signals coming from the Earth's core.

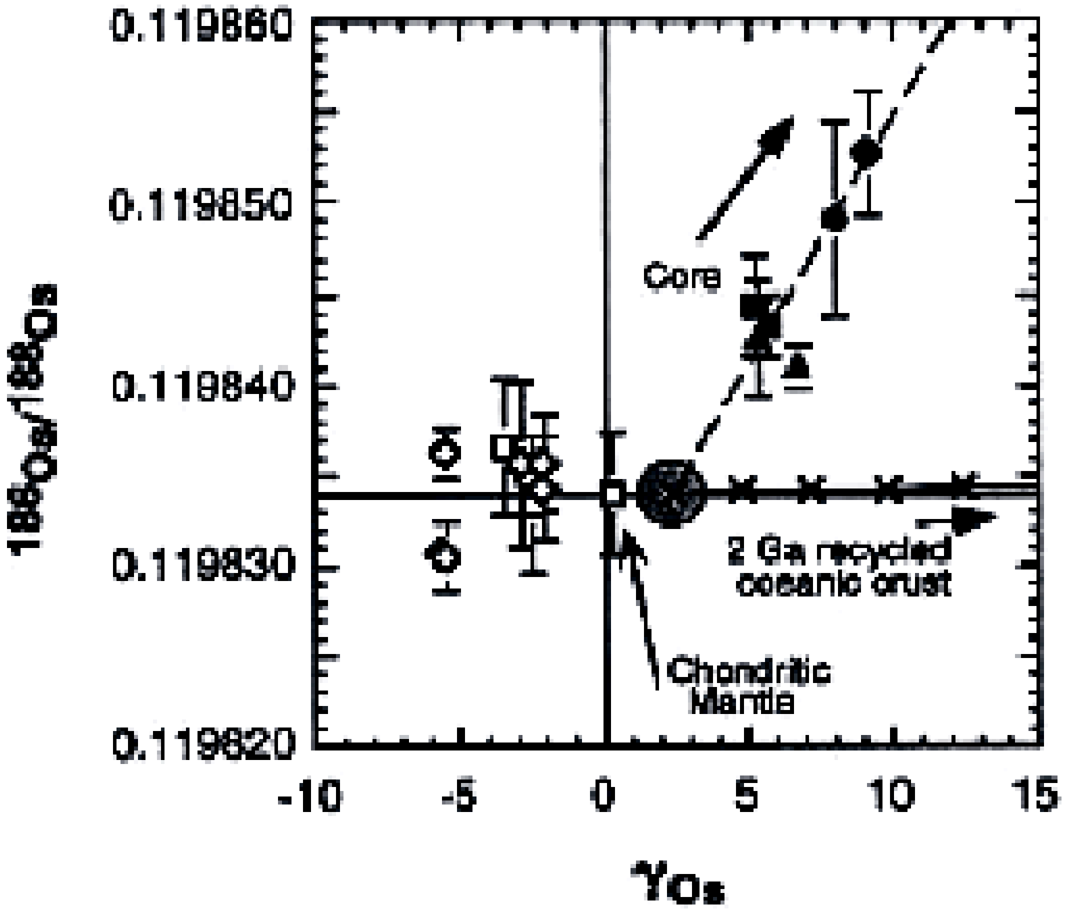

Fig. 1.**Synchronous positive deviations from chondritic values of $^{186}Os/^{188}Os$ and $^{187}Os/^{188}Os$ ratios for Hawaiian picrites and Norilsk ores (BRANDON et al., 1998). It suggests the involvement of core material in the source of plume related magmas.**

$\gamma Os = ((^{187}Os/^{188}Os)_{sample}/ (^{187}Os/^{188}Os)_{Chond} - 1)*100$

The observed variations of $^{186}Os/^{188}Os$ ratios are very small (1-2*10^{-5} units), and therefore their measurements require high precision technique, available only in a few laboratories. It would be desirable to find some simpler criteria of the interaction of core with the overlying geospheres. For this reason I analysed how the entrainments of material from core into very large mantle plumes would affect the behaviour of major elements of which the metallic core is composed. The major components of core are Fe (ca 80%) and Ni (ca 5%). The addition of 1% of such material to pyrolite will reduce after its oxidation the Mg/Mg+Fe ration approximately by 1%. Regarding that in peridotites NiO enters almost completely into olivine, its content in olivine would increase approximately by 0.1% after the addition and oxidation of 1% of alloy with 5% of Ni. In result we would have lherzolite with somewhat lower Mg# and significantly higher NiO content in olivine (trend opposite to the trend of fractional crystallization). This feature would be later inherited by olivines crystallizing from the magmas formed by partial melting of such peridotitic material. Thus, in order to check the hypothesis concerning the participation of core material in the source of plume-related magmas, one may compare NiO contents in olivines from basaltic and picritic rocks of various origin. Highly magnesian volcanics from Siberian trap province are the most likely materials for the finding of the indications of the participation of the core in the source of superplumes, because they are much closer to primary melts by comparison with the much more widespread tholeiitic plateaubasalts, and these picritic rocks are not affected by the contamination by the material of continental crust [8]. From Fig. 2 one can see substantial difference between Ni content in olivine phenocrysts from plume-related magmatic rocks of Siberian trap province and MORB-type asthenospheric melts. This does not contradict the suggestion that large plumes were formed at the core–mantle boundary and captured about 1% of the metallic phase.

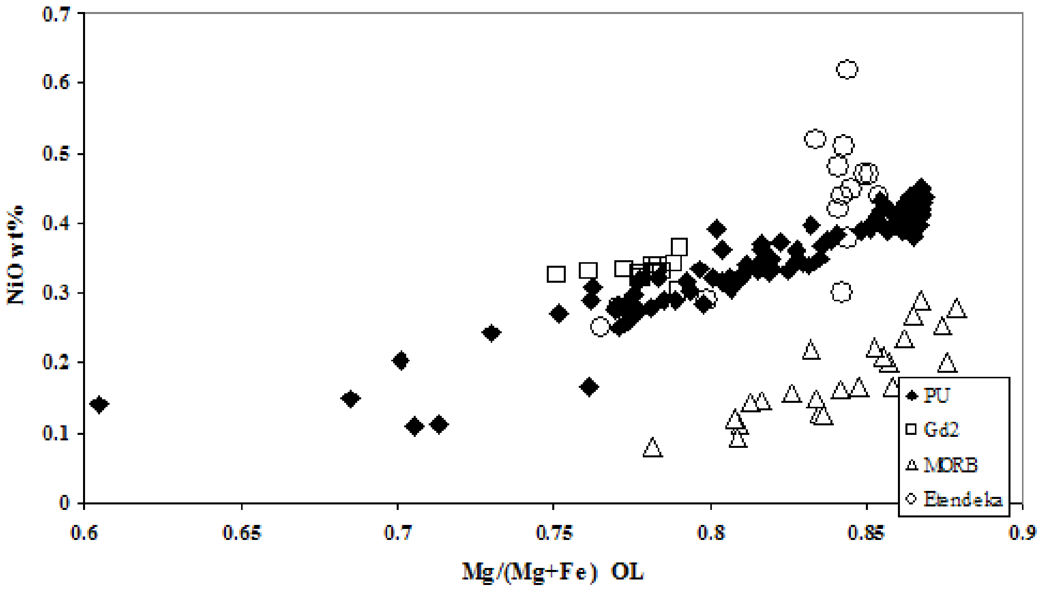

Fig. 2. **The NiO content vs. Mg/(Mg + Fe) atomic ratio relationship in olivine. (PU) Subalkaline picrobasalt from the Putorana Plateau; (Gd2) picrite from the upper unit of the Gudchikha formation in the Noril’sk–Talnakh district; Etendeka ferropicrites and MORB [8].**

VOLATILE COMPONENTS IN THE MATERIAL OF MANTLE PLUMES

Under high pressures and low contents of volatile components they do not form separate fluid phase in the mantle. Instead they enter rock-forming minerals as isomorphous admixture, and they behave themselves as usual incompatible elements (Fig. 3). The correlation of volatile components with their nonvolatile geochemical analogues (elements which have similar bulk partition coefficients in magmatic systems) permit to find the relation between the content of volatiles in quenched glasses or melt inclusions and their concentrations in mantle source.

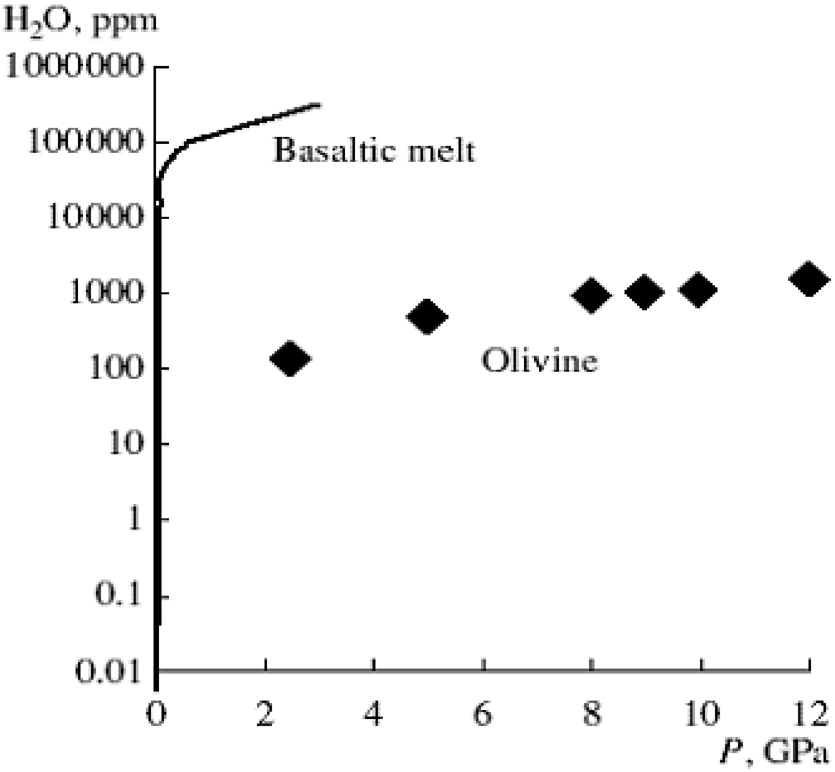

Fig. 3. **Water solubility in olivine at 1100 C [6] compared with water solubility in basaltic melt.**

A geochemical analogue of water is Ce under such conditions. Both MORB and magmas of plume environments, for instance, the basaltoids of the Hawaiian hot spot, fall on a common H_2O –Ce correlation trend. The melts of the Siberian plume (meimechites) lie on the extension of the same trend (Fig. 4). The sympathetic variations of H_2O and Ce suggest that water behaves as an incompatible element in the magmatic process, and there is no evidence for fluid mass transfer in the plume environment (gas phase will certainly show much higher H_2O/Ce ratio by comparison to melt). Furthermore, the parallel behavior of volatile and incompatible elements suggests that the occurrence of magmas with high contents of volatile components in plume environments does not necessarily imply an enrichment of their mantle source in volatiles: all strongly incompatible elements including volatiles are merely extensively extracted by melt at low degrees of partial melting. Indeed, water content was estimated as 250–400 ppm for the source of Hawaiian magmas and 230–310 ppm for the high-magnesia magmas of the Siberian plume. These values are only slightly higher than the water content of the MORB source and much lower than the estimate for the primitive mantle.

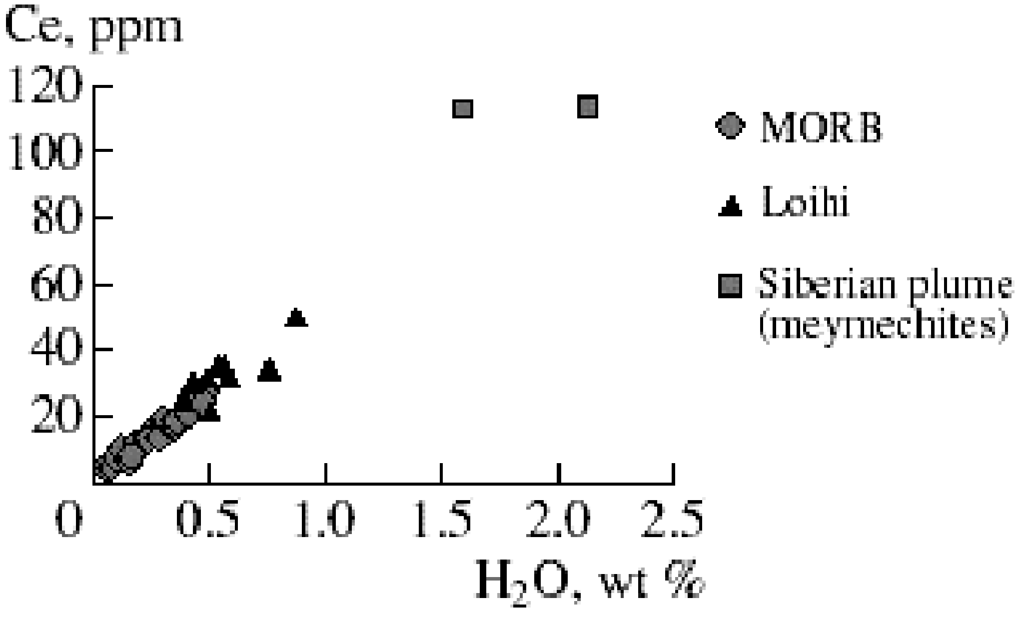

Fig. 4. **Correlation of water and Ce contents in basaltic magmas of various origins. (1) Glasses from the mid-ocean ridge basalts of the Pacific and Indian oceans [2]; (2) glasses from the basalts of the Loihi Seamount, Hawaii [3] and (3) estimate for the alkali picrites of the Maimecha–Kotui region [9].**

In the absence of residual carbonates, the concentration of oxidized carbon in magmas is correlated with the abundances of the most incompatible elements, such as thorium, niobium, or barium. Variations in CO_2/Th ratio suggest that the concentrations of CO_2 in the high-magnesia melts of the Siberian plume (about 3 wt % according to fluid and fluid–melt inclusion evidence) and even in kimberlites (about 20 wt % for protokimberlite estimated on the basis of phase equilibrium studies by [11] can be produced by low-degree melting of the ordinary primitive mantle (Fig. 5). Thus, the concentrations of volatiles in the material of mantle plumes are not anomalously high as compared to the abundances of other incompatible elements, i.e., there are no geochemical signals indicating an additional input of volatile compounds by deep-seated fluids.

Among the melts related to the ascend of mantle plumes diamond-bearing magmas – kimberlites and lamproites are the richest in volatile components. This is reflected in the explosive mode of their eruptions and in the presence of primary carbonates and phlogopite. Our estimates give 10 – 20% CO_2 for protokimberlite melts, i.e. they are intermediate between silicate and carbonate melts. However, diamond-bearing rocks are enriched not only in volatiles, which belong to incompatible elements, but also in nonvolatile highly incompatible elements. High concentrations of volatiles in kimberlites are due to the very intense extraction of volatile compounds by melt at low extent of partial melting, and they do not require anomalous enrichment of their mantle source.

The observed close correlation between volatile components and their nonvolatile geochemical analogues in the mantle-derived magmas imply the absence of large-scale fluid mass transfer of material in inner geospheres.

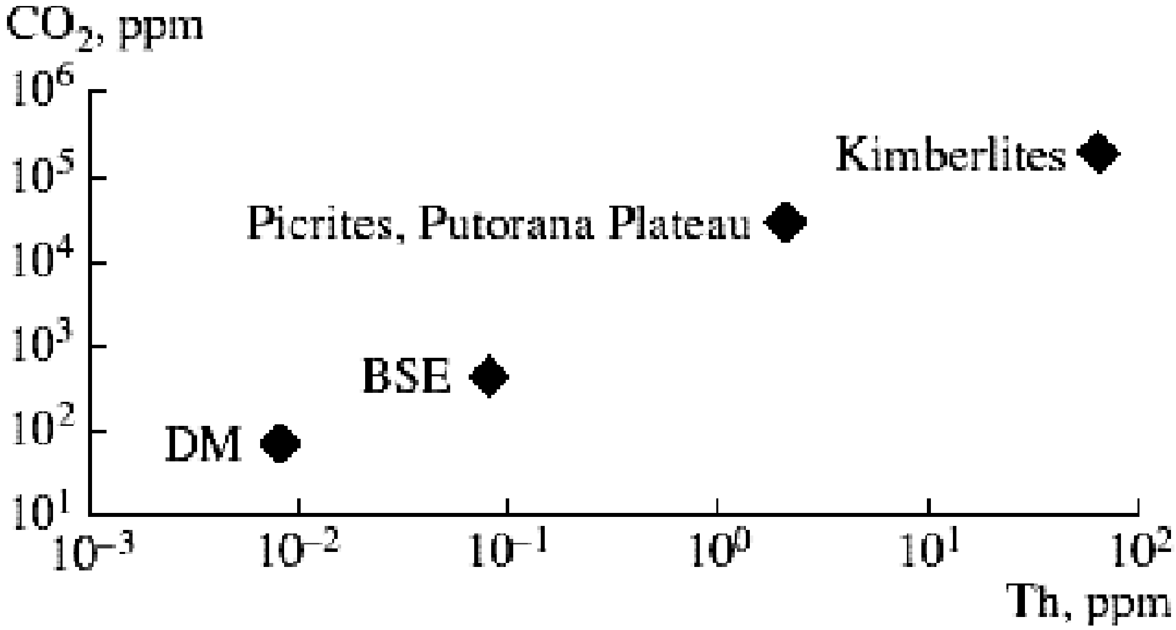

Fig. 5. **Correlation between the CO_2 contents of plume magmas and the concentrations of strongly incompatible elements (exemplified by thorium), which is a consequence of the concentration of magmaphile components in melt at low degrees of partial melting. DM is the source of midocean ridge basalts (SAAL et al., 2002), and BSE is the bulk silicate Earth. Also shown are the subalkaline picrite magmas of the Putorana Plateau estimated from the investigation of combined melt–fluid inclusions and group I kimberlite magmas**

CO_2 contents in tholeiitic plateaubasalts of Siberian trap province were estimated from correlation with Nb. Minimal estimate of the total amount of outgassed CO_2 (1.5×10^{13} t) is comparable with the mass of CO_2 (about 2×10^{13} t), sufficient for the considerable global warming (for the rise of average temperature by 1 – 2^o). The eruptions of the immense volumes of magmas, created by the rise of superplumes, are likely to cause global environmental changes and catastrophic biocrises.

VOLATILE COMPONENTS OF INNER GEOSPHERES

The estimated average contents of volatile components in the mantle are rather low, but their intense fluxes at the depth can be related either to the degassing of fossil oceanic lithosphere in subduction zone environments or to the entrainment of the material of the metallic core into mantle convection systems, provided the core contains considerable amounts of the elements producing volatile compounds. If the amounts of volatiles in the bulk Earth are known, their concentrations in the Earth's core can be determined by subtracting the masses of volatiles in the silicate Earth from their amounts in the bulk Earth. The abundances of volatiles in the bulk Earth can currently be estimated only from cosmochemical principles. Dreibus and Palme [4] estimated sulfur content in the core as about 1.8% assuming similar degrees of S and Zn depletion in the bulk Earth by comparison with CI carbonaceous chondrites (these elements have similar condensation temperatures under conditions of the protoplanetary nebula).

Table 1.

H/^{36}Ar ratios in diverse geochemical reservoirs

CI carbonaceous chondrites	$3.34 \cdot 10^8$
Atmosphere and hydrosphere	$7.74 \cdot 10^5$
Depleted mantle	$3.34 \cdot 10^8$

To estimate the terrestrial budget of hydrogen we used the comparison of ratios of H to other volatile components in geospheres and cosmos. We have chosen argon as a reference element, or rather isotope ^{36}Ar, which is undoubtedly more volatile by comparison with water, and whose mass on the Earth remained constant after the termination of accretion. H/^{36}Ar ratio in carbonaceous chondrites is order of magnitude higher than in atmosphere + hydrosphere (Table 1). It implies that the mass of hydrogen approximately equivalent to 9 hydrospheres was lost from the upper geospheres and Earth's mantle. The selective loss to cosmos of water in relation to argon seems not very likely due to higher volatility of argon.

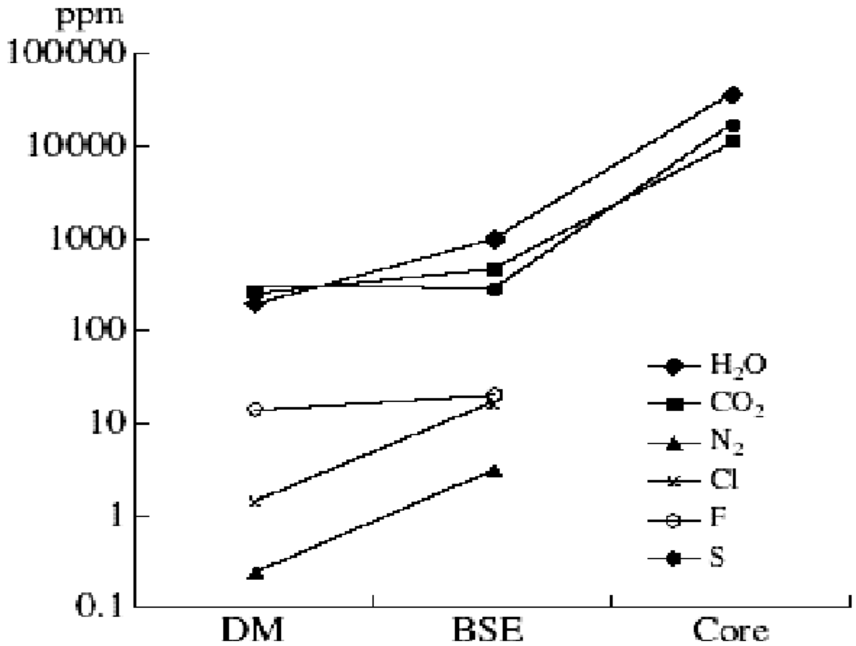

Fig. 6. **Estimated contents of volatile components in global geospheres: DM, depleted and degassed upper mantle and BSE, bulk silicate Earth.**

The alternative assumption is the loss of hydrogen to the core in the form of hydrides as a result of interaction of water with metallic iron at great depths. In this case the estimated content of H in metallic core is about 0.1% (Fig. 6).

The comparison of the estimated masses of water and other volatile components in global geospheres shows, that they may be an order of magnitude higher in the core by comparison with silicate Earth including exosphere (Fig. 7). The possibility of the transport of volatiles from the core to overlying geospheres depends on the possibility of the involvement of core into convective systems operating in the mantle.

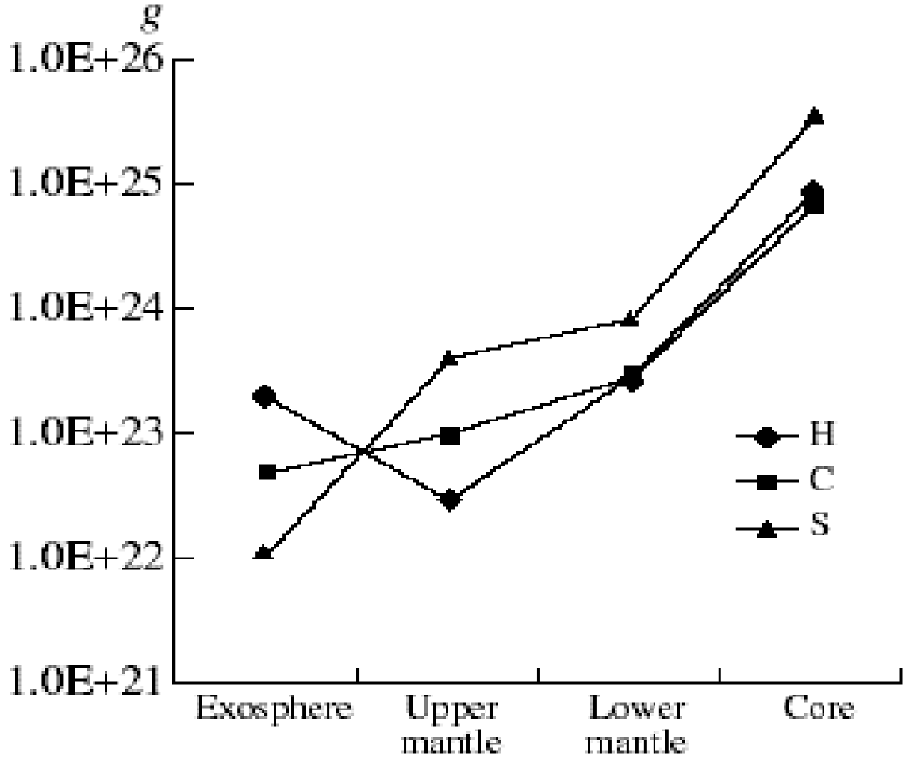

Fig. 7. **Masses of main fluid-generating elements in global terrestrial shells.**

The separation of hydrogen from core in the form of fluid phase seems not to be likely due to the very high stability of iron hydride at superhigh pressures (according to experimental data by [7].Certain amounts of volatiles may be transported from the core into the material of superplumes due to the capture of metallic phase by plumes. As we have mentioned, the interpretation of isotope data for the system ^{190}Pt/^{186}Os (BRANDON et al., 1998), as well as the behaviour of Ni may imply that approximately 1% of metallic material may be added to plume. For the compounds of H and C these additions would be insignificant.

TEMPERATURES OF PLUMES

Thermodynamic parameters of the generation of near-solidus melts permit to estimate temperatures of plume material and thereby to resolve the dilemma of thermal or fluid nature of plumes. For this one has to estimate the pressure of the beginning of magma generation and to compare it with the experimentally measured solidus of peridotitic material. It is also necessary to take into account the effect of volatile components on the melting of peridotite. For this we need to find near-solidus magmas of deep origin. By far the prevailing magmas in Siberian trap province are plateau basalts, which are not very suitable for our purpose, because they correspond to relatively high degrees of partial melting and were affected by crustal contamination. Highly magnesian magmatic rocks from the same region are much more appropriate for our purpose: they manifest indications of near-solidus melts formed at very high pressures – high incompatible elements contents at high MgO concentrations, steep spidergram in the region of HREE, no indication of contamination by continental crust (no Nb-Ta minima).

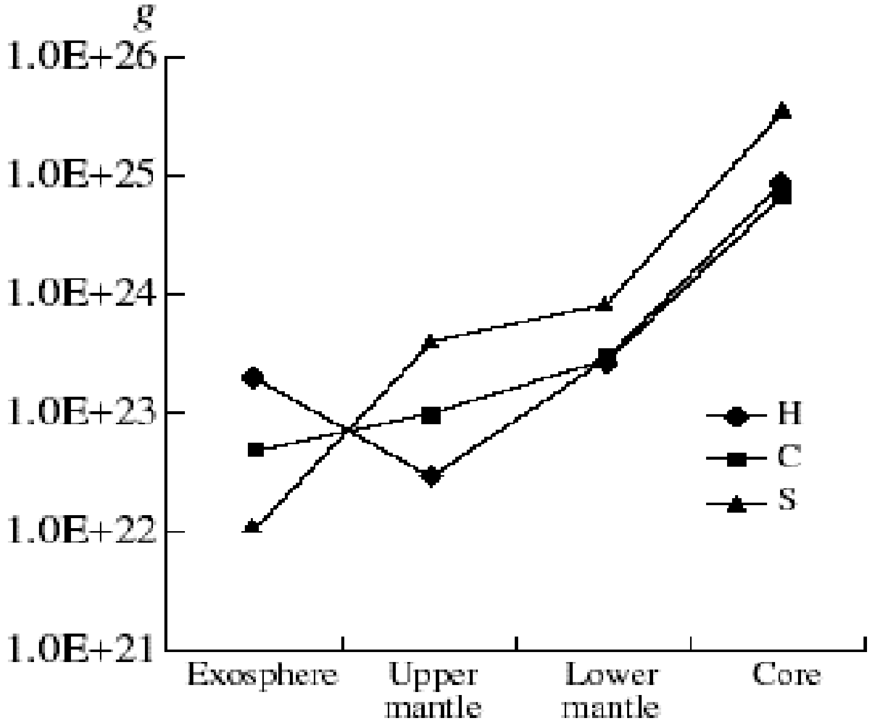

Fig. 8. **Titanium–sodium ratio calculated on the basis of experimental data for liquids derived by partial melting of the pyrolite bulk composition as a function of pressure and degree of melting. Also shown are the ranges of titanium–sodium ratio in the melt inclusions in olivine from the meymechites and alkali picrites of the Maimecha– Kotui region. *FL* is the degree of partial melting.**

Taking into account that sodium partitioning into pyroxene increases with increasing pressure, and that of titanium decreases (Fig. 8), the titanium–sodium ratio can be used as an efficient barometer for the processes of mantlemagma formation. Indeed, this ratio is much higher in deep-derived magmas than in the mantle and MORB (Fig.9). A comparison of the compositions of melt inclusions with the titanium–sodium ratio of melt derived from pyrolite as a function pressure and degree of melting calculated from experimental data (Fig. 8) suggests that the beginning of melting of the material of the Siberian plume corresponded to a pressure of no lower than 7 GPa, and this value probably approached 9 GPa for meimechites. Judging from TiO_2/Na_2O ratios the pressure of kimberlite magma formation was even higher.

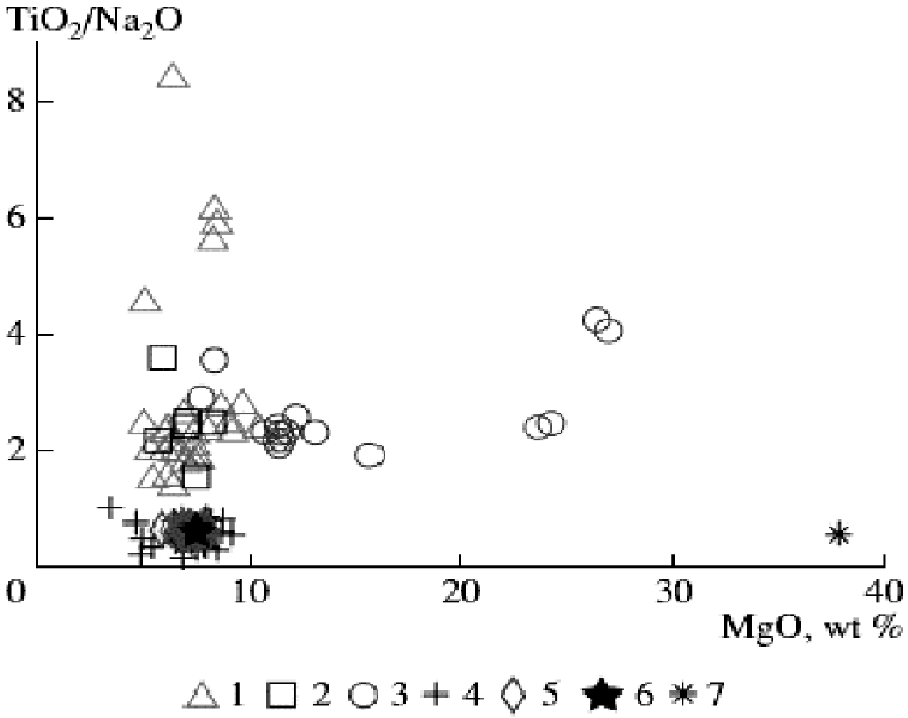

Fig. 9. **Titanium–sodium ratios in the rocks and melt inclusions from the subalkaline picrobasalts and plateau basalts of the Putorana Plateau.**

(1) Melt inclusions in olivine from picrobasalts (Putorana Plateau); (2) inclusions in clinopyroxene from picrobasalts; (3) bulk compositions of picrobasalts; (4) inclusions in plagioclase from plateau basalts (Putorana Plateau); (5) bulk compositions of plateau basalts; (6) average composition of N-MORB; and (7) pyrolite.

Another approach to the estimation of near-solidus pressures in the plume material is based on a comparison of the estimated major-element compositions of primary magmas with experimental data on the subliquidus equilibria in mantle peridotites. The compositions of melt inclusions from the rocks studied were recalculated to the conditions of equilibrium with mantle olivine (*Fo* 90) at TiO_2 concentrations corresponding to the pyrolite solidus (about 3 wt %). The projections of these compositions within the CaO– (Mg, Fe)O–Al_2O_3 – SiO_2 system were compared with the melts derived from pyrolite at varying pressure. This yielded pressure estimates of 7–9 GPa for both meimechites and picritic rocks of the Siberian trap province. These values are in agreement with the estimates obtained on the basis of titanium–sodium ratios (Figs. 10, 11).

The peridotite solidus lies at 1750°C at 7 GPa and 1800°C at 9 GPa. The interpretation of these data for the estimation of the temperature of plume material requires accounting for the possible influence of volatile components. The presence of 1.5-2% H_2O in such magmas (see above) will decrease the melting temperature by approximately 50° , i.e., to 1700– 1750°C . The corresponding potential temperatures are 1630–1660°C. For comparison, in the absence of perturbations caused by plume upwelling, the potential temperature of

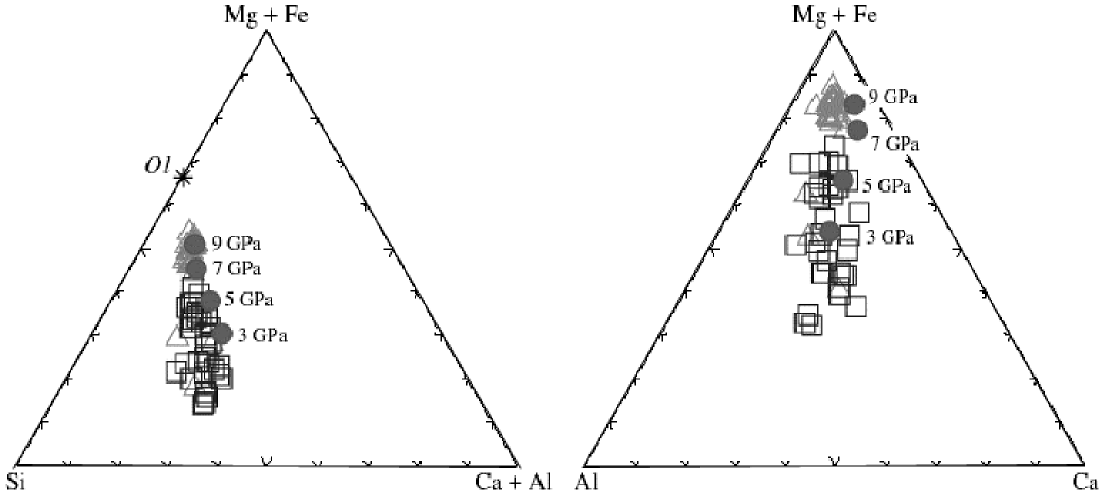

Fig. 10**. Cation fraction diagrams for the compositions of melt inclusions from the subalkaline picrites of the Putorana Plateau recalculated to the conditions of equilibrium with *Fo_{90}* at a TiO_2 content of 2.7 wt % (triangles) and at arbitrary TiO2 contents (squares) compared with the melts generated near the pyrolite solidus (WALTER, 1998).**

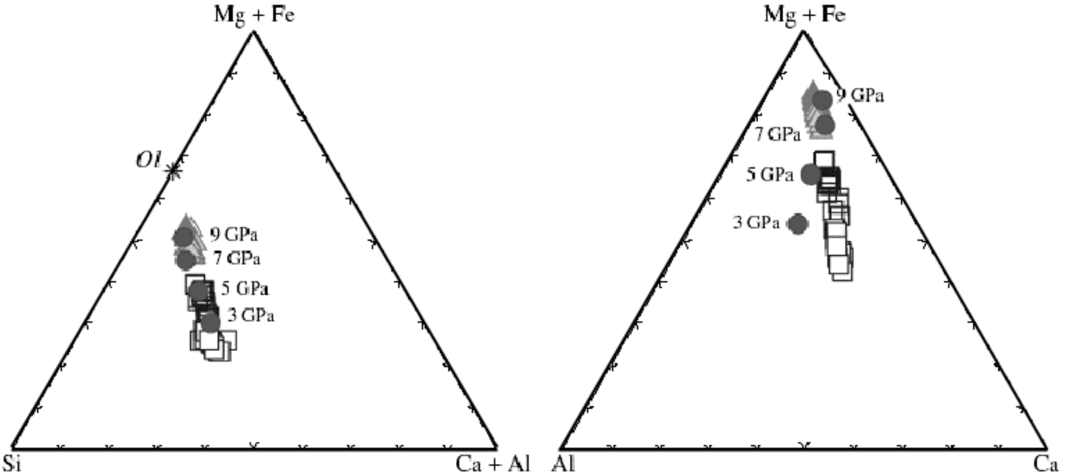

Fig. 11**. Cation fraction diagrams for the compositions of melt inclusions from the meymechites and alkali picrites of the Maimecha –Kotui region recalculated to the conditions of equilibrium with *Fo_{90}* at a TiO_2 content of 2.85 wt % (triangles) and at arbitrary TiO_2 contents (squares) compared with the melts generated near the pyrolite solidus (Walter, 1998).**

material may be 350–400°C higher than the temperature of the enclosing mantle (Fig. 12), which is somewhat higher than suggested for modern plumes on the basis of seismic tomography (for instance, in Iceland). Estimates based on seismic tomography correspond to temperatures averaged over considerable volumes, whereas, according to geochemical studies, plumes display a zonal distribution of temperature and geochemical characteristics: their axial parts contain the hottest material with the maximum fraction of deep-derived material, and peripheries have lower temperatures and a higher contribution from the colder upper mantle asthenosphere and lithosphere. The temperature estimates based on the geochemical characteristics of high-magnesia melts correspond most likely to the conditions in the axial part of the plume (or possibly plume tail), whereas lower temperatures are obtained for plateau basalts owing probably to an admixture of the upper mantle material.

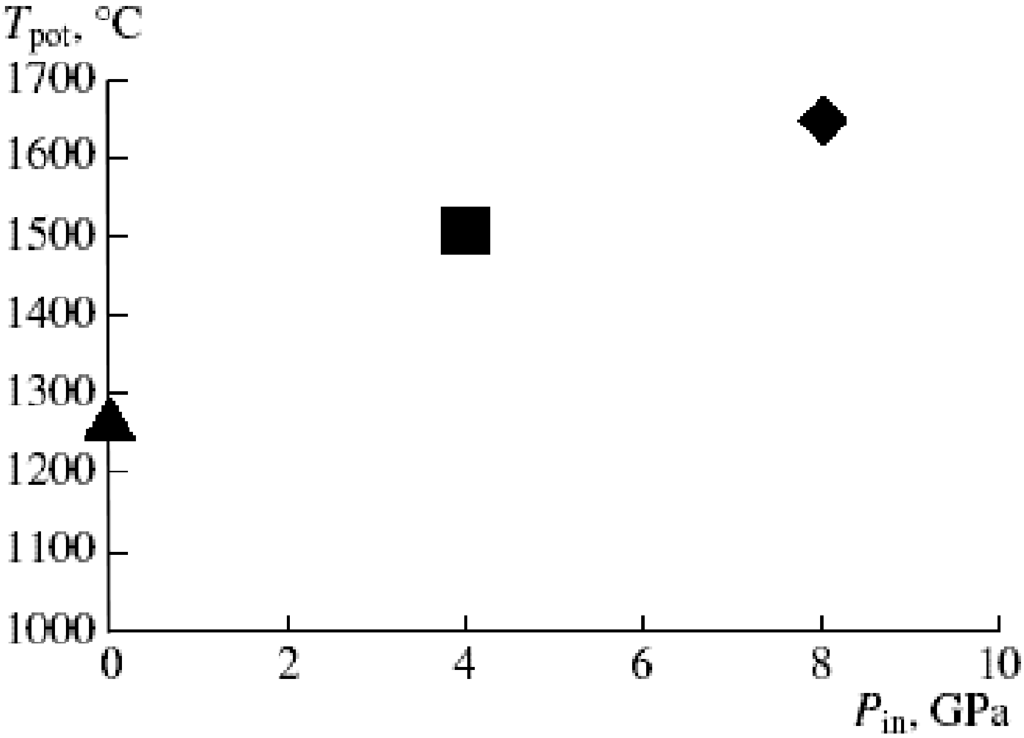

Fig. 12. **Estimates of potential temperatures, *T*pot, and initial pressures at the base of magma-forming columns, *P*in, for the magmas of meymechites (square), plateau basalts of the Siberian trap province (diamond), and average mantle adiabat (triangle).**

Our estimates compare more favourably with conclusions from the analysis of the uplift of the Hawaiian Islands. According to [16] the excess plume temperatures to be greater than 400 K

The conclusions drawn from the geochemical characteristics of high-magnesia melts are of fundamental importance for the understanding of the nature of mantle plumes and mechanisms of magma formation in plume environments. As I have mentioned above, in addition to the concept that the reason for the generation of mantle plumes is the ascent of hot low-density material from the core–mantle boundary and plume melting within the upper mantle in response to adiabatic decompression, there are alternative models disputing the necessity of high temperatures. In particular, several researchers proposed that the main reason for magma formation in plume environments was related to the flows of reduced fluid from the Earth’s core. Such fluids decreased the melting temperatures of silicate material after oxidation[5,13]. These authors proposed to change the model of hot spots by that of “wet spots”. Other hypotheses assume that the lowering of melting temperatures can be provided by the predominant entrainment of subducted basaltic material instead of peridotite into the processes of magma formation [12].

The data presented in this contribution demonstrate that the deep seated material was characterized by very high temperatures, and the role of volatiles in mantle plumes was limited. It is thought that these conclusions are of special importance for the determination of the thermal structure of the Earth. It supports abrupt temperature jump near the CMB, which was deduced from experimental data on the melting of Fe-rich alloys at super high pressures [1]. This also favours the hypothesis, maintaining that the part of the global thermal flux comes from the energy stored in slowly crystallizing core.

This work was supported by Russian Foundation for Basic Research (RFBR). Project 02-05-62192

CONCLUSIONS

1. The material of deep seated plumes is characterised by the ordinary contents of volatile components similar to BSE or even lower

2. The appearance of magmas with high concentrations of volatile components at the base of magma generating plumes is due to the extraction of incompatible elements (including volatile components) by near-solidus melts at very small degrees of partial melting.

3. There is no evidence of additional contribution of volatile components (e.g. in the form of deep seated fluid fluxes) from the Earth’s core. The conception of “wet spots” instead of “hot spots” is not supported.

4. Even taking into account the presence of volatile components the estimated temperatures of plume material at the initial stages of magma generation significantly exceed temperatures of the upper part of asthenosphere, which is consistent with the thermal nature of mantle plumes.

REFERENCES

1. **Boehler R**. (1996) Melting temperature of the earth's mantle and core: Earth's thermal structure. Annual Review of Earth and Planetary Sciences 24, 15-40.
2. **Brandon A. D., Walker R. J., Morgan J. W., Norman M. D., and Prichard H. M**. (1998) Coupled 186Os and 187Os evidence for core-mantle interaction. Science 280(5369), 1570-1573.
3. **Danyushevsky L. V., Eggins S. M., Falloon T. J., and Christie D. M.** (2000) H2O abundance in depleted to moderately enriched mid-ocean ridge magmas: Part I: Incompatible behaviour, implications for mantle storage, and origin of regional variations. Journ. Petrol. 41(1329-1364).
4. **Dixon J. E. and Clague D. A**. (2001) Volatiles in basaltic glasses from Loihi seamount, Hawaii: evidence for a relatively dry plume component. Journal of Petrology 42(3), 627-654.

5. **Dreibus G. and Palme H**. (1996) Cosmochemical constraints on the sulfur content in the Earth's core. Geoch. Cosm. Acta 60, 1125-1130.
6. **Green D. H., Falloon T. J., and Taylor W. R.** (1987) Mantle-derived magmas - roles of variable source peridotite and variable C-O-H fluid compositions. In Magmatic processes: physicochemical principles, Vol. 1 (ed. B. O. Mysen), pp. 139-154. Geochem. Soc. Spec. Pub.
7. **Kohlstedt D. L., Keppler H., and Rubie D. C**. (1996) Solubility of water in the alpha, beta and gamma phases of (Mg,Fe)2SiO4. Contrib. Mineral. Petrol. 123, 345-357.
8. **Okuchi T. (**1997) Hydrogen partitioning into molten iron at high pressure: implications for Earth's core. Science 278, 1781-1784.
9. **Ryabchikov I. D**. (2003) High NiO Content in Mantle-Derived Magmas as Evidence for Material Transfer from the Earth's Core. Doklady Earth Sciences 389A, 437-439.
10. **Ryabchikov I. D., Solovova I. P., Kogarko L. N., Brey G. P., Ntaflos T., and Simakin S. G.** (2002) Thermodynamic Parameters of Generation of Meymechites and Alkaline Picrites in the Maimecha-Kotui Province: Evidence from Melt Inclusions. Geochemistry International 40(11), 1031-1041.
11. **Saal A. E., Hauri E. H., Langmuir C. H., and Perfit M. R**. (2002) Vapour undersaturation in primitive mid-ocean-ridge basalt and the volatile content of Earth's upper mantle. Nature 419, 451-455.
12. **Рябчиков И.** Д. (2002) Источники вещества и механизмы формирования алмазоносных магм. In *Российская Арктика - геологическая история, минерагения, геоэкология* (ed. Д. А. Додин and В. С. Сурков), ВНИИОкеангеология. pp. 444-451.
13. **Takahashi E., Nakajima K., and Wright T. L**. (1998) Origin of Columbia River basalts: melting model of a heterogeneous plume head. Earth Plan. Sci. Lett. 162, 63-80.
14. **Taylor W. R. and Green D. H.** (1988) Measurements of reduced peridotite-C-O-H solidus. Nature 332, 349-352.
15. **Walter M. J**. (1998) Melting of garnet peridotite and the origin of komatiite and depleted lithosphere. Journal of Petrology 39(1), 29-60.
16. **Yaxley G. M.** (2000) Experimental study of the phase and melting relations of homogeneous basalt + peridotite mixtures and implications for the petrogenesis of flood basalts. Contrib Mineral Petrol 139, 326-338.
17. **Zhong S. and Watts A. B.** (2002) Constraints on the dynamics of mantle plumes from uplift of the Hawaiian Islands. Earth and Planetary Science Letters 203, 105-116.

UDK 552.33+550.42

Sr and Nd isotopes geochemistry of alkaline and carbonatite complexes of Siberia and Mongolia and some geodynamic consequences.

Vladykin N.V. [1], Morikiyo T. [2], Miyazaki T. [3]

[1] *Institute of Geochemistry of Siberian Branch, Irkutsk, Russia, e-mail: vlad@igc.irk.ru*
[2] *Department of Geology, Shinshu University, Asahi, Matsumoto, Japan*
[3] *Japan Institute for Geothermal Sciences, Kyoto University, Kyoto, Japan*

Introduction

Carbonatites are one of the most complex natural formations, associated with deep-seated silicate ultrabasic and alkaline rocks. Their magmatic genesis and the mantle pattern of initial magmas, which gave rise to these rocks as their differentiates does not call any doubts. As the surface does not always contain all members of carbonatite complexes and due to a poor outcropping of areas it is problematic to classify carbonate rocks as carbonatites. The mineralogical (availability of rare-metal Nb, Zr, TR-minerals) and geochemical criteria (heightened Ba, Sr, Nb, TR concentrations) are used for this purpose. The geochemistry of stable isotopes is of particular interest as it can be used for defining the type of mantle, which gave rise to carbonatites. However, there are a lot of problems of isotope geochemistry, which still remain unsolved, and the accumulation of new data leads to expanding of isotope limits, established earlier. For example, 20 years ago only rocks having the ratio of Sr isotope to be 0.703-0.704 were considered as mantle rocks. Progress in isotope Nd geochemistry and Nd isotope, Nd/Sr isotope ratio data show, that the ratio of Sr isotopes as 0.703 are characteristic of depleted mantle, while for enriched mantle EM-1 and particularly EM-2 mantle these values increase up to 0.720 (for example, in mantle lamproites of Australia and Spain)[15,18,33]. The scope of rocks which are associated with carbonatites has enlarged (for example, alkaline rocks of K- series) and occurrences of carbonatitic complexes [1,27]. It was earlier considered, that the carbonatitic complexes originate only on margins of platforms and shields. However, they are also abundant in areas of completed folding (e.g. Mongolia, Buryatia) [7-11]. As the carbonatitic complexes have the mantle genesis, associations of geodynamic settings and the type of primary mantle substratum are of particular interest [11,23]. The given article discusses isotope data, obtained for carbonatitic occurrences of the Siberian Platform framing, Aldan shield, South Mongolia, Primor'e. It also gives the date concerning the massifs of the Kola Peninsula and Central Asia for comparison. Geochemical samples of carbonatites have been collected for the last 30 years by N.V. Vladykin, the isotope data were obtained by T.Morikiyo and T.Miyazaki in Shinshi, Kyoto and Niigata Universities (Japan). Besides, isotope determinations for samples obtained by E.A. Chernysheva, L.I. Panina and N.M. Podgornykh, the results of investigations were published in the joint article [14], which discusses the procedure of isotope analysis. Therefore, here we give only a brief specification of this method. The present article is a continuation of former studies devoted to carbon and oxygen isotopes, published in the

Proceedings of the 4th Seminar [31]. C, O, Sr and Nd isotopes were measured in the same samples. In terms of geologic location of carbonatitic massifs three genetic (geodynamic) areas of their occurrences are found. They include 1) carbonatite of the Siberian Platform framing, 2) carbonatites of mobile belts; 3) carbonatites of rift zones of the joint of the Anabar shield and the Siberian Platform.

ANALYTICAL PROCEDURE

The details of Sr and Nd isotopic analysis have been given in Miyazaki and Shuto [12]. Initial Sr and Nd isotopic ratios were calculated from the measured $^{87}Sr/^{86}Sr$, $^{87}Rb/^{86}Sr$, $^{143}Nd/^{144}Nd$, $^{147}Sm/^{144}Nd$ ratios and ages for the bodies which were taken from literatures. Initial $\varepsilon Sr(t)$ and $\varepsilon Nd(t)$ values were also calculated. For the calculation of εvalues, the following parameters for Bulk Earth were employed: $(^{87}Sr/^{86}Sr)pr=0.7045$, $^{87}Rb/^{86}Sr=0.0827$, $(^{143}Nd/^{144}Nd)pr=0.512638$, $^{147}Sm/^{144}Nd=0.1966$ [11,4]. Isotopic analyses were conducted at Niigata University using a Finnigan MAT 262 mass spectrometer.

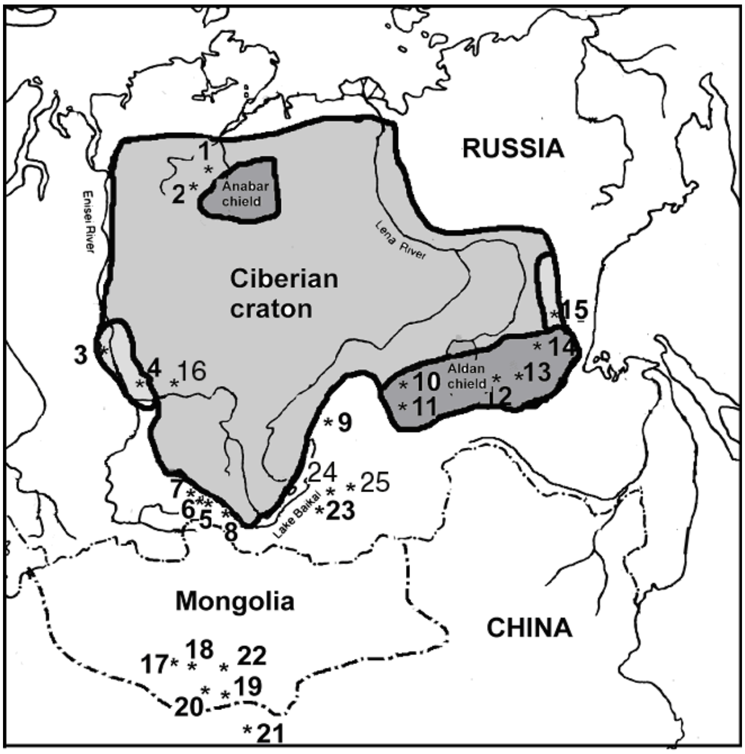

FIG. 1. **GEOGRAPHIC POSITION OF CARBONATITE MASSIFS.**
Massifs: 1 - Guli, 2 - Essei, 3 - Kiya, 4 - Tatar, 5 - Belaya Zima, 6 - Srednaya Zima, 7- Tagna, 8 - Zhidoi, 9 - Burpala, 10 - Murun, 11- Khani, 12 - Bilibin, 13 - Arbarastakh, 14 - Ingili, 15 - Gornoe Ozero, 16 - Chadobez, 17- Mushugai, 18 - Bayan- Khushu, 19 - Lugingol, 20 - Khan-Bogdo, 21 - Bayan-Obo, 22 - Ulugei, 23 – Khaluta, Arschan, Uznii, 24-Oschurkovo, 25- Ermakovka

CARBONATITES OF THE SIBERIAN PLATFORM FRAMING

The given article considers the data on carbon and oxygen isotopes for the East-Sayan Province (Bolsheziminskyi, Sredneziminskyi, Tagninskyi and Zhidoi massifs), Maimecha-Kotui province (Guli and Essei massifs), Yenisei Ridge (Kiya and Tatarskyi massifs) as well as the Eastern Aldan and Sete-Davan provinces (Arbarastakh, Ingili and Gornoe Ozero massifs). The location of massifs is shown in Fig. 1. The values of carbon and oxygen isotopes are given in Table 1. The massifs are described in [2,3,5,17-19,23,26-28]. The massifs Gornoe Ozero, Ingili and Arbarastakh are located in the South-Eastern framing of the Siberian Platform.

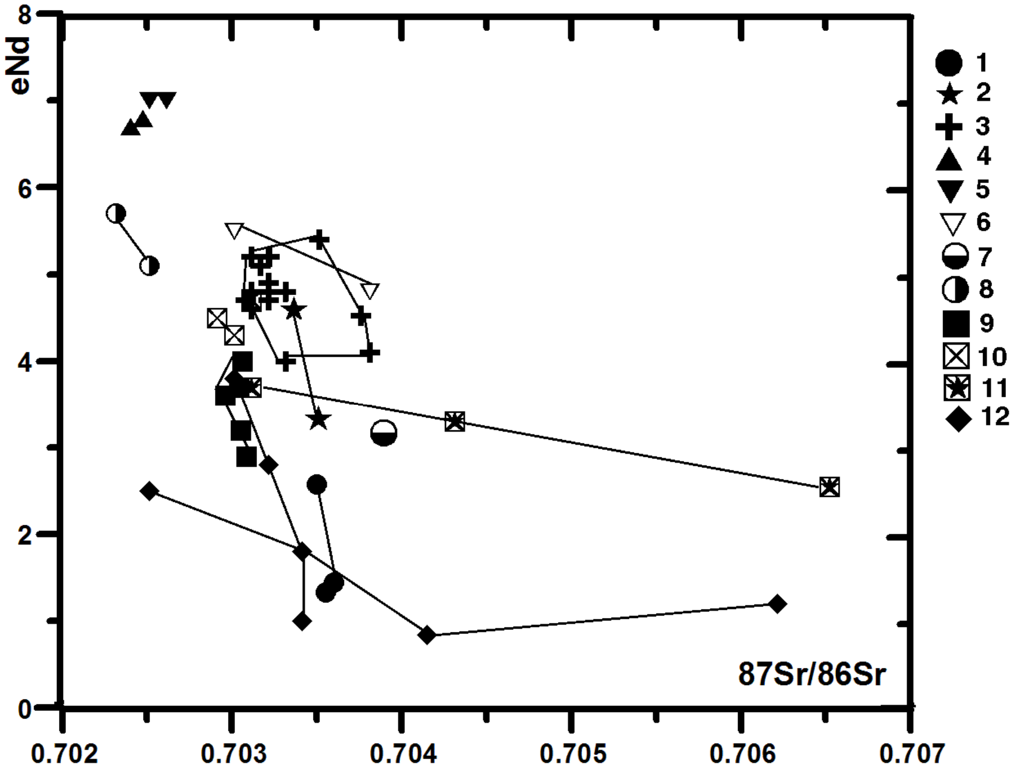

Fig. 2. **Carbonatite of the Siberian Platform framing**.
Massifs: 1 – Chadobez, 2 - Essei, 3 - Guli, 4 - Ingili, 5 - Arbarastakh, 6 - Gornoe Ozero, 7 - Kiya, 8 - Tatar 9 - Belaya Zima, 10 - Srednaya Zima, 11-Tagna, 12 – Zhidoi

Arbarastakh massif. The area of the massif is 42 km^2, the age is 675 Ma. The major phase of the massif contains pyroxenites with sites of biotite pyroxenites. The whole massif is cut by ring-type dikes of carbonatites and in some cases by cancretite and alkaline syenites. The center of the massif is composed of foskorites (apatite-magnetite-forsterite-calcite rocks). Carbonatites and foskorites are potential for Nb and Ta. Calcite rare-metal carbonatites have been analyzed. They demonstrate the highest values of epsilon Nd being equal to 7. The values of Sr isotope ratio amount to 0.70250-0.70285.

Ingili massif. The area of the massif is 20 km^2. The age of the massif determined from carbonatite zircon is 647 Ma. The massif contains amphibole-pyroxenites rocks and biotite pyroxenites, which are cut by dikes of ijolites, syenites and calcite carbonatites with amphibole and mica [23]. The authors use samples from the drill core to refine the magmatic scheme of the massif. Diatremes composed of basaltoid rocks (ingilites) with numerous xenoliths of the earth's lower crust have been found beyond the massif's contact. Carbonatite both from cores and dyke body found on the surface have been analyzed. On the diagram (Fig.2) the points of the carbonatites from the Ingili massif are located close to the points of the Arbarastakh carbonatites. They correspond to values of Epsilon Nd as 6.7-6.8 and 87Sr/86Sr as 0.70239-0.70246.

Gornoe Ozero massif. The area of the massif is 9,3 km^2. The age is 360 Ma. It contains pyroxenites, ijolites, syenites, magnetite forsterite and carbonatite (calcite and rare-earth) rocks [5]. The calcite carbonatite and rare-earth carbonatite (calcite+berbankite) were analyzed.

In the calcite carbonatite epsilon Nd is 5.5, and 87Sr/86Sr ratio is 0.70298, while in rare-earth carbonatite they amount to 4.8 and 0.70376, correspondingly.

The Yenisei ridge is located in the western framing of the Siberian Platform. The Kiya and Tatarskyi carbonatitic massifs are found within this ridge.

Tatarskyi (Penchenginskyi) massif. It is located in the southeast part of the Yenisei Ridge [5]. The age of the massif is 672 Ma. The massif is composed of dolomite, calcite-forsterite and ankeritic carbonatites. Silicate rocks have not been found in the massif. Xenoliths of strongly chloritized and serpentized rocks, which could be possibly the early rocks of the massif, are available.

Dolomite and calcite carbonatites have been analyzed. Values of Epsilon Nd amount to 5.1-5.7, and those of 87Sr/86S are equal to 0.70233-0.70252. Isotope ratios of the Arbarastakh, Ingili, Gornoe Ozero and Tatarskyi massifs form a small field in the left corner on the diagram and demonstrate the highest values of Epsilon Nd.

Kiya massif. The massif is located in the North-West part of the Yenisei Ridge, the area is 15 km2. The age of the massif is 250 Ma. The massif contains ijolites, nephelinic and alkaline syenites and carbonatites. We analyzed calcite carbonatites. Epsilon Nd values amount to 3.2 , 87Sr/86Sr ratio is 70388.

Guli massif. This is the largest massif of carbonatitic complexes. The area of the massif is 600 km^2 (from geophysical data it is 2000 km^2). The age of the massif is 240 Ma. It is located in the north of the Siberian Platform and is included into the Maimecha–Kotui province. The massif has concentrically-zonal structure and contains [3]: dunites-peridotites, pyroxenites, melilitic rocks, olivine melanephelinites, ijolites, nephelinic and alkaline syenites. The magmatic series is terminated by calcite and dolomitic carbonatites. We analyzed the calcite and dolomitic carbonatites, the isotope values of silicate rocks are taken from [Kogarko 1997]. Both carbonatites and silicate rocks demonstrate similar Sr isotope values aepsilon Nd Nd. Lower Epsilon Nd values are found for dunites and koswites of the first

Table 1.

Sr and Nd isotopic results for the carbonatites from Siberia and Mongolia.

Sample	Sm (ppm)	Nd (ppm)	^{147}Sm/ ^{144}Nd	^{143}Nd/^{144}Nd (measured)	^{143}Nd/^{144}Nd (initial)	Rb (ppm)	Sr (ppm)	^{87}Rb/^{86}Sr	^{87}Sr/^{86}Sr (measured)	^{87}Sr/^{86}Sr (initial)	εNd	εSr
1	2	3	4	5	6	7	8	9	10	11	12	13
Arbarastakh (675Ma)												
273	66.7	453.0	0.0890	0.51252	0.51213	1.7	7980	0.0006	0.70250	0.70249	7.0	-17.2
275	39.8	279.0	0.0860	0.51251	0.51212	28.5	3480	0.0237	0.70282	0.70260	7.0	-15.7
Ingili (665Ma)												
314	74.2	522.0	0.0860	0.51250	0.51213	48.2	12200	0.0114	0.70257	0.70246	6.8	-17.8
309	58.0	393.0	0.0893	0.51251	0.51212	44.1	6600	0.0193	0.70257	0.70239	6.7	-18.9
Ozernyi (360Ma)												
Go1	19.4	150.0	0.0778	0.51264	0.51246	34.2	3690	0.0268	0.70312	0.70298	5.5	-15.6
Go2	1250	16800	0.0450	0.51253	0.51242	0.6	1530	0.0011	0.70376	0.70376	4.8	-4.5
Tatarskii (640Ma)												
162/35	93.5	552.0	0.1024	0.51250	0.51208	45.2	7220	0.0181	0.70268	0.70252	5.1	-17.4
1704/27	5.0	32.4	0.0943	0.51250	0.51211	1.4	6690	0.0006	0.70233	0.70233	5.7	-20.2
Kiiskii (250Ma)												
K240	11.6	66.1	0.1062	0.51265	0.51248	10.6	928	0.0331	0.70400	0.70388	3.2	-4.5
Chadobez (160Ma)												
436/4	35,0	227.0	0.0932	0.51263		2.0	3070	0.0022	0.70352	0.70350	1.37	-10.5
436/5	17,8	93.1	0.1159	0.51267		1.0.	2470	0.0008	0.70344	0.70340	2.86	-12.4
436/8	41,1	287.0	0.0881	0.51262		1.0	1490	0.0016	0.70357	0.70360	1.48	-10.6
Guli (230Ma)												
G1	5.57	32.3	0.1042	0.51274	0.51258	14.3	7370	0.0056	0.70309	0.70307	4.7	-16.4
G2	34.3	234.0	0.0889	0.51274	0.51261	0.6	4370	0.0004	0.70321	0.70321	5.2	-14.5
G3-4	12.0	80.8	0.0895	0.51273	0.51260	1.2	3720	0.0010	0.70316	0.70315	5.1	-15.2
Essei (230Ma)												
2000	8.69	45.5	0.1155	0.51269	0.51252	2.8	2890	0.0028	0.70344	0.70343	3.5	-11.3
2014	7.68	48.9	0.0950	0.51272	0.51258	1.2	4190	0.0008	0.70334	0.70333	4.7	-12.7
Nizhnesayanskii (600Ma)												
HC1b	39.5	240.0	0.0995	0.51246	0.51207	22.0	4040	0.0157	0.70318	0.70305	4.0	-10.6
HC1c	16.4	130.0	0.0764	0.51235	0.51205	62.0	5800	0.0309	0.70321	0.70294	3.6	-12.1
HC2a	49.2	320.0	0.0930	0.51239	0.51203	1.5	6850	0.0006	0.70304	0.70304	3.2	-10.7
HC6w	37.5	307.0	0.0739	0.51230	0.51201	0.7	8690	0.0002	0.70308	0.70307	2.9	-10.2
HC6g	43.4	510.0	0.0515	0.51226	0.51205	0.5	11300	0.0001	0.70303	0.70303	3.7	-10.9
Б31				0,51207						0,70305	4.0	
Verhnesayanskii (600Ma)												
1/1	26.0	158.0	0.0994	0.51249	0.51209	8.3	6940	0.0035	0.70295	0.70292	4.5	-12.4
86/7	19.4	118.0	0.1001	0.51250	0.51211	152.0	1580	0.2783	0.70547	0.70309	4.7	-10.0
113/3	22.7	139.0	0.0985	0.51247	0.51209	13.9	5400	0.0074	0.70303	0.70297	4.3	-11.7
Bolshetagninskii (600Ma)												
BT1	2.2	19.9	0.0672	0.51230	0.51203	0.9	645	0.0040	0.70438	0.70434	3.3	7.8
BT34	2.3	25.6	0.0545	0.51227	0.51205	83.9	1550	0.1566	0.70439	0.70305	3.7	-10.6
BT5	6.36	41.2	0.0932	0.51237	0.51200	0.6	429	0.0040	0.70662	0.70658	2.7	39.7

Table 3. Continued

1	2	3	4	5	6	7	8	9	10	11	12	13
Zhidoy (600Ma)												
Zd316/3	57.4	393.0	0.0883	0.51241	0.51206	0.5	13600	0.0001	0.70300	0.70300	3.8	-11.2
Zhd327	46.6	348.0	0.0810	0.51233	0.51201	2.7	7770	0.0010	0.70318	0.70317	2.8	-8.8
Mushugai (120-150Ma)												
Myh1986	13.8	156.7	0.0532	0.51247	0.51243	1.81	1547	0.0034	0.70625	0.70624	-0,8	26.9
Myh1910	9.7	107	0.0549	0.51246	0.51242	0.46	1327	0.0010	0.70626	0.70625	-1,0	27.2
Myh540a	22,2	168,3	0.0799	0.51253		116.4	5243	0,0642	0.70550	0.70537	-0,4	14,4
Myh1985	354,0	4172,1	0.0513	0.51241		16.8	1187	0,0410	0.70720	0.70711	-2,2	39,0
Myh1898	628,6	5072,8	0.0749	0.51246		2.4	71565	0,0001	0.70600	0.70599	-1,7	23,1
Myh1907				0.51243		1.9	20586	0,0003	0.70600	0.70595	-1,1	22,6
Bajan-Hushu (120-145Ma)												
Bax2031	86,2	969,6	0.0537	0.51251		2.8	102472	0,0001	0.70600	0.70600	0,2	23,8
Bax2029	135,1	1610,1	0.0507	0.51244		8.3	47153	0,0005	0.70600	0.70598	-1,0	23,5
Bax2032	80,7	739,4	0.0660	0.51241		3.9	2775	0,0041	0.70690	0.70691	-1,9	36,7
Ulugei-Hushu (150-175Ma)												
Yr1975-1	42,8	364,8	0.0710	0.51266		1.4	23888	0,0002	0.70410	0.70408	2,8	-3,5
Yr1975-2	43,0	366,0	0.0710	0.51268		1.3	23715	0,0002	0.70420	0.70419	3,2	-3,3
Lugingol (257Ma)												
l 1778	520	5864	0.0536	0.51238	0.51231	44	1227	0.1036	0.70831	0.70831	-1,4	57.5
l 1779	482	5836	0.0500	0.51233	0.51233	15	1325	0.0326	0.70855	0.70846	-1,0	59.5
L-4443			0.0869	0.51239				1.476	0.71345	0.70805	-1.3	
Z-4444			0.0952	0.51236				0.2286	0.70889	0.70806	-2.1	
Beltsin-Gol (400Ma)												
Blg 525/2	0,2	1,2	0.1074	0.51214		1.0	2100	0,0009	0.70783	0.70782	-5,3	53
Blg 525/6	0,2	1,0	0.1168	0.51216		0	2450	0,0003	0.70809	0.70809	-5,2	57
Blg529/4	6.0	32,8	0.1098	0.51247		1.0	1110	0,3464	0.70867	0.70867	1,2	38
Blg529/31	2,2	10,6	0.1237	0.51217		1.0	820	0,0018	0.70780	0.70781	-5,6	53
Khalyta (120Ma)												
Hl-1/6	46.4	303.0	0.0926	0.51226		118.0	13870	0.0247	0.70582		-5.7	20.1
Hl-4/1-si	106.0	1330.0	0.0482	0.51230		1.6	3620	0.0013	0.70581		-4.3	20.5
Hl-4/1-c	5.0	30.0	0.1033	0.51236		6.3	188400	0.0001	0.70589		-4.1	21.8
Hl-4/4-si	612.0	4530.0	0.0816	0.51223		0.8	7935	0.0003	0.70571		-6.1	19.1
Hl-4/4-c	39.6	275.0	0.0869	0.51228		10.2	122800	0.0002	0.70584		-5.4	21.0
Hl-4/5	47.6	359.0	0.0803	0.51222		0.4	40050	0.00003	0.70589		-6.3	21.8
Hl-136/1	47.8	331.0	0.0874	0.51224		0.5	38800	0.00003	0.70583		-6.1	30.9
Arshan (120Ma)												
AR138/2F	121	703.0	0.1037	0.51224				0	0.70592		-6.4	22.2
Ar138/2b	5004	77620	0.0390	0.51219		0.1	22460	0.00001	0.70592		-6.4	22.2
Oshurkovo (120Ma)												
Osh-1/7	33.3	231.0	0.0871	0.51236		40.1	6010	0.0193	0.70540		-3.7	14.3
Osh-2/16	36.3	235.0	0.0935	0.51237		27.1	7200	0.0109	0.70541		-3.6	14.6
Osh-1/13	27.7	188.0	0.0892	0.51239		37.6	6430	0.0169	0.70535		-3.2	13.7
Osh-1/4	14.3	102.0	0.0853	0.51240		49.6	8900	0.0161	0.70525		-2.9	12.2
Osh-2/17	6.5	44.2	0.0882	0.51242		9.00	12430	0.0021	0.70522		-2.6	12.1
Osh-2/2	41.2	331.0	0.0753	0.51236				0	0.70539		-3.6	14.7

Table 3. Continued

1	2	3	4	5	6	7	8	9	10	11	12	13
Ermakovka (140Ma)												
714	9,3	71,2	0.0788	0.51237		32.7	3258	0,0290	0.70645	0.70642	-3.2	29.6
714/16	5,5	37,0	0.0905	0.51234		276.6	2272	0,3523	0.70818	0.70745	-4.0	44.2
712/10	0,5	2,2	0.1406	0.51247		18.4	1911	0,0279	0.70778	0.70772	-2.3	48.1
712/13	3,6	20,5	0.1053	0.51242		200.0	515	1,1239	0.71103	0.70879	-2.5	63.3
713	0,4	10,4	0.0216	0.51240		58.0	1581	0,1061	0.70775	0.70754	-1.6	45.5
714/15	0,4	1,8	0.1215	0.51235		5,3	280	0,0551	0.70729	0.70718	-4.3	40.4
712/3	5.7	57.6	0.0600	0.51233		67.2	1665	0.1168	0.70706	0.70683	-3.6	35.4
7123/1	39.4	246.4	0.0967	0.51251		232.7	215	3.1286	0.71540	0.70918	-0.7	68.7
Burpalinskii (300Ma)												
311/21	4.1	14.6	0.1694	0.51226	0.51193	1.4	3230	0.0012	0.70850	0.70851	-6.3	61.9
Darai-Pios (100Ma)												
322	21.1	108.3	0.1178	0.51212	0.51200	241	1388	0.5036	0.70984	0.70872	-8,5	63
91/1	3.92	13.9	0.1187	0.51215	0.51203	180	889	0.0326	0.70967	0.70838	-7,9	58
85/3				0,51207		19.2	3832	0,0145	0.7079	0.70790	-8,5	50,0
Malomurunskii (145Ma)												
143	15.0	117.0	0.0777	0.51133	0.51125	15.7	41400	0.0011	0.70690	0.70694	23.4	37.0
136/52	25.2	199.0	0.0764	0.51141	0.51134	152.0	27200	0.0162	0.70710	0.70708	21.8	39.0
173	9.4	69.5	0.0817	0.51136	0.51128	55.5	23400	0.0069	0.70720	0.70722	22.9	41.1
137/5	2.8	18.3	0.0937	0.51139	0.51130	15.7	4730	0.0096	0.70680	0.70678	22.5	34.8
1052/2	4.6	46.2	0.0606	0.51165	0.51159	25.5	29600	0.0025	0.70680	0.70681	16.8	35.2
186	2.3	22.2	0.0635	0.51129	0.51123	50.1	8060	0.0180	0.70730	0.70727	23.9	41.7
144/2	15.4	80.7	0.115	0,51161	0.51150	123	4338	0.082	0,70708	0.70691	-18,5	
151	5.52	70.4	0.065	0,51162	0.51156	21.5	40996	0.0015	0,70626	0.70626	-17,4	
172	6.23	31.7	0.119	0,51150	0.51150	490	1443	0.981	0,70856	0.70654	-18,5	
241	9.49	31.0	0.185	0,51150	0.51151	325	1723	0.546	0,70767	0.70654	-18,4	
3/100	5.89	29.3	0.122	0,51130	0.51133	240	1255	0.554	0,70863	0.70750	-21,5	
Bilibinskyi (132Ma)												
lam1	6.2	24.3		0,51165		4.5	1299		0.70679	0.70677	-18,7	34.3
lam2	7.1	27.3		0,51178						0.70700	-16,3	37.7
Khani (3200Ma)												
205	74.0	539.0	0.0831	0.51047	0.50946	126.0	4370	0.0837	0.70670	0.70450	15.7	31.1
206	146	1060	0.0834	0.51042	0.50942	16.1	4790	0.0097	0.70531	0.70506	-16.6	39.0
Riabinovyi (140Ma)												
48/9	20,5	103,6	0.1198	0.51182		83.4	34303	0,0070	0.70504	0.70503	-14.5	9,8
Iakokut (140 Ma)												
Як1	1.2	3.98		0.51210		0.86	224		0.70574	0.70572	-10.2	19.7
Zidoi (600 Ma)												
Zd316/3	57.4	393.0	0.0883	0.51241	0.51206	0.5	13600	0.0001	0.70300	0.70300	5.0	-9.9
Zhd327	46.6	348.0	0.0810	0.51233	0.51201	2.7	7770	0.0010	0.70318	0.70317	4.0	-7.5
Z-1	52.4	295	0.1075	0.51244	0.51196	0.67	768	0.0025	0.70249	0.70246	3.8	-17
Z-3	10.2	67.8	0.0910	0.51227	0.51186	33.6	1240	0.0785	0.70414	0.70338	22.0	-4.5
Z-4	4.3	25.8	0.1006	0.51234	0.51189	105	882	0.3458	0.70618	0.70618	2.6	-12
Z-5	42.9	314	0.0827	0.51226	0.51198	1.03	6050	0.0005	0.70335	0.70335	2.6	-5.0
Z-6	43.9	324	0.0883	0.51230	0.51194	1.79	4660	0.0011	0.70339	0.70338	3.5	-4.5

intrusive phase, while higher values are observed for ijolites-melteigite-yakuperangite series of rocks. 87Sr/86Sr values are the highest in early dunite and late nephelinic syenite. Sr isotope ratios for rocks of the Guli massif vary within 0.70309-0.70376 aepsilon Nd Nd equals to 3.97-5.35.

Essei massif. It is located in the same province. The area of the massif is 6 km^2. The age of the massif is 230 Ma. It is composed of olivinites and peridotites, ijolites, forsterite–apatite- magnetite rocks (phoskorites), dolomite and calcite carbonatites [3]. Dolomite carbonatites and foskorites were analyzed. Foskorites as opposed to carbonatites show lower Epsilon Nd value and slightly higher value of Sr isotope ratio. Variations of 87Sr/86Sr equal to 0.70333-0.70334, while those of Epsilon Nd amount to 3.5-4.7.

East-Sayan province. The province includes 4 massifs: Belya Zima, Srednyaya Zima, Tagninskyi and Zhidoi [5]. Sr and Nd isotope values are given in Table 1 and on Fig. 2.

Belaya Zima massif (Nizhesayanskyi). The area of the massif is 17 km^2. The age of the massif is 650 Ma. It contains [5] pyroxenites, ijolites, melilitic rocks, syenites and carbonatites. The massif also involves calcite, dolomitic and ankeritic carbonatites, which are divided into 5 stages of carbonate formation. We analyzed calcite carbonatites with forsterites, diopside, magnetite, apatite and pyrochlore of the first and second stages of generation. Sr isotope values range within 0. 70303-0.70321 and those of Epsilon Nd vary within 2.9-4.0 and do not depend on the stage of generation.

Srednyaya Zima Massif (Verkhnesayanskyi). The area of the massif is 7 km^2. The age of the massif is 600 Ma. It is composed of ijolites, nephelinic syenites and carbonatites. Carbonatites are calcite with biotite and pyroxene. We analyzed calcite carbonatites with pyroxene, biotite, pyrochlore. Variations of ^{87}Sr/^{86}Sr are 0.70295-0.70547 and those of Epsilon Nd amount to 4.3-4.7.

Tagninskyi massif. The area of the massif is 9 km^2. The age of the massif is 600 Ma. It involves ijolites, alkaline syenites, microclinites, carbonatites and dikes of picrites, tinguaites and nephelinites. The carbonatites are divided into calcitic, calcite-fluoritic and ankeritic. Calcite carbonatites with magnetites, hematite were analyzed. Variations of ^{87}Sr/^{86}Sr are 0.70305-0.70658 and those of Epsilon Nd equal to 2.7-3.7. Carbonatites show significant variations in Sr isotope value.

Zhidoi massif. The massif is located southwards as opposed to the above three massifs. The massif is composed of pyroxenites, ijolites and dikes of syenites and carbonatites [25]. Carbonatites are of calcite composition with scarce apatite. The age of the massif is 650 Ma. A separate article is dedicated to a problem of isotope geochemistry of the Zhidoi massif [13]. We analyzed the main varieties of rocks from the massif. The silicate rocks demonstrate the following variations ^{87}Sr/^{86}Sr as 0.70249-0.70618 aepsilon Nd Nd as 0.5-2.5 while carbonatites show ^{87}Sr/^{86}Sr values as 0.70300-0.70338 aepsilon Nd Nd as 1.0-3.4. There is a gradual increase of ^{87}Sr/^{86}Sr value from early pyroxenites through ijolites to syenites, while carbonatites show a significant scatter in Epsilon Nd values.

Chadobetskoe carbonatite occurrence. Outcrops of the Precambrian rocks of the Chadobetskyi uplift, which are cut by dikes and diatremes, composed of Mesozoic carbonatites, picrites and ultrabasic rocks occur in the south-western part of the Siberian Platform [5]. We analyzed calcite carbonatites. Sr isotope shows variations as 0.7034-0.7036 while Epsilon Nd have variations being 1.5-2.9.

CARBONATITES OF MOBILE BELTS

The given section considers the carbonatites of Mongolia, North Baikal Area as well as lamproites of Australia, Spain and carbonatites of North Tien Shan. Occurrences of carbonatites of K-series are found in Mongolia, South Gobi. They include volcanic rocks of Mushugai-Khuduk, Ulugei-Khud, Bayan-Khushu [7,9,24] and Lugingol [6] massifs of pseudoleucite syenites. The latter is located in 100 km from the occurrence of carbonatites with TR ores in China (Bayan-Obo). On the North of Mongolia in the Hovsgol area there is jolite-syenite massif with Beltsin-Gol carbonatites. In Buryatia one can find carbonatite occurrences of the Khalyutinskaya group (Khalyuta, Arshan, South) [19], carbonatites in the Oshurkovskyi shonkinite massif and Be-F- carbonatite occurrences of Ermakovka, genetically similar to carbonatites. Sr and Nd isotope values are given in Table 1 and Fig.5.

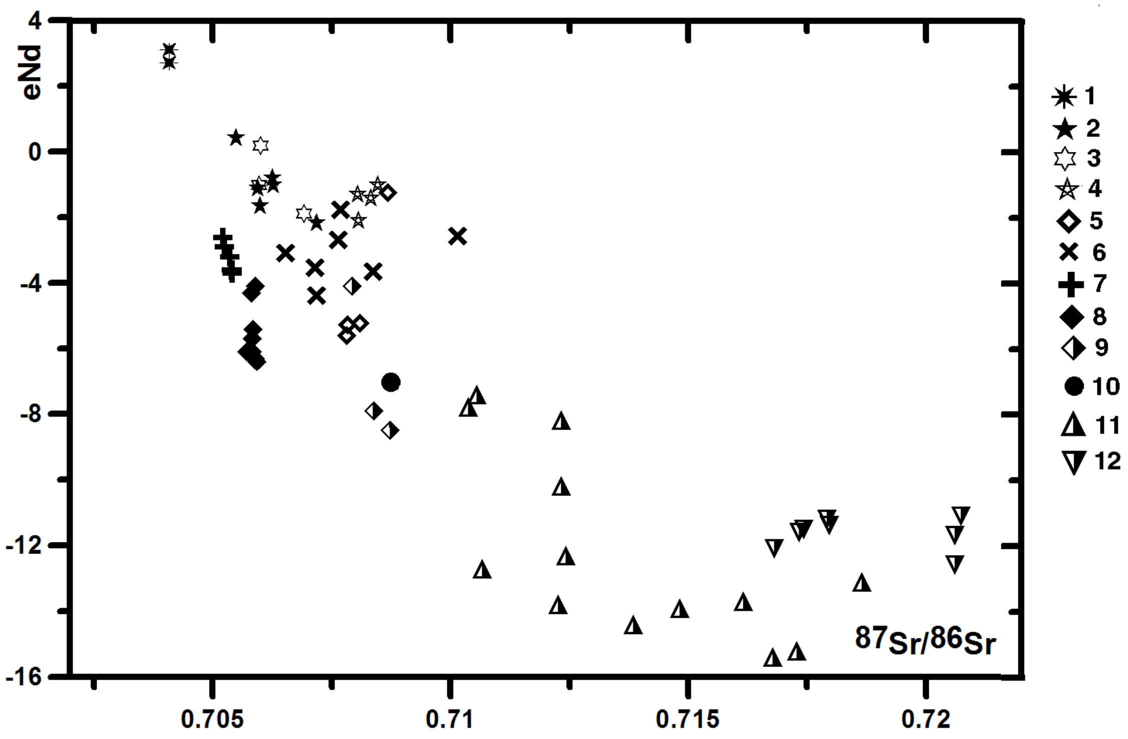

Fig. 3. **Carbonatite and lamproite of mobile belts.**
Massifs: 1 – Ulugei, 2 - Mushugai, 3 - Baian-Khushu, 4 - Lugingol, 5 - Beltsin-Gol 6 – Ermakovka, 7 - Oshurkovo, 8 – Khaluta, 9 - Darai-Pioz, 10 - Burpala , 11- Australia, 12 – Spain.

Mushugai-Khuduk volcanic area. It is located in 100 km to the south of Dalandzagad city (Mongolia). The flows of lava and tuff lava of melanephelenites, trachytes, phonolites, stocks of nepheline and alkaline syenites occur on the area of over 100 km^2. They are cut by dikes and diatremes of apatite-magnetite and carbonatitic composition. Carbonatites are mainly calcitic and calcitic-fluoritic[7-9]. Cerussite-containing tuffs are found as well [24, 27]. The age of the complex is 120-150 Ma. We analyzed calcite carbonatites, apatite-fluorite-celestite-magnetite rocks, apatite-magnetite rocks, cerussitic tuffs and carbonatite separations in lavas of melenephelenites. 87Sr/86Sr ratio varies within 0.70548-0.70717 aepsilon Nd Nd ranges within +0.42 - 2.16. The earlier drop-like inclusions of carbonatites occurring in lavas of melanephelenites, show the lowest Sr isotope values, while in carbonatites and apatite-magnetite rocks these values are similar. The highest Sr isotope values are found in cerussite-jarosite tuffs. Negative Nd values increase in the same order.

Bayan-Khushu massif. It is located in 50 km eastward of Mushugai-Khuduk. The massif is composed of shonkinites, nephelinic and alkaline syenites, which are cut by dikes of calcite-fluorite-celestine (and barite) carbonatites. The hosting rocks contain the veined body of dolomitic tuff. The age of rocks is 120-145 Ma. We analyzed calcite carbonatites, calcite-fluorite-celestine veins and dolomite tuffs. Epsilon Nd varies within +0.2 – 1.87, 87Sr/86Sr ratio ranges from 0.70598 to 0.70692. Like in Mushugai rocks Epsilon Nd negative values increase in the series calcite, calcite-fluorite carbonatites, dolomitic tuff. Isotope values in tuffs of both complexes are similar.

Ulugei-Khud massif. This carbonatitic complex is located in 200 km eastward of Mushugai-Khuduk. The massif contains volcanic rocks of trachyte composition, alkaline and quartz syenites, apatite-magnetite rocks and calcite carbonatites. The age of rocks is 150-175 Ma.

We analyzed calcite carbonatites. Epsilon Nd varies within +2.8 - + 3.2, Sr isotope values are 0.70407. Isotope characteristics of carbonatites from this massif differ from the previous complex in positive Epsilon Nd values and lower Sr isotope ratio values.

Lugingol massif is situated in 250 km south-westwards of Mushugai-Khuduk and in 100 km eastward of the largest Khan-Bogdo agpaitic massif of alkaline granites [6, 20]. It is composed of nephelinic and pseudoleucite syenites of the major phase of the massif, which also contains the xenoliths of feld-spar pyroxenites and shonkinites. The syenites are cut by dikes of pseudoleucite syenites, pseudoleucite tinguaites and calcite carbonatites with bastnesite, sinkhisite. The carbon isotope values varying from -1,5 up to - 2,4 and very heavy oxygen from 23,3 up to 25,2 is typical of carbonatites. In coexisting calcite-bastnasite the calcite is marked by lighter isotopes. Shonkinite dikes occur in 50 km westward of Lugingol. In chemical and mineral composition they are similar to shonkinites of TR deposit Mautin-Pass (USA). The dyke of dolomitic carbonatites with bastnaesite (30 %) is found as well. We analyzed calcite-bastnaesite carbonatites of both occurrences. Epsilon Nd values range from –1.0 to –1.4, 87Sr/86Sr ratio varies from 0.7081 to 0.7085.

Beltsin-Gol massif. It is located in Hovsgol area in Mongolia. The massif contains pyroxene-nepheline ijolites and leucosyenites. Ijolites of the northern near-contact part of the massif contain small veined bodies of calcite carbonatites. We analyzed carbonatites. Epsilon Nd values vary within – 1.2 - 5.6, 87Sr/86Sr value ranges from 0.7078-0.7087.

Buryat carbonatite province is situated southwestwards and northeastwards of Ulan-Ude and includes 7-8 carbonatitic occurrences[19]. It stretches over 200 km. The most significant occurrences of carbonatites include Khalyuta, Arshan, South, Oshurkovskoe and Ermakovskoe Be- deposit with carbonatite-like rocks.

Khalyuta occurrence includes several outcrops of dykes, stocks, and volcanic flow of calcite carbonatites. There are also dykes of K-shonkinites and syenites. Carbonatites contain apatite, magnetite, sulfides and great abundances of Sr and Ba sulfates and carbonates –barite, celestine, strontianite. Isotope data are taken from [16]. We analyzed carbonatites, shonkinites and syenites. 87Sr/86Sr values vary within 0.70571-0.70590, Nd epsilon ranges from – 4.1 to - 6.3

Arshan and South occurrences. They are located in 70 km southwestwards of Ulan-Ude. They include breccia-like diatremes with carbonatite cement. On the Arshan occurrence xenoliths comprise altered host granites. Carbonatites are calcite with apatite, monazite, bastnaesite. TR contents reach as high as 5 %. Carbonatites show the following isotope values: 87Sr/86Sr =0.70592 aepsilon Nd Nd – 6.4.

Oshurkovskyi massif is located in 5 km from Ulan-Ude. The massif is composed of shonkinites, which contain xenoliths of Bt and potassium feld spar pyroxenites, of syenites and granite pegmatites. Shonkinites show small dikes of calcite carbonatites. Shonkinite and syenites are marked by high apatite contents and are apatite ore. Isotope date are given in [16]. We analyzed carbonatites, shonkinites and syenites, 87Sr/86Sr values vary from 0.70522 to 0.70541 Epsilon Nd ranges from – 2.6 to - 3.7.

Ermakovskoe occurrence is found in 100 km towards the north of Ulan-Ude. It contains dikes of basic rocks, syenites and alkaline granites [10,11]. Ore rocks contain Be silicates (phenacite, bertrandite, eudidymite etc.), fluorite, microcline, apatite, carbonatites, sulfides. Carbonate content in some rocks reaches as high as 60%. In terms of the genesis the separation of silicate-Be-fluorine-carbonate liquid from the silicate magma is similar to the separation of carbonatites. We analyzed carbonate rocks with fluorite and different Be minerals. 87Sr/86Sr values vary within 0.70648-0.71103, while epsilon Nd ranges from 1.5 to 4.3.

Burpala massif is located in the North Baikal Area, in 100 km northeastwards of the northern margin of Lake Baikal [23]. The massif contains nephelinic, alkaline and quartz syenites, which are cut by numerous dikes of rare-metal agpaitic syenites-pegmatites. The central massif’s zone comprises a large body of apatite-fluorite rocks, containing magnetite and mica (analog of phoskorites). The carbonatitic dikes of calcite composition with brewsterite are found in the center of the massif while calcite dikes with a quartz and pyrite occur in the host rocks. Calcite carbonatite was analyzed, Epsilon Nd is –6.3, 87Sr/86Sr equals to 0.70851.

Darai-Pioz massif is found in South Tien Shan at the altitude of 5000 m. The massif is composed of nephelinic, alkaline syenites and alkaline granites, which are cut by dikes of carbonatites and rare-metal alkaline-granite pegmatites. Calcite-pyroxene carbonatites contain rare metal mineralization [22]. The carbonatites and calcite of drop-like shape in the alkaline granite have been analyzed.

For a greater representation of the diagram of Sr and Nd isotopes we plot also the data concerning lamproites of Australia, Spain and North America [18,33,15]. The Australian lamproites show 87Sr/86Sr variations as 0.71055-0.71677, epsilon Nd for them varies from –7.4 to –15.4 while the Spanish lamproites have variations of 87Sr/86Sr as 0.71681, epsilon Nd ranges from –11.1 to –12.6. Both lamproites occur in folded zones.

CARBONATITES OF RIFT ZONES OF SIBERIAN PLATFORM AND ALDAN SHIELD JOINING

The carbonatitic complexes of this structural region can be divided into 2 groups [28]. The first group includes complexes of the western and central parts while the second one comprises complexes of the south part [28]. The first group includes the Murun, Raybinovyi, Yakokutskyi and Bilibin massifs of Mz age [5, 21,26,28], while the second one involves the Khaninksyi massif of PreCm age. Values of Sr and Nd isotopes are given in table 1 and Fig. 4.

Murun massif. The area of the massif is 150 km2, the age is 145 Ma. It belongs to volcano-plutonic ultra potassium stratified alkaline complex [26,28]. The massif contains complex of Bt-pyroxenites, K -ijolites, leucite shonkinites and fergusite (early complex) with xenoliths of olivine-spinel monticellite-melilitic rocks. The rocks of the major phase involve the stratified complex of melanoctratic and leucocratic pseudoleucites, alkaline syenites and alkaline granites. At later stage tuff lavas and leucite phonolites and leucite lamproites flows were erupted and the dikes of leucite tinguites were intruded. The later phase contains a stratified silicate-carbonate complex of microclinites, microcline-pyroxene rocks, charoite rocks, as well as calcite and benstonite carbonatites [29,30]. Then all rocks were subjected to hydrothermal silicification and sulfidization, containing numerous ore mineralization. We have revealed 5 types of carbonatites and over-intrusive zone of calcite- K-rickterite-tetraferriphlogopite rocks [12]. We analyzed the silicate rocks and carbonatites, fields of their points are overlapped. Variations of 87Sr/86Sr are 0.70620-0.7730, those of Epsilon Nd are from –16.8 to –23.9. Considering negative values of epsilon Nd (to – 25) the Murun massif is the deepest amongst massifs of alkaline rocks.

Bilibin massif. The area of the massif is 150 km2. It belongs to K-leucite complex of rocks [21]. The massif is composed of the stratified complex of micaceous peridotites, Bt- pyroxenites, olivine-leucite lamproites and leucite fergusites. Shonkinites, leucite and alkaline systenites and alkaline granites were crystallized later. The second group of rocks has gradual transitions. A unique differentiation from ultrabasic rocks to granites is common to the massif. A small clump of apatite - calcite carbonatites has been found among occurrences of ultrabasic rocks. The clump could be brought from the Arbarastakh massif, located in 100 km eastwards. 87Sr/86Sr values in silicate rocks vary as 0.70580-0.70700., Epsilon Nd ranges from –16.3 to –18.7.

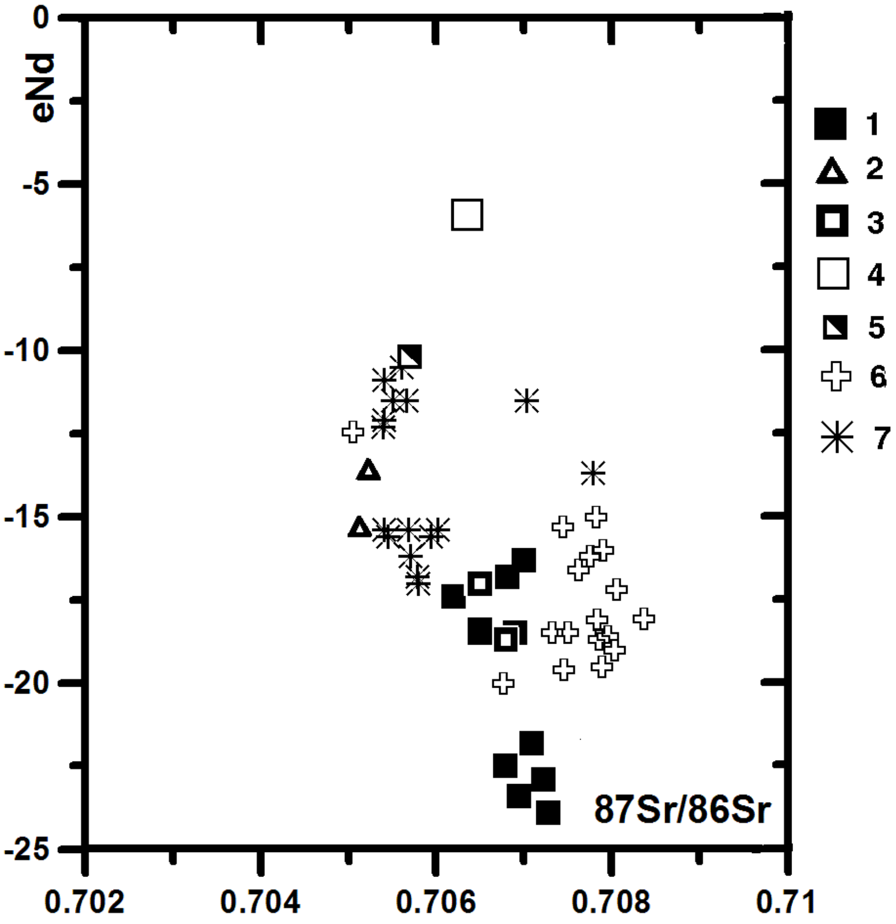

Fig. 4**. Of alkaline, lamproite and carbonatite complexes of Rift zones of Siberian platform and Aldan Shield joining and the North American Platform and Canadian shield joining.**

Massifs: 1 - Murun, 2 - Khani, 3 - Bilibinski, 4 – Jakokut, 5- Pjabinovi, 6 – Montana, 7 – Leucite Hills

Khani massif (Ukduska site). The massif is composed of apatite-biotite pyroxenites, shonkinites, syenites and granites. Pyroxenites are cut by the dike of the layered syenite-carbonatites (calcite) and dike of olivine lamproites [23]. The age of lamproites, determined from zircon is 2702 Ma. These are the most ancient lamproites of the world. 87Sr/86Sr vary within 0.70450-0.70505, Epsilon Nd ranges from –12.5 to –15.3. The massifs of the Aldan alkaline province demonstrate also values of 87Sr/86Sr as 0.70504 aepsilon Nd Nd as –14.5 for the carbonatite vein in biotite pyroxenites of the Ryabinovyi massif and 87Sr/86Sr value as 0.70570 aepsilon Nd Nd as –10.2 for lamproites of the Yakokutskyi massif.

Alkaline rocks of the North America mainly occur in rift zones between the North American Platform and Canadian shield as in the case of the Aldan alkaline rocks found between the Aldan shield and Siberian Platform. Thus, we plot them on the diagram of Sr and Nd isotope ratios using the data from [15,18,33]

THE ASSOCIATION OF STRONTIUM AND NEODYMIUM ISOTOPES WITH THE TYPE OF MANTLE AND GEODYNAMIC SETTINGS

As known, the type of primary mantle for massifs is conditioned by Sr and Nd isotope ratios, considering the age of rock origin. Three main types of mantle have been distinguished: depleted (impoverished) mantle, enriched EM-1 mantle and enriched EM-2 mantle (Fig.5,6).

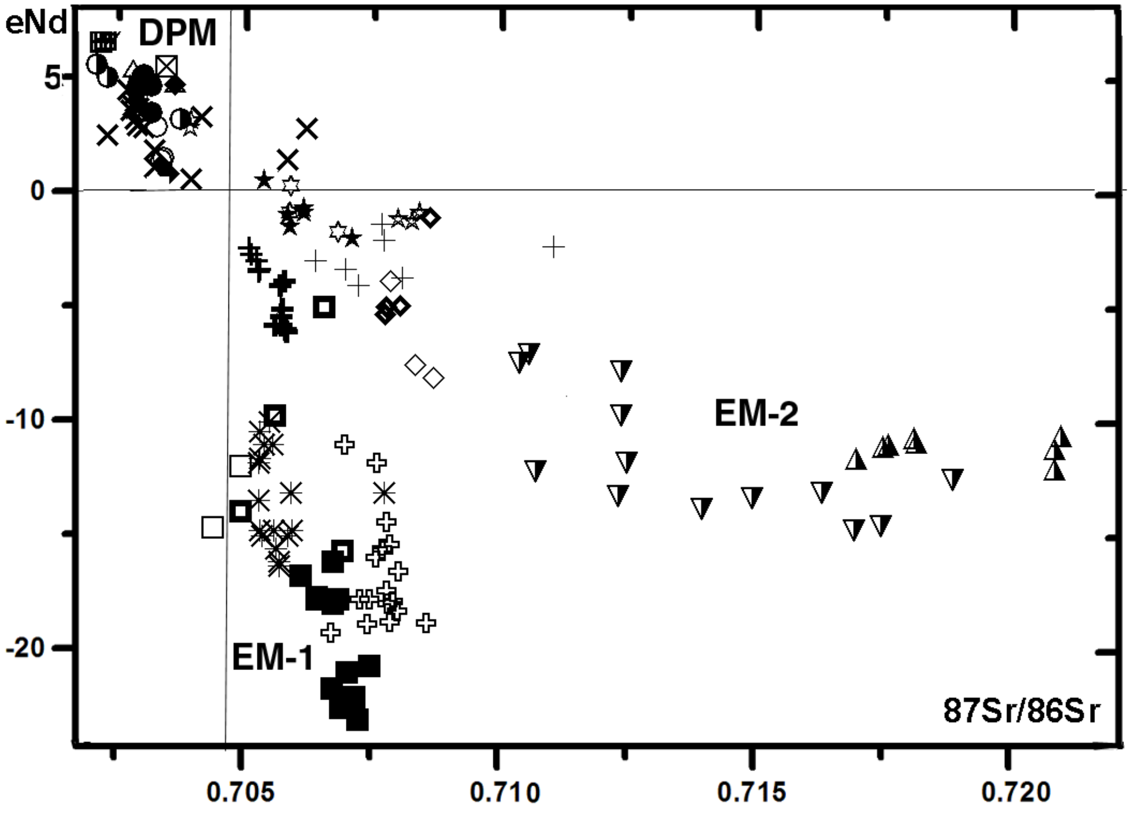

Fig. 5. **Sr/Nd isotope ratio of alkaline, lamproite and carbonatite complexes of Siberia and Mongolia and lamproites of Australia and Spain.**

Map symbols on; fig 2,3,4. **DPM** - depleted mantle.

Different types of mantle demonstrate different isotope values. Thus, depleted mantle shows positive values of epsilon Nd and 87Sr/86Sr values ranging within 0.702-0.705, while the enriched EM-1 mantle is marked by negative epsilon Nd and values 87Sr/86Sr varying as 0.705-0.709, and the enriched EM-1 mantle demonstrates negative values of epsilon Nd and 87Sr/86Sr values as 0.705-0.725. On the boundary of three mantle values there is an intermediary area. The referring of rocks having Sr values over 0.705 to mantle rocks cast some doubt. However, in Spanish lamproites and diamond-bearing Australian lamproites, which are undoubtedly mantle rocks, 87Sr/86Sr values reach as high as 0.722 [18,15]. Considering the geologic position of studied massifs and geodynamic situation of these areas [10,11,] we came to an interesting conclusion [31]. Different geodynamic settings of alkaline rock generation show different mantle types (Fig. 6) [28,31]. Thus, isotope values of massifs located within the framing of the Siberian Platform, which underwent subduction, lie in the field of the depleted mantle. They include massifs of the Eastern-Sayan province (Bolshaya Zima, Srednyaya Zima, Tagninskyi, Zhidoi), Maimecha-Kotui province (Guli and Essei), Yenisei Ridge (Kiya, Tatarskyi) as well as Eastern-Aldan and Sete-Davan provinces (Arbarastakh, Ingili and Gornoe Ozero).

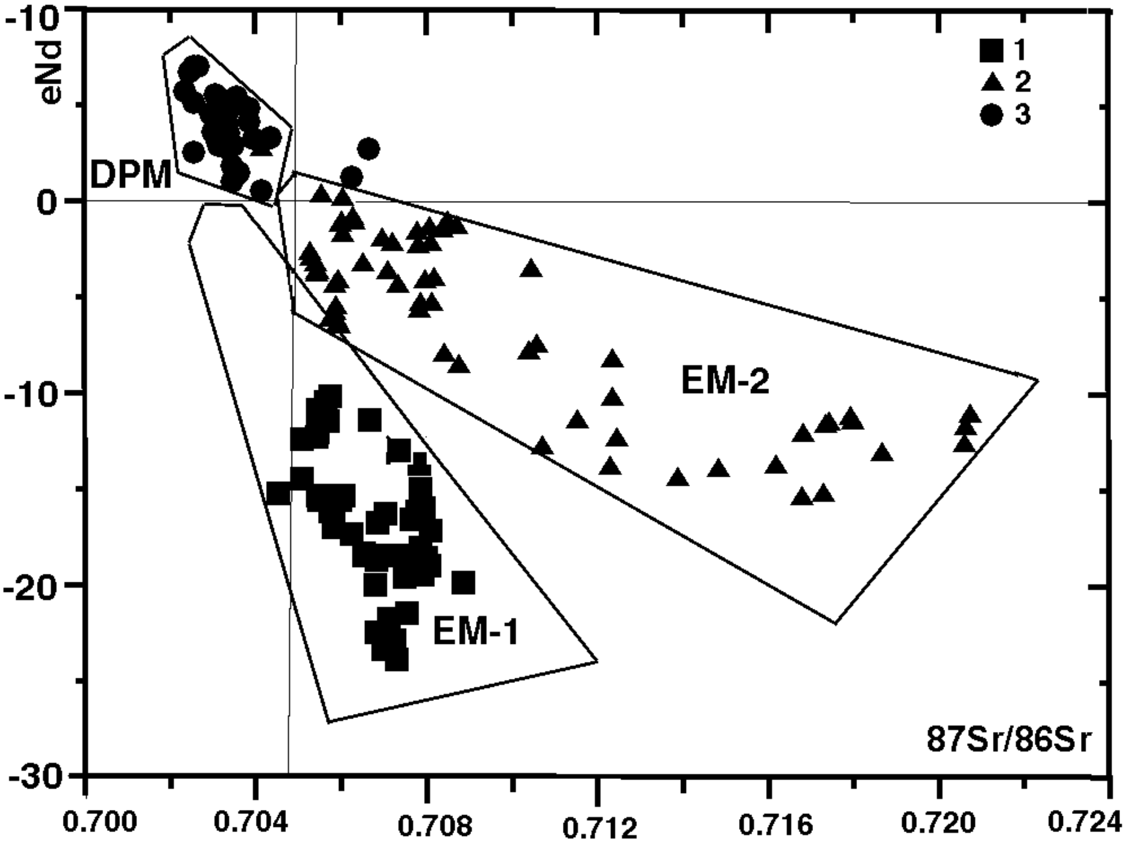

Fig. 6. **Sr/Nd isotope ratio of alkaline, lamproite and carbonatite complexes and types of the mantle**

1 - of alkaline, lamproite and carbonatite complexes of Rift zones of Siberian platform and Aldan Shield joining and the North American Platform and Canadian shield joining. 2- of alkaline, lamproite and carbonatite complexes of mobile belts 3- of alkaline and carbonatite complexes of the Siberian Platform framing. **DPM** - depleted mantle.

Massifs of mobile (folding) belts (of areas of complete folding) lie in the field with isotope values of enriched EM-2 mantle. They include carbonatitic complexes of Mongolia (Mushugai-Khuduk, Ulugei Khud and Bayan-Khushu, Lugingol Beltsin Gol), of Burytia (Khalyuta, Southern, Oshurkovo and Ermakovka), carbonatites of the North Tien Shan (Darai Pioz), Northern Baikal area (Burpala) as well as lamproites of Australia and Spain.

Massifs, generated in intracontinental rift zones between the Siberian Platform and Aldan shield (as well as between the North American Platform and Canadian shield) lie in the field of isotope values of the deepest enriched EM-1 mantle. They include the following massifs Murun, Ryabinovyi, Yakokutskyi, Bilibin, Khanan and lamproites of Leucite Hills, Montana, Smoky Butte, Praire Creek. The melting of these massifs is associated with plume processes. However, the question arises how such ore potential magmas of alkaline rocks could be melted out of depleted mantle. It can be explained by a low degree of selective melting of the mantle when magmas of alkaline rocks originated. Therewith, minerals relatively enriched in rare elements are melted (e.g. garnet).

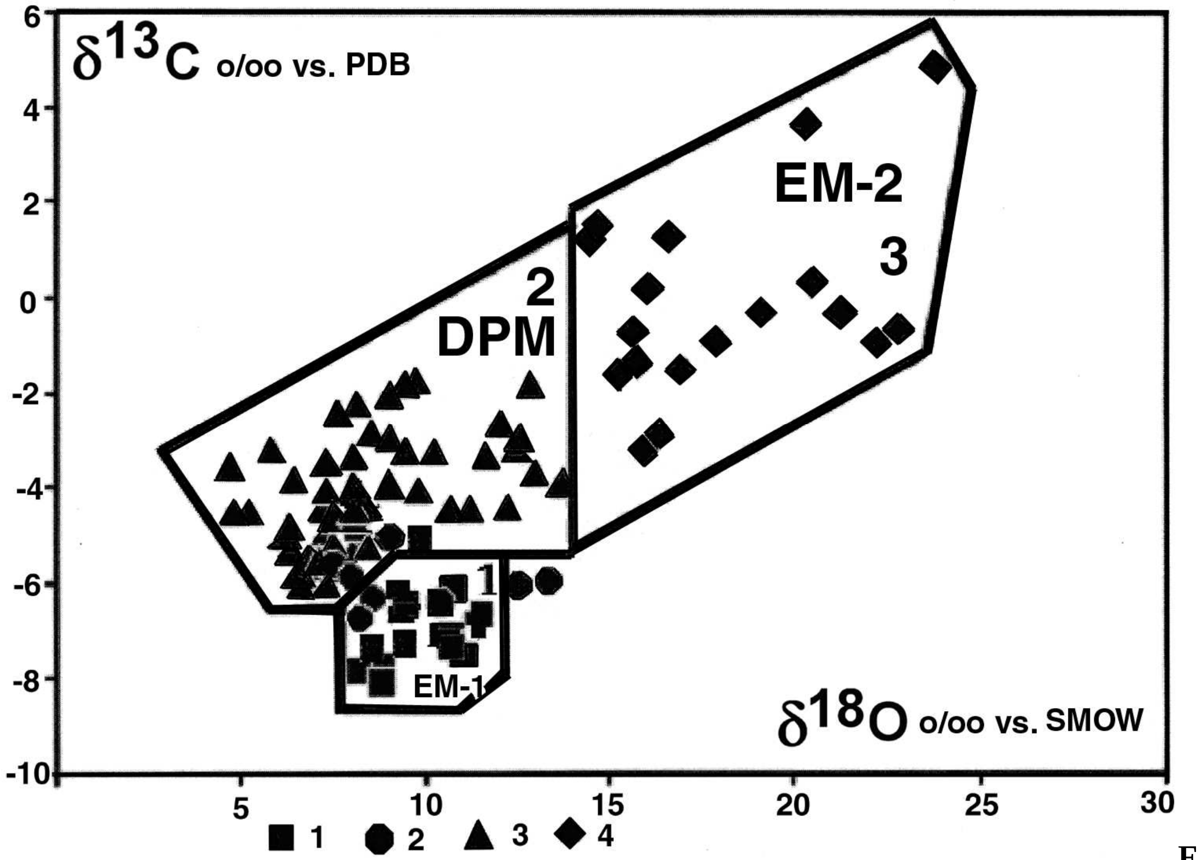

Fig. 7. Carbon/oxygen isotope ratio and types of the mantle.

Field 1 - EM-1 mantle. Field 2 - depleted mantle. Field 3 – EM-2 mantle. Conventional units. Massifs: 1 - Murun, Khani, 2 - Bilibin, Inagli, Arbarastakh, 3 - massifs of the Siberian Platform framing,4 - massifs of mobile (folded) belts.

We made an attempt to use the data concerning the mantle type obtained from the diagram of Sr and Nd ratio for the same samples on the plot of carbon and oxygen isotope ratios (Fig. 7). A rather compact pattern of separating massifs by mantle type has been obtained [19].

Massifs of the completed folding (Mongolia, Buryatia, North Baikal Area, Tien Shan etc.) fall into field 3. Their initial magmas generated from enriched mantle EM-2.

Earlier isotope determinations in the field 3 for carbonatites are conditioned by capturing of atmospheric oxygen and surface water during formation [17]. For the studied carbonatites this mechanism can act, but as secondary one. When rocks of the zone of the completed folding are generated the surface water was captured and these rocks have heightened values of heavy oxygen. When they subsided along Benioff zones to a considerable depth of the mantle they were mixed with the mantle changing isotope determinations. When the alkaline rocks were melted from this mantle they already had these new determinations. Thus, heavier oxygen is not an evidence of their contamination by crustal material as was considered by [17], but the effect of melting from contaminated mantle.

The massifs of the Siberian Platform framing, exhibiting subduction fall into field 2. The depleted mantle is typical of them. The carbonatites of massifs originated in rift zones between Aldan shield and Siberian Platform or on the shield itself fall into the field 1. This characteristic is common both to ultra potassium Mz complexes of the Aldan shield (Murun and other massifs), and to Precambrian K-massifs (Khani massif). The influencing of plume processes, occurring in Asian continent at that time, on magma melting is more probable [11]. Isotope values for ancient massifs of the Western Aldan (Arbarastakh, Ingili and Gornoe Ozero) are located on the boundary of fields 1 and 2. Such a position can be explained by lack of data concerning the geodynamic settings of areas in the Precambrian or by proximal position to the platform’s margin with the depleted mantle type.

The above indicates that the proposed diagram [19] can be applied for determining mantle type for carbonatites of the Asian continent. As the analysis of oxygen and carbon isotopes is much cheaper and easier than the analysis of Sr and Nd isotopes, such application has sense. However, for new areas of carbonatite magmatism it is necessary to confirm the definition of mantle type using also data on Sr and Nd isotopes.

CONCLUSIONS

We discussed Sr and Nd isotope values and their ratios in alkaline carbonatitic complexes of Siberia and Mongolia. On the diagram epsilon Nd ratios and 87Sr/86Sr isotope values of alkaline massifs generated in different geodynamic settings lie in fields of different mantle sources (depleted, enriched EM-1 and enriched EM-2). A similar tendency is typical of oxygen and carbon isotope ratios [19]

The investigations were supported by the Russian Foundation for Basic research (grant № 03-05-64146) and integration projects of SB RAS № 67 and RAS № 6-2-1.

REFERENCES

1. **Deines, P.** (1989). Stable isotope variations in carbonatites // Carbonatites. Genesis and Evolution (Edited by Keith Bell). London, pp. 301-359.
2. **DePaolo, B.J.,** (1988). Neodymium isotope geochemistry // An Introduction. Springer-Verlag, New York.
3. **Egorov, L.S.** (1991). Ijiolite-carbonatite plutonism // Nedra. 260 pp.
4. **Goldstein S., O'Nions, R., Hamilton, P.J.,** (1984). A Sm-Nd study of atmospheric dusts and particulates from major river system // Earth Planet. Sci. Lett.70, 221-236.
5. **Kogarko, L.N., Kononova, V.A., Orlova, M.P., Wooley, A.R.** "Alkaline Rocks and Carbonatites of the World // London, Glasgow, New York, Melbourne, Madras.
6. **Kovalenko, V.I., Vladykin, N.V., et al.** (1974). The Lugingol massiff of pseudoleucitic syenites in the MNR // Izvestia Akademii Nayk SSSR, seria geologicheskaia, N 8, p. 38-49.
7. **Kovalenko, V.I., Vladykin, N.V., Goregljad, A.V.** (1977). East Mongolia-the new province of the rare metal mineralisazion. // In: Main problems of geology in Mongolia. V.22, Nauka, p. 189-205.
8. **Kovalenko V.I., Vladykin N.V. et al.** (1977). Geochemical characteristics of rocks from near surface carbonatite kindred from Goby desert, Mongolia // Geochimia, № 9, pp.1313-1326.
9. **Kovalenko V.I., Samoilov B.S., Vladykin N.V. et al.** (1979). Rare-metal carbonatites and apatite-magnetite rocks of Mongolia // Geology and magmatismes of Mongolia, v.30, Nauka, p. 158-167.
10. **Kovalenko V.I., Yarmolyuk, V.V., Vladykin, N.V. et al.** (2002). Stages of formation, geodynamic setting and sources of rare-metal magmatism of central Asia // Petrology, v. 10, .№ 3, p. 227-253.
11. **Kovalenko V.I., Yarmolyuk V.V., Vladykin N.V., Kozlovsky A.M.** (2002). Problem of plumes and their bearing on sources of rare-metal magmatism in central asia // Deep-seated magmatic sources and the problem of plumes Vladivostok, pp. 23-42.
12. **Miyazaki T., Shuto K.,** (1998). Sr and Nd isotope ratios of twelve GSJ rock reference samples. // Geochem. J. 32, 345-350.
13. **Morikiyo T., Tokana K., Miyazaki T., Kagami H., Vladykin N.V.** (2000). Sr, Nd, C and O isotopic compositions of carbonatite and peralkaline silicate rocks from the Zhidoy complex, Russia // Journal of Mineralogical and Petrological, 2000, v. 95, pp. 162-172.
14. **Morikiyo T., Miyazaki T., Kagami H., Vladykin N.V., Chernysheva E.A., Panina L.I., Podgornych N.M.** .(2001) Sr, Nd, C and O isotope characteristics of Siberian carbonatites // Alkaline magmatism and the problems of mantle sources, Irkutsk, pp. 69 - 84.
15. **McCulloch M.T., Jaques A.L., Nelson D.R. and Lewis J.D.** (1983). Nd and Sr isotopes in kimberlites and lamproites from Western Australia: an enriched mantle origin // Nature. vol. 302, 31 March, pp. 400-403.
16. **Nikiforov A.B. et al.** (2000) Chemical and isotope composition of carbonatites of Transbaikalia // Petrology, v.8, № 3, pp. 309-336.
17. **Pokrovsky, B.G.** (2000) Crustal comtamination of mantle on evidance of isotope geochemistry // M, Nauka, 228 p.

18. **Powell J.L. and Bell K**. (1970) Sr isotopic Studies of Alkalic Rocks: Localities from Australia, Span and Western United States // Contr. Mineral. And Petrol. 27. pp.1-10.
19. **Ripp, G.S., Badmatsyrenov, M.V., Skulyberdin, A.A.** (2002). A New Carbonatite occurrence in Northern Transbaikalia // Petrology. V. 10. № 4. P. 442-4
20. **Vladykin N.V., Kovalenko V.I., Dorfman M.D.** (1981) Mineralogical and geochemical features Khan-Bogdo massiff alkaline granites // Nauka. Moskva, p.1-136.
21. **Vladykin N.V.** (1996). Bilibin-massiff K-alkali rocks // DAN, v.349, N6, p. 972-975.
22. **Vladykin N.V., Dusmatov V.D.** (1996). Chemistry composition mikas Darai-Pioz massiff. // ZVMO, N.3, p.84-94.
23. **Vladykin N.V.** (1997). "Petrology and productivity of K-alkali rocks of Mongol-Okhotsk area of magmatism // The thesis in the of an scientific report, Irkutsk, p.1-80.
24. **Vladykin N.V.** (1999), Ore-bearing tuffs and volcanics of the Mushugai Khuduk carbonatite complex, Gobi, Mongolia // Proceedings of Universities of Siberia, issue 4-5, p. 84-86.
25. **Vladykin N.V., Morikiyo T., Tokana K.** (1999). New data about Zidui massif ultrabasik-alkali rocks and karbonatite // Geology and metalogenie preCm of Siberia. Irkytsk, p. 25-28.
26. **Vladykin N.V.** (2000). Malyi Murun Volcano-Plutonic Complex: An Example of ifferentiated Mantle Magmas of Lamproitic Type // Geochemistry International, 2000, v. 38, suppl. 1, pp. 573-583.
27. **Vladykin, N.V.** (2001). Ore potential of carbonatite tuffs of K-alkaline complexes of Siberia and Mongolia // 100-anniversary of studies of carbonatites of the Kola Peninsula. S-Peterburg, p. 49-51.
28. **Vladykin N.V.** (2001). The Aldan Province of K-alkaline rocks and carbonatites: problems of magmatism, genesis and deep sources // Alkaline magmatism and the problems of mantle sources. Irkutsk, pp. 16-40.
29. **Vladykin N.V., Tsaruk I.I.** (2003). Geology, chemistry and genesis of Ba-Sr-bearing ("benstonite") carbonatites of the Murun massif // Geology and Geophysics, v. 44, № 4, pp. 315-330.
30. **Vladykin N.V., Viladkar S.G., Miyazaki T., Mohan R.V.** (2003). Chemical composition of carbonatites of Tamil Nadu massif (South India) and problem of “benstoonite” carbonatites // Plumes and problems of deep sources of alkaline magmatism. Khabarovsk, pp.130-154.
31. **Vladykin N.V., Morikiyo T., Miyazaki T.** (2004) Geochemistry of carbon and oxygenisotopes in carbonatites of Siberia and Mongolia and some geodynamic consequences .// Deep seated magma-tism it’s sources and their relation to plum processes. Irkutsk – Ulan-Ude. pp. 96-112.
32. **Volmer R., Ogden P., Schilling J.-G., Kingsley R.H., Waggoner D.G.** (1984). Nd and Sr isotopes in ultrapotassic volcanic rocks from the Leucite Hills, Wyoming // Contr. Mineral. and Petrol. vol. 87, pp. 359-368.

UDK 552.33+550.42

ORIGIN OF CARBONATITE-BEARING COMPLEXES FROM FOLD SYSTEMS: ISOTOPIC EVIDENCE FOR THE MANTLE-CRUST INTERACTION

Vrublevskii V.V., Gertner I.F.

Tomsk State University, Tomsk, labspm@ggf.tsu.ru

This paper presents isotopic evidence for mantle-crust interaction that had place during the forming of alkaline and carbonatite-bearing magmatic complexes with different ages and formation types in the setting of consolidation and late-collisional rifting of fold systems. Material of middle-depleted mantle corresponding to PREMA- or HIMU-type with probable minor component of MORB- and EMI-reservoirs was dominant in the composition of juvenile sources for Late Precambrian and Early Paleozoic carbonatite-bearing rock assotiations as well as for most of their analogs in cratons. Magma sources of Mesozoic and Cenozoic carbonatite complexes are mostly similar to the matter of enriched subcontinental lithospheric mantle zones. Such distinction for the nature of magma-generated substance proposes a development of young carbonatite-bearing associations on the continental crust with high thickness as a main control factor. According to this reason processes of rifting destruction relaxed with depth and didn't achieve areas bordered with asthenosphere. Therefore only EMI- and EMII-resevoirs in subcontinental lithosphere was single deep-seated sources that could produce alkaline and carbonatite melts.

The evolution of parental magmas was differently completed by crustal contamination on the level of feeder channels and intermediate chambers. This process proceeded without direct absorption of hard matter by magmas, but could be a result of their interaction with high-concentrated solutions that was mobilized from host sedimentary layers by the thermal influence of intrusions. For such contamination we assume to promote an additional carbonatization and enrichment of briny components in mantle alkaline silicate magmas with last isolation of strictly carbonatite liquids. The relationship between «mantle» contamination and genesis of carbonatites is less revealed and found expression in metasomatic carbonatization of mantle substrate with subsequent melting of carbonatite or CO_2-rich alkaline magmas.

INTRODUCTION

For present day the origin of carbonatites have a debatable character that relative with obvious heterogeneity of their sources and forming processes. Isotope geochemical researches began to play a most important role to understand a genesis of carbonatites on a level with traditional methods of geology, mineralogy and experimental modeling. According to modern views a primary matter of carbonatites must to have mantle-similar isotopic characteristics [9-10, 13], that usually correspond to narrow field of variations. Deviation from this parameters can be interpreted as manifestation of following processses: (a) compositional mixing of differential mantle domens, (b) contamination of mantle primary magmas including a recycling of inorganic carbon from the crust in deep parts of subduction zones, (c) selective crust contamination complicated a differentiation of carbonatizated silicate melts, (d) fractionation of carbonatite liquids, (e) fluid-rock reactions during late stages of magmatic evolution [10, 21, 24, 27, 29, 35, 45, 49-55, 63, 71-72, 82-88 et al.]. Features of carbonatite composition and its metallogeny is mostly defined by participation of mantle matter in the development of carbonatite system. Such component is predominant in most of alkaline ultrabasic and carbonatite-bearing complexes in cratons where the magma-generated substrate is usually present by middle depleted HIMU- or PREMA-type mantle corresponding to the source of oceanic island basalts [6, 8, 23-24, 39, 41]. At the same time a differ scale mixing between HIMU-plume component and EMI matter is established for many young (< 200 Ma) carbonatite complexes [1, 3, 6-8, 10, 19-20, 24, 33, 36, 56, 64-67, 73-74 et al.].

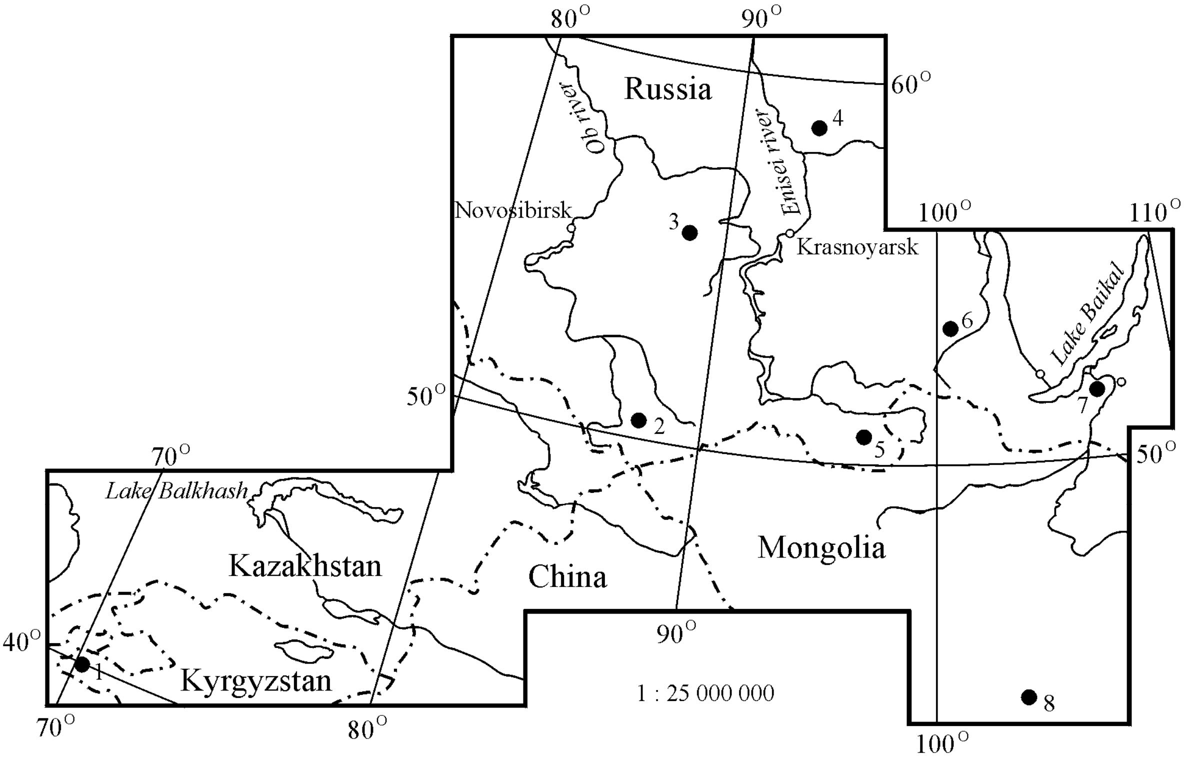

Fig. 1. **Geographic position of carbonatite-bearing complexes**

Complexes: 1 – Matcha (Turkestan Alai ridge, Southern Tien Shan), 2 – Edel'veis (Gorny Altai), 3 – Verkhnepetropavlovsk (Kuznetsky Alatau), 4 – Penchenga (Enisei ridge), 5 – Kharla (SE Tuva), 6 – complexes of the Eastern Sayan province, 7 – complexes of the Western Baikalian region, 8 – Mushugai-Khuduk (Southern Mongolia).

Forming of carbonatite-bearing rock associations in folded regions unlike platforms has more episodic character and realizes in the setting of late or postcollisional rifting. Apparently an influence of crust matter on the evolution of carbonatite systems was more significant in conditions of continued continental crust growth [51, 83]. The age, geological setting and geochemical features of alkaline rocks and carbonatite complexes of folded regions from Siberia (Gorny Altai, Kuznetsky Alatau, Eastern Sayan, Enisei ridge, Sangilen et al.) and Southern Tien-Shan (Turkestan-Alai) assume to correlated with products of late collisional rifting [83]. Therefore their isotopic parameters can be accompanying to criteria of some processes forming of final carbonatite composition in studied complexes. This processes may be as reflection of plume activity and mantle evolution beneath different lithospheric blocks, relative velocity of crust accretion and continental rifting, mantle-crust interaction and postmagmatic alterations. This paper is discussed the character of revealed isotopic heterogeneity in carbonatite complexes from orogenic areas and reasons of its origin.

PRIMARY MANTLE ORIGIN AND ND-SR-ISOTOPIC SYSTEMATIC OF CARBONATITES AND COMAGMATIC ALKALINE ROCKS

Results of combined isotope composition analysis in studied rock associations are clearly showing that a primary matter of carbonatite-formed systems had a mantle origin [80, 82-88]. At the same time a manifestation of alkaline and carbonatite magmatism in folded regions opposite to cratonic conditions must to be obviously characterized by more scale mixing of mantle and crustal material. Influence of this process was less reflected in the Nd-isotope composition parameters of that testify to two compositionally different mantle sources for primary matter of carbonatite complexes at the minimum. The material of middle depleted asthenospheric or lower mantle was dominated in the first of them. The second kind of source was obviously present by enriched subcontinental lithospheric mantle.

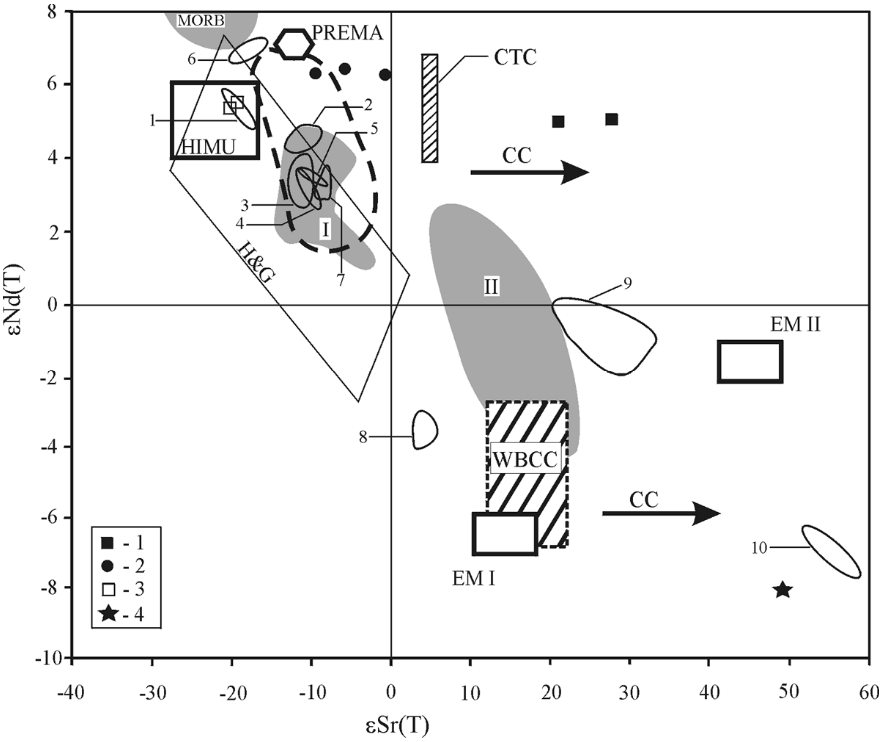

Fig. 2. **Sr-Nd-isotopic composition of carbonatite-bearing complexes from folded areas relative to «classic» carbonatites from cratons**

Symbols: 1 - Verkhnepetropavlovsk, 2 - Edel'veis, 3 - Penchenga, 4 - Matcha. Compositional fields: H&G – young (<200 Ma) carbonatite complexes of world from [24]; I – Proterozoic carbonatites from Northern America [6]; II – contaminated carbonatites from Southern America and India [24]; CTC – carbonatites from Tury massif (Kola peninsula) contaminated on the 10 % level by the matter of middle upper crust [23]; WBCC – alkaline rocks and carbonatites from the Western Baikalian region [43]. Bold dotted outline – carbonatites of alkaline ultramafic massifs from the Karel-Kola and Maimecha-Kotui alkaline provinces in Precambrian cratons [4-5, 23, 33-34, 40, 91]. Thin outlines: 1-6 – carbonatites from alkaline ultramafic massifs of Siberia [40] such as the Srednetatarsk (1), Verkhnesayansk (2), Niznesayansk (3), Zidoi (4), Bolshetagninsk (5), Ingili and Arbarastakh (6); 7-8 – carbonatites of the Koga and Jhambil (7), Loe Shilman and Sillai Patti (8) complexes from the NW Pakistan [74]; 9 – carbonatites of the Mushugai-Khuduk complex from the Southern Mongolia, 10 – carbonatites of the Darai-Pioz massif from the Southern Tien-Shan [75-76]. Mantle reservoirs (MORB, PREMA, HIMU, EM I and EM II) are shown as corresponding to their modern isotopic parameters [25, 92]. "CC" - arrows – direction of isotopic displacement during the crustal contamination.

Magmatic associations of R_3-PZ_1 age. Differently depleted (εNd_T 2,8-6,4) magma-generated substrates are typical for Late Riphean and Early Paleozoic carbonatite-bearing associations from the Altai-Sayan Fold System (ASFS), such as the Zima complex in the Eastern Sayan, Verkhnepetropavlovsk massif in the Kuznetsky Alatau and Edel'veis complex in the Gorny Altai as well as Srednetatarsk massif and Penchenga linear fenite-carbonatite complex from the Enisei ridge (Fig. 1, 2). Similar composition (εNd_T 1,5-7,0) is established for most «classic» carbonatites from different age platformic alkaline-ultramafic massifs in the Kola peninsula (Ozernaya Varaka, Sokli, Kovdor, Vuorijarvi, Tury, Khibiny), Siberia (Guli, Essei, Ingili, Arbarastakh), Northern America, Cenozoic volcanoes of Eastern Africa [4-6, 10, 23, 33-34, 40, 91]. These isotopic parameters alloy to assume a mixing in different proportions between materials of mantle plumes HIMU-or PREMA-type and enriched mantle reservoir, for example EMI that be often used to explain variations of carbonatites composition. Two versions are usually supposed for a penetration of EMI-components in the mantle plume material: (a) a recycling of continental and oceanic sediments in deep parts of subduction zones on the boundary with the asthenosphere or perhaps lower mantle, (b) an interaction between sediments and mantle plume uplifting to level of acient subcontinental lithosphere [17, 26, 39]. On the example of carbonatites from Eastern Africa some authors are also discussed a possibility of forming of isotope heterogenic plumes from HIMU and EMI reservoirs that can be spatially combined in deep (lower 1000 km) mantle or on the core-mantle boundary [10].

According to results of paleogeodynamic reconstructions structural assemblages of ASFS and Enisei ridge was components of Prevendian and Vendian-Cambrian arc island systems on the active continental margin of Siberian craton [12, 32]. Determined us ages for forming rocks of Penchenga (Enisei ridge, 672 ± 93 Ma), Verkhnepetropavlovsk (Kuznetsky Alatau, 509 ± 10 Ma) and Edel'veis (Gorny Altai, 474 ± 37 Ma) complexes [80, 82-88] in the combination of other geochronological data (630-725 Ma) for alkaline rocks and carbonatites from the Eastern Sayan and Enisei ridge [14-16, 30, 38, 69-70] are confirmed to the sequence of accretional and collisional processes on the margin of Siberian craton from Late Precambrian to Early Paleozoic. A very wide range of this age data does allow to suppose two (Late Riphean-Vendian and Cambrian-Ordovician) epochs of pulsate plume activity of mantle that was under the Northern Asia on the border between Proterozoic and Paleozoic. Folded blocks of the Enisei ridge and Eastern Sayan was subject to the Late Precambrian rifting destruction that initiate alkaline and carbonatite magmatism in this region. The Sm-Nd-isochron dating (672 Ma) for linear magnesium carbonatites of the Penchenga complex from Enisei ridge is mostly corresponding to the temporal interval of formation for ijolites, aegirine-bearing syenites and carbonatites from the near seating Srednetatarsk (Zaangarsk) massif (660-675 Ma) as well as associations of alkaline-ultramafic rocks and carbonatites from the Urick-Iisk graben of the Eastern Sayan province (630-725 Ma). This rocks have similar as Nd-Sr-isotopic parameters (Fig. 2) as a model age (T_{DM} 830-960 Ma) for depletion of mantle substrate [15-16, 40, 84], that can assume a kindred origin of their sources. Small existent distinguishing features of Nd- and Sr-isotopic composition between rocks of mentioned complexes can be explained either as a different grade mixing of matter from few mantle domains, or as processes of crustal contamination. At the same time need to remark that in spite of similar to HIMU isotopic parameters (εNd_T 5,1-5,7; εSr_T -17,4÷ -20,4) rocks from the Enisei ridge are characterized by a very low initial $^{87}Sr/^{86}Sr_T$ ratios (0,70229-0,70252) relative to most of famous carbonatites in the Siberian craton and its folded framework [40, 43-44, 48, 50-51, 75-76, 83-84 et al.]. Only carbonatites with near age (~ 650-720 Ma) from the Arbarastakh and Ingili massifs in the Aldan alkaline province have such level of initial $^{87}Sr/^{86}Sr_T$ (0,70239-0,70260) data [40], but their forming was relative with more young (T_{DM} 760-780 Ma) and more depleted (εNd_T 6,7-7,0) mantle source. Usually unaltered basalts from middle oceanic ridges have a similar isotopic composition of strontium, but it is often observed in Precambrian with age more 550-600 Ma carbonatites of intrusive complexes in ancient cratons [6, 41, 68 et al.]. It allow to assume an existence of MORB-component in the magmatic source specially in the case when fragments of middle oceanic ridge will be strike up subduction zone. The drawing of different mantle materials into magma melting processes and the degree of their mixing can be apparently defined by as a slope as a penetrating deep of subduction zones that lead to spatial combination of different substrates. The effect of mixing between HIMU and EMI is more significant in the composition of carbonatites with near age from the Eastern Sayan that are similar to Proterozoic carbonatites from Northern America and more young complexes of mantle origin in platforms according to Nd-Sr-isotopic peculiarities (Fig. 2).

Despite the isotopic composition of neodymium like to HIMU and PREMA reservoirs whole rock samples of Early Paleozoic carbonatite-bearing complexes from the Kuznetsky Alatau and Gorny Altai have more high $^{87}Sr/^{86}Sr_T$ from 0,7033 to 0,7065. Take features of their O-C-isotopic composition we propose a relationship with process of selective crustal contamination of melts on the level of intermediate chambers and feeder channels, but not with a geochemistry of mantle sources [50, 81, 83, 85-87]. The analogous deviation from mantle array is also observed for likely contaminated carbonatites from complexes of South America (Jacupiranga, Barra do Itapirapuã), India (Sevathur, Amba Dongar) [3, 36, 41, 59, 65-66] and the Tury massif in the Kola peninsula [23]. It is important that Nd-isotopic composition in rocks from the Tury and Verkhnepetropavlovsk massifs are preserved parameters of depleted mantle under significant level of crustal contamination (Fig. 2). The PREMA material had more significant participation in the source of carbonatites and alkaline rocks from the Gorny Altai that corroborate a dominate role of this substrate in the mantle superplume controlling an evolution of Early and Middle Paleozoic basic magmatism on the territory of Northern Asia [90].

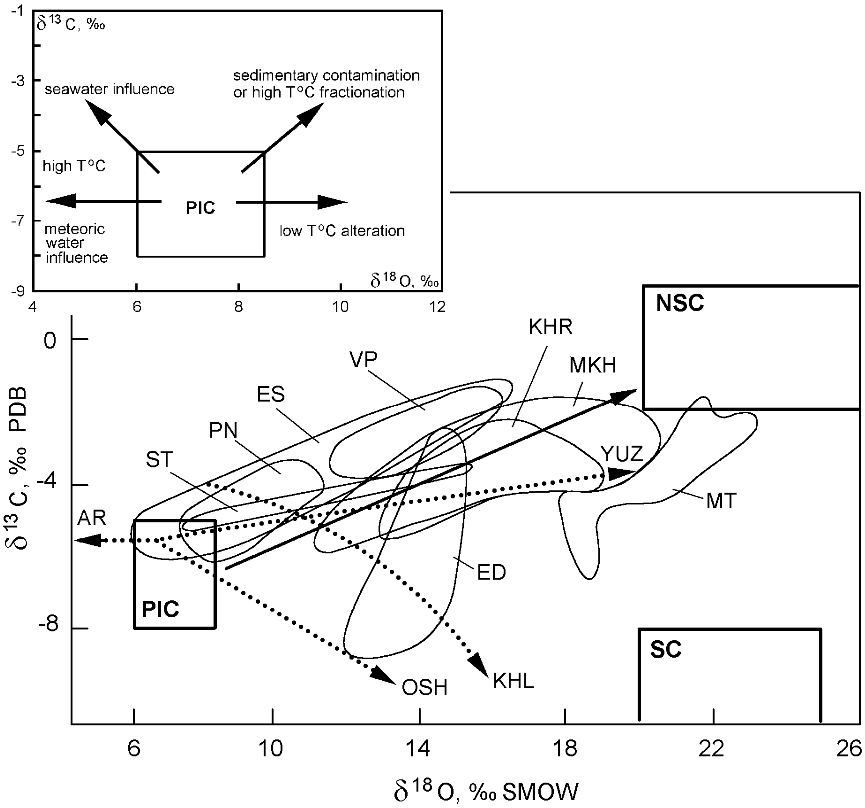

Fig. 3. **Carbon and oxygen isotope variations of carbonatites relative to a character and scales of crustal contamination**

Thin outlines of rock-forming carbonates for different complexes: PN - Penchenga, VP - Verkhnepetropavlovsk, ED - Edel'veis, MT - Matcha, KHR - Kharla, MKH - Mushugai-Khuduk, ES - Eastern Sayan, ST - Srednetatarsk massif from the Enisei ridge [31, 35, 37, 49, 62, 77-79, 82, 84, 86]. Dotted arrows are evolution trends of isotopic compositions of carbonatites from the Western Baikalian region (carbonatite bodies: AR - Arshan, OSH - Oshurkovsk, KHL - Khaluta, YUZ - Yuznoe) [42, 44, 57]. Compositional fields: PIC - primary igneous carbonatites [18], NSC - normal sedimentary carbonates, SC - soil carbonates [51, 61]. PIC and NSC fields are connected by line wuth an arrow showing an increase role of crustal matter. Small figure demonstrated an influence of different processes on isotopic evolution of primary carbonatite matter (from [22]).

Magmatic associations of MZ-KZ age. Significant amount of crustal ^{87}Sr was penetrated in magmatic melts during a forming of the Mesozoic and more young carbonatite-bearing complexes from folded areas. According to isotopic composition of neodymium their initial source was strongly differ from depleted mantle reservoirs a matter of that was dominant in rocks of the Late Riphean and Early Paleosoic association. This source is compositionally characterized by negative values of εNd_T and highest $^{87}Sr/^{86}Sr_T$ ratios that like to enriched mantle parameters.

For example, the composition of carbonatites and middle rich by potassium comagmatic alkaline rocks of Khaluta, Arshan, Oshurkov and other little massifs from the western part of Western Baikalian volcanic rifting region (εNd -2,6÷ -6,4; εSr 12,1-22,2; Fig. 2) [11, 43-44, 58] is more similar to the EMI component. According to revealed features of carbon and oxygen isotopic compositions in rock-forming carbonates a participant of mantle matter was very significant in the initial source of mentioned rocks. Observed extreme deviation of $\delta^{13}C$ and $\delta^{18}O$ values can be mainly proposed as hydrothermal alterations or on interaction with meteoric and underground waters and more less as a direct contamination of melts by crustal components (Fig. 3) [11, 42-43, 57]. The wide diapason of εNd and εSr values in rocks with a near age assumes to activate two sources of enriched mantle with a different degree of depletion. One of them was apparently present a relict zone preserving its depleted composition in spite of probable metasomatism. Isotope geochemical features of carbonatite complexes from the NW Pakistan are important for this situation. They are spatially localized in the Ind suture zone that form as a result of collision between the Indian craton and Asian continent. Tilton et al. [74] show that Oligocenic (~30 Ma) synorogenic complexes as the Loe Shilman and Sillai Patti have a mixing source between HIMU and EMI types with a predominate role of enriched mantle matter (εNd -3,1÷ -3,8; εSr 2,4-5,6). Authors propose a transport of this lithospheric source into the collision zone with Indian plate migrating from the Eastern African continental segment. The Koga and Jhambil preorogenic carbonatite complexes with the Late Paleozoic (~300 Ma) have Sr-Nd-isotopic characteristics (εNd 3,2-3,7; εSr -8,5÷ -9,4) of depleted mantle substrate that is usual for most of carbonatites (Fig. 2). Isotopic parameters of carbonatites (εNd ~ 0÷ -2; I_{Sr} ~ 0,7058-0,7066) from the Mushugai-Khuduk complex of alkaline volcanic and plutonic rocks in the Southern Mongolia demonstrate slightly to rise a grade of mixing between a material of depleted mantle and EMI type matter (Fig 2). Isotopic features of this rocks was early interpreted an evidence of initial source like to the hypothetical enriched mantle reservoirs of EMII type [75]. Moreover mentioned carbonatites have a large isotopic composition of oxygen and carbon ($\delta^{18}O$ ~11,5-20,4 ‰; $\delta^{13}C$ ~-2,1÷ -5,5 ‰) as well as high $^{87}Sr/^{86}Sr_T$ values [35]. We assume to regard a more true model of interaction between matters of HIMU and EMI sources that complicate with a selective crustal contamination of magmatic melts.

Carbonatites of the Matcha massif from the Turkestan Alai ridge are differ in a very high level of contamination by crustal matter. Nevertheless a value of εNd = -8,21 (Fig. 2) calculated for Late Triassic (~ 223 Ma) age [83] is nearly corresponding to lower boundary of that in the EMI reservoir (εNd ~ -6,5). Similar values εNd (from -8 to -6) was also determined in vein-forming contaminated carbonatites (I_{Sr} ~ 0,7082 - 0,7086) from the nearest Darai-Pioz alkaline intrusion

[76]. Despite the fact that carbonatites from Southern Tien-Shan and Western Baikalian region have an unconformity in spatial position and real age their modeling T_{DM}-values are enough similar (T_{DM} ~1300-1500 Ma) [43, 83] and indirectly show an isotopic coherence of magma-generated substrates. Mesozoic and more young carbonatite-bearing complexes of folded systems are obviously formed on the crust with a high thickness. According to this reason processes of late-collisional rifting destruction relaxed with depth and didn't achieve areas bordered with asthenosphere. In such situation reservoirs of enriched lithospheric mantle are only able to generate magmatic melts. It is mostly caused a high level of crustal contamination for mentioned rocks.

ROLE OF CRUSTAL CONTAMINATION AND LATE-POSTMAGMATIC ALTERATION IN THE FORMATION OF CARBONATITE-BEARING COMPLEXES

Two different ways to transport a crust matter in deep magmatic melts are existent according to modern views. The «mantle» contamination is assumed a direct impregnation of crust material in magma-generated mantle zones during subduction processes. Other more wide spread variant can be a crustal contamination of melts in feeder channels and intermediate chambers on the level of upper lithospheric sections. In this case an impregnation of contaminant in the melt is selective, for example, as a mobilization of solutions localized in sedimentary formations [47, 51]. The conduct of stable isotopes and radiogenic strontium in rocks of carbonatite-bearing complexes are shown a significant role of crustal contamination that compete with crystalline fractionation and late-postmagmatic alteration determined a final face of carbonatites [83].

Distribution of stable isotopes. The effect of contamination is remarked in different rocks of studied complexes but it is more reveal for the isotopic balance of carbonatites. Most of $\delta^{13}C$ (‰, PDB) and $\delta^{18}O$ (‰, SMOW) values of rock-forming carbonates are corresponding to linear areas from the field of initial magmatic carbonatites to the field of sea sedimentary carbonates with an immediate position (Fig. 3). According to some views [21, 29, 45, 55] we can't deny a possibility to form an obtained correlation as a result of the Rayleigh isotopic fractionation that may be during high temperature (about 600-800°C) stages of carbonatite melts differentiation with sequent forming of impoverished by ^{13}C and ^{18}O solid carbonate mineral phases and isolation of enriched by this isotopes CO_2-H_2O-bearing fluid. Probably this process was only realized during the initial stage of carbonatite forming. To assume a limited scale of such fractionation (no more 13,5 ‰ of $\delta^{18}O$) and enough high values of $^{13}C/^{12}C$ and $^{18}O/^{16}O$ ratios in carbonates we can propose a crustal contamination with mixing between deep-seated and sedimentary cycle carbon dioxides as a dominant process [35, 77-78, 82-84, 86 et al.].

The calcite of carbonatites from Early Paleozoic complexes of the Kuznetsky Alatau , Gorny Altai and SE Tuva is characterized by similar level of contamination with variations of δ^{13}C from -2,0 to -8,4 ‰ and δ^{18}O from 11,8 to 18,6 ‰ (Fig. 3). The matter mobilized from «heavy» isotopic (δ^{13}C 0,1-2,3 ‰; δ^{18}O 21,1-24,9 ‰) carbonate sedimentary rocks in the frame of alkaline intrusions could be assumed as a probable contaminant that was mixed with a mantle substance. A specific evidence of hybrid origin is a clear tendency to grow an heavy oxygen isotope composition in other rock-forming minerals from as well as carbonatites and associated alkaline rocks of this complexes. More high δ^{18}O values relative to mantle parameters ($\delta^{18}O = 5{,}5 \pm 0{,}5$ ‰ SMOW according to [72] et al.) are striking for typical minerals of carbonatites such as phlogopite (7,5-8,1 ‰) of the Edel’veis complex, magnetite (7,1-7,5 ‰) and diopside (9,0 ‰) of the Verkhnepetropavlovsk complex and apatite (11,9-13,9 ‰) from rocks of the Kharla massif in Sangilen upland (Fig. 4). Oxygen isotope systems of clinopyroxenes, micas,

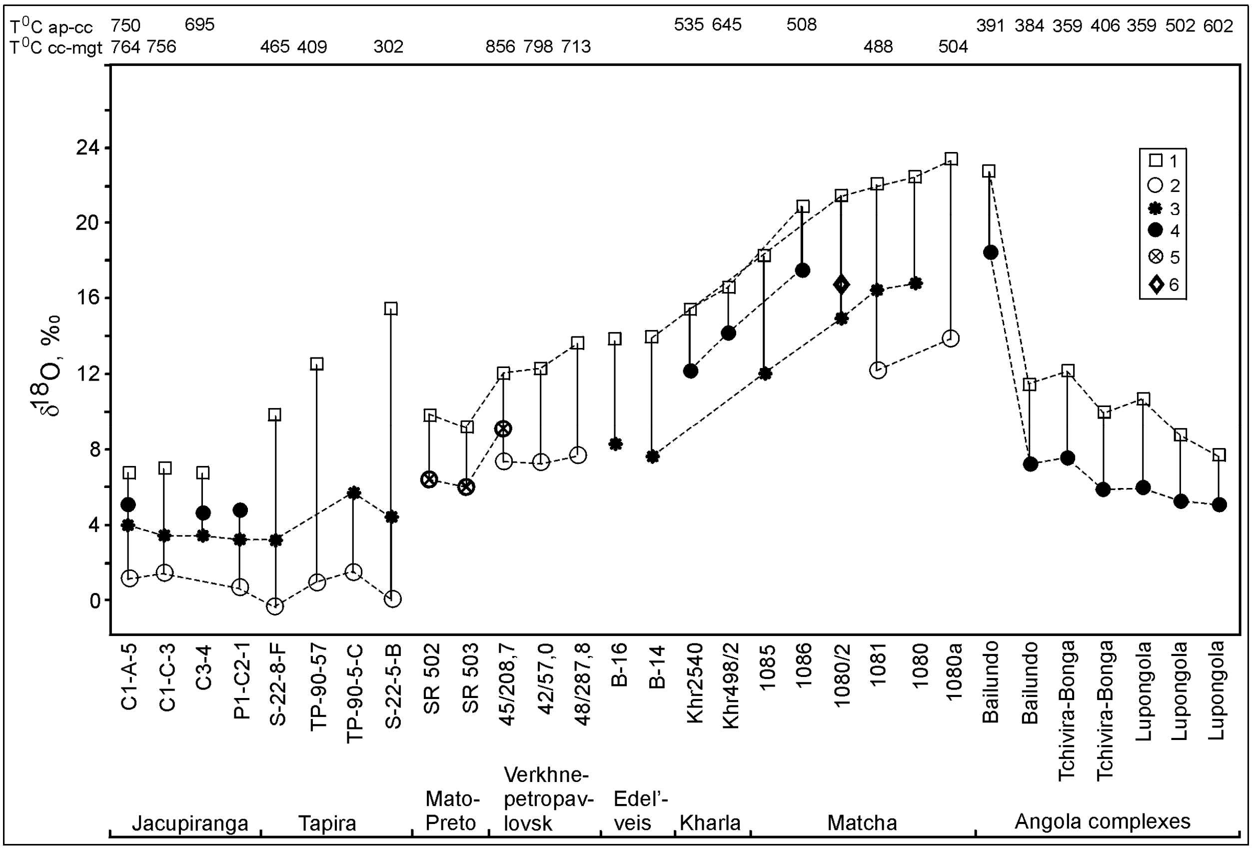

Fig. 4. **Character and scale of oxygen isotopic fractionation between rock-forming minerals of carbonatites**

1 – calcite, 2 – magnetite, 3 – brown mica, 4 – apatite, 5 – clinopyroxene, 6 – amphibole. Thin lines connect a compositions of coexisting mineral phases. Dotted lines demonstrate variations in a single minerals. Numbers and locations of studied samples and temperature values of isotopic equilibrium apatite-calcite (T°C ap-cc) and calcite-magnetite (T°C cc-mgt) are corresponding to author’s data [1, 49-50, 63, 79, 82, 86].

feldspars and nepheline from comagmatic silicate rocks are likely reactive on the crustal contamination. Features of progressive making melts «dirty» by the matter of sedimentary origin on depths of feeder chambers are mostly clear in minerals and whole rock composition of some differentiate alkaline basic intrusions in the northern part of Kuznetsky Alatau ridge including the Verkhnepetropavlovsk carbonatite-bearing pluton. We defined a regular trend to increase $\delta^{18}O$ middle values from 8,4 ‰ in early subalkaline gabbroides to 9,6 ‰ in theralites and foidolites and to 10,4 ‰ in nepheline syenites [81]. A similar tendency of $\delta^{18}O$ growth with small exception is obtained for rock-forming clinopyroxenes (7,2-9,3 ‰), feldspars (8,6-10,6 ‰) and nepheline (9,2-10,7 ‰). In spite of the high level of contamination one example a breach of local isotopic equilibrium between main minerals was only found in rocks of Paleozoic complexes from ASFS. This is a very inverse association of clinopyroxene and nepheline ($\delta^{18}O$ are 13,4 and 7,8 ‰ SMOW relatively) that was formed in the calcite-bearing contaminated ijolite of the Kharla massif from the SE Tuva. On the base of that we can surely speak about real entry of crustal material in magmatic system during stage of melt existence. The obtained range of $\delta^{18}O$ values and enrichment by heavy oxygen isotope isn't mostly relative with postmagmatic processes. Hydrogen isotope data for rocks of the Edel'veis complex are confirmed to last conclusion. Measured δD values in phlogopites from micaceous clinopyroxenites (-85 ‰ SMOW) and carbonatites (-61 ‰ SMOW) are mostly correlated with primary magmatic origin of water containing in this rocks [82-83, 86].

Isotopic compositions of carbon and oxygen in ancient Late Precambrian carbonatites from the Eastern Sayan province ($\delta^{13}C$ -1,5÷ -6,0 ‰; $\delta^{18}O$ 6,6-16,4 ‰) and the Enisei ridge ($\delta^{13}C$ -1,8÷ -5,9 ‰; $\delta^{18}O$ 7,4-15,3 ‰) are widely range [40, 62, 84], but also similar to the general trend of crustal contamination (Fig. 3). Nevertheless, more 50 % total amount of points of this rocks are located near a field of primary igneous carbonatites unlike Paleozoic complexes that show a highest role of mantle component in the rock composition.

A participant of mantle carbon dioxide in the composition of carbonate component from more young complexes is successively decrease and their $\delta^{13}C$ and $\delta^{18}O$ values are bringing closer to that of sedimentary carbonate rocks despite the fact that isotopic variational fields of this carbonatites intersect themselves (Fig. 3). Marbleized limestones with similar isotopic composition ($\delta^{13}C$ 0,1-2,3 ‰; $\delta^{18}O$ 21,1-24,9 ‰) are usually either acted as a host rocks for examined carbonatite complexes, or widely spread in the regional stratigraphic cross section. Increased concentration of radiogenic strontium in magmatic rocks together with lightly changing isotope composition of neodymium can be considered as an additional argument for participation of limestone matter in the carbonatitic genesis. Sometimes contamination trends can become distorted in the result of interaction between magmatic rocks and meteoric or underground waters bearing an organic carbon dioxide. This processes are assumed for carbonatites from the Western Baikal region (Fig. 3).

The appreciable presence of atmospheric hydrous component with $\delta^{18}O<0$ in the carbonatite fluid-magmatic system is distinctly revealed for the Penchenga linear complex that spatially controlled by the Tatarsk lineament in the Enisei ridge. The highest permeability of this structure promoted more deep circulation of atmospheric waters. Their action could contributed to remobilization of carbonatite matter with a disappearance of features of primary magmatic origin and a loss of oxygen isotope equilibrium between minerals that was stable during early contamination process. It is corroborated by more light oxygen isotope composition in silicates (δ^{18}O 3,8-7,1 ‰) and apatite (δ^{18}O 4,7 ‰) relative to rock-forming carbonate as well as negative δ^{18}O values in accessory pyrochlore (-2,8÷ -3,2 ‰) and magnetite (-0,3÷ -0,5 ‰) lesser to that from magmatic carbonatites [84]. At the same time wide variation of oxygen and hydrogen isotope composition in rock-forming micas (δ^{18}O 3,8-7,1 ‰; δD -30÷ -93 ‰) and amphiboles (δ^{18}O 3,1-5,0 ‰; δD -98÷ -154 ‰) of the Penchenga complex are able to propose a crystallization of this minerals under the influence of heterogeneous fluid in conditions of quickly changed thermal regime [84]. The obvious loss of mineral equilibrium is revealed in a scale of sample where amphibole has less 60 ‰ of deuterium relative to biotite or phlogopite. The evidence of this processes is a coefficient of isotopic fractionation Δ^{18}O between coexistent amphiboles and micas that range from +0,3 to -0,3 ‰. It isn't corresponding to equilibrated associations where Δ^{18}O values are always positive with 4,5-5,0 ‰ for 400°C and 1,5-2,0 ‰ for 800°C [28]. In this situation the total impoverishment by deuterium for mineral phases accompanying to isotopic non-equilibrium and regular correlation between water content and δD value could be interpreted as a result of gas release from carbonatitic magmas and mixing between magmatic and meteoric waters with a forming of specific heterogeneous fluid. The wide-spread fenitization of host rocks surrounding carbonatite bodies is demonstrated a significant role of such gas release during formation of the Penchenga complex that was completed with a melt contamination by a sedimentary material [83-84]. The obvious inclusion of sediments is confirmed by prevalent positive δ^{34}S values that are range from -0,8 to +9,2 ‰ in the pyrrotite from this carbonatites. A level of mixing between sulfur of sedimentary cycle and mantle source was defined by the heterogeneous composition and different proportions of selective assimilation [84]. Pyrrotite from other studied carbonatites in the Kuznetsky Alatau (δ^{34}S +4,6 ‰) [49] and Southern Tien Shan (δ^{34}S +12,6÷12,8 ‰) [79, 83] are also enriched by heavy isotope ^{34}S relative to the «Sikhote-Alin» meteorite standard (δ^{34}S ~ 0 ‰) and middle value δ^{34}S (~ -3 ‰) in sulfides of carbonatites [21]. This data show an acceptation of significant amount of crustal matter into juvenile carbonatitic systems.

Features of most scale crustal contamination are displayed in rocks of Mesozoic carbonatite-bearing alkaline complexes from the Southern Tien Shan, Southern Mongolia and Western Baikalian region that was forming on the crust with a highest thickness. This carbonatites have wide variation of oxygen and carbon isotope composition that are closer or partially higher to typical sedimentary carbonates (Fig. 3). For example, calcite of carbonatites from the Mushugai

Khuduk complex (Southern Mongolia) is characterized by followed parameters as $\delta^{18}O$ = 11,5-20,4 ‰ and $\delta^{13}C$ = -5,5÷ -2,1 ‰. Rock-forming minerals of carbonatites from the Matcha complex (Turkestan Alai) are mostly enriched by heavy ^{18}O and ^{13}C isotopes (Fig. 4) with values of $\delta^{18}O$ = 18-23 ‰ and $\delta^{13}C$ = -6,5÷ -1,9 ‰ for calcite, $\delta^{18}O$ = 11,9-13,5 ‰ for magnetite, $\delta^{18}O$ = 17,2 ‰ for apatite, $\delta^{18}O$ = 11,9-16,5 ‰ for micas and amphiboles [79, 83]. As well as for studied complexes from the Kuznetsky Alatau and Gorny Altai there isn't an obvious evidence of inverted isotopic fractionation realizing under an action of hot atmospheric waters with $\delta^{18}O$ < 0 ‰. Nevertheless scales of real isotopic fractionation in carbonatitic systems can be more small. We don't exclude a postmagmatic alteration of calcite during the low temperature stage (75-100°C) and reaction type of hydroid fluid with rock so this mineral has most high $\delta^{18}O$ values [83]. Relations between δD (-57÷ -41 ‰) and $\delta^{18}O$ (14,7-16,5 ‰) values in the phlogopite and magnesioarfvedsonite from carbonatites of the Matcha massif are alloyed to propose an influence of «metamorphogenic» waters isolated during the dehydration of metasedimentary rocks as some fluid source [51].

According to character and variation of $\delta^{13}C$ and especially $\delta^{18}O$ parameters studied carbonatites from Mesozoic complexes are typical examples of wide-scale mixing between mantle and crust materials where the isotopic effect of such mixing was «masked» during the low temperature late and postmagmatic action of heterogeneous thermal waters. Isotope compositions of carbon and oxygen in subvolcanic carbonatites from the Western Baikalian region are mostly significant [42, 44, 57]. The calcite with low $\delta^{13}C$ values (-4,1÷ -6,5 ‰) is enriched by heavy oxygen isotope ($\delta^{18}O$ 6,0-12,9 ‰) that show an addition of crustal component. The following regular increase or decrease of $\delta^{13}C$ and $\delta^{18}O$ values are legitimately interpreted by some researches as a result of hydrothermal alteration of carbonatites with participation of meteoritic and underground waters of brine-type or organic CO_2 enriched fluids.

Origin of contaminant and its quota in magma. The analysis of Nd-, Sr- и O-isotope distribution in studied rocks alloy to recognize the composition of contaminant and the degree of its involvement in processes of carbonatite genesis. The locality of varied fields on the «εNd - $^{87}Sr/^{86}Sr$» plot relative to lines of mixing between mantle and crust matters is mainly defined by a nature of continental crustal source (Fig. 5). Precambrian associations from the Enisei ridge and Eastern Sayan province have an obvious autonomic positions on this plot. It is showed a lower crust as a main contaminant with most role of ancient sedimentary dolomites having low $^{87}Sr/^{86}Sr$ (~ 0,7045-0,705) and εNd (-10,4÷ -5,0) parameters. This fact is a possible to explain an obtained in carbonatites low initial $^{87}Sr/^{86}Sr$ ratio that are usually typical for MORB- and HIMU-type mantle reservoirs. The quota of crustal component absorbed by the magma was significant according to variations of $\delta^{13}C$ and $\delta^{18}O$ values, so we can't fully exclude an interaction between MORB-domen and crust. Complexes from the Kuznetsky Alatau, Gorny Altai, Western Baikalian region, Southern Mongolia and Tien Shan are formed more similar group of points distribution of that is controlled by a line of mixing between a mantle material and middle upper continental crust (εNd ~ -26; $^{87}Sr/^{86}Sr$ ~ 0,717). Compositional fields of alkaline rocks and carbonatites from Paleozoic and Mesozoic associations with different mantle sources of matter are located near total trend of contamination. At the same time obtained deviations from the dominant mixing line can be explained by features of regional statigraphic sections where are widely spread carbonate sediments of Phanerozoic (Kuznetsky Alatau) or Riphean (Gorny Altai and Western Baikalian region) age (Fig. 5). This interpretation may to explain an obvious upper crust origin of matter that contaminated Mesozoic carbonatite-bearing complexes as the Matcha from the Turkestan Alai and Mushugai-Khuduk from the Southern Mongolia. This rocks have a prevalent crustal component in their isotopic composition if to take actually proposed the enriched mantle of EMI-type as initial source [83].

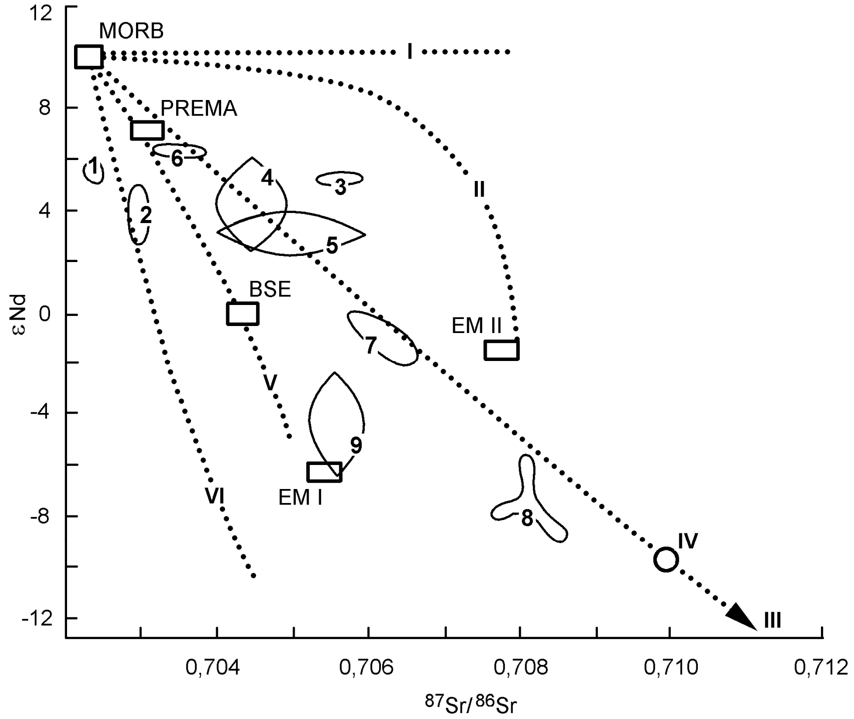

Fig. 5. **εNd and $^{87}Sr/^{86}Sr$ isotope correlation plot showing a mixing between mantle carbonatite-bearing alkaline magmas and the matter of different crustal reservoirs**

Thin outlines: 1 – carbonatites from the Enisei ridge (Penchenga complex and Srednetatarsk massif); 2 – carbonatites from the Eastern Sayan province (Niznesayansk, Verkhnesayansk, Bolshetagninsk, Zidoi massifs); 3 – alkaline rocks and carbonatites of the Verkhnepetropavlovsk complex from the Kuznetsky Alatau; 4-5 – Ordovician basalts (4) and trachytes (5) of the Imir formation in the Eastern Kuznetsky Alatau and it's surrounding Minusa depressions; 6 – carbonatites and alkaline rocks of the Edel'veis complex from the Gorny Altai; 7 - carbonatites of the Mushugai-Khuduk complex from the Southern Mongolia; 8 - carbonatites from the Southern Tien Shan (Matcha and Darai-Pioz massifs); 9 – rocks of carbonatite complexes from the Western Baikalian region (after [40, 43, 49-50, 60, 75-76, 80, 82-87]). Nd-Sr-isotopic trends of mixing between mantle matter and crustal contaminant are showing as a dotted curves from [51]. This trends: I – crustal contamination of altered oceanic basalts; II – contamination by Phanerozoic sea carbonates (εNd = -2, Nd = 2 г/т, $^{87}Sr/^{86}Sr$ = 0,7078, Sr = 470 г/т); III - contamination by middle upper continental crust (εNd = -26, Nd = 32 г/т, $^{87}Sr/^{86}Sr$ = 0,717, Sr = 510 г/т); IV - contamination by the lower crust (εNd = -10, Nd = 30 г/т, $^{87}Sr/^{86}Sr$ = 0,710, Sr = 400 г/т); V - contamination by Precambrian sedimentary dolomites (εNd = -5, Nd = 2 г/т, $^{87}Sr/^{86}Sr$ = 0,705, Sr = 50 г/т); VI - contamination by the lower crust (εNd = -10,4, Nd = 32 г/т, $^{87}Sr/^{86}Sr$ = 0,7045, Sr = 370 г/т). Isotopic parameters of mantle domens (EM I, EM II, BSE, PREMA, MORB) are showing after [25, 92].

The correlation between simultaneously increased $\delta^{18}O$ and $^{87}Sr/^{86}Sr_T$ values in rocks of studied complexes can be an indicator of contamination character. Compositional trends are closer to mixing lines that connect compositions of mantle source and corresponding sedimentary contaminant (Fig. 6). Such tendency must to include a strong enrichment of magma-generated zones by the strontium in the result of mantle metasomatism. It is an evidence of dominant crust level for the

enter of strontium in melts. Some deviations of compositions according to curve lines of mixing between primary magmas and contaminant more enriched by strontium relative to typical crust can be explained not a hole but selective contamination with a participation of high concentrative solutions that was mobilized from sedimentary carbonate rocks by a heat of alkaline intrusions [47, 50-51, 83]. Their composition must to be similar to Sr-bearing brines (Sr to 10 g/l) that are buried in Late Precambrian and Early Paleozoic sedimentary formations of the Siberian craton and its folded framework [2, 46]. For example, a higher concentration of strontium (> 2000 ppm) are known for separate parts of the Vendian and Cambrian carbonate formations that locate in the Northern Kuznetsky Alatau and have an initial $^{87}Sr/^{86}Sr$ ratios equal 0,70802-0,70829 [49]. The isotopic

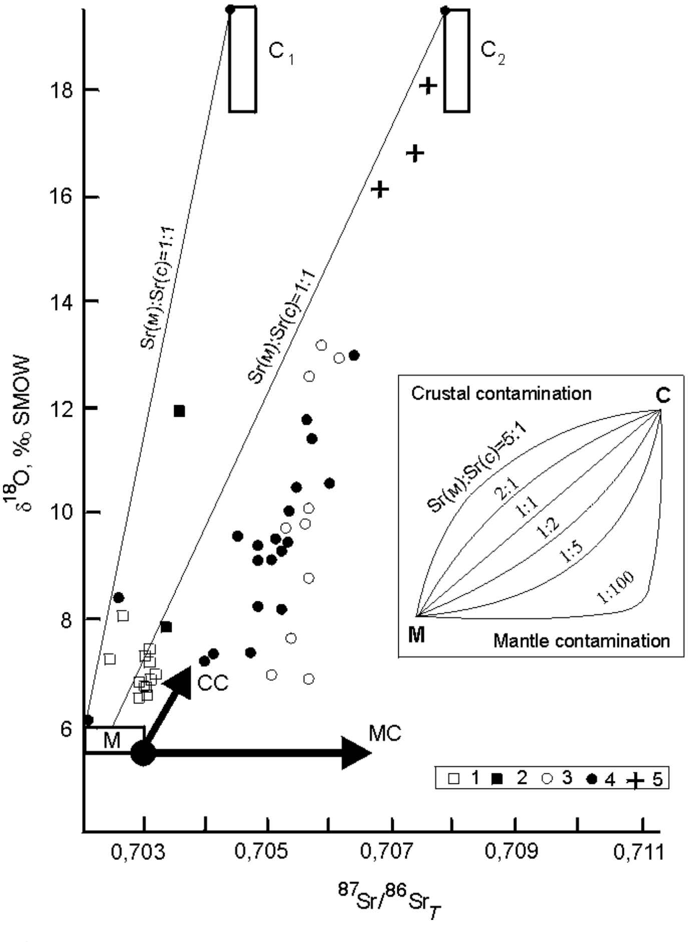

Fig. 6. **Distribution of whole rocks and minerals isotopic composition from studied carbonatite-bearing complexes on the $\delta^{18}O$ versus $^{87}Sr/^{86}Sr$ plot demonstrated a scale mixing between mantle and crustal matters**

composition of strontium in brines is usually closed to that in host carbonate rocks. Isotopic parameters of moderately depleted mantle can be assumed as an initial for the parental alkaline basic magma according to lowest $^{87}Sr/^{86}Sr$ ratio (~ 0,7025) that was defined in clinopyroxenes from alkaline gabbroids. In this case on the base of approximate calculation we must to propose a significant part (~ 40-70 %) from a total amount of radiogenic strontium in alkaline rocks and carbonatites of the Kuznetsky Alatau to be taken from sedimentary formations. Similar level of contamination is found for complexes from the Western Baikalian region. Such significant transport of matter couldn’t be able without wide participation of fluids. More high (no less 80 %) of crustal strontium is typical for carbonatites of the Matcha complex from the Southern Tien Shan (Fig. 6) that include any doubts about great volume of fluid phase in forming of this rocks.

The matter balance of strontium is less established for Riphean and Vendian carbonatites from the Eastern Sayan province and Enisei ridge, so a material of Precambrian carbonate sediments with low initial $^{87}Sr/^{86}Sr$ (~ 0,7045) must to be involved in carbonatite-generated processes. Like rocks with $^{87}Sr/^{86}Sr$ = 0,7040-0,7052 are spread among Proterozoic formations hosted bodies of the Penchenga complex in the Enisei ridge [37]. A possible assimilation of such matter by a mantle carbonatite melt with the initial $^{87}Sr/^{86}Sr$ ~ 0,702-0,7025 (according to lowest ratio in minerals of the Enisei ridge carbonatites) can be considered a real if about 30 % of strontium came from a crustal source. The inconstancy in isotopic compositions of oxygen and carbon revealed for this rocks is also confirmed such calculations [40, 84].

CONCLUSION

A comparative analyses of isotope geochemical data for carbonatite-bearing complexes from folded areas is able to make following basic inferences.

Firstly, all magmatic rocks including carbonatites of studied complexes have mantle sources of primary matter. At the same time their initial substrates are differed between themselves specially in the isotopic composition of neodymium depending on the real time of alkaline and carbonatite magmatism, the depth of magma generation and probably a thickness of continental lithosphere. Carbonatites of ancient from Riphean to Vendian and from Cambrian to Ordovician epochs of riftogenic magmatism as well as their cratonic analogues are characterized by positive values of εNd that are typical for a moderately depleted matter of asthenospheric or low mantle plumes. Observed variations of this isotopic parameter in postorogenic carbonatites with such age are showed the drawing of material from HIMU-, PREMA- and probably MORB-type reservoirs with different but mostly limited participation of EMI matter into magma melting processes. We can assume that obtained variety and degrees of relative mixing between mantle components was defined by a slope and penetrate depth of subduction zones as well as a close vertical matching for fragments of ancient oceanic lithosphere (HIMU-source) and middle oceanic ridges (MORB-source) immersed in the mantle, if to pay special attention to subduction and accretion processes that was in the frame of Siberian craton during the Late Precambrian and Early Paleozoic time [12].

Secondly, Mezosoic and more young carbonatite-bearing complexes from folded regions formed on the continental crust with a high thickness. Perhaps, it was a main reason of more limited depth for a penetration of late orogenic rifting destruction that didn't achieve mantle zones bordered with the asthenosphere. In this case EMI- and EMII-type reservoirs in the enriched subcontinental lithosphere was only able to generate alkaline and carbonatite melts.

Thirdly, the evolution of primary magmatic melts was differently complicated by the crustal contamination during an emplacement of alkaline rocks and carbonatites complexes with different formation types and ages. This contamination has a selective character. It isn't realized by direct assimilation of hard matter, but is a result of interaction between magma and strongly concentrated solutions that was mobilized from host sedimentary units owing to a thermal influence of intrusions. An absorption of such brine-type substance by melts took place mostly in the crust on the level of feeder channels and intermediate chambers.

Fourthly, this mechanism of contamination could contribute to additional carbonatization and enrichment by briny components in mantle alkaline silicate magmas. It was late conductive to an isolation of strictly carbonatite liquids. The convincing argument for such supposition can be a more significant degree of contamination in rocks from Phanerozoic carbonatite complexes accompanied by a total activation of carbonatite magmatism during a geological history of Earth [89]. The relationship between «mantle» contamination and carbonatite-forming processes is less appeared and probably realized as a carbonatization of mantle substrate that later contribute to melting of direct carbonatite or enriched by carbon dioxide alkaline magmas.

Fifthly, features of initial magmatic origin of carbonatites are concealed by effects of late- and postmagmatic alteration in favorable condition such as a forming on small depths or near large-scale faults. This alteration was going with a participation of heterogeneous fluid that was a product of mixing between juvenile and atmospheric waters.

The study was funded by the Russian Foundation for Basic Research (grant № 04-05-64331) and Ministry of Education and Science of Russia (grants №№ E 02-9.0-92, UR 09.01.042).

REFERENCES

1. **Alberti, A., Castorina, F., Censi, P., et al.** (1999) Geochemical characteristics of cretaceous carbonatites from Angola. J. African Earth Sci. V. 29. № 4. P. 735-759.
2. **Antsyferov A.S.** (1989) Hydrogeology of ancient oil-bearing sediments of the Siberian craton. Moscow: Nedra. 176 p. (in Russian)

3. **Andrade, F.R.D., Möller, P. and Höhndorf, A.** (1999) The effect of hydrothermal alteration on the Sr and Nd isotopic signatures of the Barra do Itapirapua carbonatite, Southern Brazil. J. Geol. V. 107. P. 177-191.
4. **Balaganskaya, E.G., Verhulst, A., Demaff, D. and Liferovich, R.P.** (2000) Kovdor alkaline-ultramafic massif: new petrological and geochemical characteristics of rocks. Abstracts of XIXth Ross. meeting «Geochemistry of magmatic rocks». Moscow. P. 20-21. (in Russian)
5. **Balaganskaya, E.G., Dauns, H., Subbotin, V.V., et al.** (2000) Mantle sources of the Kola carbonatites: new Sr, Nd-isotopic and geochemical data for the Vuoriyarvi massif, Kola peninsula. Ibid. P. 21-22.
6. **Bell, K., Blenkinsop, J.** (1989) Neodymium and strontium isotope geochemistry of carbonatites. In: Carbonatites: Genesis and Evolution. Ed. K.Bell. London: Unwin Hyman. P. 278-300.
7. **Bell, K. and Simonetti, A.** (1996) Carbonatite magmatism and plume activity: implications from the Nd, Pb and Sr isotope systematics of Oldoinyo Lengai. J. Petrol. V. 37. № 6. P. 1321-1339.
8. **Bell, K.** (1998) Radiogenic isotope constraints on relationships between carbonatites and associated silicate rocks – a brief review. J. Petrol. V. 39. № 11/12. P. 1987-1996.
9. **Bell, K., Kjarsgaard, B.A. and Simonetti, A.** (1998) Carbonatites - into the twenty-first century. J. Petrol. V. 39. № 11/12. P. 1839-1845.
10. **Bell, K. and Tilton, G.R.** (2001) Nd, Pb and Sr isotopic compositions of East African carbonatites: evidence for mantle mixing and plume inhomogeneity. J. Petrol. V. 42. № 10. P. 1927-1945.
11. **Bulnaev, K.B. and Posokhov, V.F.** (1995) Isotopic and geochemical data about the nature and age of endogenic carbonate rocks from the Baikalian region. Geokhimiya. № 2. P. 189-195. (in Russian)
12. **Berzin, N.A. and Kungurtsev, L.V.** (1996) Geodynamical interpretation of geological complexes of the Altai-Sayan region. Russian Geology and Geophysics. № 1. P. 63-81.
13. Carbonatites: Genesis and evolution (1989) Ed. by K. Bell.Unwin Hyman,London. 600 p.
14. **Chernyshova E.A., Sandimirova G.P., Pahol’chenko U.A. and Kuznetsova S.V.** (1992) Rb-Sr age and some specific features of the genesis of the Bolshetagninskii carbonatite complex (East Sayan). DAN SSSR. V. 323. № 5. P. 942-947. (in Russian)
15. **Chernyshova, E.A., Sandimirova, G.P., Bankovskaya, E.V. and Kuznetsova, S.V.** (1995) Rb-Sr age and Sr-isotopic composition in alkaline rocks from dikes of carbonatitic complexes from the PreSayan region. Dokl. Ross. Akad. Nauk. V. 345. № 3. P. 388-392. (in Russian)
16. **Chernyshova, E.A. and Morikiyo, T.** (1999) Source characteristics of alkaline rocks from carbonatitic complexes of the PreSayan region on Nd-Sr-isotopic data in dike serie rocks. Dokl. Ross. Akad. Nauk. V. 369. № 3. P. 381-384. (in Russian)
17. **Cochen R.S. and O'Nions R.K.** (1982) Identification of recicled continental material in the mantle from Sr, Nd and Pb isotope investigations.Earth Planet.Sci. Lett.V.61.P.73-84.
18. **Conway, C.H. and Taylor, H.P.** (1969) $^{18}O/^{16}O$ and $^{13}C/^{12}C$ ratios of coexisting minerals in the Oka and Magnet Cove carbonatite bodies. J. Geol. V. 77. № 5. P. 618-626.
19. **Cooper, A.F. and Reid, D.L.** (1998) Nepheline sövites as parental magmas in carbonatite complexes: evidence from Dicker Willem, Southwest Namibia. J. Petrol. V. 39. № 11/12. P. 2123-2136.
20. **Cooper, A.F. and Reid, D.L.** (2000) The association of potassic trachytes and carbonatites at the Dicker Willem complex, Southwest Namibia: coexisting, immiscible, but not cogenetic magmas. Contrib. Mineral. Petrol. V. 139. P. 570-583.
21. **Deines, P.** (1989) Stable isotope variations in carbonatites. In: Carbonatites. Genesis and Evolution. Unwyn Hyman, London. P. 301-359.

22. **Demény, A., Ahijado, A., Casillas, R. and Vennemann, T.W.** (1998) Crustal contamination and fluid/rock interaction in the carbonatites of Fuerteventura (Canary Islands, Spain): a C, O, H isotope study. Lithos. V. 44. P. 101-115.

23. **Dunworth, E.A. and Bell, K.** (2001) The Turiy massif, Kola peninsula, Russia: isotopic and geochemical evidence for multi-source evolution. J. Petrol. V. 42. № 2. P. 377-405.

24. **Harmer, R.E. and Gittins, J.** (1998) The case for primary, mantle-derived carbonatite magma. J. Petrol. V. 39. № 11/12. P. 1895-1903.

25. **Hart, S.R.** (1988) Heterogeneous mantle domains: signature, genesis, and mixing chronologies. Earth Planet. Sci. Lett. V.90. P. 273-296.

26. **Hoernle, K., Tilton, G., Le Bas, M.G., et al.** (2002) Geochemistry of oceanic carbonatites compared with continental carbonatites: mantle recycling of oceanic crustal carbonate. Contrib. Mineral. Petrol. V. 142. P. 520-542.

27. **James, D.E.** (1981) The combine use of oxygen and radiogenic isotopes as indicators of crustal contamination. Annual Rev. Earth Planet. Sci. V. 9. P. 311-344.

28. **Javoy, M.** (1977) Stable isotope and geothermometry. J. Geol. Soc. London. V. 133. N. 6. P. 609-636.

29. **Javoy, M., Pineau, F. and Delorme, H.** (1986) Carbon and nitrogen isotopes in the mantle. Chem. Geol. V. 57. N1/2. P. 41-62.

30. **Kononova, V.A.** (1976) Jacupirangite-urtite serie of alkaline rocks. Moscow: Nauka. 215 p. (in Russian)

31. **Kononova, V.A. and Yashina, R.M.** (1984) Geochemical criteria for differentiating between rare-metallic carbonatites and barren carbonatite-like rocks. The Indian Mineralogist. P. 136-150.

32. **Kornev, T.Ya., Kachevskii, L.K., Nozhkin, A.D., et al.** (1999) Working correlation scheme of magmatic and metamorphic complexes of the Enisei ridge. In: Regional correlation schemes of magmatic and metamorphic complexes of the Altai-Sayan folded area. Новосибирск. P. 17-46.

33. **Kramm, U.** (1993) Mantle components of carbonatites from the Kola alkaline province, Russia and Finland: a Nd-Sr study. Eur J. Mineral. V. 5. P. 985-989.

34. **Kramm, U. and Kogarko, L.N.** (1994) Nd and Sr isotope signatures of the Khibina and Lovozero agpaitic centres, Kola alkaline province, Russia. Lithos. V. 32. P. 225-242.

35. **Kuleshov, V.N.** (1986) Isotopic composition and origin of deep carbonates. Moscow: Nauka. 124 p. (in Russian)

36. **Kumar, A., Charan, S.N., Gopalan, K. and Macdougall, J.D.** (1998) A long-lived enriched mantle source for two proterozoic carbonatite complexes from Tamil Nadu, southern India. Geochim. Cosmochim. Acta. V. 62. № 3. P. 515-523.

37. **Lapin, A.V., Guschin,V.N. and Lugovaya, I.P.** (1986) Isotopic interaction features between carbonatites and metamorphic carbonate sediments. Geokhimiya. № 7. P. 979-986. (in Russian)

38. **Lapin, A.V., Ploshko, V.V. and Malyshev, A.A.** (1987) Carbonatites of the Tatar deep fault in the Enisei ridge. Geologiya rudnykh mestorozgdenii. № 1. P. 30-45. (in Russian)

39. **McCenzie, D. and O'Nions, R.K.** (1983) Mantle reservoirs ocean island basalts. Nature. V. 301. P. 229-231.

40. **Morikiyo, T., Miyazaki, T., Kagami, H., et al.** (2001) Sr, Nd, C and O isotope characteristics of Siberian carbonatites. In: Alkaline magmatism and the problems of mantle sources (ed. N.V. Vladykin). Proc. International Workshop, Irkutsk. P. 69-84.

41. **Nelson, D.R., Chivas, A.R., Chappell, B.W. and McCulloch, M.T.** (1988) Geochemical and isotopic systematics in carbonatites and implications for the evolution of ocean-island sources. Geochim. Cosmochim. Acta. V. 52. P. 1-17.

42. **Nikiforov, A.V., Yarmolyuk, V.V., Pokrovskii, B.G., et al.** (1998) Isotopic composition of oxygen, carbon and sulfur in rocks of the Khalyuta volcanic carbonatite complex (Western Baikalian region). Dokl. Ross. Akad. Nauk. V. 363. № 6. P. 815-818. (in Russian)

43. **Nikiforov, A.V. and Yarmolyuk, V.V.** (2000) Sr, Nd- isotopic composition of rocks from carbonatitic associations of the Western Baikalian region. Abstracts of XIXth Ross. meeting «Geochemistry of magmatic rocks». Moscow. P. 106-107. (in Russian)

44. **Nikiforov, A.V., Yarmolyuk, V.V., Pokrovskii, B.G., et al.** (2000) Late Mesozoic carbonatites of the Western Baikalian region: mineralogy, chemistry and isotopic (O, C, S, Sr) composition and relationships with alkaline magmatism. Petrologiya. V. 8. № 3. P. 309-336. (in Russian)

45. **Pineau, F., Javoy, M. and Allégre, C.J.** (1973) Etude systématique des isotopes de l’oxygéne, du carbone et du strontium dans les carbonatites. Geochim. Cosmochim. Acta. V. 37. P. 2363-2377.

46. **Pinneker, E.V.** (1968) Brines of the Angara-Lena artesian basin. Moscow: Nauka. 332 p. (in Russian)

47. **Pokrovskii, B.G. and Vinogradov, V.I.** (1987) Isotopic composition of some elements in alkaline-ultramafic rocks from the Meimecha-Kotui province. Sovetskaya geologiya. № 5. P. 81-91. (in Russian)

48. **Pokrovskii, B.G., Belyakov, A.Yu., Kravchenko, S.M. and Gryaznova, Yu.A.** (1990) Origin of carbonatites and ore deposit of the Tomtor massif (N-W Yakutiya) on the base of isotopic data. Geokhimiya. № 9. P. 1320-1329. (in Russian)

49. **Pokrovskii, B.G., Vrublevskii, V.V. and Grinev, O.M.** (1991) The role of host rocks in forming of alkaline-gabbroid intrusions from the northern part of Kuznetsk Alatau after isotopic data. Izv. AN SSSR. Seriya geologicheskaya. № 8. P. 81-94. (in Russian)

50. **Pokrovskii, B.G., Andreeva, E.D., Vrublevskii, V.V. and Grinev, O.M.** (1998) Contamination mechanisms of alkaline-gabbroid intrusions in the southern framing of the Siberian platform: evidence from strontium and oxygen isotopic compositions. Petrology. V. 6. N 3. P. 237-251.

51. **Pokrovskii, B.G.** (2000) Crustal contamination of mantle magmas on evidence of isotopic geochemistry. Moscow: Nauka. 228 p. (in Russian)

52. **Ray, J.S.** (1998) Trace element and isotope evolution during concurrent assimilation, fractional crystallization, and liquid immiscibility of a carbonated silicate magma. Geochim. Cosmochim. Acta. V. 62. № 19/20. P. 3301-3306.

53. **Ray, J.S. and Ramesh, R.** (1999) Evolution of carbonatite complexes of the Deccan flood basalt province: stable carbon and oxygen isotopic constraints. J. Geophys. Res. V. 104. № B12. P. 29,471-29,483.

54. **Ray, J.S., Ramesh, R.** (1999) A fluid-rock interaction model for carbon and oxygen isotopic variations in altered carbonatites. J. Geol. Soc. India. V. 54. P. 179-186.

55. **Ray, J.S. and Ramesh, R.** (2000) Rayleigh fractionation of stable isotopes from a multicomponent source. Geochim. Cosmochim. Acta. V. 64. № 2. P. 299-306.

56. **Riley, T.R., Bailey, D.K., Harmer, R.E., et al.** (1999) Isotopic and geochemical investigation of a carbonatite-syenite-phonolite diatreme, West Eifel (Germany). Miner. Mag. V. 63. N 5. P. 615-631.

57. **Ripp, G.S., Posokhov, V.F. and Kobylkina, O.V.** (1998) O, C and S isotope features Late Mesozoic carbonatites from the Western Baikalian region. Abstracts of XVth isotope geochemistry symposium. Moscow. P. 241-242. (in Russian)

58. **Ripp, G.S., Posokhov, V.F. and Kobylkina, O.V.** (1998) Strontium isotopic composition in Late Mesozoic carbonatites from the Western Baikalian region. Ibid. P. 243-244. (in Russian)

59. **Roden, M.F., Murthy, R.V. and Gaspar, J.C.** (1985) Sr and Nd isotopic composition of the Jacupiranga carbonatite. J. Geol. V. 93. P. 212-220.

60. **Rublev, A.G., Chergina, Yu.P. and Krymskii, R.Sh.** (1998) Age and genesis of the Byskar volcanic rocks (central part of ASFA) according to isotopic data. Abstracts of International Conf. «Problems of origin of magmatic and metamorphic rocks». St-Peterburg. P. 128.

61. **Salomons, W.** (1975) Chemical and isotopic composition of carbonates in recent sediments and soils from Western Europe. J. Sediment. Petrol. V. 45. № 2. P. 440-449.

62. **Samoilov V.S**.(1984) Geochemistry of carbonatites. Moscow: Nauka. 190 p. (in Russian)

63. **Santos, R.V. and Clayton, R.N.** (1995) Variations of oxygen and carbon isotopes in carbonatites: a study of Brazilian alkaline complexes. Geochim. Cosmochim. Acta. V. 59. № 7. P. 1339-1352.

64. **Schleicher H., Keller J., Kramm U.** (1990) Isotope studies on alkaline volcanics and carbonatites from the Kaisershtul, Federal Republic of Germany. Lithos. V. 26. P. 21-35.

65. **Schleicher, H., Kramm, U., Pernicka, E., et al.** (1998) Enriched subcontinental upper mantle beneath Southern India: evidence from Pb, Nd, Sr, and C-O isotopic studies on Tamil Nadu carbonatites. J. Petrol. V. 39. № 10. P. 1765-1785.

66. **Simonetti, A., Bell, K. and Viladkar, S.G.** (1995) Isotopic data from the Amba Dongar carbonatite complex, west-central India: evidence for an enriched mantle source. Chem. Geol. V. 122. P. 185-198.

67. **Simonetti A., Goldstein S.L., Schmidberger S.S., Viladkar, S.G.** (1998) Geochemical and Nd, Pb, and Sr isotope data from Deccan alkaline complexes – inferences for mantle sources and plume-lithosphere interaction. J. Petrol. V. 39. № 11/12. P. 1847-1864.

68. **Smithies, R.N. and Marsh, J.S.** (1998) The Marinkas Quellen carbonatite complex, southern Namibia; carbonatite magmatism with an uncontaminated depleted mantle signature in a continental setting. Chem. Geol. V. 148. P. 201-212.

69. **Sobachenko, V.N., Plyusnin, G.S., Sandimirova, G.P. and Pahol'chenko U.A.** (1986) Rb-Sr-isotopic age of alkaline metasomatites and granites near the Tatar-Penchenga fault zone (Enisei ridge). Dokl. Akad. Nauk SSSR. V. 287. № 5. P. 1220-1224. (in Russian)

70. **Sveshnikova, E.V., Semenov, E.I. and Khomyakov, A.M.** (1976) Zaangar alkaline massif: rocks and minerals. Moscow: Nauka. 80 p. (in Russian)

71. **Taylor, H.P.** (1980) The effect of assimilation of rocks by magmas: $^{18}O/^{16}O$ and $^{87}Sr/^{86}Sr$ systematics in igneous rocks. Earth Planet. Sci. Lett. V. 47. N 2. P. 243-254.

72. **Taylor, H.P. and Sheppard, P.M.N.** (1986) Igneous rocks: I. Processes of isotopic fractionation and isotope systematics. Reviews in Mineralogy. V. 16. P. 227-271.

73. **Tilton, G.R. and Bell, K.** (1994) Sr-Nd-Pb isotope relationships in late archean carbonatites and alkaline complexes: applications to the geochemical evolution of archean mantle. Geochim. Cosmochim. Acta. V. 58. N 15. P. 3145-3154.

74. **Tilton G.R., Bryce J.G. and Mateen A.** (1998) Pb-Sr-Nd isotope data from 30 and 300 Ma collision zone carbonatites in Northwest Pakistan.J.Petrol.V.39.№11/12.P.1865-1874.

75. **Vladykin, N.V., Morikiyo, T. and Miyazaki, T.** (2000) Sr-Nd-systematics of carbonatites from Siberia and Mongolia. Abstracts of XIXth Ross. meeting «Geochemistry of magmatic rocks». Moscow. P. 34-36. (in Russian)

76. **Vladykin, N.V.** (2001) The Aldan province of K-alkaline rocks and carbonatites: aspects of magmatism, origin and deep sources. In: «Alkaline magmatism and problems of deep sources». Proc. of International meeting. Irkutsk. P. 18-45. (in Russian)

77. **Vrublevsky, V.V. and Kuleshov, V.N.** (1988) Isotopic composition and origin of carbonatites of the Verkhnepetropavlovsk massif (Kuznetsk Alatau). Dokl. Akad. Nauk SSSR. V. 298. № 5. P. 1214-1218. (in Russian)

78. **Vrublevsky, V.V., Pokrovsky, B.G., Kuleshov, V.N., et al.** (1999) Geochemistry of carbon and oxygen isotopes of carbonatites from the western part of Altay-Sayan folding system. In: Ninth Annual V.M. Goldschmidt Conference. Lunar and Planetary Institute, Houston. LPI Contribution N 971. P. 311-312.

79. **Vrublevsky, V.V., Gertner, I.F. and Toporkova, A.A.** (2000) New data for carbonatites of the Matcha complex (South Tyan-Shan). In: «Problems of geology and geochemistry of South Siberia». Proc. Conf. Tomsk. P. 116-122. (in Russian)

80. **Vrublevsky, V.V., Gertner, I.F. and Zhuravlev, D.Z.** (2001) Sr-Nd system evolution and geochronology of carbonatite-bearing complexes from the western part of Altai-Sayan fold region and the Enisei ridge. In: IGCP Project 420 «Continental Growth in the Phanerozoic: Evidence from Central Asia». Third Workshop Abstracts. Novosibirsk: Publishing House of SB RAS, Department «Geo». P. 119-122.

81. **Vrublevsky, V.V., Gertner, I.F. and Voitenko, D.N.** (2002) Oxygen isotope ratios in alkaline basites from Kuznetsky Alatau ridge (South Siberia). Geochim. Cosmochim. Acta. V. 66. N 15a (S1). Twelfth Goldschmidt Conference Abstracts. P. A813.

82. **Vrublevsky, V.V.** (2003) Geochemistry, geochronology and sources of the carbonatitic complexes of South Siberia // Alkaline complexes of Central Siberia. Krasnoyarsk: KNIIGGMS. P. 113-130. (in Russian)

83. **Vrublevsky, V.V.** (2003) Petrology of carbonatitic complexes from consolidated fold systems (on example of South Siberia and Tyan-Shan). Science Doctoral thesis. Novosibirsk. 40 p. (in Russian)

84. **Vrublevskii, V.V., Pokrovskii, B.G., Zhuravlev, D.Z. and Anoshin, G.N.** (2003) Composition and age of the Penchenga linear carbonatite complex, Yenisei range. Petrology. V. 11. N 2. P. 130-146.

85. **Vrublevskii, V.V., Gertner, I.F., Zhuravlev, D.Z. and Makarenko, N.A.** (2003) The Sm-Nd isotopic age and source of comagmatic alkaline mafic rocks and carbonatites of Kuznetsk Alatau. Doklady Earth Sciences. V. 391A. N 6. P. 832-835.

86. **Vrublevskii, V.V., Krupchatnikov, V.I. and Gertner, I.F.** (2004) The Edel’veis carbonatite-bearing complex (Gornyi Altai): new data from composition and age. In: Natural resours of Gornyi Altai. Gorno-Altaisk. № 1. P. 38-48. (in Russian)

87. **Vrublevskii, V.V., Zhuravlev, D.Z., Gertner, I.F., et al.** (2004) Sm-Nd isotopic systematics of alkaline rocks and carbonatites from the Edel'veis complex, Northern Chuya, Gornyi Altai. Doklady Earth Sciences. V. 397A. № 6. P. 870-874.

88. **Vrublevskii, V.V., Gertner, I.F., Vladimirov, A.G., et al.** (2004) Geochronological boundaries and geodynamic interpretation of the alkaline mafic magmatism in Kuznetsk Alatau. Doklady Earth Sciences. V. 398A. № 7. P. 990-994.

89. **Woolley, A.R.** (1989) The spatial and temporal distribution of carbonatites. In: Carbonatites: Genesis and evolution. Ed. By K. Bell. Unwin Hyman, London. P. 15-37.

90. **Yarmolyuk, V.V. and Kovalenko, V.I.** (2003) Deep geodynamics, mantle plumes and their role in forming of the Central Asian fold belt. Petrologiya. V. 11. № 6. P. 556-586. (in Russian)

91. **Zaitsev, A. and Bell, K.** (1995) Sr and Nd isotope data of apatite, calcite and dolomite as indicators of source, and the relationships of phoscorites and carbonatites from the Kovdor massif, Kola peninsula, Russia. Contrib. Mineral. Petrol. V. 121. P. 324-335.

92. **Zindler, A. and Hart, S.R.** (1986) Chemical geodynamics. Ann. Rev. Earth Planet. Sci. V. 14. P. 493-571.

UDK 553.3:539.183.2(571.54)

Composition, sources and conditions of magmatism in the North Mongolia – Trans-Baikal Early Mesozoic rift zone

Vorontsov A.A.[1], Yarmolyuk V.V.[2], Kovalenko V.I.[2], Lykhin D.A[2] , Dril S.I[1], Tatarnikov S.A[1], Sandimirova G.P.[1]

[1] Institute of Geochemistry, SB RAS, Irkutsk, e-mail: voron@igc.irk.ru
[2] IGEM, RAS, Moscow, e-mail: volya@igem.ru

In the Early Mesozoic a sizable region of the Central Asian fold belt (CAFB) was affected by the magmatic activity of intraplate type. It resulted in formation of vast zonally structured magmatic areas with the batholith cores in the center and rift zones on their margins [40]. One of the most representative structures reflecting the intra-plate regime over the region at that time was the North Mongolia – West Trans-Baikal (NMWTB) rift zone. It actually is the northern margin of the Khentey-Dauria zonal magmatic area with specific structural position. It is determined by the extensive North Mongolia – Transbaikalia belt of large faults running from the Altay mountains in Mongolia in the west to the Vitim plateau in the east. This belt of faults, striking for 2000 km, is associated with the boundaries of the large Precambrian terranes: (i) Sangilen and Khangay in the west and Barguzin in the east of the belt. Thus, it is referred to the category of structural sutures. Through entire Phanerozoic this suture boundary repeatedly became the zone for intraplate activity to take place. This is the reason why some of its segments evolved due to rifting in the Middle and Late Paleozoic, Early and Late Mesozoic and Cenozoic, having transformed this zone into multi-staged Mongolian-Transbaikalian rift system [28]. A significant event in the development of this rift system was formation of the NMWTB rift zone in the Early Mesozoic. It was initiated by intra-plate processes, which covered enormous regions of East Mongolia and Trans-Baikal. However, up to the recent time no systematic data on structural specifics were available. The paper provides the data featuring the structure of the rift zone, composition of magmatic assemblages, geochemical and isotope characters of rocks in these assemblages. Besides, it offers a discussion of the magmatic evolution occurring through the rift zone formation.

GEOLOGICAL POSITION AND STRUCTURE OF THE RIFT ZONE

The Early Mesozoic NMWTB rift zone (Fig.1) extends for over 1200 km, its width being 250 km, is characterized by the development of the depressions, grabens, dividing uplifts and horsts. These structures are largely eroded, so the rift zone is comprehensively represented by magmatic formations, i.e. volcanic sequences composed of basalt or bimodal basalt-comendite assemblages and numerous massifs of alkaline granites. The boundaries limiting the distribution of these magmatic rocks are interpreted as the boundaries of the rift zone. The age of these formations,

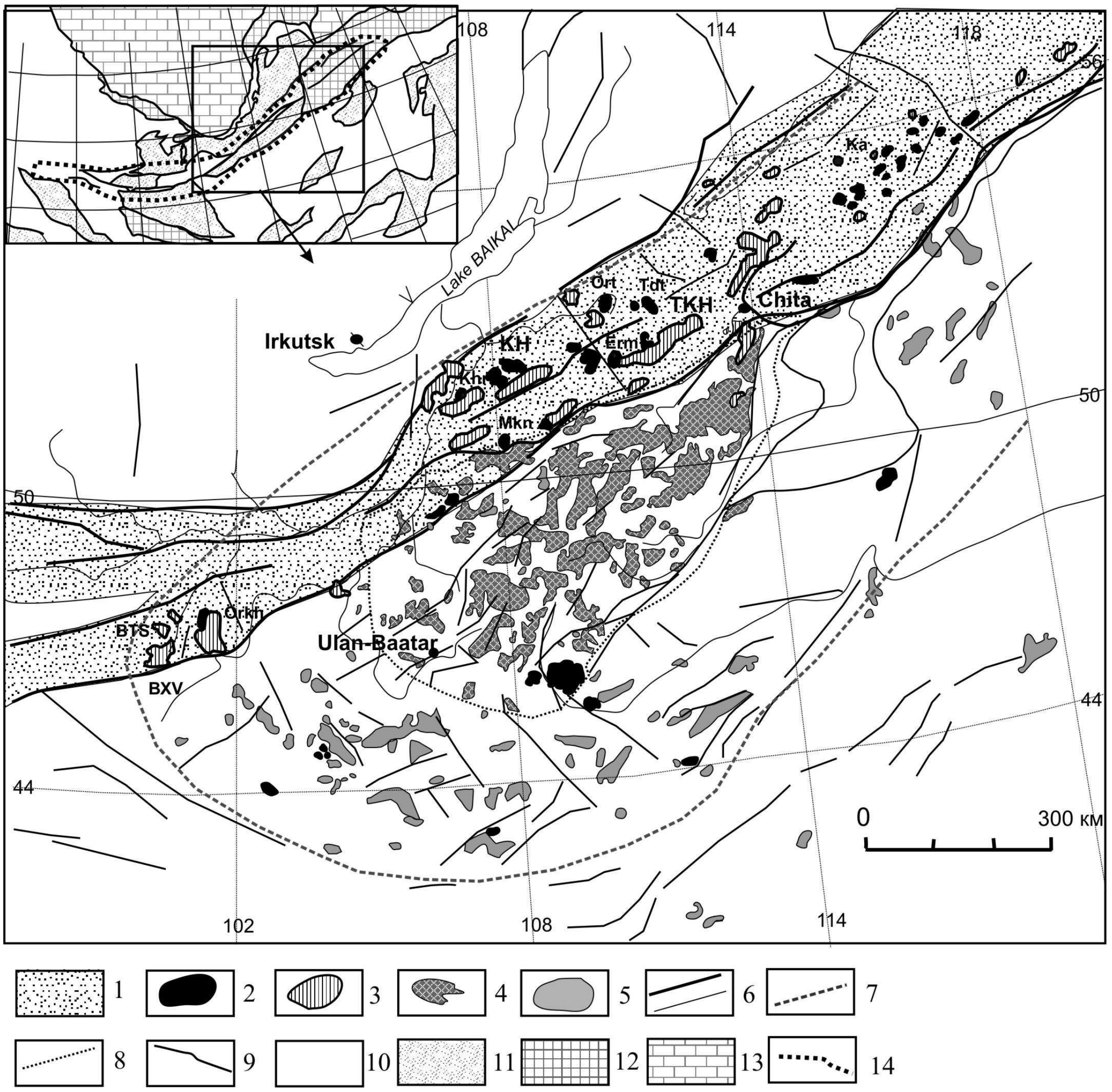

Fig.1. **Position of the North Mongolian – West Trans-Baikal rift zone within the Early Mesozoic magmatic area, with the Khentey-Dauria batholith core in the center and rift zones on its margins. The inlet displays multi-staged Mongolian - Trans-Baikal rift system**.

1 – North Mongolian – West Trans-Baikalian rift zone, 2 – 3 – magmatic assemblages of the North Mongolian – West Trans-Baikal rift zone: 2 – alkaline granitoids, 3 – alkaline -bimodal trachybasalt-comendite and trachybasalt, 4 – 5 – rocks of zonal magmatic area: 4 – granitoids of Khentey-Dauria batholith, 5 – rifting volcanic assemblages of the Khentey-Dauria batholith surroundings, 6 – belt of large faults referred to the category of sutures and outlines of North Mongolian – West Trans-Baikal rift zone, 7 – external contour of the zonal Early Mesozoic magmatic area, 8 – outlines of Khentey-Dauria batholith, 9 – faults, 10 – 14 – legend to inlet: 10 – Caledonides, 11 – terranes of the Riphean crust, 12 – Pre-Riphean continental blocks, 13 – Siberian platform, 14 – boundaries of polychronous rift system.

Reference massifs: Khrt – Kharitonovsky, Mkn – Malokunaleisky, Erm – Ermakovsky, Ort – Orotskiy, Tdt – Tadutskiy.

Volcanic fields of the West Trans-Baikal sector: KH – Kharitonovsky assemblage, TKH - Tsagan Khurtey assemblage, Ka – Karengskiy volcanic area.

Volcanics of the North Mongolian sector filling the depressions: Orkh – Orkhonsky, BTS – Bat–Tsengelsky, VKH – Verkhne-Khanuisky.

--

defined by different methods to lie within the range 233 – 188 Ma, is regarded as Late Triassic – Early Jurassic.

The structure of NMWTB rift zone consists of the two sectors – North Mongolian and West Trans-Baikalian, distinguished by the composition of magmatic assemblages.

North Mongolian sector of the rift zone strikes for 600 km, being about 120-150 km wide. It runs along the Orkhon River valley and is vividly divided into the eastern and western segments. The eastern segment hosts plutonic formations as massifs of gabbroids and alkaline granites [19]. The western segment incorporates a series of differently sized depressions, e.g. Orkhon, Bat-Tsengel, Verkhne-Khanguy, filled with the Early Mesozoic sedimentary and volcanic formations. The largest Orkhon depression [18] is sized as ≈120x150 km. It basically consists of some angular basins and one-sided grabens divided by the faults of northwestern and submeridional strike. The depression is filled with two sequences: Abzogsky lower terrigenous sequence and Mogodsky upper volcanogenic sequence. Both sequences are closely related by facial transitions represented by alternating layers of sedimentary and volcanogenic rocks. The lower Abzogsky sequence is composed of conglomerates and sandstone-silty sediments containing floristic remains of the Middle – Late Triassic plants [20]. The Mogodsky volcanogenic sequence encompasses rocks of the basic and medium composition. These are trachyandesite basalts, basalts are not so common; trachyandesites and trachytes occur as irregular flows. The Urtyngolsky graben, with the thickness over 2500 m, is filled with the lavas of pyroxene porphyry and pyroxene-plagioclase porphyry trachyandesite basalt. The section locally contains layers of ball lavas with hyaloclastic cement, which is the evidence of lava flows proceeding in aqueous conditions, and locally interbedded red agglomerates and abundantly porous lavas formed in the subaerial environment.

The Bat-Tsengel depression is located in the northern margin of Khoit-Tamira river. Having dimensions about 15x30 km, it extends to the north-east. It is distinguished from the volcanic grabens of the Orkhon depression by absence of sedimentary rocks in its structure. The age of the depression formation is defined through volcanics by K-Ar method. In the basalts of the middle part of the volcanic pile it is 220 Ma [40], which corresponds to Late Triassic. Within the depression volcanic rocks discordantly lie on the rocks of the Early and Middle Paleozoic and produce the sequence over 1200 m thick. The eastern end of the depression is dominated by massive or amygdaloidal lavas of plagioclase-porphyry, rarely pyroxene-plagioclase porphyry, as well as aphyric trachyandesite basalts and trachyandesites. Tuffs and agglomerates are not common, only the lower part locally contains some thin layers of trachyrhyolite tuffs. In the western edge of the depression tuffs and lavas of trachyrhyolites predominate. This can be linked with their location close to the effluent channel. In general, the volcanic association of the Bat-Tsengel depression can be regarded as bimodal.

The Upper Khanuy depression represents the field of volcanic rocks development (≈30x30 km). A group of diverse rocks, including trachybasalts, basalt trachyandesits, trachytes and sintered tuffs of trachytes is available. Volcanic formations occur on the Early Mesozoic weathering crust after Late Paleozoic complexes of the Khangay trough. They are compositionally close to the rocks of Bat-Tsengel depression and Late Triassic and Early Jurassic volcanic sequences of the Western Trans-Baikal area. Therefore, the age of the rocks of the depression is considered as Late Triassic – Early Jurassic [19].

The plutonic rocks of this sector [10] form syenite-leucogranite assemblages, their age varying within 245-186 Ma.

Table 1

Sites, depressions and typesof the Early Mesozoic volcanic assemblages of the North Mongolian - West Trans-Baikal rift zone.

Units	Rocks assemblages
	West Trans-Baikal segment ***Kharitonovsky assemblage***
Monostoisky site	trachybasalt-trachybasaltic andesite-trachyte-alkaline trachydacite
Ust-Sukharinsky site	trachyrhyodacite-pantellerite
Ulantuisky site	trachybasalt-trachybasaltic andesite-trachyte-pantellerite with teschinite
Novospassky site	pantellerite
Malokunaleisky and Kharitonovsky massifs	alkaline granite and syenite
	Tsagan-Khurtey assemblage
Saransky site	trachybasalt-trachybasaltic andesite-trachyte-trachyrhyolite-pantellerite-comendite
Zunnemetey site	trachybasalt-trachybasaltic andesite-trachyrhyolite-pantellerite-comendite
Taidutsky and Kudunsky sites	trachyte-trachyrhyolite-pantellerite-comendite
Khushegovsky site	trachyte-trachyrhyolite-comendite
Ermakovsky, Orotsky, Tadutsky and Atkhinsky massifs	leucogranite-alkaline granite-syenite
	North-Mongolian segment
Orkhon depression	basalt-trachybasaltic andesite-trachyandesite-trachyte
Bat-Tsengelskaya depression	trachybasaltic andesite-trachyandesite-trachyrhyolite
Verkhne-Khanuy depression	trachybasalt-trachybasaltic andesite-trachyte-phonolite

The West Trans-Baikal sector extending for 80 km, covers that part of the rift zone, which is traced from the confluence of the Dzhida and Selenga Rivers through the basins of rivers Uda, Tunguy, Khilok to the basin of the Vitim River upstream. In the Early Mesozoic in this zone great volcano-plutonic structures (area 2000 km^2) were formed. They contain fields of volcanics of trachybasalt and

--

alkaline-bimodal trachybasalt-comendite assemblages and massifs of alkaline granites and syenites [13,39], confined to the systems of horsts and grabens. In the western part of the sector magmatic rocks produce the Kharitonivsky assemblage, and Tsagan-Khurteisky one in the eastern part.

The Kharitonovsky assemblage unites magmatic rocks of the Tugnuy depression, i.e. the Kharitonovsky massif of subalkaline and alkaline syenites and granites (about 230 km^2) and framing sequences of trachytes, alkaline trachyandesites, pantellerits, as well as trachybasalts-trachyandesite basalts and teshenites. Based on Rb-Sr dating the age of alkaline granites and syenits of the Kharitonovsky massifs is assessed within the interval 209-221 Ma [40, 12]. Close to the Kharitonovsky massif the Early Mesozoic volcanic sequences Close to the Kharitonovsky massif the Early Mesozoic volcanic sequences are associated with Monostoysky (≈20x8 km) and Ust-Sukharinsky (≈2x2 km) volcanic fields. The structure of the Monostoysky lava field define alternating covers of trachybasalts, trachyandesite basalts and trachytes-alkaline trachydacites, their age defined by Rb-Sr isochron to be 194,3 Ma [37]. The volcanic sequence of Ust-Sukharinsky field is composed of beds of massive aphyre and porphyry trachyrhyodacites-pantellerites, alternating with lava breccias, tuffs and ignimbrites of the same composition. The isochron Rb-Sr age of trachyrhyodacites-pantellerites is assessed as 215 Ma [38]. In the northreastern part of the Tuguy depression the Early Mesozoic volcanics are revealed within Ulantuy (≈50x10 km) and Novospassky (≈1x1 km) lava fields. The former consists of the bed covers and extrusive bodies of trachytes, trachyrhyolites-pantellerites, infrequent beds of black aphyre and large leucite trachybasalts and some interbedded sequences of sedimentary rocks, as well as abundant dykes of alkaline basalts and pantellerites. The upper part of cross-section contains teshenite sill, its K-Ar age, after two determinations, varies from 208 and 212 Ma [40]. Within the Novospassky lava field there are bed covers of porphyry pantellerites close in composition to those of Ust-Sukharinsky volcanic field. The youngest volcanic formations of the Kharitonovsky association produce the lava field in the region of Chernoyarovo village, consisting of trachybasalts and trachytes of the Chernoyarovsky suite with the age 188-198 Ma (K-Ar method for bulk samples, following data by V.G.Ivanov).

The Tsagan-Khurtey assemblage includes magmatic rocks of the Kizhinga and Tsagan-Khurtey depression. The assemblage involves alkaline-bimodal volcanic rocks of the Tsagan-Khurtey suite and alkaline granites and granosyenites of the Maly Kunaley complex with the age 233 Ma [26]. In the Kizhinga depression these are alkaline rocks occurring in the surroundings of the Orotsky and Kinzhinga depressions, having the age 232-225 Ma [14,15]. In the Tsagan-Khurtey depression volcanic fields are intruded by alkaline granites and quartz syenites of some massifs as well as numerous longitudinal dykes of basalts and comensites. Volcanic assemblages consist of trachybasalts, trachyrhyodacites – trachyrhyolites and pantellerites-comendites with predominant comendites among acid rocks and limited involvement of acid rocks, e.g. trachyandesite basalts and trachytes. The isochron Rb-Sr ages of rocks correspond to the range 209 - 212 Ma [29], which practically coincided with the estimates of K-Ar dates of trachybasalts (207 ± 5 Ma, sample TH-1/7) [40].

In addition, some rock assemblages close in composition have similar age dates in the other regions of the West Trans-Baikal. Thus, in its northeastern part, between the Vitim and Karenga rivers, as follows from the data by Stupak F.M. [22], alkaline granitoids formed about 209 Ma.

Completing description of the Early Mesozoic magmatism in NMWTB rift zone, we are to emphasize an evident relation to the formation of the system of grabens, bimodal character with predominance of basic volcanic and acid magmatic rocks: comendites, pantellerites, trachyrhyolites and their plutonic analogs – alkaline granites and syenites. Similar features of the composition and conditions of magmatism occurrence are typical for continental rifts, which is the foundation for distinguishing NMWTB area of magmatism as the rift zone.

ANALYTICAL METHODS

This study is based on processing of 170 samples collected from volcanic fields in different parts of the rift zone. The compositions were defined by various methods. Some analyses were made at the Institute of Geochemistry SB RAS(Irkutsk): (i) petrogenic elements and Zr contents were defined by XRF followoing procedure proposed Afonin et al. [1], (ii) Rb contents were determined by flame photometry, (iii) the contents of other trace elements were measured by neutron-activation analysis at the UIGGM SB RAS (Novosibirsk), IGCP-MS at Precambrian Institute RAS (St.Petersburg) and in Analytical Center of the Irkutsk Science Center (ACISC).

The isotope compositions of Rb and Sr in basaltoids were defined at IGEM RAS (Moscow), Institute of Geochemistry and Geology Institute SB RAS. The measurements were executed by mass spectrometer Finnigan MAT-262 and MI-1201 "T" in a single-ray regime. The isotope composition of Sr and its concentration were detected by the double isotope dilution, and the content of Rb was determined by a simple isotope dilution. To control the isotope composition of Sr a reference sample with the attested value $^{87}Sr/^{86}Sr = 0.70801$ was used. The ratio $^{87}Sr/^{86}Sr = 0.70796 \pm 0.00009$ was obtained during our work . The errors in ratio determination, with regard to parallel measurements for $^{87}Sr/^{86}Sr$ and $^{87}Rb/^{86}Sr$, were not higher than 0,05 and 2 %, accordingly. The isotope compositions of Sm and Nd were measured at IGEM RAS and the university of Rennes (France), respectively, by mass-spectrometer Finnigan MAT-262 and Finnigan MAT-261 under statistical regime of measurements with the standard technique applied [41]. The precision of Sm и Nd concentration determination was ±0,5% (2σ). The isotope measurements were made with precision (2σ): $^{147}Sm/^{144}Nd$ - 0.5% and $^{143}Nd/^{144}Nd$ - 0.005%. The average weighted value

---

--

^{143}Nd/^{144}Nd in Nd-standard La Jolla amounts to 0.511841 ± 4 (2σ). The value εNd(T) was estimated relative to model homogeneous chondrite reservoir CHUR with parameters ^{143}Nd/^{144}Nd = 0.512638, ^{147}Sm/^{144}Nd = 0.1967 [5].

The isotope composition of Pb was defined in rocks by 7-collector thermal ionization mass-spectrometer Finnigan MAT-262 at ACISC. The data obtained were corrected by the standard NBS-981 (^{206}Pb / ^{204}Pb = 16,914 ± 0,004, ^{207}Pb / ^{204}Pb = 15,461 ± 0,004, ^{208}Pb / ^{204}Pb = 36,605 ± 0,009, n=19). The composition of femic minerals was analysed at IGC SB RAS by microprobe “Superprobe-733” Jeol Co.

COMPOSITION OF VOLCANIC ASSEMBLAGES OF NORTH MONGOLIAN – WEST TRANS-BAIKAL RIFT ZONE

Petrographic features of rocks. As was mentioned, the composition of magmatic assemblages in the NMWTB rift zone is dominated by basic and mid-basic rocks (trachybasalts, trachyandesite basalts) on the one hand, and alkaline-salic rocks (trachytes, alkaline trachydacites, trachyrhyolites, pantelerites, comendites and alkaline granites and syenites) on the other hand. The main varieties of rocks have close petrographic characteristics in different parts of the rift zone, they will be considered in general terms.

Trachybasalts (olivine, pyroxene-plagioclase, plagioclase) have porphyric, rarely aphyre structure. Phenocrysts of porphyry varities consist of basic plagioclase (up to 50%), olivine (to 20%), titanium-augite (to 40%). The matrix is composed of microlites of plagioclase and pyroxene, immersed in the brown devitrified volcanic glass. They are also composed of pyroxene and plagioclase (labrador, 64-66 % An [11]. Besides, the basic mass contains fine crystals of olivine (Fo_{70-75}), locally alkaline feldspar, biotite, kersutite, as well as ore and accessory minerals.

Subalkaline-alkaline gabbro-dolerites (teshenites) possess hypidiomorphic grained, poikillitic structure. They are made of plagioclase (up to 40%), titanium-augite (40%), olivine (to 30%), biotite (20%), barkevekite (20%), ore and accessory minerals make up 15%. In mostly alkaline varieties, compositionally close to teshenite, there appears fresh or slightly pilitic analcite (5%), as well as nepheline (5%), replaced by albite and ceolite.

Trachyandesite basalts and trachyandesites are not as widespread as trachybasalts and are characterized by poprhyre and aphyre structures. Phenocrysts represent widely tabular andesite-labradorite and augite. The basic mass consists of hardly discernible long prismatic microlites of plagioclase and augite, chloritized amphiboles and biotite, isometric ore minerals immersed in the fine-grained chloritized matrix.

Salic effusive rocks – trachytes, alkaline trachydacites, trachyrhyolites, pantellerites and comendites are characterized by poprhyric, rarely glassy aphyre structures. Trachytes contain phenocrysts of alkaline feldspar with pertite structure, aegerine and aegerine-augite (locally hypersthene), rarely quartz and zonal plagioclase (10-30 % An). The basic mass consists of grains of feldspar, rare prismatic crystals of alkaline amphiboles, microlites of acid plagioclase (10-12 % An) and ore minerals. Not so abundant is quartz and brownish devitrified glass.

Alkaline trachydacites, trachyrhyolites, pantellerites and comendites in phenocrysts contain alkaline feldspar, less widespread is quartz, amphibole and biotite. The matric represents microfelsitic and microspherolitic structure, is actually made of micrographic growths of quartz and K-Na feldspar. They are surrounded by glassy basis enclosing spicular microlites of aegerine varying in composition in rhyolites with different contents of silicic acid (from highly magnesian in trachydacites to low magnesian in comendites). Compositions of some femic minerals of trachybasalts, trachytes, trachydacites and comendites are listed in Table 2.

Table 2.

Composition of femic minerals in the Early Mesozoic volcanic rocks of the West Trans-Baikal segment of the North Mongolian-West Trans-Baikal rift zone.

Sample	TKH 1/1	TKH 1/19	TG 13/6				TG 1/8			
Rock	trachybasalt	trachyte	Alkaline trachydacite				comendite			
Mineral	Ti-augite	kaersutite	High-Mg aegerine				Low-Mg aegerine			
SiO_2	51,00	38,65	49,38	52,08	51,79	51,82	48,95	61,86	48,75	49,00
TiO_2	1,87	9,31	1,48	0,95	1,10	1,01	3,83	3,45	2,40	2,69
Al_2O_3	2,19	11,19	0,96	1,33	1,01	1,53	0,50	0,48	0,59	0,56
FeO*	11,60	13,17	21,64	20,96	18,61	17,15	26,11	26,41	26,70	25,45
MnO	0,20	0,32	1,83	1,46	2,15	1,85	1,50	1,54	1,45	1,39
MgO	12,89	12,20	6,91	8,09	8,85	10,46	1,36	1,72	2,42	2,53
CaO	19,94	10,46	3,82	3,13	5,16	6,37	1,16	2,03	2,69	2,73
Na_2O	0,00	2,48	7,10	6,32	6,07	5,89	7,97	8,07	7,44	7,37
K_2O	0,00	0,64	1,43	0,86	1,27	1,04	1,23	1,32	1,28	1,33
Total	99,68	98,42	94,55	95,17	96,01	97,12	92,61	96,88	93,72	93,05

Alkaline granites and syenites involve pertitic feldspar and quartz in different voluminous ratios. The rocks consist of grains and micro-grains. In alkaline feldspar varieties of rocks femic minerals are represented by biotite and subcalcic amphibole, mostly alkaline rocks contain riebekite-arfvedsonite, calcic riebekite, aegirine, kataforite [42, 15]. Accessory minerals are apatite, sphene, zircon and fluorite. Alkaline syenites are mainly mid-grained rocks consisting of alkaline feldspar, nepheline, albite, aegerine, ore and accessory minerals.

Petrochemical characterization of rocks. The chemical compositions of representative varieties of rocks are listed in Table 3 On the chart SiO_2 – Na_2O+K_2O the rocks of the Early Mesozoic magmatic assemblages produce a sequence of figurative points of the compositions, which is statistically divided into two groups (Fig. 2). The first group contains rocks of the basic composition, among which are trachybasalts and trachyandesite basalts (SiO_2 varies within the range 46-59 mass %). The second group represents salic rocks, i.e. trachytes, alkaline trachyrhyodacites, trachyrhyolites, pantellerites and comendites and their intrusive analogs - syenites, granosyenites and alkaline granites (SiO_2 varies within

Table 3.

Compositions of representative rocks of Early Mesozoic magmatic assemblages of North Mongolian - West Trans-Baikal rift zone.

West Trans-Baikal segment										
Kharitonovsky assemblage										
Monostoisky site, volcanic rocks										
Sample	TG 13/5	TG 13/6	TG 13/8	TG 13/9	TG 13/11	TG 13/12	TG 13/13	TG 13/15	TG 13/17	TG 13/19
SiO_2	66,50	65,98	66,00	51,37	50,88	50,64	52,39	61,98	65,04	50,55
TiO_2	0,60	0,60	0,73	1,54	1,80	1,75	2,27	0,95	0,70	1,44
Al_2O_3	17,03	16,40	16,75	17,57	18,04	17,75	16,39	17,52	16,93	16,32
Fe_2O_3	3,13	3,79	3,99	8,08	11,51	11,01	9,54	4,48	3,36	9,63
MnO	0,04	0,14	0,11	0,18	0,11	0,12	0,14	0,12	0,06	0,16
MgO	0,10	0,36	0,13	3,41	2,23	3,40	2,19	0,87	0,43	3,66
CaO	0,20	0,32	0,20	7,42	4,98	5,93	5,63	2,10	1,03	10,02
Na_2O	5,52	5,73	5,69	3,73	4,03	4,26	4,14	5,01	5,13	3,58
K_2O	6,07	5,65	5,76	2,44	2,20	2,39	3,67	5,60	6,28	1,92
P_2O_5	0,08	0,09	0,11	0,56	0,54	0,52	1,55	0,31	0,17	0,59
LOI	0,71	0,82	0,46	3,62	3,64	2,09	1,66	0,78	0,68	1,93
Total	99,98	99,88	99,93	99,92	99,96	99,86	99,57	99,72	99,81	99,80
c.a.	0,92	0,95	0,93	-	-	-	-	0,82	0,9	-
Rb	150	140	140	42	40	52	64	130	160	28
Ba	45	35	35	1190	960	1030	2410	1788	1182	860
Sr	22	20	30	1110	890	1070	1500	798	327	1470
Zr	820	709	648	302	263	264	451	556	642	207
Nb	19,96	21,00	25,66	15,14	10,34	11,15	22,44	24,50	27,65	9,94
Hf	37,11	44,35	16,82	6,07	5,37	5,23	8,41	22,44	20,59	4,12
Ta	3,87	1,97	2,13	0,76	0,49	0,48	1,11	3,53	1,83	0,54
Y	33,00	39,00	34,00	29,00	30,00	30,00	30,00	23,00	22,00	21,00
Th	22,86	23,59	14,94	4,79	3,50	3,26	5,49	12,67	18,11	3,62
U	3,49	4,67	1,52	1,52	0,76	0,70	1,10	2,47	3,00	1,00
Pb	34,69	39,40	22,34	13,00	10,00	10,00	16,00	22,68	21,62	10,00
La	89,81	99,79	103,11	44,35	34,90	35,42	83,54	89,34	87,21	39,74
Ce	210,97	212,09	224,33	96,82	73,97	76,12	175,20	184,71	180,92	83,15
Pr	23,64	23,00	24,93	11,22	9,30	9,27	23,27	19,99	18,90	9,91
Nd	92,83	90,44	89,54	44,38	39,68	38,67	93,64	72,16	66,51	40,02
Sm	15,06	14,90	13,76	8,15	7,51	7,35	14,59	10,75	9,85	6,94
Eu	1,98	2,04	1,44	2,34	2,28	2,27	4,33	2,72	1,98	2,27
Gd	10,93	12,27	10,33	7,59	7,37	7,77	12,89	8,22	7,73	7,31
Tb	1,62	1,80	1,23	0,99	1,02	1,03	1,47	0,88	0,89	0,94
Dy	9,21	10,64	6,58	5,32	5,85	6,06	6,56	4,48	4,38	4,40
Ho	1,95	2,18	1,10	0,99	1,12	1,16	1,20	0,78	0,77	0,80
Er	5,37	6,48	3,36	2,88	2,82	2,87	2,73	2,25	2,22	2,06
Tm	0,85	1,05	0,51	0,44	0,45	0,41	0,36	0,30	0,29	0,33
Yb	5,53	6,51	2,72	2,74	2,41	2,52	2,09	1,75	1,84	1,75
Lu	0,87	1,06	0,46	0,42	0,39	0,35	0,34	0,26	0,27	0,26

Table 3. Continued.

West Trans-Baikal segment										
Kharitonovsky assemblage										
Kharitonovsky massif, intrusive rocks					Ust-Sukharinsky and Ulantuisky sites, volcanics					
Sample	B 163/3*	A 254-2*	B 163/11*	V 336/1*	TG 1/1	TG 1/2	TG 1/3	TG 1/4	TG 1/5	TG 1/7
SiO_2	65,60	73,26	49,10	48,60	67,94	70,29	62,25	70,15	69,14	68,87
TiO_2	0,63	0,26	2,44	2,13	0,49	0,38	0,71	0,48	0,38	0,38
Al_2O_3	16,02	13,87	16,01	16,90	16,34	15,09	17,69	15,23	15,33	15,24
Fe_2O_3	2,56	2,44	10,70	11,33	2,20	2,05	3,67	2,45	1,66	1,27
MnO	0,02	0,01	0,14	0,13	0,05	0,02	0,12	0,07	0,18	0,15
MgO	0,63	0,00	4,87	6,17	0,08	0,15	0,73	0,16	0,19	0,20
CaO	1,55	0,45	7,49	6,64	0,17	0,07	0,85	0,07	0,25	0,30
Na_2O	4,43	4,47	3,63	3,66	6,04	4,88	5,95	5,93	6,11	6,20
K_2O	7,20	5,05	2,13	1,75	5,09	5,63	6,55	3,88	5,28	5,34
P_2O_5	0,11	0,01	0,62	0,75	0,09	0,09	0,23	0,16	0,04	0,04
LOI	0,75	0,45	2,3	1,52	0,54	0,56	0,38	0,74	0,32	0,29
Total	99,50	100,27	99,43	99,58	99,03	99,21	99,13	99,32	98,88	98,28
c.a.	0,94	0,92	-	-	0,95	0,94	0,96	0,92	1,03	1,05
Rb	110	271	32	23	145	194	140	128	202	218
Ba	610	106	1200	720	81	126	380	84	25	27
Sr	180	49	845	910	47	57	75	33	12	10
Zr	1400	344	370	230	770	849	510	840	915	848
Nb	61,00	43,50	16	11	28,76	30,97	30,09	19,00	29,01	32,21
Hf	-	-	-	-	6,35	11,81	41,19	5,58	35,28	36,47
Ta	-	2,42		7,70	3,16	2,35	3,60	1,49	3,39	4,16
Y	140,00	29,00	41,00	30,00	31,86	41,43	28,08	24,33	56,00	58,06
Th	199,00	-	8,00	2,00	12,26	17,86	18,21	12,06	33,50	35,00
U	-	-	-	-	3,12	2,66	3,37	2,23	4,83	4,91
Pb	-	-	-	-	36,00	25,00	39,00	37,00	51,00	52,00
La	120,00	39,25	30	26	142,81	90,05	100,51	131,48	108,84	110,36
Ce	420,00	70,85	65	58	225,51	177,13	200,00	227,21	205,00	229,58
Pr	-	-	-	-	33,14	22,54	25,16	30,11	26,77	26,34
Nd	190,00	20,00	34	30	111,38	76,62	101,51	100,27	99,54	101,32
Sm	25,00	3,17	7,1	6,4	14,41	12,83	16,88	14,20	16,43	17,81
Eu	3,50	0,32	2,2	2,1	1,38	1,29	3,33	1,40	1,60	1,71
Gd	-	2,83	-	-	11,81	11,28	11,83	11,37	13,74	14,06
Tb	-	-	-	-	1,39	1,45	1,55	1,19	2,24	2,23
Dy	4,80	2,30	1,2	1,1	7,20	8,53	8,01	6,03	13,14	14,01
Ho	-	-	-	-	1,30	1,63	1,45	0,99	2,74	2,82
Er	-	0,21	-	-	3,94	5,06	4,19	2,96	7,99	8,64
Tm	-	-	-	-	0,56	0,78	0,62	0,39	1,35	1,34
Yb	11,00	1,25	3,6	2,5	3,79	5,36	3,68	2,73	8,59	8,32
Lu	1,40	0,18	0,52	0,34	0,56	0,78	0,61	0,37	1,39	1,31

Table 3. Continued.

West Trans-Baikal segment										
Kharitonovsky assemblage		*Tsagan-Khurtey assemblage*								
Ust-Sukharinsky and Ulantuisky sites,sill		Saransky site, volcanic rocks							Zunnemetey site, volcanic rocks	
Sample	TG 16/2	TKX 1/1	TKX 1/2	TKX 1/6	TKX 1/7	TKX 1/8	TKX 1/14	TKX 1/19	TKX 7/2	TKX 7/5
SiO_2	48,18	49,36	57,74	48,48	46,93	75,38	74,97	61,73	77,23	53,02
TiO_2	1,71	2,11	1,98	2,02	2,69	0,29	0,30	1,13	0,11	1,48
Al_2O_3	16,83	16,46	15,07	17,03	16,19	10,83	12,09	16,91	11,20	17,73
Fe_2O_3	11,41	10,41	8,73	10,76	12,48	4,08	2,97	5,26	2,85	8,88
MnO	0,16	0,17	0,12	0,14	0,17	0,12	0,07	0,12	0,01	0,17
MgO	7,47	5,78	1,79	6,21	6,37	0,12	0,17	1,11	0,07	4,51
CaO	8,29	7,55	5,21	8,06	8,12	0,16	0,19	2,59	0,09	4,97
Na_2O	3,72	3,81	4,81	3,98	4,02	3,84	3,81	5,73	3,65	4,51
K_2O	1,35	1,45	2,72	1,09	1,10	4,80	4,82	4,25	4,69	3,85
P_2O_5	0,46	0,74	0,84	0,80	1,02	0,03	0,02	0,38	0,03	0,66
LOI	0,36	2,07	0,83	1,36	0,90	0,22	0,45	0,59	0,07	0,00
Total	99,93	99,91	99,83	99,92	99,98	99,86	99,85	99,80	99,99	99,78
c.a.	-	-	0,72	-	-	1,06	0,95	0,83	0,99	-
Rb	16	-	48	13	10	162	114	107	130	68
Ba	647	876	1002	703	608	19	18	686	100	1590
Sr	1049	981	656	1263	1536	15	17	293	40	935
Zr	166	325	409	177	228	787	732	424	491	258
Nb	6,92	11,30	14,70	5,44	10,79	28,06	32,00	15,00	13,80	15,00
Hf	6,92	6,91	9,66	3,67	5,64	10,45	9,37	6,26	6,35	5,42
Ta	2,55	-	-	-	-	0,79	2,00	1,85	1,13	1,41
Y	30,72	-	52,60	28,40	30,30	56,41	44,08	28,65	28,30	25,80
Th	1,41	2,57	6,66	2,01	2,07	17,65	8,89	7,63	8,51	3,36
U	0,32	0,75	2,24	0,43	0,56	4,02	2,32	2,15	1,54	0,65
Pb	5,80	7,30	11,00	6,60	7,30	30,00	28,00	15,50	11,50	8,80
La	24,09	47,30	47,20	34,20	39,80	85,96	56,38	41,26	32,80	43,10
Ce	57,04	100,00	104,00	62,00	94,30	161,51	117,87	83,46	59,20	96,90
Pr	7,07	12,10	12,90	9,25	11,40	19,29	14,90	10,89	6,72	10,90
Nd	32,33	56,30	59,40	43,90	54,80	70,31	52,71	39,80	24,40	42,30
Sm	6,89	11,10	13,00	8,79	10,40	13,42	9,80	7,77	4,74	7,42
Eu	2,03	3,44	3,87	3,00	3,36	1,62	1,35	2,11	0,12	2,06
Gd	6,21	9,21	10,60	7,14	8,26	10,69	9,29	7,33	4,42	6,67
Tb	0,90	1,44	1,78	1,13	1,26	1,64	1,37	1,10	0,72	0,89
Dy	5,17	7,68	9,48	5,92	6,43	9,73	8,16	6,07	4,22	4,58
Ho	0,96	1,54	1,98	1,17	1,27	1,84	1,62	1,17	0,87	0,83
Er	2,67	3,86	5,08	2,74	3,08	5,67	4,94	3,40	2,80	2,37
Tm	0,41	0,63	0,82	0,43	0,48	0,89	0,69	0,55	-	-
Yb	2,47	3,89	5,22	2,72	2,85	5,59	4,62	3,22	2,86	2,01
Lu	0,36	0,54	0,77	0,36	0,37	0,41	0,64	0,47	0,46	0,29

Table 3. Continued.

West Trans-Baikal segment									
Tsagan-Khurtey assemblage									
Zunnemetey site, volcanic rocks						Ermakovsky massif, intrusive rocks		Orotsky massif, intrusive rocks	
Sample	TKX 7/6	TKX 7/8	TKX 7/9	TKX 7/10	TKX 7/11	805**	400**	Oro-1***	Oro-9***
SiO_2	75,89	51,08	70,20	55,82	67,90	54,26	75,16	75,70	73,28
TiO_2	0,12	2,15	0,62	1,41	0,65	1,18	0,28	0,34	0,38
Al_2O_3	11,99	16,87	13,84	17,64	15,05	16,52	11,90	11,62	15,42
Fe_2O_3	2,83	9,20	3,96	10,31	3,38	7,83	2,47	4,37	1,36
MnO	0,03	0,17	0,06	0,12	0,11	0,05	0,02	0,15	0,03
MgO	0,16	3,08	0,35	3,13	0,39	2,95	0,20	0,35	0,21
CaO	0,27	6,24	0,22	2,67	0,54	5,58	0,35	0,51	0,52
Na_2O	2,97	4,70	3,75	4,74	5,96	5,4	4,25	2,21	2,98
K_2O	5,11	2,75	6,39	1,88	5,31	2,93	4,66	4,71	5,65
P_2O_5	0,02	1,16	0,09	0,33	0,14	0,24	0,03	0,01	0,02
LOI	0,61	2,62	0,57	2,11	0,59	3,10	0,56		
Total	99,99	100,02	100,06	100,16	100,02	100,04	99,88	99,97	99,85
c.a.	0,87	-	0,95	-	1,03	-	1,01	0,72	0,69
Rb	160	46	150	60	82	94	335	235	271
Ba	140	1150	120	520	730	813	58	63	121
Sr	240	889	65	548	52	650	43	13	30
Zr	426	437	358	139	452	146,74	712	1102	714
Nb	42,00	28,60	26,40	6,10	24,90	7,88	38,0	77,50	97,85
Hf	13,30	10,60	7,60	2,37	7,29	4,4	38,00	29,28	20,12
Ta	3,93	2,60	2,32	1,23	2,76	0,46	4,89	4,40	6,02
Y	69,00	36,40	44,70	20,40	42,30	21,7	-	66,38	83,59
Th	19,60	7,94	7,03	3,00	6,84	5,09	39,70	29,60	32,98
U	2,12	1,55	2,22	0,77	0,91	1,15	8,30	5,44	8,41
Pb	32,10	15,50	16,30	6,30	15,40	5,9	23	80,53	44,77
La	36,00	89,90	42,40	18,30	64,30	26,66	60,30	56,97	123,20
Ce	87,10	162,00	97,30	34,60	133,00	54,16	91,70	117,40	252,10
Pr	10,10	20,30	12,20	5,54	14,30	6,55	7,23	11,62	30,14
Nd	36,10	81,00	48,40	23,30	54,60	24,80	19,10	36,68	103,50
Sm	8,13	13,60	9,39	4,63	9,03	4,78	2,66	7,42	18,59
Eu	0,17	3,38	2,27	1,20	1,71	1,39	0,25	0,80	1,88
Gd	8,02	11,40	8,77	4,40	8,15	4,54	2,20	7,02	13,98
Tb	1,50	1,36	1,25	0,62	1,18	0,74	0,42	1,41	2,33
Dy	9,62	6,88	7,39	3,54	6,81	4,04	3,30	9,32	13,25
Ho	2,07	1,18	1,41	0,68	1,33	0,79	0,90	3,26	2,93
Er	6,60	3,08	4,20	1,88	4,21	2,16	3,61	7,91	8,90
Tm	-	-	-	-	-	0,29	0,68	1,43	1,56
Yb	6,87	2,41	3,60	1,78	3,96	1,79	5,31	10,07	9,81
Lu	1,10	0,37	0,56	0,23	0,63	0,26	0,92	1,54	1,49

--

Table 3. Continued.

North Mongolian segment												
	Orkhon depression		Bat-Tsengelskaya depression			Verkhne-Khanuy depression						
Volcanic rocks												
Sample	MOG-1/4	MOG-1/8	BTS-7/3	BTS-7/6	BTS-7/7	4155/10	4152/1	4152/7	4152/8	4150/4	4150/3	4150/5
SiO_2	54,34	51,47	51,24	51,78	55,06	53,33	52,25	54,85	53,88	54,22	54,25	54,65
TiO_2	0,89	1,20	1,90	1,94	1,25	1,38	1,66	1,42	1,44	1,38	1,47	1,39
Al_2O_3	17,61	16,22	16,31	15,14	16,28	15,65	16,90	16,97	17,11	16,90	17,17	17,30
Fe_2O_3	7,28	7,24	9,39	9,30	7,33	7,65	9,00	8,50	8,72	8,15	8,40	8,27
MnO	0,11	0,10	0,10	0,15	0,10	0,07	0,05	0,06	0,10	0,04	0,11	0,04
MgO	3,83	4,58	4,27	2,31	3,05	3,54	2,80	2,57	2,48	2,75	2,90	2,70
CaO	7,59	8,16	5,70	7,38	6,16	4,34	4,85	4,33	4,97	5,30	5,09	4,61
Na_2O	4,19	4,82	3,94	3,53	3,41	4,67	5,85	5,40	5,36	5,01	5,28	5,13
K_2O	2,38	2,57	3,04	2,85	2,69	2,96	3,55	3,58	3,00	3,75	3,45	3,61
P_2O_5	0,39	1,03	1,21	1,22	0,57	0,85	1,19	0,95	0,94	1,05	1,11	1,10
LOI	1,32	2,08	2,55	4,03	3,80	6,22	3,00	1,34	1,66	1,84	1,44	1,60
Total	99,93	99,47	99,67	99,63	99,70	100,66	102,20	99,97	99,66	100,39	100,67	100,40
c.a.	-	-	-	-	-	-	-	-	-	-	-	-
Rb	30	48	63	71	66	82	68	101	74	78	72	80
Ba	842	2152	1510	1490	1170	1029	2299	1652	1603	2500	2600	2800
Sr	1707	2975	1040	957	800	1457	1420	1000	1219	1500	1700	1200
Zr	132	333	319	589	380	399	287	319	308	410	360	450
Nb	3,98	7,11	25,60	31,50	18,20	16,00	26,98	34,06	32,39	13,00	12,00	12,00
Hf	4,05	8,90	7,21	11,50	8,10	11,00	9,18	11,30	10,94	12,00	9,50	11,00
Ta	0,21	0,33	1,44	1,48	1,06	1,10	1,16	1,77	1,67	1,05	1,09	1,15
Y	12,29	28,35	22,20	39,40	23,80	28,00	25,99	26,59	26,14	25,40	21,10	22,30
Th	12,80	9,53	4,86	4,13	6,15	5,80	4,22	7,20	6,85	-	-	-
U	3,64	2,68	1,52	1,26	1,70	1,55	1,44	2,21	1,67	-	-	-
Pb	28,96	29,76	15,80	22,30	17,40	-	22,79	27,19	24,75	-	-	-
La	45,71	76,98	81,50	105,00	59,40	84,40	93,55	91,27	87,88	72,60	72,90	76,20
Ce	100,81	181,33	169,00	208,00	122,00	135,40	186,08	178,48	174,80	149,00	145,00	148,00
Pr	11,62	24,03	18,60	23,00	13,00	-	20,69	19,77	19,31	16,00	16,10	16,90
Nd	45,20	100,50	77,00	96,80	53,90	58,70	75,89	70,35	69,30	56,10	56,10	59,80
Sm	7,08	20,04	12,20	16,50	8,90	10,00	11,32	10,80	10,62	7,97	7,96	8,47
Eu	2,06	5,37	3,48	3,70	2,06	3,50	2,80	2,64	2,71	2,01	2,17	2,34
Gd	5,51	14,85	9,75	12,60	7,33	10,40	8,99	8,14	7,91	6,09	6,02	6,56
Tb	0,19	0,26	0,29	0,56	0,35		0,30	0,33	0,33	0,24	0,26	0,27
Dy	0,67	1,72	1,18	1,74	1,07	1,46	1,18	1,08	1,12	0,80	0,76	0,85
Ho	2,81	6,82	5,08	7,86	4,67	-	5,53	5,31	5,32	3,93	4,06	4,10
Er	0,54	0,99	0,91	1,46	0,89	-	0,93	0,94	0,91	0,72	0,63	0,73
Tm	1,36	2,22	1,99	3,98	2,30	-	2,44	2,34	2,32	1,97	1,95	1,94
Yb	1,28	1,51	1,65	3,20	2,00	2,10	2,02	2,10	1,86	1,50	1,63	1,71
Lu	0,17	0,23	0,23	0,48	0,28	0,26	0,28	0,33	0,30	0,20	0,24	0,25

Note.: (1) - dash - no data; (2) - Fe2O3* denotes total iron; (3) - c.a. - coefficient of agpaite content; (4)* - data borrowed from paper by Yarmolyuk et al., (2001); (5)**- data borrowed from paper by Lykhin et al., (2001); (6)***- data borrowed from paper by Lykhin et al., (2004).

the range 62-77 mass %). All rocks show high alkalinity. Relative to the ratio of silica and the sum of alkalies they belong, as part of basic volcanics to the subalkaline series, and as part of salic volcanics to the subalkaline and alkaline K-Na (Na_2O/K_2O ranges from 1 to 2,5) petrochemical series. Regarding salic rocks, mostly alkaline are trachydacites, pantellerites and comendites, the coefficient of agpaite content is always higher than 1 and varies from 1,00 to 1,27. This agrees well with the common presence of alkaline dark color minerals, among which aegerine is diagnosed by microprobe analyses. In less alkaline trachyrhyolites the coefficient of agpaitic content reduces to 0,87.

The petrochemical magmatic rocks indicate the differences in the composition (from SiO_2 content) of one type volcanics both in the strike of NMWTB rift zone in its different sectors and in particular on the eastern and western flanks of the West Trans-Baikal sector. Thus, in the last sector in the basc rocks of the Kharitonovsky assemblage the range of SiO_2 variations 48-53 mass % in acid volcanics, trachytes included. SiO_2 ranges from 62 to 70 mass %. In the Tsagan-Khurtey assemblage the most common are highly siliceous rock varieties: in the rocks of the basic and mid-basic compositions of SiO_2 reaches 58 mass %, in acid volcanics 76,5 mass %. In the North Mongolian sector the silica acid content in granitoids varies within narrow ranges from 51 to 55 mass %.

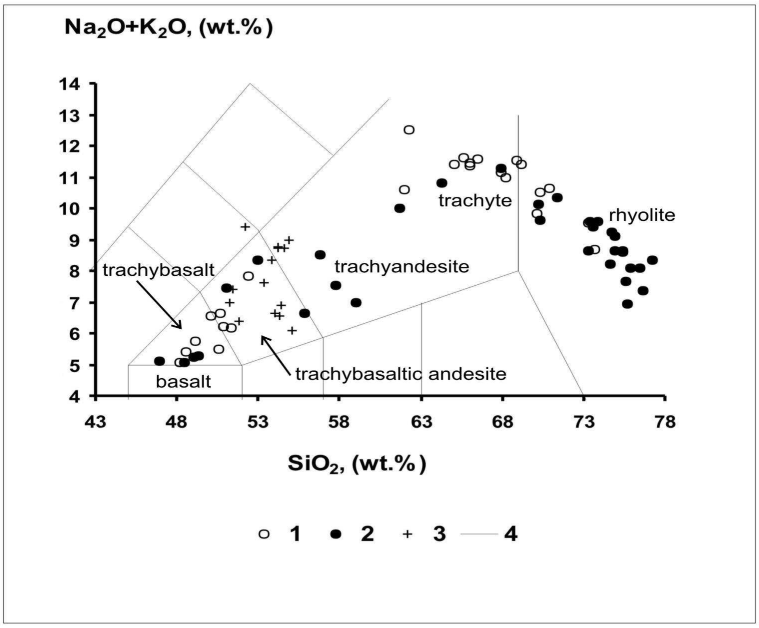

Fig.2. **Position of compositions of the Early Mesozoic magmatic associations of North Mongolian – West Trans-Baikal rift zone on the classification diagram SiO_2 – (Na_2O+K_2O).**

1-2 – West-Trans-Baikal sector: (1 – Kharitonovsky and 2 – Tsagan Khurtey assemblages), 3 – North Mongolian sector, 4 – boundaries of fields of rock compositions [17].

Figure 3 yields the data on the distribution of minor elements in the Early Mesozoic magmatic assemblages. As evident from the Figure, the spectrum of their distribution in trachybasalts is located above the spectrum of MORB compositions and close to OIB compositions, accepted as the reference enriched in

--

---

lithophyle elements of basic melt sources [25]. As compared to OIB trachybasalts and trachyandesite basalts of assemblages are marked Ba maximum (plus Th, U и Pb in the North Mongolian sector), less expressed maxima of K, Rb and Sr, sharp minimum of Nb and small minima Ta and Ti.

The rocks of the basic composition are more enriched in LREE rather than HREE and the spectrum of REE distribution corresponds to that of OIB basalts. The rocks of the North Mongolian sector are highly enriched in LREE.

All salic rocks, particularly their alkaline varieties, are enriched in lithophyle elements. Alkaline granites, panetellerites and comendites are marked by maximally high contents of Th, U, Rb, TR, Pb, Zr, Hf, with steadily low concentrations of Sr (from 10 to 65 ppm) and Ba (from 20 to 80 ppm). REEs are accumulated in salic rocks simultaneously with emergence of europium minimum in trachytes and its increase in alkaline trachyrhyodacites – trachyrhyolites and pantellerites – comendites, which is defined by plagioclase fractionation. The most vivid negative europium anomaly are typical for copmendites having maximum silicic acid content amongst all salic rocks. This is the evidence of crystallization differentiation of magmas of basic composition.

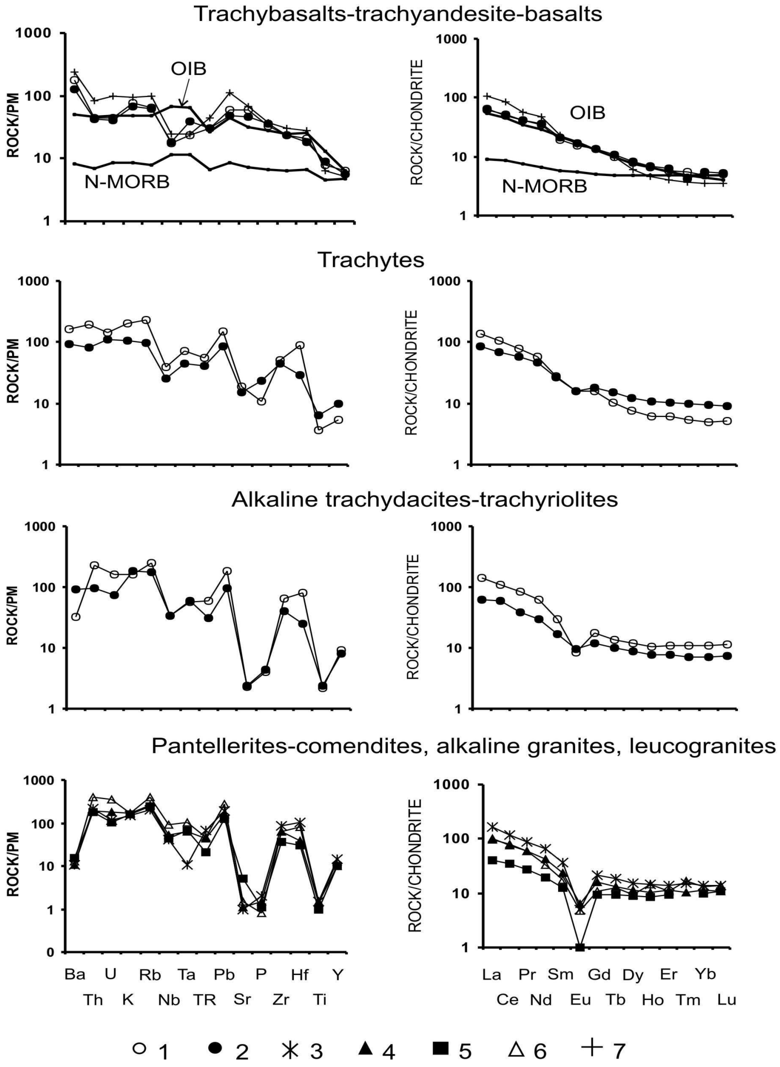

Fig.3. **Plots of the normalized distribution of rare and rare-earth elements in the Early Mesozoic magmatic rocks of the North Mongolian – West Trans-Baikalian rift zone**.

1-5 – West Trans-Baikal sector (1 – rocks of Kharitonovsky assemblage, 2 – rocks of Tsagan Khurtey assemblage, 3-5 – comendites of Tsagankhurtey assemblage, differing in the sum of REE: 3 – with relatively high TR, 4 – with intermediate TR, 5 – with relatively low TR), 6 – granites (Kharitonovsky, Ermakovsky and Orotskiy massifs), 7 – trachybasalts and trachyandesite basalts of the North-Mongolian sector.

Volcanics of the western and eastern parts of the West Trans-Baikal sector differ in the rare and rare-earth elements contents. The alkaline-salic rocks of the Kharitonovsky assemblage, comparing with the same type of rocks of the Tsagan-Khurtey assemblage, are enriched in majority of lithophyle elements (except for P and Hf in trachytes and Ba in alkaline trachydacites – comendites). Figure 4 provides the data on the distribution of some petrogenic and rare elements and their ratios relative to each other and SiO_2, referred to as the parameter reflecting the degree of evolution of parental magmas. The analysis of the plots provides the following considerations. The entire range of compositions displays positive correlations with SiO_2 c K_2O, Rb, Zr, Nb, La, Th, U, and negative one with MgO and Sr, that is typical for the series generated by fractionation of mineral phases in the differentiated magmatic system. Such correlations indicate that bomodal series belong to the genetic series united by the common composition of sources of primary melts and conditions of crystallization differentiation. While SiO_2 contents are increasing Al_2O_3 and Ba rise from trachybasalts to trachytes, which is explained by reduction of olivine in the melt and increase of pyroxene and plagioclase amount. Analogous pattern is observed on the diagram Ba-K_2O. The latest differentiates – trachyrhyolites, pantellerites and comendites are impoverished in alumina, Ba, as well as Sr, which is evidently related with the change of regime of magma crystallization – disappearance of pyroxenes and emergence innthe melt of K-Na feldspars and quartz. The ratio of rare elements relative to each other in the pairs “incoherent-incoherent” (Rb-K_2O, Nb-Zr) is defined by positive linear dependences. A similar pattern of dependences between these groups of elements corresponds to their distribution in the rock-forming minerals and residual melts in fractionation crystallization of the basalt magma. Thus, accumulation of incoherent Zr and Nb reflects a deep differentiation of melts at late stages of evolution of parental magmas with decreasing proportion of residual melt. The increase of Rb concentration correlates well with the increase of potassic minerals, their amount increasing in the late differentiates. The plots also exhibit the compositions the lower and upper continental crust and entire crust, assessed for Central Asia through the example of China territory [24] and accepted as the reference of the continental crust substratum. These plots demonstrate two groups of lithophyle elements differing in the degree of coincidence of the curves in the crust substance with the trends of element content variations relative to each other and SiO_2 in magmatic rocks of NMWTB rift zone. Thus, in a series of lithophyle elements Al_2O_3, MgO, K_2O, Zr, Nb, Ba these trends do not coincide, which is the evidence in favor of formation of source magmas in the mantle. For the other elements La, Th, U, as well as ratios Nb/Zr – U/Th, Th/Ta – Rb/Ta there is only a partial coincidence, which complicates the model of crystallization differentiation of initial melts of mantle origin. It is possibly due to interaction of mantle magmas with crustal substratum as a result of assimilation of host rock substance of the continental crust by source magmas.

--

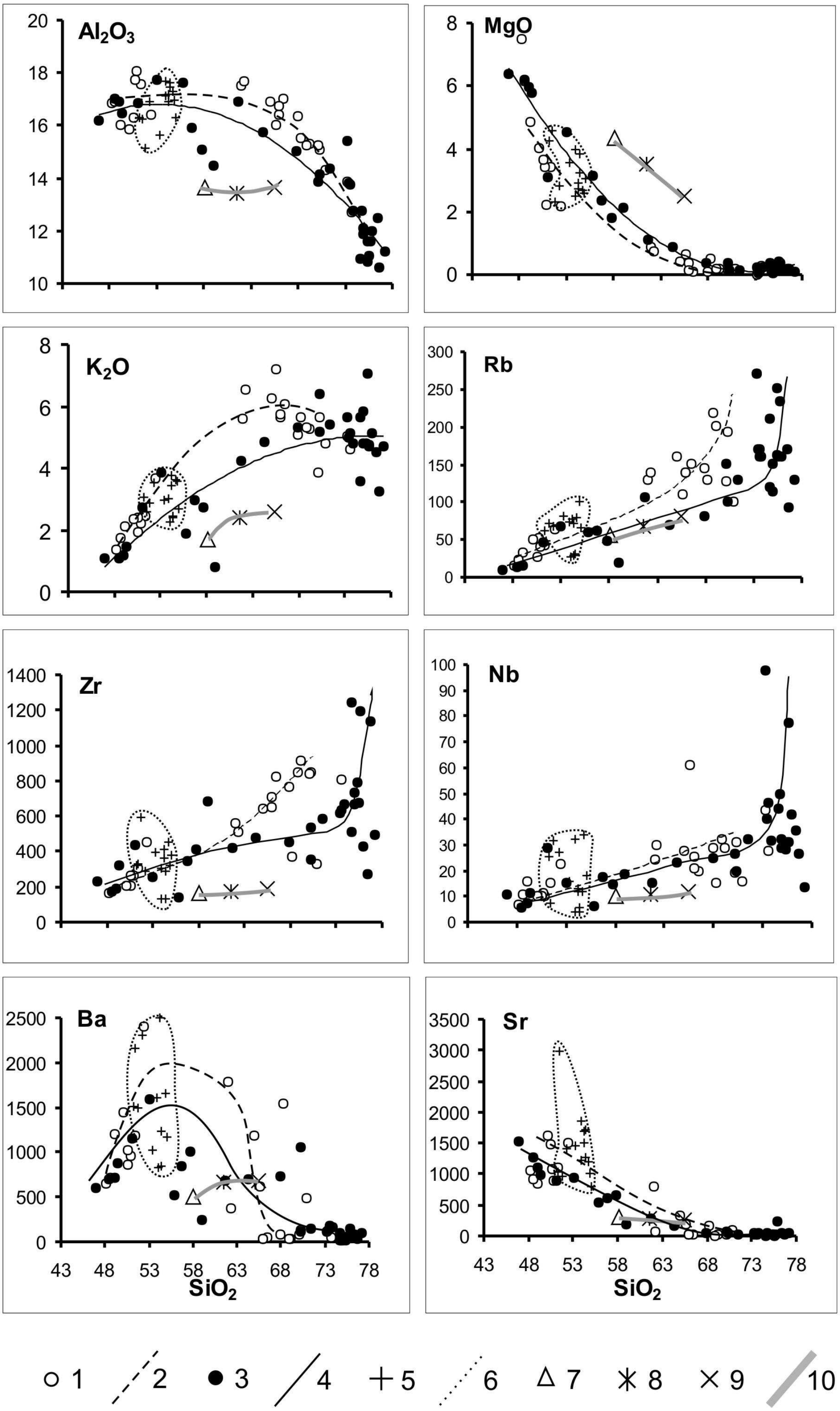
Al2O3
20
18
16
14
12
10
MgO
8
6
4
2
0
K2O
8
6
4
2
0
Rb
300
250
200
150
100
50
0
Zr
1400
1200
1000
800
600
400
200
0
Nb
100
90
80
70
60
50
40
30
20
10
0
Ba
2500
2000
1500
1000
500
0
43 48 53 58 63 68 73 78
SiO2
Sr
3500
3000
2500
2000
1500
1000
500
0
43 48 53 58 63 68 73 78
SiO2
1
2
3
4
5
6
7
8
9
10

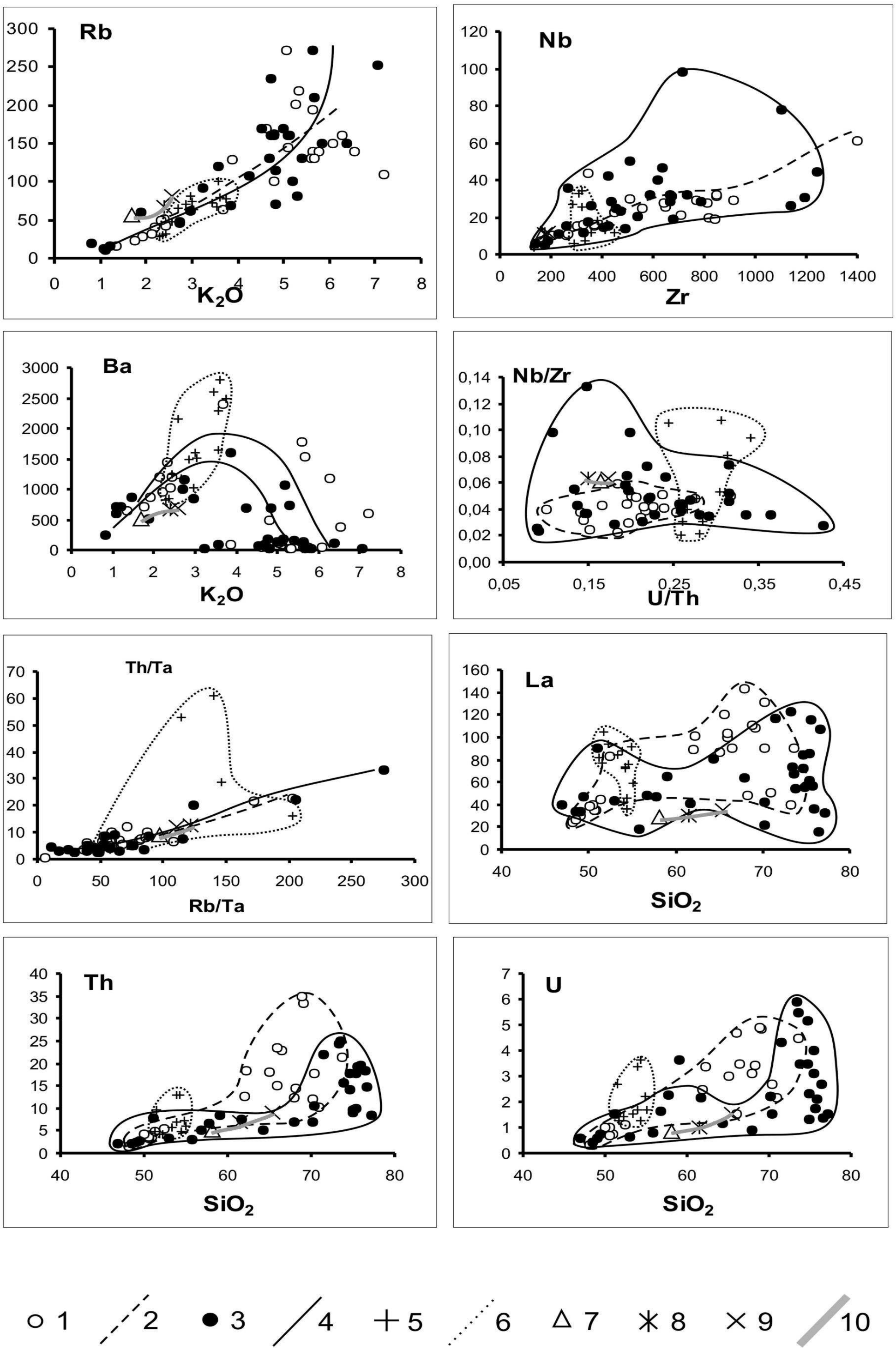

Fig.4. **Distribution of petrogenic oxides and rare elements relative to SiO_2 and correlation dependences between rare elements and their ratios in the Early Mesozoic magmatic associations of the North Mongolian – West Trans-Baikalian rift zone.**

1-4 – West Trans-Baikal sector (1 – Kharitonovsky assemblage, 2- trend of variation and field of compositions of rocks of the Kharitonovsky assemblage, 3 – Tsagan Khurtey assemblage, 4 – variation trend and field of compositions of rocks of Tsagan Khurtey assemblage), 5 – North Mongolian sector, 6 – field of compositions of rocks of the North Mongolian sector, 7-9 – average compositions of the crust of Central Asia after [24]: 7 – lower crust, 8 – entire crust, 9 – upper crust, 10 – crust trend.

--

On the background of a general pattern there are three fields and lines of correlation of rock compositions corresponding to rock assemblages of the North Mongolian sector, Kharitonovsky and Tsagan-Khurtey assemblages of West Trans-Baikal sector, which evidently explains geochemical differences and features of evolution of source magmas in different sectors of the magmatic area under study.

Considering the features of magmatic assemblage compositions of NMWTB rift zone we see their likeness to magmatic assemblages of the other continental rift zones, primarily in the bimodal character of magmatism, and in particular in a wide distribution of alkaline-salic rocks, i.e. trachytes, comendites, pantellerites and their plutonic analogs alkaline granitoids. The basic rocks of NMWTB rift zone, like the same rocks of the other rift zones, are enriched in incompatible elements and in their content approach basalts of OIB type. The differences consist in the lower contents of Ta, Nb и Ti and in higher Ba, Sr and Pb. It appears that these differences, characteristic of all Late Paleozoic – Early Mesozoic intra-plate basic rocks of North Asia, are related to the features of composition of mantle sources, controlling the intra-plate activity in the Late Paleozoic and Early Mesozoic in this sector of the Earth.

THE ISOTOPE COMPOSITION (SR, ND, PB) OF ROCKS AND SOURCES OF MAGMATISM

The composition of magmatic rocks of the rift zone varies widely from basic to acid. As stated above, there are obvious differences in the types of rocks and trend in the change of geochemical parameters when silicic acid contents increase in the bimodal assemblages of the Eastern Tsagan-Khurtey and Western Kharitonovsky segments of the West Trans-Baikal sector and in trachybasalts of the North Mongolian sector. These differences undoubtedly affect assessment of the source composition and evolution of source magmas. In this connection, the isotope compositions were defined for Sr, Nd and Pb magmatic rocks from different sectors of the area. The results of investigations are given in Tables 4 and 5 (see APPENDIX), and some are depicted in Figures 5 and 6.

Isotope composition of Sr and Nd of rocks of the rift zone is depicted on the plot $(^{87}Sr/^{86}Sr)_0$ - εNd (Fig.5-a). It is evident that compositions of rocks of the Kharitonovsky and Tsagan-Khurtey assemblages of the West Trans-Baikal sector and rocks of the North Mongolian sector primarily differ due to wide variations of salic rock compositions. The rocks of the basic composition are characterized by a certain homogeneity. On the plot their figurative points produce a linear sequence localized within the trend of correlated compositions of mantle sources of melts (mantle array). These points are basically concentrated in the lower part of the mantle sequence where the sources of the enriched mantle are located. This sequence of compositions is observed through the field of rocks of the Khentey-Dauria batholith yielding a combined composition of the continental crust in the region. It appears that granitoids and so the crust do not affect the isotope characteristics of basalts. Therefore, we assume that basalts, with the parameters displayed in the right lower quadrant of the diagram, formed from enriched mantle sources, marked by increased contents of radiogenic strontium, that is sources generated with the enriched mantle (EMII) involved. As seen on the plot, the range of compositions of basalts occurring on the magmatic area, are defined by the interaction of two mantle sources: EMII and MORB.

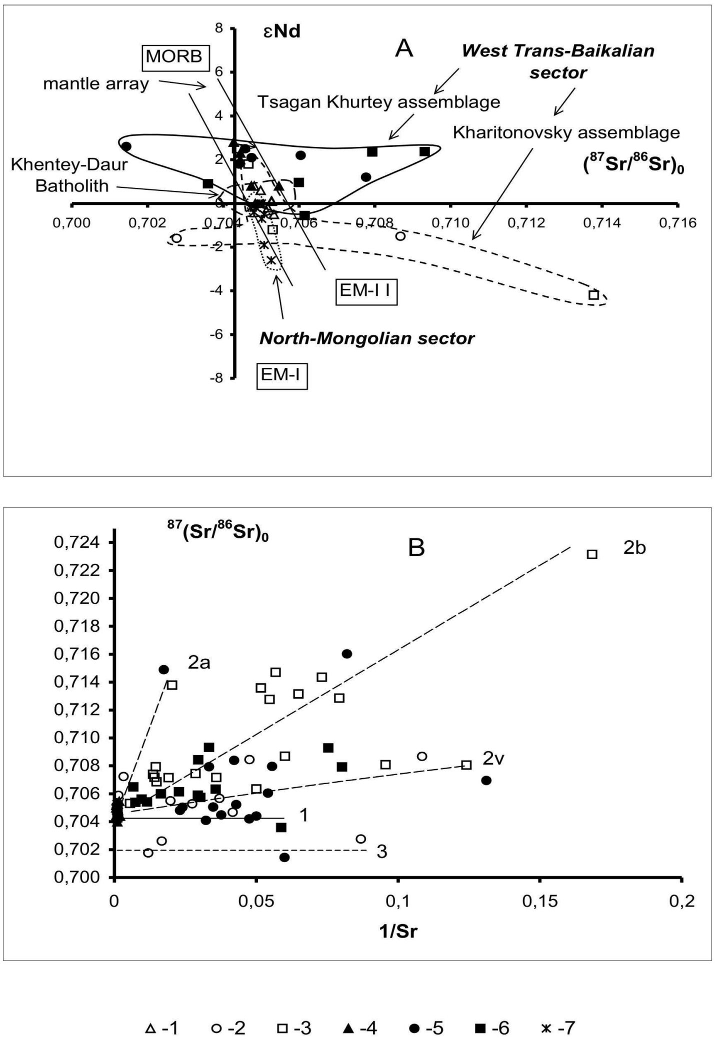

Fig.5 **(A) Position on the diagram (^{87}Sr/^{86}Sr)$_0$ - ε_{Nd} of figurative points of compositions of Early Mesozoic rock assemblages of North Mongolian – West Trans-Baikal rift zone. PREMA – moderately depleted mantle source, EM-I – mantle source enriched in neodymium, EM-II – mantle source enriched in strontium, (B) Primary (provided to the age of rock formation) isotope composition of the early Mesozoic volcanic rocks on the chart (^{87}Sr/^{86}Sr)$_0$ – 1/Sr. The lines indicate distribution of figurative points of compositions: 1 – corresponding to isotopically homogeneous source, 2(a,b,c) - generated due to interaction of isotopically heterogeneous sources, 3 – supposed sources with low values (^{87}Sr/^{86}Sr)$_0$.**

1-6 – West Trans-Baikalian sector (1-3 – Kharitonovsky assemblage: 1 – trachybasalts-trachyandesite basalts, 2 – acid volcanics, 3 – alkaline granites and syenites of Kharitonovsky massif, 4-6 – Tsagan Khurtey assemblage: 4 – trachybasalts-trachyandesite basalts, 5 – acid volcanics, 6 – alkaline granites, syenites, leucogranites and syn-ore dykes of syenite-granite composition of the Ermakovsky and Orotsky massifs, 7 – trachybasalts of North Mongolian sector.

--

Basalt-associated alkaline-salic rocks, e.g. comendites and alkaline granitoids are typified by such geochemical and isotope-geochemical relationships with basalts, that are believed to result from fractionation of the same initial magma [8]. The features of affinity of these petrochemically different rocks are observed on the plot $(^{87}Sr/^{86}Sr)_0$ - εNd (Fig.5-a), on which closely located points of compositions of basalts and alkaline-salic rocks indicate identity of their isotopic (Sr, Nd) sources. However, some alkaline granitoids and comendites have different isotope characteristics. The ranges of scatter of their isotope compositions in concrete volcano-plutonic associations are depicted on the plot as dotted lines. Exemplified by bimodal associations of the Western Trans-Baikal it was shown [39], that such types of variations are described in terms of AFC model [4] and are linked with crustal contamination of products of differentiation of basalt melts. These two simultaneously proceeding processes of differentiation and contamination eventually defined the isotope and geochemical specifics of alkaline-granitoid melts. Crustal components of these magmas are evaluated from isotope characteristics of isotope compositions of alkaline granites, being mostly contrasting with the isotope compositions of associated basalts. The parameters of some granites agree well with the isotope characteristics of enclosing blocks of the crust. Thus, NMWTB rift zone is partly overlapped on the marginal part of the Riphean Barguzin microcontinent, so formation of alkaline-salic rocks was contributed by the crustal sources with characteristics of εNd ~ -4 and T_{Nd} (DM-2st)~1300 Ma, typical for the Riphean isotope crustal province [36]. Some varieties of comendites have close to trachybasalts isotope composition of Nd, with lowered values of isotope composition of Sr (<0,703). It is assumed that the crust with low Rb/Sr ratio served as the source for melts, which can be compared to fairly young Caledonian crust involved in the crust formations of the region [36] and characterized in the Triassic by value ε_{Nd}, ranging from +2 to +4 [6].

The isotope composition of Sr rocks, formed with the crust component involved, commonly shows a wide scatter of values $^{87}Sr/^{86}Sr$. Involvement of crustal source with a high ratio $(^{87}Sr/^{86}Sr)_0$ (>0,7075) in formation of trachyrhyolites, comendites and alkaline granites is traced in the compositions with higher isotope ratio than in basalts. The rocks of the regional Late Riphean continental crust could be such a source. They are characterized by the increased values of Rb/Sr value (>0,5), which could cause the change of their isotope composition to the necessary value by the time of melting (approximately for 400 -500 Ma). In addition, it should be considered that alkaline-salic rocks show high ratios Rb/Sr and, consequently their enrichment in radiogenic ^{87}Sr could occur at the magmatic stage, particularly for granitoids [7]. Therefore, the isotope composition of such rocks cannot serve as the estimate of isotope composition of the crust.

Isotope composition of Pb was investigated for a series of rocks of basic composition and acid volcanics of the Kharitonovsky and Tsagan-Khurtey assemblages. The ratios measured Pb^{206}/Pb^{204} vary from 17.771 to 18.343,

Isotope composition of strontium and neodymium in the rocks of Early Mesozoic magmatic assemblages of North Mongolian- West Trans-Baikal rift zone

Table 4

Sample	Rock	Age	Rb (ppm)	Sr (ppm)	^{87}Rb/^{86}Sr	^{87}Sr/^{86}Sr±2σ	(^{87}Sr/^{86}Sr)$_0$	Sm (ppm)	Nd (ppm)	^{147}Sm/^{144}Nd	^{143}Nd/^{144}Nd±2σ	ε$_{Nd}$(T)
1	2	3	4	5	6	7	8	9	10	11	12	13
West Trans-Baikal segment												
Kharitonovsky assemblage												
Monostoisky site												
TG 13/5	alkaline trachydacite	194,3	160	24	19,179	0,75766±23	0,70467					
TG 13/6	-/-	194,3	151	21	20,621	0,76543±24	0,70846					
TG 13/8	-/-	194,3	152	27	16,378	0,75092±26	0,70567					
TG 13/9	trachybasalt	194,3	43,5	1077	0,1168	0,70566±16	0,70534	7,42	40,2	0,11169	0,512509±8	-0,5
TG 13/11	-/-	194,3	39,4	859	0,1327	0,70563±17	0,70526	7,07	34,1	0,12526	0,512553±8	0,1
TG 13/12	-/-	194,3	54,6	1095	0,1442	0,70568±18	0,70528	6,96	33,7	0,12478	0,512556±7	0,1
TG 13/13	-/-	194,3	67,9	1538	0,1277	0,70534±16	0,70499	13,2	78,5	0,1016	0,512553±6	0,6
TG 13/15	trachyte	194,3	130	719	0,5214	0,70733±17	0,70589					
TG 13/17	-/-	194,3	160	312	1,4581	0,71127±47	0,70724					
TG 13/19	trachybasalt	194,3	30,4	1486	0,0592	0,70534±19	0,70518	6,94	36,9	0,11385	0,512524±7	-0,2
Ust-Sukharinsky and Ulantuisky sites												
TG 1/1	pantellerite	215	145,1	50,7	8,161	0,73045±15	0,70550					
TG 1/2	-/-	215	194,1	60,0	9,232	0,73084±15	0,70261					
TG 1/3	trachyrhyodacite	215	140	83,7	4,76	0,71632±14	0,70177					
TG 1/4	pantellerite	215	128,1	36,4	10,03	0,73595±18	0,70528					
TG 1/5	-/-	215	215	11,5	53,97	0,86779±17	0,70277	14,5	83,3	0,1052	0,512430±6	-1,6
TG 1/7	-/-	215	218,2	9,2	68,71	0,91877±17	0,70868	14,3	82	0,1056	0,512438±5	-1,5
TG 16/2	teschinite	209	14,9	801	0,0539	0,704977±16	0,70482	5,74	26,6	0,13063	0,512590±7	0,8
Kharitonovsky massif (Yarmolyuk et al., 2001)												
B 275	alkaline granite, syenite	209	152,9	20	22,26	0,77251±15	0,70635					
B 278	alkaline granite, syenite	209	110,2	73,6	4,339	0,72029±10	0,70739					
B 312/1	alkaline granite, syenite	209	93,75	10,5	26,12	0,78572±13	0,70809					

Table 4.Continued

1	2	3	4	5	6	7	8	9	10	11	12	13
A 92/3	alkaline granite, syenite	209	146,30	8,1	53,31	0,86651±18	0,70806					
A 150	alkaline granite, syenite	209	201,7	67,4	8,682	0,73266±12	0,70686					
A 150*	alkaline granite, syenite	209	206,9	70,7	8,485	0,73240±12	0,70718					
A 150**	alkaline granite, syenite	209	196,5	52,4	10,8 9	0,73952±14	0,70715					
A 145/2	alkaline granite, syenite	209	173,6	16,6	30,45	0,79920±15	0,70870					
B 317	alkaline granite, syenite	209	185,2	27,8	19,36	0,76471±14	0,70717					
B 278/2	alkaline granite, syenite	209	201,4	34,9	16,77	0,75730±13	0,70746					
B 313/1	alkaline granite, syenite	209	153,8	68,8	6,484	0,72721±12	0,70794					
A 143	alkaline granite, syenite	209	114,5	12,6	26,43	0,79141±16	0,71285					
B 312	alkaline granite, syenite	209	87,3	13,7	17,58	0,76661 ±15	0,71436					
B 314	alkaline granite, syenite	209	91,9	15,4	17,35	0,76472±13	0,71315					
B 318/1	alkaline granite, syenite	209	100,2	19,4	15,03	0,75826±12	0,71359					
B 318	alkaline granite, syenite	209	125,8	18,3	20,02	0,77227±15	0, 71277					
B 276	alkaline granite, syenite	209	184,2	5,9	92,32	0,99755±18	0,72316					
B 279	alkaline granite, syenite	209	245,9	17,6	40,92	0,83633±18	0,71471					
B 163/3	alkaline granite, syenite	209	112,9	181,8	1,797	0,710645±20	0,7053 0	27,5	1,52	0,10967	0,512460±7	-1,2
A 254/2	alkaline granite, syenite	209	270,9	49,2	16,03	0,761427±19	0,71378	2,95	18,1	0,09867	0,512289±6	-4,2
basaltic dykes (Yarmolyuk et al., 2001)												
B 163/11	basaltic dyke	209	32,4	844,8	0,1108	0,704688±18	0,70436	7,2 1	34,2	0,12745	0,512671±8	2,5
V 336/1	basaltic dyke	209	24,1	916	0,0762	0,704889±17	0,70466	6,8	32,5	0,12648	0,512634±8	1,8
Tsagan -Khurtey assemblage												
Saransky site												
TKH 1/1	trachybasalt	209,3	17,7	793	0,0646	0,704928±13	0,70474	7,79	39,3	0,11983	0,51257 3±8	0,8
TKH 1/2	trachybasaltic andesite	209,3	48	500	0,24916	0,70514±30	0,70440					
TKH 1/5	trachybasalt	209,3	16	974	0,04817	0,70413±44	0,70399					
TKH 1/6	-/-	209,3	12,7	988	0,0372	0,704553±15	0,70444	6,09	30,9	0,11921	0,512632±7	2
TKH 1/ 7	-/-	209,3	10	1188	0,0245	0,70452±12	0,70445	7,22	37,4	0,11078	0,512646±7	2,3
TKH 1/8	comendite	209,3	162	12,2	38,87	0,82044±23	0,70474	12,1	66,7	0,1099	0,512625±7	2,1
TKH 1/9	-/-	209,3	150	18	23,6892	0,78654±21	0,71603					

Table 4.Continued

1	2	3	4	5	6	7	8	9	10	11	12	13
TKH 1/11	trachyrhyolite	209,3	252	30	24,732	0,78158±27	0,70797					
TKH 1/14	-/-	209,3	114	20	16,3687	0,75666±51	0,70794					
TKH 1/19	trachyte	209,3	107	330,2	0,935	0,707194±13	0,70441	7,99	42,9	0,11276	0,512616±6	1,8
Tsagankhurtey assemblage (Yarmolyuk et al., 2001)												
B 440	pantellerite	209,3	207,1	21,03	28,72	0,79006±14	0,70458	11,43	61,28	0,1128	0,512651±4	2,5
B 456	-/-	209,3	243,7	30,99	22,89	0,77234±10	0,70421					
B 461-1	-/-	209,3	144,7	16,67	25,30	0,77940±15	0,70410					
B 444	comendite	209,3	131,8	18,49	20,73	0,76314±10	0,70144	18,74	100,5	0,1127	0,512657±4	2,6
B 445-1	-/-	209,3	172,3	57,49	8,69	0,73192±8	0,70605					
B 462	-/-	209,3	162,9	7,63	62,96	0,90229±18	0,71489					
B 461	-/-	209,3	129,3	22,47	16,73	0,75675±16	0,70695					
B 446/1	trachybasalt	209,3	10,54	1144,6	0,03	0,70435±9	0,70427	8,08	41,09	0,1189	0,512675±4	2,8
B 463-3	-/-	209,3	37,94	1400,7	0,08	0,70470±8	0,70447					
Zunnemetey site												
TKH 7/2	comendite	211,5	135,2	23,7	16,594	0,75486±3	0,70495					
TKH 7/3	trachyrhyolite	211,5	181,6	30,2	17,520	0,76110±23	0,70840					
TKH 7/5	trachybasalt	211,5	76,3	979	0,225	0,70552±21	0,70484	7,42	42,3	0,1056	0,512513±4	0
TKH 7/6	trachyrhyolite	211,5	170,2	227,3	21,673	0,71179±21	0,64660					
TKH 7/8	trachybasalt							13,6	81	0,10108	0,512596±4	1,8
TKH 7/9	pantellerite	211,5	155	36,8	12,250	0,74289±22	0,70604	9,39	48,4	0,11679	0,512640±6	2,2
TKH 7/10	trachybasaltic andesite	211,5	69,6	591	0,341	0,70649±21	0,70546	4,63	23,3	0,11962	0,512573±6	0,8
TKH 7/11	pantellerite	211,5	85,7	56,4	4,399	0,72100±22	0,70777	9,03	54,6	0,09956	0,512562±8	1,2
Ermakovskoe Be-ore deposite (Lykhin et al., 2001)												
398	syn-ore dykes of granites and syenites	224	255	104	7,09	0,72821	0,70562					
2-95		224	259	87	8,59	0,73279	0,70542					
3-95		224	182	17	30,50	0,80076	0,70359	3,394	22,897	0,08957	0,512527	0,90
311		224	206	33	17,97	0,76299	0,70574					
313		224	427	136	9,08	0,73432	0,70539					
483		224	313	61	14,90	0,75346	0,70599	13,928	71,731	0,11733	0,512571	0,96

Table 4.Continued

1	2	3	4	5	6	7	8	9	10	11	12	13
805	basaltic dyke	224	92,88	679,22	0,40	0,70716	0,70590	5,2	26,54	0,1184	0,512468	-1,08
1-95	leucogranites of massif "Shtok"	224	311	28	32,60	0,81020	0,70634					
300		224	303	150	5,85	0,72513	0,70649					
479		224	342	34	29,50	0,79988	0,70590					
400		224	324	44	21,80	0,77560	0,70615	4,31	29,72	0,08796	0,51245	-0,56
Orotskoe Be-ore deposite (Lykhin et al., 2001)												
Oro-2	trachydacite	236,4	145,5	43,31	9,75	0,73758±7	0,70481					
Oro-3	trachydacite	236,4	139,2	41,72	9,68	0,73761±7	0,70504					
Oro-4	rhyodacite	236,4	222,2	23,31	27,83	0,79882±8	0,70523					
Oro-8	rhyolite	236,4	220,5	28,72	22,37	0,78029±7	0,70506					
Oro-22	rhyodacite	236,4	236,3	26,54	25,98	0,79184±7	0,70449					
Oro-1	leucogranite	223	233,6	12,47	55,12	0,88286±7	0,70793	8,15	40,5	0,1217	0,51265±4	2,35
Oro-9	leucogranite	223	288,8	29,98	28,12	0,79856±7	0,70932	17,7	99,5	0,1072	0,51263±6	2,37
Oro-10	alkaline granite	223	269,4	33,81	23,22	0,78214±7	0,70844					
Oro-35	alkaline granite	223	211,1	13,26	46,72	0,85756±7	0,70928					
North-Mongolian segment												
Bat-Tsengelskaya depression												
BTS-7/3	trachybasalt	220	63,8	1187	0,1554	0,705498±15	0,70501	11,40	69,60	0,09861	0,512463±7	-0,7
BTS-7/6	trachybasalt	220	70,9	1113	0,1843	0,705842±15	0,70527	15,10	90,20	0,1013	0,512366±5	-2,6
BTS-7/7	trachybasaltic andesite	220	68,0	945	0,2082	0,705728±14	0,70508	8,53	50,40	0,1024	0,512403±7	-1,9
4155/10	trachybasaltic andesite	220	68,3	1350	0,1585	0,705453±17	0,70496	9,63	62,9	0,09252	0,512487±8	0
Verkhne-Khanuy depression												
4152/1	trachybasaltic andesite	190	59,40	1700,0	0,1014	0,705282±16	0,70501	9,00	58,50	0,09307	0,51251±6	0
4152/7	trachybasaltic andesite	190	93,20	983,0	0,2743	0,705607±15	0,70487	10,50	68,50	0,09296	0,512497±8	-0,2
4152/8	trachybasaltic andesite	190	62,80	1180,0	0,1536	0,705490±18	0,70508	10,00	64,70	0,09380	0,512485±8	-0,5
4150/4	trachybasaltic andesite	220	74,2	1320	0,1632	0,705318±17	0,70481	9,35	62,9	0,08978	0,512466±7	-0,4
4150/3	trachybasaltic andesite	220	61	1630	0,1084	0,705286±15	0,70495	9,97	64,9	0,09384	0,512490±8	0
4150/5	trachybasaltic andesite	220	97,3	992	0,2838	0,705605±15	0,70472	9,94	65,1	0,0922	0,512479±8	-0,2

Note. * - salic and ** - femic fraction of rocks. Solid font denotes samples used for isochrone calculations

Pb^{207}/Pb^{204} from 15.404 to 15.531, Pb^{208}/Pb^{204} from 37.709 to 38.266. Threse ratios were recalculated for the age 210 Ma and plotted on the charts $^{07}Pb/^{204}Pb$ - $^{206}Pb/^{204}Pb$ and $^{208}Pb/^{204}Pb$ - $^{206}Pb/^{204}Pb$ (Fig.6). With regard to the isotope composition of lead the rocks of the basic and salic composition are close between each other, which is the evidence of their formation from the same magmatic source and formation of trachyrhyolites-comendites via crystallization differentiation. The figurative points of isotope compositions of Pb in basic and acid volcanics of the West Trans-Baikal sector produce the general evolution trend adjacent to the line of evolution of uranium-generating lead in the mantle (Fig.6-a) and to the line of evolution of thorium-generating lead in the bulk composition of the continental crust (Fig.6-b). The general trend direction is somewhat discordant to both evolutionary curves, and the fields of figurative points of isotope compositions of Pb rocks of the western (Kharitonovsky assemblage) and eastern (Tsagan-Khurtey assemblage) exhibit different position on the chart. The most depleted isotope compositions are typical for lead of the Kharitonovsky association rocks, which is the evidence of undoubtful contribution in their genesis of depleted mantle reservoir and (or) depleted lower crust substratum. The more radiogenic isotope compositions are common for basalts and acid volcanics of the Tsagan-Khurtey assemblage, which is the evidence of enrichment with radiogenic lead of their magmatic sources. It should be marked that these differences verify the differences in the types of rock assemblages, trends of evolution of petrogenic and rare lithophyle elements and in the isotope composition of Sr and Nd. These plots also show the fields of isotope compositions, corrected for the age 210 Ma, for oceanic basalts of plateau Kergelen, basalts of mid-oceanic ridges in general and basalts from the East Pacific uplift in particular. They characterize the source of MORB type and Siberian traps. However, these compositions differ from those characterizing participation of crust sources, e.g. island arc basalts (Aleutian and South Sandwich island arcs), granites of East Trans-Baikal and sediments of passive margins of the Atlantics. The field of compositions of volcanics of the Tsagan-Khurtey assemblage practically coincides with the field of model compositions of Siberian traps characterizing the intra-plate (plume) mantle source, also with the field of compositions of mid-oceanic ridge basalts (MORB). On the plot $^{208}Pb/^{204}Pb$ - $^{206}Pb/^{204}Pb$ the points of volcanics compositions of the Kharitonovsky assemblage entirely fall within the field of compositions of the Kergelen plateau basalts. The trend of Pb isotope composition variation for the Early Mesozoic volcanics of the West Trans-Baikal sector may be interpreted as the line of mixing between the substance of depleted mantle source, plume source, and possibly crustal source, represented by the volcanogenic-sedimentary (greywacke) material of island arc prisms and turbidites of passive continental margins.

Completing the isotope-geochemical description of the Early Mesozoic magmatic assemblages it should be marked that their formation proceeded both with participation of both mantle and crust sources of melts. The processes of

---

--

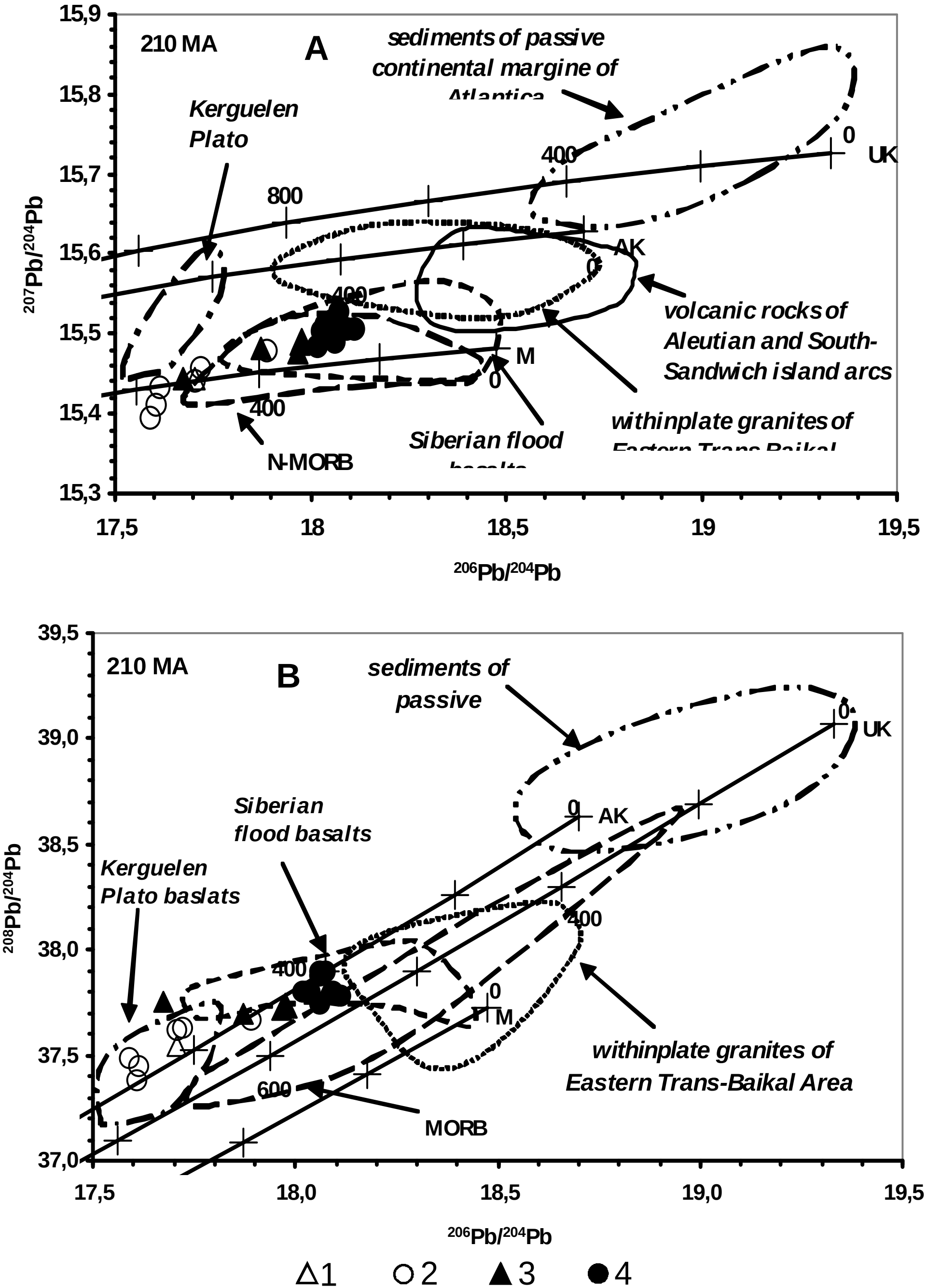

Fig.6 (A) Diagram $^{207}Pb/^{204}Pb$-$^{206}Pb/^{204}Pb$ and (B) Diagram $^{208}Pb/^{204}Pb$-$^{206}Pb/^{204}Pb$ for Early Mesozoic volcanic rocks of the West Trans-Baikal sector of the North Mongolian – West Trans-Baikal rift zone.

1 - 2 – rocks of the Kharitonovsky assemblage (Ust-Sukharinsky and Ulantuysky sites): 1 – trachybasalts, 2 – acid volcanics, 3 - 4 – rocks of the Tsagankhurtey assemblage (Saranskiy and Zynnemetey sites): 3 – trachybasalts; 3 – acid volcanics. Lines indicate model curves of Pb evolution in the mantle (M), upper crust (BK), middle crust (CK). Figures on the lines denote age in mln. years. Reference fields of compositions of rocks recalculated for the age 210 Ma: intraplate granites of East Trans-Baikal [27], volcanics of the Aleutian and South Sandwich island arcs [3], Siberian traps [33], sediments of passive margins of the Atlantics [30], N-MORB [2], MORB from the East-Pacific uplift [32, 21], basalts of Kergelen plateau [31,23,16]

Table 5

Isotope composition of lead in the rocks of the Early Mesozoic magmatic assemblages of the West Trans-Baikal segment of the North Mongolian - West Trans-Baikal rift zone

Sample	Rock	U (ppm)	Pb (ppm)	Th (ppm)	$^{206}Pb/^{204}Pb$	+/-2σ	$^{207}Pb/^{204}Pb$	+/-2σ	$^{208}Pb/^{204}Pb$	+/-2σ
Kharitonovsky assemblage										
Ust-Sukharinsky and Ulantuisky sites										
TG-1/1	pantellerite	3,12	36,14	12,26	17,771	0,002	15,404	0,002	37,715	0,05
TG-1/2	-/-	2,66	25,18	17,86	17,943	0,007	15,469	0,008	38,123	0,027
TG-1/3	trachyrhyodacite	3,37	39,54	18,21	18,069	0,004	15,489	0,005	37,984	0,018
TG-1/4	pantellerite	2,23	37,08	12,06	17,833	0,005	15,447	0,005	37,842	0,02
TG-1/5	-/-	4,83	49,9	33,5	17,810	0,019	15,420	0,002	37,843	0,0041
TG-1/7	-/-	4,91	49,39	35	17,821	0,003	15,445	0,003	37,931	0,0117
TG-16/2	teschinite	0,32	5,77	1,41	17,822	0,0033	15,450	0,004	37,709	0,014
Tsagan-Khurtey assemblage										
Saransky site										
TKH 1/1	trachybasalt	0,75	7,04	2,57	18,195	0,0045	15,499	0,005	37,988	0,015
TKH 1/2	trachybasaltic andesite	2,24	16	6,66	18,164	0,005	15,496	0,006	37,976	0,025
TKH 1/6	trachybasalt	0,43	6,81	2,01	18,098		15,484		37,920	
TKH 1/7	-/-	0,56	7,11	2,07	17,836	0,0064	15,452	0,007	37,948	0,0254
TKH 1/8	comendite	1,33	26,77	9,69	18,122	0,0016	15,489	0,002	38,045	0,0055
TKH 1/14	trachyrhyolite	2,32	21,83	8,89	18,283	0,006	15,515	0,007	38,175	0,022
TKH 1/19	trachyte	2,15	15,53	7,63	18,364	0,0021	15,452	0,002	38,235	0,0066
Zunnemetey site										
TKH 7/2	comendite	1,54	12	8,51	18,334	0,0016	15,505	0,001	38,234	0,0034
TKH 7/5	trachybasalt	0,65	8,9	3,36	18,134	0,0016	15,501	0,001	37,988	0,0034
TKH 7/6	trachyrhyolite	2,12	32,4	19,6	18,231	0,0018	15,513	0,002	38,218	0,0038
TKH 7/8	trachybasalt	1,55	15,6	7,94	18,291	0,0026	15,525	0,002	38,166	0,0054
TKH 7/9	pantellerite	2,22	16,6	7,03	18,343	0,0092	15,531	0,007	38,174	0,0019
TKH 7/10	trachybasaltic andesite	3,5	26,5	17,6	18,317	0,0011	15,526	9E-04	38,266	0,0023
TKH 7/11	pantellerite	0,91	15,4	6,84	18,239	0,0009	15,512	8E-04	38,094	0,0021

crystallization differentiation occurred with mantle sources of MORB and OIB types involved. In the western and eastern sites of the magmatic area these processes were differently directed, that affected the types of magmatic assemblages and composition of final products of differentiation.

GEODYNAMIC RECONSTRUCTIONS

The NMWTB rift zone originated as a result of formation of the Mongol-Trans-Baikal Early Mesozoic zonal magmatic area and thus, consideration of conditions of its formation should be considered with beyond the relationship with geodynamics of formation of the zonal area. The structure of the latter is defined by the Khentey-Dauria granitoid batholith located in the core of the area and zones of bimodal and alkaline magmatism developed over margins [40, 9], the NMWTB

--

rift zone included. The area originated within the interval between 230 – 195 Ma. This was proved by geochronological correlation under complete synchronous activity of different-natured magmatic processes in the central and marginal domains of the area. The unusual character of magmatism of the area was due to specific geodynamic setting, which consists in synchronous occurrence of zonally spread conditions of extension (peripheric system of rift zones) around the central area of compression (domal uplift and batholith core). As was shown [40], the reason for generating such a constrasting tectonic setting was determined by lithosphere and sub-lithosphere location of sources at different depths. Thus, the intra-lithosphere setting of compression accompanied by batholith formation, was caused by closing of Dzhargalantuinsky trough, which occupies the axial position in the structure of the area and tectonic collision of its edges. Judging from presence of the Early – Mid-Triassic marine sediments in the trough, as well as presence of plagiogranites with the age 207 Ma, the collision processes occurred nearly at the same time as formation of batholith. The influence of sub-lithosphere source of extension resulted in rift zone formation, accompanied by the mantle basalt and bimodal and alkaline-granitic magmatism. The rift zones frame the batholith core of the area and are characterized by fairly homogeneous isotope-geochemical composition of basic rocks of mantle genesis [9]. This fact suggests that the magmatic area covering the territory about 1500x800 km, corresponded to the projection of the large sub-lithosphere source of magmatic melts or mantle plume.

The geodynamic setting of formation of the zonal area should be linked with plume action on the lithosphere segment, occurring under collision compression conditions. In the zone of collision itself the mantle magmas could not move onto the surface and heated the crust causing its anatectic melting fusion of batholith. Beyond the zone of collision in the peripheral parts of the area mantle melts reached the surface forming assemblages with predominance of rocks of mantle genesis.

Position of NMWTB rift zone within the magmatic area is controlled by the system of large fractures being the suture boundary of the Barguzin microcontinent. This system of fractures, being the lithospehere boundary, traced weakened zones in the basement of lithosphere. In the epochs of mantle plume origination under the Central Asia lithosphere such zones became peculiar asthenospheric traps, in which asthenosphere affected greatly the lithosphere and therefore contributed to the rifting process to proceed along suture boundaries [34]. This could also take place in the early Mesozoic, when asthenosphere of the mantle plume searching for exit onto the earth surface displaced into the asthenosphere trap of the suture boundary and gave rise to rifting processes along this boundary .

Appearance of the mantle plume in the basement of the of the study area in the Early Mesozoic should be viewed in the context of the geological history of the region. Thus, it should be reminded that the intra-plate activity in the Late

Paleozoic and Early Mesozoic of Central Asia led to formation of gigantic rift system covering the territory of NW China, Mongolia and Trans-Baikal [7,38]. Its formation is linked with mantle plume overlapped by the southern margin of the Late Paleozoic North Asian continent. In time of overlapping the zone of intraplate activity traveled deep into the continent throughout Late Carboniferous and Permian, and in the Late Permian rifting processes covered the territory of Central Mongolia [35]. As a result, the zonal-symmetric magmatic area similar to that in the Early Mesozoic was derived. Its central part enclosed the Khangay batholith, and in the southern and northern margins there were accordingly the Gobi-Altay and North Mongolia rift zones with alkaline granitoid and bimodal magmatism. It is remarkable that the North Mongolian zone originated within the same North Mongolian – Trans-Baikal system of suture faults, that NMTB rift zone, that underlines the role of this system of suture boundaries in placement of asthenosphere traps. In the Early Mesozoic due to the change of direction of lithoshhere plate some of its eastern (in recent coordinates) parts turned out to be above the mantle. These are territories of the western and eastern Trans-Baikal and Northeastern Mongolia [38], where the Mongolian - Trans-Baikal area, NMWTB rift zone included, were formed.

CONCLUSIONS

The North Mongolian – West Trans-Baikal rift zone is one of the largest rift systems in Central Asia. It extends for over 1200 km, its width 250 km. The rift zone formed within the interval between 233 and 188 Ma as the system of depressions and grabens, their development accompanied by volcanic eruptions of the bimodal and alkaline specifics and intrusions of alkaline granites. The rift zone consists of two great eastern and western segments. The western segment incorporates volcanic associations composed of rocks of basic composition. The eastern segment is dominated by bimodal basalt-comendite-pantellerite volcanic assemblages of mostly common alkaline-salic rocks. In addition, widespread are alkaline granitoids.

Magmatic rocks of the rift zone occur in subalkaline and alkaline petrochemical series. On the plots the compositions of rocks of the magmatic assemblages agree with the trends of composition variations modeled by the conditions of fractionation crystallization of highly alkalic basalt melts. Primary basalt melts are marked by enrichment in many incompatible elements. Initial basalt melts are enriched in many incompatible elements. The level of their content the rocks approach composition of OIB-type basalts. The differences consist in the lower content of Ta, Nb and Ti and in higher Ba, Sr и Pb. But these differences are typical for all Late Paleozoic – Early Mesozoic intra-plate basites of North Asia and are probably predetermined by the composition of mantle sources controlling the intraplate activity in the region at that time.

The isotope composition of basic rocks is characterized by variations of values $(^{87}Sr/^{86}Sr)_0$ and εNd, lying in the lower part of the mantle array

---

--

corresponding to enriched mantle sources. It is assumed that formation of melts was related to interaction of two mantle sources: (i) enriched source of EMII type and (ii) depleted source of MORB type. A significant part of alkaline-salic rocks of the rift zone is marked by composition variations which agree with the model AFC. They are expressed in enrichment of rocks with radiogenic strontium.

The isotope composition of lead of the rift zone rocks, both basic and alkaline-salic compositions, is fairly homogeneous and indicates the same type of their sources. This composition is close to that of rocks of oceanic plateau mid-oceanic ridges, as well as Siberian traps and is somewhat different from the composition of rocks which generated in settings of a significant contribution of crustal material to magma formation, in island arc setting included. The observed trend of Pb isotope composition variation in the rocks of the rift zone may be interpreted as a result of mixing between the substance of depleted and plume mantle source which agrees well with isotope data on Sr and Nd.

The rift zone formation was associated with formation of the Mongolian-Trans-Baikal zonal magmatic area, which generated due to the mantle plume action on that part of lithosphere of Central Asia, which occurred in the state of collision compression. In the zone of collisional suture rifting processes were responsible for formation of sizable batholith under the effect of mantle plume. Extension zones with rifting magmatism were produced on the margins of the latter. Localization of rifting processes was much affected by asthenospheric traps in the basement of lithosphere under the boundaries of suture type. Formation of NMWTB rift zone was related to the existence of such a boundary represented by the North Mongolian – Trans-Baikal system of suture faults, in the site of its intersection with the head of mantle plume.

Acknowlegments. This work was done with financial support of grants RFBR 03-05-64579, 05-05-64332 and Integration Project RAS 6.5.3.

REFERENCES

1. **Afonin V.P., Gunicheva T.N., Piskunova L.F.** X-ray fluorescence analysis. Novosibirsk: Nauka. 1984. 328 p.
2. **Cohen R.S., O'Nions R.K.** The lead, Neodymium and Strontium Isotopic Structure of Ocean Ridge Basalts.//Journal of Petrology, vol.23, part 3, pp. 299-324, 1982
3. **Cohen R.S., O'Nions R.K**. Identification of recycled continental material in the mantle from Sr, Nd and Pb isotope investigations.//Earth and Planetary Science Letter. 61 pp.73-84, 1982.
4. **DePaolo D.J**. Neodymium isotope geochemistry: an introduction // New York: Springer Verlag. 1988. 187 p.
5. **For G.** Basics of isotope geology: Translated from English. Moscow: Mir. 1989. 590 P.
6. **Kovalenko V. I., Yarmolyuk V. V., Kovach V. P. et al**. Sources of Phanerozoic granitoids of Central Asia: Sm-Nd isotope data //Geochemistry.1996 № 8.P. 699-713.
7. **Kovalenko V.I., Kostitsyn Yu.A., Yarmolyuk V., et al.** Sources of magma and isotope (Sr and Nd) evolution of rare-metal Li-F granitoids //Petrology. 1999. V. 7. № 4. P

8. **Kovalenko V.I., Yarmolyuk V., Kozlovsky A.M., Ivanov V.G.** Sources of magmas of alkaline granitoids and related rocks of intra-plate magmatic assemblages of Central Asia // Doklady. PAS. 2001. V. 377. № 5. P. 672-676.
9. **Kovalenko V.I., Yarmolyuk V., Salnikova E.B. et al.** Sources of magmatic rocks and origin of the Early Mesozoic tectonic-magmatic area of the Mongol – T.-B. magmatic area (geological evidence and isotope geochronology)//Petrology. 2003. № 2. P. 164-178.
10. **Koval P.V.** Regional geochemical analysis of granitoids. – Novosibirsk: Publ.H. SB RAS. 1998. 492 p.
11. **Kuzmin D. V., Chupin V. P., Litvinovskiy B. A.** Temperatures and compositions of magmas of trachybasalt-comendite assemblage of the Tsagan-Khurtey Ridge, West Trans-Baikal area (after inclusions in minerals) // Geology and Geophysics. 1999. V. 40. № 1. P. 62-72.
12. **Litvinovskiy B.A., Posokhov V.F., Zanvilevich A.N**. Uncommon rubidium-strontium data on the age of the two reference alkaline-granitoids massifs of Trans-Baikal area// Geology and Geophysics. 1995. V. 36. № 12. P. 65-72.
13. **Litvinovskiy B.A., Yarmolyuk V.V., Vorontsov A.A., Zhuravljov D.Z., Posokhov V.F., Sandimirova G.P., Kuzmin D.V.** Late Triassic stage of formation of Mongol-Trans-Baikal alkaline-granitoid province: data of isotope-geochemical studies // Geology and Geophysics. 2001 V. 42. № 3. P. 445-456.
14. **Lykhin D.A., Kovalenko V.I., Yarmolyuk V.V**. Rb-Sr age and magma sources of the Early Mesozoic beryllium province of Central Asia, exemplified by the Orotsky deposit // Doklady RAS. 2002. V 385. № 4. P. 529-532.
15. **Lykhin D.A., Kostitsyn Yu.A., Kovalenko V.И., Yarmolyuk V.V., et al.** Ore-bearing magmatism of the Ermakovsky beryllium deposit in West Trans-Baikal area: age, magma sources and relationship to mineralization // Geology of Ore Deposits. 2001. № 1. P. 52-70.
16. **Lassiter J. C., DePaolo D. J., Mahoney J. J.** Geochemistry of the Wrangellia Flood basalt province: implications for the role of continental and oceanic lithosphere in flood basalt genesis // Journal of Petrology. 1995. V. 36. № 4. pp. 983-1009.
17. **Le Bas M.J., Le Maitre R. W., Streckeisen A. & Zanettin B.** Chemical Classification of Volcanic Rocks Based on the Total Alkali-Silica Diagram // Journal of Petrology. 1986. V. 27. pp. 745-750.
18. Mesozoic and Cenozoic deposits and magmatism of Mongolia. Moscow: Nauka. 1975.
19. Map of geological formations, Mongolia. Scale 1:1 500 000. Geodesy and Cartography Management. Moscow. 1989.
20. **Mossakovskiy A.A., Saltykovskiy A.Ya., Tomurtogoo O.** Triassic volcanogenic and molassa formations of the Orkhon depression, Central Mongolia. In.: Volcanogenic rock assemblages of rocks in Mongolia, their composition and stratigraphic position. Moscow: Nauka. 1973. P. 94-106.
21. **Prinzhofer A., Lewin E., Allegre C.J.** Stochastic melting of the marble cake mantle: evidence from local study of the East Pacific Rise at 12°50’N // Earth and Planetary science Letters. 1989. V. 92. pp. 189-206.
22. **Stupak F. M**. New data on geology, age and tectonics of the Early Mesozoic volcanic assemblages of North Trans-Baikal area // Doklady PAS. 1999. V. 369. № 4. P.
23. **Salters V. M. J., Storey M., Sevigny J.H., Whirechurch H**. Trace element and isotopic characteristics of the Kerguelen-Heard Plateau basalts. Proceedings, Ocean Drilling Program,Scientific Results,120. College Station,TX:Ocean Drilling Pr-m 1992.pp. 55-62.
24. **Shan Gao, Ting-Chuan Luo, Ben-Ren Zhang, Hong-Fei Zhang, Yin-wen Han, Zi-Dan Zhao, and Yi-Ken Hu**. Chemical composition of the continental crust as revealed

--

---

by studies in East China // Geochimica et Cosmochimica Acta. 1998. V. 62. № 11. pp. 1959-1975.

25. **Sun S.-s, McDonough W.F.** Chemical and isotopic systematcs of oceanic basaits: implications for mantle composition and processes // Saunders A.D., Narry M.J. (eds) Magmatism in the Ocean Basins. Geol. Society Special Publ-n. 1989. № 42. pp. 313-345.
26. **Shergina Yu.P., Murina G.M., Kozubova L.A., Lebedev P.B**. Age and some genetic features of rocks of the Kunaley complex in the West Trans-Baikal area from Rb-Sr data // Proceedings AN SSSR. 1979. V. 246. № 5. P. 1199-1202.
27. **Tatarnikov S.A., Vladimirova T.A., Zhitova N.N.** K-feldspar phenocrysts as indicators of substance source of intra-plate granites of East Trans-Baikal area. Isotope geochronology and solution pf problems of geodynamics and ore genesis. SPb. 2003. P.
28. **Vorontsov A.A., Yarmolyuk V.V.** North Mongol – Trans-Baikal polychronous rift system (stages of formation, magmatism, melt sources, geodynamics) // Lithosphere. 2004. № 3. P. 17-32.
29. **Vorontsov A.A., Yarmolyuk V.V., Baikin D.N.** Structure and composition of the Early Mesozoic volcanic series of the Tsagan-Khurtey graben (West Trans-Baikal area): geological, geochemical and isotope data // Geochemistry. 2004. № 11. P 1186-1202.
30. **William M., Dupre B., Vidal P**. Isotope and trace element geochemistry of sediments from the Barbados Ridge-Demerara Plain region, Atlantic Ocean.// Geochimica et Cosmochimica Acta, vol. 49 pp.1875-1886, 1985.
31. **Weis D., Bassias Y., Gautier I., Mennessier J.P.** Dupal anomaly in existence 115 Ma ago: evidence from isotopic study of the Kerguelen Plateau (South Indian Ocean) // Geochimica et Cosmochimica Acta. 1989. V. 53. pp. 2125-2131.
32. **White W. M.** ^{238}U/^{204}Pb in MORB and open system evolution of the depleted mantle // Earth and Planetary Science Letters. 1993. V. 115. pp. 211-226.
33. **Wooden J.L., Gerald K., et. al.** Isotopic and trace-element constraints on mantle and crustal contribution to Siberian continental flood basalts, Norilsk area, Siberia // Geochimica et Cosmochimica Acta. 1993. V. 57. pp. 3677-3704.
34. **Yarmolyuk V.V., Kovalenko V.I.** Position of continental rift structures of Mongolia // Izvestia AN SSSR. Ser. Geol. 1986. № 9. P. 3-16.
35. **Yarmolyuk V.V., Kovalenko V.I**. Rifting magmatism of active continental margins and ore-bearing capacity. Moscow: Nauka. 1991. 263 P.
36. **Yarmolyuk V.V., Kovalenko V.I., Kovach V.P. et al**. Nd-isotope systematics of crustal magmatic protoliths of West Trans-Baikal and the problem of Riphean crust formation in Central Asia // Geotectonics. 1999б. № 4. P. 3-20.
37. **Yarmolyuk V.V., Vorontsov A.A., Ivanov V.G., Kovalenko V.I., et al.** Epochs of bimodal and alkaline granitoid magmatism in the West Trans-Baikal area: geochronological data on the Tugnuy depression area // DAN. 2000a V.373. 1. P. 78-83.
38. **Yarmolyuk V.V., Kovalenko V.I., Kuzmin M.I**. North Asian super plume in the Phanerozoic: magmatism and deep geodynamics // Geotectonics. 2000б. №5. C. 3– 29.
39. **Yarmolyuk V.V., Litvinovskiy B.A., Kovalenko V.I., Bor-ming Jahn, et al.** Stages of formation and sources of alkaline granitoid magmatism, North Mongolia – Trans-Baikal rift belt in Permian and Triassic // Petrology. 2001. V. 9. № 4. P. 351-380.
40. **Yarmolyuk V.V., Kovalenko V.I., Salnikova E. B., Budnikov S. V., Kovach V. P., Kotov A. B., Ponomarchuk V. A.** Tectono-magmatic zonation, sources of magmatic rocks and geodynamics of the Early Mesozoic Mongol - Trans-Baikal magmatic area // Geotectonics. 2002. № 4. P. 42-63.
41. **Zhuravljov D. Z., Chernyshov I. V., Agapova A. A., Serdjuk N. I**. Precision isotope analysis of Nd in rocks //Izvestia AN SSSR. Ser. Geol. 1983. № 12. P.23-40.

UDK 552.33; 550.42

PETROGENETIC IMPLICATIONS AND CHEMICAL EVOLUTION OF LOPARITE IN THE LAYERED, PERALKALINE LOVOZERO COMPLEX, KOLA PENINSULA, RUSSIA

L.N. Kogarko[1], C.T. Williams[2*] and A.R. Woolley[2]

[1] *Vernadsky Institute, Kosygin Street 19, Moscow 117975, Russia*
[2] *Dept of Mineralogy, Natural History Museum, Cromwell Road, London SW7 5BD, UK*

Lovozero, the largest of the world’s layered peralkaline intrusions, includes gigantic deposits of Nb + REE-loparite ore. Loparite became a cumulus phase after crystallisation of about 35% of the ‘Differentiated complex’, and its chemical evolution has been investigated through a 2.35 km section of the intrusion. The composition of the cumulus loparite changes systematically upwards through the intrusion with an increase in Na, Sr, Nb and Th and decrease in REE and Ti. This main trend of loparite evolution records differentiation of the peralkaline magma through crystallisation of 1600 m of the intrusion. The formation of the loparite ores was the result of several factors including the chemical evolution of the highly alkaline magma and mechanical accumulation of loparite at the base of a convecting unit. At later stages of evolution, when concentrations of alkalis and volatiles reached very high levels, loparite reacted with the residual melt to form a variety of minerals including barytolamprophyllite, lomonosovite, steenstrupine-(Ce), vuonnemite, nordite, nenadkevichite, REE,Sr-rich apatite, vitusite-(Ce), mosandrite, monazite-(Ce), cerite and Ba,Si-rich belovite. The absence of loparite ore in the “Eudialyte complex” is likely to be a result of the wide crystallisation field of lamprophyllite, which here became a cumulus phase.

INTRODUCTION

The most alkaline igneous systems are represented by more than 70 occurrences of peralkaline nepheline syenite including the large intrusions of Lovozero and Khibina (Kola Peninsula, Russia), Ilimaussaq (Greenland), Pilanesberg (South Africa) and Poзos de Caldas (Brazil). These rocks are extremely enriched in volatiles (F, Cl, S) and rare elements, as well as alkalis. The alkalinity of these systems is related to the agpaitic coefficient, (Na+K) /Al (molar), which is >1 in peralkaline nepheline syenites and usually increases during crystallisation, owing to early separation of nepheline and feldspar leading to the enrichment of alkalis in the residual melt, and may reach values of >2 [9]. The high alkalinity is the reason, owing to the changing of the melt structure, for the presence in these rocks of a broad range of minerals such as chemically complex sodium-rich zirconium-, niobium- and titanium-bearing silicates containing abundant volatile components. It has been demonstrated [11] that the high alkalinity of agpaitic magmas inhibits the separation of volatile and rare components into the fluid phase, while the magmatic system remains closed with regard to the rare metal components.

--

Loparite, a member of the perovskite structural group, is an accessory mineral in a number of occurrences of agpaitic rocks but is only present in significant amounts in the Lovozero complex, where it is concentrated in some layers up to 25% by volume [4], and forms the world's largest known (Nb + REE) deposit. Loparite mineralisation is closely connected with the igneous layering at Lovozero [5, 28, 33] and one of the principal aims of the present study of the mineralogy of Lovozero was to investigate the compositional evolution of the loparite during crystallisation in this highly alkaline igneous environment. It is generally assumed that in giant intrusions magmatic sedimentation leads to crystal accumulation and, in closed systems, element concentrations in the melt will change, mostly depending on the partition coefficients of the crystallising phases. This process must certainly influence loparite composition (as a cumulus phase) through the vertical section of Lovozero and will be expressed as cryptic variation in the loparite.

We demonstrate in this paper the existence of cryptic variation in the loparite through most of the Lovozero intrusion, which constitutes strong evidence of the magmatic origin of the loparite deposits, in contrast to the suggestion of some authors [3,8] that the loparite ore is of metasomatic origin.

During the very late evolution of the peralkaline magma, when concentrations of volatile components and alkalis reached very high levels, hyperagpaitic minerals [9] might be expected to form. At this stage very early-formed mineral phases became unstable. We report in this paper that loparite at the very last stage of differentiation of the agpaitic magma became unstable and reacted with the residual melt, resulting in the formation of lamprophyllite, lomonosovite, vitusite, nordite, steenstrupine, REE, Sr-rich apatite, nenadkevichite, mosandrite, cerite, monazite, vuonnemite and Ba,Si-rich belovite.

This study forms part of a continuing research programme to re-examine the mineralogy and petrology of the Lovozero layered complex employing modern microanalytical techniques.

GEOLOGICAL SETTING

The Lovozero complex is located in the central part of the Kola Peninsula (Fig 1). The massif is rectangular in plan, has an area of 650 km^2 and lies in a northwesterly striking tectonic zone within which a sunken, east-west-trending belt of Palaeozoic rocks has been preserved. Immediately west of Lovozero is the even larger Khibina alkaline massif [15].

The Lovozero intrusive complex is emplaced in Archaean granite gneisses and has the form of a lopolith with a broad base [4]. According to Arzamastsev et al. [1] the gigantic magma chamber of Lovozero is trough-shaped with a feeding channel situated in the south-western part of the intrusion. The geophysical work of Shablinskiy [27] indicates that the alkaline rocks can be traced to a depth of more than seven kilometres, but their lower limit has not been determined.

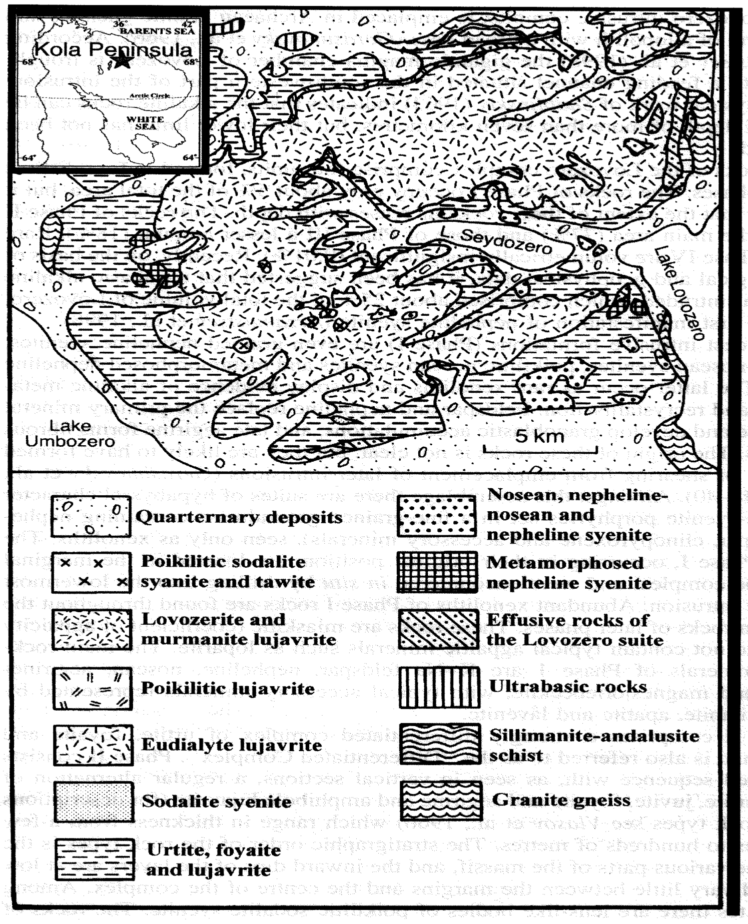

Fig 1**. Geological map of the Lovozero complex with inset showing location of Lovozero (star) within Kola Peninsula**

The rocks of the Lovozero complex comprise four units, formed in four distinct intrusive phases. The rocks of Phase I occupy only about 5% of the total area, but it is possible that the extent of these rocks increases with depth. The rocks of Phase II comprise the main area (77%) and those of Phase III a lesser amount (18%). Rare dykes of Phase IV are volumetrically insignificant (0.01%). Recently, on the basis of new geological and geophysical data, it has been suggested that ultrabasic alkaline magma was intruded, which comprised about 25% of the total volume of Lovozero, before the first manifestation of nepheline syenite [1].

The oldest intrusive formations (Phase I) are even-grained nepheline syenites, nepheline-nosean syenites, poikilitic nosean syenites and metamorphosed nepheline syenites. Amongst this assemblage there are suites of hypabyssal character (nepheline-syenite porphyries). The rocks of Phase I, occurring in their original position, are located in the marginal parts of the complex, and were encountered *in situ* by drilling into the lowermost part of the intrusion. Abundant xenoliths of Phase I rocks are found throughout the complex in rocks of later phases. These rocks are miaskitic (coefficient of agpaicity <1) and do not contain typical agpaitic minerals such as loparite. The main rock-forming minerals of

--

Phase 1 are K-Na feldspar, nepheline, nosean, aegirine-diopside and magnesioriebeckite, with typical accessory minerals represented by ilmenite, titanite, apatite and l⊖venite.

Phase II comprises a strongly differentiated complex of urtite, foyaite and lujavrite, and is also referred to as the “Differentiated complex”. Phase II consists of a layered sequence with, as seen in vertical sections, a regular alternation of layers of urtite, juvite, foyaite and aegirine and amphibole lujavrite (for descriptions of these rock types see [33]) which range in thickness from a few centimetres to hundreds of metres. The stratigraphic order of the rock types is the same in the various parts of the massif, and the inward dips of the layers are at low angles and vary little between the margins and the centre of the complex. Among the lujavrites there are lens-like bodies of poikilitic sodalite syenite. The rocks of Phase II are more alkaline than Phase I (agpaicity >1) and contain abundant peralkaline minerals. The main rock-forming minerals are nepheline, microcline, sodalite, aegirine and arfvedsonite. The accessory phases are typically enriched in elements such as Sr, Zr, Nb, Ba and REE, and include eudialyte, lomonosovite, murmanite, lamprophyllite, villiaumite, loparite, lorenzenite, apatite and titanite.

The rocks of intrusive Phase III comprise a suite of eudialyte lujavrites which cut, and overlie, the upper part of the rocks of Phase II (Phase III is also known as the “Eudialyte complex”). The plane of contact between rocks of Phases II and III dips towards the centre of the complex with the angle increasing from the margins towards the centre. The rocks of Phase III form the summits of the mountains of the Lovozero Massif, and the thickness of this suite reaches 450m but, because of erosion, decreases from northwest to southeast. The rocks of Phase III include leucocratic, mesocratic and melanocratic eudialyte lujavrites, eudialyte foyaite and juvite and a coarser layering is developed than in the rocks of Phase II. At the boundary with the rocks of Phase II there are bodies of porphyritic lujavrite, which are probably partly quenched varieties of eudialyte lujavrite. Individual veins of porphyritic lujavrite, which are late derivatives of Phase III, up to several kilometres long and 50 m wide, cut the rocks of Phases I and II. Poikilitic sodalite syenite and tawite (sodalitite with some aegirine and minor nepheline, alkali feldspar and eudialyte) are found in the form of equidimensional, sharply defined bodies (generally some 10s of metres across) amongst the eudialyte lujavrites of Phase III and rocks of Phase II. The main rock-forming minerals of Phase III are nepheline, microcline, aegirine, eudialyte, lamprophyllite and arfvedsonite. Eudialyte in this complex is euhedral, which is the principal difference from that in the lujavrite of Phase II. The common accessory minerals are lomonosovite-murmanite, loparite, lovozerite, pyrochlore and sodalite.

The rocks of intrusive Phase IV consist of rare dykes of alkaline lamprophyres (monchiquite, fourchite, tinguaite, etc.) which cut all the older alkaline rocks and the surrounding granite gneisses.

SOURCE OF SPECIMENS

In spite of extensive drilling the exact form of the Lovozero complex is not known. In Fig. 2 a generalised section (not to scale) is presented to illustrate the broad relationships of the principal units and the approximate positions of the drill holes from which the specimens on which this study are based were collected. It should be noted that drill holes 144 and 178 penetrated most of Phase III. Drill hole 272B is confined to the lower part of Phase II, the lowest part of which was sampled by drill holes 469, 904 and 905. The upper part of Phase II is mostly covered by drill hole 521. The samples from the middle zone were collected from surface outcrop.

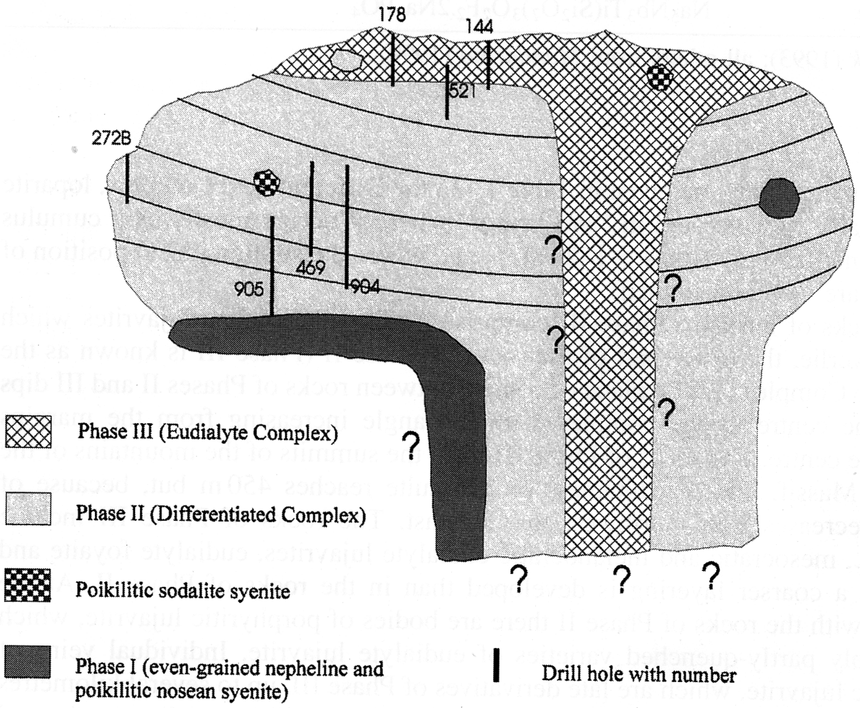

Fig. 2. **Stylised cross-section of the Lovozero intrusion to show the general relationships of the principal rock types and the relative positions, and numbers, of the drill holes sampled during this study**.

The layering of the Differentiated complex is illustrated in a simplified form. Bodies of poikilitic sodalite syenite and poikilitic nosean syenite are shown schematically to indicate their relative positions. The geophysical information is not sufficient to constrain the form of the deeper levels of the intrusion. Note that the upper and lower parts of the Differentiated complex have been extensively drilled but that a section in the lower upper part is unrepresented.

The samples that were collected from the surface could not be correlated very accurately with the stratigraphy determined from the various drill cores. Numerous samples of loparite were also collected from mines and from many shorter cores from holes drilled into individual units. In total, 673 microprobe analyses of

---

--

loparite from 136 samples spanning 2.6 km were obtained from the Lovozero massif.

DISTRIBUTION OF LOPARITE

The chemistry of loparite has been studied principally in Phases II and III of the Lovozero massif (Table 1). Although it is very rare in pegmatites, loparite in three pegmatite samples from Phase II and one sample from a Khibina pegmatite were also studied. According to our investigations, and the data of Gerasimovsky *et al.* [4], loparite is absent from the rocks of Phase I and it is extremely rare in late veins of porphyritic eudialyte lujavrite. In the upper zone of Phase II loparite is particularly enriched in thin seams of malignite (nepheline, a little alkali feldspar and aegirine) where its concentration may reach about 25 % by volume. Usually, however, the loparite is concentrated in urtite and juvite layers (up to 2-3 vol. %) and in the upper part of lujavrite layers.

Table 1.

	1	**2**	**3**	**4**	**5**	**6**	**7**	**8**	**9**	**10**	**11**	**12**	**13**
Spec No	469-717	11374	469-593	469-589	469-586	L-10	57	1_90	9	54-19	904-1495	521-4371	328
Depth	-1317	-1331	-1143	-1140	-1136	-830	-305	50	150	300	-2045	-181	175
Location	Phase II	Phase II	Phase II	Phase II	Phase II	Phase II	Phase II	Phase III	Phase III	Phase III	Phase II	Phase II	Phase III
Cumulus /intercum.	Cum	Cum	Cum	Cum	Cum	Cum	Cum	Cum	Cum	Cum	Inter	Inter	Inter
Na2O	8.49	8.73	8.65	8.62	8.59	8.42	8.71	8.86	9.62	8.60	9.59	11.35	15.89
K2O	0.04	0.07	0.11	0.04	0.05	0.06	0.06	0.07	0.05	0.08	0.00	0.05	0.03
CaO	4.93	4.75	3.94	4.06	4.32	4.48	4.66	4.13	2.98	2.88	3.77	2.76	0.64
TiO2	41.35	40.90	40.72	40.47	40.48	40.42	39.35	38.61	35.19	36.62	36.35	33.18	11.41
FeO	0.54	0.29	0.53	0.35	0.44	0.27	0.35	0.12	0.09	0.06	0.04	0.03	0.24
SrO	1.13	1.17	1.45	1.40	1.54	2.40	3.64	4.46	5.24	7.68	3.05	2.06	3.08
Y2O3	0.01	0.00	0.00	0.02	0.01	0.00	0.00	0.00	0.00	0.00	0.00	0.00	0.00
Nb2O5	6.92	6.61	7.50	7.58	7.10	7.67	8.73	10.56	16.56	13.35	15.06	21.88	57.83
BaO	0.10	0.39	0.07	0.04	0.05	0.20	0.10	0.24	0.31	0.36	0.01	0.02	0.06
La2O3	9.03	9.10	9.51	9.14	9.40	8.95	8.36	8.32	8.06	7.80	7.41	7.72	2.95
Ce2O3	19.43	19.65	19.73	19.21	19.50	18.34	17.50	16.43	14.69	14.77	14.76	14.60	3.86
Pr2O3	1.62	1.76	1.64	1.67	1.50	1.64	1.62	1.57	1.47	1.35	1.28	1.02	0.19
Nd2O3	4.27	4.53	4.23	4.37	3.99	3.99	4.44	4.41	3.57	3.47	4.55	2.63	0.43
Sm2O3	0.17	0.24	0.11	0.24	0.11	0.30	0.16	0.25	0.21	0.19	0.36	0.02	0.00
Gd2O3	0.11		0.00	0.00	0.03	0.00					0.11	0.00	0.00
Ta2O5	0.69	0.51	1.04	0.82	0.60	0.64	0.71	0.72	1.15	0.95	0.92	1.19	0.89
PbO			0.00	0.06	0.00	0.00					0.14	0.30	0.45
ThO2	0.53	0.44	0.52	0.79	0.42	0.63	0.86	0.84	0.65	0.74	1.16	1.33	0.47
UO2	0.10	0.25	0.00	0.00	0.07	0.00	0.10	0.10	0.10	0.14	0.04	0.21	0.25
Total	99.66	99.40	99.75	98.88	98.20	98.41	99.14	99.59	99.84	99.04	98.61	100.35	98.66

Note.1 - Poikilitic sodalite syenite (average of four analyses from one thin section); 2, 3 - Juvite; 4 - Foyaite; 5 - Lujavrite; 6 - Loparite-apatite ore; 7 - Loparite urtite; 8 - Loparite juvite; 9, 10 - Eudialyte lujavrite; 11 - Lujavrite; 12 - Foyaite; 13 - Eudialyte lujavrite.

In Phase III, loparite is commonly an accessory mineral and its concentration is about 0.2 vol. %. Only one layer of eudialyte-bearing juvite contains as much as 2-3 vol. % of loparite.

In the rocks of Phases II and III loparite forms two distinctive morphologies:

(a) Well-defined idiomorphic cubes, octahedra (Fig. 3) or twins on the Fluorite law. Commonly this loparite is associated with aggregates of aegirine and amphibole. Such crystals vary in diameter from 0.1 to several millimetres. There is some indication of sorting by size of loparite grains in the urtite seams, which is particularly noticeable when the loparite concentration is higher.

(b) In the rocks of the lowest part of Phase II (1,500-2,350m below upper contact of Phase II) only interstitial, anhedral, loparite occurs (Fig. 4). It should be emphasised that in this part of the intrusion interstitial loparite is associated with titanite, ilmenite and apatite, all as cumulus phases, and the layering is less marked. Some urtite layers have been found that contain 3-5 vol. % of cumulus titanite. In the Eudialyte complex loparite forms euhedral cumulus crystals only in the lower zone (about 150 m thick). In the upper parts of this complex loparite is commonly developed in the interstices of other minerals as irregular and poikilitic crystals. Idiomorphic cumulus loparite in the upper part of the Eudialyte complex is very rare. This feature of loparite morphology in Phase III was also reported by Ifantopulo and Osokin [8]. Commonly, loparite is partially replaced by fibrous aggregates of lomonosovite-murmanite, lamprophyllite, mosandrite, nenadkevichite, steenstrupine and phosphates of REE, Ca and Sr.

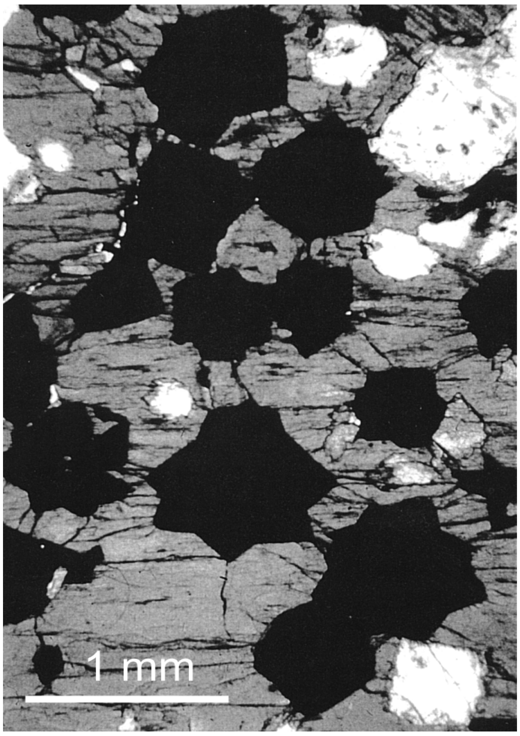

Fig. 3**. Photomicrograph of loparite ore. Black, loparite; grey, pyroxene; white, nepheline. Plane polarised light. The loparite crystals are 0.7-0.8 mm across**

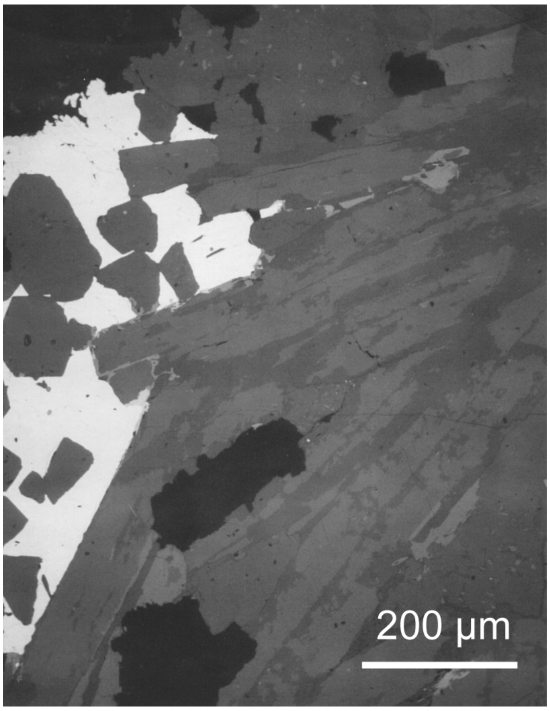

Fig. 4. **Backscattered electron image showing loparite (white) interstitial to pyroxene (dark grey). The black areas are holes in the section**.

--

CHEMICAL EVOLUTION OF LOPARITE RELATED TO MAGMATIC FRACTIONATION TRENDS

Loparite was first documented in the Lovozero Massif in 1894 by Ramsay and Hackman [26] and subsequently studied in detail by a number of researchers [5, 8, 18, 20, 23, 28; 32, 33]. Some systematic changes were noted in the loparite chemistry through the Lovozero differentiated complex, but the majority of these earlier studies were based on analyses of loparite concentrates separated from polymineral fractions.

Progress in the accurate measurement of major and trace elements in individual mineral grains by electron microprobe now makes it possible to study the loparite composition in detail, its zoning and chemical variation in individual grains within particular horizons and through the vertical section of the differentiated and eudialyte-bearing complexes. The analyses were made on a CAMECA SX50 wavelength-dispersive electron microprobe at the Natural History Museum, London. Operating conditions were an accelerating voltage of 15kV and 20nA probe current. Standards used were a combination of natural minerals, synthetic compounds and pure metals, which included synthetic $NaNbO_3$, $SrTiO_3$, $CaTiO_3$, and individual REE-doped glasses for the major components. Background positions were carefully selected to avoid interferences, particularly for the REE, and inter-element empirical corrections made following the procedure in [34].

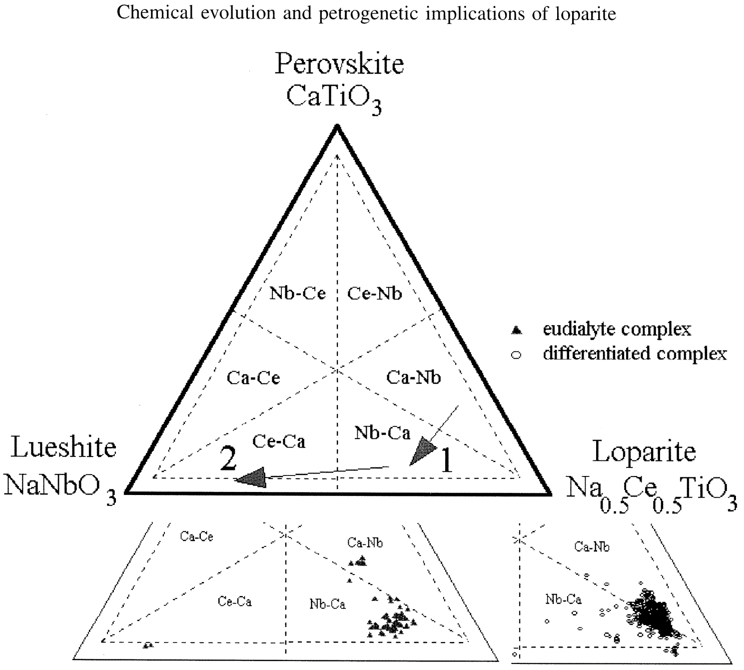

Fig. 5 a. Plot of loparite composition in terms of the lueshite, perovskite and loparite end-member molecules. The change of composition of the loparite with increasing height through the Lovozero intrusion is indicated by the arrow. b Loparite composition in terms of tausonite-loparite-lueshite.

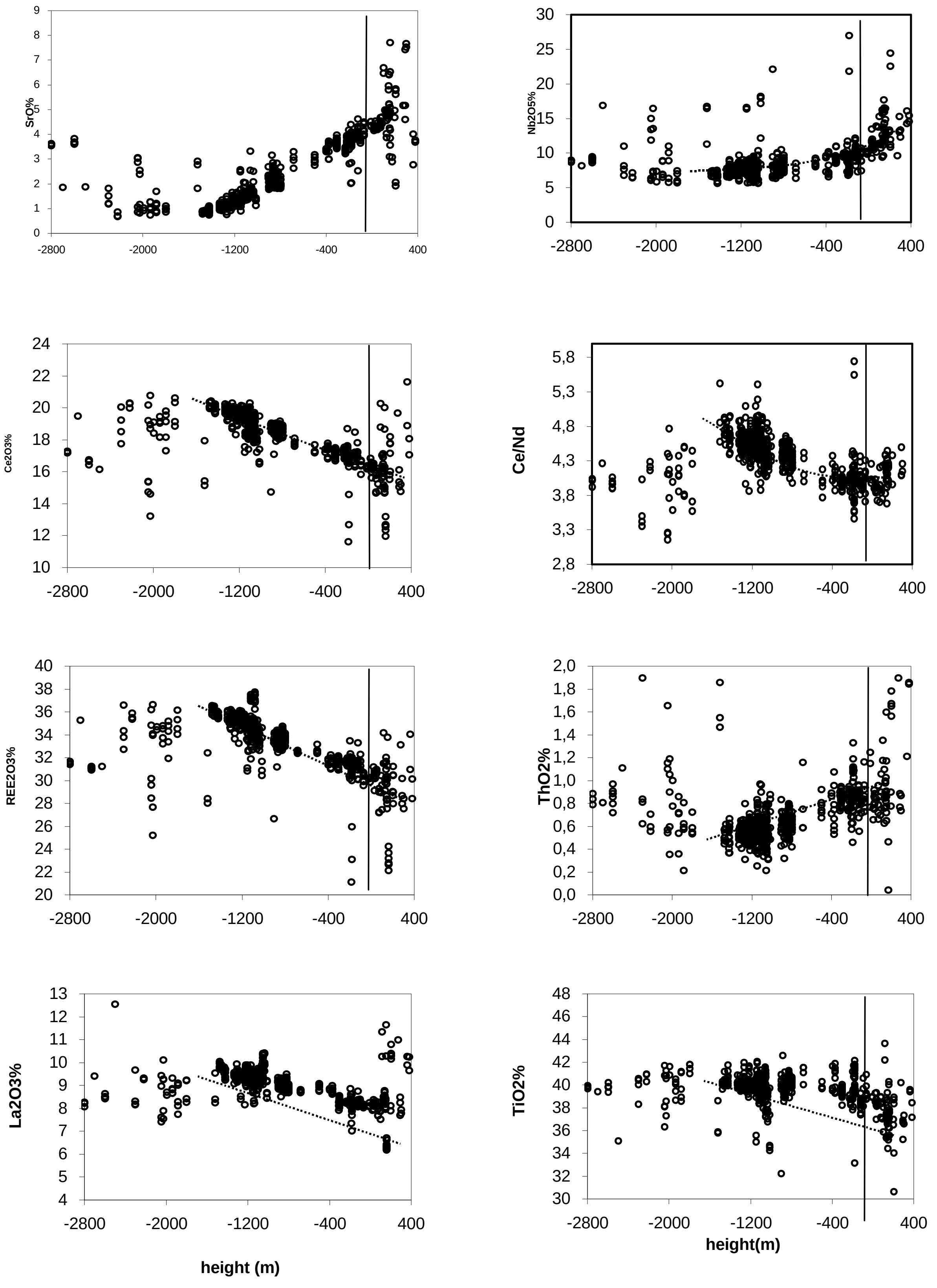

Fig. 6**. Chemical variation of loparite plotted against height in the Lovozero complex. The line at 0 metres is taken at the top of the Differentiated complex**.

a SrO, **b** Nb_2O_5, **c** total REE_2O_3, **d** ThO_2, **e** Ce_2O_3, **f** Ce/Nd.

--

Loparite is a member of the perovskite structural group which may be written as $A_2B_2O_6$, in which A includes Ca, Sr, Na, REE and Ba and B includes Ti, Nb, U, Th and Ta. In spite of the rather variable composition, the majority of natural loparite have compositions which fall within the quaternary system represented by four major end-member components: perovskite ($CaTiO_3$), tausonite ($SrTiO_3$), lueshite ($NaNbO_3$) and loparite ($Na(REE)Ti_2O_6$) (Figs 4a and b) (see [22] for a recent classification scheme). The very good negative correlations between Ti and Nb and (Ca+Sr) and (Na+REE) in the data from this study are in good agreement with this conclusion.

The variation in the composition of the loparite can be seen in the leushite-perovskite-loparite (Fig.5a) and the lueshite-tausonite-loparite ternary diagrams. The majority of analyses plot in the field of loparite, as was shown by earlier workers [5, 18, 23, 32]. However, some compositions lie in the fields of niobian loparite and cerian lueshite (nomenclature from [23]).

The composition of loparite reflects the fractional crystallisation of the highly alkaline melt and, in this work, the evolution of the Lovozero magma was monitored through about 2,350 m of layered nepheline syenites using the loparite compositional changes, which have been plotted as a function of the structural depth in the intrusion (Fig. 6). As has been shown by many authors (e.g. [6,7] the compositions of cumulus phases in layered intrusions might be changed dramatically by subsequent reaction with intercumulus melts and by re-equilibration processes.

In order to minimize the influence of post-cumulus factors on genuine cryptic variations in loparite composition, we used analyses of about 400 grains of loparite from 63 samples from the so-called ‘ore layers’, where loparite occurs mostly as a cumulus mineral at modal proportions >1-2 vol. %, and where their relative heights are well-constrained. We also investigated loparite in about 50 further thin sections, mainly from drill-core, from the Differentiated and Eudialyte complexes.

If the Lovozero intrusion is examined as a whole (including the differentiated and eudialyte-bearing complexes) we see that there is a clear coherence between concentrations of Sr, Nb, Ta, Th, Ca, REE, Ti and Na in the cumulus loparite and the depth within the intrusion (Figs 5a) show some of these element plots). In these figures, where oxides, or element ratios are plotted against depth, the zero line is taken at the top (contact) of the Differentiated complex with the Eudialyte complex. All depths in the differentiated complex are expressed as negative numbers, and in the Eudialyte complex as positive numbers (see also Fig. 2). Our petrographic data indicate that loparite is a cumulus phase in the Differentiated complex from a depth of about -1500 m up to about +150 in the Eudialyte complex. Moving stratigraphically upwards through the intrusion the cumulus loparite becomes progressively enriched in Sr, Nb, Ta, Th and Na and depleted in Ca, Fe, Ti, Ce, La, Nd and total REE. This is the principal trend of cumulus loparite evolution in Lovozero, which is observed through some 1600 m of the intrusion. There is a degree of scattering of the compositional data because some of the loparite analysed in this zone is intercumulus, seen from thin section examination (and backscattered electron images), where it has crystallised within localised, trapped, interstitial melt. As mentioned above, loparite is intercumulus in the lower part of the Differentiated complex (from -2300 to -1500 m), and its composition here reflects crystallisation within an evolving trapped liquid, which resulted in large variations in its composition (Figs 5a).

It is noteworthy that the same trends for Sr, Nb, Th, and REE that are observed for cumulus loparite in the structural section of the massif, can be demonstrated within one interstitial loparite grain. In the lowest part of the Differentiated complex (2029 m depth) in one zoned grain of interstitial loparite the values shown in Table 2 were obtained (across the grain from the centre to the edge).

Table 2.

Chemical variation across a zoned, interstital loparite grain.

	Centre of grain			**Edge of grain**
SrO	0.83	2.78	2.57	2.4
ThO_2	0.36	0.83	0.60	1.19
Nb_2O_5	6.6	12.76	13.56	16.5
Ce_2O_3	20.7	13.32	14.61	13.23
$N_{d2}O_3$	4.36	3.46	3.88	3.17
Nb:Ta ratio	13.75	22.57	26.07	48.5
Ce:Nd ratio	4.74	3.84	3.77	4.17

Comparison of these data with the distribution of Nb, Sr, Th and REE in cumulus loparite throughout the structural section of the Lovozero intrusion indicates that the complete evolution of this large magma chamber can be represented in one interstitial loparite grain.

During the evolution of the Eudialyte complex, when about 30% of the magma had crystallised, lamprophyllite is likely to have become a cumulus phase, together with nepheline, K-feldspar, aegirine, eudialyte and arfvedsonite. Petrographic investigations show that lamprophyllite in the lower part of the Eudialyte complex (up to approximately 100-150 m from the contact with Phase II) occurs as irregular plates or interstitial crystals, but in the upper part the abundance of lamprophyllite increases substantially and it forms euhedral, elongate crystals among aegirine needles. Lamprophyllite is a major sink for Ti and Sr, containing up to 30 wt% TiO_2 and 16 wt% SrO, thus early crystallisation of lamprophyllite will result in a depletion of these elements in the fractionated magma. Our investigation also indicates that in the uppermost part of the Eudialyte complex pyrochlore, containing up to 52 wt% Nb_2O_5, forms euhedral crystals and so probably also became a cumulus phase. As a result of the appearance of cumulus lamprophyllite and pyrochlore the field of crystallisation of loparite dramatically decreased. This feature also may be related to an increase in the alkalinity of the magmatic system at this stage of the evolution of the intrusion. Experimental data of [17] have shown that the concentration of loparite at the

--

eutectic in the nepheline-loparite system is ~17 wt%, but in the system lueshite-nepheline the content of the more alkali-rich lueshite reaches 48%. Saturation of the alkaline melt in more lueshite-rich loparite takes place at a much lower temperature which led to the interstitial crystallisation of loparite. This is probably the reason for the wide scatter of the Sr, Nb, REE and Th data of the loparite from the upper part of the Lovozero intrusion (Figs 5a). The crystallisation of lamprophyllite led to a decrease in the content of Sr in the cumulus loparite in the upper part of Phase III (for instance, up to 1.9% SrO) at depths of 205 m (from the contact with the Differentiated complex).

The Nb:Ta ratio in the cumulus loparite increases continuously upwards from an average value close to 12 in the lower part of the differentiated complex to 32 in some loparite grains from the eudialyte complex. Very high Nb:Ta ratios up to 48.5 were observed in one grain of interstitial loparite of Phase II and exceptionally high, up to 299, in intercumulus loparite of Phase III. In loparite from pegmatite at Khibina the Nb:Ta ratio is also high (38.5). It is interesting to note that pyrochlore co-existing with the intercumulus loparite is also characterised by similar very high Nb:Ta ratios. For example, pyrochlore from the sample of eudialyte lujavrite in which the Nb:Ta ratio of the loparite is 299 has a ratio of 326.

With increasing stratigraphic height the Ce/Nd ratio in cumulus loparite decreases slightly from a mean value of 4.7 in the lower part of the differentiated complex to a mean of 4.0 in loparite from the upper part (Fig. 6f). In Phase III there is an inverse correlation in the Ce: Nd ratio with height in cumulus loparite. This ratio increases slightly from the lower part of the Eudialyte intrusion, where it has a mean value of 4.0, up to 4.2 in loparite from the upper part of the Eudialyte complex (Fig. 6f).

Cumulus loparite is the major host of REE in the Lovozero peralkaline magma, particularly in the Differentiated complex. The mineral-mineral partition coefficient of REE in loparite and apatite which are in equilibrium, they are both cumulus minerals in Phase II, is relatively high i.e. KdCe = 5.5, KdNd = 4.3 and KdSm = 1.

The initial Ce:Nd ratio in the primary magma of the Differentiated complex, according to the data of Balashov and Turanskaya (1960), is 3.36. In cumulus loparite from intrusion II this ratio varies from 4.69 (from the lower part of the complex at 1,500-1,400 m depth) to 4.0 in the upper part (0-100 m) (Fig. 6f). Consequently, crystallisation of loparite will decrease the Ce:Nd ratio in the melt during its crystallisation. This study shows that many interstitial minerals, such as monazite, vitusite, steenstrupine and mosandrite, also have higher Ce:Nd ratios than the primary melt of the Differentiated complex (i.e. >3.36), thus their crystallisation will also decrease the Ce:Nd ratio in the residual liquid.

The migration of less dense interstitial melt through the pores of the partly consolidated rocks, as a result of compaction and convection within the settled crystals, is an important process in layered intrusions [24], and such melts may interact with the main portion of the magma. Thus, in the case of an open system , in respect of movement of residual melt, the crystallization of interstitial, REE-bearing mineral phases from this interstitial melt would also have contributed to a decrease in the Ce:Nd ratio of the Phase II melt during differentiation. It should be noted that the average Ce:Nd ratio in the rocks of a very large pegmatite body of Phase II falls as low as 1.54 [4]. An inversion in the trend of the Ce:Nd ratio in loparite during the evolution of the Eudialyte complex may be attributed to the early crystallisation of eudialyte which here becomes a major cumulus phase. The Ce:Nd ratio of the eudialyte is approximately 2.0 throughout the Eudialyte complex, and its crystallisation will increase the initial Ce:Nd ratio in the melt and consequently affect its ratio in loparite crystallising from this melt.

The composition of loparite from the poikilitic sodalite syenite body in the lower part of the 'Differentiated Complex' (Phase II) was also investigated (analysis 1, Table 1). Loparite from this sample contains very low Na and Nb, and high total REE. The poikilitic sodalite syenite sample is from an isolated oval-shaped body approximately 16 m in diameter; it displays sharp contacts against the surrounding juvite and does not have feeding channels. It consists of sodalite (~ 60%), microcline and albite (~15%), aegirine and arfvedsonite (~5%), nepheline (~15%) and accessory eudialyte, villiaumite, loparite, lorenzenite, monazite and thorianite. As has been demonstrated [16] the composition of sodalite syenites lies in the immiscibility field in the system nepheline-albite-halite, and many geological and geochemical features of these rocks are consistent with the model of poikilitic sodalite syenite originating by a process of liquid immiscibility. The evidence includes very high concentrations of chlorine and fluorine, the presence of primary micro-inclusions containing halite, and characteristic distribution patterns of some rare elements between the country rocks and poikilitic sodalite syenites [4].

The separation of immiscible liquids demands equilibrium not only between them, but also between all the solid phases. Our data show that the composition of loparite is similar in both the poikilitic sodalite syenites and the enclosing juvite (analysis 2, Table 1). Thus, these data are in general agreement with other geochemical and petrological evidence of the major role of liquid immiscibility in the origin of sodalite syenites.

ZONING IN LOPARITE

Loparite zoning was considered earlier by Mitchell and Chakhmourdian [23], but only in the sense of core-rim zonation. Our study has shown that individual loparite crystals can display very complex zoning, best illustrated using backscattered electron images (Figs 6a and b). Darker (lower mean atomic number) zones are usually enriched in Na, Nb and Sr, while the lighter zones are characterised by higher concentrations of REE, Th, Ti and Ca .Several types of zoning are distinguishable.

--

1. Marginal zoning, in which there is enrichment in Sr, Nb and Na in the outer rim (Fig. 7a).

2. Reverse zoning, in which the outer rim is depleted in Sr, Nb and Na.

3. Oscillatory zoning in which there is repetition of zones enriched and depleted in Sr, Nb and Na.

4. Sector zoning.

5. Irregular zoning (Fig. 7b).

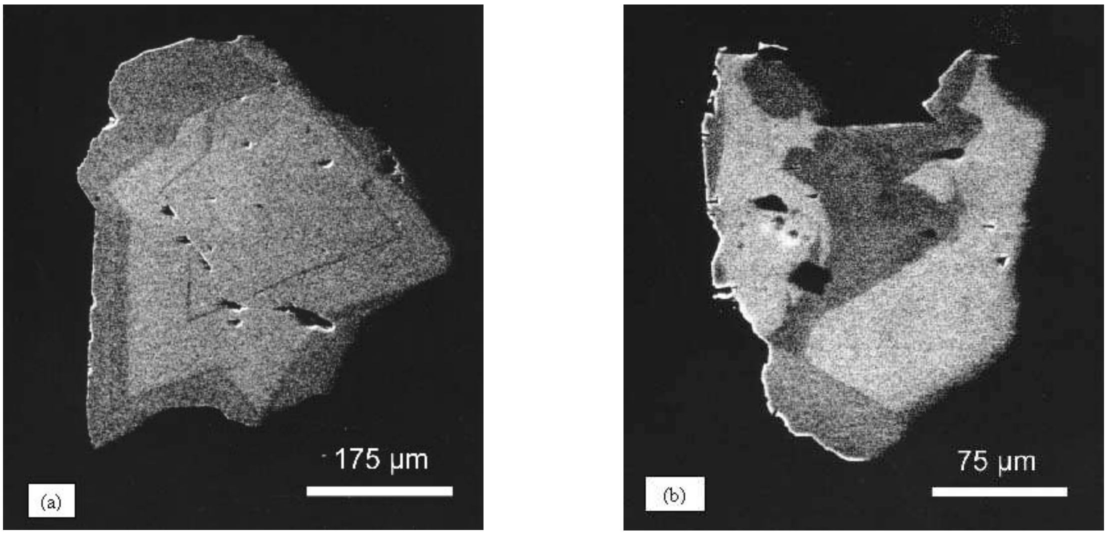

Fig. 7**. Backscattered electron images of loparite showing a marginal zoning, and (b patchy zoning.**

The marginal zoning is undoubtedly caused by loparite crystallisation in equilibrium with a restricted amount of interstitial melt, when the loparite rapidly becomes enriched in the lower temperature components lueshite and tausonite. The same trend was reported by Veksler *et al.* [31] in experimental studies involving decreasing temperatures. Reverse zonation is probably the result of crystallisation of the loparite in interstitial melt simultaneously with mineral phases having higher partition coefficients for Sr, Nb and Na. These minerals include lamprophyllite, Sr-apatite, murmanite-lomonosovite, pyrochlore and nenadkevichite, which are abundant as interstitial minerals in rocks of Phases II and III.

Oscillatory zonation is probably the result of the interplay of several factors such as the variations in rates of crystal growth of loparite and minerals competing for the major components of loparite, differential element diffusion rates, and localised dis-equilibrium conditions adjacent to growing loparite crystal faces. Such mechanisms have been described previously in peralkaline magmas [12], and are a relatively common feature described in a range of minerals from other magmatic environments.

One of the reasons for the irregular and sector zoning might be the partial recrystallisation of the loparite after accumulation. Such processes are widespread in cumulus rocks of layered intrusions [7]. Another factor that may contribute to these types of zoning is the formation of glomeroporphyritic crystal aggregates in the melt, which retain their distinctive composition in the sedimented mush where they anneal and recrystallise into zoned crystals. These aspects will be considered further in a separate publication.

LOPARITE - MELT REACTIONS

The agpaitic order of crystallisation results in a continuous increase of the alkalinity. High alkalinity prevents the separation of volatile components and rare elements into the gas phase (H_2O, F, Cl, S etc.) [10], which is a fundamental geochemical feature of peralkaline magmas. The very high solubility of water in peralkaline melts [10,11] will cause the very gradual transition from magmatic peralkaline residual melt into hydrothermal solution (brine). Extremely high concentrations of F and Cl [4] enhance this process. The accumulation of volatile components in the melt, but not in the vapour phase, is the reason for the extremely low temperature of the solidus of these rocks, up to 425°C [16] and a very prolonged interval of peralkaline rock crystallisation. This feature facilitates the post-cumulus reactions.

Our study has demonstrated that loparite primocrysts may not only change their composition, but may be replaced by other minerals during the late stages of high alkaline magma evolution (Figs 8a-d).

The petrography indicates that the urtites are typical adcumulates, usually with a very small percentage of intercumulus material, and that compaction was an important process in their formation. The foyaite and lujavrite, in contrast, contain much more interstitial material and loparite here is more commonly replaced by another phase.

We have recognised seven reactions between loparite and the trapped residual liquid (L_1 and L_2).

1. $(Ce,La)(Ca,Sr,Na)(Nb,Ti)O_3$ (*loparite*) + L_1 = $Na_2Ca_4CeTiSi_4O_{15}F$ (*mosandrite*) + $Na_6(Sr,Ba)_3FeTi_6Si_8O_{34}F_2$ (*lamprophyllite*) + $(Ce,La,Nd)(PO_4)$ (*monazite*) + L_2

2. $(Ce,La)(Ca,Sr,Na)(Nb,Ti)O_3$ (*loparite*) + L_1 = $Na_6Ba_3FeTi_6Si_8O_{34}F_2$ (*baritolamprophyllite*) + $Na_{10}Ti_4Si_4P_2O_{26}$ (*lomonosovite*) + $Na_3Ce\ (PO_4)_2$ (*vitusite*) + $(Ce,La,Th,Ca,Na)_2(Mn,Fe)[SiO_3]_4.5H_2O$ (*steenstrupine*) + $(Ca,Na,Sr,Cl,La)_5(PO_4)_3F$ (*REE,Sr-rich apatite*) + L_2

3. $(Ce,La)(Ca,Sr,Na)(Nb,Ti)O_3$ (*loparite*) + L_1 = $(Na,K)_2(Ca,Mg,Fe,Mn)_{0.88}Ba_{0.93}Nb_{0.77}Ti_2Si_{4.09}O_{17}(F,OH,H_2O)x$ (*unknown phase*) + $(Ce,La,Nd)(PO_4)$ (*monazite*) + $(Ce,La)_3Si_2O_8(OH)$ (*cerite*) + $Na_6Ba_3FeTi_6Si_8O_{34}F_2$ (*baritolamprophyllite*) + L_2

4. $(Ce,La)(Ca,Sr,Na)(Nb,Ti)O_3$ (*loparite*) + L_1 = $(Na,Ca)(Nb,Ti)(Si_2O_7).2H_2O$ (*nenadkevichite*) + $(Ce,La,Nd)(PO_4)$ (*monazite*) + L_2

5. $(Ce,La)(Ca,Sr,Na)(Nb,Ti)O_3$ (*loparite*) + L_1 = $(Ce,La)(Sr,Ca)Na_2(Na,Mn)(Zn,Mg)\ Si_6O_{17}$ (*nordite*) +$Na_{10}Ti_4Si_4P_2O_{26}$ (*lomonosovite*) + L_2

6. $(Ce,La)(Ca,Sr,Na)(Nb,Ti)O_3$ (*loparite*) + L_1 = $Na_5TiNb_3Si_6O_{25}F_22Na_3PO_4$ (*vuonnemite*) + $(Ce,La,Nd)(PO_4)$ (*monazite*) + L_2

7. $(Ce,La)(Ca,Sr,Na)(Nb,Ti)O_3$ (*loparite*) + L_1 = $Na_6Ba_3FeTi_6Si_8O_{34}F_2$ (*baritolamprophyllite*) + $Na(Ce,La)(Sr, Ba)_3(PO_4)_3F$ (*Ba,Si-rich belovite*) + L_2

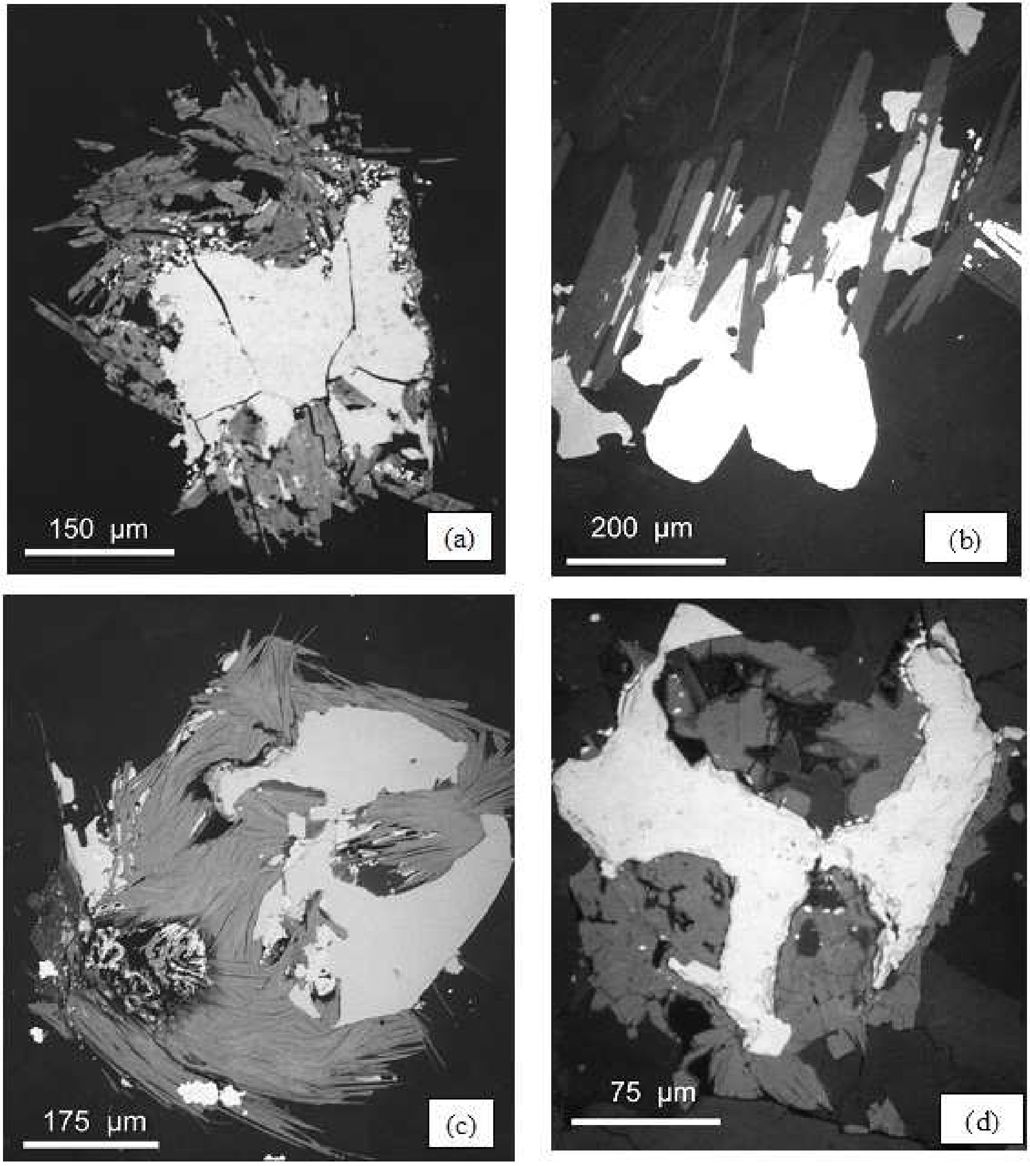

Fig. 8. **Backscattered images showing reactions of loparite with residual melt.**

a Loparite (white) replaced by lamprophyllite (grey, acicular), mosandrite (grey, more platy crystals) and monazite (small white crystals). **b** Loparite (large white crystals) replaced by lamprophyllite (dark grey acicular crystals), lomonosovite (black, immediately above steenstrupine crystal on left margin), vitusite (medium grey, irregular crystals), steenstrupine (white grain on left margin) and REE,Sr-rich apatite (white needle to right of loparite). **c** Loparite is replaced by Ba lamprophyllite, monazite and an unknown phase. **d** Loparite (pale grey) replaced by nenadkevichite (medium grey) which includes small pyroxenes (black); the small white spots are monazite crystals.

These reactions indicate a dramatic increase in the concentrations of volatiles (F,H_2O), Na, P, Th, Ba and Zn in the residual interstitial melt in which loparite became unstable. The migration of the interstitial melt from the urtite layers is probably one of the reasons for the preservation of the loparite ore in these rocks. These aspects will be considered further in a separate publication.

MECHANISMS OF LOPARITE FRACTIONATION

The large amount of data on layered intrusions from different parts of the world accumulated during recent decades has provided new evidence and mechanisms to explain the observed phenomena (Parsons, 1987). The role of *in situ* processes has been considered including different patterns of convection, flow segregation, nucleation density, compaction, textural equilibration and recrystallisation. However, the origin and differentiation of layered intrusions still remains largely unresolved because of the complexity of this process and participation of many different genetic mechanisms. The compositions of cumulus minerals in layered intrusions provide invaluable information about the fractionation processes and melt evolution in the magma chamber.

Given the concentrations of a component in loparite as a function of depth in the layered intrusion and assuming that the behaviour of this component obeys the Rayleigh law (ideal fractional crystallisation with constant partition coefficients), we may estimate partition coefficients and the fraction of loparite in the total mass of crystallising solid phases. The Rayleigh equation is:

$CL = Co^* (F_L)\ K_B\text{-}1$

Where CL is the concentration in melt at a given stage; Co is the initial concentration in the melt prior to crystallisation (taken here as an average abundance in the intrusion); F_L is the fraction of melt remaining in the system at a given moment, calculated as the ratio of distance of a given layer from the top of the intrusion divided by the thickness of the intrusion, and K_B is the bulk (weighted average) partition coefficient.

Where Klop is the partition coefficient of some element in loparite = Clop/C_L the concentration in loparite (Clop) may be expressed as:

$\mathrm{Clop} = \mathrm{Klop}^*\mathrm{Co}^*\ (F_L)\ K_B\text{-}1$, or in the logarithmic form:-

$\ln(\mathrm{Clop}) = \ln(\mathrm{Klop}^*\mathrm{Co}) + (K_B\text{-}1)^*\ln(F_L)$.

From the available analytical data we estimate (K_B-1) and ln (Klop*Co) applying the least squares procedure to the linear regression of ln (Clop) against ln (F_L). For REE and a number of other components we make the assumption that loparite is the only crystallising phase which incorporates these elements in substantial amounts, and therefore

$K_B = \mathrm{rlop}^*\mathrm{Klop}$,

where rLop is the fraction of loparite in the total mass of crystallising solid phases.

Using the data on the distribution of Sr, REE, Nb, Ta and Th in loparite we obtained estimated values for the fraction of loparite in the total mass of crystallizing solid phases in the Differentiated complex to be in the range of 0.6 - 4 % which is consistent with the experimental data of [17] who estimated the proportion of loparite in eutectic with lujavrite to be 1-2%.

The calculated partition coefficients between loparite and alkaline melt for Sr, REE, Nb, Ta and Th are 22.6, 100-157, 80, 85, 133 respectively. The bulk partition

---

--

coefficients were estimated to be for Sr = 0.52-0.38, REE = 1.06-0.91, Nb = 0.87, Ta = 0.92, TiO_2 = 1.01, and Th = 0.77. The partition coefficients of Ce and La for loparite/alkaline melt have also been obtained, based on the distribution of these elements between cumulus loparite and apatite from the same Lovozero samples. WЦrner *et al*. [35] have reported melt distribution coefficients for rare earths for apatite/Laacher See phonolite i.e. La, 14.4 and Ce, 24.3, which we used for calculation, because of the similarity in composition of this rock with Lovozero. The estimated loparite/melt partition coefficients of La and Ce (80-135) for Lovozero are close to the previously calculated data, given above (i.e. 100-157).

In spite of the relatively low concentrations of the loparite component necessary to saturate peralkaline magma (1-2%) according to the experimental data [17, 31], the initial Lovozero melt was not saturated with respect to loparite, which is confirmed by the fact that loparite is absent from Phase I [4]. In Phase II loparite becomes a cumulus phase only after about 35% crystallisation of the magma. Deeper than -1500 m in Phase II loparite is an interstitial phase and its composition reflects the rapid evolution of trapped melt. In this part of the intrusion the main Ti and Nb cumulus phases are titanite, ilmenite and titanomagnetite. With the increasing alkalinity and concentration of REE and Nb in the melt, loparite started to crystallise as a cumulus phase. The composition of loparite changed systematically through about 1600 m towards the top of the intrusion and correlates with stratigraphic level with an increase in the lower temperature components lueshite and tausonite (Na, Sr, Nb). There are no discontinuous changes in the cumulus loparite composition throughout the Differentiated complex, which indicates the absence of magma replenishment in this intrusion, but instead implies a closed system fractionation. The initial melt of the Eudialyte complex, in contrast to the Differentiated complex, is saturated with respect to eudialyte, which is a cumulus phase throughout. As outlined above, lamprophylite probably became a cumulus phase after crystallisation of approximately 30% of the Eudialyte complex. Loparite still occurs, but only as a relatively rare phase. However, the experimental phase relationships between loparite and lamprophyllite are not known for this stage. The reaction of loparite with peralkaline interstitial melt producing lamprophylite in the Differentiated complex suggests that in the more peralkaline Eudialyte complex, this reaction controls the whole of the evolution of the later stages of the melt, which precludes the formation of loparite accumulation (i.e. loparite ore) in the rocks of phase III.

From the observed data of the significant cryptic variation in loparite through the intrusion (Fig. 6), it is clear that differentiation from lower to higher levels was the dominant process occurring in the magma chamber, and therefore that the loparite-rich horizons were formed during the magmatic stage. Geological evidence, including continuous layers of lujavrite, foyaite and urtite, together with isotopic studies [17, 19], point to fractionation of the Lovozero magma within a closed magma chamber. Plots of Sr, Nb, REE and Th concentrations against depth (Figs 6a-d) also indicate the closed character of the fractionation at Lovozero. The linear correlation of log-element concentrations in plots of cumulus loparite against log-depth (not shown) testify to the relatively constant bulk partition coefficients of these elements in loparite in the Differentiated complex, which are independent of changes in melt composition. These data show a good correspondence with the experimental data of [17, Veksler *et al.* [30], which indicates that the partition coefficients of Sr, Nb and REE in the equilibrium loparite-lujavrite-melt and loparite-nepheline-melt did not change. As outlined above, bulk partition coefficients for LREE, HREE and Sr in loparite changed in Phase III, because here eudialyte, lamprophyllite and pyrochlore became cumulus mineral phases. Thus, it is possible to suggest that fractional crystallisation, combined with continuous settling of loparite, was the most important process responsible for the observed chemical trend of loparite through the stratigraphic section and for the genesis of the loparite ore. The sorting phenomenon of loparite grains in the ore layers supports this conclusion.

As demonstrated by [29] in magmatic systems containing minerals with different settling velocities, and different critical concentrations, a sequence of layers can result from steady convection and steady cooling. Crystals in melts may remain in suspension only until the settling velocity is small as compared with the velocity of convective currents [13, 21, 29]. We may speculate that the formation of rhythmic units in Phase II, consisting of loparite-bearing urtite, foyaite and lujavrite, may be attributed to sedimentation from relatively steady convection. During this process the alkaline magma contained cumulus phases, including nepheline, loparite, feldspar, aegirine and amphibole, but only the nepheline and loparite separated to form the loparite-bearing urtite layers. Petrographic examination demonstrates the striking cumulate textures of the urtite layers. Loparite, as the most dense cumulus phase, sank to the lowest part of the urtite layers and even, in some cases, into the upper zone of the partially solidified underlying lujavrite. Grains of nepheline and feldspar, probably having a lower settling velocities, because of their smaller size, accumulated later forming the foyaite layers having an orthocumulate texture, using the nomenclature proposed by Hunter [7]. Subsequently, aegirine, which usually forms smaller needle-like crystals than nepheline or feldspar, started to crystallise and sink simultaneously, or even later, with these minerals so that foyaite gradually graded into lujavrite. The overlying urtitic units probably formed from successive convection pulses resulting in sharp contacts with the underlying lujavrite, which can be seen clearly throughout the Differentiated complex. There is evidence for sorting of the minerals within some of the units such that larger crystals accumulate in the lower part of the urtite layers, whereas smaller crystals are confined to the upper part of the lujavrites. The succession of rocks in these units was probably partially facilitated by the very large field of crystallisation of nepheline and feldspar in the Lovozero peralkaline magmatic system [10].

This hypothesis for the formation of rhythmic layering is supported firstly by the correlation of the thickness between urtite, foyaite and lujavrite in each unit,

--

the disturbance of this regularity probably being related to magmatic erosion, and secondly, by the presence of centimetre-scale lamination, this being especially well exhibited by feldspar and aegirine, which is evidence for the existence of convection currents within the magma chamber. Deviation from this regularity might be attributed to the fluctuations in the degree of compaction, strength of convection, and different other factors, during the formation of loparite-bearing layers.

As mentioned above, the high alkalinity of the Lovozero magma and the accumulation of volatile components in the peralkaline melt, but not in the fluid phase, was the main reason for the gradual transition from the magmatic to the hydrothermal stage and the very long period of crystallisation. This geochemical feature of the peralkaline magma system initiated the wide-scale development of the late-stage processes such as recrystallisation, reactions with interstitial melt and textural equilibration, which partly overprinted the characteristic primary features of the loparite in the Lovozero intrusion.

CONCLUSIONS

From the data it is clear that there is a significant systematic cryptic variation in cumulus loparite throughout the Lovozero layered intrusion, so that fractional crystallisation combined with settling of the fractionating phases, in a closed system, was the dominant differentiation process of the Lovozero magma. Thus, the massive loparite deposits are magmatic in origin, and not the result of a metasomatic event as suggested by some workers (e.g. [3]).

The process of fractional crystallization is recorded in the composition of the loparite throughout the whole layered intrusion. The composition of intercumulus loparite reflects crystallization in a ‘trapped magma’ environment and gives a similar trend, but to a greater degree of evolution, than that of the cumulus loparite. The parent magma of the Lovozero intrusion, Phases II and III, was initially undersaturated with respect to loparite and only after the crystallization of about 30% of the original melt did loparite appear as a cumulus phase (together with nepheline, microcline, clinopyroxene and amphibole), and accumulate to form the loparite ores. The principal processes involved were probably a combination of magmatic convection coupled with settling of loparite at the base of units of urtite, foyaite and lujavrite. Each unit consists of three seams enriched in nepheline + loparite, followed by nepheline + feldspar, and finally nepheline + feldspar + aegirine.

The partition coefficients of REE, Sr, Nb and Th between loparite and melt are relatively constant and independent of temperature and melt composition, which is in good agreement with the experimental data [17].

During the evolution of the peralkaline nepheline syenite magma there was enrichment of alkalis and volatiles in the residual melt. Loparite became unstable during the post-cumulate stage and was replaced by a range of minerals including barytolamprophyllite, lomonosovite, steenstrupine-(Ce), vuonnemite, nordite, nenadkevichite, REE,Sr-rich apatite, vitusite-(Ce), mosandrite, monazite-(Ce), cerite and Ba,Si-rich belovite.

This work was supported by The Royal Society and RFBR Grant 05-05-64144

REFERENCES

1. **Arzamastsev A.A., Arzamastseva L.V., Glasnev V.N., Raevsky A.B.** (1998). Deep structure and the composition of deep parts of Khibina and Lovozero complexes, Kola Peninsula, petrological and geophysical model. J Petrol 6: 478-496
2. **Balashov Yu.A., Turanskaya N.V.** (1960) Regularities in the distribution of rare-earth elements in rocks of the Differentiated complex of the Lovozero alkaline massif in connection with some problems of the genesis of this complex. Geokhimiya 701-713
3. **Eliseev N.A., Fedorov E.E.** (1953) Lovozero pluton and its mineral deposits. Trans Laboratory Geol of the Precambrian, St Petersburg
4. **Gerasimovsky V.I., Volkov V.P., Kogarko L.N., Polyakov A.I., Saprykina T.V., Balashov Yu.A.** (1966) The Geochemistry of the Lovozero alkaline massif. Part 1. Geology and Petrology. Part 2. Geochemistry. Translated 1968 by *DA Brown*. Australian National University Press, Canberra. 224 and 369 pp. (Translation of original Russian text published in 1966)
5. **Gerasimovsky V.I., Kostyleva E.E.** (1937) Loparite minerals of Khibina and Lovozero tundras (in Russian). St Petersburg: Acad Sci, 408-419
6. **Henderson P.** (1975) Geochemical indicator of the efficiency of fractionation of the Skaergaard Intrusion, East Greenland. Min Mag 40: 286-291
7. **Hunter R.H.** (1996) Texture development in cumulate rocks. In: *Cawthorn RG* (ed) Layered intrusions. Developments in Petrology 15. Elsevier, Amsterdam, pp 77-101
8. **Ifantopulo T.N., Osokin E.D.** (1979) Accessory loparite from stratified alkaline intrusions. In: New Data on Mineralogy of Mineral Deposits from Alkaline Rocks. Trans Institute Mineral Geochem and Crystallog Rare Elements, pp 20-28
9. **Khomyakov A.P.** (1995) Mineralogy of Hyperagpaitic Alkaline Rocks. Clarendon Press, Oxford. 223 pp
10. **Kogarko L.N.** (1977) Genetic problems of agpaitic magmas. Nauka, Moscow. 294 pp
11. **Kogarko L.N.** (1990) Ore-forming potential of alkaline magmas. Lithos 26: 165-175
12. **Kogarko L.N., Volkov V.P.** (1963) Physical-chemical evolution of differentiated complex of Lovozero massif in connection with its layering. In Chemistry of the Earth's Crust 1. Nauka, Moscow 111-127
13. **Kogarko L.N., Khopaev V.** (1987) The modelling of formation of apatite deposits of the Khibina massif (Kola Peninsula). In: *Parsons I* (ed) Origin of igneous layering. Reidel Publishing Company, Dordrecht. pp 589-611
14. **Kogarko L.N., Burnham C.W., Shettle D.** (1977) The water regime in hyperalkaline magmas (in Russian). Geokhimiya 5: 643-51
15. **Kogarko L.N., Kononova V.A., Orlova M.P., Woolley A.R.** (1995) Alkaline Rocks and Carbonatites of the world. Part 2. Former USSR. London: Chapman and Hall 226 pp
16. **Kogarko L.N., Ryabchikov I.D., Sцrensen H.** (1974) Liquid fractionation. In: *Sцrensen H* (ed) The Alkaline Rocks. John Wiley, London. pp 488-500
17. **Kogarko L.N., Veksler I.V., Krigman L.D.** (1983) Magmatic crystallization of loparite in the system loparite-nepheline. Dokl, Acad Sci USSR, Earth Sci Sect 268: 1213-1215
18. **Kogarko L.N., Williams T., Osokin E.D.** (1996) The evolution of loparite compositions in the Lovozero massif. Geochem Int 34: 262-265

--

---

19. **Kramm U., Kogarko L.N.** (1994) Nd and Sr isotope signatures of the Khibina and Lovozero agpaitic centres, Kola alkaline province, Russia. *Lithos* 32: 225-*242*
20. **Kravchenko S.M., Saytsev Ye.I., Shatagina Ye.V.** (1974) Uranium as an indicator of magmatic processes of formation of differentiated intrusives (with Lovozero pluton as an example). Dokl, Earth Sci Sect 218: 215-218
21. **Marsh B.D., Maxey M.R.** (1985) On the distribution and separation of crystals in convecting magma. J Volc Geotherm Res 24: 95-150.
22. **Mitchell R.H.** (1996) Perovskites: a revised classification scheme for an important rare earth element host in alkaline rocks. In: *AP Jones, F Wall, CT Williams* (eds), Rare Earth Minerals: Chemistry, origin and ore deposits Mineralogical Society Series 7, Chapman and Hall, London, pp 41-76
23. **Mitchell R.H., Chakhmouradian A.R.** (1996) Compositional variation of loparite from the Lovozero alkaline complex, Russia. Can Min 34: 977-990
24. **Naslund H.R., McBirney A.R.** (1996) Mechanisms of formation of igneous layering. In: *Cawthorn RG* (ed) Layered Intrusions. Developments in Petrology 15. Elsevier, Amsterdam, pp 1-43
25. **Parsons I**. (1987) Origins of Igneous Layering. Reidel Publishing Company, Dordrecht, 531
26. **Ramsay W., Hackman V.** (1894) Das Nephelinsyenitgebiet auf der Halbinsel Kola, I. Fennia. Bull Soc Geogr Finlande. Helsingfors, 11 (2): 1-225
27. **Shablinskiy G.N.** (1963) On the minor structure of the Khibina and Lovozero plutons. Trans Leningrad Nat Hist Soc 74: 41-43
28. **Smirnov V.I.** (1976) Rare earth deposits. In: Geology of Mineral Deposits. NEDRA, Moscow. pp. 116-119
29. **Sparks R.S.J., Huppert H.E., Koyaguchi T., Hallworth M.A.** (1993) Origin of modal and rhythmic igneous layering by sedimentation in a convecting magma chamber. Nature, London 361: 246-249
30. **Veksler I.V., Kogarko L.N., Krigman, L.D.** (1983) Phase equilibria in the loparite-nepheline system. Geokhimiya 1203-1208
31. **Veksler I.V., Kogarko L.N., Krigman L.D., Senin V.G.** (1989) Loparite crystallization from lujavrite under dry and saturated conditions. Geochem Int, 26(9): 15-24
32. **Vlasov K.A.., Kuz'menko M.V., Es'kova E.M.** (1966) The Lovozero Alkali Massif. Oliver and Boyd, Edinburgh 627 pp (first published 1959 by Akademii Nauk SSSR, Moscow)
33. **Vorob'eva O.A.** (1938) On the genesis of the loparite deposits of the Lovozero massif. Izvestia Akad Sci USSR, Geol, Ser, 3
34. **Williams C.T.** (1996) Analysis of rare earth minerals. In: *AP Jones, F Wall, CT Williams* (eds) Rare Earth Minerals: Chemistry, origin and ore deposits, Mineralogical Society Series 7, Chapman and Hall, London, pp 327-348
35. **Wцrner G., Beusen J.-M., Duchateau N., Gijbels R., Schminke H.-U.** (1983) Trace element abundances and mineral/melt distribution coefficients in phonolites from the Laacher See volcano (Germany). Contr Min Pet 84: 152-173

UDK 552.323.6

Kimberlites of Yakutia: Standard and Anomalous Indications

A.Y. Rotman, I.N. Bogush, O.V. Tarskikh

Yakutian Geological Enterprise of Exploration, Research and Development (YaGEER&D) CNIGRI, ALROSA Co. Ltd., 678170, Chernyshevsky sh. 7, Mirny, Republic Sakha (Yakutia), Russia

In the result of performed investigations as well as analysis and systematization of available data sufficiently kimberlite nature of Mirny, Nakyn, Alakit-Markhinsky, Daldyn and Verkhne-Munsky fields' bodies has been established. Kimberlites and convergent to them rocks take part in the structure of pipes and veins of Kuranakhsky, Luchakansky, Dyukensky, Birigindinsky, Ary-Mastakhsky and Starorechensky fields and carbonatites prevail in the structure of Orto-Yarginsky field bodies. Specific features of petrographic-mineralogical composition and petrogeochemical properties of various fields' kimberlite rocks are shown, and specifics of diamond indicator minerals is reflected: garnet, picroilmenite, spinel, in particular.

Original and literary materials on petrography, mineralogy and geochemistry of kimberlites – the basic magmatic source of diamonds, are given. Each kimberlite body represents an individual target by totality of heterogeneous indications not repeating in nature. At the same time there are some typical for all of them features which are as follows: a) complicated geological structure of most diatremes; b) narrowing of diatremes with depth and gradual transition into dyke bodies – intake channels; c) the share of admixture material of country rocks becomes smaller with depth; d) the content of deep kimberlite minerals in the vertical section varies with their relatively consistent correlation; composition of minerals practically does not change with depth; e) the scales of secondary kimberlite reprocessing with depth usually decrease. Composition of abyssal (mantle) minerals (pyrope, picroilmenite, chromospinelide and others), crystal morphology and physical properties of diamonds are differentiated at the level of a province, field and each pipe. The registered variations of kimberlite occurrence composition from south to north and north-east of Yakutian kimberlite province indicate elements of lateral zonality of its lithosphere mantle, probable reason of which was the change of deep geodynamic situations.

INTRODUCTION

Kimberlites are distinctive volcanic ultrabasic sufficiently olivine rocks with increased alkalinity at their potassic bias. The presence of unique accessory – diamond in many occurrences is one of its characteristic indications. In connection with this kimberlites represent the main magmatic type of primary deposits of this mineral from which about 80% of natural diamond raw material is mined. In spite of half a century period of studying kimberlite pipes of Yakutia and even longer period – of South Africa the form of their occurrence, composition and indications of diamondiferousness remain the most interesting questions of geological science and practice. The problems of their genesis, nature of diamondiferousness, mechanism of diatreme formation and structural control of occurrences are actual and debatable as before.

--

The received original and literary materials about petrography, mineralogy and geochemistry of kimberlites – basic magmatic source of diamonds, testify about heterogeneity of kimberlite formation processes and polyfacial structure of diatremes. Mantle parageneses of minerals from kimberlites and related to them rocks were studied for purposes of making diamondiferous paragenetic associations specific. Spectra of rare earth elements in rocks of various pipes were determined. Petrologic-mineralogical characteristics of industrially diamondiferous kimberlites and xenoliths of mantle rocks from them were shown; basic petrologic-mineralogical characteristics of different in age diamondiferous rocks with various parameters of diamondiferousness were determined. The registered composition variations of kimberlite occurrences from south to north and north-east of Yakutian kimberlite province indicate elements of lateral zonality of its lithosphere mantle.

In the result of performed investigations, analysis and systematization of available data sufficiently kimberlite nature of Mirny, Nakyn, Alakit-Markhinsky, Daldyn, and Kuranakhsky fields' bodies has been established. Kimberlites and convergent to them rocks take part in the structure of pipes and veins of Luchakansky, Dyukensky, Birigindinsky, Ary-Mastakhsky and Starorechensky fields and carbonatites prevail in the structure of Orto-Yarginsky field bodies. Specific features of petrographic-mineralogical composition and petrogeochemical properties of various fields' kimberlite rocks are shown, and specifics of diamond indicator minerals is reflected: garnet, picroilmenite, chromospinelides, in particular.

INTERNAL STRUCTURE SPECIFIC FEATURES OF KIMBERLITE OCCURRENCES

Pipes of explosion (or diatremes) are the main form of kimberlite occurrence. Upper parts of these pipes are crowned by crater erections and at depth (down to 1000-2500 m from surface) the bodies change into dykes, rarely sills and independent dykes (veins) are registered. Integrity of crater parts depends on their thickness and size of "postkimberlite" erosion slice of the territory and root parts are exposed only in individual pipes due to large depth of bedding. Conformably to generalized section of diatremes in kimberlite occurrences one can observe representatives of three facies – hypabyssal (subvolcanic), diatreme (volcanic, and crater (explosive). The first one is represented by porphyric kimberlites (PK), infilling dykes, veins, and stocks. Diatremes are composed as a rule be kimberlite breccias (KB) and autolithic kimberlite breccias (AKB). Fragments of crater parts are filled with kimberlite tuffs (KT) and tuff breccias (KTB). Among the main rock types of different facial attachment differences in quantitative-qualitative spectrum of minerals and in chemical composition are found. Sometimes tearing contacts are observed, as well as presence of fragments of some of them in others. Composition of kimberlites differs from other magmatic rocks by mineral combination of the deepest mantle paragenesis including, together with diamond, its paragenetic indicator minerals – pyrope, chrome-spinel, picroilmenite, and prevailing in volume low-temperature mineral associations (carbonates, serpentine, micas and others).

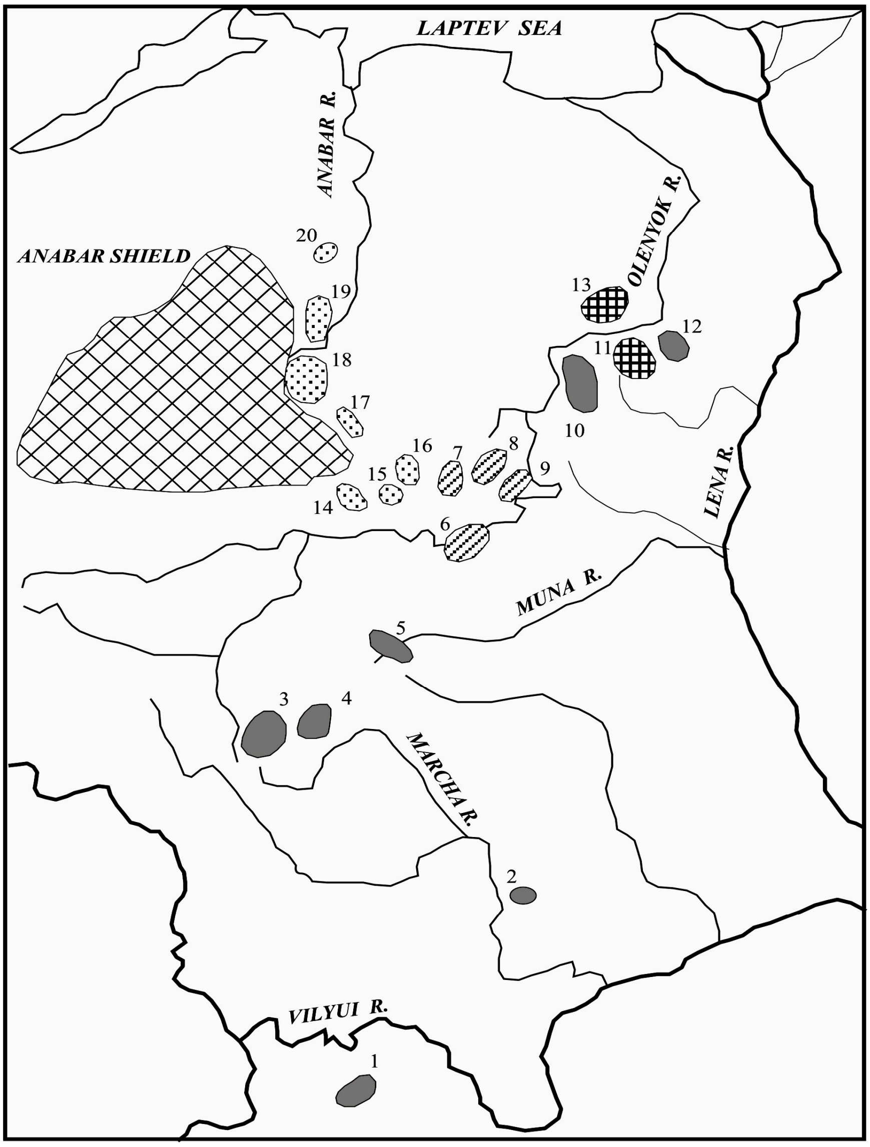

Fig. 1. **Scheme of kimberlite fields' location in Yakutian kimberlite province.**

Numerals stand for fields: 1 – Mirny, 2 – Nakyn, 3 – Alakit-Markhinsky, 4 – Daldyn, 5 – Verkhne-Munsky, 6 – Chomurdakhsky, 7 – West-Ukukitsky, 8 – East-Ukukitsky, 9 – Ogoner-Yuryakhsky, 10 – Merchimdensky, 11 – Molodinsky, 12 – Toluopsky, 13 – Kuoyksky, 14 – Kuranakhsky, 15 – Birigindinsky, 16 – Luchakansky, 17 – Dyukensky, 18 – Ary-Mastakhsky, 19 – Starorechensky, 20 – Orto-Yarginsky.

Group disposition and formation of zones or belts (Fig. 1) are one of characteristic indications of kimberlite occurrences of both Yakutia and other regions of the World. Aggregates of bodies often form chains in addition. Diatremes with preserved fragments of crater parts are notable for Alakit-Markhinsky kimberlite field – pipes Yubileynaya, Krasnopresnenskaya and others.

--

The firs one is the largest in Russia with 59 hectare area [16]. Aggregates of kimberlite occurrences (fields) occupy hundreds of square kilometers, discovering the tendency of direct correlation of a field's area and quantity of kimberlite bodies and reverse correlation of vein bodies' density per unit of area with diamondiferousness of the field. In most cases various stratigraphic levels of terrigenous-carbonaceous thickness of Lower Paleozoic serve as the hosting environment.

Researchers acknowledge complexity and inconsistency of many material characteristics of kimberlite rocks, and in the first turn of mineral composition. Heterogeneity of kimberlites is stipulated by availability of deep and country cocks' xenoliths, availability of numerous mineral-phenocrysts enclosed in serpentine-carbonaceous binding mass, which represent products of abyssal nodules' disintegration in most cases. Inconsistency of interpretation of kimberlite mineral composition is aggravated by dualism of their chemism. They simultaneously possess indications of both ultrabasic and alkaline-basaltic rocks [11].

At the same time it seems undoubted that part of indicative kimberlite minerals has its own kimberlitic but polygenic nature.

The aspect about origin of kimberlite rocks' varieties in poly-phase systems in the result of differentiation of unified initial melt seems to be very fruitful with origin of secondary hotbeds in a number of cases at a definite stage of the process, segregating from the basic one and further evolving as independent systems [29]. It is possible that formation of non-diamondiferous kimberlite from in-pipe veins of pipe Mir owes to this very process. Without going into details of kimberlite formation models we'll note that in all cases kimberlite (or protokimberlitic) magma is considered as the result of partial melting of upper mantle material and subsequent evolution of melts.

By present time vast actual data have been collected on material composition of prevailing mantle paragenesis carried by kimberlites to the surface in the form of abyssal xenoliths and mineral-products of their disintegration. To a sufficiently smaller degree systematic geochemical investigations were carried out, which still brought most significant results concerning specific features of two basic processes in the depths of the Earth – mantle metasomatism and partial melting of mantle substrata, bringing to the appearance of protomelts, crystallizing later on surface in the form of broad spectrum of diamondiferous kimberlites and related rocks.

The problem of interrelation of mantle material fragments and hosting them kimberlites remains in a number of core ones in modern petrology, for it can uncover additional evidence about formation processes of various especially deep melts under ancient platforms. Consideration of all these questions requires in its turn generalization and analysis of accumulated data on material composition of discrete groups of various mantle rocks – dunites, garnet and spinel peridotites, pyroxenites, eclogites, ilmenite- and phlogopite-bearing paragenesis, - being potential suppliers of diamonds and other abyssal material into kimberlites. In other words it is necessary to consider those parameters and processes, analysis of which can help in deeper understanding of kimberlite origin mechanisms and reasons of their different productivity.

The main morphological type of kimberlite occurrences of Yakutia, as well as other provinces of the World, - diatremes, which discover large variety in size, morphology, depth of magmatic hotbeds' location, internal structure, specific features of infilling rocks' composition, content and composition of abyssal material, degree and character of reprocessing kimberlites by postmagmatic processes, content, morphology, and physical properties of diamonds. Mechanism of kimberlite occurrence formation is most close to volcanoes of central type. Diatremes of kimberlites are characterized as a rule by multi-phase structure with distribution of rocks of not less than two phases of intrusion: of the first hypabyssal one, represented by porphyric kimberlites, the second volcanic one, represented by various kimberlite breccias, and the third explosive one, represented by tuff breccias and tuffs. Distinguishing differences between them by mineral composition of the basic mass and indicator minerals (pyrope, chromospinelides, picroilmenite), abyssal xenoliths and petrogenic oxides (SiO_2, TiO_2, FeO, MgO, CaO, K_2O, Cr_2O_3) is of important significance. Studying paragenesis of kimberlite indicator minerals and xenoliths of mantle rocks is an actual constituent of scientific research of diamond primary deposits, as well as investigation of broad spectrum of secondary minerals, the quantity of which is about eighty which in the result contribute to the solution of a number of theoretical and practical questions.

Is it was stated above, the structural scheme of diatremes responds to typical volcanic erections of maar-diatreme type [19] and is confirmed by actual material received in the result of studying complex in structure pipes Yubileynaya, Krasnopresnenskaya, Odintsova [16], results of studying pipes of Arkhangel'sk province [2], and it is also described by many researchers in Australia [15], in South Africa [4 et al.], in Angola [26], in Canada [25], in USA [22], starting from the known work of D. Hawthorne on the model of a kimberlite pipe [9], generalizing works on kimberlites by G. Dowson [6], C. Clement and E. Skinner [5], R. Mitchell [23, 24] and others. The main specific features of kimberlite diatremes may comprise the following: absence of large volumes of displaced rocks; absence of abyssal complexes; specifics of petrographic-mineralogical and petrogeochemical indications (relative to other ultrabasic rocks); mainly carrot-like shape (the shape of upturned cone); spectrum of volcanic formations, characterizing three-phase section (crater, diatreme, and root hypabyssal zone) and differing from each other; saturation with volatiles at high share of CO_2; relatively low-temperature character of prevailing part of kimberlite materials; presence of poorly crystallized sites and other indications of fast intrusion; availability of xenoliths of mantle, crust, and country rocks with most angular shape of the latter; presence of diamonds; examples of diatreme transition into dykes; indications of explosive genesis; availability of pre-pipe, sin-pipe, and post-pipe dykes; absence of thermal metamorphism; broad qualitative-quantitative variations of mineral

---

--

composition between communities of bodies and individual occurrences. One should take into account the factor of different ages of kimberlite occurrences as well. In spite of wide value spread of absolute age, received with the help of applying different methods, kimberlite fields may be unified into four age ranges [1, 8, 7 and others]: 1) S_1-D_2 (420-380 Ma) – Chomurdakhsky, West-Ukukitsky, East-Ukukitsky, Ogoner-Yuryakhsky; 2) D_2-C_1 (380-340 Ma) – Mirny, Nakyn, Alakit-Markhinsky, Daldyn, Verkhne-Munsky, Merchimdensky, Toluopsky; 3) T_1 (245-240 Ma) – fields of Anabar group – Kuranakhsky, Birigindinsky, Luchakansky, Dyukensky, Ary-Voltakhsky, Starorechensky (Nizhniy-Kuonamsky), and Orto-Yarginsky; 4) J_2-K_1 (170-140 Ma) – Molodinsky (Verkhne-Molodinsky) and Kuoyksky (see Fig. 1). According to the materials of Zaitsev A.I., executive of the Institute of diamond and precious metals geology SB RAS, and his colleagues, kimberlites of Middle Paleozoic age are present in Dyukensky and Ary-Mastakhsky fields together with kimberlites of Mesozoic age.

When describing kimberlite rocks following terms were used: Porphyric kimberlites represent rocks of massive, in some sites of breccia or breccia-like texture, in which heterogeneous clastic material is cemented by macrocrystalline, rarely microcrystalline kimberlite having massive texture and porphyric structure. Porphyric structure is determined by phenocrysts of olivine or pseudomorphs on them, and the basic mass is composed by micro-grained or cryptocrystalline serpentine-carbonaceous mixture with microlite of olivine, monticellite, perovskite, phlogopite, apatite, ilmenite, and magnetite at usual presence of accessory phenocrysts of pyrope, chromites, picroilmenites, and pyroxenes. The basis for distinguishing structural varieties of this kimberlite type is constituted by specific features of structure (shape, value, grade, distribution character of rock-forming phenocrysts) and qualitative correlation of microlites and serpentine-carbonaceous formations in the basic mass. It is notable that two, sometimes three generations of olivine and phlogopite are distinguished, and varying number of fine (to powder-like) secretions of magnetite, small crystals of perovskite, apatite, secondary mica, calcite, and sulphides are registered in the basic mass of rocks. In order to divide rock-forming minerals-phenocrysts according to stages (generations) of crystallization the following sizes and morphological features are used: relatively small (up to 1-2 mm) crystals of the second generation with distinctly expressed crystallographic faceting respond to kimberlite stage of crystallization proper, and the first (proto-kimberlitic) generation is represented by clastic secretions of larger than above noted size.

Manifestation of breccia texture and availability of noticeable (more than 7 – 10 vol.%) number of inclusions of hypabyssal facies kimberlites, fragments of enclosing rocks (cover and basement) and macrocrysts of mantle minerals serves as indication of eruptive-fragmental rocks and is the basis for distinguishing eruptive kimberlite breccias (or kimberlite breccias). Availability in the latter different in size spherical, subspherical, often irregular in shape macro- or micro-inclusions “kimberlite in kimberlite” – autoliths allows distinguishing the group of autolithic kimberlite breccias. In addition to autoliths noteworthy are sporadically occurring taxitic textural heterogeneities in kimberlites (ataxites and eutaxites) which, in opinion of B.M. Vladimirov and co-authors [17], could arise in melt owing to irregular distribution of water in it. Therefore, one can distinguish three varieties among eruptive kimberlite breccias: autolithic, ataxitic, and eutaxitic. By the size of fragments kimberlite breccias are divided into coarse-fragmental, medium-fragmental, and fine-fragmental, and by character of kimberlite-cement – porphyric, clastoporphyric, autolithic (or lavoclastic) and lithocrystalloclastic (lavocrystalloclastic) structures. The binding mass in most cases consists of varying quantities of serpentine and carbonate in coarse grains. Rather often besides serpentine and carbonate the same minerals as in autolithic formation are present in it but in smaller quantities. Xenoliths and abyssal inclusions are located in autoliths and outside them.

On the whole, according to available geological data, KB and AKB at subordinate share of PK sub-volcanic phase occupy the main part of volume in most kimberlite pipes of Yakutia, except diatremes of Verkhne-Munsky field. AKB is a petrographic type in industrial deposits of diamonds, determining productivity of targets (pipes Mir, International, Botuobinskaya, Nyurbinskaya, Aykhal, Yubileynaya, Udachaya and others). However, reverse regularity is observed in medium- and low-diamondiferous pipes (pipes Zapolyarnaya, Komsomol’skaya-Magnitnaya, Dal’nyaya, Iskorka and others). By character of interrelations of sub-volcanic (PK) and volcanic (KB and AKB) intrusion phases within the province one can distinguish three groups of pipes. Kimberlite bodies where PK are preserved in primary bedding and form individual ore columns are referred to the first group. Their volume correlations with KB (AKB) of volcanic phase vary from 1:1 (pipes Zapolyarnaya, Baitakhskaya and others); 1:2 (Dal’nyaya, Sytykanskaya, Molodost’ and others); 1:4 (Yubileynaya, Botuobinskaya, Udachnaya); 1:10 (Komsomol’skaya, Geophysicheskaya and others). The pipes where PK is present in AKB in the form of multiple fragments and individual large (tens of meters) blocks are referred to the second group, but they already do not form ore columns (pipes Krasnopresnenskaya, Kylakhskaya, Vostok, Mir, Nyurbinskaya and others). Volumetric correlations of PK and AKB in these bodies are from 1:30 to 1:100. The third group unifies kimberlite bodies where PK is present in AKB in the form of multiple small fragments (pipes Dolgozhdannaya, Zarnitsa, Zarya, 325 years of Yakutia, Markhinskaya, Leningradskaya, Yakutskaya and others). Primary deposits of diamonds and high-diamondiferous kimberlite bodies enter the first and the second groups, low-diamondiferous – are open-end for these three groups.

Kimberlite rocks of the crater part are discovered in pipes Yubileynaya, Krasnopresnenskaya and named after Odintsov, which encompass the whole spectrum of formations including representatives of explosive-fragmental, sedimentary-volcanoclastic, volcanogenic-sedimentary and sedimentary-clastic groups of rocks. The group of explosive-fragmental rocks is represented by: a)

--

tuffs and tuff breccias, consisting of clastic material of kimberlites without sufficient admixtures, b) xeno-tuffs and xeno-tuff breccias, containing admixture of extraneous rocks' fragments of various size in less than 50% quantity. Tuff breccias – breccia kimberlite rocks formed in the result of condensing and cementing of unsorted coarse-fragmental porous angular or low-rounded volcanoclastic material submerged into more fine-grained tuff cement. Tuffs are formed from hard products of kimberlite eruptions and fragments of hosting environment, subsequently packed and cemented. The rocks are divided by size of prevailing fragments: coarse-fragmental (agglomerate), large-fragmental (psephitic), medium-fragmental (psammitic), thin-fragmental (silty), and by character of fragments – lithoclastic (from fragments of rocks), crystalloclastic (from crystals and their debris), occur very seldom, and mixed crystalloclastic, most widely distributed. In a number of cases, when observing sharp contacts with other rocks, it would be more correct to call them tuffisites – intrusive tuffs. Sometimes intensive hydrothermal cementation of rocks gives the rocks the appearance of kimberlite breccias and their belonging to tuffs may be detected by stratified textures and saponite (montmorillonite)-chlorite-hydromicaceous (with alternative correlations) character of the cement.

Sedimentary-volcanoclastic rocks (tuffites) are distributed in kimberlite erections rather restrictedly and may be conventionally distinguished in individual samples of pipe Krasnopresnenskaya. Among the basic mineral types of cement carbonaceous, montmorillonitic, chlorite, chlorite-hydromicaceous and others are distinguished.

The group of volcanogenic-sedimentary rocks includes formations with more than 50% content of sedimentary material, where kimberlite material (40-20% and less) is present in the form of debris of breccias, autoliths, grains of indicator-minerals, etc.

Synchronous to intrusion of kimberlites and asynchronous to intrusion phases formations developed mainly after the previous groups should be referred to sedimentary-clastic formations. Most of them are distinguished under the name "epiclastic sediments" which include the spectrum of sedimentary formations with less than 1-2% content of kimberlite material, heterolithic breccias with less than 1-2% content of kimberlite material, consisting of rock fragments of the region's geological section. They are often combined with the previous group in foreign classifications and distinguished as redeposited formations - resedimented volcanoclastic deposits, formed in the result of deposition in water, fall of the stones, rockslide, avalanches, flows of grains and viscous mass flows. Broad development of temporary flows' deposits is referred to characteristic features of crater erections, which is expressed in formation of sedimentary sections with repeating mini- and micro-foliation, which is emphasized by distribution of psephitic material or argillaceous interlayers. It is natural to distinguish alluvial sediments with gravel-shingle material in craters, which possess very strong placer-forming properties, as a rule, and due to it are enriched by kimberlite indicator minerals.

Analyzing distribution of the noted spectrum of kimberlite rocks in the volume of weakly eroded diatremes of Alakit-Markhinsky field one can ascertain that pyroclastic kimberlite tuffs and tuff breccias compose upper parts of craters forming bodies with thickness from 30-35 m (the Odintsov pipe) to 230-250 m (pipe Yubileynaya). In the latter case the thickness of pyroclastic formations was disturbed by much later intrusion phase of autolithic kimberlite breccia. The thickness of tuff breccia in the crater part of pipe Krasnopresnenskaya reaches 50 m, and the thickness of occurring higher epiclastic tufogenic material in the form of interlayers and lenses in terrigenous rocks of Lower Carboniferous Tegeryukskaya suite (crater-lacustrine sediments) – 10-57 m. The supposed general thickness of crater deposits of the pipe’s central part reaches 100-110 m.

GEOCHEMICAL PROPERTIES OF KIMBERLITE ROCKS

Analysis of petrogeochemical properties of kimberlite and convergent to them rocks allows to ascertain noticeable variations in the content of petrogenic and admixture elements which are determined both by endogenous and exogenous factors. Petrogeochemical investigations allow concretizing diagnostics of rocks and determine their specifics within fields, groups, and individual bodies. On the whole, by chemical composition the rocks of all fields of both southern and northern parts of the province respond to ultrabasic rocks, characterized by approximately equal quantity of SiO_2 and MgO, high content of magnesium and increased ratios of magnesium to iron. This tendency preserves both in the least altered and eroded rocks and in intensively carbonatizated kimberlites and picrites. The latter ones, as well as carbonatites of Orto-Yarginsky field indicate evidence of decreased (in comparison with clarkes for ultrabasic rocks) concentrations of Si, Fe, Mg, Cr, Ni at raising the proportion of Ti, Al, K, P, Sr, Zr, Nb, Ta and other elements peculiar to alkaline rocks. Kimberlite rocks proper differ, together with the highest contents of Mg, Cr, and Ni, by the largest values of Mg/Fe and Ni/Co ratios. Kimberlites of Yakutia, and in the first turn of industrially diamondiferous bodies, correspond to kimberlites of group I of South Africa by correlation of oxides of potassium and titanium, aluminium and calcium (Fig. 2, 3), as well as by correlation of zirconium and niobium, niobium and lanthanum, cerium and strontium. In a number of bodies of individual northern fields (Luchakansky, Ogoner-Yuryakhsky) at this, increased (more than 3 wt.%) contents of TiO_2 (Table 1) are observed. Besides, medium compositions of individual pipes (Dachnaya, Sputnik), distinguished by low concentration of titanium oxide, fall into the field of orangites with the increase of K2O proportion. Kimberlites of Nakyn field pipes also stand apart by chemism, in which rather low – less than 0.5 wt.% - content of TiO_2 is registered, as in pipes Aykhal and Collectivnaya (Alakit-Markhinsky field), Gornyatskaya (Daldyn field). Correlation analysis of alumina

--

and calcium oxide indicates most consistent kimberlite structures of Verkhne-Munsky field. In other fields with industrial diamondiferousness enrichment by CaO is registered, which is expressed by high average content of lime in kimberlites of Mirny and Alakit-Markhinsky fields (see Table 1), and in the fields of Anabar group - Al_2O_3 (Ary-Mastakhsky and Dyukensky fields) or both oxides simultaneously (Birigindinsky and Luchakansky fields). On the whole kimberlites of Anabar group fields are distinguished by higher concentrations of TiO_2, K_2O, FeO, and often P_2O_5 with regard to those with commercially significant productivity.

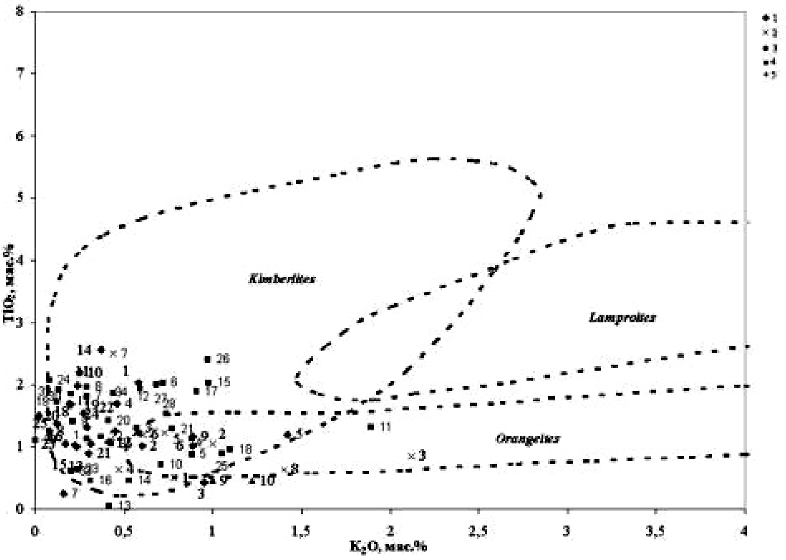

Fig. 2. **Diagram of K_2O и TiO_2 (wt.%) correlations in kimberlites of the southern part of Yakutian kimberlite province.**

Notation conventions: 1 – Mirny field (pipes” 1 – International, 2 – Mir, 3 – Dachnaya, 4 – XXIIIrd CPSU Congress, 5 – Tayezhnaya, 6 – Amakinskaya, 7 – anomaly A-21, 8 – Sputnik); 2 – Nakyn field (pipes: 9 – Nyurbinskaya, 10 – Botuobinskaya), 3 – Alakit-Markhinsky field (pipes: 1 – Komsomol’skaya, 2 – Yubileynaya, 3 – Aykhal, 4 – Druzhba, 5 – Iskorka, 6 – Kismet, 7 – Collectivnaya, 8 – markoka, 9 – Nachal’naya, 10 – neva, 11 – NIIGA, 12 – Odintsova, 13 – Octyabr’skaya, 14 – Olympiyskaya, 15 – Ottorzhenets, 16 – Pobeda, 17 – Podtrappovaya, 18 – Geophysicheskaya, 19 – Smezhnaya, 20 – Souvenir, 21 – Svetlaya, 22 – talisman, 23 – Veselaya, 24 – Yunost’, 25 – Zarya), 4 – Daldyn field (pipes: 1 – Dolgozhdannaya, 2 – Zarnitsa, 3 – Irelyakhskaya, 4 – Udachnaya, 5 – Udachnaya-western, 6 – Festival’naya, 7 – Aeromagnitnaya, 8 – Aerosyemochnaya, 9 – Academicheskaya, 10 – Daikovaya, 11 – Electra, 12 – Evrika, 13 – Gornyatskaya, 14 – Iksovaya, 15 – Il’menitovaya, 16 – Letnyaya, 17 – Lyubimaya, 18 – Mastakhskaya, 19 – Malyutka, 20 – Nevidimka, 21 – Nyurbinskaya, 22 – Osennyaya, 23 – Oval, 24 – Polyarnaya, 25 – Polunochnaya, 26 – Rot-Front, 27 – Saratovskaya, 28 – Sibirskaya, 29 – Sosednyaya, 30 – Studencheskaya, 31 – Ugadaika, 32 – Ukrainskaya, 33 – vesnushka, 34 – Volzhanka, 35 – Zimnyaya). Composition boundaries of magmatic diamondiferous rocks’ basic types according to Mitchell, 1995, Smith et al., 1985.

Comparing industrially diamondiferous kimberlites of southern part of Yakutian province (Mirny, Nakyn, Alakit-Markhinsky, Daldyn, and Munsky kimberlite fields) with low-diamondiferous and non-diamondiferous occurrences of the northern part (all fields north of the Munsky field) by distribution of elements-admixtures one can ascertain higher contents of Ni, Cr, Li, and Pt in the first ones, Co, Mn, V, Ti, Sc, Be, Ga, Ba, Sr, Zr, Nb, Ta, REE, Zn and Sn in the second ones, at approximately equal quantities of Rb, Pb, Mo, Th, and U. It should also be noted that most of the mentioned elements, except Ni, Co, Cr, Mn and Pt, are accumulated in concentrations many times prevailing the clarke ones for ultrabasic rocks.

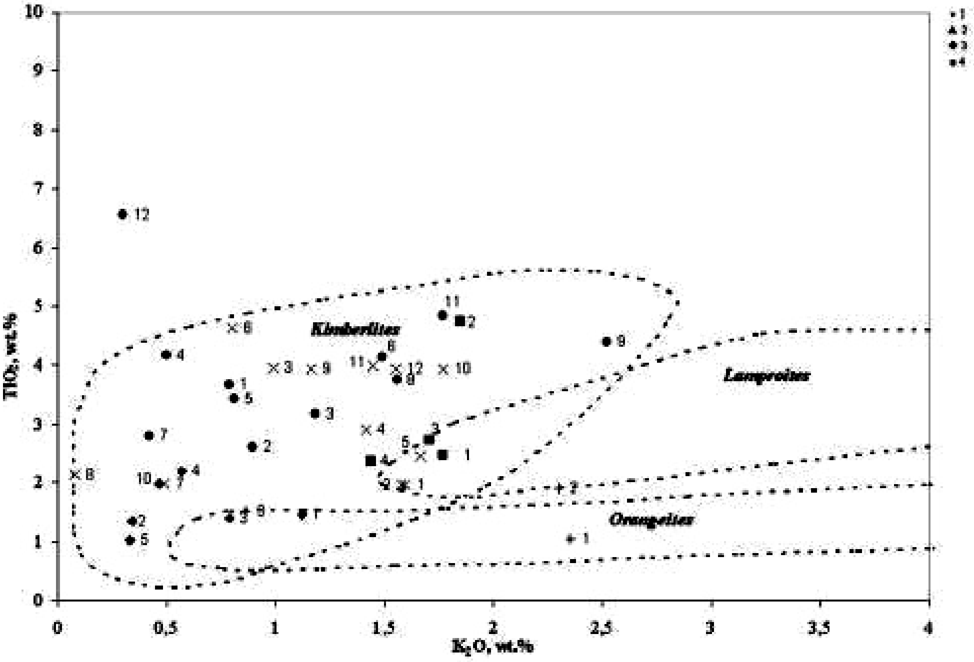

Fig. 3. **Diagram of K_2O и TiO_2 (wt.%) correlations in kimberlites of the northern part of Yakutian kimberlite province.**

Notation conventions: 1 – Verkhne-Munsky field (pipes: 1 – Deimos, 2 – Zapolyarnaya, 3 – Poiskovaya, 4 – Novinka, 5 – Komsomol’skaya-Magnitnaya); 2 – Dyukensky field (anomalies: 1 – 67/63, 2 - 12/63, 3 - 32/89, 4 - 33/89, 5 – 37/63, 6 – 41/63, 7 – 44/89, 8 - 51/89, 9 – 52/89-2, 10 – 52/89-1, 11 – 55/89, 12 – 114/63), 3 – Ary-Mastakhsky field (anomalies:1 – 1/98, 2 - 12/89, 3 - 10/98, 4 - 11/98, 5 – 103/91, 6 – 104/91, 7 – 106/91, 8 - 109/91, 9 – 194/63, 10 – 72/63, 11 – 85/89, 12 – 98/91); 4 – Luchakansky field (1 – 124, 2 – 106, 3 – 101, 4 – 103), 5 – Birigindinsky field (1 – 95/65, 2 – 96/65, 3 – 98/65). Composition boundaries of magmatic diamondiferous rocks’ basic types according to Mitchell, 1995, Smith et al., 1985.

Competence of distinguishing three petrogeochemical kimberlite groups of Yakutia is confirmed, which was suggested earlier in the process of joined investigations with colleagues from IGEM RAS [3], differing by content of titanium and a number of HFSE and LILE as well: low-titanium kimberlites (TiO_2 < 1 wt.%, Zr 44–77 ppm, Ce 21–70 ppm) developed in the Nakyn field, and represented in pipes Nadezhnaya (Chomurdakhsky field) and Ruslovaya (Kuoyksky field), moderately titaniferous kimberlites (TiO_2 1.0–2.5 wt. %, Zr 50–280 ppm, Ce 58–240 ppm), widely represented in southern fields of the province (Mirny, Alakit-Markhinsky, Daldyn, Verkhne-Munsky), but also in some pipes of northern fields (Dama, Dyanga, Mgrishnitsa and others); high-titaniferous (TiO_2 > 2.5 wt.%, Zr 125–690 ppm, Ce 100–284 ppm) diversities are registered only in a

Table 1.

--

Average chemical composition (wt.%) of kimberlite fields of Yakutia

№	FIELDS	SiO_2	TiO_2	Al_2O_3	Fe_2O_3	Cr_2O_3	MnO	MgO	CaO	Na_2O	K_2O	P_2O_5	L.O.I.	Total
1	Mirny (311 an.)	27,11	1,07	3,01	5,62		0.13	17.85	20.14	0.32	0.94	0.63	23.17	99,89
2	Nakyn (547)	29.21	0.46	3.99	5.51		0.13	23.07	14.12	0.01	1.11	0.47	22.16	100,21
3	Alakit-Markhinsky (437)	26,25	1,43	2,55	6,50	0,15	0,18	20,80	18,07	0,08	0,63	0,52	22,98	99,91
4	Daldyn (658)	27,00	1,30	2,64	6,45		0,13	25,08	14,99	0,08	0,46	0,39	21,30	100,08
5	Munsky (347)	26,50	1,51	2,76	7,94	0,14	0,11	26,73	12,38	0,16	0,74	0,81	20,17	99,96
6	Chomurdakhsky*	25,55	2,62	3,18	9,49	0,10	0,14	23,95	13,37	0,16	0,99	0,86	19,45	99,86
7	West-Ukukitsky*	26,55	3,72	4,04	11,31	0,09	0,18	21,28	13,14	0,13	1,53	0,96	16,94	99,87
8	East-Ukukitsky**	34,04	3,32	3,52	15,57	0,10	0,12	23,83	5,95	0,09	1,34	0,54	11,36	99,78
9	Ogoner-Yuryakhsky*	28,04	3,90	4,46	9,68	0,14	0,16	21,75	11,77	0,09	2,12	0,68	17,40	100,18
10	Merchimdensky*	24,98	2,87	3,44	8,52	0,11	0,13	19,57	16,28	0,17	1,63	0,74	21,12	99,56
11	Molodinsky*	21,12	2,42	2,63	8,96	0,11	0,24	16,16	22,51	0,22	0,98	1,12	23,39	99,86
12	Toluopsky*	29,35	2,48	4,89	9,50		0,19	13,09	18,41	0,98	1,65	0,49	19,48	100,51
13	Kuoyksky*	30,11	1,44	2,00	8,56	0,13	0,17	27,09	10,54	0,15	0,66	0,41	18,69	99,95
14	Kuranakhsky*	29,66	2,12	3,58	10,01	0,18	0,18	24,37	10,54	0,11	1,49	0,95	16,61	99,80
15	Birigindinsky (12)	22,74	1,53	4,23	10,55		0,18	8,54	25,82	0,03	1,70	1,45	23,18	99,95
16	Luchakansky (31)	36,30	2,75	5,69	10,85		0,16	20,18	11,13	0,12	1,67	0,49	10,96	100,30
17	Dyukensky (34)	25,97	2,98	3,43	12,17		0,17	23,78	14,91	0,01	1,36	1,01	14,66	100,45
18	Ary-Mastakhsky (55)	26,47	3,48	4,27	13,10		0,17	17,42	16,04	0,01	1,04	1,07	17,02	100,09
19	Starorechensky*	26,51	2,94	4,39	11,20	0,11	0,19	18,39	16,23	0,21	1,17	0,72	17,88	99,93

Note: Published data are used from works of *[14], **[18].

number of northern kimberlite fields of the province. It has been proven experimentally that with the growth of temperature silicate melts are enriched by titanium and zirconium. Taking this regularity into account one can assume that, evidently low-titaniferous kimberlites of the Nakyn field, characterized by low concentrations of titanium and zirconium, cerium, niobium, and rare-earth elements, were formed at somewhat decreased temperatures in comparison with kimberlites of other fields of the province. It should be noted that in most kimberlite pipes of the northern part of the province higher (more than 300 ppm) total content of rare-earth elements is registered (Table 2) while in southern fields this indicator notably varies: concentration of REE is usually lower of the registered level in kimberlite breccias of pipes Mir, Botuobinskaya, Komsomol’skaya, Sytykanskaya, Yubileynaya, in most of the Daldyn field pipes, and it is higher in pipes Sputnik, International, 23rd CPSU Congress, Tayezhnaya, Aykhal, Krasnopresnenskaya, Molodost’, and Feinshteynovskaya. The determining contribution to these concentrations is made by La, Ce, and to a smaller degree by Nd. Sierophile and lithophile elements discover rather high span of contents both between the pipes and in individual pipes, in radioactive plan most consistent are distributions in kimberlites of individual bodies and as a consequence pipes vary by this indicator.

Table 2.

Average content of rare-earth elements (ppm) in kimberlite pipes of Yakutia

№	**Pipes**	**La**	**Ce**	**Nd**	**Sm**	**Eu**	**Gd**	**Tb**	**Tm**	**Yb**	**Lu**	**Total**
1	Mir (7 an.)	71,0	120,0	43,1	6,71	1,80	4,50	0,58	0,13	0,67	0,09	248,5
2	Sputnik (2)	154,1	264,1	95,3	15,54	3,80	9,40	1,18		1,15	0,14	544,8
3	International (5)	99,7	163,3	60,3	8,83	2,22	5,90	0,68		0,71	0,08	341,8
4	XXIIIrd CPSU Congress (1)	127,0	194,0	67,0	11,00	2,82	6,90	0,91		0,89	0,10	410,6
5	Tayezhnaya (1)	224,1	319,6	89,0	12,98	3,03	7,40	0,99	0,18	0,91	0,15	658,4
6	Amakinskaya (1)	46,0	74,0	24,0	4,10	1,11	2,80	0,42		0,54	0,05	153,0
7	Botuobinskaya (5)	32,6	62,0	29,8	6,95	1,78	5,35	0,82		1,39	0,18	140,9
8	Markoka (1)	65,0	104,0	35,0	4,70	1,05	2,50	0,33		0,38	0,05	213,0
9	Aykhal (4)	125,0	203,3	73,0	10,53	2,46	5,63	0,77		0,82	0,10	421,5
10	Komsomol'skaya (1)	36,0	61,0	24,0	4,11	0,95	2,40	0,34		0,43	0,06	129,3
11	Krasnopresnenskaya (2)	83,0	150,0	48,5	7,32	1,70	4,01	0,55		0,62	0,08	275,4
12	Molodost' (1)	110,0	175,0	61,0	8,20	2,11	4,70	0,65		0,69	0,08	362,4
13	Sytykanskaya (4)	46,8	73,3	26,0	4,00	1,00	2,33	0,35		0,41	0,05	154,1
14	Radiovolnovaya (1)	76,0	123,0	39,0	5,90	1,53	3,90	0,50		0,55	0,06	250,4
15	Feinshteynovskaya (1)	103,0	168,0	62,0	9,20	2,01	6,50	0,76		0,82	0,09	352,4
16	Yubileynaya (5)	60,1	91,6	30,3	4,86	1,14	2,57	0,38	0,03	0,39	0,05	191,4
17	Udachnaya (29)	48,2	81,9	28,8	4,31	1,07	2,70	0,37	0,08	0,48	0,07	167,9
18	Zarnitsa (5)	77,0	123,8	48,2	7,06	1,70	4,00	0,56		0,68	0,08	263,1
19	Dolgozhdannaya (1)	45,0	68,0	25,0	3,58	0,85	2,30	0,35		0,50	0,06	145,6
20	Irelyakhskaya (1)	84,0	132,0	46,0	6,45	1,68	4,30	0,51		0,58	0,07	275,6
21	Dal'nyaya (1)	76,0	126,0	48,0	7,30	1,68	4,00	0,48		0,51	0,07	264,0
22	Leningradskaya (1)	48,0	72,0	28,0	4,47	1,04	2,70	0,40		0,65	0,09	157,3
23	Ukrainskaya (1)	54,0	80,0	30,0	4,58	0,82	2,50	0,37		0,49	0,06	172,8
24	Yakutskaya (2)	40,5	69,0	25,4	3,90	0,96	2,55	0,34		0,49	0,06	143,2
25	Chomur (1)	140,0	245,0	105,0	18,90	4,84	11,10	1,51		1,74	0,20	528,3
26	Snezhinka (1)	97,0	146,0	50,0	7,30	1,70	3,60	0,50		0,53	0,08	306,7
27	Malo-Kuonamskaya (1)	118,0	205,0	75,0	12,00	2,62	5,50	0,80		0,71	0,08	419,7
28	Ivushka (1)	76,0	140,0	58,0	9,80	2,20	5,50	0,79		1,05	0,14	293,5
29	Ruslovaya (1)	37,0	63,0	24,0	3,60	0,89	1,70	0,27		0,34	0,04	130,8
30	Obnazhennaya (2)	145,5	224,0	77,0	11,85	2,99	6,90	0,92		0,93	0,10	470,2

Note. Analyses were performed in Analytical Center of United Institute of Geology Geophysics and Mineralogy SD RAS (Novosibirsk) by INAA method in 2002-2003.

SPECIFIC FEATURES OF MANTLE XENOLITHS' COMPOSITION

Xenoliths of mantle rocks are usual constituents in most kimberlite pipes. Their petrographic spectrum is rather wide and includes the following groups [6]: 1) peridotites-pyroxenite rocks, 2) eclogites and grospydites, 3) metasomatisated peridotites enriched by amphibole and (or) mica, 4) glimmerites and "marides" (mica + amphibole + rutile + ilmenite + diopside), 5) other xenoliths. Classification of deep inclusions, based on the scheme of facies and subfacies of

--

upper mantle and composition of rocks, enjoys great popularity, which also takes into account conceptions of N.V. Sobolev [27] about typomorphic properties of garnets being in association with one or two pyroxenes: harzburgite-dunites, lherzolites, vehrlites, websterites, and free of olivine clinopyroxene-garnet associations – eclogites, identified with basalt systems. When characterizing xenoliths of deep rocks from the row of kimberlite diatremes of Yakutia Z.V. Spetsius and V.P. Serenko [28] distinguish peridotites and pyroxenite series of eclogites and eclogites-like rocks.

The shape of xenoliths is rounded as a rule, less frequently angular-rounded. The surface is smooth. The sizes usually vary from fractions of centimeter to the first centimeters. Very seldom they exceed 0.3-0.5 m in diameter. The contacts of xenoliths with hosting them kimberlite rocks are sharp. It is necessary to note that there are two points of view on probability of their falling into kimberlites: 1) as captured fragments of mantle material, 2) as cumulates (glomeroporphyric growths). Not to go into analysis of this or that point of view’s predominance it is necessary to point to a rather important role of deep rocks’ xenoliths in perception of processes of magma, kimberlite and diamond formation. Xenoliths are distributed in kimberlite bodies both by size and by quantity very irregularly.

Analysis data of various in composition xenoliths from pipes Mir, Udachnaya, Sytykanskaya, and Obnazhennaya [28] testify about prevalence of ultrabasic and basic paragenesis with garnet independently of the degree of the rocks’ diamondiferousness. A rather wide spectrum of petrographic-mineralogical varieties of xenoliths was registered in the first three mentioned pipes, therewith, and in pipe Obnazhennaya they are represented mainly by lherzolites, pyroxenites, and eclogites. Garnet and spinel peridotites and pyroxenites, dunites, various eclogites, including diamondiferous ones, metasomatisated ultramafites with ilmenite and phlogopite, glimmerites and some other types of abyssal rocks were registered in pipe Mir, with prevalence of garnet peridotites and pyroxenites among them. Pipe Udachnaya stands apart by broad distribution of broken down peridotites, and pipe Sytykanskaya – by frequent occurrence (about 15%) of ilmenite varieties. On the whole, increased quantity of hypogene inclusions is peculiar to diamondiferous kimberlite explosion pipes of Malo-Botuobinsky and Daldyn-Alakit regions. One should make a reservation here that the above described is not a regularity but a taking shape tendency: for example, in Mirny kimberlite field, together with rich pipes (Mir, International) by quantity of hypogene rocks’ xenoliths there are bodies with very low (pipe Sputnik) quantity of nodules, or almost without any at all (pipe Amakinskaya).

Quantitative variations of mantle nodules are also peculiar to kimberlite bodies of Verkhne-Munsky field – pipes both with rather high content of hypogene rocks’ xenoliths (pipes Zapolyarnaya, Novinka, Zimnyaya, and Komsomol’skaya) and the bodies in which inclusions of deep-seated rocks are not discovered yet, are present here. Low quantity of hypogene rocks’ inclusions is peculiar to most kimberlite pipes of Nizhne-Oleneksky diamondiferous region, but here a number of bodies (pipes Obnazhennaya, Ruslovaya and Slyudyanka) with rather high frequency of deep-seated nodules' occurrence is also registered. Kimberlite pipes of Sredne-Oleneksky region distinguish by higher qualitative-quantitative spectrum of hypogene inclusions, and increased quantity of ilmenite hyper-basic rocks is registered in pipes Druzhba and Chomur. Rather rare are xenoliths in kimberlite diatremes of Kuonamsky and Prilensky regions, though in the first of them nodules of deep-seated rocks occur more frequently in a number of bodies (pipes Universitetskaya, named after Komarov, and Kuranakhskaya). They are represented usually by serpentinous olivinites and peridotites, and serpentine-phlogopite and ilmenite-phlogopite rocks [10] were found in pipe Djo-northern, which is a specific feature of Kuonamsky region's kimberlites.

The analysis of data on chemical composition of hypogene inclusions indicates that among the studied samples [17] magnesia hyper-basic rocks (dunites, harzburgites, lherzolites, ortopyroxenites, clinopyroxenites, and websterites) prevail with subordinate proportion of their magnesia-ferruginous varieties – ilmenite and garnet-ilmenite lherzolites and pyroxenites. By correlation of petrogenic oxides MgO, CaO, and FeO analyzed xenoliths vary within compositions of dunite-harzburgite (magnesia hyper-basic rocks), dunite-vehrlite-pyroxene and olivinite-vehrlite (magnesia-ferruginous hyperbasic rocks) formations. Z.V. Spetsius and V.P. Serenko [28] indicated that the calculated average chemical composition of the mantle in Malo-Botuobinsky and Daldyn-Alakitsky regions corresponds to harzburgite-lherzolites by content of basic rock-forming oxides, and in Nizhne-Oleneksky – to vehrlites. Hypogene xenoliths of pipes Mir and Sytykanskaya are enriched by titanium (ilmenite varieties of peridotites and pyroxenites are its concentrator), of pipes Sytykanskaya and Obnazhennaya – by alkali, the sources of which are varieties with phlogopite and amphibole, and of pipe Mir – by chrome.

Thus, fragments of various ultrabasic and basic mantle formations are present in kimberlite pipes, qualitative-quantitative spectrum of which together with some "continuous" varieties can noticeably differ even within one region, which is seen from compositions of a number of closely located diatremes. This reflects laminar character of the mantle, variations between fields and pipes – lenslikeness and lateral changeability on the one hand, and coverage of various levels of the mantle by hotbeds of kimberlite-formation – on the other hand.

KIMBERLITE INDICATOR MINERALS

Qualitative-quantitative spectrum of deep-seated minerals, significant part of which represents the products of mantle nodules' disintegration, is much larger in kimberlites. Characteristic indications (grade and size, integrity and fissuring, colour, character of surface and its various physical-chemical alterations, internal structure and some others) of pyrope row garnets, chrome-spinellids, picroilmenites and, to smaller degree, chrome-diopsides and olivines, are used in the basis of comparative analysis of hypogene mineralogy of kimberlites.

--

Distribution of pyrope and picroilmenite in pipes is most indicative, which allows comparing individual pipes between each other (or blocks inside complex pipes). Their contents in kimberlites vary within rather wide limits – from isolated characters to 0.8-1.0% for pyrope and to 3.5% for ilmenite. Other deep-seated minerals – olivine (relics of fresh olivine), chrome-spinellids, chrome-diopside – occur more seldom in noticeable quantities in the heavy fraction. By total content (wt.%) of pyrope and picroilmenite kimberlites are conventionally divided into 4 groups: group I >1 (Mir, Zarnitsa, Dal'nyaya, Komsomol'skaya, Sytykanskaya and others); II – from 0.5 to 1 (Yubileynaya, Olimpiyskaya, Kylakhskaya and others); III – from 0.1 to 0.5 (Dachnaya, International, Botuobinskaya, Nyurbinskaya, Krasnopresnenskaya, Udachnaya, Zapolyarnaya and others); IV – less than 0.1 (Aykhal, Sputnik, named after Odintsov, Radiovolnovaya, Poiskovaya and others), and by correlation of these two minerals – into two groups: 1) with prevalence of pyrope over picroilmenite – International, Sputnik, Aykhal, Krasnopresnenskaya, Udachnaya-western, Zapolyarnaya and others; 2) with inverse correlation of these minerals – Mir, Dachnaya, Komsomol'skaya, Udachnaya-eastern and others [16]. Aykhal, International, Zapolyarnaya noticeably distinguish in the first group, and Komsomol'skaya and Iskorka – in the second. Pipes with extremely low content of picroilmenite (Botuobinskaya, Nyurbinskaya) at increasing proportion of chrome-spinellids should be noted separately.

Concentration of indicator minerals (together with properties of diamond), their correlations and some other specific features in kimberlites of Yakutia have tendency to regular change in the direction from central diamondiferous regions to northern ones. Within Yakutian kimberlite province one can distinguish two areas or subprovinces: southern – Vilyuyskaya (Mirny, Nakyn, Alakit-Markhinsky, Daldyn, and Munsky kimberlite fields) and northern – Anabar-Olenekskaya (other kimberlite fields – see Fig. 1), the bodies of which differ by content of indicator minerals, together with distinctions by diamonds and other indications.

According to the data of works [31] in Mirny kimberlite field three groups of kimberlite bodies are distinguished, which sharply differ by typomorphic features of diamonds, related probably with three separated in time phases of kimberlite magmatism (I – vein A-21, II – pipes Tayezhnaya and Amakinskaya, and III – pipes Mir, International, 23rd CPSU Congress, Dachnaya, and Sputnik). The first (the earliest) group is characterized by low content of octahedrons with prevalence of rhombic dodecahedron habit individuals. Approximately equal correlation of crystals of octahedral and rhombic dodecahedral habits at comparatively low (first percents) content of typically rounded diamonds and prevalence of diamonds with blue-pale blue photoluminescence is distinguished in the second group. The third, most high-productive group of kimberlite bodies, is characterized by sharp prevalence of coarse-laminar crystals of octahedral and transitive from it to rhombic dodecahedral habits at low (less than 10%) content of rhombic dodecahedral habit individuals, among which typically rounded diamonds are practically absent. On the whole kimberlites in Mirny field are distinguished by sharp prevalence of colorless octahedrons with increased content of admixture nitrogen in the form of A-center and noticeable contents of twins at low content of growths. This testifies about comparatively moderate temperatures of formation and increased oversaturation, which appears in high content of individuals with polycentrically growing facets and twins.

Prevalence of crystals of octahedral and transitive from octahedral to rhombic dodecahedral habits of variety I according to Y.L. Orlov, at comparatively high content of shapeless debris (especially in fine classes of size) and practical absence of typical rounded diamonds are characteristic features of the Nakyn kimberlite field diamonds. Increased content of admixture nitrogen in the form of A-center and low content of B1 and B2 defects are peculiar to dominating colorless crystals of octahedral habit, which testifies about comparatively moderate temperature of formation and low degree of oversaturation, annealing and plastic deformation. Increased content of eclogites association inclusions has been established among them. High content of coloured diamonds with coating of variety IV according to Y.L Orlov, presumably of eclogite genesis, is typomorphic feature of diamonds.

Prevalence of crystals of rhombic dodecahedral habit at variable (depending on the degree of productivity) contents of typical rounded diamonds of variety I according to Y.L. Orlov is peculiar to diamonds from kimberlite bodies of Daldyn-Alakit region. Increased aggregation of nitrogen centers at significant concentration of B_2 and B_2 (P) – centers, are characteristic of them, testifying about maximum temperatures of formation in comparison with other regions, which brought to annealing and plastic deformation of crystals. Genesis of most diamonds – ultrabasic, and for diamonds of the Aykhal and Yubileynaya pipes increased contents of crystals with coating, presumably of eclogites genesis, are typical. The content of hail-crystalline growths of variety VIII diamonds is maximal among explotable primary deposits.

Diamonds of Verkhne-Munsky field kimberlites are similar to those from kimberlite bodies with hail-industrial diamondiferousness of Daldyn-Alakit region and are characterized by prevalence of rhombic dodecahedral habit crystals at high content of typical rounded diamonds being unfavorable factor of diamondiferousness [31]. This testifies about significant dissolution and subsequent etching of diamonds in the process of kimberlite magma ascent and at autometamorphism of kimberlites. Laminar crystals of octahedral, rhombic dodecahedral and transitive between them habits prevail in pipe Malokuonapskaya (Kuranakhsky field) at sufficient proportion of admixture nitrogen in the form of A-center. Consequently high-nitric are diamonds both from kimberlite bodies of Malo-Botuobinsky and Sredne-Markhinsky diamondiferous regions of Vilyuy are and of Anabar-Olenekskaya area.

Increased content of pyrope, picroilmenite, and chrome-spinellid is characteristic of Vilyuy area kimberlites. Rocks of groups I and II prevail by quantity of hypogene parageneses minerals, though quite often kimberlites of groups III and IV are registered. Here the content of pyrope is increased in relation

--

to other indicator minerals, the share of high-chromic varieties of pyrope and chrome-spinellid is also increased, especially in pipes with economically significant productivity.

Kimberlites of Anabar-Olenekskaya area are characterized mainly by low content of diamond indicator minerals, though there are pipes with their increased quantity (Obnazhennaya, Ruslovaya, Dyanga). In Picroilmenite prevails over pyrope in overwhelming majority of the pipes and dykes.

The size of phenocrysts of deep-seated minerals is one of characteristic features of the pipes (blocks). According to the data of I.P. Ilupin [12] large nodules of ilmenite and garnet are by far not always attributed to those pipes where there is much of this mineral. Thus, in most rich in garnet (about 0.9% in vol.) pipes Zagadochnaya and Snegopadnaya of Daldyn field the garnet is fine, mainly less than 5 mm in diameter, while in massive kimberlite of pipe Geophysicheskaya (0.07% of garnet) nodules of garnet measured by first centimeters in diameter were found.

It has been established during investigation of various fields' kimberlite rocks that the content of KIM (kimberlite indicator minerals) even in closely located bodies and within complex in structure or twinned bodies may vary in the interval of several orders taking sometimes abnormally high or very low values.

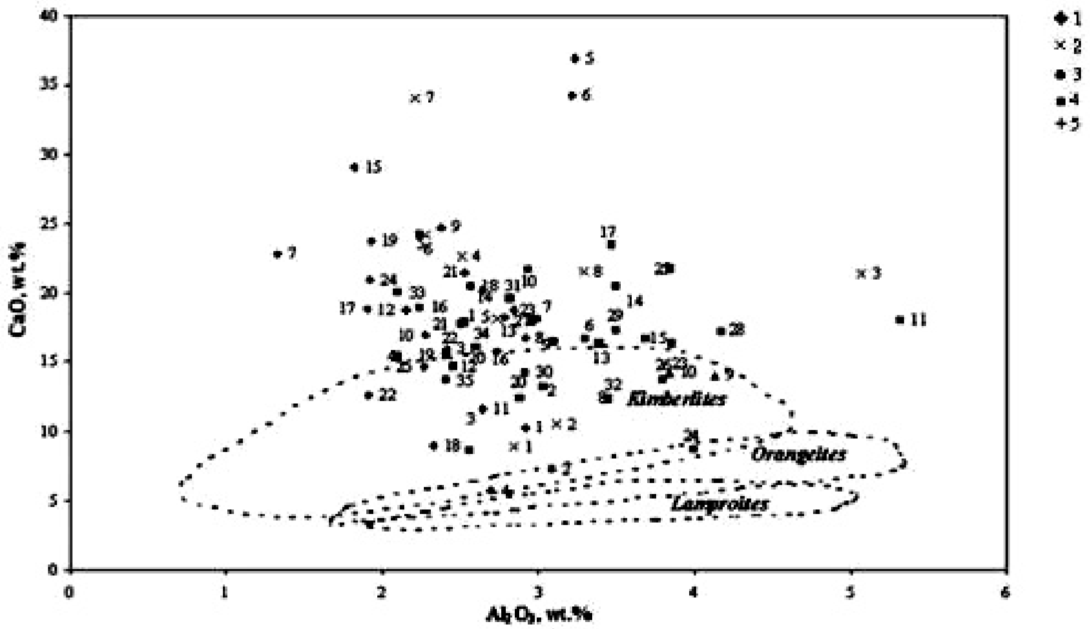

Fig. 4. **Diagram of Al_2O_3 и CaO (wt.%) correlations in kimberlites of the southern part of Yakutian kimberlite province.**

Notation conventions correspond to Fig. 2.

It has been established that availability of garnets of diamondiferous parageneses is one of most important indications of diamondiferousness and depth of kimberlites, that is, direct correlation of diamondiferousness and content of chromic knorringite-bearing pyropes (pyropes of diamond association) is observed.

Composition and coloring of garnets bear rather broad information about their paragenetic belonging and also about probable diamondiferousness of their primary source. Diversity of coloring is stipulated by assortment and concentration of admixtures, the main of which are Cr^{3+}, Fe^{2+} , Fe^{3+} and to smaller degree Ti^{3+} [20, 21], and studying of this important crystallochemical factor is performed with the help of optical spectroscopy [21]. Garnets from kimberlites are characterized by rather complicated composition: together with pyrope, almandine, and grossular minals, present in various quantitative proportions, they contain knorringite, uvarovite, andradite, Ti-andradite and spessartine minals, allowing to presume availability of chromorphous centers Cr_6^{3+}, Fe_6^{3+}, Fe_4^{3+}, Ti_6^{3+}, Fe_8^{2+}, Mn_8^{2+}, Fe_8^{2+}, Ti_6^{4+} and some others [20]. Their various combinations stipulate various optical absorption spectra of garnets of ultrabasic (peridotites-pyroxenite) and basic (eclogites) parageneses, including diamondiferous ones, subdividing into two series: magnesia (spinel ultrabasic rocks, websterites, and eclogites) and magnesia-ferruginous (ilmenite ultrabasic rocks, pyroxenites, and eclogites).

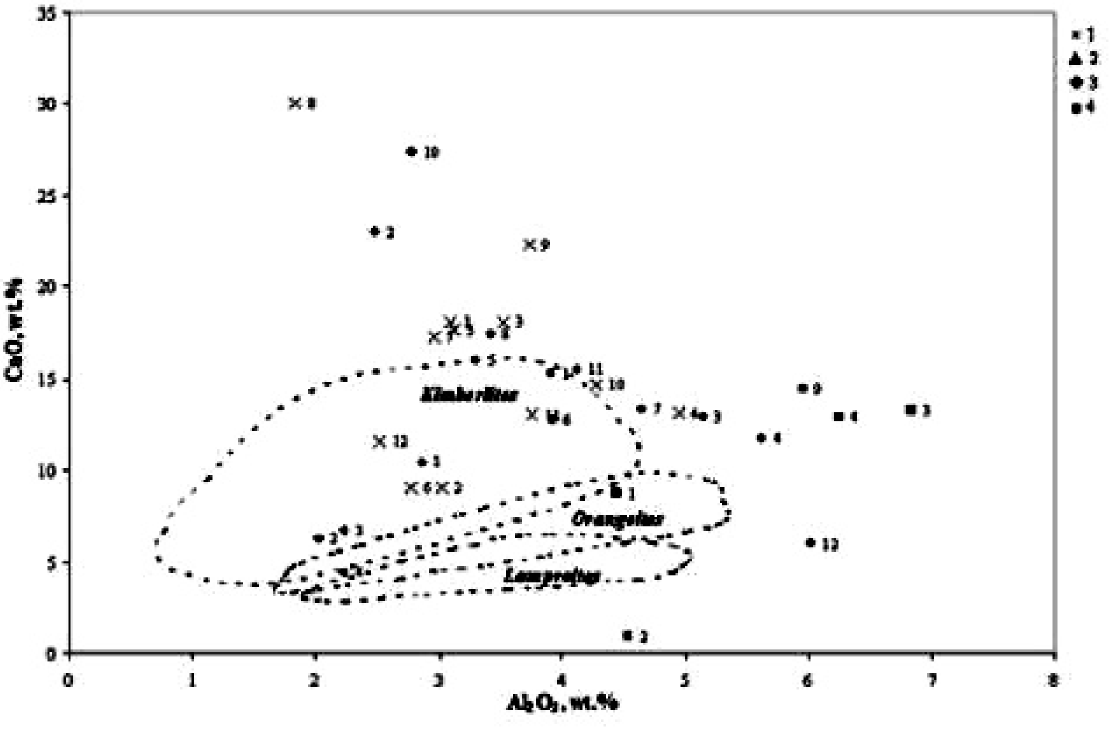

Fig. 5. **Diagram of Al_2O_3 и CaO (wt.%) correlations in kimberlites of the northern part of Yakutian kimberlite province.**

Notation conventions correspond to Fig. 3.

Traditionally important parameter of kimberlites – specific features of chemical composition of indicator minerals. Differences between pipes by content of chrome in garnets were shown by N.V. Sobolev with co-authors [10, 27 and others]. Proportion of garnet containing more than 10% Cr_2O_3 (with respect to the whole garnet) constitutes from 0.6 (pipes Vostok and Oval) to 16.1% (Aykhal). Most of industrially diamondiferous kimberlite pipes contain garnets figurative points of which are located in the field of diamond association (Fig. 4-6).

--

Exclusions are constituted by pipes of the Nakyn field, in which occasional selections from about 100 grains may not contain the mentioned garnets, which requires increase of selection volumes for micro-X-ray-spectral analysis. More successful results are shown by optical-spectroscopic investigations. Basing on comparative detailed analysis of the results received by T.A. Antonova during performance of optical-spectroscopic study of garnets from various petrographic varieties of Botuobinskaya pipe kimberlites the following conclusions were made:

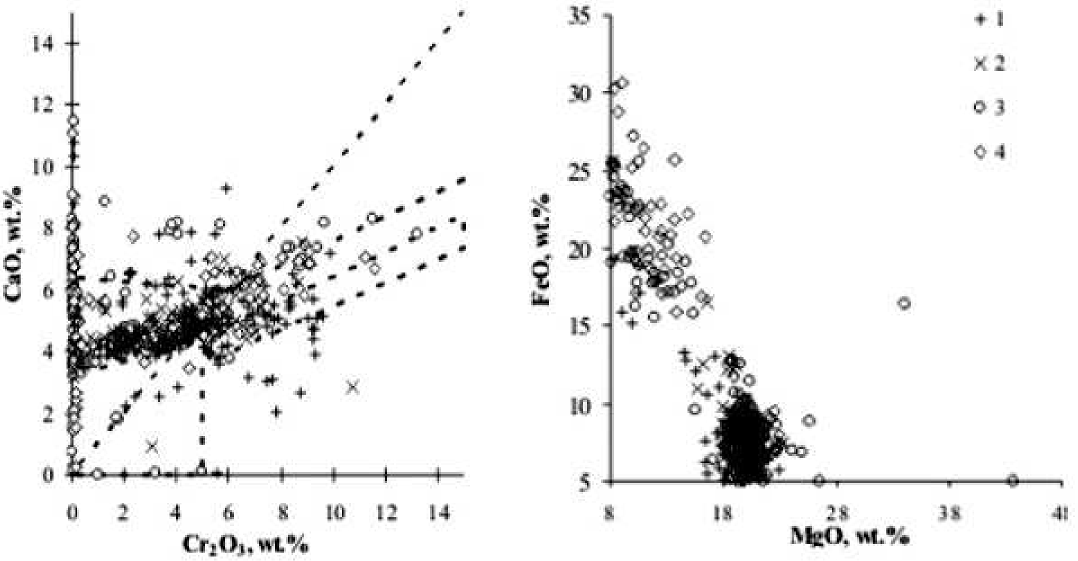

Fig. 6. **Diagrams of chemical composition of garnets from kimberlites of Mirny and Nakyn fields.**

Notation conventions of pipes: 1 – International, 2 – Mir, 3 – Botuobinskaya, 4 – Nyurbinskaya.

1.Investigated varieties of kimberlites (KB, AKB, and PK) have close qualitative and quantitative correlation of garnets of various genetic types, which correspond practically to all known peridotite and eclogites parageneses. Garnets of ultrabasic hypogene associations prevail over eclogites ones with proportion 2:1, therewith.

2. Pyropes from evenly granular lherzolites (20-25%), pyrope-almandines from magnesia-ferruginous eclogites (18-19) and magnesia almandines from eclogites-like rocks (17-23%), which in total constitute more than half of all the studied grains, are distributed at the most. Knorringite-pyropes from harzburgites and dunites, uvarovites and uvarovite-pyropes from vehrlites, high-chromic pyropes from spinel ultrabasic rocks, low-chromic pyropes from websterites, broken down lherzolites and ilmenite ultrabasic rocks, pyrope-almandines from magnesia eclogites and almandines from metamorphic rocks of the Siberian platform’s basement play the subordinate role (not more than 5 – 10% each paragenesis individually). Similar correlation of garnet-bearing parageneses is in a way the “passport” of pipe Botuobinskaya. There is prevalence of garnets of chromic-magnesia series of reduced titaniferous and ferruginous properties from harzburgites, spinel ultrabasic rocks, evenly granular lherzolites, magnesia

websterites and magnesia eclogites in this pipe, which in total constitute about 66%.

3. Among the garnets of diamondiferous and potentially diamondiferous parageneses eclogites ones domain, namely: pyrope-almandines from magnesia-ferruginous eclogites. The second place is taken by knorringite-pyropes from harzburgites, and the third – from dunites. The total number of garnets of diamond-bearing parageneses is somewhat higher in autolithic kimberlite breccia (16%) than in kimberlite breccia (14%) of pipe Botuobinskaya.

Kimberlite rocks of pipe Nyurbinskaya are noted for prevalence of purple and red garnets, the content of which reaches 90%. Insignificantly developed are garnets of pink colour, the quantity of which does not exceed 10%. Studied by method of optical spectroscopy garnets were divided into 13 genetic types, from which 11 correspond to known deep-seated garnet-bearing ultrabasic and eclogites parageneses of the Yakutian province kimberlite bodies [20]. Garnets of sufficiently almandine composition from eclogites-like and metamorphic rocks of the Siberian platform’s crystalline basement have been found in noticeable quantities (26%). All registered deep-seated mineral associations can be divided into 5 colour (genetic) groups by chromic centers in garnets. The first group includes garnets of harzburgites, spinel ultrabasic rocks, evenly granular lherzolites and websterites, the second – dunites, vehrlites, broken down lherzolites, ilmenite ultrabasic rocks and nodules, the third group includes magnesia-ferruginous and magnesia eclogites. Within each group garnets are located from more deep-seated (diamond-pyrope) to less deep-seated (graphite-pyrope) facies of depth, which is explained by various conditions of differentiation of initial material of the upper mantle. Garnets of chromic-magnesia series of reduced titaniferous and ferruginous properties from harzburgites, spinel ultrabasic rocks, evenly granular lherzolites, magnesia websterites and magnesia eclogites prevail and constitute 65% in total. Among garnets of diamondiferous and potentially diamondiferous parageneses eclogites ones predominate, namely: pyrope-almandines from magnesia-ferruginous eclogites (6% of all grains). Knorringite-pyropes from harzburgites and from dunites are in subordinate approximately equal quantity. The total number of garnets of diamond-bearing parageneses is equal to 10%.

Basing on comparative detailed analysis of the results, received during optical-spectroscopic study of garnets from the Botuobinskaya and Nyurbinskaya pipe kimberlites one can distinguish both general and distinctive indications for them. The number of indications characteristic of both pipes of the Nakyn field can include: a) noticeable prevalence of garnets of evenly granular lherzolites (Gr+Ol+Cpx+Opx) over the garnets of all other mineral associations; b) by frequency of different type garnets’ occurrence the dominating role is played by representatives of their chromic-magnesia branch with decreased titaniferous and ferruginous properties from harzburgites, spinel ultrabasic rocks, evenly granular lherzolites, magnesia websterites and magnesia eclogites; c) about 30% of the studied garnets have sufficiently almandine composition and correspond to those

--

from eclogites-like and metamorphic rocks of the Siberian platform’s crystalline basement. The distinctive indications reflecting formation specifics of each pipe are: a) increased content of garnets from broken down lherzolites and, rarely, from nodules is registered in pipe Nyurbinskaya; garnets from nodules are not registered in pipe Botuobinskaya and the quantity of eclogites paragenesis garnets including diamond-bearing is noticeably higher.

Occurrence comparison of various genetic types’ deep-seated garnets of the Nakyn field pipes was performed with those of some industrially diamondiferous kimberlite bodies of Malo-Botuobinsky (pipes Mir, International, 23rd CPSU Congress) and Daldyn-Alakitsky (Udachnaya, Sytykanskaya, Aykhal, Yubileynaya) regions and kimberlite pipes of Muno-Tyungsky region as well. The comparison has shown that the structure of upper mantle in the region of pipes Botuobinskaya and Nyurbinskaya resembles more that of Malo-Botuobinsky region than of Daldyn-Alakitsky and Muno-Tyungsky. Among them two mineralogical models are distinguished. The first one unifies all high-productive kimberlite bodies of Daldyn-Alakitsky and Muno-Tungskay regions and high content of garnets of magnesia-titanium-ferruginous branch from dunites, vehrlites, broken down lherzolites, ilmenite hyperbasic rocks and nodules, and from magnesia-ferruginous pyroxenites and magnesia-ferruginous eclogites, is typical. The second model includes diamond deposits of industrial significance of Mirny and Nakyn fields. Prevalence of garnets of magnesia-chronic branch of decreased titaniferous and ferruginous properties from harzburgites, spinel ultrabasic rocks, evenly granular lherzolites, magnesia websterites and magnesia eclogites is peculiar to it.

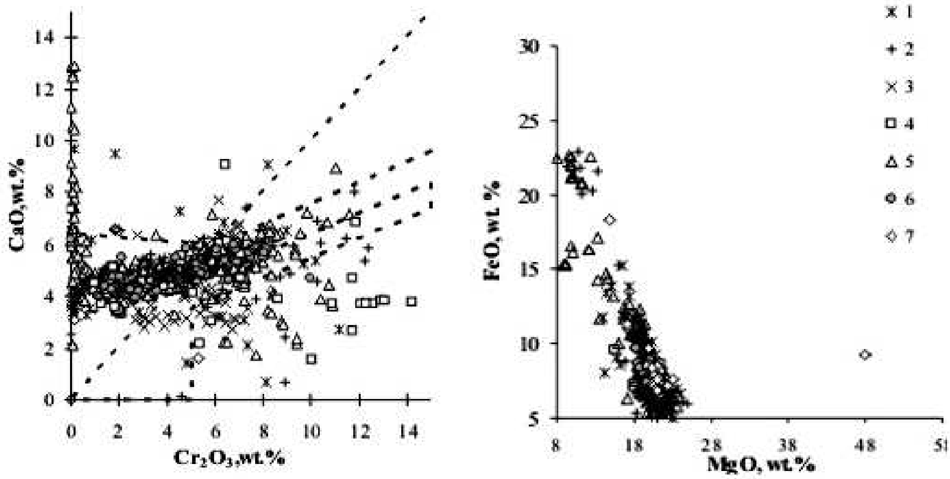

Fig. 7. **Diagrams of chemical composition of garnets from kimberlites of Alakit-Markhinsky and Daldyn fields.**

Notation conventions of pipes: 1 – Aykhal, 2 – Yubileynaya, 3 – Komsomol’skaya, 4 – Udachnaya, 5 – Zarnitsa,
6 – Dolgozhdannaya, 7 – Festival’naya.

Specific features of ilmenite (Fig. 7-9) composition are also successfully used, the longest trend of which by correlation of titanium and magnesium oxides is registered in kimberlites of Mirny field (pipe Mir). Cr_2O_3 in ilmenites of Daldyn-Alakitsky diamondiferous region (average by pipes) varies from 0.30 (pipe Kollektivnaya) to 4.33% (Smezhnaya). The results of ilmenite composition relation with specific features of hypogene evolution of mantle melts were considered in the work of I.P. Ilupin and co-authors [13]. Concentration of Ta in ilmenites from kimberlites of Daldyn-Alakitsky region changes from 101 (pipe

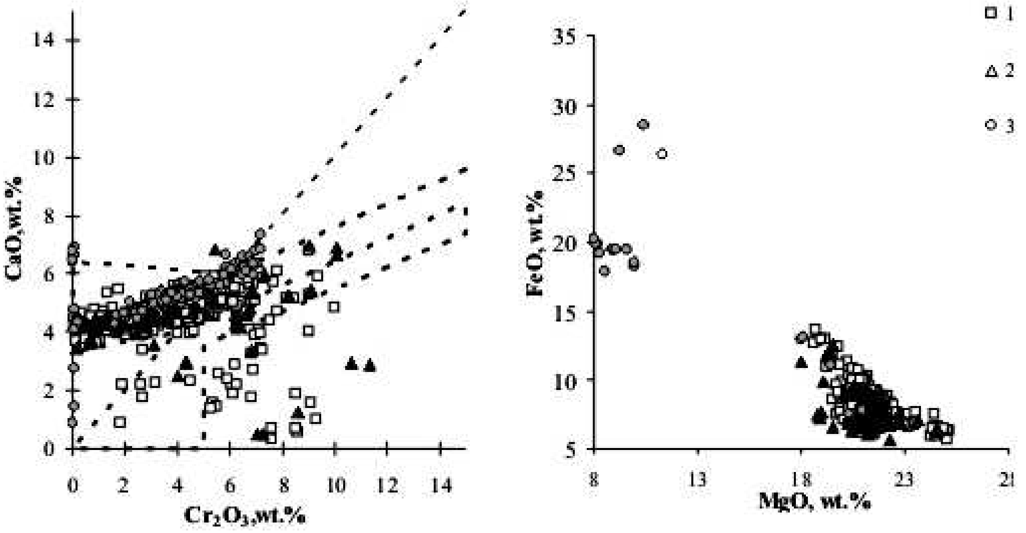

Fig. 8. **Diagrams of chemical composition of garnets from kimberlites of Verkhne-Munsky field and fields of PreAnabariya.**

Notation conventions of pipes: 1 – Zapolyarnaya, 2 – Novinka, 3 – kimberlites and convergent to them rocks of PreAnabariya.

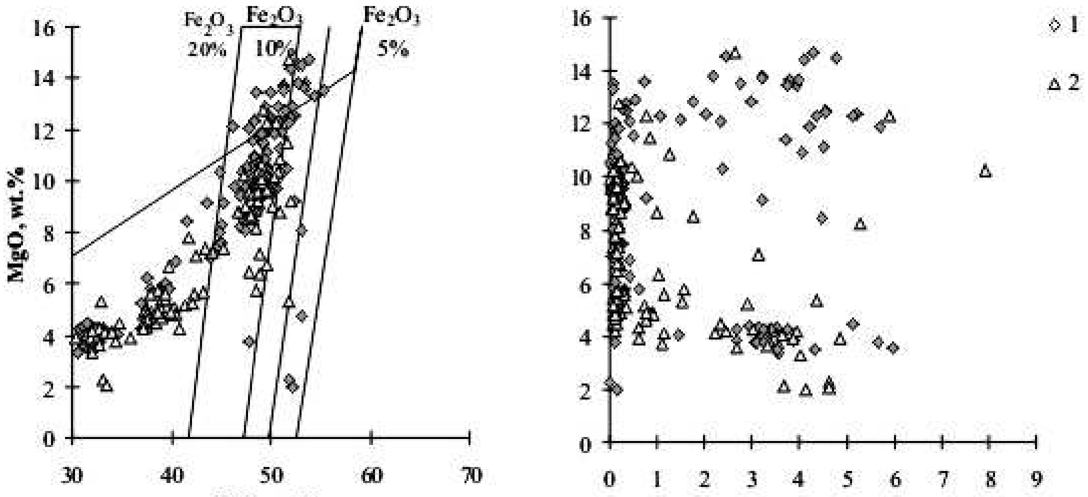

Fig. 9. **Diagrams of chemical composition of ilmenite from kimberlites of Mirny field.**

Notation conventions of pipes: 1 – International, 2 – Mir.

--

Baitakhskaya) to 324 g/t (Rot-Front), and Hf from 7.4 (Zagadochnaya) to 30.9 g/t (Lyubimaya). Supposition was made that different magmatic hotbeds, as a rule, served as the source of picroilmenite for pipes of different clusters. And only pipes of one linear cluster could have common unified hotbed.

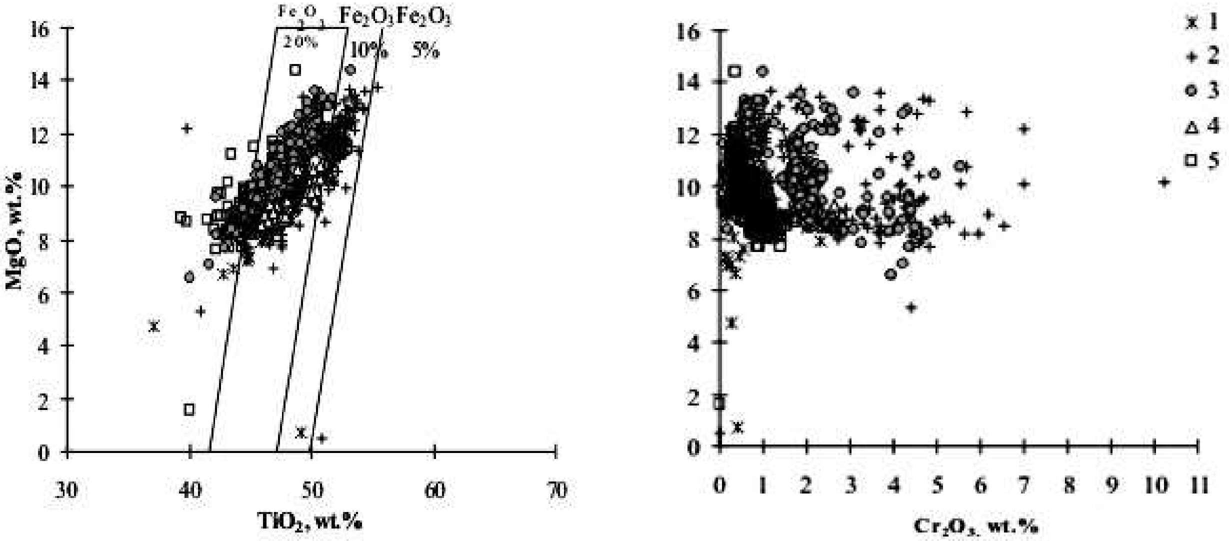

Fig. 10. **Diagrams of chemical composition of ilmenite from kimberlites of Alakit-Markhinsky and Daldyn fields.**

Notation conventions of pipes: 1 – Aykhal, 2 – Yubileynaya, 3 – Komsomol’skaya, 4 – Udachnaya, 5 – Zarnitsa.

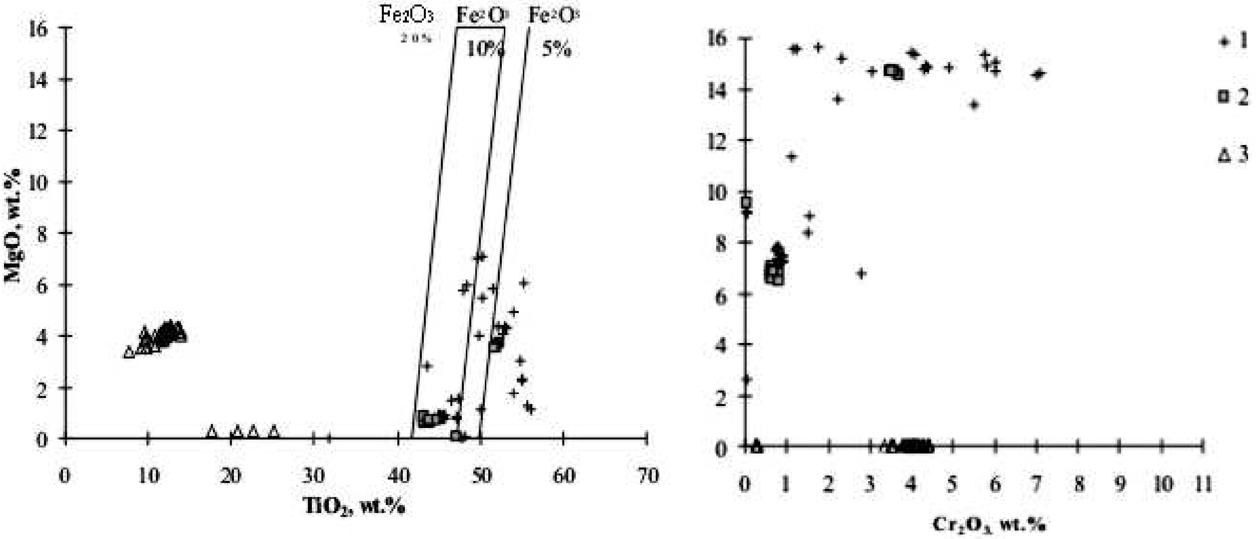

Fig. 11. **Diagrams of chemical composition of ilmenite from kimberlites of Verkhne-Munsky field and PreAnabariya.**

Notation conventions of pipes: 1 – Zapolyarnaya, 2 – Novinka, 3 – kimberlites and convergent to them rocks of PreAnabariya.

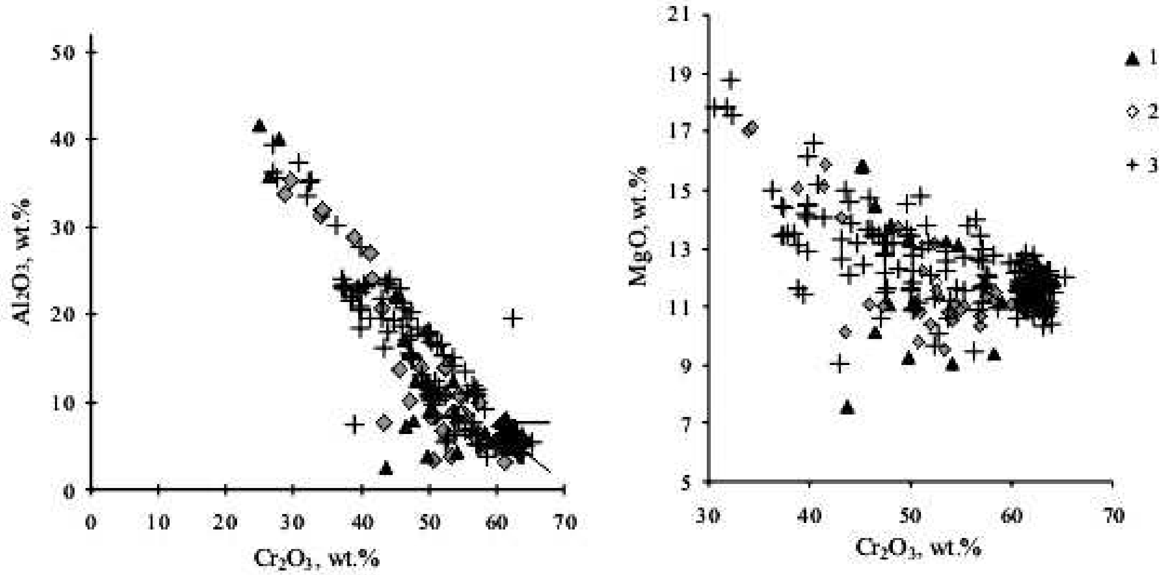

Fig. 12. **Diagrams of chemical composition of chrome-spinellids from kimberlites of Mirny and Nakyn fields.**

Notation conventions of pipes: 1 – Mir, 2 – International, 3 – Botuobinskaya.

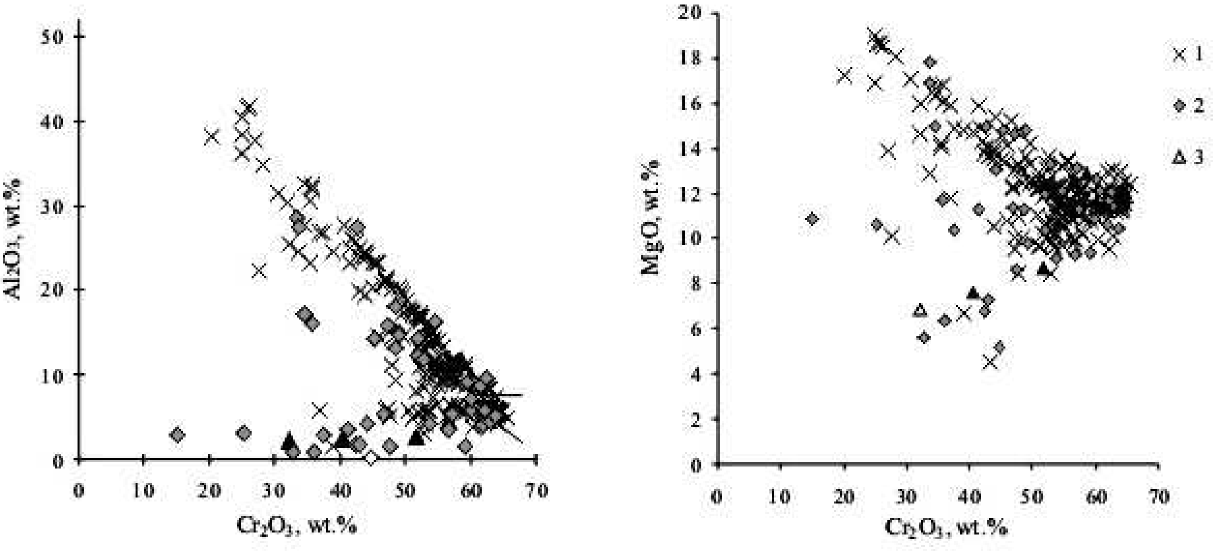

Fig. 13. **Diagrams of chemical composition of chrome-spinellids from kimberlites of Alakit-Markhinsky and Daldyn fields.**

Notation conventions of pipes: 1 – Aykhal, 2 – Yubileynaya, 3 – Zarnitsa.

Noticeable quantities of chrome-spinel are registered in kimberlites of many pipes, the presence of diamond association individuals (more than 61 wt.% Cr2O3) among grains of which serves as the premise of industrial diamondiferousness of rocks (Fig. 10-12). Kimberlites of the Nakyn field are an example of it. Cr_2O_3 22.1-67.9 (average 55,1 wt.%), Al_2O_3 3.8-39.6 (11.6), TiO_2 0.0-3.8 (0.6), MgO 9.7-19.1 (12.0), FeO 11.3-25.1 (18.1) and MnO 0.0-0.3 (0.1) contents are typical for chrome-spinellids of pipe Botuobinskaya kimberlite rocks. Strong positive correlation between Al_2O_3 and MgO, and negative between Cr_2O_3 and Al_2O_3,

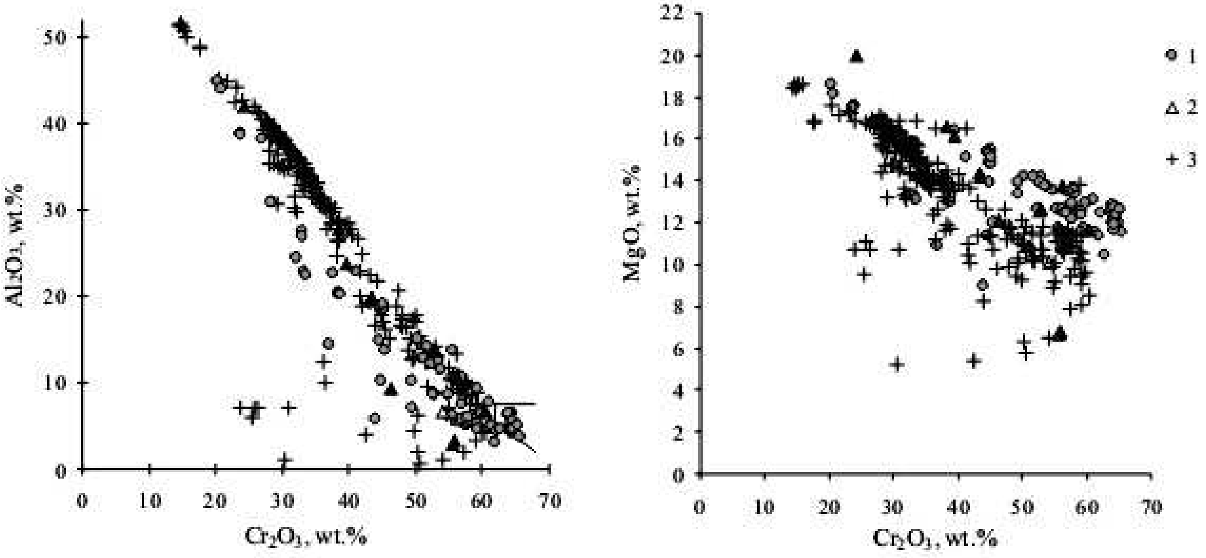

Fig. 14. **Diagrams of chemical composition of chrome-spinellids from kimberlites of Verkhne-Munsky field and fields of PreAnabariya.**

Notation conventions of pipes: 1 – Zapolyarnaya, 2 – Novinka, 3 – kimberlites and convergent to them rocks of PreAnabariya.

Cr_2O_3 and MgO are registered. High-chromic spinellids of ultrabasic, including harzburgite, parageneses of diamond facies of depth, of which are 51.4% of all the studied grains, are most numerous in the heavy fraction. Let us notice for comparison that similar chrome-spinellids in pipe Aykhal constitute only 23%. High-chromic spinellids mainly of lherzolite (about 16.8%) and medium-chromic ones of peridotite (17.4) parageneses are widespread. Low-chromic spinellids from peridotites, including harzburgites, and from garnet websterites play the subordinate role (not more than 6 – 8.4% each paragenesis separately).

BASIC ASSOCIATIONS OF SECONDARY MINERALS IN KIMBERLITE ROCKS

Consideration of basic associations of secondary minerals in kimberlite rocks of Yakutia made it possible to distinguish about 10 types among them. Most distributed among them, according to the data of L.V. Liskovaya, are the following: chlorite-serpentine, talc-serpentine and pyroaurite-serpentine. Average contents of chlorite and pyroaurite do not exceed 10% and talc – 2% at this. Calcite-serpentine association with admixture of dolomite is registered in all deposits of Yakutia, while serpentine-calcite association with admixture of dolomite is peculiar only to pipes of Daldyn and Munsky fields. Intensive development of brucite-serpentine association as well, most intensively developed in pipe Novinka, is one more their peculiarity. A broad selection of carbonate-serpentine associations due to the minerals contained in subordinate quantities is registered for pipes of Mirny, Nakyn and Alakit-Markhinsky fields, apart from

Daldyn and Munsky fields, where the spectrum of secondary minerals is more homogeneous at sufficient predominance of serpentine and carbonates.

Tendency to preferential development of a definite type of carbonate-serpentine associations depending on productivity of deposits is observed. Thus, high-diamondiferous diamond deposits have wide selection of serpentine-carbonaceous associations except serpentine-calcite one with admixture of dolomite, which distinguishes them from non-industrial where the latter prevails. All medium-diamondiferous deposits have calcite-serpentine association with admixture of dolomite. Analysis of carbonates distribution in kimberlites shows that contact carbonatization is not related directly with assimilation of carbonaceous xenoliths of hosting terrane but is caused by infiltration of carbonate-bearing solutions from country rocks. Extremely uniform substitution of all structural components of kimberlite rocks by calcite is an additional proof of it: from the basic mass and serpentine pseudomorphs on phenocrysts of olivine to xenoliths of crystalline schists. As far as xenoliths of limestones are concerned, their content in intensively carbonatizated contact zones is often not as high as in moderately carbonatizated central parts of the pipe.

Employment of such individual characteristics of serpentine as correlation of lizardite and chrysotile, belonging to septochlorite and structures with low perfection of crystalline structure, do not allow distinguishing sustained regularities in their development degree in the basic mass of kimberlites depending on productivity of the body or its location. Nevertheless, some tendencies concerning the degree of septochlorite and lizardite distribution were revealed.

Lizardite is the predominant mineral from the group of serpentines in the basic mass of kimberlites of most Yakutian deposits. Chrysotile is in the lead only in kimberlite rocks of pipes Aykhal, Deimos, and Novinka, and proportions of these type serpentine in pipes Udachnaya and Dolgozhdannaya most often are equal. Among industrial deposits chrysotile-calcite-dolomite association prevails only in kimberlites of pipe Aykhal. In other high-diamondiferous pipes the majority of associations are formed mainly by lizardite.

Septochlorite is most of all distributed in deposits of Daldyn and Munsky fields, among which pipes Zarnitsa, Festival’naya, and Zapolyarnaya take first place by the quantity of the mineral, and in pipe Botuobinskaya of the Nakyn field. Relatively rarely this mineral is registered in deposits Aykhal, International, Mir, Nyurbinskaya, Yubileynaya, Novinka, Komsomol’skaya, Deimos. Other pipes occupy intermediate position between the mentioned kimberlite bodies. The tendency to increasing the degree of septochlorite distribution in medium-diamondiferous and half-industrial deposits has been revealed. Probably it is connected with higher temperatures of serpentinization processes which took place in these kimberlite bodies.

Serpentine with defective structure prevails in the basic mass of most Yakutian deposits’ kimberlites. Only kimberlites from deposits Komsomol’skaya, Zarnitsa, Zapolyarnaya, and Novinka are distinguished by formation of the mineral

--

---

with relatively perfect structure. Poorly crystallized serpentine is most distributed in pipes Nyurbinskaya, Aykhal, and Deimos. No any persistent regularities on prevailing development of poorly crystallized serpentine depending on belonging to fields or productivity of kimberlite bodies have been found.

Analysis of secondary minerals' distribution shows some features of their development in various deposits. Individual character of secondary processes, typical of high-diamondiferous deposits, may be characterized with the help of the following associations:

Mir – calcite-serpentine association with admixture of dolomite with prevalence of lizardite, feeble development of septochlorite and serpentine of defective structure;

International – calcite-dolomite-serpentine association with admixture of chlorite, with prevalence of lizardite and feeble development of septochlorite and serpentine with defective structure.

Botuobinskaya – dolomite-serpentine-calcite association with prevalence of lizardite, moderate development of septochlorite and serpentine with defective structure.

Nyurbinskaya – calcite-serpentine-dolomite association with prevalence of lizardite, feeble development of septochlorite and high - serpentine with defective structure.

Aykhal – serpentine-calcite-dolomite association with prevalence of chrysotile, feeble development of septochlorite and high – serpentine with defective structure;

Udachnaya – dolomite-serpentine-calcite association with prevalence of lizardite, moderate development of septochlorite and serpentine with defective structure;

In the result of analysis of the received data it has been established that each diamond deposit of Yakutian kimberlite province has individual character of developing various types of serpentine, carbonates, talc, and chlorite, which testifies about differences in initial composition of kimberlite rocks and diversity of secondary processes' behavior in them. Intensity of secondary minerals development decreases to central parts of pipes with depth.

DISCUSSION

Petrographic-mineralogical and petrogeochemical features of kimberlites and convergent to them rocks practically of all kimberlite fields of Yakutian province have been analyzed. Its southern part (from Mirny to Verkhne-Munsky and, perhaps, Kuranakhsky fields) sufficiently differs by kimberlite character of composition. Bodies of convergent to kimberlites formations are present in the zone of kimberlite rocks' occurrences in the fields of Anabar group, which stretches out along eastern and south-eastern borders of Anabar crystalline massif, actually repeating its outline. Pipe bodies of carbonatites are distributed in the northern part of this zone (basins of rivers Staraya, Yaryga), and kimberlites prevail in the center and at the southern flange of the zone. Significant part of occurrences is represented by rocks of intrusive facies which are located among explosive formations. Pipes in Luchakansky and Kuranakhsky fields have both simple and complex structure. Pipes in Dyukensky, Starorechensky, and Ary-Mastakhsky fields are infilled usually by some one variety of rocks. The age of kimberlite and kimberlite-like rocks of the region is considered by most researchers as Mesozoic (Middle Triassic – Early Jurassic), the bodies of carbonatites (mainly Orto-Yarginsky field) are of younger age: Jurassic – Early Cretaceous.

On the whole, correlation of various types of rocks in the fields is various – from south to north, and in the fields of Sredne-Oleneksky region the tendency to the increase of the role of picrite porphyrites is registered. Specifics of the pipes' mineral composition is expressed in noticeable increase of titanium-magnetite and monticellite quantity in submeridional direction from south to north, gradual disappearance of picroilmenite, together with the increase of alkalinity, ferruginous and titaniferous properties of rocks. The stated above is also confirmed by specialized petrochemical investigations on creating models of kimberlite bodies [30]. Compositions of the studied Yakutian kimberlites are subdivided into 7 quasihomogeneous by chemical composition groups – populations in the work, ranged average compositions of which form the row in which all elements subordinate to unified petrochemical trand: increase of Ti, Fe, Mg contents and decrease of K, Al and Ca from the 1st to the 7th population by decrease of magma-formation depth (230 - 150 km – kimberlites, 140 – 100 km – picrites and alkaline picrites). The latter rocks, together with kimberlites, were verified by these petrochemical data in Chomurdakhsky, West-Ukukitsky, East-Ukukitsky, Ogoner-Yuryakhsky, Merchemdensky, Molodinsky, and Kuoyksky fields, and in the fields of Anabar group as well.

Among the exploited and being at the stage of exploration deposits pipes Yubileynaya and International distinguish by complicated petrographic composition at picroilmenite-pyrope association of indicator minerals in the first pipe, and picroilmenite-chromite-pyrope in the second one, and in autolithic kimberlite breccia of more simple in structure pipe Zarnitsa increased proportion of heavy fraction and pyrope-picroilmenite association of diamond indicator minerals have been registered. Tufogenic-sedimentary formations of pipe Yubileynaya crater part, apart from typical rocks of diatreme facies, are usually characterized by low grade of diamonds and their somewhat decreased size. With the quantity increase of tufogene material down along the section of crater formations the grade of diamonds increases. Varieties of diatreme facies kimberlite rocks, composing upper levels of diatremes, have increased contents (grades) of diamonds varying in plan either naturally in conformity with the change of kimberlite types, or accidentally with interchange of relatively rich and poor sites. Increased diamondiferousness is registered in autolithic breccias with rare xenoliths, porphyric kimberlites, decreased – in xeno- and tuff breccias, which are sometimes referred to non-industrial types.

The lowest concentrations of heavy minerals at chromite-pyrope association of KIM are peculiar to kimberlites of the Nakyn field, and sufficiently pyrope association – to kimberlites of the Munsky field, at the highest degree of garnet kelyphitization. Differences in distribution of minor, rare, and trace elements in kimberlites of the considered pipes and KIM are registered. Associations of secondary minerals noticeably vary.

General content of nitrogen and hydrogen admixtures is one of main distinctive features of diamonds, together with the most important indication – crystallomorphology [31]. In diamonds of Munsky field pipes these admixtures constitute 490 at. ppm. and 1.6 cm^{-1}, crystals from pipe Zarnitsa differ by aggregation of N admixture (45%) at H admixture of 2.1 cm^{-1}, diamonds of pipe Yubileynaya are enriched by N admixture to 450 at. ppm. at 1.4 cm^{-1} H, and enrichment by N admixture up to 450-540 at. ppm. in feebly aggregated state (28-33%) are general for stones of pipes International, Nyurbinskaya, and Botuobinskaya. Among other main distinctive features of diamonds are small size of laminar formations (B2-centers), small contents of N3-defect and admixture H (0.6-1.6) and also crystals which underwent postgrowth deformation and annealing at more than 500° C temperature.

It is supposed that the growth of diamonds is mainly related with metasomatism of upper mantle rocks in the infiltration result of carbonate-bearing, enriched by rare elements fluids and melts. Metasomatism in most cases directly precedes kimberlite magmatism, simultaneously formation of kimberlite source and growth of diamonds in this source take place. During formation of a kimberlite source fraction crystallization of asthenosphere metasomatic melt takes place, the result of which is association of megacrysts (ilmenite, garnet, clino- and ortopyroxene, olivine, phlogopite) observed in composition of kimberlites. Diamond is probably also genetically related with this association, grows preferably in separate parts of the source, in which favourable conditions for its growth and integrity form in the result of evolution. Kimberlites in their turn inherit rare-element composition of metasomatic melt, while petrochemical composition is inherited from peridotite of upper mantle. Petrochemical composition of the latter also changes under the influence of metasomatism. The rocks of initially dunite-harzburgite composition are transformed into lherzolites due to the growth of metasomatic clinopyroxene. Large part of garnets is evidently captured by diamonds at early stages of source formation and that is why inclusions in diamond most often correspond to dunite-harzburgite paragenesis, and kimberlites are melted from a little later formed metasomatizated carbonate-bearing lherzolite.

In the result of carried out studies and analysis and systematization of available data sufficiently kimberlitic nature of the bodies of Mirny, Nakyn, Alakit-Markhinsky, Daldyn, and Verkhne-Munsky fields has been established.

Kimberlites and convergent to them rocks take part in the structure of pipes and veins of Kuranakhsky, Luchakansky, Dyukensky, Birigindinsky, Ary-Mastakhsky, and Starorechensky fields, and carbonatites dominate in composition of Orto-Yarginsky field bodies. Specific features of petrographic-mineralogical composition and petrogeochemical properties of various fields' kimberlite rocks are shown, and specifics of diamond indicator minerals – garnet, picroilmenite, chrome-spinellid, is also indicated.

Conclusion

As the result of proper studies and generalization of other authors' materials it is established that kimberlite diatremes of Yakutia are characterized by variations of petrographic and mineral composition, geochemical properties, differences in depth of magmatic hotbeds' initial stage, internal structure, content and composition of hypogene minerals, degree and character of kimberlite recycling by postmagmatic processes, content, morphology and physical properties of diamonds and other indications. It is established that each kimberlite body represents an individual target not repeating in nature. At the same time there are typical features among them, which are as follows: a) complicated geological structure; b) narrowing with depth and gradual transition into dyke bodies – incurrent canals; c) proportion of admixture material of country rocks decreases in kimberlite pipes with depth; d) the content of mantle nodules and hypogene minerals of kimberlites among pipes and in sections of individual pipes varies at their relatively consistent correlation; composition of minerals practically does not change with depth; e) the grade of diamonds, their morphology and physical properties do not change to the depth of 1-1.5 km; f) the scales of secondary recycling of kimberlites as a rule do not reduce with depth.

Among specific features of kimberlite magmatism of Yakutia one should note the following: sufficiently kimberlitic composition of occurrences of Vilyuy area (Mirny, Nakyn, Alakit-Markhinsky, Daldyn, and Verkhne-Munsky kimberlite fields) with increased content of pyrope, picroilmenite, chrome-spinellid (at increased proportion of high-chromic varieties of pyrope and chrome-spinellid, especially in pipes with economically significant productivity) and appearance, together with kimberlites, of picrites and alkaline picrites in the fields of Anabar-Olenekskaya area with predominantly low content of diamond indicator minerals (except pipes Obnazhennaya, Ruslovaya, Dyanga with their increased quantity) at prevalence of picroilmenite over pyrope in most pipes and dykes; regional variations of geochemical properties; availability of crater parts in single diatremes of Alakit-Markhinsky field. By mineralogical-geochemical indications kimberlites of Nakyn field stand apart. On the whole wide variations of composition are peculiar to kimberlite fields, which is caused by heterogeneity of mantle source, time and PT-conditions of melt formation, admixture of crust material and specifics of intrusion.

--

Garnet ultrabasic (peridotite-pyroxenite) and basic (eclogites) parageneses are extremely characteristic material-indicative features of primary diamond sources of Yakutian kimberlite province. By specific features of chemical and mineral composition they are subdivided into two series: magnesia (spinel ultrabasic rocks, websterites, and eclogites) and magnesia-ferruginous (ilmenite ultrabasic rocks, pyroxenites, and eclogites). Among ultrabasic varieties dunite, harzburgite, vehrlite, lherzolite, and pyroxenite parageneses are distinguished. Depending on TP-conditions of crystallization and depth of formation they are correlated with spinel, graphite-(chrome-spinel-) pyrope and diamond-(chrome-spinel-)pyrope facies of depth. Analysis of composition and optical properties of garnets from kimberlites of southern part of the province shows possibility of their attribute to two mineralogical models. The first one, which unifies all high-productive kimberlite bodies of Daldyn-Alakitsky and Muno-Tyungsky regions, is characterized by high content of garnets of magnesia-titaniferous-ferruginous branch from dunites, vehrlites, broken down lherzolites, ilmenite hyperbasic rocks and nodules, and from magnesia-ferruginous pyroxenites and magnesia-ferruginous eclogites as well. The second one includes diamond deposits of industrial significance of Mirny and Nakyn fields. Prevalence of magnesia-chromic branch garnets of decreased titaniferous and ferruginous properties from harzburgites, spinel ultrabasic rocks, evenly granular lherzolites, magnesia websterites and magnesia eclogites is peculiar to it.

The reasons of regional differences of typomorphic features of diamonds form individual kimberlite bodies of spatially disconnected regions of Yakutian province are related with heterogeneity of their mantle sources. Long staying of diamonds both in stable and unstable situations of kimberlite formation hotbeds is accompanied by annealing, dissolution, oxidizing, corrosion, mechanical disturbances and other alterations. Growth of diamonds is predominantly related with metasomatism of upper mantle rocks in infiltration result of carbonate-bearing enriched by rare elements fluids and melts. Metasomatism in most cases directly precedes kimberlite magmatism. Simultaneously formation of kimberlite melts' source and growth of diamonds in this source take place.

Composition of mantle minerals (pyrope, picroilmenite, chrome-spinellid and others), crystallomorphology and physical properties of diamonds are differentiated at the level of a province, field, and each pipe. Individual features of composition and physical properties of kimberlite indicator minerals, occurring at the statistic level, allow carrying out identification of kimberlite minerals of placers and link them with known sources or forecast unascertained primary ones.

References

1. **Agashev A.M., Orikhashy Y., Vatanabe T., Pokhilenko N.P., Serenko V.P.** Isotopic-geochemical characteristics of the Siberian platform's kimberlites in connection with the problem of their origin // Geology and geophysics, 2000. V. 41. № 1. P. 90-99.

2. Arkhangel’sk diamondiferous province (geology, petrography, geochemistry, and mineralogy) / Under ed. of O.A. Bogatikova. M.: Publishers MSU, 1999. P. 524.
3. **Bogatikov O.A., Kononova V.A., Golubeva Y.Y., Zintchouk N.N., Ilupin I.P., Rotman A.Y., Levsky L.K., Ovchinnikova G.V., Kondrashov I.A**. Petrogeochemical and isotopic composition variations of Yakutian kimberlites and their reasons. – Geochemistry, 2004, № 9, p. 915-939.
4. **Clement C.R. and Reid A.M.** The origin of kimberlite pipes: an interpretation based on a synthesis of geological features displayed by southern African occurrences. Geological Society of Australia Special Publication, 1989, 14, 1. P. 632-646.
5. **Clement C.R. and Skinne, E.M.W**. A textural-genetic classification of kimberlites. Transactions of Geological Society of South Africa, 1985, 88. P. 403-409.
6. **Dowson G.** Kimberlites and xenoliths in them. M.: Nedra, 1983. P. 300.
7. **Griffin W.L., Pearson N.J., Belousova E. et al.** The Hf isotope composition of cratonic mantle: LAM-MS-ICPMS analysis of zircon megacrysts in kimberlites// Geoch. et Cosmoch. Acta, 2000, V. 64. № 1. P. 133-147.
8. **Griffin W.L., Ryan C.G., Kaminsky F.V. et al.** The Siberian lithosphere traverse: mantle terranes and assembly of the Siberian Cratons// Tectonophysics, 1999. V. 310. P. 1-35.
9. **Hawthorne, J.B**. Model of a kimberlite pipe. Physics and Chemistry of the Earth, 1975, 9. P. 1-15.
10. Hypogene xenoliths and upper mantle / Under edition of V.S. Sobolev, N.L. Dobretsov, N.V. Sobolev. – Novosibirsk, 1975. P. 271.
11. **Ilupin I.P., Kaminsky F.V., Frantsesson Y.V.** Geochemistry of kimberlites. – M.: Nedra, 1978. P. 352.
12. **Ilupin I.P.** Kimberlites of Yakutia – linear location of pipes and material composition / Ores and metals, 2003, # 5-6. P. 60-68.
13. **Ilupin I.P., Kuligin V.M., Rakovsky A.Y.** Specific features of chemical composition of ilmenite as indication of deep-seated magmatic hotbeds’ specifics // Physical-chemical investigations of hypogene magmatism products. M., 1982. P. 158-171.
14. **Ilupin I.P., Vaganov V.I., Prokopchuk B.I**. Kimberlites / Reference boor. – M.: Nedra, 1990. P. 248.
15. **Jakes A., Luis G., Smith K**. Kimberlites and lamproites of Western Australia: Transl. from Engl. M.: World, 1989. P. 430.
16. **Khar’kiv A.D., Zintchouk N.N., Kryuchkov A.I**. Primary diamond deposits of the World. – M.: Nedra, 1998. P. 555.
17. **Vladimirov B.M., Soloviyeva L.V., Kiselev A.I. et al.** Kimberlites and kimberlite-like rocks: Kimberlites – ultrabasic formation of ancient platforms /– Novosibirsk: Science. Siberian branch, 1990. P. 264.
18. **Koval’sky V.V., Nikishov K.N., Yegorov O.S.** Kimberlite and carbonatites formations of eastern and south-eastern slopes of Anabar anteclise. – M.: Science, 1969. P. 288.
19. **Lorenz V.** Maars and diatremes of phreatomagmatic origin: a review. Trans. Geol. Soc. S. Afr., 1985, 88. P.459-470.
20. **Matsyuk S.S., Platonov A.N., Sobolev N.V.** Influence of crystallochemical factors on optical spectra and coloring of chrome-bearing garnets // Journ. of appl. spectroscopy, 1994, 60, # 1-2. P. 141-151.
21. **Matsyuk S.S., Zintchouk N.N.** Optical Spectroscopy of the Upper Mantle Minerals. – M.: “Nedra-Businesscenter Ltd.”, 2001. P. 428.
22. **McCallum, M.E.** The Sloan 1 and 2 kimberlite complex near the southern boundary of the State Line district of the Colorado-Wyoming kimberlite province. Wyoming Geological Association Guidebook for 42nd Field Conference, 1991. P. 229-250.

--

23. **Mitchel, R.H.** Kimberlites: mineralogy, geochemistry and geology. Plenum Press, New York, 1986. P. 442.
24. **Mitchell R.H.** Kimberlites, Orangeites, and Related Rocks//Plenum Press: New York and London, 1995. P. 410.
25. **Mogg T., Kopylova M., Smith B.S., Kirkley M.** Petrology of the Snap Lake kimberlite, NWT, Canada // 8th IKC, 2003.
26. **Rotman A.Y., Zintchouk N.N., Nosyko S.F., Kryuchkov A.I., Yegorov K.N., Stegnitsky Y.B.** Geology and material composition of kimberlite pipe Catoca (Angola) // Problems of forecasting, prospecting and studying mineral deposits on the threshold of the XXIst century. Voronezh, Voronezh State University, 2003. P. 111-122.
27. **Sobolev N.V.** Deep-seated inclusions in kimberlites and the problem of upper mantle composition. – Novosibirsk: Science, 1974. P. 264.
28. **Spetsius Z.V., Serenko V.P.** Composition of continental upper mantle and crust bottoms under the Siberian platform. – M.: Science, 1990. P. 272.
29. **Vaganov V.I.** Diamond deposits of Russia and the World. Moscow: Geoinformmark. 2000. P. 371.
30. **Vasilenko V.B., Zintchouk N.N., Kuznetsova L.G.** Petrochemical models of diamond deposits of Yakutia. Novosibirsk, Science, Sib. branch of RAS, 1997. P. 574.
31. **Zintchouk N.N., Koptil' V.I**. Typomorphism of the Siberian platform's diamonds. – M.: Nedra, 2003. P. 603.

UDK 552.48; 552.321.6

Exsolution textures and minerals inhomomgeneity in xenoliths from Yakutian kimberlites: evidence for the mantle evolution

Spetsius Z. V.[a] and Spetsius V. Z.[b]

[a]*Institute of Diamond Industry, ALROSA Co. Ltd, Mirny, Russia*
[b]*Moscow State University, Russia*

More and more evidence is being discovered on the later mantle evolution after the formation of subcontinental lithosphere and stabilization of the Platform. The main high-pressure mineral indicators for that are coesite, diamonds and exsolved phases in different minerals of mantle xenoliths. Recent discoveries of pyroxene exsolution in garnet as well as the presence of majoritic garnets among inclusions in diamond and xenoliths from kimberlites suggest ultra-high pressure and deep levels of their possible origin. Exsolution textures in different minerals of mantle xenoliths from kimberlites represent another line of evidence for some complicated history of mafic and ultramafic mantle rocks.

In this paper we have tried to combine different indicators features of transformation and evolution rocks and minerals that are present among mantle xenoliths from kimberlites of Yakutia. Zonation and other possible heterogeneities of minerals are discussed. These heterogeneities are mainly caused by the presence of oriented lamellae of rutiles and other phases in garnets, ilmenites in rutiles and kyanites and different kind of exsolution textures. Variations of major and trace elements caused by these processes are present and possible PT-conditions and path of mineral evolution after their origin also are discussed. Special attention was paid to difference in distribution of exsolution textures and evolution of xenoliths from individual pipes and kimberlite fields of Yakutian Province.

KEY WORDS: *exsolution textures; eclogite xenoliths; garnet; coesite; kimberlites; mantle evolution; Yakutia*

Email address: Spetsius@yna.alrosa-mir.ru

INTRODUCTION

In many papers devoted to mantle petrology and in particular to mantle composition under Siberian Platform it is shown that lithospheric mantle under Yakutian kimberlite Province was formed about 3 Ga years ago (e.g. Pearson et al., 1995; Griffin et al., 2002). These data have been obtained as a result of mantle rocks and minerals dating with using Sm-Nd, Re-Os and others modern methods of isotope system analyses. All these methods are based on the statement that minerals in mantle xenoliths are in equilibrium that is correct and in most cases represents the facts according to the dates of investigations of mantle xenoliths from kimberlite pipes.

As a rule in most mafic and ultramafic mantle xenoliths the main rockforming minerals do not show evidence of zonality and are in equilibrium behavior with each other. That suggests that they were formed in stable termodynamic conditions or have been completely reformed and re-equilibrated by subsequent metamorphic or metasomatic processes on mantle levels (Spetsius and Serenko, 1990). At the same time exsolution textures, zonal minerals and exsolved phases as in rockforming and accessory minerals occur in separate samples of mantle xenoliths especially of eclogitic and pyroxenitic compositions.

For the past two decades different evidence for the ultrahigh-pressure (UHP) formation of some mantle and crustal rocks has been recognized through the finding of exsolved phases and substitution in their minerals. These occurrences include exsolved phases in host minerals that suggest that the original mineral had a composition indicative of the UHP (Haggerty and Sautter, 1990; Zhang and Liou, 1999; Leost et al., 2002). Different examples of exsolution due to decompression from UHP minerals include rods of ilmenite in olivines from the Alpe Arami garnet peridotites (Dobrzhinetskaya et al., 1996) and the Dabie-Sulu UHP terrane (Hacker et al., 1997), K-feldspar lamellae in clinopyroxene and coesite in titanite from the UHP diamondbearing metamorphic rocks of the Kokchetav massif, Kazakhstan (Sobolev and Shatsky, 1990; Ogasawa et al., 2002), K-feldspar lamellae in clinopyroxene inclusions in eclogitic garnets from kimberlites (Harlow and Veblen, 1991) and rods of pyroxene in garnet from kimberlite xenoliths (Haggerty and Sautter, 1990).

Another line of evidence for the ultrahigh-pressure (UHP) has been summarized by Chopin (2003), which shows that in many cases UHP metamorphism could be traced between the mafic and ultramafic rocks due to the presence of several mol.% majorite component that gives micro structural evidence for exsolution of orthopyroxene in coarse garnet, implying a‘super-silicic’ precursor garnet (e.g. Haggerty and Sautter, 1990; Van Roermund and Drury, 1998). Experimental evidence is the clearest for incorporation of supersilicic, majoritic components ($MSiO_3$ or better written $Mg_3\,Mg\,{}^{VI}Si\,{}^{IV}Si_3O_{12}$) in garnets at pressures greater than 50 kbar (e.g., Irifune 1987; Gasparik, 1989). Excess of Si in the octahedral site of garnet is a signature of its UHP origin. If majoritic garnet reequilibrates in lithosphere, the supersilicic component exsolves as pyroxene.

There are other element substitutions (Ti, P, Na without excess Si) which may also indicate very high pressures (e.g. Sobolev and Lavrent’ev, 1971; Bishop et al., 1976). Na-, Ti- and P-rich garnets are evidenced by relatively high abundances of these elements in homogeneous grains of this mineral or exsolved phases such as rutile, ilmenite, clinopyroxene, and apatite which contain appreciable amounts of these constituents (Roden et al., 2003). For example, garnets equilibrated (both in nature and in experiments) at moderate to high PT-conditions are known to contain up to 2.5 wt% TiO_2, 1.6 wt% Na_2O and 0.6 wt% P_2O_5 (Sobolev and Lavrent'ev, 1971; Bishop et al., 1978; Moore and Gurney, 1985; Haggerty et al., 1994). Other garnets have exsolved rutile, Na-bearing diopside and apatite inclusions indicating that the initial garnet had appreciable amounts of Ti, Na and/or P (e.g., Roden et al., 2003; Mproskos and Kostopoulos, 2001).

The present paper particularly concentrates on the exsolution textures and some mineral inhomogeneity especially of garnets predominantly in two types of mantle xenoliths from kimberlites – eclogites and garnet pyroxenites (websterites). It should be stressed that these rocks provide the most spectacular examples of different exsolved minerals and a wide variety of exsolution textures between mantle xenoliths from kimberlites worldwide as well as from the Yakutian kimberlites.

The Siberian craton occupies about $4x10^9$ km^2, mostly buried beneath Riphean-Phanerozoic sedimentary cover 1-8 km thick, averaging about 4 km. According to the concept of terranes, which appeared and developed independently as isolated sialic masses (microcontinents), the craton's structure resulted from the collision and amalgamation (accretion) of heterochronous microcontinents, which were transformed into terranes or tectonic blocks of varying genesis (Rosen et al., 2002). Situated in the northeastern part of Siberian craton, Yakutian kimberlite province occupies mostly the territory of the Anabar superterraine, including the Magan and Daldyn granulite-gneiss terranes and the Markha granite-greenstone terrane. Kimberlite diatremes occur from the Vilyuy River in the south to the lower reaches of the Olenek and Kotui Rivers in the north, over an area of more than 1100 km in longitude and 800 km in latitude. A more detailed description is given by Rosen et al. (2002) and locations of main pipes, which were mentioned in the text, are shown on the map that is provided in the paper (Spetsius, 2004).

SAMPLES AND ANALYTICAL TECHNIQUES

More than 1000 samples of mantle xenoliths from kimberlite pipes situated in different parts of the Yakutian kimberlite province were studied. Modal analyses have been performed for the major part of xenoliths. For most samples major rock chemistry was determined. Major-element analyses were performed for the rock-forming and minor minerals. Trace element compositions were obtained for some minerals. All the samples were classified into different varieties of eclogites or pyroxenites according to their petrographic and chemical features. Particular attention has been focused on the investigation of the minerals inhomogeneity and the presence of exsolution textures or exsolved phases in rockforming and accessory minerals.

Major element compositions of silicate and oxide minerals in the xenoliths were determined with a Superprobe JXA-8800R electron microprobe at ALROSA Co Ltd. (Mirny, Russia) and partly using a CAMECA SX-50 electron microprobe at Institute of Geology (Yakutsk) and Moscow State University (MGU). Analytical conditions included accelerating voltage of 15 keV, a beam current of 20 nA, beam

---

size of 5 µm, and 20 seconds counting time for all elements. All analyses underwent a full ZAF correction.

The trace elements (TRE) have been measured in rockforming garnets and exolved grains and needles of eclogites by laser Ablation ICP-MS (LAM) at the Macquarie University in Sydney, with NIST 610 glass as external standard and Ca as internal standard; pit diameters were 40 –50mm. The trace elements in rockforming and zoned grains of garnet were obtained by Iron microprobe in the standard conditions at Yaroslavl (Russia) and partly by proton probe at CSIRO (Sydney, Australia).

PETROGRAPHY AND SAMPLE DESCRIPTION

Xenoliths of eclogites in general population of xenoliths from kimberlite pipes are fairly abundant and represent at least three varieties chemically similar, but different by mineralogy and conditions of formation. Eclogites are of a particular importance for understanding a number of problematic issues of the upper mantle petrology and greater abundance of diamond-bearing xenoliths among them in comparison with ultramafic rocks.

Varieties of ferrian, magnesian, and highly-aluminous line (groups A, B, and C eclogites according to Taylor and Neal, 1989) are distinguished among mantle eclogites that differ from each other in paragenises and also in composition of rocks and minerals. Intertransient samples are noted among some varieties.

Magnesian eclogites **(**group **A**) are coarse-grained rocks of mosaic or cataclastic and rarely poikilitic texture composed of orange garnet (to 70%), pale-green omphacite (to 50%), and admixture of rare rutile grains. They have elevated Mg# (53.2-73.8%), contain 13-21 wt% MgO and have reduced alkalinity and bulk iron content (less than 11.80 wt% $FeO+Fe_2O_3$). Rutile, sulfides, and rare ilmenite represent accessory minerals.

Ferrian eclogites **(**group **B**) are coarse-grained rocks of mosaic texture composed of orange-red garnet (about 40%) 1-10 mm size and dark-green clinopyroxene, accessories: rutile, sulfides, and ilmenite sometimes. They have low Mg# (59-66%), high content of bulk iron (from 10.07 to 14.42 wt%), and elevated content of titanium. Rutile, sulfides, and ilmenite represent accessory minerals.

Highly-aluminous kyanite eclogites **(**group **C**) are pale-grey rocks and distinguished by the presence of kyanite (to 30%), sometimes coesite (to 12%), corundum eclogites occur rarely; specimens with sanidine are solitary (Spetsius and Serenko, 1990). Wide variations of garnet (20-80%) and clinopyroxene (20-60%) content may be observed. Ore and accessory minerals are represented by rutile, rare segregation's of sulfides, ilmenite, and graphite.

Garnet websterites that sometimes are combined in croup A eclogites (Taylor and Neal, 1989) are close to magnesian eclogites by chemical composition. They represent medium-grained rock with orange-red garnet (30-40%), grass-green clinopyroxene, and pale-green orthopyroxene. The quantity of the orthopyroxene represented by enstatite having high Mg# varies from several units to 50%. Clinopyroxenes have moderate Mg# and insignificant content of jadeite component.

The quantity of xenoliths of eclogite series in different pipes is variable: kyanite eclogites are present in pipes Udachnaya, Zarnitsa and Sytykanskaya of Daldyn-Alakitsky region; grospydites (by definition contain > 50% of the grossular component) are discovered in pipe Zagadochnaya (Sobolev, 1974). In spite of a detailed investigation of xenoliths contained in pipe Mir only one specimen of corundum eclogite is found; similar formations are also rare in pipe Obnazhennaya (Spetsius and Serenko, 1990). Garnet websterites and other types of pyroxenites are abundant in pipe Obnazhennaya but bimineral eclogites are rare. Bimineral **(**group **B**) eclogites dominate in the Mir pipe.

As far as the presence of exsolution textures and mineral inhomogeneity are concerned special attention could be paid to a sample of magnesian eclogite (U-2279) from the Udachnays pipe. This sample is an ovoid eclogite block that was approximately 12 cm (maximum dimension) before sectioning. Modal composition of sample is: Cpx – 61.0 vol.%, Gt - 37.0 vol.%, Ru - 1.5 vol.% and Sf - 0.5 vol.%. It is inequigranular with large (up to 20 mm) clinopyroxene grains and rounded (up to 10 mm) grains of orange garnet. Heterogeneous distribution of garnet and clinopyroxene in different parts of eclogite and presence of large and little grains of garnet should be noticed. Little rounded garnet grains (about 0.5 mm) are situated in omphacite matrix and probably have exsolved from a formerly high-Al clinopyroxene. This sample contains both rare zonal garnet grains and exsolution lamellas of garnet in omphacite (Fig. 1a). Besides, most rutiles in this sample contain both needles of ilmenite and have outer ilmenite rims as it will be shown later.

The eclogite xenolith (U-2338) is similar to this sample that is rather close by mineral compositions, petrographic peculiarities and presence of oriented lamellas of garnet in clinopyroxene (Fig. 1b). It should be pointed that by the rock and mineral chemistry this sample belongs to the Group A eclogites and contains small rounded garnets grains (around 0.5 mm in size), besides of large garnet grains of (2-3mm in size), that are present as exsolved phases in large porphyroblasts of clinopyroxene.

Kyanite eclogite (sample U-795) from the Udachnaya pipe has been chosen for detailed studying due to the presence of exolved needles of kyanite in omphacite (Fig. 1c) that are quite similar to elongated intergrowth of this mineral in eclogite-like rocks from the same pipe (Spetsius, 2004). By its modal composition this xenolith consists of: Cpx - 47,0 vol.%, Gt - 34.0 vol.%, Ky – 17.0 vol.%, Ru - 1.5 vol.% and Cs - 1.5 vol.%.

Special attention should be paid to rare intergrowth of garnet and coesite that was found only in two samples of kyanite eclogites with coesite from the Udachnaya pipe (Fig. 1d). Both these samples are rounded coarse grained

---

eclogites. In particular sample U-168 by its modal composition consists of: Cpx - 47,0 vol.%, Gt - 34.0 vol.%, Ky – 17.0 vol.%, Ru - 1.5 vol.% and Cs - 1.5 vol.%.

It is a coarse grained partly deformed rock with strongly altered clinopyroxene, which fresh relicts come to about 3%. Coesite is present as single grains that are strongly replaced by secondary quartz with the formation of characteristic pseudomorphs and intergrowth with garnet also mostly replaced by the quartz of pronounced palisade texture.

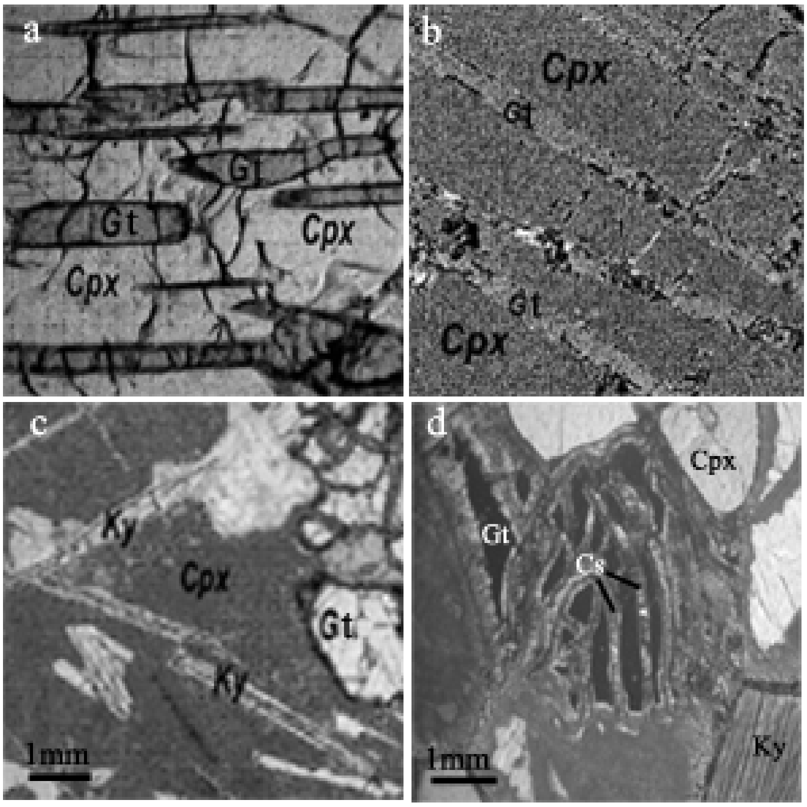

Fig. 1**. Exsolution textures in eclogite xenoliths from the Udachnaya pipe.**

(a, b) Lamellae of garnet in clinopyroxene (thickness of lamellae about 50 micron), sample U-2279 & U-2338; (c) Newly formed needles of kyanite after omphacite, sample U-795; (d) Intergrowth of garnet with coesite replaced by the quartz of pronounced palisade texture, sample U-168. Legend for these and other photomicrograph figures is as follows: Gt = garnet, Cpx = primary omphacite, Cpx_2 = secondary clinopyroxene in spongy texture, Opx = orthopyroxene, Ky = kyanite, Cd = corundum, Cs = coesite, Ilm = ilmenite, TiMt = titanomagnetite.

Spectacular exsolution textures have been met in a sample of eclogite from the Obnazhennaya pipe (Fig. 2a). This eclogite represents ovoid xenolith approximately 6 cm (maximum dimension) that consists of coarse grained light green omphacite, which is cut by tiny lamellas of orange garnet. Unusual in composition exsolution texture has been met in corundum eclogite from this pipe (Fig. 2b) that consists of tiny lamellae of garnet and corundum in clinopyroxene.

It should also be pointed to the presence of garnet exsolution in orthopyroxenites. One of such sample is shown on (Fig. 2c) and by some garnet lamellae close to the exsolved lherzolites that are discovered and described in Monastery pipe (Dawson, 1994). Coarse rod-shaped lamellae or elongate pods of garnet are abundant in porphyroclastic enstatite. Such xenoliths are frequently found in the Udachnaya pipe and they are worth of additional investigation. Wide distribution of specific textures in garnet websterites and eclogites group A is important both for their recognizing and for understanding of their origin. These xenoliths are distinguished by the presence of small rounded garnet grains in clinopyroxene matrix (Fig. 2d).

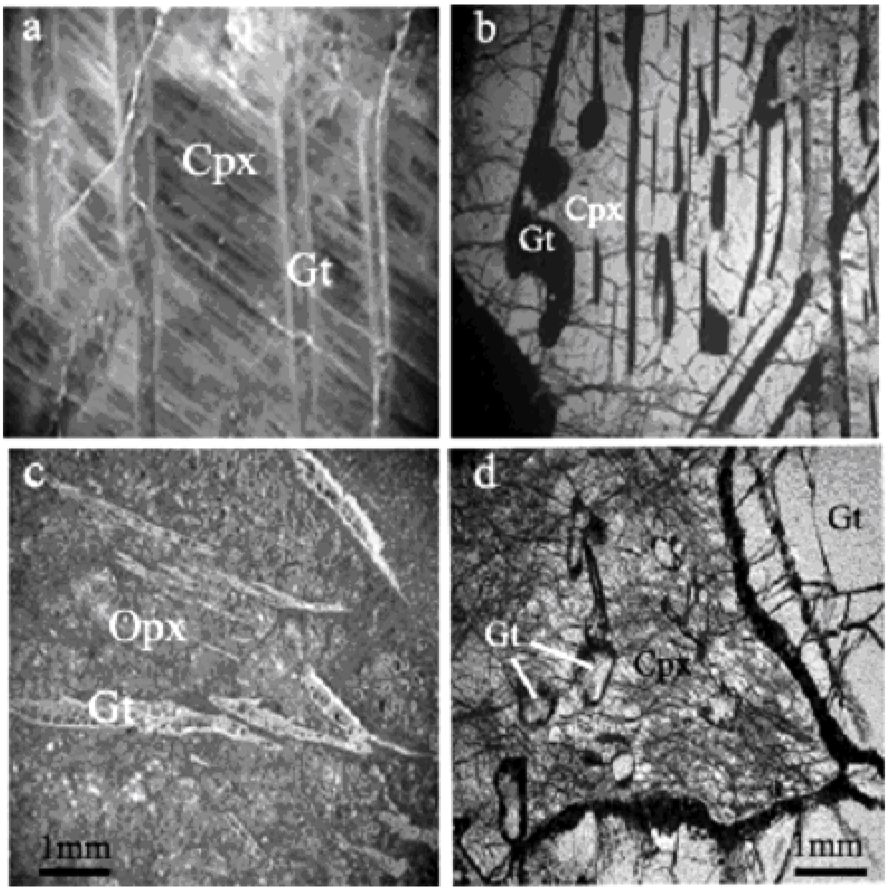

Fig. 2. **Typical types of exsolution textures.**

(a) Needles of garnet in eclogite clinopyroxene, sample O-88 from the Obnazhennaya pipe; (b) Exsolved garnet and corundum in eclogite from Obnazhennaya, sample O-3465; (c) Needles of garnet in orthopyroxene, sample U-30-80; (b) Rockforming garnet and exsolved small rounded garnet grains in clinopyroxene matrix of magnesian (group A), sample **U-68.**

MINERAL CHEMISTRY

Zoned Garnet

Garnet is a major mineral of eclogite and pyroxenite xenoliths especially garnet websterites. Chemical composition of this important constituent of eclogites largely reflects their nature. Garnets from the majority of eclogites and websterites exhibit intra- and intergrain homogeneity (e.g. Spetsius and Serenko, 1990; Taylor et al., 2003). Garnets from eclogites show a wide variation in content of Mg, Fe and Ca oxides. Eclogitic garnets usually are poor in chrome content but in websterites and pyroxenites they could contain up to 1.0 wt% Cr_2O_3. Analyses of garnets were made in different types of eclogites with the attention to possible

---

zoning of this mineral (Table 1). We presented here only our original data that show a rather wide difference in Mg/(Mg+Fe) ratio from sample to sample and obvious variation in content of major elements from core to rim. It should be pointed that zoning in garnets probably could be formed as a result of at least two different processes: (1) magmatic crystallisation or subsolidus transformation that is subsequent in time with the exsolution textures as in sample U-2279 (Fig. 3a) and (2) zoning could be a result of metasomatic events. Last statement is obvious from the picture (Fig. 3b) that demonstrates a relationship of zonality with the intergranular space and boundaries between the mineral grains and cracks. It correlates with intensity of metasomatic processes and was formed under fluids incorporation. It should be stressed that changing of major elements from the core to the

Table 1.

Zoned garnet in eclogite xenoliths

Sample.	**Description**	**SiO_2**	**TiO_2**	**Al_2O_3**	**Cr_2O_3**	**FeO**	**MnO**	**MgO**	**CaO**	**Na_2O**	**Total**
U-2340	core	38.74	0.62	21.14	0.07	21.83	0.43	8.15	8.65	n.a.	99.62
U-2340	rim	38.23	0.56	20.21	<0.03	23.44	0.42	7.6	9.28	n.a.	99.77
U-2279	core	39.08	0.4	22.16	0.04	17.28	0.36	8.54	12.33	0.29	100.5
U-2279	rim	39.04	0.44	22.03	0.03	16.36	0.32	8.06	12.7	0.28	99.29
U-2279	coarse gr	39.41	0.44	22.11	0.06	16.49	0.36	8.27	12.54	0.27	99.95
U-2279	lammella	41.08	0.46	22.86	0.07	10.38	0.49	18.13	6.24	0.17	99.88
B-18	core	39.81	n.d.	22.04	n.d.	19.49	0.55	12.52	5.52	n.a.	99.93
B-18	rim	39.02	n.d.	21.44	n.d.	22.22	0.5	10.24	6.27	n.a.	99.68
B-20	core	40.18	0.17	23.60	0.09	16.32	0.32	16.49	1.14	0.15	98.45
B-20	rim	40.26	0.22	23.73	0.08	14.27	0.35	18.26	0.9	0.16	98.23
N-24	core	41.72	0.29	22.85	0.10	17.07	n.d.	14.87	4.01	0.12	101.03
N-24	rim	41.87	0.31	23.00	0.07	16.88	n.d.	14.54	4.00	0.11	100.77
N-66	core	41.17	0.20	22.41	0.19	9.46	n.d.	12.31	13.71	0.08	99.52
N-66	rim	41.44	0.49	22.31	0.21	9.50	n.d.	16.21	9.25	0.11	99.52
N-150	core	40.81	0.46	21.90	0.08	12.58	0.21	13.87	9.23	0.15	99.29
N-150	rim	41.91	0.44	22.39	0.04	12.50	0.29	14.49	8.84	0.15	101.05
N-155	core	41.33	0.48	22.06	0.00	13.69	0.53	17.81	3.64	0.16	99.70
N-155	rim	40.53	0.45	21.87	0.01	14.20	0.56	17.14	3.39	0.15	98.30

Note. Abbreviations (here and further): B-pipe Botuobinskaya, M-pipe Mir, N-pipe Nyurbinskaya, O-pipe Obnazhennaya, U-pipe Udachnaya; n.a: not analized; n.d: not detected.

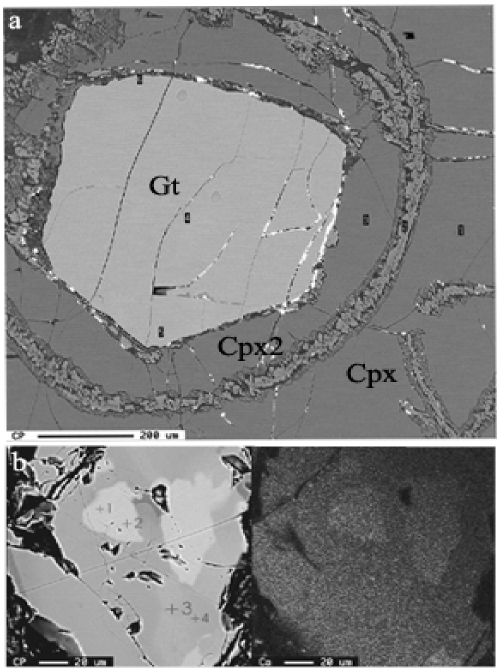

Fig. 3. **Zoning garnets in eclogite xenoliths.**

(a) Idiomorphic garnet (size – 4 mm) in eclogite, sample U-2279. Notice a newly formed clinopyroxene (Cpx_2) around garnet; (b) Zoned garnet in diamondiferous eclogite (Botuobinskaya pipe, sample B-20). Inhomogeneous elements distribution as a result of metasomatose is obvious.

rim is different in these two cases (see Table 1).

Clinopyroxene

Clinopyroxene is characterized by high Mg#, high-Al content and it is a typical omphacite. Clear correlation of jadeite (Jd) content in omphacites of eclogite rocks both bimineral and with kyanite is observed along with their Al_2O_3 and CaO-content (Table 2), and therewith this relationship is maintained in eclogite clinopyroxenes from all the pipes studied before (Spetsius and Serenko, 1990; Taylor et al., 2003). The clinopyroxene, unlike the garnet, is of homogeneous composition regardless of its relationship with the garnet and practically never shows any zonality. Analyses of the clinopyroxene show no detectable compositional variation between grain cores and rims, or between different grains. Analyses were carried out in

Table 2

Clinopyroxenes in eclogitetes with exolution textures

Sample.	**U-2279**	**U-2279***	**U-2279$^+$**	**U-534**	**U-795**	**U-593**	**U-2245**	**U-420**	**U-2278**
SiO_2	56.11	55.14	53.15	55.77	55.1	55.81	56.37	55.47	54.69
TiO_2	0.42	0.34	0.51	0.21	0.28	0.3	0.27	0.23	0.24
Ai_2O_3	13.42	2.9	7.82	14.81	15.17	13.85	12.87	10.01	8.53
Cr_2O_3	0.07	0.02	0.11	n.d.	0.04	0.06	0.09	0.06	0.06
FeO	4.02	3.44	5.19	3.56	1.88	1.38	2.12	4.71	5.18
MnO	0.03	0.11	0.05	0.04	0.03	0.02	0.09	0.05	0.07
MgO	6.94	15.94	11.24	6.39	7.6	7.68	8.27	8.83	9.91
CaO	10.49	19.98	17.41	11.56	13.09	11.39	11.89	14.74	16.42
Na_2O	8.06	2.21	3.55	7.6	7.21	7.61	6.18	5.45	4.8
K_2O	0.09	0.07	0.04	0.05	0.07	0.07	0.01	0.02	0.05
Total	99.65	100.15	99.07	99.99	100.47	98.17	98.48	99.57	99.94

Note.*: clinopyroxene from the rim around garnet; $^+$: clinopyroxene between garnet needles; U-534, 593, 795: from Ky-eclogites; other abbreviations as in Table 1.

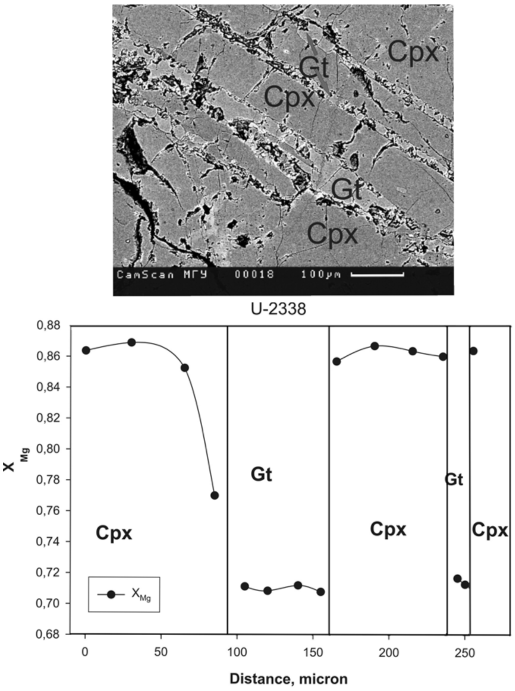

Fig. 4. **Composition profile (Mg#) in garnet lamellae and adjacent omphacite.**

Sample U-2338 is presented by bimineral (Group A) eclogite from the Udachnaya pipe.

different areas in the porphyroclasts (close to, and away from, areas of exsolved garnet lamellae; the lamella-free grain-margins). A striking feature is its remarkably uniform composition (Fig. 4 and Table 3).

Table 3.

Composition profiles of garnet lamellae and adjacent omphacites

Profile 2920 µm

Distance	Sample	O-88	SiO_2	TiO_2	Al_2O_3	Cr_2O_3	FeO	MnO	MgO	CaO	Na_2O	Total
0	1	Cpx	53.91	n.a.	8.35	0.36	1.84	n.a.	12.68	19.23	3.37	99.73
200	2	Cpx	54.04	n.a.	8.25	0.28	2.06	n.a.	12.96	19.17	3.19	99.95
200	3	Cpx	54.45	n.a.	7.36	0.26	1.72	n.a.	13.17	19.83	3.15	99.93
50	4	Cpx	54.84	n.a.	6.77	0.26	1.69	n.a.	13.45	19.89	2.97	99.86
50	5	Cpx	55.03	n.a.	5.77	0.31	1.71	n.a.	14.34	20.29	2.51	99.96
50	7	Grt	41.56	n.a.	23.58	n.a.	10.14	n.a.	17.81	6.49	n.a.	99.57
50	8	Grt	42.35	n.a.	23.53	n.a.	9.73	0.24	17.79	6.13	n.a.	99.78
50	9	Grt	41.92	n.a.	23.55	0.22	10.06	0.34	17.70	6.21	n.a.	100.00
50	10	Grt	41.47	n.a.	23.64	n.a.	9.88	n.a.	18.31	6.27	n.a.	99.57
100	11	Grt	41.36	n.a.	23.60	0.28	9.86	n.a.	18.25	6.34	n.a.	99.68
300	12	Grt	41.82	n.a.	23.35	0.22	9.83	n.a.	18.31	6.19	n.a.	99.72
300	13	Grt	41.75	n.a.	23.36	0.22	9.85	n.a.	17.93	6.36	n.a.	99.46
320	14	Grt	41.37	n.a.	23.35	0.3	10.02	0.29	17.87	6.66	n.a.	99.85
50	15	Grt	41.47	n.a.	23.68	n.a.	10.15	0.37	17.61	6.55	n.a.	99.84
50	16	Grt	41.93	n.a.	23.34	n.a.	10.07	0.22	17.58	6.66	n.a.	99.80
50	18	Cpx	54.62	n.a.	5.35	0.35	1.49	n.a.	14.80	21.10	2.14	99.85
50	19	Cpx	54.40	n.a.	6.88	0.39	1.60	n.a.	13.64	20.07	2.95	99.93
50	20	Cpx	54.25	n.a.	7.54	n.d.	1.95	n.a.	13.14	19.87	2.91	99.67
50	21	Cpx	54.32	n.a.	8.02	0.39	1.83	n.a.	12.83	19.42	2.93	99.76
900	22	Cpx	53.86	n.a.	9.12	n.d.	1.93	n.a.	12.10	19.65	3.16	99.81

Profile 255 µm

Distance	Sample	U2338	SiO_2	TiO_2	Al_2O_3	Cr_2O_3	FeO	MnO	MgO	CaO	Na_2O	Total
0	29	Cpx	54.67	0.24	2.29	n.d.	4.56	n.d.	16.22	20.32	1.51	99.80
30	30	Cpx	54.69	0.19	2.01	n.d.	4.39	0.21	16.33	20.61	1.48	99.90
35	31	Cpx	54.19	0.19	1.92	0.21	5.07	n.d.	16.48	20.04	1.58	99.67
20	32	Cpx	48.80	0.58	7.82	n.d.	8.19	0.58	15.40	18.29	n.d.	99.65
20	33	Grt	40.89	0.46	21.93	n.d.	12.80	0.53	17.69	5.44	n.d.	99.74
15	34	Grt	41.22	0.56	21.63	0.22	12.82	0.45	17.48	5.54	n.d.	99.91
20	35	Grt	41.08	0.52	21.87	n.d.	12.69	0.45	17.61	5.63	n.d.	99.85
15	36	Grt	40.98	0.56	21.59	0.25	12.89	0.50	17.52	5.73	n.d.	100.00
10	37	Cpx	54.41	n.d.	1.98	n.d.	4.84	n.d.	16.28	20.56	1.48	99.54
25	38	Cpx	53.99	0.26	1.94	n.d.	4.56	n.d.	16.72	20.50	1.72	99.68
25	39	Cpx	54.45	0.22	1.97	n.d.	4.63	n.d.	16.51	20.69	1.37	99.84
20	40	Cpx	54.53	0.20	1.92	n.d.	4.78	n.d.	16.54	20.61	1.23	99.80
10	41	Grt	41.42	0.54	22.24	n.d.	12.26	0.46	17.41	5.52	n.d.	99.84
5	42	Grt	41.02	0.48	21.97	n.d.	12.67	0.45	17.64	5.42	n.d.	99.65
5	43	Cpx	54.41	0.21	1.79	n.d.	4.63	n.d.	16.52	20.60	1.69	99.85

Orthopyroxene

Analyses of orthopyroxenes have been taken predominantly from the published paper, but some analyses were obtained from the orthopyroxenes containing lamellae of garnets (Table 4). A striking feature is its remarkably uniform composition. Orthopyroxenes occur as primary assemblage in garnet websterites of Obnazhennaya pipe and as exsolution lamellae (Taylor et al., 2003). In the latter case the mineral is more Al_2O_3- and FeO-rich than its discrete granular counterparts in the same sample (see Table 4)

Table 4.

Orthopyroxenes and other minerals in websterites with exsolution textures

Sample	**U3080p***	**O3207w**	**O-3199p**	**O-926e**	**O-1103e**	**O-1108e**	**O901w**		**O1109w**	
	exsol	exsol	exsol	exsol	exsol	exsol	coarse	exsol	coarse	exsol
SiO_2	56.92	56.69	57.33	56.6	56.2	54.9	56.1	55	57.8	55.3
TiO_2	0.09	0.08	0.11	0.03	0.08	0.09	0.06	0.07	0.09	0.07
Al_2O_3	0.37	1.28	0.94	0.76	1.97	3.67	1.18	3.47	1.17	3.46
Cr_2O_3	0.25	0.35	0.25	0.05	0.04	0.18	0.14	0.14	0.14	0.08
FeO	4.45	2.48	5.05	9.15	8	6.94	6.77	7.53	4.44	5.25
MnO	0.16	0.07	0.1	0.07	0.11	0.13	0.09	0.11	0.07	0.1
MgO	36.68	38.85	36.77	32.6	32.5	33.2	34.6	32.9	36.7	35.4
CaO	0.31	0.19	0.2	0.23	1.29	0.2	0.24	0.2	0.2	0.2
Na_2O	0.14	0.01	0.12	0.06	0.25	0.05	0.05	0.07	0.04	0.06
K_2O	<0.03	0.02	0.01	<0.03	<0.03	<0.03	<0.03	<0.03	0.03	<0.03
Total	99.35	100.01	100.87	99.55	100.44	99.34	99.23	99.49	100.65	99.92

Note.*Designation of eclogite (e), websterite (w) or pyroxenite (p) lithology. Analyses 4-10 from (Taylor et al., 2003),

RUTILE

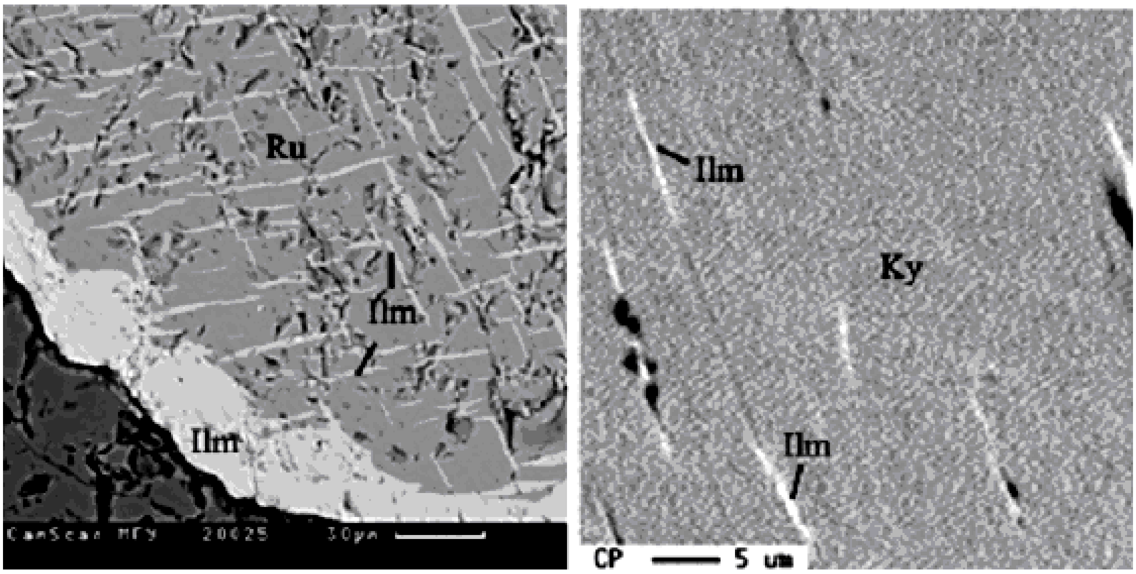

Fig. 5. Exsolved lamellae of ilmenite.

(a) Lamellae and rim of ilmenite in rutile, sample U-2279; (b) Needles of ilmenite in kyanite of diamondiferous eclogite from the Nyurbinskaya pipe, sample N-1.

Rutiles are common minerals for all types of eclogites and they are often present in garnet websterites. By their composition rutiles are not distinguished between different eclogite varieties. Rutiles from eclogites often contain tiny lamellas of ilmenite and titanomagnetite and also the rims of the latter mineral that suggests changing of oxygen and temperature conditions and probably as a result of the metasomatic fluids action. Such textures are widespread in eclogites from the Udachnaya pipe, as for example in sample U-2279 (Fig. 5a). The detailed EMP study of the rutiles was performed especially for the minerals with inclusions. As a rule rutiles are homogenous in the given samples (Table 5). The major variables are Al_2O_3 and FeO contents.

Table 5

Rutiles in eclogitetes and pyroxenites with exolution textures

Sample	**U-2279**	**U-534**	**U-795**	**U-795**	**U-593**	**U-420**	**U-420**	**U-34**	**U-2278**	**U-2278**
	Ru-gr	Ru-gr	Ru-gr	Ru-n*	Ru-gr	Ru-gr	rim Ru	Ru-gr	Ru-gr	TiMt**
SiO_2	0.11	n.d.	n.d.	0.18	n.d.	n.d.	38.27	n.d.	n.d.	n.d.
TiO_2	89.01	94.78	99.74	99.16	99.14	99.58	4.52	99.33	97.01	81.87
Ai_2O_3	3.73	0.22	<0.03	<0.03	0.1	0.09	18.02	0.14	<0.03	<0.03
Cr_2O_3	0.2	0.02	0.08	0.11	0.08	0.06	0.03	0.02	n.d.	n.d.
FeO	2.23	4.95	0.7	0.53	0.3	0.66	13.08	0.08	0.24	15.41
MnO	0.03	0.04	0.05	0.05	0.08	<0.03	0.27	0.01	<0.03	<0.03
MgO	1.63	0.36	n.d.	0.04	<0.03	0.04	9.53	0.09	0.03	0.52
CaO	0.04	0.04	0.11	0.45	0.01	0.03	10.42	<0.03	<0.03	0.01
Na_2O	0.13	0.04	n.d.	<0.03	<0.03	<0.03	2.56	n.d.	n.d.	n.d.
K_2O	0.04	0.01	0.07	0.14	0.01	0.04	1.4	0.02	0.02	0.01
Total	97.15	100.46	100.75	100.66	99.72	100.49	98.6	99.69	97.3	97.9

Note.*-rutile needles in Cpx, **- rim on rutile

Inclusions in rutile

A typical feature of some samples of rutile is the presence of regular lamellae of other mineral phases, which in most cases are presented by ilmenites, different in compositions, and titanomagnetites (Table 6). These minerals mould also outer

Table 6

Exsolved phases in rutiles from eclogies and pyroxenites

Sample	**U-593**	**U-534**	**U-2278**	**U-593**	**U2245**	**U420**	**U-948**	**U2278**	**U-2278**	**U-534**
	nd* in Ru	incl in Ru	nd in Cpx	nd in Ru	nd in Ru	Ru rim	incl.in Ru	TiMt rim	nd in Cpx	incl in Ru
SiO_2	0.12	n.d.	2.38	0.12	0.05	38.27	n.d.	n.d.	2.38	n.d.
TiO_2	25.37	63.87	94.09	25.37	23.61	4.52	63.76	81.87	94.09	65.93
Ai_2O_3	70.46	0.61	0.84	70.46	49.33	18.02	<0.03	n.d.	0.84	n.d.
Cr_2O_3	0.54	0.02	0.09	0.54	0.68	0.03	0.01	<0.03	0.09	0.07
FeO	1.32	34.58	0.79	1.32	11.89	13.08	29.12	15.41	0.79	30.54
MnO	<0.03	0.01	0.02	<0.03	0.05	0.27	0.18	n.d.	0.02	0.14
MgO	0.39	2.15	0.24	0.39	13.23	9.53	5.88	0.52	0.24	2.77
CaO	0.02	0.02	1.26	0.02	0.03	10.42	<0.03	0.01	1.26	0.01
Na_2O	0.09	0.02	0.23	0.09	0.04	2.56	n.d.	n.d.	0.23	n.d.
K_2O	<0.03	0.02	0.01	<0.03	<0.03	1.4	0.03	0.01	0.01	0.03
Total	98.31	101.31	99.94	98.31	98.92	98.6	98.99	97.9	99.94	99.49

Note. nd* - needles in rutiles or clinopyroxenes.

rims on rutiles. In most cases ilmenite of lamellae and rims is the same in composition. The recognized heterogeneities in the latter mineral in one given sample, coupled with increased or decreased Mg and Fe concentrations, suggest that these lamellae are probably picroilmenites (Sobolev and Yefimova, 2000). It should be also noticed that tiny ilmenite lamellae have been recognized in kyanite of diamondiferous eclogite from the Nyurbinskaya pipe (Fig. 5b).

OTHER MINERALS

Among other minerals that participate in the process of mineral transformation corundum could be recorded, which sometimes is associated with possible partial melting of eclogites (Spetsius, 2004). Corundum occurs in the form of small needles 0.01-0.2 mm long in this case. Usually corundum replaces kyanite in eclogites, and more rarely forms separate lamellar crystals up to 2 mm in kyanite eclogites, which have undergone a high degree of partial melting. In this case it has a dark-blue color and it is referred to as sapphire. In some eclogites of Obnazhennaya, the corundum is ruby-red in color but this might be formed as exsolution from clinopyroxene (see Fig. 2).

Trace element chemistry

Rare occurrences and a usual little size of exsolved minerals didn't allow us to obtain a lot of data on their trace element content. The trace element contents as zoned garnet grains and exsolved lamellae determined by proton-probe analysis are given in Table 7 and trace element content in the garnet exsolution as well. Some data are shown graphically in Fig. 6.

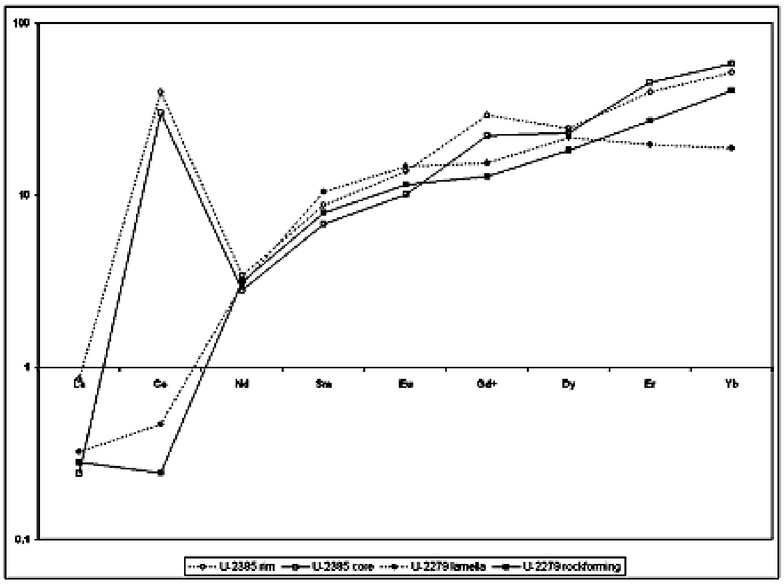

Fig. 6. **Chondrite-normalized REE diagram for the garnets of eclogites from the Udachnaya kimberlite pipe.**

U-2385 – zoned garnet of eclogite (Group A); U-2279 – exsolved garnet of eclogite (Group B) xenolith. Normalized against chondrite values of McDonough & Sun (1995).

Table 7.

Trace element content in zoned garnet and clinopyroxene in eclogite
(sample U-2279, proton probe data, in ppm)

Description	**Mn**	**Fe**	**Ni**	**Cu**	**Zn**	**Ga**	**Rb**	**Sr**	**Y**	**Zr**	**Ba**
Gt - grain1	0.255	12.6	47	n.d.	89.9	19.4	n.d.	3.79	41.5	92.3	n.d.
Gt - grain2	0.264	12.7	45.5	n.d.	89.5	17.4	n.d.	2.2	39.9	94.6	23.1
Gt - grain3	0.26	12.8	45	0.594	88.9	18	n.d.	2.04	41	100	57.4
Gt - grain4	0.257	12.4	40.2	1.1	89.5	19.4	n.d.	3.98	41.7	93.6	46.7
Gt - grain5	0.257	12.1	76.2	n.d.	89.1	16.9	1.15	67.2	39.5	95.6	71.7
Gt - grain6	0.222	10.8	120	8.02	93.5	22.5	3.5	20	27.7	74.6	43
Gt - grain7	0.392	11.2	10.2	n.d.	28.4	13.9	1.04	4.33	28.7	62.1	95.2
Gt - grain8	0.345	9.02	18	n.d.	22.5	16.5	3.71	7.77	22	69.6	n.d.
Gt - grain9	0.297	7.78	31.5	1.85	19.1	16.5	10.5	47.4	16.3	80.8	36.6
Gt - grain10	0.365	7.79	51.1	n.d.	22.3	17.5	5.91	18.1	25.2	109	60.6
Gt - grain11	0.387	8.2	28.5	n.d.	22.3	15.7	4.52	12.9	25.8	95.8	45.9
Gt-core01	0.227	13.7	51	n.a.	97.7	21	n.a.	4.12	45.1	100	n.a.
Gt-core02	0.287	13.8	49.5	n.a.	97.3	18.9	n.a.	2.39	43.4	103	n.a.
Gt.- core03	0.283	13.9	48.9	n.a.	96.6	19.6	n.a.	2.22	44.6	109	n.a.
Gt - perif04	0.279	13.4	43.7	n.a.	97.3	21.1	n.a.	4.32	45.3	102	n.a.
Gt - perif05	0.299	13.2	82.9	n.a.	96.8	18.4	n.a.	73.1	42.9	104	n.a.
G t- perif06	0.241	11.7	130	n.a.	102	24.4	n.a.	21.8	30.2	81.1	n.a.
Gt - grain near Ru	0.426	12.2	11.1	n.a.	30.9	15.1	n.a.	4.71	31.2	67.5	n.a.
Cpx-rim1	277	3.08	399	n.d.	70	38.9	n.d	147	1.72	42.4	39.2
Cpx-rim2	249	3.25	394	2.57	70.2	40.4	1.5	141	n.d.	40.6	83.8
Cpx-rim3	269	3.16	401	1.83	67.9	41.2	0.432	138	0.595	34.4	n.d.
Cpx1, relict	199	1.63	444	20.1	37.3	16.4	0.062	131	n.d.	3.13	74
Cpx2, relict	277	1.67	429	24.8	40.1	17	1.29	172	n.d.	2.76	101
Cpx3, relict	214	1.57	422	17.7	34.3	13.4	0.562	127	n.d.	2.04	73.2
Cpx4, relict, big gr.	273	2.77	331	n.d.	31.7	37.4	0.453	88.9	n.d.	32.8	36.7
Cpx5	253	2.82	364	n.d.	32.4	37.4	n.d	88.2	0.893	31.8	70
Cpx6 - betw.Gt needles	703	2.69	271	n.d.	18.7	13.4	2.21	176	2.45	56.7	72.4
Cpx7- betw.Gt needles	579	2.57	277	n.d.	18.9	13.6	1.67	188	3.64	55.5	37.4

DISCUSSION

Importance of the presence of exsolved phases and solution textures

Some garnets from high-Mg garnet pyroxenite xenoliths from the Mir pipe have triangular arrays of mineral inclusions consistent with an origin by exsolution (Roden et al., 2003). The inclusions are small (~100 micrometers), controlled by the garnet structure and concentrated in the centers of the grains. They have identified 6 high Mg garnet clinopyroxenites and websterites that contain garnet that is rich in these inclusions. The mineral assemblages contained in the garnets were variable, and consist of: diopside + rutile, diopside alone, rutile + high Mg (13-17 wt.% MgO) ilmenite and high Mg ilmenite alone (see Table 2).

Somewhat similar assemblages have been reported in the garnets from the Jagersfontein kimberlite and in garnets of Norwegian orogenic peridotites (Haggerty and Sautter, 1990; Van Roermund et al., 2000). Exsolution of diopside by itself indicates that the garnet was supersilicic and formed at very high pressures. The other exsolved mineral assemblages do not require an originally supersilicic garnet, and experimental evidence is lacking to constrain the pressure and temperature of origin.

Exsolution of diopside and rutile could result from coupled substitution of Na and Ti in the garnet and exsolution of ilmenite may reflect an Al- and Si- poor garnet component. These substitutions may represent high temperature rather than high pressure substitutions if the pyroxenites formed as cumulates from an alkaline magnesian magma that intruded into the lithosphere. Thermobarometric calculations based on experiments (Brey and Kohler, 1990) for two of these pyroxenites show that they were equilibrated in the lithosphere at relatively low temperatures (750-800^{o}C) and moderate pressures (20-30 kb, Roden et al., 2003).

Possible PT-conditions of solution textures formation

Equilibrium pressures and temperatures for both garnet peridotites and the websterites were estimated using clinopyroxene–orthopyroxene, Fe–Mg exchange, and the Al_2O_3 solubility in orthopyroxene, according to the calibrations of Brey and Kohler (1990). Olivine does not appear in the group A eclogites. However, the geothermometer and geobarometer are still applicable, because this does not affect the element partitioning between clinopyroxene–orthopyroxene and garnet–orthopyroxene. Additionally, as shown by Sobolev et al. (1999), it is not possible to accurately calculate Fe3+ from electron microprobe analyses. Therefore, all Fe in clinopyroxene and garnet is assumed to be Fe2+. With this assumption, the temperature estimates reported by Taylor et al. (2003) were considered to represent maximum equilibration temperatures. Nevertheless, if the same thermometer or barometer is applied to all the rocks, the uncertainties in comparison arise mainly from the precision of the EMP analyses. The estimated pressures are from 21.0 to 37.6 kbar, and the temperatures from 711 to 923^{o}C, for the Udacnaya and predominantly for the Obnazhennaya pipe according to the data from (Taylor et al., 2003).

Basically, no systematic differences between the websterites and peridotite groups are detected. This can be interpreted as indication that all these xenoliths, including the group A and B eclogites/websterites and the peridotites, were captured by the ascending kimberlitic melt from the same level within the upper mantle. Overall, the results of these estimations show that all of the xenoliths from Obnazhennaya were formed within the graphite stability field, a fact consistent with the barren nature for diamond of these xenoliths and host kimberlite.

In contrast to xenoliths from Obnazhennaya, those from the Udachnaya and Mir kimberlites contain diamonds, and pressure estimations for these xenoliths are mostly above 40 kbar, some 10–20 kbar higher than for most from Obnazhennaya (Boyd et al. 1997; Spetsius and Serenko, 1990). Similar conclusions about the mantle geotherm at Udachnaya were also reached by Griffin et al. (1996), by studying garnet xenocrysts in kimberlites. As shown by (Taylor et al., 2003) P–T

---

estimations correspond to a mantle geotherm of 40–45 mW/m2 at Obnazhennaya, definitely higher than that for the mantle beneath Udachnaya. This is probably related to the location of Udachnaya at the center of the Siberian platform, near the keel of the craton, whereas Obnazhennaya is near the edge (i.e., more shallow).

Besides, we should point on the difference in content of Al_2O_3 in descret enstatite and exsolution lamellae in the same samples that to average about 2 wt.% (see Table 3). Such a difference in solubility of Al in orthopyroxene that in according with the experimental data predominantly depends of pressure (Brey and Kohler, 1990) allowed to estimate a difference in pressure formation of rockforming and solved minerals not less than 10 kbars. In this case a possible PT-path for origin of exsolution textures could be explained by apvelling of intruding magmas on the distance 30-50 km.

Zonality as evidence for the mantle evolution

Zonality of garnet grains in xenoliths is rare occurrence. Nevertheless it has been ascertained for many pipes of the Yakutian Kimberlite Province namely Udachnaya, Mir, Obnazhennaya, Botuobinskaya (e.g. Spetsius and Serenko, 1990) and for the pipes of some other kimberlite provinces of the world (e.g. Dawson et al., 1990; Griffin et al., 1999). Generally it is possible to distinguish 4 types of processes during which zonary garnets are formed. Each process is being corresponded with its own type of zonality of the mineral:

1. Slow cooling of the system: zonality is not characteristic of the process or there is a too weakly distinguished direct zonality (the first percentage of petrogenic oxides - MgO, FeO, CaO).
2. Prompt cooling system: the most rare case owing to which feebly marked direct zonality is formed.
3. Intrusion of partly crystallized magmas to higher levels of the mantle: medium, sometimes very strongly pronounced reverse zonality up to several, sometimes almost up to ten major petrogenic oxides - MgO, FeO, CaO and Cr_2O_3.
4. Formation of zonality under action of metasomatic fluids, probably, also connected with the changing of PT-environmental conditions.

Let's stop at considering each type of processes and zonalities generated owing to them. The basic accent in this operation is made on studying the 3-rd type of above processes of zonalities, as on the proof of composite evolution and polyphase nature of mantle rocks and an explanation of the mechanism of such type zonality formation in garnets from xenoliths. Prior to considering mechanisms of zonary garnets formation, we shall stop at the description of the investigated system. In this case we shall understand partly crystallized magma, in which garnet is a mineral on liquidus, as "the system".

Sluggish cooling of the system results in that the melt is counterpoised with already formed garnet which thereof reacts with a melt, with formation of garnet of already other, more ferrous composition. Visual this process is represented by viewing the diagram of fusibility of garnet (in this case a solid solution pyrope and almandine) in coordinates Mg-Fe^{2+} (Fig. 7A). Owing to processes of such type direct zonality of garnet is developed exhibited in decreasing of Mg# and in slight increase of Ca#, from the centre to edges of grains, within the first percent shares of relevant petrogenic oxides.

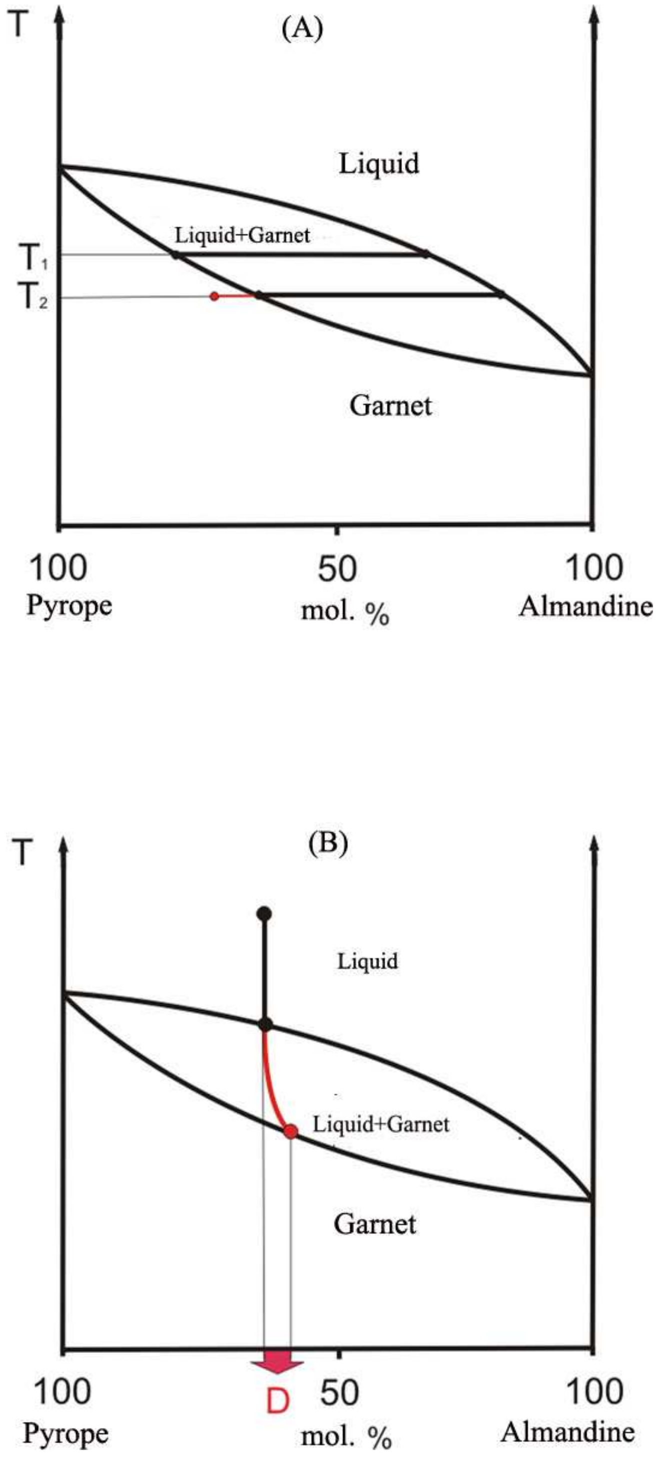

Fig. 7. **Schematic diagram of garnet zonality formation by mechanism of sluggish** (A) and prompt cooling (B).

Prompt cooling of the system results in shifting of a melt composition point to ferrous area of the garnet fusibility diagram (solid solution pyrope and almandine), that is, the melt has not time to be counterpoised with already formed garnet, and bias of a point of composition of a melt is featured by parameter that depending on temperature. Direct zonality is formed. The considered type of the process, resulting in formation of zoning garnets is most rare of the reviewed ones. Such process as intrusive propagation to higher levels of the mantle in partly crystallized magmas in which garnet is a mineral on a liquidus, finds the reflection in sharp change of exterior PT-parameters, and with one important feature: in this case the effect of pressure decrease prevails over effect of temperature decrease, as the system will react (will donate heat) on decreasing of temperature (exterior parameter) not so promptly as on pressure decrease. In this case, the effect of "throwing off" pressure prevails over temperature effect (Fig. 7B).

What does the mechanism of garnets zoning formation consist of, at such path of mantle rocks evolution? We shall consider the diagram of fusibility of garnet (solid solution of pyrope and almandine), as a projection of the threefold diagram in coordinates Ca-Mg-Fe^{2+} on plane Mg-Fe^{2+}. The system will react to pressure decrease by bias of solidus and liquidus of garnet in magnesian field of the diagram that will actually be evidenced in formation of garnets of more magnesian composition. The pressure is decreasing, as the result of magma advance to higher levels of the mantle and that causes the nature of reverse zoning of garnets from kimberlite xenoliths, sometimes reaching almost ten percent in changing of oxide content of Mg, Fe, Ca. Cases of such zonality have been described by some authors (e.g. Spetsius and Serenko, 1990) and found out by us in a sample (U-2385). In this case the content of Mg, Fe and Ca oxides is changed from the core to rim, subsequently.

Some authors consider (e.g. Anand et al., 2004) that compositions of garnets from inclusions in diamond and host-garnets do not display special differences in compositions in comparison with each other. On the contrary we want to note that, very much the other way, compositions of garnets from inclusions in diamond and host-garnets within one sample display changes of composition. On the whole, it is expressed in decrease of the content of iron in a series: inclusions of garnet in diamonds - garnet from diamondiferous xenoliths - garnet from barren xenoliths. This change of compositions of garnets, generally, with confidence, is traced on the diagram in coordinates Ca-Mg-Fe^{2+}. In that specific case (in limits of one sample) such legitimacies of change of compositions of garnets are described in a series of papers (e.g. Ireland et al., 1994; Anand et al., 2004). Taking into account the above mentioned explanation of the mechanism of zoning garnets formation during movement of partly crystallized magmas to higher levels of the mantle it becomes clear why inclusions of garnets in diamond are more ferrous than garnets from the host rock. Here the "track" of effect of pressure lowering down both from the physicochemical side of zoning garnets formation and from modal (presence and lack of diamond in xenoliths - the diagram, composition of garnet from inclusions in diamond and from the host rock containing this diamond) side of the question is legiblly traced. And it is possible to explain such effect of sharp "relief" of pressure only by intruding of xenoliths to higher levels of the mantle (for example from a field of diamond stability, to a field where diamond is not so stable), it is possible up to the boundary of the upper mantle - the Earth's crust or even into the Earth's crust. That once again confirms the complicated evolution of mantle rocks.

During studying garnet composition in xenolith (sample U-2385) zonality has been revealed concerning content Cr_2O_3. Usually Cr# is considered in correlation with Ca#. Low (up to 1.0 wt.%) content of Cr_2O_3 and moderate contents of CaO varying from the centre to edges of grains are characteristic of the garnet from the sample (U-2385). Variations of composition of garnets concern not only basic oxides (MgO, FeO, CaO, Cr_2O_3), but also trace elements. As shown by (Ireland et al., 1994; Anand et al., 2004) contents of rare earth elements (REE) in diamond inclusions and in host-minerals of eclogite, containing this diamond are different. Inclusions in garnet and clinopyroxene in diamond are enriched in light REE more than the same minerals in the host-eclogite. Instead, heavy REE of garnet inclusions in diamond are 2-3 times more depleted than in garnet from the host-eclogite. Comparing these data, we came to a deduction, that at the beginning moment of eclogite crystallization the mantle had garnet composition. It makes our guess lawful that garnet was a mineral on liquidus at the beginning moment of eclogitic magmas crystallization.

During studying eclogite U-2385 analyses of zoning garnet on the content of rare earth elements have been carried out. By normalization on chondrite contents of rare earth elements they get in a field allocated Sobolev et al. (1998), as a field of garnets from mantle xenoliths. Zoning of garnet, concerning the content of trace elements, indicates that its peripheral parts are enriched by heavy REE and depleted by light REE, in comparison with the central part of a grain (see Fig. 6). The greatest differences are characteristic of contents La, Sm, Eu and Gd. The gush on normalizing graphs for centre and rim of a garnet grain occurs on Dy that contents are within the grain proper.

It should be stressed that zoning garnets have been met in about 1/10 parts of xenoliths (based on collection of 200 samples) among diamondiferous ones from the Botuobinskaya and Nyurbinskaya pipes. This is only preliminary data but in about all the cases the garnet zoning has evidence of its formation under influence of metasomatic events as shown in Fig. 5b. In any case we could state that zoning of garnets in mantle rocks is widely spread and this confirms complicated evolution in the subcontinental lithosphere under Yakutian kimberlite province.

Summary

It is possible to divide the following main groups of inhomogeneous textures among eclogite and pyroxenite minerals: a) exsolved textures in garnets, which are presented by the following mineral phases: diopside ± rutile, rutile and ilmenite; b) rare cases zonality of garnets and others minerals; c) exsolution textures that are presented by tiny intergrowths of garnet and omphacite in eclogites, elongated lamellas of garnet and diopside in orthopyroxenes of garnet vebsterites; d) small exsolved garnets grains in magnesian eclogites (group A) and garnet websterites, where they are present simultaneously with the coarse-grained garnet with which they are similar in composition; e) acicular intergrowths of kyanite and clinopyroxene of radiant form in eclogitelike rocks and needles of kyanite in omphacite in eclogites; f) graphic intergrowths of garnet and coesite.

The most distinctive types of exsolution textures were shown in Figs. 1-2. Rutiles from eclogites often contain tiny lamellas of ilmenite and titanomagnetite and also the rims of the latter mineral that suggests the changing of oxygen and temperature conditions, probably as a result of the metasomatic fluids action. It should be pointed out that the occurrence of the exsolution textures even in the identical rock types is not similar in different pipes (Spetsius and Serenko, 1990). Distribution and presence of exsolved phases in minerals of xenoliths is very inhomogeneous and varies from pipe to pipe. Such textures have been met in

---

bimineral and Ky-eclogites from the Udachnaya pipe and are not described in eclogite samples from the Mir pipe. Prismatic needles of rutiles in clinopyroxenes are present in kyanite and coesite eclogites from the Udachnaya pipe, which could be interpreted as a result of exsolution from high titanium omphacites by decreasing of environmental PT-parameters. Spectacular exsolution textures are widespread in pyroxenites from the Obnazhennaya pipe, which consist of elongated lamellas of clinopyroxene in orthopyroxene and garnet in clino- and orthopyroxenes (see Fig. 2). Comparison of exsolution textures in minerals of xenoliths from the Mir, Udachnaya and Obnazhennaya pipes shows that pyroxenites of the latter have the most complicated minerals evolution.

CONCLUSIONS

The presence of exsolution textures and inhomogeneities in eclogite and pyroxenite minerals points to possibility of manifestation of PT-perturbation in the lithospheric mantle of the Siberian Platform after its formation and stabilization. These textures could be direct evidence in support for the possible plumes formation on mantle levels.

Differences in composition of exsolved phases in identical minerals and PT-conditions of minerals transformation between similar petrographic types of mantle xenoliths in different pipes suggest on the distinction of transformation processes intensity and character of evolution of the lithospheric mantle in different regions of the Siberian Platform.

Availability of different types of exsolution textures in separate varieties of mantle eclogites and pyroxenites points to possible origin of these rocks as a result of magmatic processes of melting and differentiation.

ACKNOWLEDGEMENTS

Bill Griffin and Suzanne O’Reilly are thanked for the collaborative work done on trace elements by ICPMS. We are grateful to Alexander Ivanov who kindly helped with the electron microprobe analyses and SEM images. Thanks are given to Bill Griffin also for discussions on eclogite~~s~~ petrology that helped in understanding of their nature and providing some proton probe analyses.

REFERENCES

1. **Anand M., Taylor, L.A., Misra K.C., Carlson W. D., Sobolev N.V**., 2004. Nature of diamonds in Yakutian eclogites: views from eclogite tomography and mineral inclusions in diamonds. Lithos 77, 333– 348.
2. **Bishop F.C., Smith J.V., Dawson J.B.,** 1978. Na, K, P and Ti in garnet, pyroxene and olivine from peridotite and eclogite xenoliths from African kimberlites. Lithos 11, 155-173.
3. **Brey G., Kohler T.,** 1990. Geothermobarometry in fourphase lherzolites II. New thermobarometers and practical assessment of existing thermobarometers, J.Petrol. 31. 1353-1378.

4. **Chopin C**., 2003. Ultrahigh-pressure metamorphism: tracing continental crust into the mantle. Earth and Planetary Science Letters 212, 1-14
5. **Chopin C., Schertl H.P**., 1999. The UHP unit in the Dora-Maira massif, Western Alps, Int. Geol. Rev. 41, 765-780.
6. **Dawson J.B**., 2004. A fertile harzburgite–garnet lherzolite transition: possible inferences for the roles of strain and metasomatism in upper mantle peridotites. Lithos 77, 553– 569
7. **Dawson J. B., Carswell D.A**., 1990. High temperature and ultrahigh pressure eclogites. In: Carswell D.A. (Ed.), Eclogite-facies rock. Chapman Hall, New York, pp. 316-319.
8. **Dawson J.B., Smith J.V., Hervig R.L**., 1980. Heterogeneity in upper-mantle lherzolites and harzburgites. Philos. Trans. R. Soc. Lond., A 297, 323– 331.
9. **Dobrzhinetskaya L., Green H.W. II, Wang, S.,** 1996. Alpe Arami: A peridotite massif from depths of more than 300 kilometers. Science 271, 1841-1845.
10. **Gasparik T**., 1989. Transformation of enstatite - diopside - jadeite pyroxenes to garnet. Contr. Mineral. Petrol.102, 389-405.
11. **Griffin W.L., Shee S.R., Ryan C.G., Win T.T., Wyat, B.A.,** 1999. Harzburgite to lherzolite and back again: metasomatic processes in ultramafic xenoliths from the Wesselton kimberlite, Kimberley, South Africa. Contrib. Mineral. Petrol.134, 232– 250.
12. **Griffin W.L, Spetsius Z.V., Pearson N.J., O'Reilly S.Y**., 2002. In-situ Re-Os analysis of sulfide inclusions in kimberlitic olivine: new constraints on depletion events in the Siberian lithospheric mantle. Geochem. Geophys. Geosystems. V.3, №11 (1069).
13. **Haggerty S.E., Sautter V**., 1990. Ultradeep (greater than 300 kilometers), ultramafic upper mantle xenoliths. Science 248, 993-996.
14. **Haggerty S.E., Fung A.T., Burt D.M**., 1994. Apatite, phosphorus and titanium in eclogitic garnet from the upper mantle. Geophys. Res. Letters 21, 1699-1702.
15. **Harlow G.E., Veblen**, 1991. Potassium in clinopyroxene inclusion from diamonds. Science 251, 652-655.
16. **Ireland T. R., Rudnick R. L & Spetsius Z. V.** (1994). Trace elements in diamond inclusions from eclogites reveal link to Archean granites. Earth and Planetary Science Letters 128, 199-213.
17. **Irifune T**., 1987. An experimental investigation of the pyroxene-garnet transformation in a pyrolite composition and its bearing on the constitution of the mantle. Phys. Earth Planet. Int. 45, 324-336.
18. **Lappin M.A.,** 1978. The evolution of a grospydite from Roberts Victor Mine, South Africa. Contribution to Mineralogy and Petroogy 66, 229-241.
19. **Leost I., Stachel T., Brey G.P., Harris J.W**., 2003. An unusual suite of inclusions in diamonds from Namibia. Extended Abstracts, 8th Int. Kimberlite Conf. Victoria, Canada.
20. **McDonough W. F., Sun S. S.** 1995. The composition of the Earth. Chemical Geology 120, 223-253.
21. **Moore R.O., Gurney J**.J., 1985. Pyroxene solid solution in garnets included in diamond. Nature 318, 553-555.
22. **Mposkos E.D., Kostopoulos D.K**., 2001. Diamond, former coesite and supersilicic garnet in metasedimentary rocks from the Greeek Rhodope: a new ultrahighpressure metamorphic province estlbished. Earth Planet. Sci. Lett. 192, 497-506.
23. **Ogasawa Y., Fukasawa K., Maruyama S**., 2002. Coesite exsolution from supersilicic titanite in UHP marble from the Kokchetav Massif, northern Kazakhstan. Am. Min. 87, 454-461.
24. **Pearson D.G., Shirey S.B., Carlson R.W., Boyd F.R., Pokhilenko N.P., Shimizu N.,** 1995. Re– Os, Sm–Nd, and Rb–Sr isotope evidence for thick Archaean lithospheric

---

mantle beneath the Siberian craton modified by multistage metasomatism. Geochim. Cosmochim. Acta 59, 959– 977.

25. **Phillips D., Harris J.W., Viljoen K.S**., 2004. Mineral chemistry and thermobarometry of inclusions from De Beers Pool diamonds, Kimberley, South Africa. Lithos 77, 155–179.
26. **Ponomarenko A.I., Spetsius Z.V., Lybushkin V.A**., 1977. Kyanite eclogite with coesite. Dokl. Akad. Nauk SSSR. 236 (1), 215-219 (in Russian).
27. **Roden M.F., Patino-Doucea A., Laz'ko E.E., Jagoutz E**., 2003. Exsolution textures in high pressure garnets, Mir kimberlite, Siberia. Extended Abstracts, 8th Int. Kimberlite Conf. Victoria, Canada.
28. **Rosen O.M., Serenko V.P., Spetsius Z.V., Manakov A.V., Zinchuk N.N**., 2002. Yakutian kimberlite province: position in the structure of the Siberian craton and composition of the upper and lower crust. Russian Geology and Geophysics 43, 3-26 (in Russian).
29. **Saltzer R.L., Chatterjee N., Grove T.L**., 2001. The spatial relationship of garnets and pyroxenes in mantle peridotites; pressure-temperature history of peridotites from the Kaapvaal craton. J. Petrol. 42, 2215–2229.
30. **Sautter V., Harte B**., 1988. Diffusion gradients in an eclogite xenolith from the Roberts Victor kimberlite pipe; (1) mechanism and evolution of garnet exsolution in Al2O3-rich clinopyroxene. J. Petrol. 29, 1325– 1358.
31. **Smith, D.C**., 1984. Coesite in clinopyroxene in the Caledonides and its implications for geodynamics. Nature 310, 641-644.
32. **Sobolev N.V., Yefimova E.S**., 2000. Composition and petrogenesis od Ti-oxides associated with diamonds. Intern. Geol. Rew. 42, 758-767.
33. **Sobolev N.V., Sobolev V.N., Snyder, G.A. Yefimova E.S., Taylor L.A.,** 1999. Significance of eclogitic and related parageneses of natural diamonds. Int. Geol. Rev. 41, 129–140.
34. **Sobolev N.V., Lavrent'ev J.G**., 1971. Isomorphic sodium admixture in garnets formed at high pressure. Contrib. Mineral. Petrol. 31, 1-12.
35. **Sobolev N., Shatsky**, V., 1990. Diamond inclusions in garnets from metamorphic rocks. Nature 343, 742-746.
36. **Spetsius Z.V**., 2004. Petrology of highly aluminous xenoliths from kimberlites of Yakutia. Lithos 77, 525– 538
37. **Spetsius Z.V., Serenko, V.P**., 1990. Composition of continental upper mantle and lower crust beneath the Siberian platform. Nauka, Moscow (in Russian).
38. **Spetsius Z.V., Taylor L.A**., 2002. Partial melting in mantle eclogite xenoliths: connection with diamond paragenesis. Intern. Geol. Rew. 44, 973-987.
39. **Taylor L. A., Snyder G. A., Keller R., Remley D. A., Anand M., Wiesli R., Valley J., Sobolev N.V.**, 2003. Petrogenesis of group A eclogites and websterites: evidence from the Obnazhennaya kimberlite, Yakutia. Contrib Mineral Petrol 145, 424–443.
40. **Taylor L.A., Keller R.A., Snyder G.A., Wang W.Y., Carlson W.D., Hauri E.H., McCandless T., Kim K.R., Sobolev N.V**., 2000. Diamonds and their mineral inclusions, and what they tell us: a detailed ‘‘pull-apart’’ of a diamondiferous eclogite. Int. Geol. Rev. 42, 959– 983.
41. **Van Roermund H.L.M., Drury, M.R.** 1998. Ultra-high pressure (P>6 Gpa) garnet peridotites in western Norway: exhumation of mantle rocks from > 185 km depth. Terra Nova 10, 295-301.
42. **Van Roermund H.L.M., Drury M.R., Barnhoorn A., De Ronde A.,** 2001 Relict majoritic garnet microstructures from ultra-deep orogenic peridotites in Western Norway, J. Petrol.42, 117-130.

43 **Zhang R.Y., Liou J.G.**, 1999. Exsolution lamellae in minerals from ultrahigh-pressure rocks. International Geology Review, 41, 981-993.

UDK 551.22 +552.11

VARIATIONS OF THE MANTLE MINERALOGY AND STRUCTURE BENEATH UPPER - MUNA KIMBERLITE FIELD

Ashchepkov I.V.[1], Vladykin N.V.[2], Rotman A.Y.[3], Afanasiev V.P.[1],
Logvinova A.M.[1], Kuchkin A.[1], Palessky V.S.[1], Nikolaeva I.A.[1],
Saprykin A.I.[1], Anoshin G.N.[1], Khmel'nikova O.S.[1]

[1] *United Institute of Geology Geophysics and Mineralogy SD RAS, Novosibirsk*
[2] *Institute of Geochemistry SD RAS, Irkutsk*
[3] *Central Science and Research Geology And Prospecting Institute Of The Stock Company "ALROSA" Mirny*

Minerals from the concentrate from three large kimberlite pipes from Upper Muna field Russia Deimos, Zapolyarnaya and Novinka studied with EPMA and LAM ICP methods show the difference from the mineral features and their TRE signatures. Monomineral thermobarometry with the Cpx, Gar, Cr-Sp and Ilm revealed the layered structures of the lithospheric mantle columns beneath these pipes with the enrichment in pyroxenite material the lower horizons –up to 40 kbars. At least three stages of the PT paths formed the incline geotherms, the hotter one that is close to 45 mv/m^2, was suggested to be produced during the stage of the growths of the feeding systems for kimberlite eruptions. The ilmenite TP estimates trace the separate parts of the TP trajectories suggesting also multistage creation of feeding channels and associated multistage metasomatism. Heating associated with this process possibly may be favorable for the growth of diamonds. TRE signatures of the minerals show enriched in Ba-U HFSE and Zr -Pb depleted compositions what is similar to the concentrate of Angola pipes as well as the PT diagrams.

INTRODUCTION.

Traditional diamond exploration regions in the Siberia: Daldyn, Alakite and Malo- Botuobinsky have now difficulties in finding the productive kimberlites that may be easy to be involved in exploration. One of the perspective regions for diamond production is Upper Muna kimberlite field counting more the 20 kimberlite bodies and several large pipes such as Zapolyarnaya, Deimos and Novinka. The features of concentrate minerals differ from those of kimberlites from regions as well as the diamond inclusions. Here we present the characteristics of the compositions of minerals and the reconstructions of the mantle structures of this kimberlite field.

The EPMA compositions were determined by Ashchepkov and Khmelnikova on CamebaxMicro mass-spectrometer in UIGGM SD RAS and TRE analyses

---

made using LAM ICP method on mass-spectrometer Finnigan Element [23], operators: Kuchkin A.M., Palessky V.S.

MINERALOLGY

Garnets from the Upper Muna kimberlites in Cr_2O_3-CaO diagram trace the lower part of the lherzolite field [18,56] up to 12% Cr_2O_3 but continuous trend are over at 6% for Zapolyarnaya pipe at 7 for Novinka and at 9% for Deimos pipe (fig.1). Subcalcic garnets [18,28] appear from 5% Cr_2O_3 forming 3 parallel subtrends mostly upper at the boundary of the harzburgites fields but dunite garnets also appear at 11% Cr_2O_3 and earlier for other pipes. Typical pyroxenite trends [38,49] are not usual for these pipes judging on the CaO content but essential enrichment of the garnets from Novinka in TiO_2 and Na_2O rising together with the Cr_2O_3 content suggest the influence of the magmatic plum material rising from the deep sources. Similar trends are found for Deimos garnets but for those from Zapolyarnaya TiO_2 rapidly fall down with the depth.

Clinopyroxenes are relatively wide spread (fig.2) in the concentrate from the Upper Muna pipes. The main amount of them belongs to typical Cr-diopsides except for those from Deimos which contain hybrid metasomatic [22,62] and eclogite types [14,17] of Cpx also. Novinka and Zapolyarnaya Cpx show the trend of decreasing NaCr (kosmochlor) minal with the FeO rise together with MgO decrease while Deimos show discrete trend with the other tendency of rising of Na-Cr with FeO to 3% and then decreasing again.

Ilmenites are not characteristic for Novinka and Zapolyarnaya pipes (fig.3) where they form sometimes fibrous aggregates. While in Deimos ilmenites are rather abundant and demonstrate the variations typical for those from kimberlites of Alakite field [2,10] and Daldyn region [1] usually considering to be fractionation trend [13,16,31,36,37]. The trend consists from the 4 parts. The most TiO_2 (54-52%) - MgO rich varieties are Cr_2O_3 – enriched and correspond to metasomatites [22,51,60] . This interval contain also varieties with high FeO content. For the more differentiated and lower in TiO_2 ilmenites the slitting into two branches with different Cr_2O_3 level are typical. In interval 49-52% those with rather low to 0.5% Cr_2O_3 ilmenites prevail but starting from 49% TiO_2 ilmenite with 2-2.5% Cr_2O_3 became more abundant and in 44-46% TiO_2. Those containing 4 up to 6 Cr_2O_3% usually corresponding to metasomatites finish the ilmenite trend [60]. Al_2O_3 content fall down in three lineal trends from 54 to 52% TiO_2 possibly show the three groups separating different garnet amount.

Chromites from the larger pipes are not studied in detail. Those from Zapolyrnaya pipe demonstrate rather restricted trend in Cr_2O_3 65-40% (fig.4). The most Cr rich varieties 65-61% typical for diamond inclusions [54] are mainly Ti-less but those lower in Cr separated from them are belonging mainly to the ulvospinel branch and demonstrate the enrichment in TiO_2 up to

8 % together with the rising of NiO% content with the slowly decreasing V_2O_5 content and rising at the end of the trend up to 1 %.

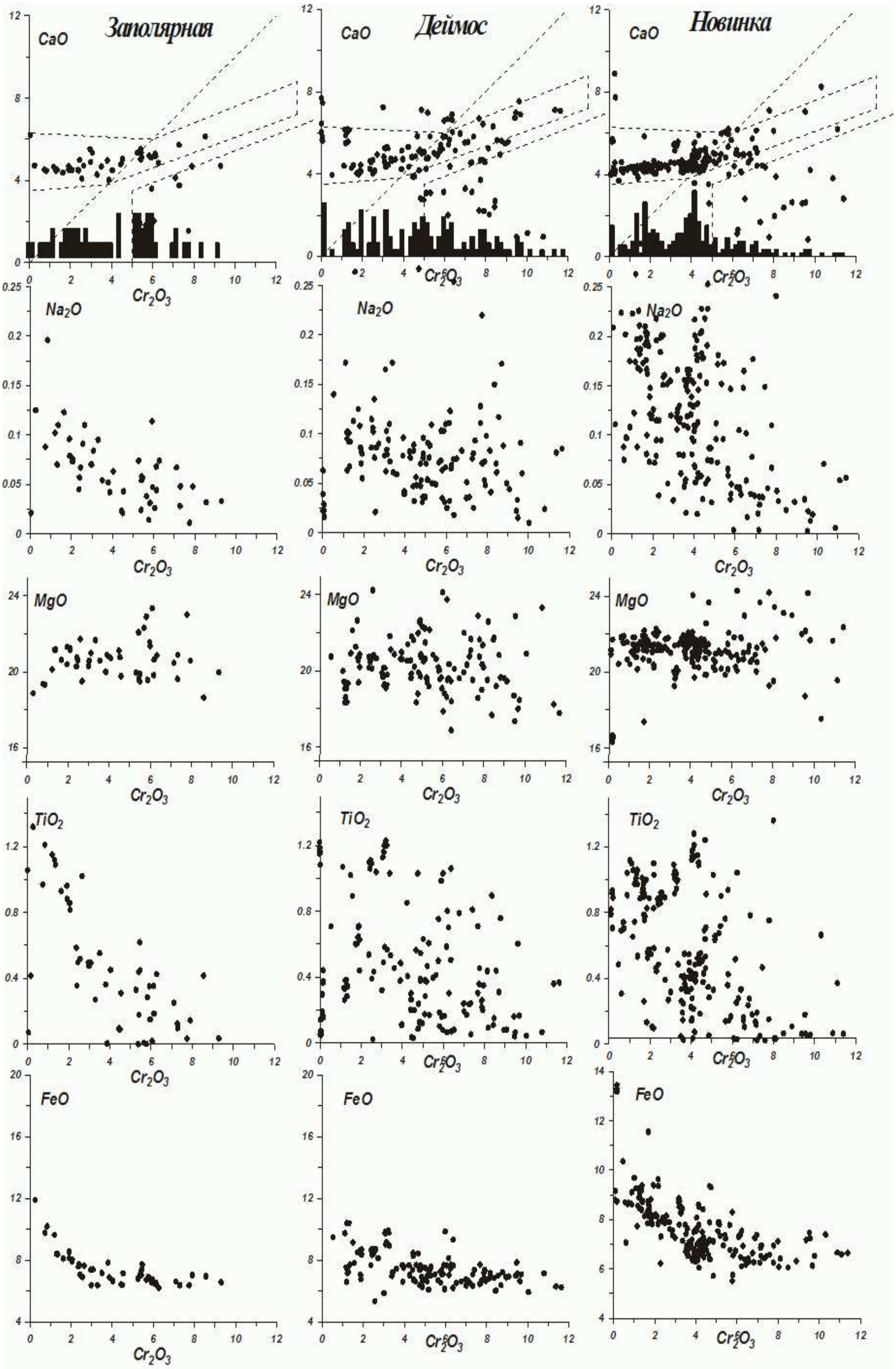

Fig.1 **Variation of the garnet compositions from the concentrate of three large kimberlite pipes in Upper Muna field.**

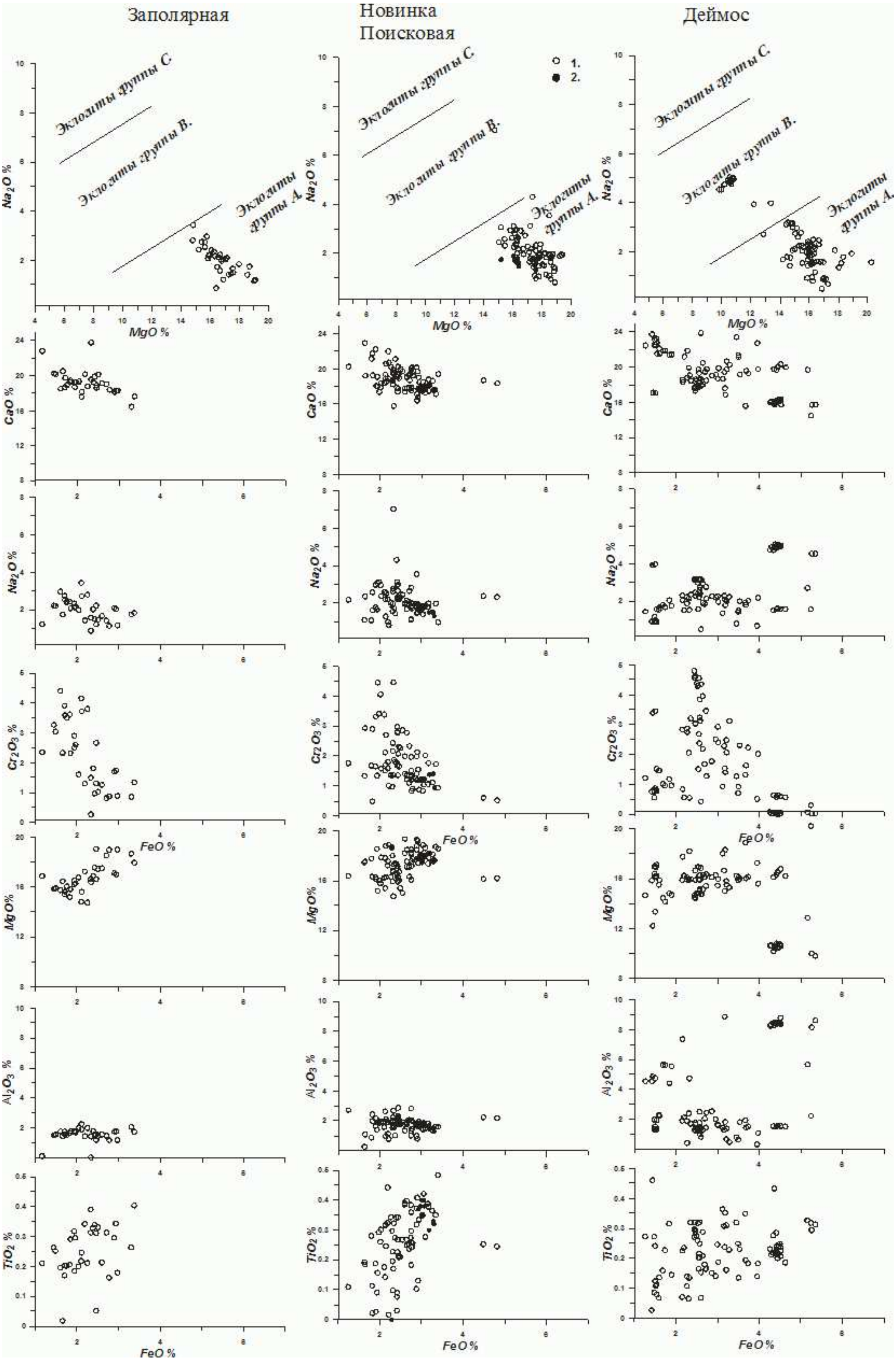

Fig.2 **Variation of the clinopyroxene compositions from the concentrate of three large kimberlite pipes in Upper Muna field**

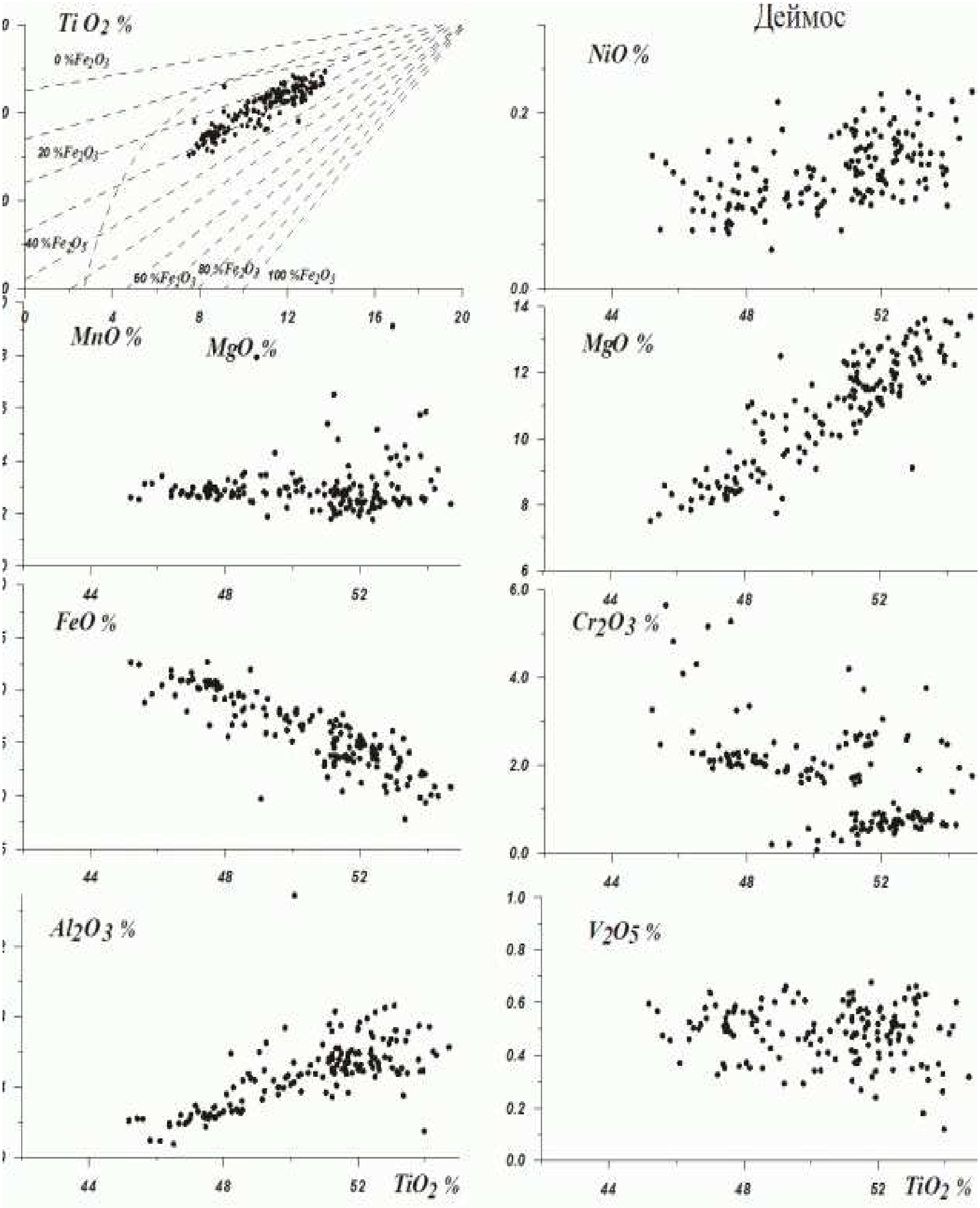

Fig.3 **Variation of the ilmenite compositions from the concentrate of Deimos kimberlite pipes of Upper Muna field**.

Amphiboles which are wide spread in Deimos pipe concentrate all are Cr- Ca horn blendes which demonstrate low Ti content and may be subdivided in to two groups where K_2O, Cr_2O_3 and Al_2O_3 are slightly decreasing together with rising FeO content (fig.5). The amphibole from Novinka pipe belong to the low Al type close to the Cpx in composition but containing 1.9% of K_2O [14].

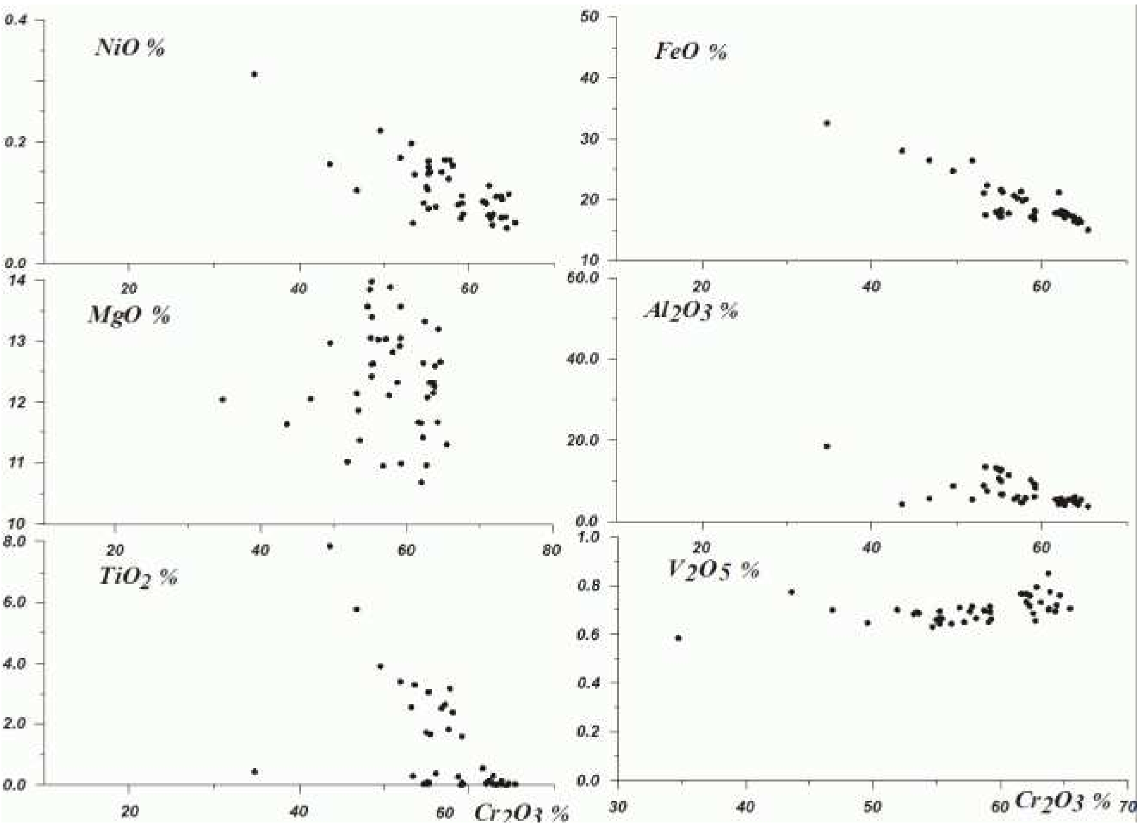

Fig.4 **Variation of the chromite compositions from the concentrate of Zapolyarnaya kimberlite pipes of Upper Muna field.**

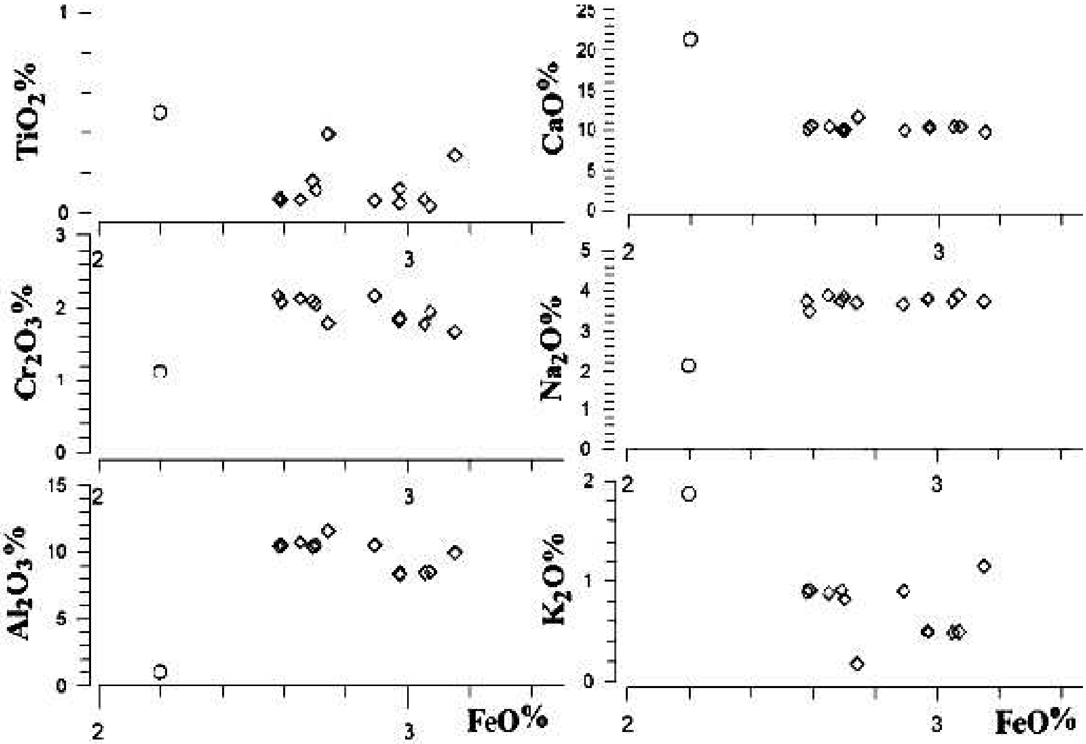

Fig.5 **Variation of the amphiboles compositions from the concentrate of Deimos (1) and Novinka (2) kimberlite pipes of Upper Muna field.**

TP RECONSTRUCTIONS

Since there were no good polymineral xenoliths were found in concentrate all the TP reconstruction were made using monomineral versions of thermometers using Garnet [3-5,32,53], Clinopyroxene [6,7,44], Orthopyroxene [40], Chromite [12] and Ilmenite [13] compositions. The different methods give sometimes not coinciding TP fields because definite minerals possibly were captured from varying in modal compositions rocks;

The clinopyroxenes [6] from Zagadochnaya pipe show on the diagram 3 trends in interval (40-60kbars) with the inclination similar to those from South Africa kimberlite deep seated xenoliths cutting the conductive geotherms. The lower part is heated up to 45 mv/m^2. Garnets [3,5] give similar TP values but most of them are more heated in interval to 65-45 kbar corresponding to 40 mv/m^2 heat flow. The estimates based on the chromite values exactly repeat three layers of the clinopyroxene geotherm. For Novinka pipe geotherm slightly differ: Cpx thermobarometry [7,44] give also three slices with the irregular heating from 35 to 45 mv/m^2. Several values in garnet – spinel facies are tracing SEA geotherm. Garnets [3,5] produce three branches in TP diagram from 35 to 43 mv/m^2 garnet pyroxenite geotherm is more hot then 45 mv/m^2. TP diagram for Deimos pipe are close differ – Cpx values give the dense cluster in 60-50 kbar rather with low T^o conditions those lower then 35mv/m^2 gradient are referring to the eclogitic pyroxenes. Upper 40 kbar the geotherm splits on those close to conductive type and more HT brunches close to 47 and 85 (SEA) mv/m^2. Garnet peridotite TP values coincides with the 40 mv/m^2 geotherm. The pyroxenite scheme of calculations [3,5] give hot geotherm in 50 -25 kbar interval. The ilmenite TP values [13] produce 5 separate clots – two from the lower part of the section from 65 to 55 kbar give the heating degree between 35 and 40 mv/m^2. The next step in interval 40 -50 kbar is more heated in average up to 43 mv/m^2 the in the upper interval between 25 and 40 mv/m^2 and the more hot 45 mv/m^2 branch appears (fig.6).

Layering of the mantle columns was reconstructed in the similar manner as for the Malo-Botuobinsky, Alakite, Daldyn and Nakyn pipes [4,9-11] separately for each mineral. Garnets for Novinka and Zapolyarnaya show close P intervals with similar garnet compositions bum or continuous for Zagadochnaya in the lower part of the section. Garnets for Deimos part produce even more complete mantle section but they definitely differ are separating in to several branches according to Cr and Ca content and FeO values in the upper part of the section are higher in 2 % then for two previous pipes (fig.7).

Layering according to the clinopyroxenes is close but the compositions of the pyroxenes are essentially different excluding the basement where the

---

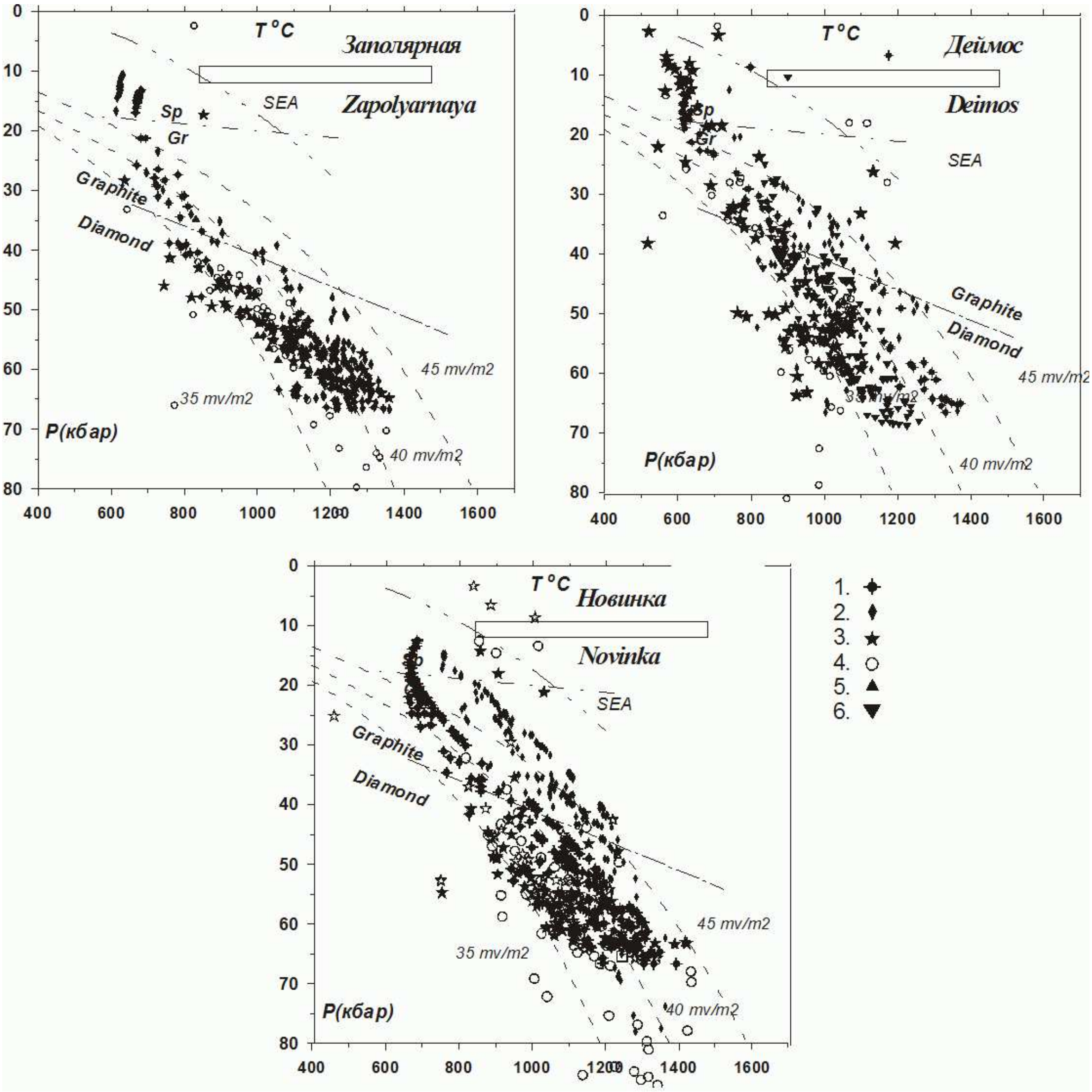

Fig.6. **TP diagram obtained with monomineral thermobarometry based o the concentrate of three large kimberlite pipes in Upper Muna field.**

1. Garnet peridotite scheme [3,5], 2. The same pyroxenite scheme [3,5], 3. Clinopyroxene [6,7], 4. The same [44]; 5. Chromite [12]; 6. Ilmenite [13].

most Fe rich pyroxenes close to those sheared one were found. Clinopyroxenes from Zapolyrnaya demonstrate gradual Fe decrease upward. Those from Deimos demonstrate three trends with the different Fe content. Clinopyroxenes from Novinka show wide variations in this interval. Cr- rich pyroxenes for Zapolyarnaya are correspondent to 50-55kbar, in mantle column under the Deimos pipe they plot in more strict interval near 55 kbar. For Deimos Na- rich pyroxenes correspond to the same interval and other pipes appear close compositions at the same pressures. Nevertheless Al content for the pyroxenes slightly varies for these pipes. Mantle Cpx from Deimos are nearly constant in composition and are slightly varying for the Zapolyarnaya while for Novinka pipe Al content is rising with the decreasing pressure .

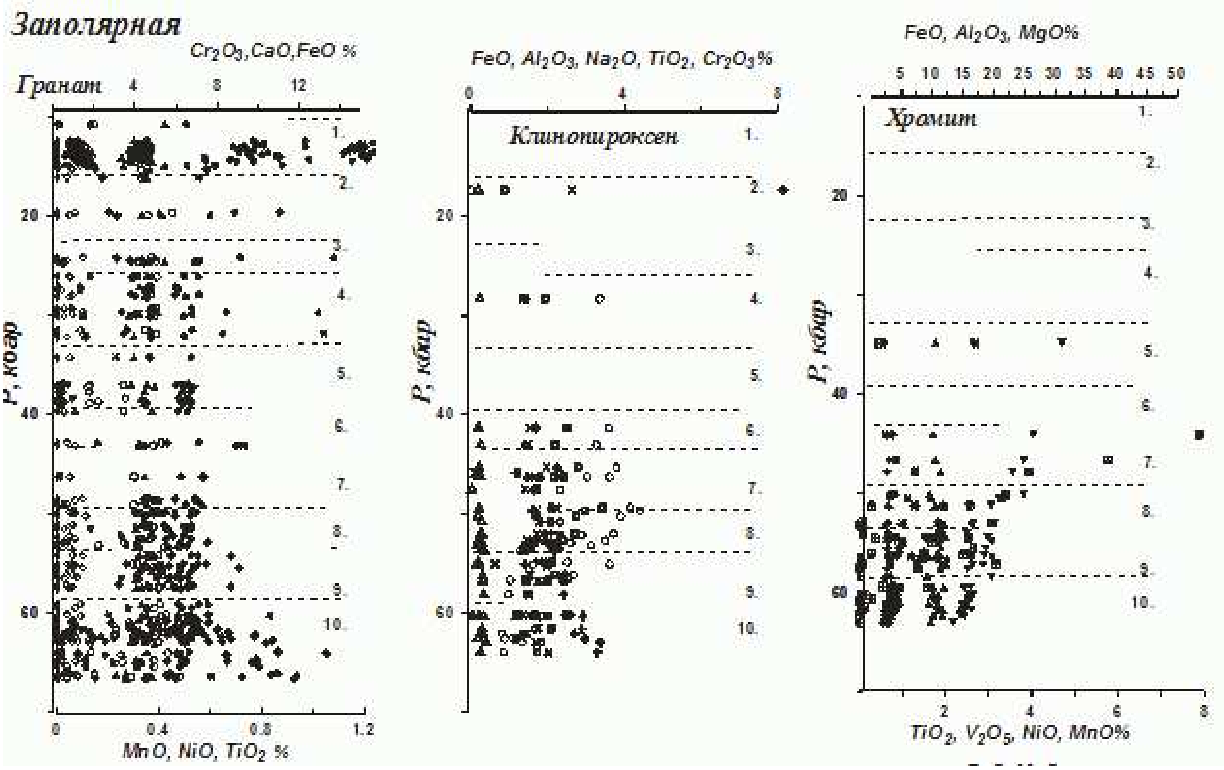

Fig.7a **Reconstruction fo the mantle layering for three pipes from the Upper Muna field**

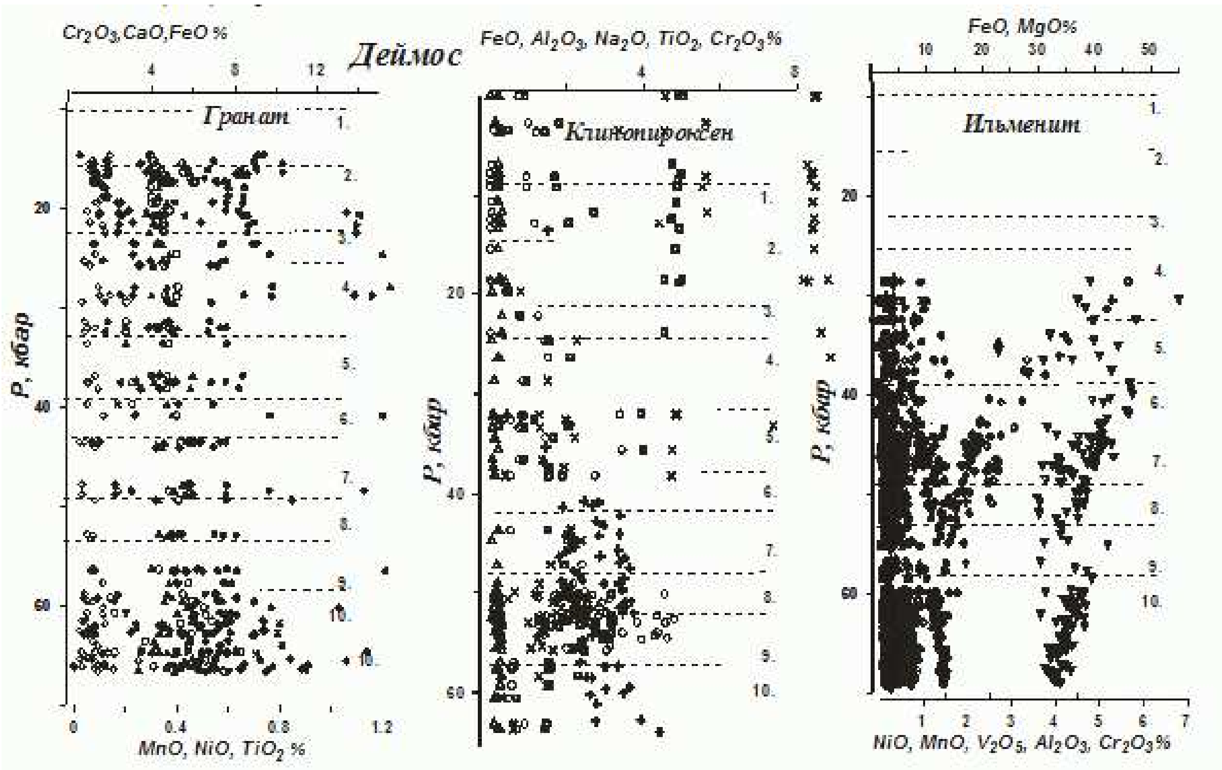

Fig.7b **Reconstruction fo the mantle layering for three pipes from the Upper Muna field**

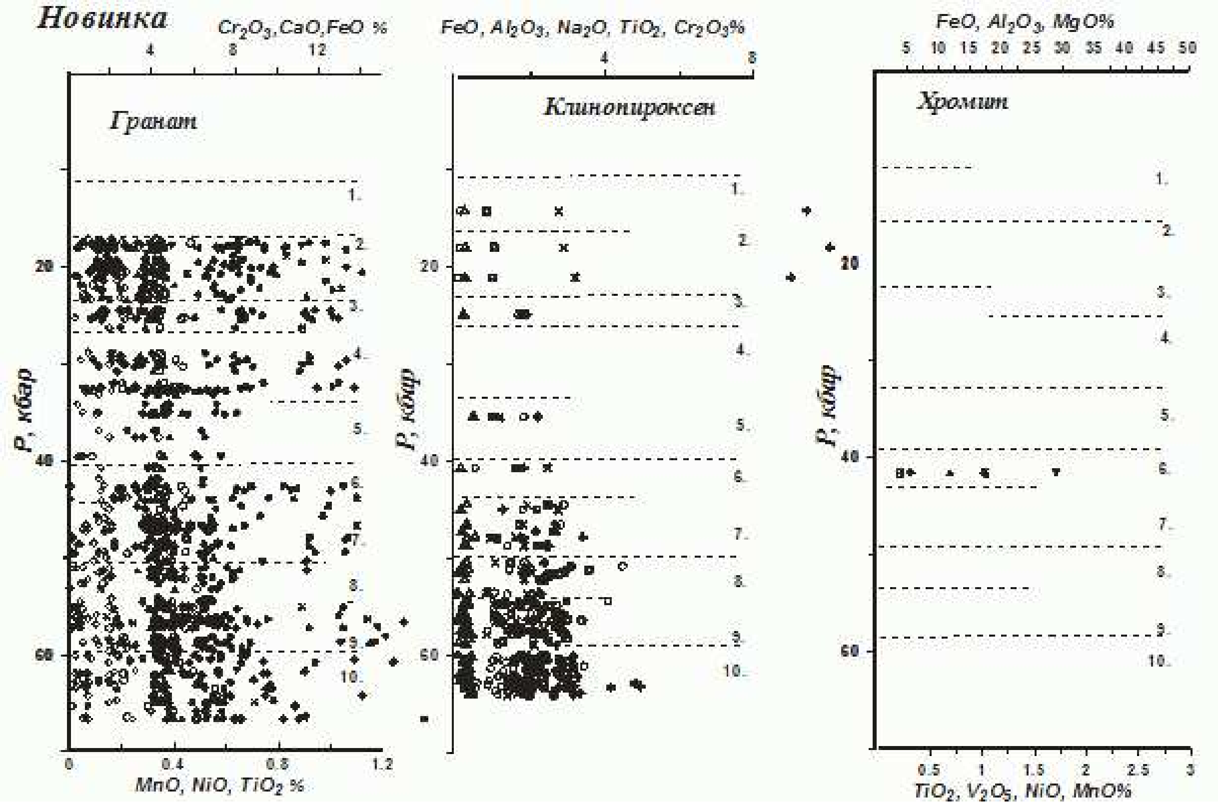

Fig.7c **Reconstruction fo the mantle layering for three pipes from the Upper Muna field**

Ilmenite layering for the Deimos pipe shows three major intervals. Lower one in upper part is restricted part by the rough of the convective layer [45,46] close to 60 kbar, the second interval is well correspondent to those produced by the clinopyroxene (55-45 kbar). The last one with the more irregular seems to be referred to the branching metasomatic system [51] at the finishing stage of the evolution of magma produced megacrystalline ilmenites [13,41-43]. Continuous rise of the Cr content possibly may be explained by the constant contamination of the magma in ascending system.

Chromite ulvospinel trend is correspondent to the 65-45 kbar coinciding with the 2nd interval of the magmatic chamber (or conduit) of the magma for parental ilmenites Rising of the Ti content in chromite seems to be caused by the contact interaction of these magmas with peridotites.

GEOCHEMISTRY

Geochemical features of the minerals from Zapolyarnaya and Novinka pipes were analyzed by LAM ICP [43] method in Analytic Center of UIGGM SD RAS. They demonstrate similar REE patterns for garnets and clinopyroxenes more different at the TRE spidergrams. Most of the clinopyroxenes show the asymmetric REE distributions with moderate Gd/Yb_n and La/Sm_n <1 what corresponds to the Gar/Cpx ratios higher then for Cpx from Yubileynaya [2]. Eclogitic pyroxenes found between the Zapolyarnaya Cpx have nearly lineal REE distributions sometimes with Eu minimums or maximums. On the TRE spidergrams Cpx from

Zapolyarnaya show Ba peaks and smaller ones for the Pb though some of them display small Pb dips. Some eclogitic Cpx show the peak in Sr. All of them reveal the Zr minimums as a rule deepening with the rising of the average TRE level, nevertheless the other HFSE are not lower then normalized REE values and even LILE do not show depletion. One analyzed subcalsic garnet demonstrate S-type REE the depletion for Rb, Ba. Elevated U, Nb,Ta and minimums in Sr and stronger one for Zr.

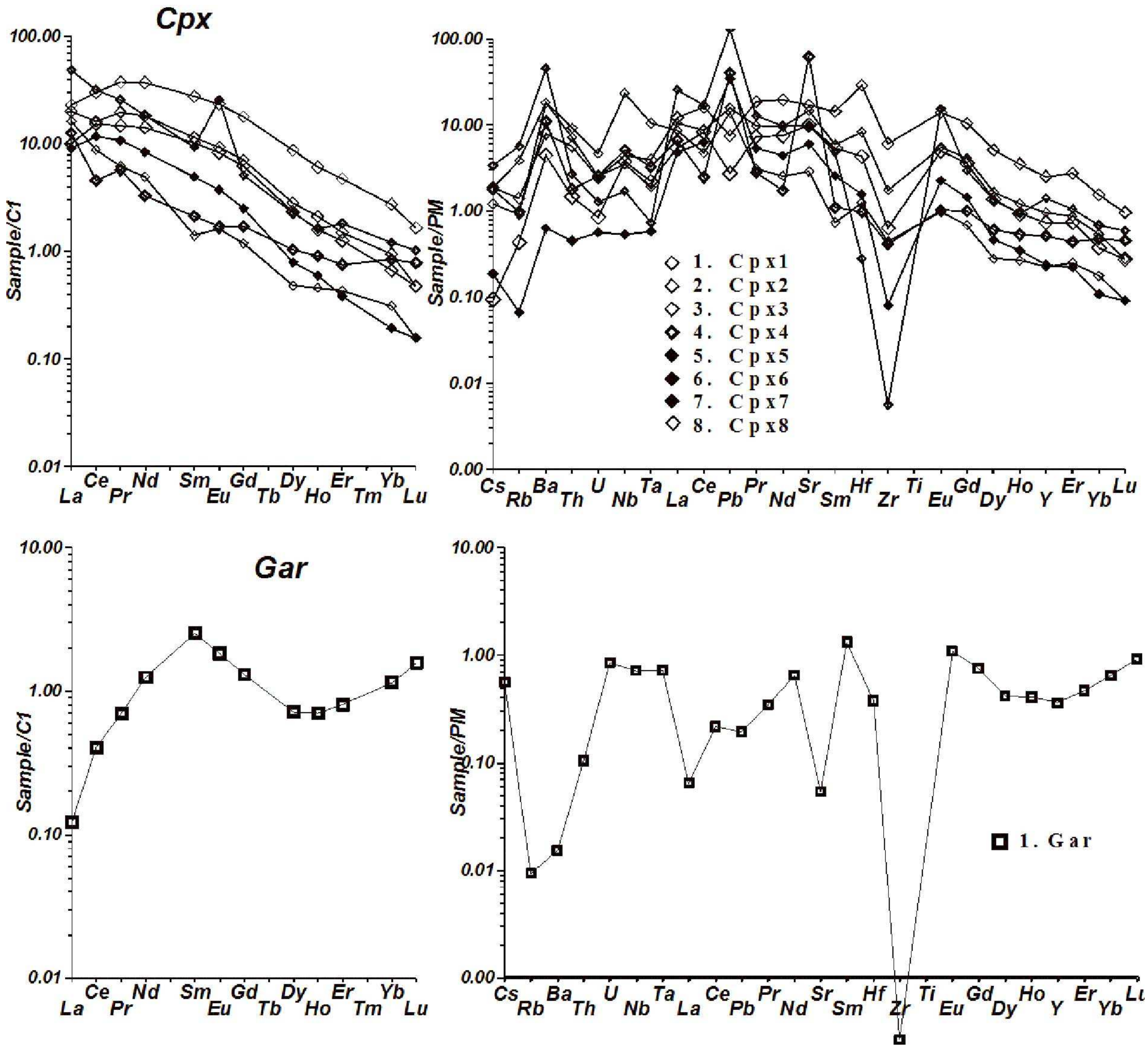

Fig.8 **TRE diagram for he minerals from the concentrate of the Zapolyarnaya pipes.**

Clinopyroxenes of Cr-Di type from Novinka pipe show similar patterns analogical to minerals from Zapolyarnaya pipe with minimum of Zr and fluctuated Pb and without extremely values of the other components. Garnets of subcalsic type reveal S- type LREE enriched pattern common for diamond inclusions [54-57], the lherzolitic ones are rounded and even humped in the middle part. All of them also show not only Sr- minima but also U peak, fluctuated Pb, Ba and slightly elevated Nb, Ta. One pyroxenitic garnet with elevated MREE shows strong Pb and smaller Nb-Ta-U peaks suggesting remelting of metasomatites with participation of the ilmenites – sulfides (fig.8).

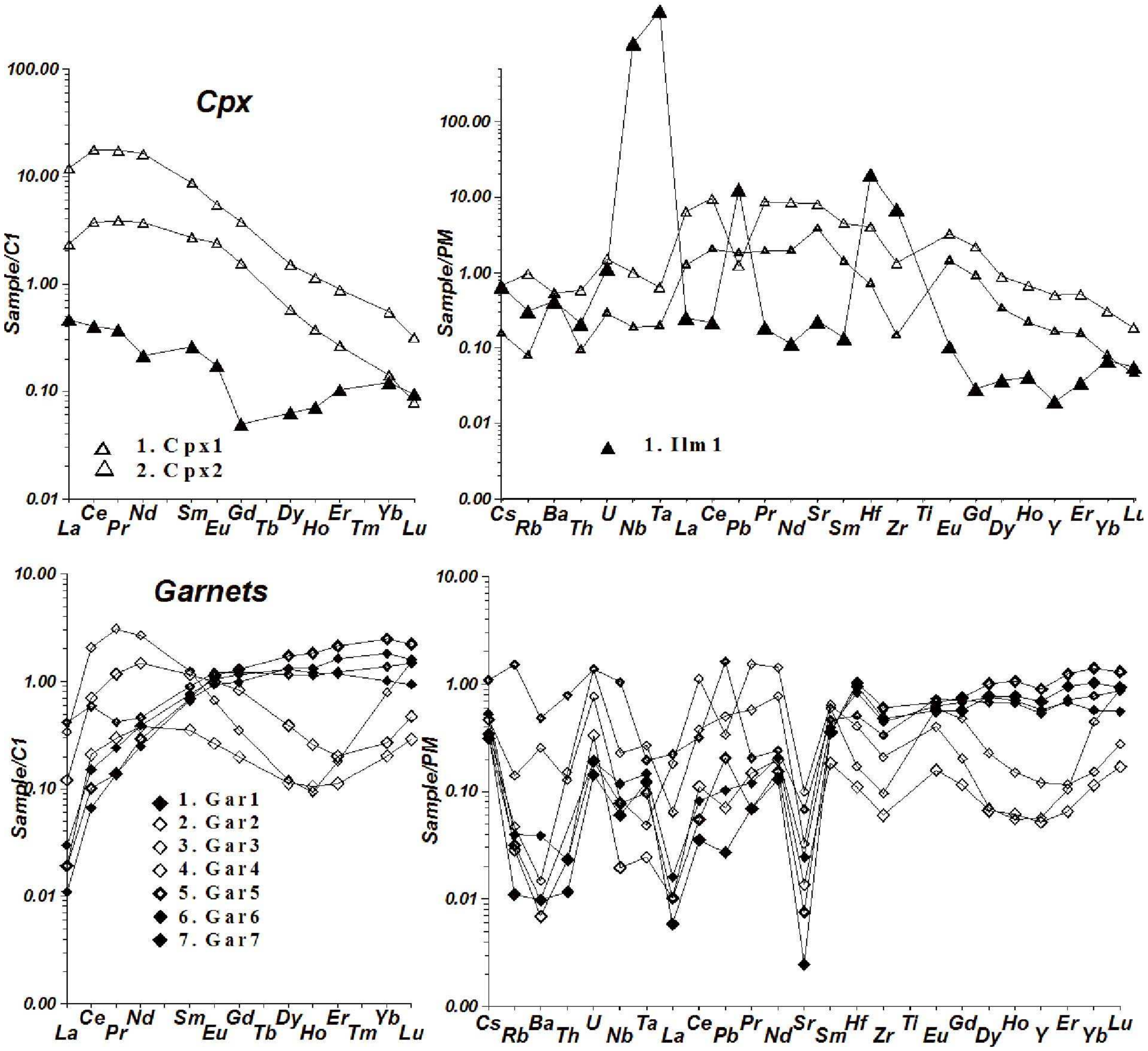

Fig.8a **TRE diagram for he minerals from the concentrate of the Novinka pipes**.

DISCUSSION

Study of the mineral concentrate of the large pipe in Upper Muna field demonstrate that the level of the xenoliths capture is low enough and the abundance of the perspective for the diamond production depleted peridotite and subcalcic garnet associations are rather high. The mineralogical features of the Upper Muna mantle minerals slightly differ from those of the other regions of Siberian platform as well the structure of the mantle columns. Wide spread enriched Cr- diopsides that are found between the mantle inclusions also [55,57] are quite unusual for the Daldyn and even Alakite region [9,11,34]. Rather low concentration of ilmenites are more similar for Nakyn field then for central region. The structure of the mantle columns shows also the abundance of the pyroxenite material in the lower horizons of the mantle what is more typical for the mantle column of Gondwana type mantle with the enriched peridotites [25,29,45,46,60,62] often having continental TRE signatures. Similar mantle structure and even mineralogical features show the groups of the pipes in the Angola [52], close to the largest in the World pipe Catoca. There are at least two types of the mantle section. Beneath the Deimos and Novinka pipes the pyroxenite – rich rocks in the basement display irregular heating with the more heated conditions typical for Deimos. Zapolyarnaya pipe.

The heating of the lower horizons that is more pronounced for the Zapolyarnaya pipe and it is suggested to be more perspective for the large god quality diamonds [24] then the other ones. Nevertheless lack of the deeply depleted horizons of the basement may suggest also that there is a possibility of the presence of more large and productive pipe in this region. Relative enrichment of the basement in the pyroxene material and it's rather enriched type including HFSE together with the fractionated character Pb- minima may suggest the enrichment of the lower horizons if the mantle by the metasomatic fluids and melts [27] having primary continental signatures. The Zr dips for the most of the minerals in the concentrate from the same pipe may mean the high P potential during melt percolation possibly from the subducted deep ocean sediments reactivated in the stage of the continental growth. All this means rather permeable low lithospheric horizons in this region that were subjected by the influence of the subducted related metasomatism [50]. At least three stages of the melt percolation with the different TP may be suggested from the TP diagram. Ti- rich garnet are referred to the rather hot stages that may be correspondent to the processes of the rising feeding systems for the protokimberlite melts produsing ilmenite vein network large channels and possibly magmatic chambers. The ilmenite TP estimates trace separate discrete arrays at the PT paths possibly also referring to the different stages of the melt percolations.

The mantle layering that was reconstructed with the minerals thermobarometry show the presence of at least two or three stages for the melt percolation from the Cpx P- Fe-trends (fig.7) for Deimos pipe. The trends of the chromites with strong enrichment in the ulvospinel component may also suggest the interaction with Ti – rich melts that produce ilmenite mmegacrysts. Several pipes in Upper Muna and Prianabarie show the preferential distribution of the ilmenite and chromite in the concentrate. In some cases it possible to suggest the dissolution of the ilmenite and crystallization of the chromite or more likely the opposite processes of the chromite dissolutions and crystallization of the Cr-bearing ilmenites. The similarity on the REE patterns for the chromites and ilmenites in many pipes may be the argument for this possibility.

The processe of the enrichment by the influence of the subduction related plum and carbonatitic or protokimberlite melts may brings to heating and growth of the diamonds [14,18, 24,33,35,47,58,59].

CONCLUSIONS

1. The Upper Muna field include the pipes which contain deep material typical for the basement of the continental keel. They carry mantle material and reveal the structure of mantle column differ then the other regions of Siberian platform close to the some pipes of the Central Africa (Angola).
2. The geochemical features of peridotite minerals show rather enriched continental or metasomatic signatures.
3. Multistage processes of the melt percolation recorded at the PT paths in mantle columns suggest rather permeable lithospheric mantle structure.
4. The structure and mineralogical features and their TRE signatures may be rather perspective for the diamond exploration.

Supported by RFBR grants 99-05-65688, 00-05-65288, 03-05-64146; 05-05-64718. The article contain the materials from the REPORTs of the Areements beween UIGGM SD RASc and ALROCA Company; projects 77-02; 65-03

References

1. **Amshinsky A.N., Pokhilenko N.P.** Characteristic features of the picroilmenite compositions from the kimberlite pipe Zarnitsa. Russian Geol Geophys. 1983. N11.pp .116-119.
2. **Ashchepkov I. V. Vladykin N. V., Nikolaeva I. V., Palessky S. V., Logvinova A. M., Saprykin A. I., Khmel'nikova O. S., and Anoshin G. N**. Mineralogy and Geochemistry of Mantle Inclusions and Mantle Column Structure of the Yubileinaya Kimberlite Pipe, Alakit Field, Yakutia. Doklady Earth Sciences, Vol. 395A, No. 3, 2004, pp. 378–384**.**
3. **Ashchepkov I., Vishnyakova E.** New garnet thermobarometry for mantle peridotites and garnet mantle geotherms // 32nd International Geological Congress, Florence, Italy, August 20-28, 2004: Abstracts Volume. - Florence, 2004. - P. 466. - CD-ROM.
4. As**hchepkov I., Vladykin N., Pokhilenko N., Sobolev N., Malygina E., Kuligin S., Ovchinnikiv Y., Afanasiev N., Mkrtychan G., Rotman A.,Kostrovitsky S., Tolstov A., Khmel'nikova J., Pokhilenko L., Logvinova A.** Clinopyroxene geotherms for the mantle columns beneath кimberlite pipes from Siberian craton. 8 th International Kimberlite Conference Long Abstract. FLA_0355.
5. **Ashchepkov I.V.** Empirical garnet thermobarometer for mantle peridotites. Seattle Annual Meeting (November 2-5, 2003). Abstract ID: 65507.
6. **Ashchepkov I.V.** Jd-Di barometer for mantle peridotites and eclogites. //Experiment in Geosciences v.10, N1, 137-138.
7. **Ashchepkov I.V.** More precise equation of the Jd-Di Barometr. Herald f of the Earth department RAS. 2003, N1. pp.45-46.
8. **Ashchepkov I.V., André L.** Pyroxenite xenoliths in picrite basalts (Vitim plateau):origin and differentiation of mantle melts. Russian Geol. Geophys. 2002. v. 43(4). pp.343-363.
9. **Ashchepkov I.V., Vladykin N.V., Rotman A.Y., Logvinova A.M. , Afanasiev V.P. , Palessky V.S., Saprykin A.I., Anoshin G.N., Kuchkin A., Khmel'nikova O.S.** Mir and International'naya kimberlite pipes – trace element geochemistry and thermobarometry of mantle minerals. Deep seated magmatism It's sources and their relation to plum

processes. //Irrutsk – Ulan-Ude 2004. Publishing house of the Institute of Geography SB RAS 2004, pp. 194-208

10. **Ashchepkov I.V., Vladykin N.V., Rotman A.Y., Logvinova A.M., Nikolaeva I.A., Palessky V.S., Saprykin A.I., Anoshin G.N., Kuchkin A., Khmel'nikova O.S.** Reconstructions of the mantle layering beneath the Alakite kimberlite field: comparative characteristics of the mineral geochemistry and TP sequences. //Deep seated magmatism It's sources and their relationto plum processes. Irkutsk – Ulan-Ude 2004. Publishing house of the Institute of Geography SB RAS 2004, pp.160-178
11. **Ashchepkov I.V., Vladykin N.V., Saprykin A.I., Khmelnikova O.S.** Composition a thermal structure of the mantle in peripheral parts of the ancient shields within Siberian craton. // Revista Brasileira de Geociencias .2001, 31(4), pp.527-636.
12. **Ashchepkov I.V., Vishnyakova E.V.** Monomineral Cr-Spinel thermobarometry for kimberlite peridotite xenoliths. Abstracts of EUG 2005.
13. **Ashchepkov I.V.,Vladykin N.V., Pokhilenko N.P., Rotman A.Ya., Afanasiaev V.P., Logvinova A.M., Kuligin S.S., Saprykin A.I., Kuchkin A.M., Nikolaeva I.V., Palessky S.V., Anoshin G.N., Khemelnikova O.S.** Ilmenite trends from the kimberlites of Siberia :Do they represent the mantle feeding vein system? Abstracts of EUG 2005.
14. **Aulbach S, Stachel T, Viljoen K.S., Brey G.P., Harris J.W**. Eclogitic and websteritic diamond sources beneath the Limpopo Belt —is slab-melting the link? //Contrib. Mineral. Petrol. .2002. v.143. pp.56 –70
15. **Aulbach S.; Griffin W.L.; Pearson N.J.; O'Reilly S.Y.; Kivi K.; Doyle B.J.** Mantle formation and evolution, Slave Craton: constraints from HSE abundances and Re-Os isotope systematics of sulfide inclusions in mantle xenocrysts // Chem. Geol. - 2004. - Vol. 208. - Iss. 1-4. - P. 61-8
16. **Baumgartner M, Ankar E, Grutter H.** Compositional Classification of 'Kimberlitic' and 'Non-Kimberlitic' Ilmenite, with Implications for Visual Selection and Discrimination. //Extended Abstracts of the 8International Kimberlite Conference. 2003. FLA_0281
17. **Beard B.L., Fraracci K.N., Taylor L.A., Snyder G.A., Clayton R.N., Mayeda T.K., Sobolev N.V.** Petrography and geochemistry of eclogites from the Mir kimberlite, Yakutia, Russia. //Contrib. Mineral. Petrol., 1996. v.125, pp.:293 –310
18. **Boyd F.R., Pearson D.G., Nixon P.H., Mertzman S.A.** Low-calcium garnet harzburgites from southern Africa: their relations to craton structure and diamond crystallization // Contrib. Mineral. Petrol. 1993. V. 113. P/ 352-366.
19. **Boyd F.R.; Pokhilenko N.P.; Pearson D.G.; Mertzman S.A.; Sobolev N.V.; Finger L.W.** Composition of the Siberian cratonic mantle: evidence from Udachnaya peridotite xenoliths. //Contrib. Mineral. and Petrol. 1997., V. 128. N 2-3. P. 228-246.
20. **Brey G.P., Kohler T.** Geothermobarometry in four-phase lherzolites. II. New thermobarometers, and practical assessment of existing thermobarometers // J. Petrol 1990. V. 31. P. 1353-1378.
21. **Dawson JB** Kimberlites and their xenoliths. Springer,Berlin Heidelberg New York 1980, 295p.
22. **Dencker I., Nimis P., Zanetti A., Sobolev N.V.** Major and Trace Elements Composition of Cr-Diopsides from the Zagadochnaya Kimberlite Pipe (Yakutia, Russia): Insights into Metasomatic Processes in the Yakutian Lithosphere. //Extended Abstracts of the 8International Kimberlite Conference. 2003. FLA_0234.
23. **Eggins, S.M., Woodhead, J.D., Kinsley, L.P.J., Sylvester, P., McCulloch, M.T., Hergt, J.M. and Handler, M.R.** 1997. A simple method for the precise determination

of 40 or more trace elements in geological samples by ICP-MS using enriched isotope internal standardisation. Chemical Geology, 134, 311-326.

24. **Fedortchouk Y., Canil D., Carlson J.A.** Oxygen Fugacity of Kimberlite Magmas and their Relationship to the Characteristics of Diamond Populations, Lac de Gras, N.W.T., Canada. //Extended Abstracts of the 8International Kimberlite Conference. 2003. FLA_0098.
25. **Gregoire M., Bell D.R.; Le Roex A.P.** 2002. Trace element geochemistry of phlogopite-rich mafic mantle xenoliths: their classification and their relationship to phlogopite-bearing peridotites and kimberlites revisited. // Contrib Mineral Petrol. 2002. v 142(5) pp. 603-625.
26. **Griffin W.L., Fisher N.I., Friedman J.H., O'Reilly S.Y. and Ryan C. G.** Cr-pyrope garnets in the lithospheric mantle. 2. Compositional populations and their distribution in time and space // Geochem. Geophys. Geosyst. 2002. V. 3(12). P. 35.
27. **Griffin W.L., Shee S.R., Ryan C.G., Win T.T., Wyatt B.A.** arzburgite to lherzolite and back again: metasomatic processes in ultramaÆc xenoliths from the Wesselton kimberlite, Kimberley, South Africa. // Contrib Mineral Petrol (1999) 134: 232±250
28. **Griffin W.L., Ryan C.G., Kaminsky F.V., O'Reilly S.Y., Natapov L.M., Win T.T., Kinny P.D., Ilupin I.P**. The Siberian lithosphere traverse: mantle terranes and the assembly of the Siberian Craton. // Tectonophysics. 1999. V.310. P. 1–35.
29. **Griffin W.L.; O'Reilly S.Y.; Natapov L.M.; Ryan C.G**. The evolution of lithospheric mantle beneath the Kalahari Craton and its margins // Lithos. - 2003. - Vol. 71. - Iss. 2-4. - P. 215-241.
30. **Griffin, W.L., Fisher N.I., Friedman J.H., O'Reilly S.Y. and Ryan C.G.,** Cr-pyrope garnets in the lithospheric mantle. 2. Compositional populations and their distribution in time and space.//Geochem. Geophys. Geosyst., 2002.v.3 (12), 35 p.
31. **Griffin W.L., Moore R.O., Ryan C.G., Gurney J.J., Win T.T.,** 1997. Geochemistry of magnesian ilmenite megacrysts from Southern African kimberlites. // Russian Geol. Geophys. 1997. v. 38(2). pp.398-419
32. **Griffn W.L., Cousens D.R., Ryan C.G., Sie S.H., Suter G.F.** Ni in chrome pyrope garnets: a new geothermometer. // Contrib. Mineral. Petrol. 1989. v.103. pp. 199-202
33. **Jacob D., Jagoutz E., Lowry D., Mattey D., and Kudrjavtseva G.** Diamondiferous eclogites from Siberia: Remnants of Archean oceanic crust. //Geochim. Cosmochim. Acta 1994, v. 58, pp.5195-5207.
34. **Khar'kiv A.D. Zinchuk N.N., Kr'ychkov A.I.** Primary deposits of the diamonds in the World. Moscow /Nedra. 1998. 545p
35. **Kopylova M.G., Russell J.K., Stanley C. , Cookenboo H**. Garnet from Cr- and Ca-saturated mantle: implications for diamond exploration //J. Geochem. Explor., 2000, v. 68,. 3, P. 183-199.
36. **Kostrovitsky S.I., Alymova N.V., Ivanov A.S., Serov V.P.** Structure of the Daldyn Field (Yakutian Province) Based on the Study of Picroilmenite Composition //Extended Abstracts of the 8International Kimberlite Conference. 2003.FLA_0207.
37. **Kostrovitsky S.I.; de Bruin D.** Chromium association of minerals in micaceous kimberlites of the Daldyn field (Yakutian province) // "GEOL GEOFIZ". - 2004. - Vol. 45. - Iss. 5. - P. 565-576.
38. **Kuligin S.S., Malkovets V.G., Pokhilenko, N.P., Vavilov M.A., Griffin W.L., O'Reilly S.Y.** Mineralogical and Geochemical Characteristics of a Unique Mantle

Xenolith from the Udachnaya Kimberlite Pipe //Extended Abstracts of the 8International Kimberlite Conference. 2003. FLA_0114.

39. **Lee, C.-T., Rudnick, R.L.**, 1999. Compositionally stratified cratonic lithosphere: petrology and geochemistry of Tanzania. In: Gurney, J.J., Gurney, J.L., Pascoe, M.D., Richardson, S.H. (Eds.), Proc. 7th Int. Kimb. Conf., Red Roof Design cc, Cape Town, pp. 503-521.
40. **McGregor I.D.** The system MgO- SiO2- Al_2O_3: solubility of Al_2O_3 in enstatite for spinel and garnet peridotite compositions. // Am. Miner. 1974. V. 59. P. 110-119.
41. **Moor R.O., Griffin, W.L.** Gurney et al. 1992 Trace element geochemistry of ilmenites megacrysts from the Monastery kimberlite, South Africa. // Lithos. 1992. v. 29, pp.1-18.
42. **Moore A.E.; Lock N.P.** The origin of mantle-derived megacrysts and sheared peridotites-evidence from kimberlites in the northern Lesotho - Orange Free State (South Africa) and Botswana pipe clusters // S. Afr. J. Geol. - 2001. - Vol. 104. - N 1. - P. 23-38.
43. **Morfi L, Harte B, Hill P, Gurney J.** Polymict peridotites - a link between deformed peridotites and megacrysts from kimberlites: Abstr. 3rd International Workshop on Orogenic Lherzolites and Mantle Processes, Pavia, Sept. 12-15, 1999 // Ofioliti - 1999. - Vol. 24. - N 1a. - P. 134. S
44. **Nimis P., Taylor W.** Single clinopyroxene thermobarometry for garnet peridotites. Part I. Calibration and testing of a Cr-in-Cpx barometer and an enstatite-in-Cpx thermometer. //Contrib. Mineral. Petrol. 2000. V. 139. N5. P.541-554
45. **Nixon, P.H.** Ed.1973 Lesotho Kimberlites./Cape and Transvaal, Cape Town, 470 p.
46. **Nixon, P.H.,** 1987. Kimberlitic xenoliths, their cratonic setting./ In: P.H. Nixon (Editor). Mantle Xenoliths. Wiley, Chichester, pp.215-239.
47. **Pal'yanov N., Sokol A. G., Borzdov M., Khokhryakov A. F.** Fluid-bearing alkaline carbonate melts as the medium for the formation of diamonds in the Earth's mantle: an experimental study .// Lithos. 2002. v.60 pp. 145–159
48. **Pokhilenko N.P., Pearson D.G., Boyd F.R., Sobolev N.V.** Megacrystalline dunites: sources of Siberian diamonds // Carnegie Inst. Wash. 1991. Yearb. 90: P. 11-18.
49. **Pokhilenko, N. P., Sobolev, N.V., Kuligin, S. S., Shimizu, N.** Peculiarities of distribution of pyroxenite paragenesis garnets in Yakutian kimberlites and some aspects of the evolution of the Siberian craton lithospheric mantle. /Proceedings of the VII International Kimberlite Conference. The P.H. Nixon volume. 2000. Pp. 690-707.
50. **Prouteau G, Scaillet B, Pichavant M, Maury R** Evidence for mantle metasomatism by hydrous silicic melts derived from subducted oceanic crust. //Nature 2001. v. 410. p.197 –200
51. **Rodionov A.S., Sobolev N.V., Pokhilenko N.P., Suddaby P., Amshinsky A.N.** Ilmenite-bearing peridotites and megacrysts from Dalnaya kimberlite pipe, Yakutia // Fifth International Kimberlite Conference: Extended abstracts, United States, 1991, pp.339-341.
52. **Rotman A., Ashchepkov I., Palessky S., Saprykin A., Khemel'nikova O., Anoshin A**. Thermal structure and geochemistry of mantle minerals from three kimberlite pipes from Angola. Geophysical Research Abstracts, Vol. 7, 02879, 2004c. European Geophysical Society 2004.
53. **Ryan C. G.; Griffin W. L.; Pearson N. J.** Garnet geotherms: Pressure-temperature data from Cr-pyrope garnet xenocrysts in volcanic rocks. // J. Geophys. Res. B. 1996. V. 101. N 3. P. 5611-5625

---

54. **Sobolev N.V., Kaminsky F.V., Griffin W.L., Yefimova E.S., Win T.T., Ryan C.G. & Botkunov A.I**. Mineral inclusions in diamonds from the Sputnik kimberlite pipe, Yakutia. // Lithos. 1997. V. 39. P. 135-157.
55. **Sobolev N.V., Sobolev V.N., Snyder G.A., Yefimova E.S., Taylor L.A**. Significance of eclogitic and related parageneses of natural diamonds. Int Geol.Rev. 1999. v.41.129–140.
56. **Sobolev, N.V**. Deep-Seated Inclusions in Kimberlites and the Problem of the Composition of the Upper Mantle./Am. Geophys. Union, Washington, D.C. 1977. 279 p.
57. **Sobolev, N.V., Taylor, L.A., Logvinova, A.M., Koptil, V.A., Zinchuk, N.N., Zedgenizov, D.A., and Yefimova, E.S**., 2003, Mineral Inclusions In Diamonds From Komsomolskaya And Krasnopresnenskaya Pipes, Yakutia: Evidence For Deep Lithospheric Heterogeneities In Siberian Craton // 8th International Kimberlite Conference, Victoria, Canada.
58. **Spetsius, Z.V.,** 1995. Occurrence of diamond in the mantle: A case study from the Siberian Platform. In: W.L. Griffin (Editor), Diamond Exploration: Into the 21st Century. J. Geochem. Explor., 1995. v. 53. p. 25-39.
59. **Spetsius, Z.V., Serenco, V.P.,** 1990. Composition of Continental Upper Mantle, Lower Crust Beneath the Siberian Platform. /Nauka, Moscow, 1990. 272 pp. (in Russian).
60. **Van Achterberg E., Griffin W.L., Steinfenhofer J**. Metasomatism in mantle xenoliths from Letlhakane kimberlites estimation of element fluxes.// Contrib. Mineral. Petrol. 2001. v. 141, pp.397-414.
61. **Walter, M.J**., 1999. Melting residues of fertile peridotite and the origin of cratonic lithosphere. In: Fei, Y., Bertka,
62. **Wang W.Y.** & Gasparik T. Metasomatic clinopyroxene inclusions in diamonds from the Liaoning province, China // Geochim. Cosmochim. Acta. 2001. V. 65. P. 611-620.

UDK 9.01:552.323.6

Essentially non-kimberlitic old diamondiferous igneous rocks

Sablukov S.M., Kaminsky F.V. and Sablukova L.I.

KM Diamond Exploration, Vancouver, Canada, S.Sablukov@g23.relcom.ru

In the past decade several tens of highly diamondiferous igneous rock occurrences, likely representing a new diamondiferous rock type, neither similar to kimberlite nor to lamproite, have been discovered in Canada and French Guyana. These peculiar rocks are old (Archean to Early Proterozoic), and occur within ancient Precambrian platforms. They are strongly metamorphosed, and have a breccia-type texture. These rocks are similar in composition to minette with some characteristics typical of lamproite (Parker Lake), to calc-alkali lamprophyre with some resemblance to komatiite (Wawa and Yellowknife), and to pure komatiite (Dachin). All the newly discovered igneous rock bodies proved to contain high-pressure kimberlite indicator minerals, primarily garnet (including G10, or diamond suite, pyrope and eclogitic pyrope-almandine), with minor olivine, chrome-diopside, picroilmenite and chromite. Further evidence of mantle origin for these rocks is either found in their ultra-potassic composition (Parker Lake) or in their high “ultramafic” elements (Mg, Ni, Cr and Co) content. Among the diamonds occurring in these rocks, small (up to 0.5 mm) crystals predominate overwhelmingly, with a minor proportion of relatively large (up to 5 mm) crystals. Diamond occurs there predominantly as octahedral, cubic, cuboctahedral and tetrahexahedral crystals, mostly with various brown, green and yellow color shades (colorless crystals are rare). Diamond grade of these rocks is generally very high, varying from 0.3 to 1 ct/ton and ranging up to 7-10 ct/ton in several samples. As regards diamond quality, commercial diamond predominates there, although gem diamonds up to 0.72 ct also do occur in the samples. It is quite probable that rocks of this sort are widespread worldwide, simply having as yet attracted no attention in view of their “atypical” appearance and composition. In Russia, diamondiferous rocks of this type may occur within the boundaries of ancient shields (Baltic, Ukrainian, Aldanian and Anabar) and, probably, in some median masses (like Kolyma and Khankai), which might promise a significant increase in diamond potential of Russia.

INTRODUCTION

In the past decade several tens of highly diamondiferous igneous rock occurrences, obviously representing a peculiar diamondiferous rock type, neither similar to kimberlite nor to lamproite (recognized as “common” primary sources of diamond), have been discovered in Canada and French Guyana. These findings perfectly confirmed the hypotheses developed by Soviet scientists [9] regarding diamond potential of basaltoid rocks, lamprophyres, alkali ultramafics and other essentially non-kimberlitic igneous rocks.

The geological structure and composition of these peculiar diamondiferous rocks would be of great interest, both in terms of gaining further insight into the formation of diamond and deep-seated diamondiferous rocks and from the standpoint of diamond potential assessment and development of prognosis for diamonds and diamond exploration in Russia and abroad.

In this study, we report the characteristic features of the most representative entities, the rocks of which we examined first-hand, with varying amount of

---

sampling material and extent of thoroughness. Diamondiferous igneous rocks from the Parker Lake and Wawa areas (Canada) were studied most thoroughly and completely, whereas for the Dachin deposit (French Guyana) a more restricted set of rock samples was examined. In addition, we used here some large-volume sampling data taken from literature and published results of studies on diamonds and high-pressure minerals from some igneous rock bodies occurring in the aforementioned areas.

DIAMONDIFEROUS ROCKS OF THE PARKER LAKE AREA,

Nunavut, Canada

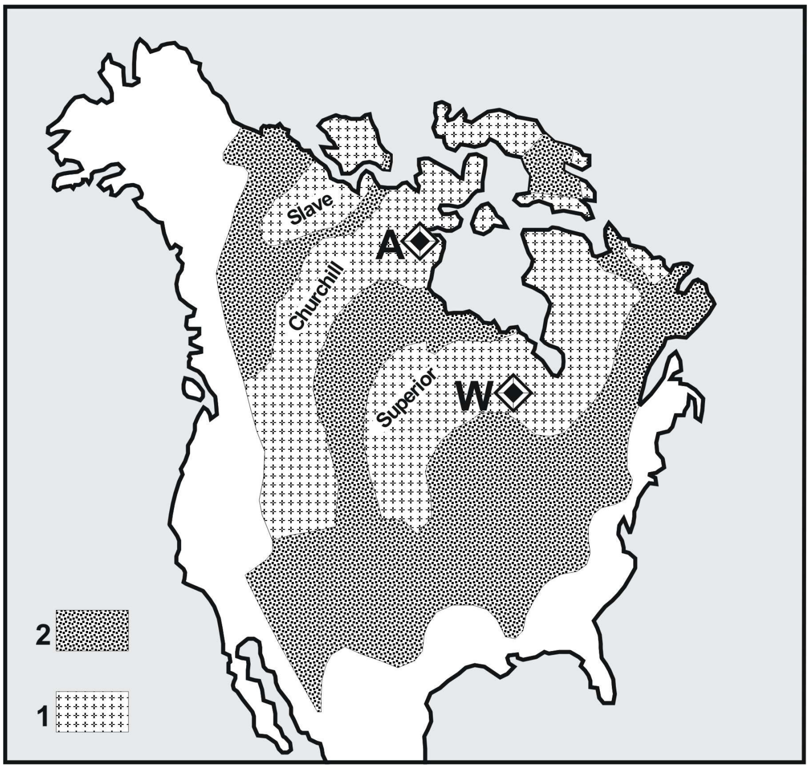

Fig 1**. Tectonic position of the non-kimberlitic diamondiferous rocks in Canadian Shield. A – Akluilak system, W – Wawa area. 1 – Archean kratons, 2 - Proterozoic orogens.**

A new type of non-kimberlitic igneous rock, not merely undoubtedly diamondiferous but showing a very high diamond grade, was discovered in the Canadian shield, within the terrain that entered the list of areas covered by diamond exploration next to latest of all. In 1994, Canadian geologists McRay and Armitage were studying the variety of CIF lamprophyre dykes (see below) in the Parker Lake area, and, in doing this, they discovered some diamondiferous rocks which, bearing no resemblance to kimberlite or lamproite (neither in appearance nor in composition), proved to be similar to minette rocks (members of the calc-alkali lamprophyre group) [16, 17].

The Parker Lake area is situated at the northwestern coast of Hudson Bay, close to the Ranking Inlet settlement, Nunavut, in the northern part of the Canadian shield, within the northern segment of the Churchill craton (Fig. 1). This part of the craton hosts the largest known Early Proterozoic province of alkali rocks occurring as numerous dykes, lava sheets and pyroclastic deposits alternating with continental sediments, known as Christopher Island Formation (CIF) [21]. As of now, four diamondiferous dykes are known in the eastern marginal zone of this alkali rock province, and all of them have been thoroughly studied by the authors [10-12]. Three of these dykes (North, Thirsty Lake and South) form the Akluilak sublongitudinal dyke system, approximately 15 km long, with rock body thickness varying from 1 to 3 m (up to 5-8 m in the swells). The fourth dyke (Victory Day), 0.5-1.1 m thick, has been traced for 300 m along the strike. It is located 10 km west of the Akluilak dyke system, thus appearing to be a small fragment of some other, also sublongitudinal, system of diamondiferous dykes. The dykes are characterized by a quite constant strike (with some elements of echelon-like structure), a nearly vertical dip and sharp (break-type) host rock contacts. Owing to the high degree of denudation characteristic of the terrain being studied, all these dykes are easy to trace and map.

Macroscopically, the rocks of all four dykes are dense and solid, with a homogeneous black coloration and a holocrystalline appearance, showing uneven, finely step-like fractures (in general, these rocks are similar in appearance to micro-to-mesocrystalline hornblendite or augitite). The structure of the rock is commonly breccia-like, and the proportion of altered metamorphic and igneous rock xenoliths varies from 1% to 60 % along th dyke strike, such that in some local zones the structure of the dyke rocks is nearly “rubbly”, with ovalized xenoliths varying in size from 5 to 15 cm (rarely, up to 20-40 cm).

All four dykes are made up of an intensely metamorphosed rock consisting essentially of potassic feldspar (50-60% of the rock volume), biotite (30-35%) and apatite (5-7%); carbonate is also present in all the examined dyke rock samples (5-10% of the rock volume), and some samples show a sizable proportion of epidote. The set of accessory minerals includes titanite, magnetite, zircon and pyrite. The texture of the rock is fine-to-medium-grained holocrystalline, poikiloblastic, clearly discernible in crossed nicols only.

The framework of the rock consists of large ***orthoclase*** poikiloblasts endowed with small (0.02-0.1 mm) biotite and apatite inclusions, with fine-grained aggregates of orthoclase, biotite, apatite, carbonate and, quite commonly, epidote occurring between some poikiloblasts. The size of orthoclase poikiloblasts varies, on the average, from1 to 3 mm (generally, from 0.2 to 8 mm). Orthoclase is characterized by a high K_2O content and very low Na_2O and CaO contents (Tab. 1).

Table 1.

Chemical composition of potassic feldspars from Parker Lake area dykes (wt. %)

No	**Sample**	**SiO_2**	**TiO_2**	**Al_2O_3**	**Cr_2O_3**	**FeO**	**MnO**	**MgO**	**CaO**	**Na_2O**	**K_2O**	**Total**
1	466/19	65.61	0.06	18.32	0.00	0.26	0.00	0.01	0.00	0.75	15.78	100.79
2	103/10	64.60	0.06	17.98	0.00	0.07	0.04	0.00	0.01	0.74	15.32	98.82
3	475/18	64.62	0.04	18.30	0.00	0.12	0.00	0.00	0.01	0.22	16.07	99.38
4	103/5	63.65	0.03	18.22	0.00	0.12	0.00	0.07	0.17	0.05	16.51	98.82

Note: 1 - North Dyke; 2 - Thirsty Lake Dyke; 3 - South Dyke; 4 - Thirsty Lake Dyke (xenolith); Electron microprobe analysis (Micro Beam Camera analyser), TsNIGRI Laboratory, analyst M.V. Shavyrina, 1996.

Biotite occurs as irregularly shaped grains, 0.02-0.5 mm in size, and as aggregates of grains, both included in orthoclase poikiloblasts and in the interstices between them. Quite commonly, biotite laths are arranged subparallel to each other around large orthoclase grains, thus forming elements of eye structure in the dyke rock. In local zones of the rock, biotite laths as large as up to 1 mm with very small, equidimensional and acicular inclusions occur. Biotite grains have a dirty-green, brown and, rarely, dark green color. Being characterized by a moderate iron index (Tab. 2, Fig. 2) and a higher than average Al_2O_3 content, biotite from the examined dyke rocks is most similar in composition to biotite from minette [20].

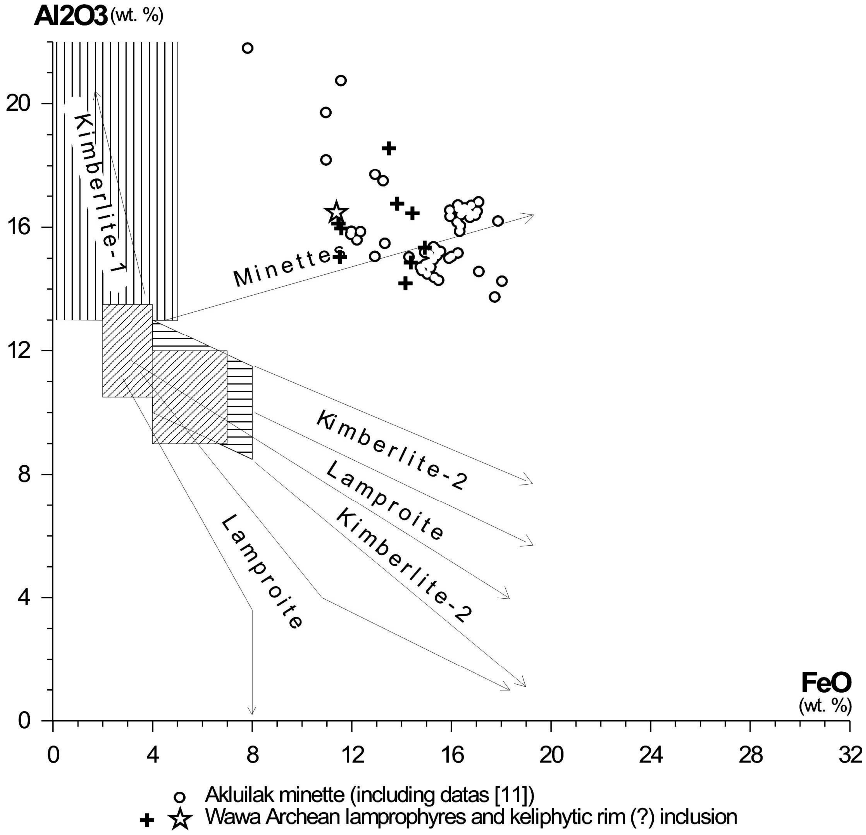

Fig. 2**. Composition of volcanic rock micas (diagram after [20]).**

Table 2.

Chemical composition of biotite from Parker Lake area dykes (wt. %)

No	**Sample**	**SiO_2**	**TiO_2**	**Al_2O_3**	**Cr_2O_3**	**FeO**	**MnO**	**MgO**	**CaO**	**Na_2O**	**K_2O**	**Total**
1	103/10	38.47	1.97	15.87	0.04	16.33	0.44	11.43	0.04	0.13	9.54	94.26
2	103/10	37.90	2.11	16.20	0.00	17.87	0.39	11.31	0.01	0.08	9.71	95.58
3	103/5	37.38	1.04	17.71	0.03	12.93	0.12	14.81	0.43	0.08	9.62	94.15
4	103/5	37.51	1.16	17.50	0.02	13.25	0.12	14.44	0.02	0.06	9.84	93.92
5	103/5	39.12	0.83	18.19	0.08	10.96	0.14	13.96	0.07	0.06	10.36	93.77
6	103/5	42.98	0.63	21.80	0.04	7.81	0.10	9.72	0.03	0.07	10.51	93.69
7	466/19	38.78	2.08	14.81	0.07	14.95	0.21	14.73	0.31	0.15	9.47	95.56
8	466/19	39.13	1.86	15.04	0.01	14.29	0.07	14.90	0.02	0.00	10.00	95.32
9	475/18	36.49	0.84	20.75	0.04	11.56	0.19	16.24	0.00	0.00	10.50	96.61
10	475/18	37.86	0.90	19.72	0.13	10.95	0.23	16.46	0.03	0.00	10.62	96.90
11	476/2	36.93	2.67	14.70	0.06	15.15	0.00	14.15	0.00	0.26	8.92	92.84
12	476/2	37.95	2.00	15.48	0.06	13.32	0.02	14.68	0.05	0.17	8.96	92.69
13	476/2	38.25	1.90	15.06	0.07	12.92	0.01	15.03	0.04	0.00	8.86	92.14
14	103/8	39.58	1.16	15.59	0.07	12.20	0.09	17.09	0.00	0.04	8.52	94.34
15	103/8	39.68	1.22	15.86	0.08	12.34	0.19	17.85	0.00	0.22	8.28	95.72
16	103/8	40.19	1.24	15.77	0.11	11.96	0.08	17.09	0.01	0.03	8.67	95.15
17	103/8	40.37	1.42	15.87	0.11	11.98	0.04	17.13	0.02	0.08	8.87	95.89

Note: 1,2 - Thirsty Lake Dyke; 3-6 - Thirsty Lake Dyke (xenolith); 7,8 - North Dyke; 9,10 - South Dyke; 11-13 – V-Day Dyke; 14-17 – CIF lamprophyre. Electron microprobe analysis (Micro Beam Camera analyser), TsNIGRI Laboratory, analyst M.V. Shavyrina, 1996.

Apatite, forming idiomorphic phenocrysts endowed with very small, highly birefringent inclusions, plays a special role in the examined dyke rocks. The size

Table 3.

Chemical composition of apatite from Parker Lake area dykes (wt. %)

No	**Sample**	**Al_2O_3**	**MnO**	**CaO**	**SrO**	**P_2O_5**	**Total**
1	103/10	0.00	0.01	55.12	0.20	39.82	95.15
2	103/10	0.06	0.51	53.53	0.07	39.93	94.10
3	103/10	0.09	0.03	55.28	0.49	40.54	96.43
4	466/19	0.00	0.00	54.19	0.99	40.36	95.54
5	466/19	0.00	0.00	54.45	0.75	40.82	96.02
6	475/18	0.00	0.00	55.71	0.41	41.87	97.99
7	475/18	0.00	0.00	56.01	0.44	41.01	97.46
8	475/18	0.00	0.09	55.36	0.65	40.95	97.05
9	476/2	0.00	0.01	53.97	1.25	38.32	93.55
10	476/2	0.01	0.00	54.71	1.06	40.40	96.18
11	476/2	0.05	0.04	53.93	0.98	39.87	94.87
12	103/8	0.06	0.12	53.95	0.19	40.23	94.55
13	103/8	0.07	0.11	53.53	0.24	39.57	93.52

Note: 1-3 - Thirsty Lake Dyke; 4,5 - North Dyke; 6-8 - South Dyke; 9-11 - V-Day Dyke; 12,13 – CIF lamprophyre. Electron microprobe analysis (Micro Beam Camera analyser), TsNIGRI Laboratory, analyst M.V. Shavyrina, 1996.

of idiomorphic apatite grains generally varies from 0.5 to 3 mm, but subangular, irregularly shaped apatite segregations, apatite proportion ranges up to 10% of the rock volume). Apatite is characterized by a higher than average Sr content (up to 1.25 wt.% SrO, see Table 3). It is probable that the apatite segregations represent the one and only preserved component of inferredly porphyritic initial texture of the dyke rock. However, the idiomorphic shape of apatite grains may be due to high crystallizing force of this mineral, and the abundance of inclusions as high as in orthoclase and biotite grains may be evidence of nearly concurrent growth of apatite, orthoclase and biotite grains in the course of metamorphic transformations of the examined rock.

Table 4.

Chemical composition of Parker Lake area minette dykes (wt. %)

No	1	2	3	4	5	6	7	8	9	10	11	12	13
Dyke	Thirsty Lake		North			South					V-Day		CIF
Sample	103/10	103X/10	466/2	466/12	466/23	475/4	475/8	475/12	475/19	475/23	476/2	476/4	103/8
SiO_2	40.31	47.84	40.65	45.45	42.70	43.31	44.94	40.98	44.75	44.06	43.78	43.14	46.60
TiO_2	1.86	0.39	1.44	1.28	0.80	1.14	1.20	1.37	1.27	1.41	1.57	1.65	1.68
Al_2O_3	11.69	25.62	15.12	15.46	12.41	14.93	15.62	13.69	15.68	16.17	13.40	12.93	12.44
Fe_2O_3	4.21	2.35	0.83	3.56	2.02	2.49	3.68	0.81	1.77	1.40	1.49	1.82	4.44
FeO	5.92	3.01	5.82	2.68	4.12	4.41	3.58	4.13	4.51	4.78	5.37	5.36	7.39
MnO	0.36	0.21	0.07	0.04	0.12	0.01	0.10	0.06	0.10	0.07	0.02	0.02	0.03
MgO	5.09	2.20	5.53	5.06	4.50	5.08	5.19	4.11	5.19	4.70	5.99	5.35	14.49
CaO	11.43	5.59	9.16	8.03	10.91	8.37	8.22	11.77	8.41	8.08	9.65	9.93	3.10
Na_2O	0.64	3.44	0.60	0.52	0.52	0.49	0.22	2.60	0.41	0.64	1.30	0.73	0.30
K_2O	8.29	6.18	9.00	11.07	9.76	10.94	11.95	10.61	11.28	10.61	7.14	9.46	6.40
P_2O_5	3.10	0.35	4.80	3.78	1.43	4.26	3.36	2.96	3.55	5.08	3.30	3.35	1.61
LOI	6.10	3.22	4.83	2.85	7.82	3.50	0.71	5.70	1.80	1.86	4.64	5.26	1.44
BaO	-	-	1.56	-	1.78	-	0.80	1.32	0.89	0.91	1.43	-	-
Total	99.00	100.40	99.41	99.78	98.89	98.93	99.57	100.11	99.61	99.77	99.08	99.00	99.92
H_2O^-	0.16	0.32	0.15	0.14	0.09	0.20	0.15	0.08	0.00	0.16	0.14	0.08	0.21
H_2O^+	0.96	2.07	1.59	0.90	5.87	0.78	0.47	0.78	0.69	0.68	0.75	0.80	1.17
CO_2	5.32	0.77	3.01	2.24	7.00	2.59	0.00	4.66	0.75	1.10	3.60	4.49	0.30
S_{tot}	0.32	0.15	0.11	0.05	0.22	0.02	0.06	0.05	0.06	0.11	0.05	0.07	0.11

Note: 1, 3-12 - diamondiferous minette; 3 - xenolith from the diamondiferous minette; 13 - CIF lamprophyre;

Chemical analysis, GIN RAS Laboratory, analyst V.V. Karpushina, 1996. (-) - not available.

Major and minor element contents were determined for twelve rock samples from four minette dykes, one altered xenoliths from the Thirsty Lake dyke and one CIF micaceous lamprophyre sample (Tables 4,5).

The rocks of the diamondiferous dykes are characterized by a low SiO_2 content (40.31-45.55 wt. %), a higher than average Al_2O_3 content (11.69-16.17 wt.

%) and a very high alkali content (8.44-13.21 wt. % ΣR_2O), with an ultra-potassic alkalinity type (K_2O/Na_2O = 4.1-54.3). Fe and Ti contents of the rock are low to moderate, and the concentrations of “typically ultramafic” compatible elements (Mg, Ni, Co and Cr) are very low. In the classification diagrams (Figures 3-5) figurative points of the dyke rocks fall into the compositional fields of foidite (Fig. 3) and Si-undersaturated, low-Mg rocks (Fig. 4). The dyke rocks contain normative leucite (up to 44%) and olivine (up to 15%), being generally similar in major elements content to foidite (leucitite) of kamafugite or tephrite-leucite series but not to that of lamproite series as they contain too much Al_2O_3, some (although not too much) normative plagioclase and nepheline, and some other components atypical of lamproite rocks.

Table 5.

Minor element composition of Parker Lake area minette dykes (ppm)

No	**1**	**2**	**3**	**4**	**5**	**6**	**7**	**8**	**9**	**10**	**11**	**12**	**13**
Dyke	**Thirsty Lake**		**North**			**South**					**V-Day**		**CIF**
Sample	103/10	103X/10	466/2	466/12	466/23	475/4	475/8	475/12	475/19	475/23	476/2	476/4	103/8
Ni	78	69	125	119	96	109	120	71	121	134	141	115	399
V	69	22	36	19	25	<10	31	<10	24	<10	30	51	170
Y	101	17	41	31	46	44	28	39	35	34	38	47	27
Nb	19	2.5	15	7.6	2.9	6.3	6.5	9.5	5.1	7.4	8.7	12	14
Zr	898	190	443	357	41	262	342	519	396	396	777	1450	636
Rb	533	610	213	353	207	378	391	342	456	386	199	274	277
Sr	909	1980	4570	1540	1060	2350	2220	4170	1300	1870	2090	2030	56
Ba	6630	3030	9180	4320	15740	8520	8150	12720	4340	4770	6850	5210	1600
La	182	47	137	77	334	134	143	145	92	102	192	166	123
Ce	364	91	270	167	512	267	280	288	222	217	370	310	215
Nd	217	55	148	95	186	118	152	148	98	128	182	144	94
Sm	52	7.4	31	21	33	30	29	29	24	26	29	31	16
Eu	20	5.7	9.8	8.1	8.5	10	9.7	11	8.4	9	11	11	4.5
Tb	5.3	0.33	3.1	2.1	1.7	2.3	2.1	3.1	2.3	1.7	1.5	2.5	1
Yb	6.7	0.33	2.9	1.1	3	2.6	1	2	1.5	1.2	1.8	3.6	2
Lu	0.68	0.07	0.23	0.14	0.32	0.28	0.15	0.34	0.18	0.19	0.29	0.37	0.39
Th	28	3.2	14	14	18	16	14	10	11	6.6	11	17	13
U	14	3.1	5.8	5.8	5.3	10	11	4.4	6.1	5.3	8	7.1	2.3
Sc	28	8.6	17	24	16	19	26	16	25	21	23	26	36
Cr	112	28	180	187	178	220	206	136	196	185	215	177	1100
Co	22	21	28	28	23	31	34	26	5.7	32	27	26	83
Hf	26	4.6	12.2	8.3	5.8	10	11	21	13.7	13	26	42	21
Ta	2.8	<0.4	<0.4	0.8	1.2	<0.4	1.6	0.48	1	0.48	<0.4	1.4	1.5
Cs	46	29	1.9	4.7	5.5	4.1	4.9	4.7	11.6	6.5	2.8	2	24

Note: 1, 3-12 - diamondiferous minette; 3 - xenolith from the diamondiferous minette; 13 - CIF lamprophyre From Ni to V - X-ray fluorescence analysis, IMGRE Laboratory, the Analyst E.P. Shevchenko, 1996. From Ba to Cs - instrumental neutron activation analysis, Kuligin V.M., Vitozhents G.Ch., TsNIGRI, 1996.

The concentration of incompatible elements in the dyke rocks is very high, and the distribution of these elements is very heterogeneous (Figures 6,7). The

rocks are characterized by very high P_2O_5 (1.43-5.08 wt. %), K_2O (7.14-11.28 wt. %), Rb (199-522 ppm), Sr (909-4570 ppm), Ba (4,320-15,740 ppm), Zr (262-1450 ppm) and REE (371-1079 ppm) contents, i.e., by a set of elements typical of Ba-KREEP-type mantle metasomatism. Small positive Eu-anomaly is marked.

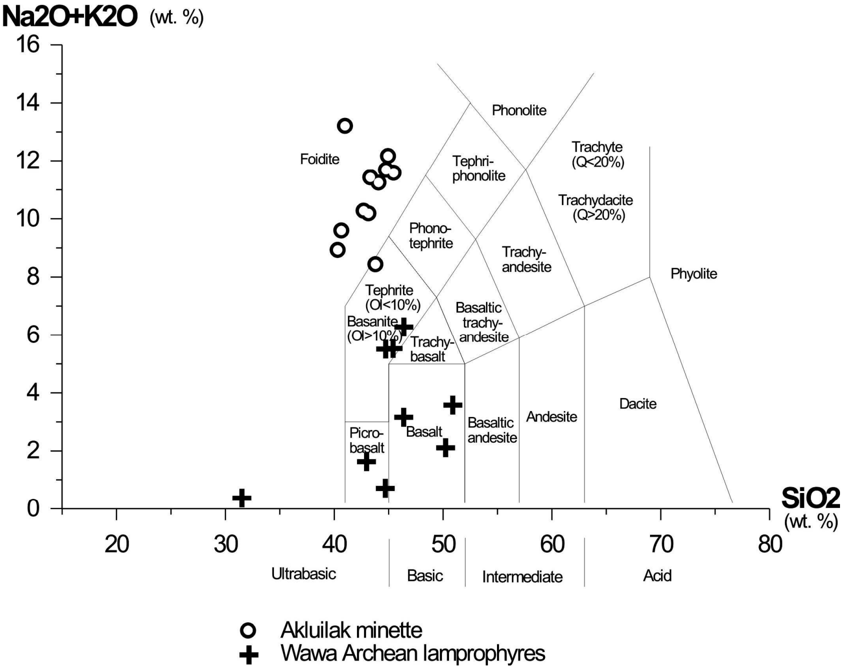

Fig. 3. **The hemical classification and nomenclature of volcanic rocks using the total alcalis versus silica (TAS), diagram [15].**

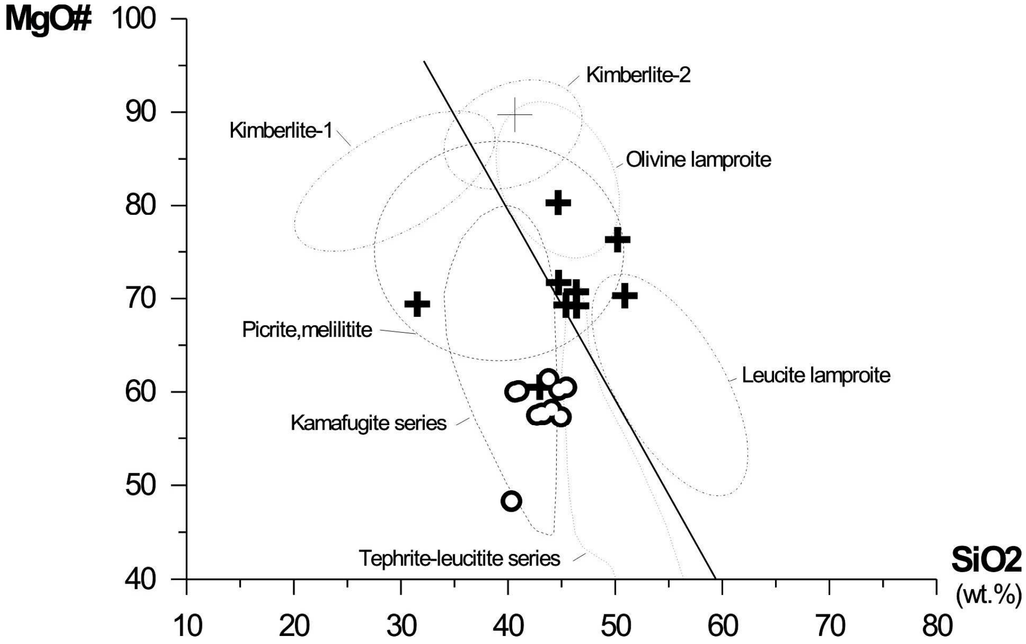

Fig. 4. **Chemical features of volcanic rocks [2]. MgO# = 100MgO/(MgO+FeO), mol. quantity.**

However, the concentrations of the elements typical of Ti-metasomatism are moderate to much lower than average (0.80-1.86 wt. % TiO_2, 2.9-19 ppm Nb, below 0.4-2.8 ppm Ta). The concentrations of radioactive elements are also moderate (4.4-14 ppm U, 6.6-28 ppm Th). Being very peculiar in their incompatible elements distribution, the rocks are yet somewhat similar to some lamproites in particular element contents. Figurative points of all the examined dyke rocks form continuous trends or compact groups in all the geochemical diagrams, which highlights their common genesis. The rock sample from the micaceous lamprophyre dyke (CIF) is similar in some geochemical characteristics to the examined rocks of diamondiferous dykes, therewith significantly differing from them by having a 3-5 times higher concentration of “ultramafic” elements (Mg, Cr, Ni, Co) and V, and 3-5 times lower Sr and Ca contents.

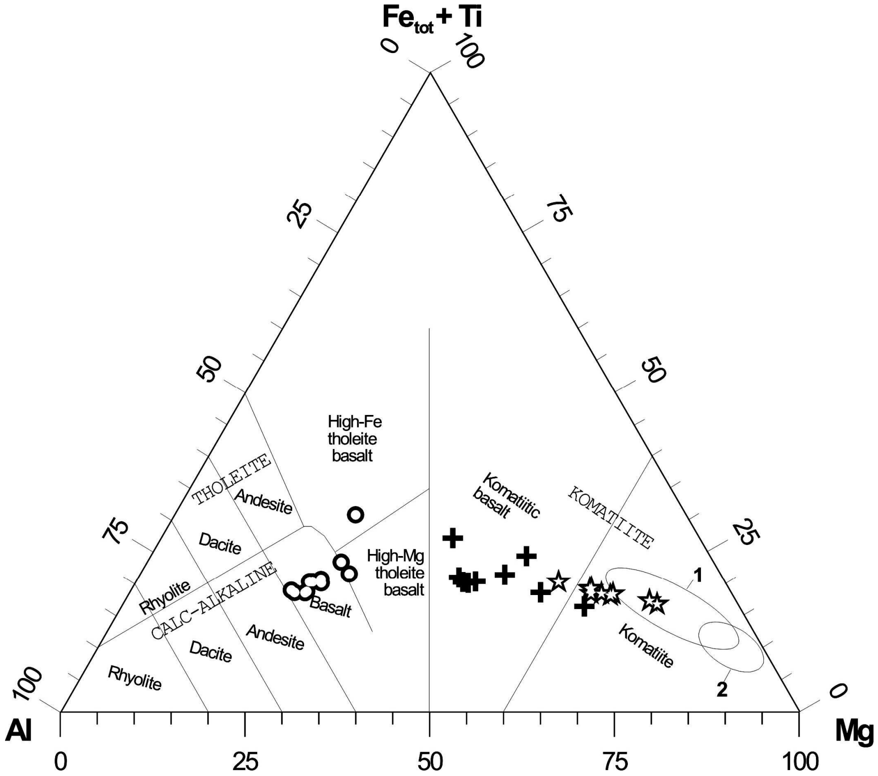

Fig. 5. **The classification of volcanic rocks according to their cation percentages of Al, (Fe_{tot} + Ti) and Mg [8, 22]. 1 – composition of kimberlites; 2 – composition of ultramafic mantle inclusions from kimberlites.**

In general, based upon the bulk mineral composition (orthoclase + biotite), biotite composition peculiarities and the essential geochemical characteristics, the examined dyke rocks can be crudely classified as minette rocks, although they differ significantly from typical minette in that they are Si-undersaturated, and have a lower MgO content and higher Al_2O_3, K_2O and P_2O_5 contents. As regards the distribution of major and minor elements, the rocks of the four dykes tend to form a separate group, differing both from lamproite and from potassic basaltoids, however, with some evidence of relationship to CIF lamprophyres.

The probable relationship of the examined diamondiferous minette dyke rocks to CIF lamprophyres is further highlighted by their similarity in Nd-Sr isotope

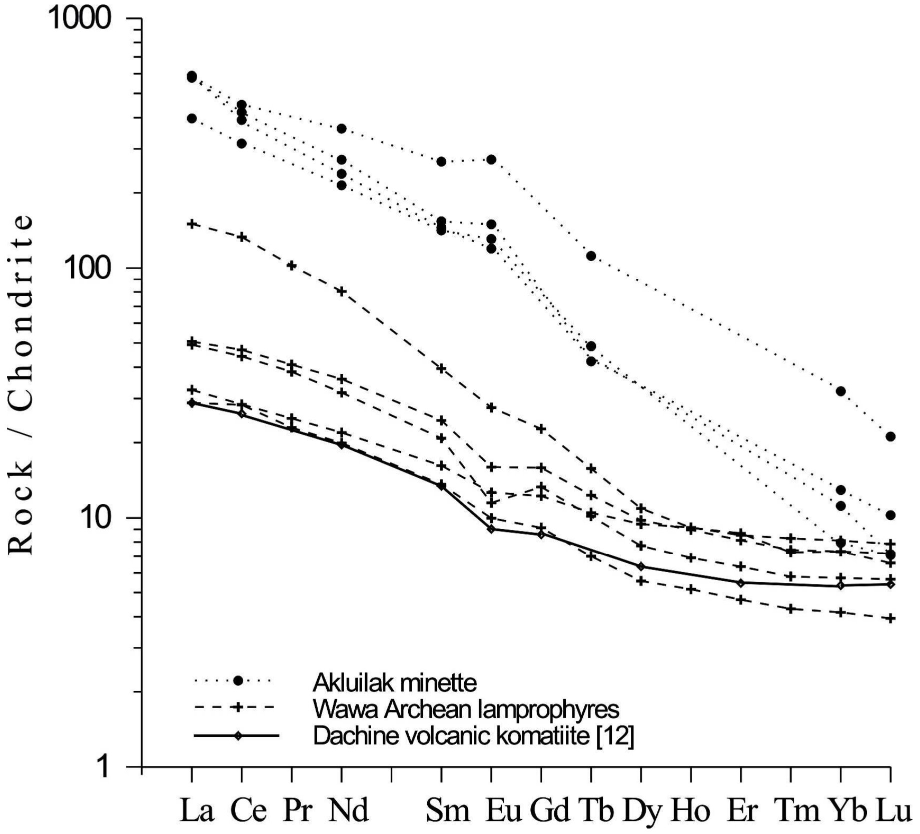

Fig. 6. **Chondrite normalized [3] REE distribution patterns for volcanic rocks.**

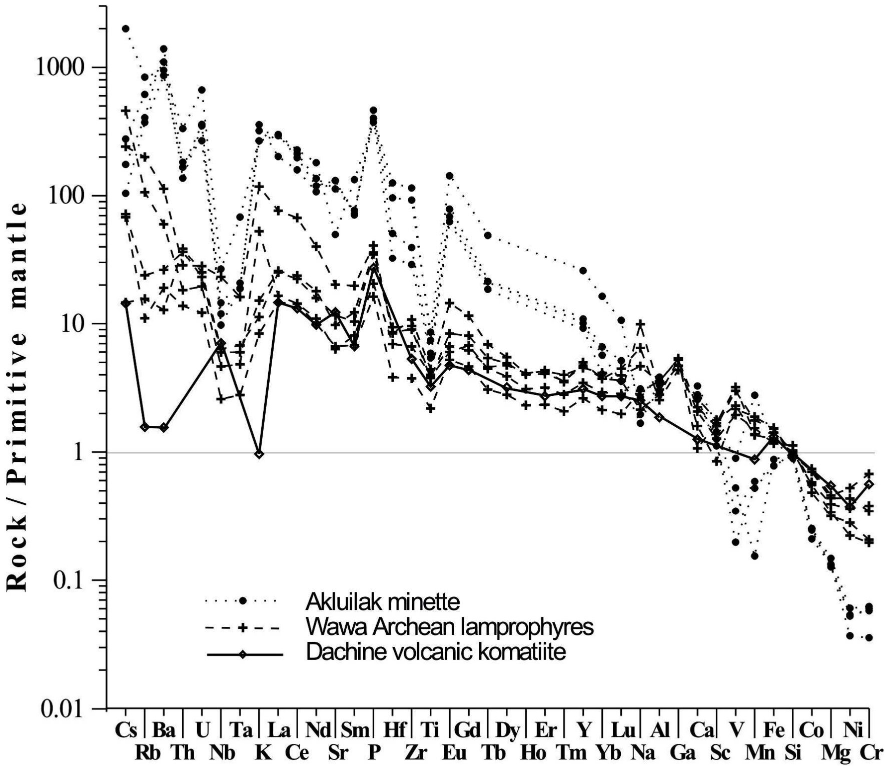

Fig. 7. **Primitive mantle normalized [6, 18] element composition of volcanic rocks**

characteristics and absolute age (Tab. 6, Fig. 8). The age of Thirsty Lake dyke, as determined by the U-Pb method for a monazite inclusion in apatite, is 1832+/-50 Ma [17]. A Sm-Nd five-point isochron plotted for bulk rock samples from the four dykes and a set of apatite grains picked from the South dyke rocks yielded an age of 1867+/-44 Ma, which agrees well with the previously determined Early Proterozoic age for the Thirsty Lake dyke [17]. This age is also close to that of Christopher Island Formation (CIF) lamprophyres [21], although it may be just the age of metamorphic transformation of an older rock affected by "steaming" in the course of the magmatic activization event responsible for the formation of CIF.

Table 6.

Sr and Nd isotope composition of the Parker Lake area dykes

No	**Kod**	**Sample**	**Rb** (ppm)	**Sr** (ppm)	**$^{87}Rb/^{86}Sr$**	**$^{87}Sr/^{86}Sr$**	**εSr_t**	**Sm** (ppm)	**Nd** (ppm)	**$^{147}Sm/^{144}Nd$**	**$^{143}Nd/^{144}Nd$**	**εNd_t**	**$T_{(DM)}$**	**$T_{(CHUR)}$**
1	N/12	466/12	355	1556	0.6611+/-27	0.721654+/-19	26.2	17.73	80.62	0.13295	0.511377+/-8	-9.6	3.325	2.995
2	A/10	103/10	550	933	1.7120+/-6	0.75073+/-16	44.0	43.92	189.0	0.14050	0.511457+/-6	-9.8	3.501	3.180
3	S/19	475/19	469	1298	1.049+/-4	0.731571+/-19	21.2	20.22	97.7	0.12510	0.511274+/-7	-9.7	3.207	2.885
4	V/4	476/4	273	2100	0.3766+/-16	0.712799+/-16	7.3	25.92	134.5	0.11653	0.511235+/-6	-8.5	2.987	2.653
5	SA/9	475/9	3.22	2912	0.0032+/-4	0.705197+/-15		68.09	197.0	0.20897	0.512296+/-7			

Note: 1-4 - minette, 5- apatite; 1- North Dyke; 2 - Thirsty Lake Dyke; 3,5 - South Dyke; 4 - V-Day Dyke. □Sr_t and □Nd_t corrected for emplacement an age 1.84 Ga. Rb-Sr and Sm-Nd isotope analyses were carried out by D.Z. Zhuravlev at the IGEM RAS Isotope Laboratory,1997 with a Finningan™ MAT-262 mass-spectrometer in a static measurement mode. Blank levels were, respectively no higher than 0.3; 0.1; 2.0 and 0.5 ng for Nd, Sm, Sr and Rb. The concentrations were measured in micrograms per 1 gram of sample weight. Analytical accuracies were equal to +/- 1% for concentrations and +/- 0.2% for Sm/Nd ratios. Standards: Eimer & Amend: $^{87}Sr/^{86}Sr = 0.708041$+/-18 (2s, n = 9); La Jolla: $^{143}Nd/^{144}Nd = 0.511840$+/-15 (2s, n = 25). Model reservoirs: CHUR: $^{147}Sm/^{144}Nd = 0.1967$, $^{143}Nd/^{144}Nd = 0.512638$; UR: $^{87}Rb/^{86}Sr = 0.0825$, $^{87}Sr/^{86}Sr = 0.7045$.

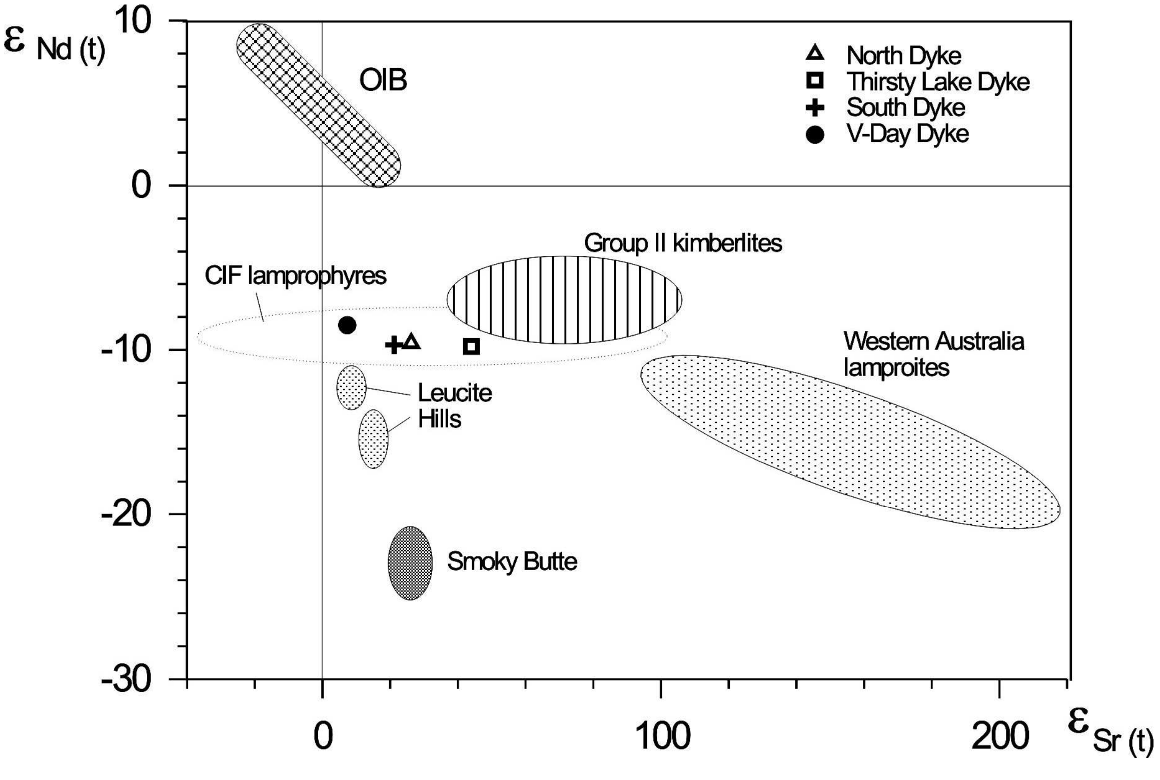

Fig. 8. **Sr and Nd isotope composition of the diamondiferous minette dykes and CIF lamprophyres [21] corrected for an age 1.84 Ga.**

The assumption that the Akluilak minette is somewhat older appears to be confirmed by the fact that this rock occurrence bears evidence of having been shifted sharply (over 6 m) by a CIF lamprophyre dyke. Absolute dating by the K-Ar method (Table 11) also yields for the Akluilak system (dykes Thirsty Lake and North) an age approximately 200 Ma older than that of a CIF lamprophyre dyke. Although the K-Ar age of these rocks is younger than actual (due to superimposed processes), the difference in absolute age of the minette and lamprophyre dykes is still evident. Probable more old (in relation to CIF) age of the diamondiferous minette dykes can specify the settlement data of Nd-modelling age according to which the source of magma minette dykes were separated from depleted mantle source 3,26 billion years back (Tab. 6), and a lamprophyre CIF magma - 2,80 billion years back [21].

Table 7.

Results of K-Ar isotope analyse of the Parker Lake area dykes

No	Sample	Dyke	K, (wt.%) +/-1σ	^{40}Ar$_{rad}$, (ngr/gr)+/-1σ	Age, Ma +/-1.6σ
1	103/10	Thirsty Lake (minette)	6.29+/-0.05	1244+/-10	1710+/-50
2	103/10-1	Thirsty Lake (xenolith)	5.26+/-0.07	892+/-8	1545+/-50
3	466/4+11	North (minette)	8.96+/-0.07	1840+/-35	1750+/-50
4	466/4+6	CIF lamprophyre	4.80+/-0.05	808+/-8	1540+/-50

Note: measurements of radiogenic Ar isotope concentration were carried out on a MI-1201 IG mass-spectrometer through the isotope dilution technique (tracer: ^{38}Ar). K determinations were performed by means of flame photometry. Age estimates were made with the following constant parameter values used: Lk = 0.581*10^{-10} year $^{-1}$; Lb = 4.962 *10^{-10} year $^{-1}$; ^{40}K=0.01167 (at.%). IGEM RAS, Laboratory of isotope geochemy and geochronology, analyst M.M.Arakelyants, 1996.

In addition to Nd-Sr characteristics, the presence of high-pressure (diamond indicator) minerals (olivine, garnet, chrome-diopside and picroilmenite) is another evidence of mantle origin for the Akluilak minette dyke rocks. The grains of these minerals are of moderate size (0.2-0.7 mm) and, few as they are, vary rather widely in mineral chemistry (Tab. 8): among them are eclogitic suite minerals (pyrope-almandine), as well as Cr-association (violet pyrope, chrome-diopside, olivine) and Ti-association (orange pyrope, picroilmenite) minerals of peridotite suite.

The high-pressure minerals are dominated by garnets, among which are orange ***pyrope-almandine*** (G5 group, according to the classification scheme of [6]), ***pale violet Cr-pyrope*** (group G9) ***and red-orange Ti-pyrope*** (group G1). Chemically, all the pyropes are of lherzolite suite, with Cr_2O_3 content varying from 1.48 to 6.12 wt. %. Not one G10 (diamond association) pyrope was found in the examined rock samples.

Clinopyroxene corresponds in mineral chemistry to typical ***chrome-diopside*** with high Cr_2O_3 and Na_2O contents, having a higher than average CaO content (47 wt. %) and a very low Al_2O_3 content (0.33 wt. %).A single ***olivine*** grain is a colorless grain fraction with a faint yellowish tint. It represents a high-Mg olivine variety (Fo 94), typical of kimberlite and lamproite rocks.

Table 8.

Chemical composition of kimberlite indicator minerals from Parker Lake area dykes (wt. %)

No	Sample	SiO_2	TiO_2	Al_2O_3	Cr_2O_3	FeO	MnO	MgO	CaO	Na_2O	K_2O	Total
1	06	55.50	0.10	0.36	2.81	2.17	0.08	16.41	20.82	1.75	0.01	100.01
2	03-8	-	51.70	0.58	0.77	33.68	0.27	12.97	3.51	-	-	103.48
3	06-1	-	54.22	0.79	1.14	29.03	0.70	14.66	5.87	-	-	106.41
4	03-7	39.38	0.07	21.91	0.08	23.87	0.40	9.55	5.70	-	-	100.96
5	03-8	39.89	0.09	21.72	0.09	20.46	0.56	11.28	5.66	-	-	99.75
6	03-1	41.17	1.04	18.10	4.89	8.55	0.35	19.80	5.27	-	-	99.17
7	03-2	41.35	0.27	18.71	6.12	7.74	0.40	19.32	5.48	-	-	99.39
8	03-3	41.92	0.09	20.23	3.97	6.43	0.38	20.42	5.32	-	-	98.76
9	03-4	41.96	0.39	21.98	1.48	7.69	0.25	20.50	4.57	-	-	98.82
10	03-5	42.29	0.01	20.13	4.55	6.84	0.99	19.57	5.26	-	-	99.64
11	03-6	42.03	0.66	19.61	2.41	9.48	0.31	19.51	5.16	-	-	99.17
12	06-1	41.83	0.13	20.94	3.41	7.62	0.32	20.00	-	-	-	94.25
13	06-2	42.12	0.09	20.81	3.78	7.21	0.34	20.41	-	-	-	94.76
14	03	41.23	-	-	0.08	6.23	0.17	51.61	0.03	-	-	99.80

Note: 1 - emerald-green chrome diopside; 2,3 – picroilmenite; 4,5 - orange pyrope-almandine; 6,9,11 - red-orange pyrope; 7,8,10,12,13 - pale violet pyrope; 14 - colorless olivine, NiO – 0.45. Electron microprobe analysis (Micro Beam Camera analyser), TsNIGRI Laboratory, analyst M.V. Shavyrina, 1997.

Picroilmenite is represented by an angular grain fraction and a fragment of an oval grain with a leucoxene rim. Chemically, these grains are high-Mg picroilmenites (>12 wt. % MgO) with a moderate Al_2O_3 content and a persistent Cr_2O_3 admixture (0.77-1.14 wt. %), which is typical of kimberlite rocks.

Table 9.

Results of $^{13}C/^{12}C$ isotope analyses of the diamonds from the Thirsty Lake Dyke (Sample 103/10)

o	**1**	**2**	**3**	**4**	**5**	**6**	**7**	**8**	**9**	**10**	**11**	**12**
Crystal No	1	6	7	19	35	36	37	40	42	44	51	60
δ ^{13}C, $^0/_{00}$	-11.8	-5.7	-11.8	-5.0	-5.2	-6.7	-3.3	-12.5	-9.0	-9.3	-16.4	-15.0

Note: GEOkHI RAS, Laboratory of carbon geochemy, analyst K. Mal'tsev, 1997.

Diamond grade of the examined rocks is very high: for instance, we extracted about 120 diamond crystals, 0.08-0.5 mm in size, from a common 3-kg crushed sample of the Thirsty Lake dyke rock. Indirect evidence for the very high diamond grade of the examined rocks is found in the facts that pits repeatedly appeared on the diamond disk after saw-cutting of the rock samples, and that we failed to avoid (and do away with) the emergence of numerous grooves and scratches on the polished surface of a minette rock sample. Most of the diamond crystals are dirty-green and brown, with a minor proportion of green, black, yellow and colorless crystals. Among the diamonds (most of them are full crystals, with only single crystal fragments) are cubes, tetrahexahedroids, combination-type crystals and,

Table 10.

Chemical composition of some minerals from Wawa area rocks (wt. %)

No	SiO_2	TiO_2	Al_2O_3	Cr_2O_3	FeO	MnO	MgO	CaO	Na_2O	K_2O	ZnO	Total
1	37.98	1.53	15.34	0.14	14.93	0.20	15.67	0.04	0.08	10.34	-	96.25
2	37.87	1.46	14.19	0.18	14.15	0.18	15.76	0.03	0.16	10.47	-	94.45
3	38.20	1.53	14.86	0.15	14.36	0.16	15.48	0.24	0.16	9.95	-	95.09
4	69.06	0.09	19.20	0.03	0.19	0.01	0.01	0.17	11.76	0.04	-	100.56
5	48.03	0.45	4.38	0.13	10.53	0.24	16.37	9.83	0.67	2.44	-	93.07
6	56.74	0.02	0.66	0.15	5.94	0.21	19.95	12.82	0.13	0.02	-	96.64
7	-	0.22	12.69	47.88	32.93	1.67	0.42	-	-	-	2.89	98.70
8	38.92	1.06	16.47	1.56	11.38	0.17	16.41	0.03	0.13	10.70	-	96.83
9	41.65	0.97	16.12	0.48	11.46	0.18	17.24	0.00	0.12	10.66	-	98.88
10	40.73	0.57	15.96	0.76	11.57	0.15	17.45	0.00	0.15	10.12	-	97.46
11	41.20	0.79	15.04	0.67	11.51	0.18	18.12	0.07	0.05	10.13	-	97.76
12	37.90	1.15	16.45	0.53	14.43	0.21	13.81	0.19	0.00	9.77	-	94.44
13	38.08	1.26	16.76	0.47	13.82	0.16	14.63	0.43	0.00	7.30	-	92.91
14	39.01	1.38	18.56	0.46	13.49	0.18	14.06	0.64	0.06	4.41	-	92.25
15	52.98	0.14	3.65	0.09	9.27	0.27	20.78	10.94	0.57	0.12	-	98.81
16	1.46	0.09	3.98	50.61	36.47	3.29	0.35	-	-	-	-	96.25

Note: 1-5 – Sandor lamprophyre, sample WS-5-2/1; 6,7 - Sandor lamprophyre (xenolith), sample WAW-1/1x; 8-11 - Cristal pyroclastic breccia, sample WN-2/1-1; 12-16 - #512631, sample WN-4/2-1. 1-4, 9-14 – biotite; 8 – biotite (keliphite?); 5,6,15 – amphibole; 7,16 – chrome spinel.
Electron microprobe analysis (Micro Beam Camera analyser), TsNIGRI Laboratory, analyst M.V. Shavyrina, 1997.

more rarely, flat-faced octahedral, their intergrowths and spinel twins (Fig. 9). In the -0.5+0.25 mm size class, deeply colored cubic and combination-type crystals predominate, whereas -0.25+0.1 mm diamonds show a somewhat higher proportion of pale octahedral.

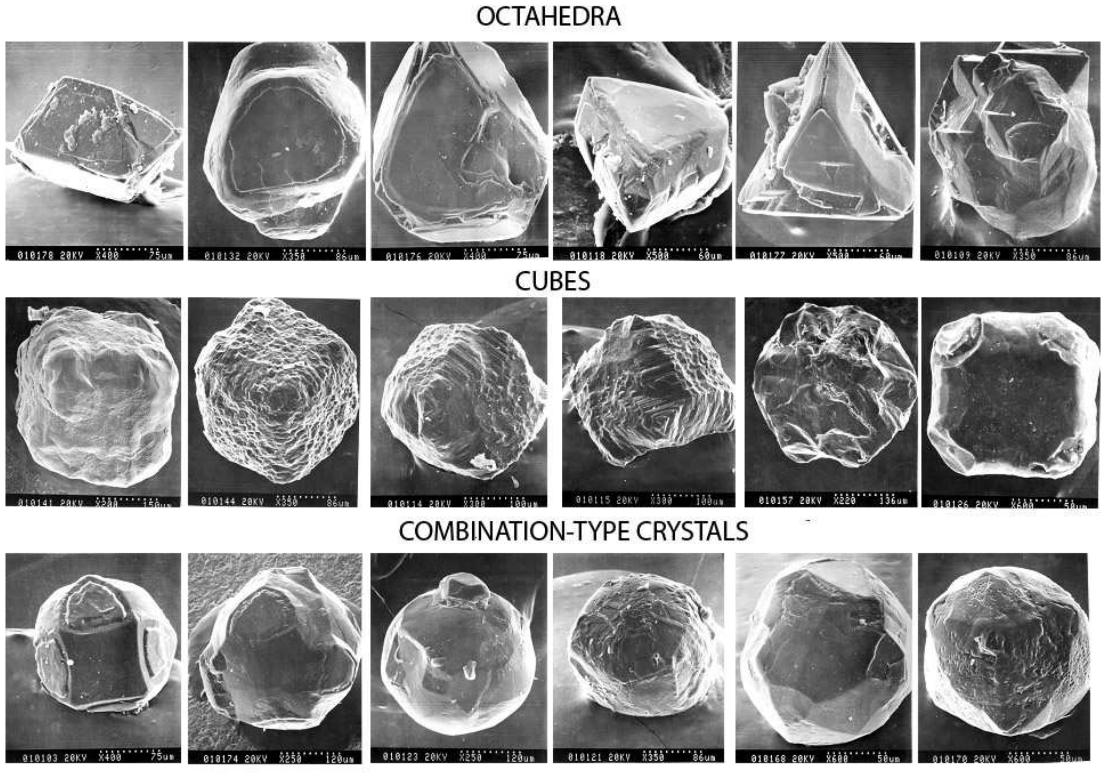

Fig. **9. Diamonds from the Thirsty Lake dyke.**

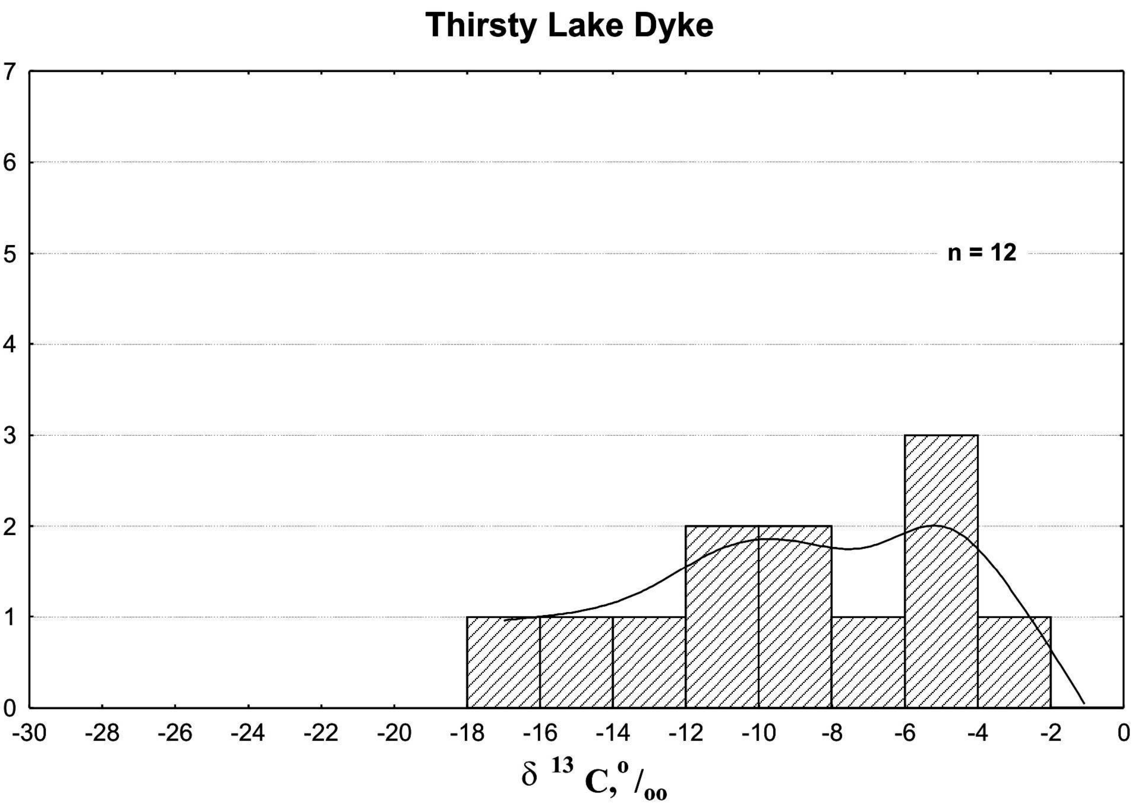

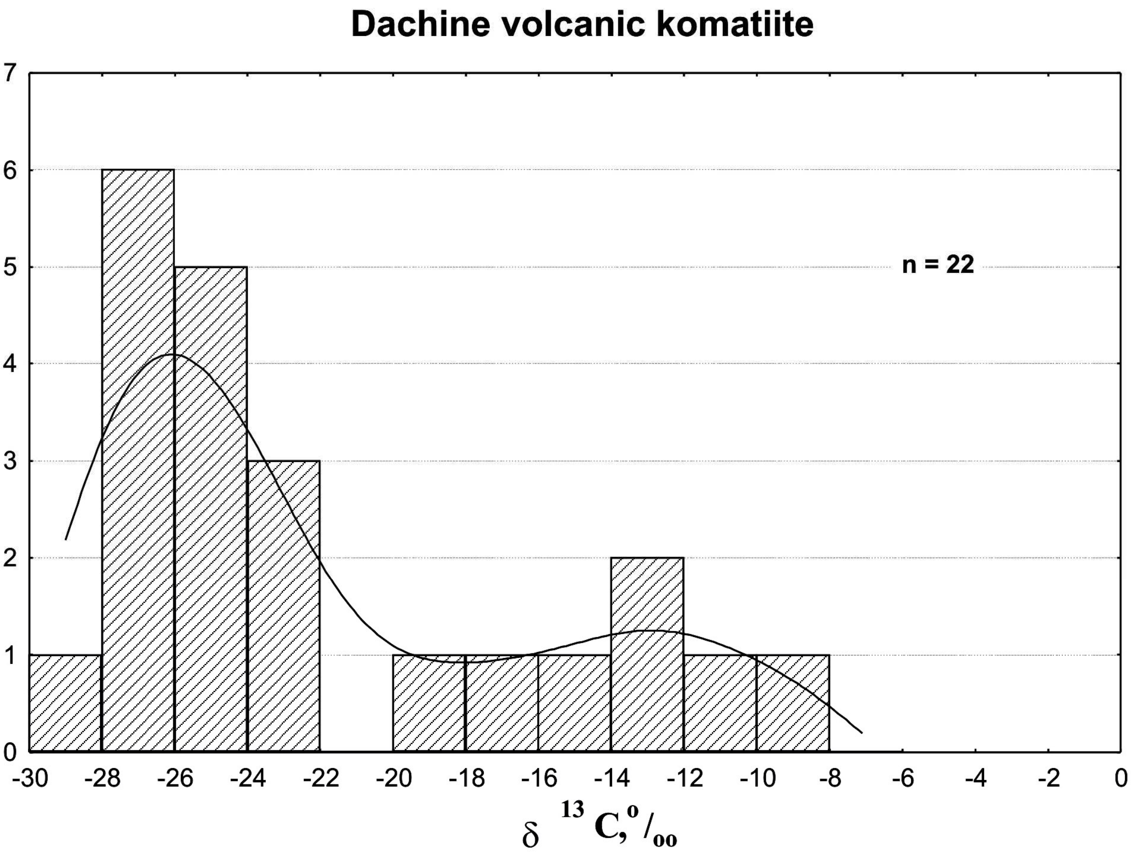

Fig. 10. **Carbon isotope composition of diamonds from the Thirsty Lake dyke (top) and from volcanic komatiites of Dachin deposit [18].**

According to thermochemical dissolution data (samples up to 50 kg) and results of small-volume sampling (sample volume 1.5 tons) performed by Cumberland Resource Ltd, diamond grade of the rocks is as high as 0.3-1 ct/ton, and even up to 7-10 ct/ton in some samples [16,17]. Maximum size of the diamond crystals extracted from the samples is 1.5 mm.

As regards carbon isotope composition of the diamonds, their $\delta^{13}C$ varies rather widely (Tab. 9), from -3.3 % to -16.4%, with two peaks of the distribution curve at -5% (typical mantle carbon) and -10% (Fig. 10, top).

DIAMONDIFEROUS ROCKS OF THE WAWA AREA, NORTHERN ONTARIO, CANADA

As soon as one year after the discovery of diamondiferous minette dykes in the Parker Lake area i.e., in 1995, a diamondiferous dyke which received the name Sandor and, next to it, several tens of non-kimberlitic diamondiferous rock occurrences have been discovered in the southern part of the Canadian shield, in the Ontario province. As of now, much of the Wawa area is a subject of licensed activity of major companies, such as DeBiers and Kennecott Co., being persistently involved in exploration programs including large-volume sampling (hundreds of tons).

The Wawa area is situated in the southern part of the Canadian shield, within the Superior ancient craton (Fig. 1). More than 30 diamondiferous, inferredly dyke-like rock occurrences are known as of now within this area [12-14,24]. We have examined six of them: Sandor, Crystal volcanic breccia, Crystal pyroclastic breccia, Moet volcanic breccia, # 51263 and # 68880 [12,13].

These rock occurrences appear to be dyke-like bodies, the outlines and host rock contacts of which are in places unclear; anyway, this is true for the Sandor rock occurrence, which we had inspected during the 1998 field season.

Rocks of all six bodies have a breccia-type clastic lava texture (up to agglomerate breccia) due to the presence of diversified rock xenoliths (in amount varying from single inclusions to 40-60% of the rock volume) in a greenish-dark-grey, metamorphosed, diversely foliated, microcrystalline matrix with a lava appearance.

Xenoliths vary in size from several millimeters to 0.5 m. There occur both oval (“ovalized”) xenoliths (prevailing in the Sandor dyke) and flattened xenogenic clasts with fusiform outlines elongated along the foliation (most common in the remaining five dykes).

Xenogenic material consists predominantly of diversified metamorphosed epidote-plagioclase-biotite-amphibole rocks, microquartzite, diabase, microdolerite and, more rarely, altered volcanic glass having a spherulitic texture with rare plagioclase phenocrysts, i.e., of xenoliths with well preserved volcanic rock textures. It is only in the Sandor dyke where most of the xenoliths consist of amphibolized peridotite transformed into a macro-to-megacrystalline actinolite aggregate, having a radical or crystalline-diverse structure, without any relicts of initial rock texture.

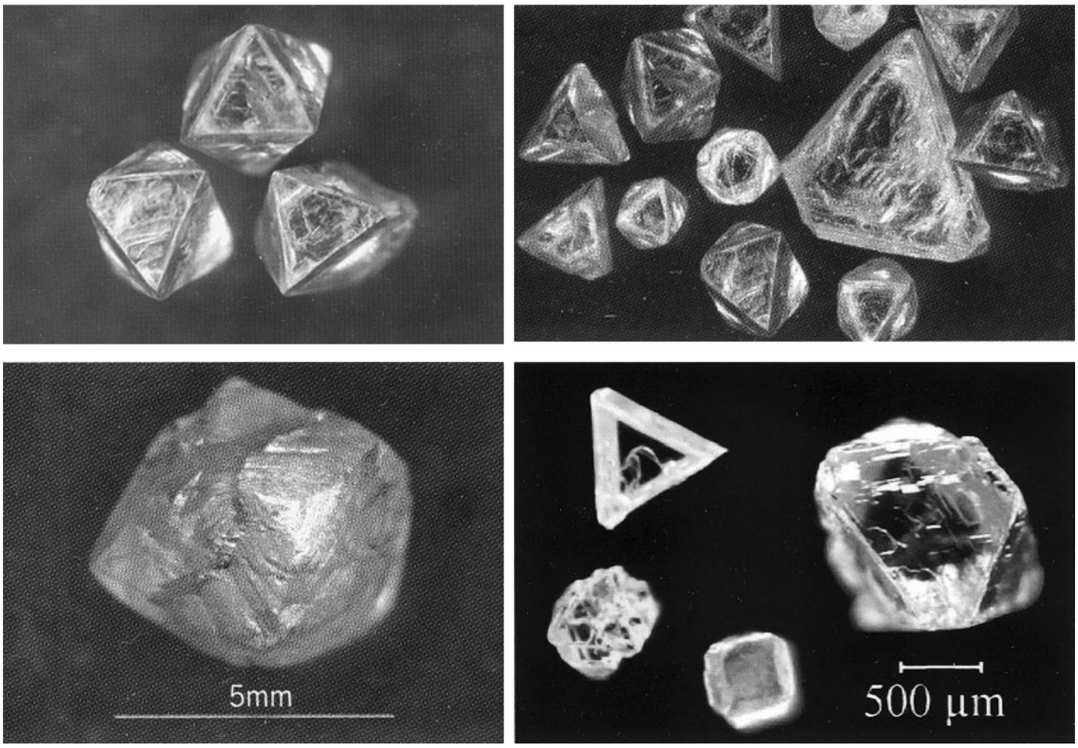

Fig**. 11. Diamonds from the Wawa area Archean lamprophyres [23, 24].**

In all the examined dyke rocks, the cementing matrix has a quite constant mineral composition, consisting predominantly of altered (to a variable extenet), tobacco-colored, clearly pleochroic biotite (35-45% of the rock volume) and light green, weakly pleochroic amphibole (actinolite) (35-45%), occasionally with minor proportions of feldspar (albite) and carbonate. The rock matrix usually has a porphyroblastic texture, with relatively large (0.3-1 mm) biotite segregations and idiomorphic amphibole grains (present in varying proportions) developed in a fine-grained crystalline granolepidoblastic mass with the same mineral composition. Some samples contain a sizable amount of feldspar (up to 5-10% of the rock volume) playing different structural roles in different dykes: in the Sandor dyke, feldspar (albite) segregations, being the least idiomorphic, cement all the remaining rock-forming minerals, whereas in dyke # 68 880 and Moet volcanic breccia feldspar forms rare, small segregations appearing like porphyroblasts or leucocratic rock microxenoliths. Carbonate (up to 10% of the rock) is only present in Sandor dyke rocks, where it forms irregularly shaped segregations cementing the remaining rock-forming minerals, and, more rarely, occurs as elongate irregular segregations subconcordant to rock foliation. The set of accessory minerals present in the dyke rocks includes titanite, epidote and, rarely, apatite. Biotite is characterized by a high Al_2O_3 content and moderate TiO_2 and FeO contents, owing to which it is very similar in composition to biotite from Akluilak minette rocks, differing from them just by having a higher Cr_2O_3 content (Tab. 10, Fig. 2).

In general, the examined rocks are somewhat similar in bulk mineral composition (amphibole + biotite +/- feldspar) to calc-alkali lamprophyres like spessartite or kersantite, therewith differing from them both in structure and in mineral chemistry. The dyke rock norm is characterized by the presence of orthoclase, plagioclase, diopside, olivine and (except in the Sandor dyke) hypersthene, which roughly corresponds to trachybasalt.

The present-day geochemical characteristics of the examined dyke rocks, while probably somewhat differing from the original ones owing to metamorphic transformation of the rocks, are yet deemed to reflect the initial rock geochemistry. By basicity, the examined rocks are clearly intermediate between the mafic and ultramafic rocks. In the TAS classification diagram (Fig. 3), Sandor dyke rocks correspond to basanite, while rocks of the remaining five dykes correspond to picrobasalts and basalts. By the Al-(Fe+Ti)-Mg relationship, rocks of all six dykes are similar to komatiite basalt (Fig. 5), and in the AFM diagram the Sandor dyke rocks correspond in composition to rocks of the calc-alkali series, whereas rocks of the remaining dykes fall into the field of tholeite series rocks.

The distribution of incompatible elements (generally present in the examined rocks in very low abundance) is rather interesting (Fig. 7). By the Th-Hf-Ta relationship, rocks of all six dykes correspond to calc-alkali volcanic arc basalts. Alternatively, REE distribution is different in rocks of different dykes. In particular, the Sandor dyke rocks are characterized by a 2-3 times higher REE content as compared to rocks of the remaining five dykes, and the Sandor dyke REE distribution curve shows no Eu minimum, which is present (while unequally pronounced) in REE distribution plots for the remaining dykes (Fig. 6,7).

Incompatible minor elements content, rocks of the examined dykes are generally similar to ultramafic rocks and, in particular, to kimberlites, which highlights their deep-seated origin. In particular, their Co content ranges up to 60-100 ppm, Ni content up to 600-1500 ppm, and Cr content up to 600, 1000 and even 3400 ppm!

In addition, there is another evidence of deep-seated origin for the studied dyke rocks. For instance, rocks of the Sandor dyke abound with ovalized inclusions, up to 0.5 m in size, made up of a megacrystalline actinolite aggregate. Geochemically (particularly in their very high Ni, Co and Cr content), rocks of these inclusions are very close to mantle peridotite modules from kimberlite pipes, which suggests they play a similar part in the Sandor dyke, unrecognizable as they are due to severe alteration (transformation). In rocks of the remaining five dykes, inclusions of this sort are rare and small (just a single inclusion, 2 mm in size, was encountered in the Moet volcanic breccia sample).

Along with this, a 2-mm segregation of ***Cr-phlogopite*** (1.56 wt. % Cr_2O_3) with a brownish-yellow color and a characteristic radial-fibreous structure was found in a sample of Crystal pyroclastic breccia (Tab. 10). This inclusion may be a completely kelyphitized pyrope grain. In addition, a 3-mm zoned inclusion, with intensely altered but quite pure ***chromite*** (50.61 wt. % Cr_2O_3) in its core and a fine-grained crystalline amphibole (tremolite) aggregate in its marginal zone, was found in dyke # 51263 (Tab. 10). According to data reported by Canadian geologists, several tens of picroilmenite, chrome spinel and pyrope grains (including G10 pyropes) were identified in large-volume samples [23,24].

The rock of the Sandor dyke differs significantly from rocks of the remaining five examined dykes, both in structure and in composition. In addition, it differs from them in absolute age, as is evident from the following results of our Rb-Sr dating:

Dyke ***Sandor***: 2802+/-59 Ma (two samples with different biotite content);

Dyke ***Crystal pyroclastic breccia***: 2023+/-11 Ma (rock + selected biotite grains);

Dyke ***# 51263***: 1548+/-44 Ma (two samples with different biotite content).

This difference in formation age obtained for different dykes appears to be due to inequal intensity of post-metamorphic alteration (biotite chloritization, etc.) of the material subjected to isotope dating; along with this, it is not inconceivable that the Sandor dyke and the remaining dykes intruded not quite synchronously.

This point, as well as some other issues related to structure and composition of the unique rocks being studied, invites further detailed investigation.

According to the results of sampling (including the large-volume one) [23,24], diamond grade of Wawa area rocks varies from 0.2 to 1 ct/ton (occasionally, up to 2.6 ct/ton). The diamonds are dominated by colored microcrystals (octahedra, cubes and combination-type crystals); diamond macrocrystals are mostly colorless. Most of the diamonds are commercial, but gem stones also do occur (Fig. 11). The as-yet largest (0.72 ct; larger than 5 mm) gem diamond from the Wawa area received the name “The Big Goose” (“wawa” is the American Indian for “goose”).

In 2003, a report on new diamondiferous lamprophyre occurrences (similar in composition to Wawa lamprophyres) discovered in the Yellowknife area within the Slave craton in the north of Canada appeared [1]. Thus, essentially non-kimberlitic diamondiferous rocks are now known within all Archean cratons of the Canadian shield.

DIAMONDIFEROUS ROCKS OF THE DACHIN DEPOSIT, FRENCH. GUYANA

Another zone of occurrence of essentially non-kimberlitic highly diamondiferous rocks is situated in South America, within the Guiana shield (French Guyana). The Dachin deposit is a large massif, 5 km long and 0.35-1.1 km wide [4]. Estimated ore reserves of this deposit are as large as 2-3 billion tons. We examined just the petrological and geochemical characteristics for a set of rock samples. According to data reported by French researchers [4], rocks of this deposit represent different varieties of old, metamorphosed volcanoclastic

---

komatiite transformed into talc schists with relicts of porphyritic and clastic textures. These rocks are characterized by high Mg, Cr and Ni contents and very low concentrations of incompatible elements, which is typical of komatiine family rocks. The rocks contain high-pressure minerals represented exclusively by eclogite garnets and pyrope (including G10 pyropes).

Most of the diamonds occurring in the Dachin rocks are octahedral, cubes and combination-type crystals, predominantly brown, yellow and grey, rarely colorless, smaller than 1 mm [4]. The largest as-yet-found diamond is 4.6 mm across. Almost 100% of the diamonds are of commercial quality. Diamond grade of is up to 4.2 ct/m^3 in the alluvium overlying the bedrocks and up to 1 ct/ton in the bedrocks.

Most of the diamonds from the Dachin deposit are “isotopically light” (their $\delta^{13}C$ varies from -8.1% to -28.9%), obviously being of eclogitic suite [18]. It is interesting that among the Dachin diamonds, much like among the diamonds from the Akluilak minette rocks, are representatives of two groups with differing carbon isotope composition characteristics (Fig. 10). One of these groups (with $\delta^{13}C$ varying from -8% to -20%) is common to the two deposits, whereas the second groups are very dissimilar: in Dachin komatiites, the second group includes the “isotopically lightest” diamonds (with $\delta^{13}C$ varying from -22% to -30%), and in the Akluilak minette the second group of diamonds is characterized by typical mantle $\delta^{13}C$ values (from -3% to -8%).

CONCLUSIONS

The examined rocks have some distinctive features in common, which must be kept in mind when organizing exploration programs in previously unexplored areas.

The new, peculiar diamondiferous rock type was found to occur in very different structural settings within Precambrian ancient platforms, namely, in Archean cratons (Parker Lake, Yellowknife) and in Archean and Early Proterozoic greenstone belts (Wawa, Dachin). The age of these rocks is also old, varying from the Archean (Wawa, Sandor dyke) to the Early Proterozoic (Parker Lake, Wawa, Dachin).

The rocks have a breccia-type texture, which points to their igneous (magmatic) origin and indicates that the formation of these igneous rock bodies was accompanied by intense shattering, melting and, probably, explosive activity. This is evidence of fast magma ascent to the surface, which protected diamond from oxidation and graphitization.

The rocks are intensely metamorphosed. They are similar in composition to minette with some characteristics typical of lamproite (Parker Lake), to calc-alkali lamprophyres with some characteristics of komatiite (Wawa and Yellowknife) and pure komatiite (Dachin). In the A-FT-M diagram, these rocks form a row extending from the kimberlite field to the basalt field. The rocks are characterized by lower than average concentrations of most of the incompatible elements (with the most pronounced Ta, Nb and Ti negative anomalies). Only the Akluilak ultrapotassic minette shows very high K, P, Zr and REE contents.

All the examined peculiar igneous rocks contain high-pressure kimberlite indicator minerals, primarily garnet (pyrope, including G1 group Ti-pyropes, G10 pyropes and eclogitic pyrope-almandines), with minor olivine, chrome-diopside, picroilmenite and chromite. Another evidence of mantle origin for these rocks is found either in their ultra-potassic composition (Parker Lake) or in high concentrations of typical "ultramafic" elements (Mg, Ni, Cr, Co), as well as in their carbon isotope composition $\delta^{13}C$.

The diamonds occurring in these rocks are dominated by small (0.1-0.5 mm) crystals, although crystals of up to 5 mm in size also do occur. Most of the diamonds are octahedral, cubic, cuboctahedral and tetrahexahedral crystals with various brown, green and yellow color shades; colorless crystals are minor. Diamond grade of the examined rocks is generally very high, varying from 0.3 to 1 ct/ton (in some samples, up to 7-10 ct/ton). By quality, most of the diamonds are commercial, but gem stones up to 0.72 ct also do occur.

The large size of the igneous rock bodies and their high diamond grade give ground to assess the diamond reserves (resources) of such deposits as very sizable. Findings of gem diamonds in known rock occurrences allow one to expect the discovery of new deposits with a diamond grainsize distribution somewhat more favorable from the standpoint of development feasibility.

It is quite probable that rocks of this sort are widespread worldwide, just having as yet attracted no attention owing to their "atypical" appearance and composition. In Russia, these peculiar diamondiferous rocks may occur within the boundaries of ancient shields (Baltic, Ukrainian, Aldanian and Anabar) and, probably, in median masses like Kolyma or Khankai. This appears to promise a significant increase in diamond potential of Russia.

REFERENCES

1. **Armstrong J., Barnett R.** (2003) The association of Zn-chromite with diamondiferous lamprophyres and diamonds: unique compositions as a guide to the diamond potential of non-traditional diamond host rocks. Long Abstract of 8th IKC, Victoria, Canada. FLA_0230
2. **Bogatikov O.A., Ryabchikov I.D. et al**. (1991). Lamproites. Moscow, Nauka.301 p. (in Russian)
3. **Boynton W.V**. (1984) Geochemistry of the rare earth elements: meteorite studies. In: Henderson P. (ed.)< Rare earth element geochemistry. Elsevier, pp. 63-114.
4. **Capdevila R., Arndt N., Letendre J., Sauvage J.F.** (1999) Diamonds in volcaniclastic komatiite from French Guiana.Nature. vol.399.No 3,June.P.456-458
5. **Chinn, I. and Kyser**, *K* (2000) Microdiamonds from the Thirsty Lake (Akluilak) dyke, Northwest Territories Canada. Journal Conf. Abstr, Goldschmidt, Oxford, 3-8 September, v. 5 (2), p. 307.
6. **Dawson J.B. and Stephens W.E**. [1975] Statistical analysis of garnets from kimberlites and associated xenoliths. Journal of Geology, v. 83, p. 589-607.

---

7. **Jagoutz, E., Palme, H., Baddenhausen, H. et al**. (1979) The abundances of trace elements in the earth's mantle as derived from primitive ultramafic nodules. Proc. X Lunar Planet. Sci. Conf., p. 2031-2050.

8. **Jensen L.S. and Picke D.R.** 1982. Komatiites in the Ontario portion of the Abitibi belt. In: Komatiites. George Allen and Unwin, London, p 117-157.

9. **Kaminsky F.V.** (1984) Diamondiferous igneous rocks of the non-kimberlitic type. M., Nedra, 173 p. (in Russian)

10. *Kaminsky, F.V., Sablukov, S.M., Sablukova, L.I., Shpanov, V.E. and Zhuravlev, D.Z.* (1998) Diamondiferous Minette Dykes from the Parker Lake Area, N.W.T., Canada. Seventh International Kimberlite Conference, Cape Town, April 1998, Extended Abstracts, p. 392-394.

11. **Kaminsky F.V., Sablukov S.M., Sablukova L.I. and Shpanov, V.** (2000) Diamondiferous minette: a new type of diamondiferous rocks. Izvestiya Earth Sciences Section, Rus. Academy of Natural Sciences, No. 4. Special Issue presented to the 31st Session of the Internat. Geol. Congress, Braz.,2000,p. 85-94.

12. **Kaminsky F.V. , Sablukov S.M.** Nontraditional diamond deposits (2002) // Science in Russia, No1, p. 4-12.

13. **Kaminsky, F.V., Sablukov, S.M., Sablukova, L.I.** (2003) Diamondiferous Archaean lamprophyres with komatiitic affinities from the Wawa area, Ontario, Canada.Abstract of 8thInternational Kimberlite Conference,Victoria,Canada,. 123.

14. **Lefebvre, N., Kopilova, M., Kivi, K., Barnett, R**. (2003) Diamondiferous volcaniclastic debris flows of Wawa, Ontario, Canada. Long Abstract of 8th IKC, Victoria, Canada. FLA_0298

15. **Le Maitre R.W., Bateman P., Dudek A. et al.** (1989). A classification of igneous rocks and glossary of terms. Blackwell, Oxford.

16. **MacRae, N.D., Armitage, A.E. and Miller, A.R.** (1994) Diamond-bearing potential of alkaline dykes in the Gibson Lake area, District of Keevatin, N.W.T. GAC-MAC Annual Meeting, Abstracts, p. A69.

17. **MacRae, N.D., Armitage, A.E., Miller, A.R., Roddick, J.C., Jones, A.L. and Mudry, M.P**. (1996) The diamondiferous Akluilak lamprophyre dyke, Gibson Lake area, N.W.T. In: A.N. LeChaminant, D.G. Richardson, R.N.W. DiLabio and K.A. Richardson (Editors), Searching for diamonds in Canada. Geological Survey of Canada Open File 3228, p. 101-108.

18. **McCandless T.E., Letendre J., Eastoe C.J.** (1999) Morphology and carbon isotope composition of microdiamonds from Dachine, French Guiana. Proceeding of 7th IKC, Cape Town, South Africa. P. 550-556.

19. **McDonough W.F., Sun S.** (1995) The composition of the Earth, Chemical Geology, v.120, pp. 223-253.

20. Mitchell, R.H. **(1995). Compositional variation of micas in kimberlites, orangeites, lamproites and lamprophires. Extended Abstracts 6 IKC, Novosibirsk, Russia, pp.390-392.**

21. **Peterson T.D., Esperanca. S., LeCleminant A.N.** (1994) Gejchemistry and origin of the Proterozoic ultrapotassic rocks of the Churchill Province, Canada. Mineralogy and Petrology, 51: 251-276.

22. **Rickwood P.C.** (1989) Boundari lines within petrologic diagrams which use oxides of major and minor elements. Lithos, 22. 247-263.

23. **Shiller E**. (2003) Wawa diamonds. Resource world magazine. Issue 6. P .21-24.

24. **Stott, G.M., Ayer, J.A., Wilson, A.C. and Grabowski, G.P.B**. (2002) Are the Neoarchean diamond-bearing breccias in the Wawa area related to late-orogenic alkalic and 'sanuktoid' intrusions? Summary of field work and other activities 2002, Ontario Geological Survey Open-File Report 6100, p. 9-1 to 9-10.

UDK 551.22 +552.11

USING OF THE MONOMINERAL THERMOBROMETRY FOR THE RECONSTRUCTION OF THE MANTLE SECTIONS.

Ashchepkov I.V.[1], Vladykin N.V.[2], Pokhilenko N.P.[1], Rotman A.Y.[3],
Afanasiev V.P.[1], Logvinova A.M.[1]

[1] *United Institute of Geology Geophysics and Mineralogy SD RAS, Novosibirsk*
[2] *Institute of Geochemistry SD RAS, Irkutsk*
[3] *Central Science and Research Geology And Prospecting Institute Of The Stock Company "ALROSA" Mirny*

Four original new monomineral methods used for mantle peridotite associations are compared with the traditional polymineral mantle thermobarometry. Original clinopyroxene barometric Jd-Di method gives the most coincidence with the Opx thermobarometry that practically reproduce and sometimes is giving most regular and smooth geotherms in accord with the all petrological methods. Slightly lower determined temperatures are explained by the more fast Ca-Mg-Fe exchange. Four variants of the garnet thermometers are calibrated using the correlations with estimates of Opx (Brey, Kohler, 1990), Cpx (Nimis, Taylor, 2000) and Gar-Cpx (Krogh, 1988) thermometers and last one the Ni-inGarnet thermometer/ the two variants of the barometers were made separately for pyroxenites and impregnated peridotites and garnet peridotites of complex nature. Cr- Sp thermobarometer uses the monomineral version of the Ol-Sp (Taylor et al, 1998) thermometer and new barometer were the Cr-dependence from pressure for Cr-Sp peridotites was calibrated. Pycroilmenite thermobarometer contain Ol-Sp (Taylor et al ., 1998) thermometer in monomineral version and the barometer where the dependence of geikelite minal from pressure is used. The methods are intercorrelated and give good coincidence in the TP diagram Using together all the combination of the methods allow to receive quite realistic TP sequences with the possibility of the reconstruction of the separate horizons of mantle peridotites with the different modal compositions, metasomatic associations and the vein systems where the megcrystallline associations were formed.

INTRODUCTION

Monomineral thermobarometry give possibility for the reconstructions of mantle structure and heating degree using the kimberlite mega- and xenocrystalls [20,21,31,36,38]. It allows to produce a good TP diagrams and mantle layering [22] for the pipes where polymineral mantle xenoliths are not good preserved. Even the concentrate from the diamond and other placers usually containing only garnets, ilmenites and chromites now may give the good possibility for the estimations the geotherm positions [32] and detail structure and rock sequences in the lithospheric mantle. The new version of the garnet thermobarometry [1,2] give not bad correlations with the traditional methods of the TP estimates, based on the polymineral associations [16,28, 31, 35,48 etc]. They nearly reproduce the pressures obtained with Al-Opx and Gar-OPx barometers [16,28,31]

Developing new methods our item was to construct the series of the methods that produce the estimates that are correlating each other. For this purposes we used the data base containing EPMA analyses from more then 2500 associations of polymineral xenoliths for the published literature and the great amount (> 20000) of the original analyses of xenocrysts form Siberian kimberlites. The

---

FORTRAIN program compiled by the first author of the paper contain more then 50 thermometers and 40 barometers including the original methods allow to calculate simultaneously several pairs of thermometers and barometers including those under the developing and to write the pairs of the TP estimates solved together in the matrix giving the possibility simply to find the correlations of the method and produce numbers of variants TP – FO2 and the covariations with the compositions of the minerals and rocks conditions. It allow also in several seconds receive the TP diagram for the several kimberlite pipes.

NEW METHODS

In addition to the orthopyroxene method [16]-[30] that often give very good estimates correlating with the other pairs for the T and P calculations [16, 25,30,31,48] we developed new Jd –clinopyroxene [6,7], Cr-garnet [1,2], Cr-spinel [5,13] and pycroilmenite [13] methods that give quite similar estimates to the orthopyroxene method. The older version of the garnet thermobarometer [39] usually is not correlating good with the pyroxene – based methods [7,16,30,31,32].

Clinopyroxene The methods described in the previous papers sue the correlation of the Jd content in clinopyroxene wit the pressure estimated with the Al – Opx barometer [30].

$P_o = 0.04*Kd*T^oC/(1-2.4*Fe)-5.5$ where $KD = Na/Ca*Mg/(Al+Cr)$

In previous versions [6,7] the second order of the polynomial bring to the pressure restriction at 65 kbar where the parabola have the maximum. The 3rd order polynomial continuously rises at the all realistic values of the upper mantle pressure $P = 0.00006*P_o^3 - 0.0156*P_o^2 + 1.6757*P_o$ $(R2 = 0.8245)$. The calculated temperatures e are lower at about 100-150°C that those obtained with the two pyroxene methods [16] and are corrected as following

$T^oC = -0.000001*T_o{}^oC**2+0.9575*T_o{}^oC+107.01$

Garnet Four new garnets thermometers are developed – three of them use the correlations of KD = with the estimates based on:

1) OPx’s [16], methods,

$T^oC = 5272.5*(Ln(KD)/P)^3+10265*(Ln(KD)/P)^2+6472*Ln(KD)/P+2113$ where $KD = MgO*TiO_2/((CaO+MgO)^2*FeO*Al_2O_3$

2) CPx [32] , : $T_0{}^oC = 362.05*(Ln(KD)/P)^3+1880.4*(Ln(KD))/P^2+2659.6*Ln(KD)/P+1695.5$ where $KD = Na_2O*MnO*TiO_2/(CaO+MgO)*FeO*Al_2O_{3,}$

3) Gar-Cpx [28] $KD = Na_2O*MnO*TiO_2/(CaO+MgO)*FeO*Al_2O_{3,}$

4) and the last one reproduces the Ni in garnet thermometry [23] with the approximation of Ni content by the other components $Ni(ppm) = 88,877*E^{(-5.021*Ni')}$, $(R^2=0.69)$ где $Ni" = MnO*ln(FeO)/ln(MgO)*1.1-0.193*TiO_2+0.003*ln(Na_2O)-0.003*Cr_2O_3+0.0035*CaO+0.004*Al_2O_3+0.00009*SiO_2$ {4} and further $T^oC = 0.0004*Ni^3-0.0304*Ni^2+7.6318*Ni+597.2$ (R2 = 0.69)

Chromite Dependence of the Cr/(Cr+Al) in spinel [36] from the pressure determined using Al-En barometry [30] was calibrated using >300 associations (R=0.8). $P=0.86347*(Cr/(Cr+Al)*T^oC/14+Ti*0.1$) the second approximation

$P=0.0004*P_o^3-0.0342*P_o^2+1.5323*P_o$ brings to the lineal correlations between the pressures determined using Chr and OPx . The temperatures are determined using monomineral version of the Ol-Sp thermometer [35] where the ***Fo*** is calculated with empirical equations $Fo=0.06+0.0005*P$ for P >30 kbar and $Fo=0.095+0.0001*P_o$ for the lower pressures. The oxygen fugacity calculated fO_2 with Sp-Ol oxybarometer [48] give the lineal correlation with monomineral version made in the same manner (R-0,96).

Ilmenite Dependence of the geikilite minal from the pressure was calibrated using correlation of the peridotite layering and the levels of the magmatic sources crystallizing ilmenite megacrysts for the 30 kimberlite pipes of the Siberian platform. Africa and America $P= (TiO_2-23.)*2.15-(T^oC-700)/20*MgO*Cr_2O_3-1.5*MnO)*T^oC/1273$ and further $P=10*(60-P_o)/60+P_o$. For the ilmenite temperatures are calculating using the monomineral version of the Ol-Il thermometer [48] with the similar scheme of the estimation of the Fo content in olivine in analogy with the chromite as following $Fo=0.11+0.00025*P$ for pressures lower then 30 kbar and $Fo=0.10+0.00025*P$ for greater pressures. The monomineral oxybarometer with the same change of the Fo content give the lineal correlations of fO_2 determined using bi- mineral Ol- Il version.

CORRELATIONS WITH THE ORTHOPYROXENE. THERMOBAROMETRY AND POLYMINERAL. THERMOBAROMETRIC METHODS

Clinopyroxene The temperatures used in the thermometer [32] are in most cases lower in 100-150°C the those determined by the Opx and two pyroxene method [16]. So we use in the computer variant additional polynomial approximation as following $T^oC =0.0006* T_o^2-0.4602*T_o+815.37$.

Clinopyroxene method for pressure calculating in most cases practically reproduces the values obtained with Opx barometry [30] for example for the mantle column of Udachnaya [15], South Africa pipes [33] Jericho [26,27] and other kimberlite pipes and only for metasomatic peridotites with highly alkaline pyroxene compositions it produces the overestimation of the pressure. This bring to ‘colder’ geotherm positions then the conductive geotherm 35mb/m2 [38]. To avoid these necessary to select the alkaline compositions and calculate them in a separate scheme. The other reason of the plotting of Cpx’s PT points in the cold

---

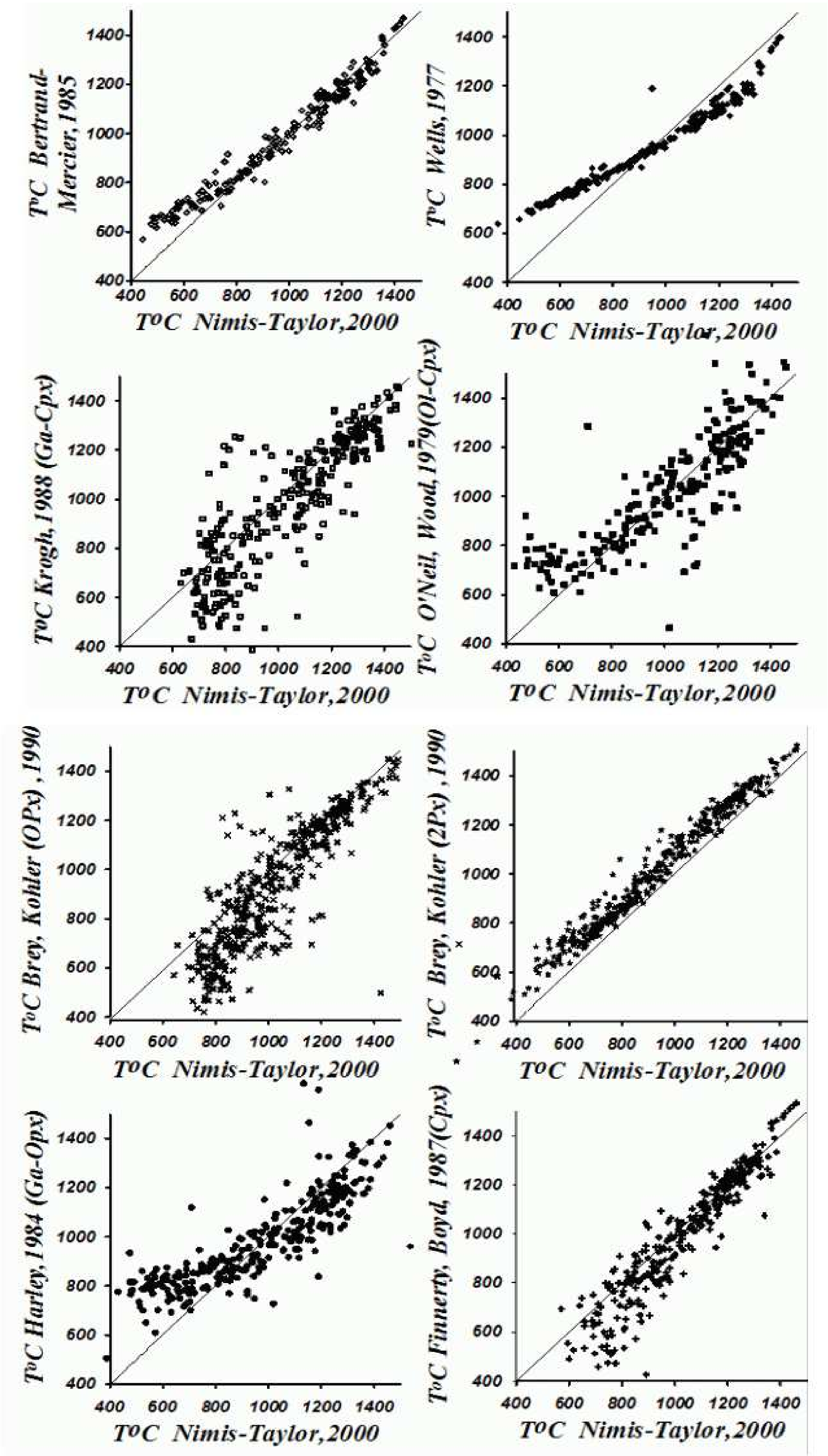

Fig.1. **Correlation diagrams for the temperatures determined with the Nimis- Taylor ,2000 [31] monomineral clinopyroxene thermometer and other thermometers used for the mantle peridotite associations.**

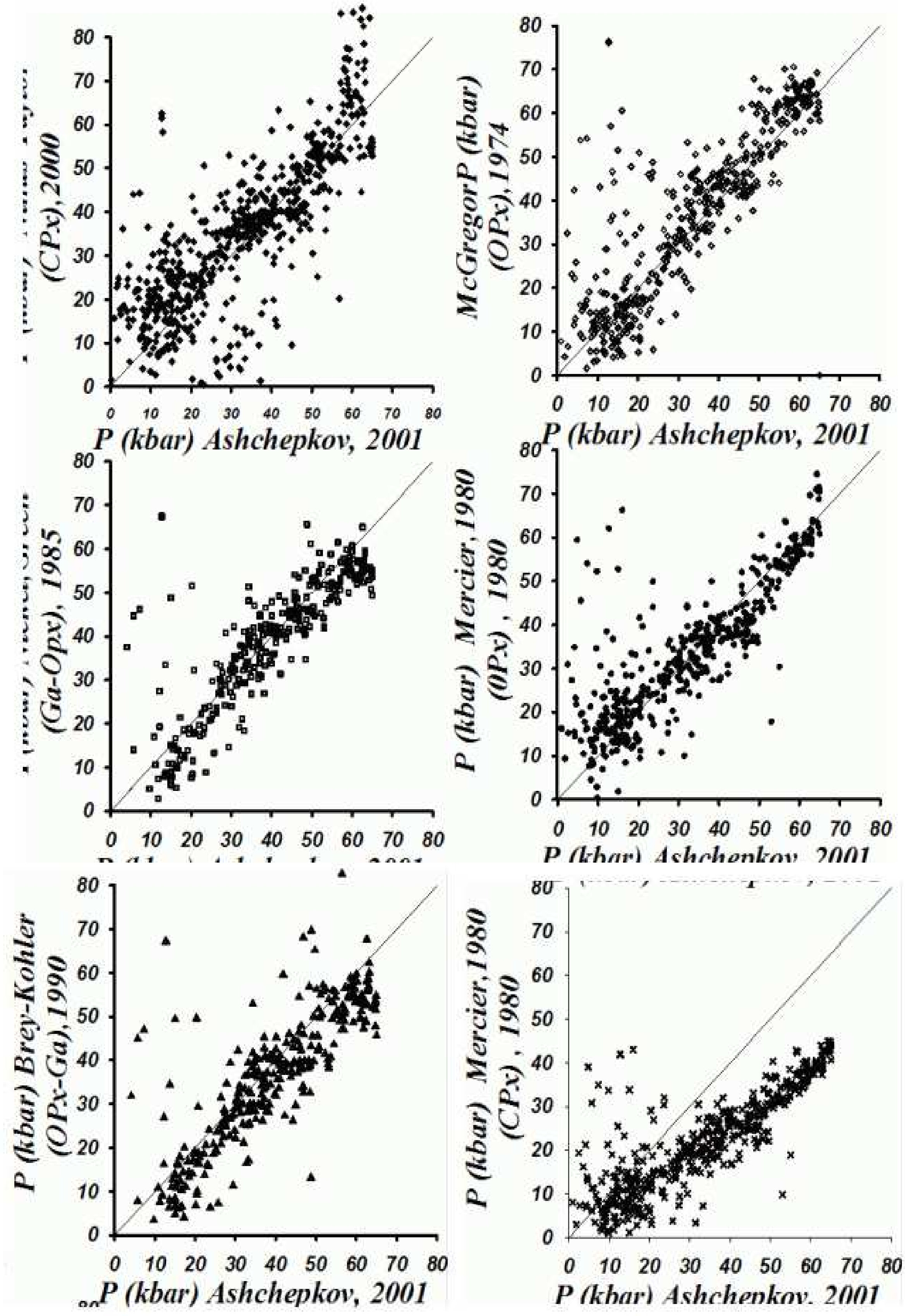

Fig.2. **Correlation diagrams for the pressure values determined with Ashchepkov 2002 Cpx [6] barometer and some other barometers used for the mantle peridotite associations.**

field is underestimations of the temperatures for the Jd rich compositions of clinopyroxenes where the Gar-Cpx thermometric methods [28] give more realistic estimates then those based on the Ca-Mg exchange [16].

Garnet The main difficulty of the themobarometric garnet methods is the high dependence of the thermometers from pressures and opposite the estimated pressures from temperatures. This brings to the dispersions of the correlation diagrams in computer variant with the high iterations number.

For the different mantle columns the variants for the temperature estimates which gives the better coincidence with the two pyroxene or other good bi- mineral methods differ, For example the Gar Opx [16] temperature approximation (1) give good coincidence with the OPx thermobarometric estimates for the Udachnaya pipe mantle column. In highly metasomatized mantle beneath Alakite field [11] the application of the approximation (2) of the clinopyroxene method [32] is more favorable. Using method based on the Ni temperatures [23] is general give good coincidence for the mantle column of Osennyaya pipe and so on. It seems to be that sometimes the equilibriums in the mantle associations are partial – garnet may be in equilibrium with CPx or OPx or both together and in the melting events usually dependent from the fluid flows related to the subduction or plum events.

The partition of the Ni may be dependent from the activity of the sulfur that may change in the multistage processes of the mantle melting.

Cr-Spinel The main problem of the Cr- spinel thermometry is not good coincidence of the temperatures produced by Ol-Sp (Opx) barometry with those obtained with the two- pyroxene and other thermometric methods for mantle peridotites. This may be explained by several reasons – 1) the diffence of the system of the calibration from the natural associations 2) disequilibrium of the Cr-spinel- Ga exchange of Fe-Mg and Cr-Al) from the Ca-Mg exchange working for the pyroxenes what may be most realistic because they may proceed with different rates and even related with the different processes.

The pressure correlations for the Cr-Sp barometer [5] represented at the fig are quite good for the Opx – and Gar-Opx methods and

Relatively low amount of the published ilmenite associations do not allow to produce a representative correlation plot. Using monomineral methods together we produce the correlation diagrams for the ilmenite thermometer and barometer [13] showing that in general ilmenite pressure calculations give the coincidence with the Garnet and Opx thermobarometry and a better with the Clinopyroxene TP estimates. But the thermometry is not good enough yet/ Nevertheless for the series of the similar type ilmenite like megacryst the relative diffence of the temperatures are quite good. In should be noted that literature data used contain not a good analyses of ilmenites. IIn addition the Fe content of the coexisting olivine essentially influence on the all the calculated parameters and it is better to find the Fo content using KD and Fe/(Fe+Mg) of the ilmenite. Nevertheless received general plot fro the ilmenite associations published in literature show not a bad coincidence with the PT plots received using other monomineral methods.

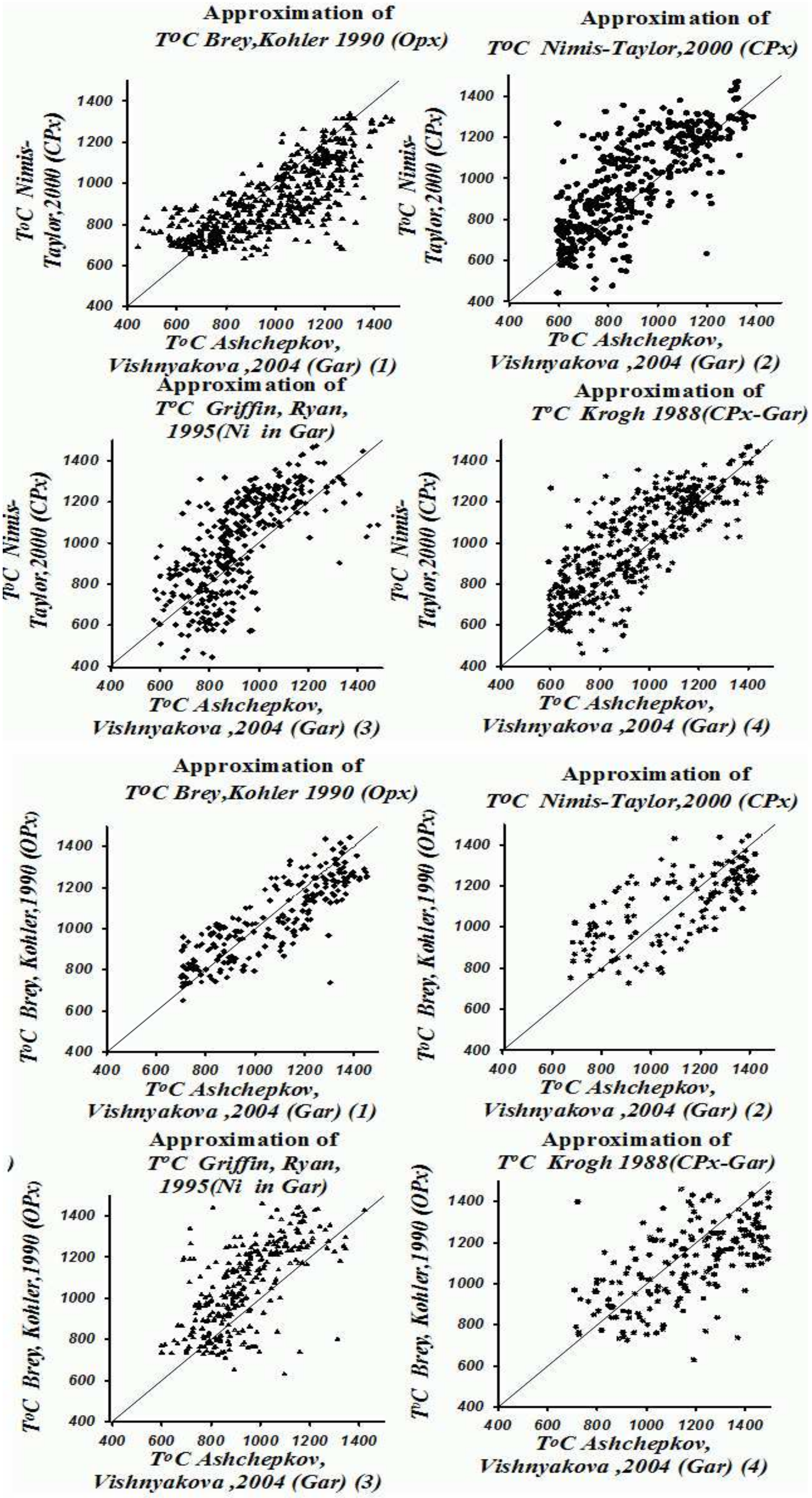

Fig.3. **Correlation diagrams for the temperatures determined with the four variants of (Ashchepkov Vishnyakova ,2005) [5] monomineral garnet thermometers and other thermometers used for the mantle peridotite associations**.

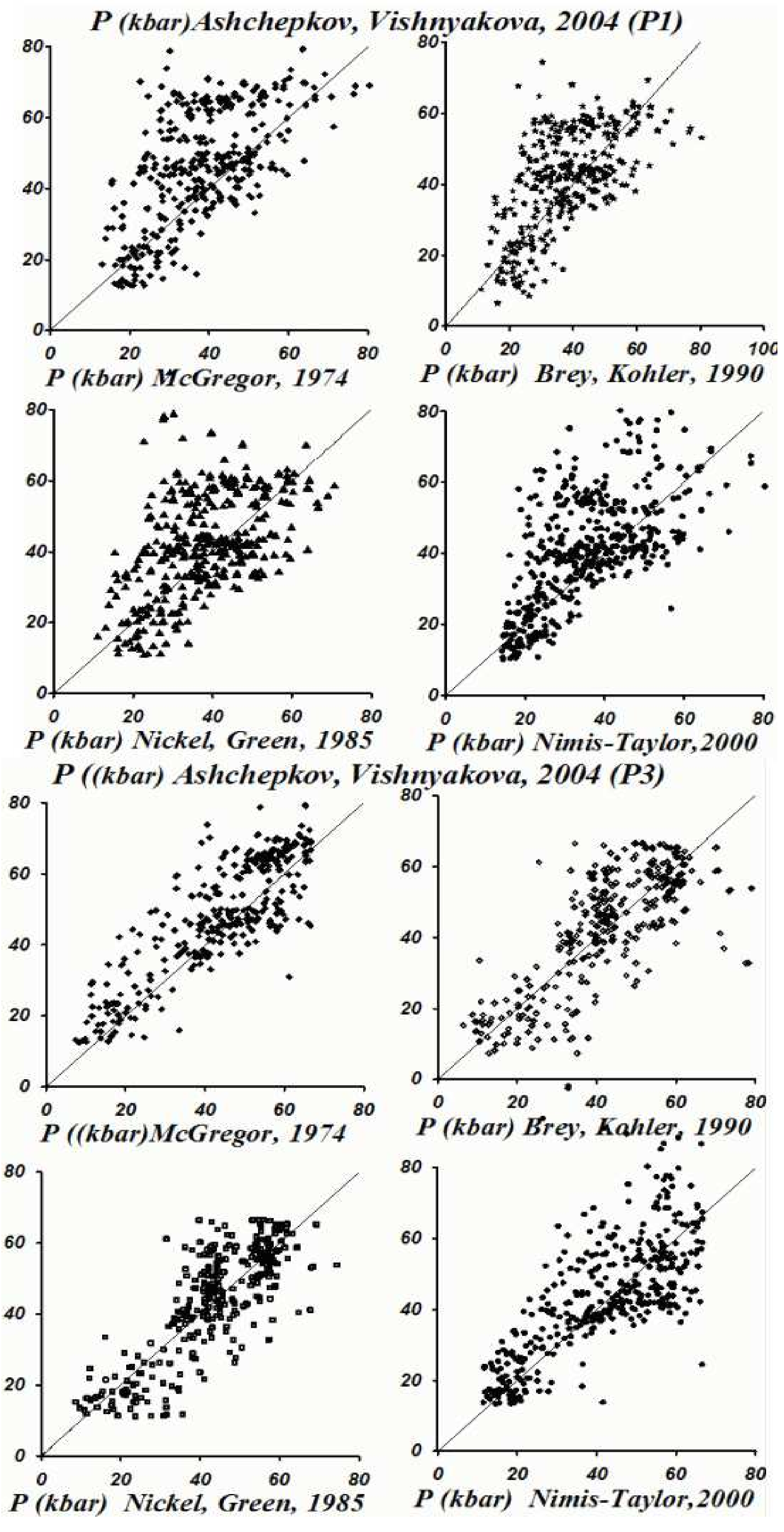

Fig.4. **Correlation diagrams for the pressure values determined with two variants of Ashchepkov, Vishnyakova 2005 [1,2] garnet barometer and some other barometers used for the mantle peridotite associations**.

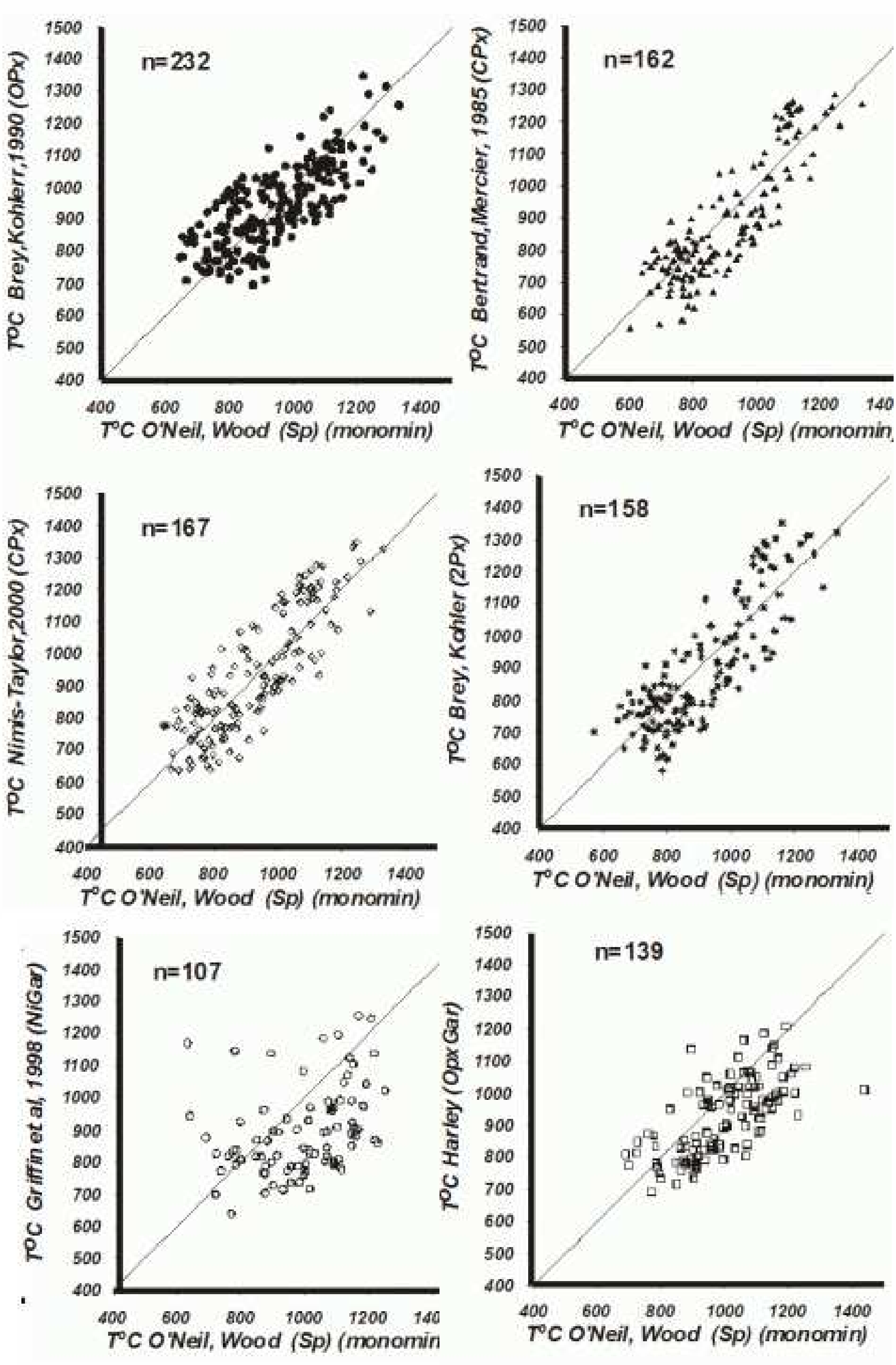

Fig.5. **Correlation diagrams for the temperatures determined with the Taylor et al ,1998 [48] monomineral chromite thermometer in the monomineral correction (Ashchepkov, Vishnyakova,2005) [2] and other thermometers used for the mantle peridotite associations.**

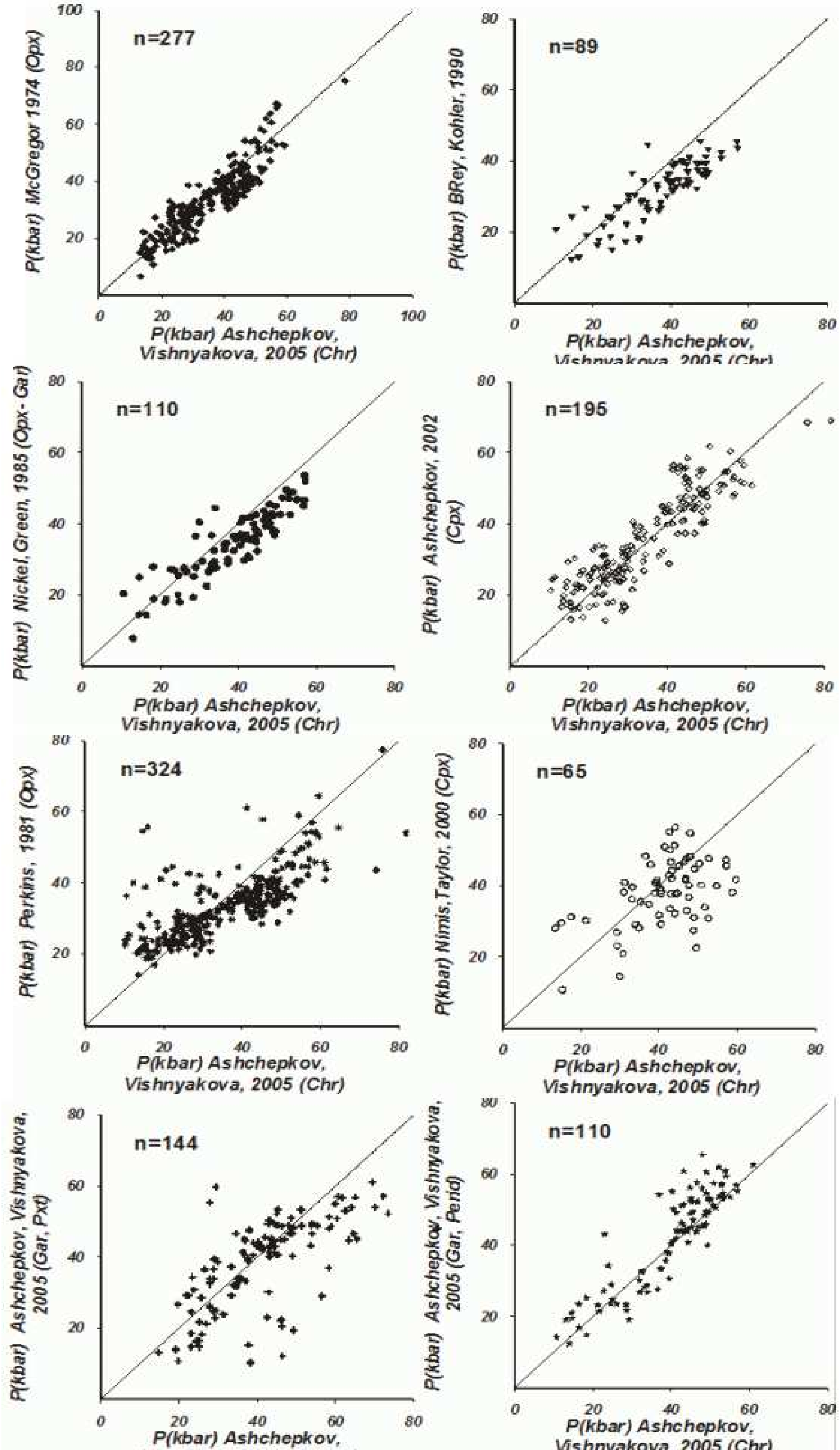

Fig.6. **Correlation diagrams for the pressure values determined with Ashchepkov Vishnyakova,2005) Cr-Sp barometer [5] and some other barometers used for the mantle peridotite associations**.

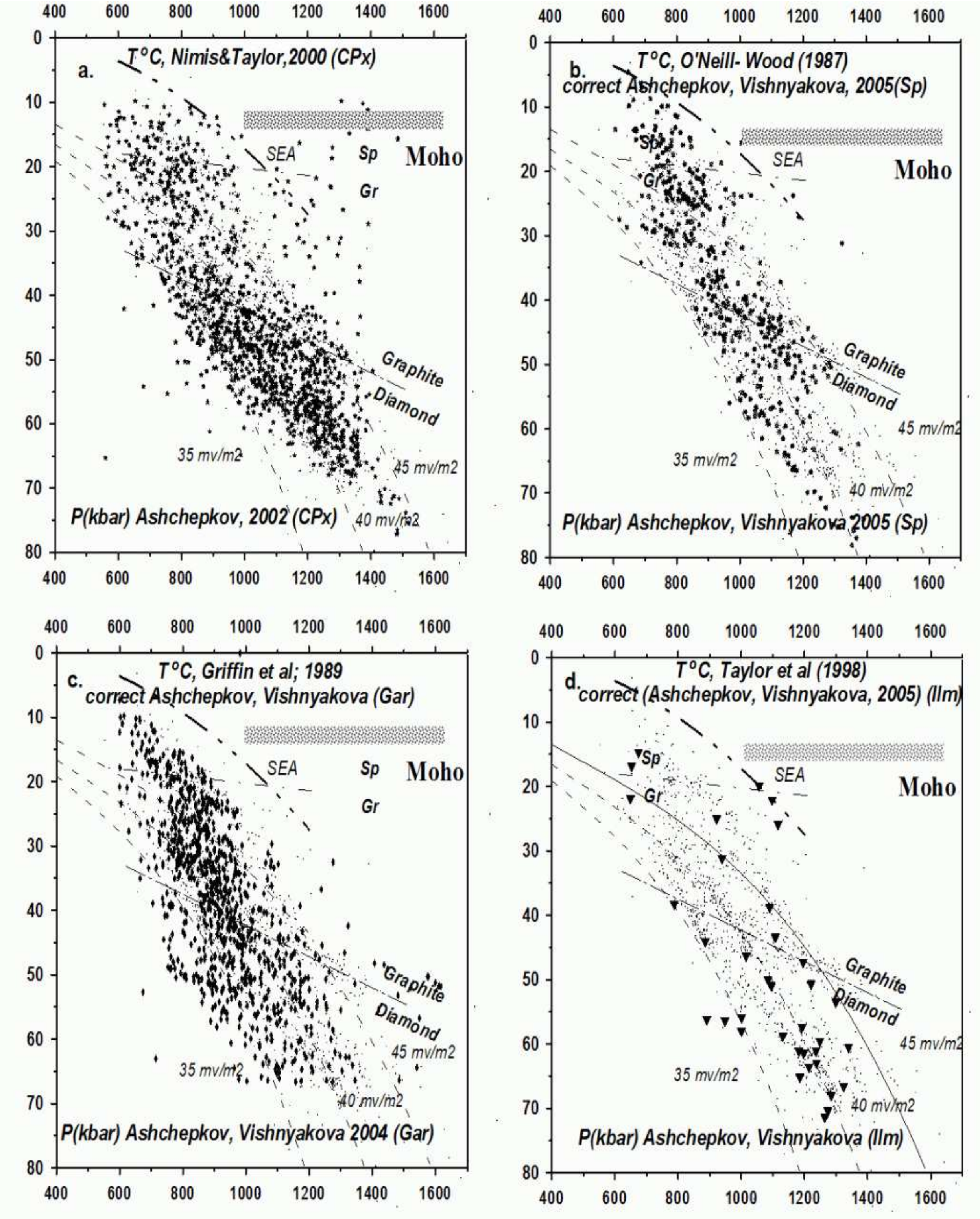

Fig 7. **Correlation diagram for the temperatures determined with the Taylor et al ,1998 [48] monomineral chromite thermometer (a) in the monomineral correction (Ashchepkov, Vishnyakova, 2005) [13] and other monomineral thermometers used for the mantle peridotite associations. Correlation diagram for the pressure values determined with Ashchepkov Vishnyakova,2005) picroilimenite barometer [13] and some other barometers used for the mantle peridotite associations.**

1. Opx [16-30] 2. Cpx [6,7], 3. Gar [1,2] and 4. Cr-Sp [5] methods

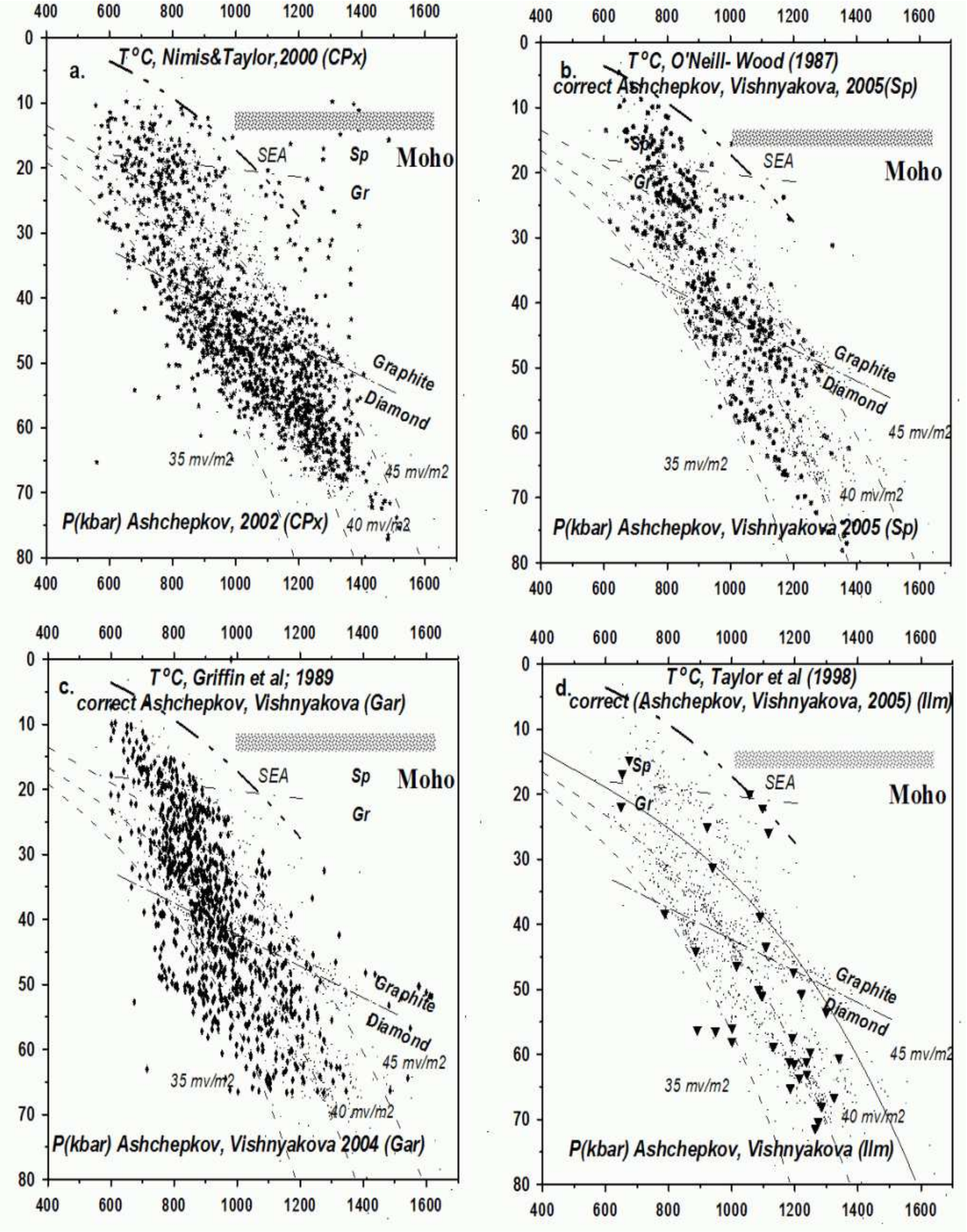

Fig8. **The TP plots for the xenoliths from whole World kimberlites (2400 associations) produced with the a) Cpx [7], Cr-Spinel [5], Garnet [2], and Pycroilmenite [13] monomineral thermobarometers plotted together with the values determined by the Opx [] thermobarometer**.

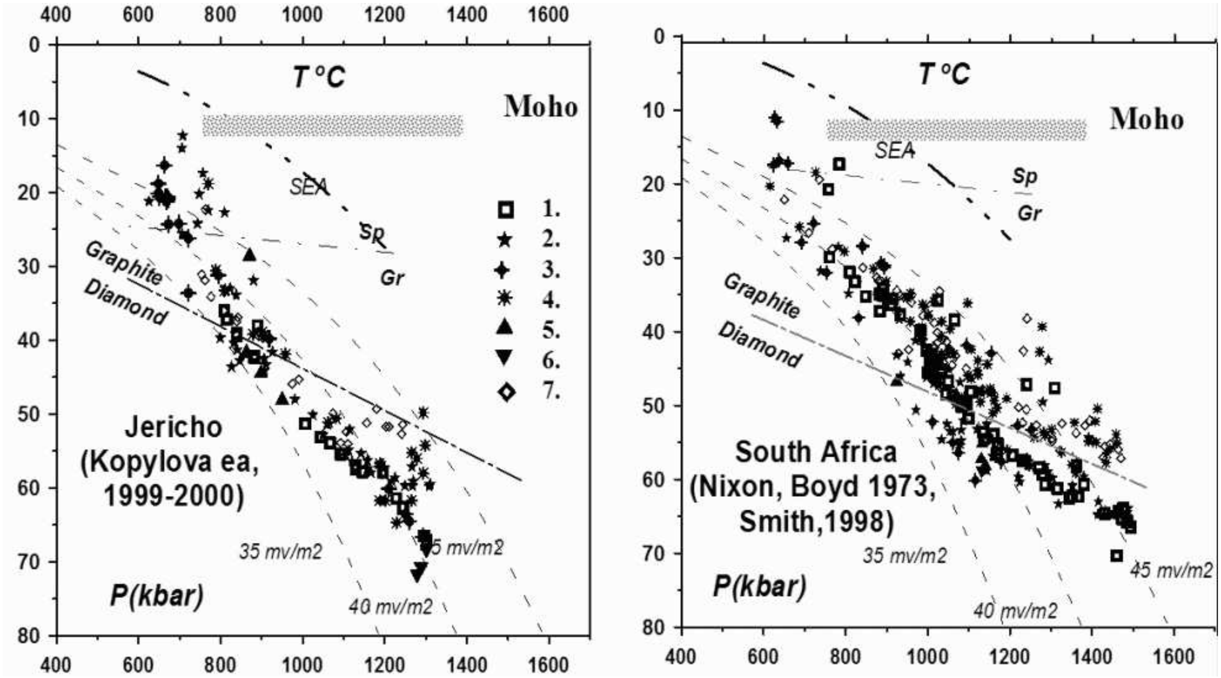

Fig 9. **The TP plot produced using Opx, Cpx, Gar, Cr-Sp And picroilmenete together with TP values determined with the most applicable polymineral thermo – and barometer methods [16] and [31].1. Opx [16,30] 2. Cpx [7,31], 3. Gar [2] and 4. Cr-Sp [5] 5. piroilmenite [13] and 6.[16] Two –Px thermometer and methods 7.[31]**

DISCUSSION

Application to the mantle columns reconstructions beneath the kimberlite pipes.

Clinopyroxene Jd-Di thermobarometry [6,7] give very good coincidence for the pipes where the composition of the mantle peridotites is relatively depleted but it also give produce realistic PT estimates and for the Mg- rich eclogites [14]. They often give the clots at 40 kbars near the inflection of the garnet Cr2O3-CaO diagram that and where the deviation to the pyroxenite fields represented by the Ga-Sp associations are common [26]. This level in the mantle is commonly marked by the relatively heated association and judging by the geochemistry to the pyroxene – rich assemblages representing the pyroxenite lens detected for the Udachnaya pipe [15] and other mantle columns.

Garnet thermobarometry [1,2] is rather specific but very useful. For the relatively depleted mantle columns it give the only good possibility for the reconstruction of the mantle layering and producing of the TP paths. Using different temperature and pressure pairs it is possible to receive the number of the variants and TP paths. The heated one near 40-42 mv/m^2 is corresponded to the Ti-rich associations that are likely related to the stages of the intrusions of the protokimberlite melts [4,12]. The most cold associations located near 35 mv/m^2 geotherm mark the depleted peridotite horizons with the subcalcic garnets. The disadvantage of the temperature methods using Ti is in the calibrations that do not allow to receive the T>1300^{o}C. Using the approximation of the Ni temperatures allow to obtain the higher values but the relatively low precision (R=0.65) sometimes give too low temperatures located lower then 35 mv/m^{2} geotherm.

The TP estimates using the chromite thermobarometer [5] give very close geothems positions and layering of the mantle columns beneath the kimberlite pipes as those determined by pyroxenes. As a rule they mark the irregularly heated harzburgite and dunite horizons [] in lower parts that are not determined by the pyroxenes and garnets. For diamond inclusions they define high To to 1500^{o}C at the basement of the mantle columns. Hi-T^{o}C estimates are found also at 40 kbar for pyroxenite lens and in the garnet- spinel facie. Cr-spinels mark sharply layered mantle referring to the low T conductive geotherm for Daldyn and Alakite regions [3,11]. For the Udachnaya pipe mantle column they show 6 horizons. The ilmenite TP estimates for Zarnitsa pipe give 3 (4) discrete intervals more HT in the upper part of the mantle as well as for Osennyaya pipe. For Aeromagnitnaya pipe the Ilm temperatures coincide with the Cpx’s estimates and are likely refer to metasomatic rocks. For the mantle columns of the Alakite the Ilm TP estimates coincides with the peridotite mantle layering especially for the Yubileynaya pipe. In mantle beneath the Upper Muna field the main part of TP estimates are plotted in the 3 layer in the middle part of the mantle section showing the irregular heating and oxidizing conditions rising linearly upward. In Malo-Botuobinsky field for Internationalnaya mantle the upper and low part of mantel columns determined by Cr-Sp are divided by irregular heated and oxidized peridotites. Ilmenites TP trace all column sequence from basement to the crust [4,12,13]. In Prianabarie chromites show irregular heated mantle partly highly oxidized. TP estimates for ilmenites mark there the lower horizons showing close conditions to Cpx [6,7] and possibly are related to the metasomatic mantle veins of glimmerites and mica pyroxenites found in dunite xenoliths [8].

The joining of the TP plots produced by the different monomineral methods give the possibility to determine the detail mantle structure. As an example we showed here the diagrams for well studied Jericho [26,27] and Lesotho [33,34]. They show not only coincidence with the PT estimates made with best polymineral thermobarometers [16,31] but also show the level of the Ilm metasomatites.

Diamond inclusion

We also produced a plot for the diamond inclusions using only published data (Fig.10) [40-46]. It is show that the majority of the garnets especially of the sub-calcic type are located at the lower and colder part of the diagram sometimes lower then 35 mv/m2. The Spinels an opposite trace the convective heated branch as well as the clinopyroxenes. The later trace more hot trend closeto adiabatic and probably reflect the conditions of the diamond growth near the rising protokimberlite system where HT good diamonds can be formed [19]. The amount of the inclusions crystallized upper then 35 kbar show that diamonds can crystallize in the metastable conditions in upper part of the mantle column. The oxygen fugasity calculated with the monomineral version of the the Sp and Ilm oxybarometers show the good coincidence with the data determined by the other methods [29].

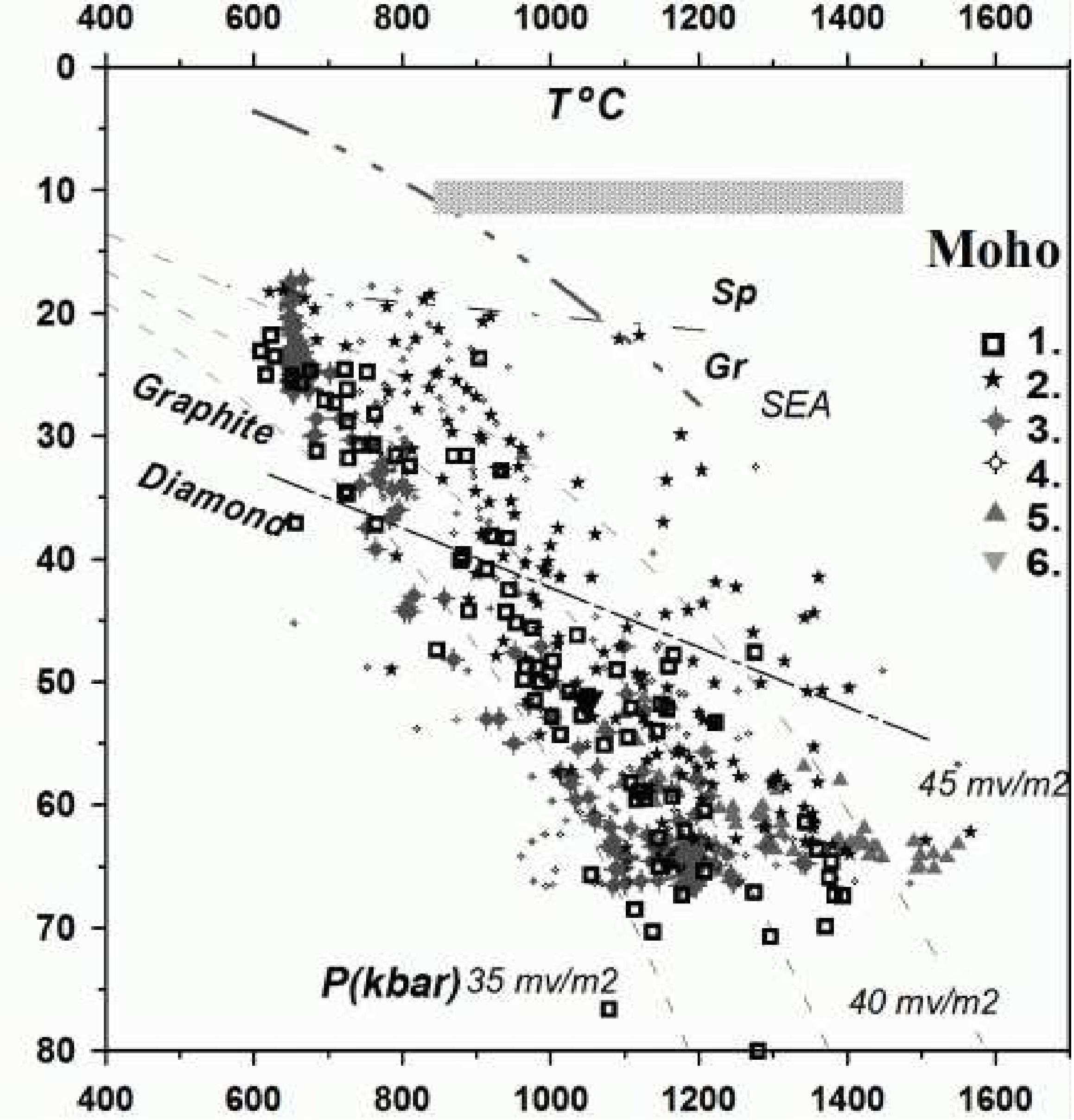

Fig 10. **The TP plot for the diamond inclusions produced using the published data.**

1. Opx [16,30] 2. Cpx [7,31], 3. and 4. Gar (P1-P2) [2] pressures or the peridotites and piroxenites and 5. Cr-Sp [5] 6. piroilmenite [13]

CONCLUSIONS

1. Monomineral thermobarometry based on the calibration of orthopyroxene method produce the PT plots that are intercorrelated and coincides with the polyminaral thermobarometry.
2. Garnet , Cpx , Opx , Sp , Ilm from the concentrates and placers may be used for the mantle reconstructions.

---

3. The Diamond inclusions show several specific TP fields For each preferential for the definite type of the mantle inclusions. Some of diamonds may growth or reshape in the metastable conditions.

Supported by RFBR grants, 03-05-64146; 05-05-64718. The article contain the materials from the REPORTs of the Agreements between UIGGM SD RASc and ALROCA Company; projects 77-02; 65-03.

References

1. **Ashchepkov I., Vishnyakova E.** New garnet thermobarometry for mantle peridotites and garnet mantle geotherms // 32nd International Geological Congress, Florence, Italy, August 20-28, 2004: Abstracts Volume. - Florence, 2004. - P. 466. - CD-ROM.
2. **Ashchepkov I.V.** Empirical garnet thermobarometer for mantle peridotites. //Seattle Annual Meeting (November 2-5, 2003). Abstract ID: 65507.
3. **Ashchepkov I., Vladykin N., Pokhilenko N., Sobolev N., Malygina E., Kuligin S., Ovchinnikiv Y., Afanasiev N., Mkrtychan G., Rotman A.,Kostrovitsky S., Tolstov A., Khmel'nikova J., Pokhilenko L., Logvinova A.** Clinopyroxene geotherms for the mantle columns beneath кimberlite pipes from Siberian craton. 8 th International Kimberlite Conference Long Abstract. FLA_0355.
4. **Ashchepkov I., Vladykin N., Rotman A., Khmelnkova O., Nikolaeva I., Anoshin G., Palessky S. Saprykin A.** Ilmenite trends from the kimberlite pipes as the result of the vertical migration of melts in the pre- eruption feeding vein system // 32nd International Geological Congress, Florence, Italy, August 20-28, 2004: Abstracts Volume. - Florence, 2004. - P. 1188
5. **Ashchepkov I.V., Vishnyakova E.V**. Monomineral Cr-Spinel thermobarometry for kimberlite peridotite xenoliths. Abstracts of EUG 2005.
6. **Ashchepkov I.V.** Jd-Di barometer for mantle peridotites and eclogites. Experiment in Geosciences. 2001. v.10, N1, 137-138
7. **Ashchepkov I.V**. More precise equation of the Jd-Di Barometer //Herald of the Earth department RAS. 2003. № 1. P. 45-46.
8. **Ashchepkov I.V., Afanasiev V.P., Pokhilenko N.P., Sobolev N.V., Vladykin N.V., Saprykin A.I., Khmelnikova O.S., Anoshin G.N.** Small note on the composition of Brazilian mantle // Revista Brasileira de Geociencias, 2001, 31, N 4, 653-660.
9. **Ashchepkov I.V., Vladykin N.V., Logvinova A.M., Rotman A.Y., Anoshin G.N., Saprykin A.I., Khmelnikova O.S.** Mantle geochemistry and construction in Mirninsky field.// Conference Supplement to Conference Supplement to Geochimica et Cosmochimica Acta. Abstracts and Program Goldschmidt Conference Copenhagen, Denmark June 5-11, 2004, Copenhagen. 5.7.P08 A724.
10. **Ashchepkov I.V., Vladykin N.V., Rotman A.Y., Logvinova A.M. , Afanasiev V.P. , Palessky V.S., Saprykin A.I., Anoshin G.N., Kuchkin A., Khmel'nikova O.S..** Mir and International'naya kimberlite pipes – trace element geochemistry and thermobarometry of mantle minerals. Deep seated magmatism It's sources and their relationto plum processes. //Irrutsk – Ulan-Ude 2004. Publishing house of the Institute of Geography SB RAS 2004, pp. 194-208
11. **Ashchepkov I.V., Vladykin N.V., Rotman A.Y., Logvinova A.M., Nikolaeva I.A., Palessky V.S., Saprykin A.I., Anoshin G.N., Kuchkin A., Khmel'nikova O.S.** Reconstructions of the mantle layering beneath the Alakite kimberlite field: comparative characteristics of the mineral geochemistry and TP sequences. //Deep seated magmatism

It's sources and their relationto plum processes. Irkutsk – Ulan-Ude 2004. Publishing house of the Institute of Geography SB RAS 2004, pp.160-178

12. **Ashchepkov I.V.,Vladykin N.V., Pokhilenko N.P., Rotman A.Ya., Afanasiaev V.P., Logvinova A.M., Kuligin S.S., Saprykin A.I., Kuchkin A.M., Nikolaeva I.V., Palessky S.V., Anoshin G.N., Khemelnikova O.S.** Ilmenite trends from the kimberlites of Siberia :Do they represent the mantle feeding vein system? Abstracts of EUG 2005.
13. **Ashchepkov I.V., Vishnyakova E.V.** Monomineral ilmenite and chromite thermo- and oxybarometry application to the mantle xenolith of Siberian platform. Evolution of the continental lithosphere origin of diamonds and their deposits. Abstract of the International Symposium devoted to 70 anniversary of N.V.Sobolev. Novosibirsk. 2005 p.45.
14. **Beard B.L., Fraracci K.N., Taylor L.A., Snyder G.A., Clayton R.N., Mayeda T.K., Sobolev N.V.** Petrography and geochemistry of eclogites from the Mir kimberlite, Yakutia, Russia. //Contrib. Mineral. Petrol., 1996. v.125, pp.:293 –310
15. **Boyd F.R.; Pokhilenko N.P.; Pearson D.G.; Mertzman S.A.; Sobolev N.V.; Finger L.W.** 1996. Composition of the Siberian cratonic mantle: evidence from Udachnaya peridotite xenoliths. //Contrib. Mineral. and Petrol. 1997., V. 128. N 2-3. P. 228-246.
16. **Brey G.P., Kohler T.** Geothermobarometry in four-phase lherzolites. II. New thermobarometers, and practical assessment of existing thermobarometers // J. Petrol 1990. V. 31. P. 1353-1378.
17. **Canil D.** The Ni-in-garnet geothermometer: calibration at natural abundances.// Contrib. Mineral. Patrol. 1999 v. 136 , pp.240-246.
18. **Eggler D.H., Mccallum M.E.** A geotherm from megacrysts in the Sloan kimberlite pipes, Colorado // Carnegie Inst. Wash. Yearb. 1976. V. 75. P. 538-541.
19. **Fedortchouk Y., Canil D., Carlson J.A.** Oxygen Fugacity of Kimberlite Magmas and their Relationship to the Characteristics of Diamond Populations, Lac de Gras, N.W.T., Canada. //Extended Abstracts of the 8International Kimberlite Conference. 2003. FLA_0098.
20. **Griffin W. L., Fisher N. I., Friedman J. H., O'Reilly S. Y., and Ryan C. G.** Cr-pyrope garnets in the lithospheric mantle. 2. Compositional populations and their distribution in time and space // Geochem. Geophys. Geosyst. 2002. V. 3(12). P. 35.
21. **Griffin W. L., Ryan C. G., Kaminsky F. V., O'Reilly S. Y., Natapov L. M., Win T. T., Kinny P.D., and Ilupin I. P.** The Siberian lithosphere traverse: Mantle terranes and the assembly of the Siberian Craton. // Tectonophysics, 1999. v.310, pp.1–35
22. **Griffin W.L., Doyle, B.J., Ryan, C.G., Pearson, N.J., O'Reilly, S.,Davies, R., Kivi, K., van Achterbergh, E., Natapov, L.M.,** 1999.Layered mantle lithosphere in the Lac de Gras area, Slave craton:composition, structure and origin. J. Petrol. 40, 705– 727.
23. **Griffn W.L., Cousens D.R., Ryan C.G., Sie S.H., Suter G.F.** Ni in chrome pyrope garnets: a new geothermometer. // Contrib. Mineral. Petrol. 1989. v.103. pp. 199-202
24. **Grutter H.S., Moore R.O.** Pyroxene Geotherms Revisited - An Empirical Approach Based on Canadian Xenoliths. //Extended Abstracts of the 8International Kimberlite Conference. 2003. FLA_0272
25. **Harley S.L.** An experimental study of partitioning of iron and magnesium between garnet and orthopyroxene. //Contrib Mineral. Petrol. 1984. v. 86. pp.359 –373.
26. **Kopylova M.G., Russell J.K., Stanley C., Cookenboo H**. Garnet from Cr- and Ca-saturated mantle: implications for diamond exploration //J. Geochem. Explor., 2000, v. 68,. 3, P. 183-199.
27. **Kopylova M.G.; Russell J.K.; Cookenboo H.** Petrology of peridotite and pyroxenite xenoliths from the Jericho kimberlite: Implications for the thermal state of the mantle beneath the Slave craton, northern Canada. // J. Petrol. 1999. V. 40. N1. P. 79-104

----

28. **Krogh, E.J.** 1988. The garnet-clinopyroxene Fe-Mg geothermometer - a reinterpretation of existing experimental data. // Contrib. Mineral. Petrol. V.99, pp.44-48
29. **McCammon C.A.; Griffin W.L.; Shee S.R.; J'Neill H.S.C.** Oxidation during metasomatism in ultramafic xenoliths from the Wesselton kimberlite, South Africa: implications for the survival of diamond. // Contrib. Mineral. and Petrol. - 2001. - Vol. 141. - N 3. - P. 287-296.
30. **McGregor I.D.** The system MgO- SiO2-Al2O3: solubility of Al2O3 in enstatite for spinel and garnet peridotite compositions. // Am. Miner. 1974. V. 59. P. 110-119.
31. **Nickel K.G., Green D.H.** Empirical geothermobarometry for garnet peridotites and implications for the nature of the lithosphere, kimberlites and diamonds. //Earth Planet .Sci. Lett . 1985. V.73: pp.158-170.
32. **Nimis P., Taylor W.** Single clinopyroxene thermobarometry for garnet peridotites. Part I. Calibration and testing of a Cr-in-Cpx barometer and an enstatite-in-Cpx thermometer // Contrib. Mineral. Petrol. 2000. V. 139. № 5. P. 541-554.
33. **Nixon P.H.** Ed.1973 Lesotho Kimberlites./Cape and Transvaal, Cape Town, 470 p.
34. **Nixon P.H., Boyd F.R.** Petrogenesis of the granular and sheared ultrabasic nodule suite in kimberlites // In Lesotho Kimberlites (P.H. Nixon, ed.). Lesotho National Development Corporation, Maseru, Lesotho. 1973. P. 48-56.
35. **O’Neill H. St. C., Wall V.J.** (1987). The olivine orthopyroxene-spinel oxygen geobarometer, the nickel precipitation curve, and the oxygen fugacity of the Earth’s upper mantle. // Journal of Petrology 28, 1169-1191.
36. **O’Neill H. St. C.** (1981). The transition between spinel lherzolite and garnet lherzolite, and its use as a geobarometer. Contributions to Mineralogy and Petrology 77, 185–194.
37. **O’Reilly S.Y., Griffin W.L.,** Poudium Diomany, Morgan P. Are lithospehers forever? // GSA Today. 2001.V. 11. P. 4-9.
38. **Pollack H.N., Chapman D.S.** On the regional variations of heat flow, geotherms and lithosphere thickness. // Tectonophysics 1977. v.38. pp 279.
39. **Ryan C. G.; Griffin W. L.; Pearson N. J.** Garnet geotherms: Pressure-temperature data from Cr-pyrope garnet xenocrysts in volcanic rocks // J. Geophys. Res. B. 1996. V. 101. P. 5611-5625.
40. **Sobolev N.V., Lavrentev Y.G., Pokhilenko N.P., Usova L.V.** Chrome-Rich Garnets from the Kimberlites of Yakutia and Their Parageneses // Contributions to Mineralogy and Petrology, 1973, 40, N 1, 39-52.
41. **Sobolev N.V., Logvinova A.M., Zedgenizov D.A., Yefimova E.S., Taylor L.A., Promprated P., Koptil V.I., Zinchuk N.N.** Mineral Inclusions in Diamonds from Komsomolskaya and Krasnopresnenskaya Pipes, Yakutia: Evidence for Deep Lithospheric Heterogeneities in Siberian Craton // 8th International Kimberlite conference, Victoria, BC, Canada, June 22-27th, 2003: Extended Abstracts, 2003, FLA_0141
42. **Sobolev N.V., Sobolev V.N., Snyder G.A., Yefimova E.S., Taylor L.A**. Significance of eclogitic and related parageneses of natural diamonds. Int Geol .Rev. 1999. v.41 pp.129 – 140.
43. **Spetsius Z.V.** Two generation of diamonds in the eclogite xenoliths. // Proc. 7th Int. Kimberlite Conf., Cape Town, 1999, pp. 823–828
44. **Stachel T, Harris J.W.** (1997) Diamond precipitation and mantle metasomatism ± evidence from the trace element chemistry of silicate inclusions in diamonds from Akwatia, Ghana. // Contrib Mineral Petrol 129: 143±154
45. **Stachel T.; Harris J.W.; Tappert R.; Brey G.P.** Peridotitic diamonds from the Slave and the Kaapvaal cratons - similarities and differences based on a preliminary data set // Lithos. - 2003. - Vol. 71. - Iss. 2-4. - P. 489-503.

46. **Taylor L.A., Anand M., Promprated P., Floss C., Sobolev N.V.** The significance of mineral inclusions in large diamonds from Yakutia, Russia // American Mineralogist, 2003, 88, N 5-6, 912-920
47. **Taylor W.R, Nimis P.** (1998) A single-pyroxene thermobarometer for lherzolitic Cr-diopside and its application in diamond exploration. //7th Int Kimb Conf Abstract Volume, Cape Town, pp 897- 898
48. **Taylor W.R., Kammerman M., Hamilton R.** New thermometr and oxigen fugasity sensor calibrations for ilmenite and chromian spinel-bearing peridotitic assemlages. . 7th International Kimberlite Conference. Extended abstracts. Cape town. 1998. Pp.891-901

UDK 550.42; 552.111

Two types of “intra-plate” lavas on Kamchatka

Avdeiko G.P. and Savelyev D.P.

Institute of Volcanology and Seismology, FED RAS, Petropavlovsk-Kamchatsky,
e-mail: gavdeiko@kcs.iks.ru

Two types of lavas with intra-plate geochemical characteristics are distributed in Kamchatka. One of them form a part of the Cretaceous ophiolite complex. This complex contains assemblage of MORB-like tholeiites and high-K_2O alkali basalts occurring among jaspers, limestone and cherts. Geochemical characteristics of the alkali basalts correspond to those of ocean island basalts (OIB). High content of K, P, Nb and LREE in the studied rocks is similar to alkali basalts of the Emperor Seamount Chain. Spinel compositions of investigated basalts are within the OIB spinel field. Melt inclusions in spinel from tholeiitic basalts extend the compositional field of basalts toward compositions, which are extremely depleted in incompatible trace elements. Selective enrichment of these melt inclusions in K, Sr, Ba and LREE compared to elements of similar incompatibility mimics geochemical peculiarity of melt inclusions from Hawaiian and Icelandic tholeiites. Composition and age of the studied rocks allow connecting the formation of the Kamchatsky Mys ophiolite to the activity of the Hawaiian mantle plume. This complex was formed in the anomalous segment of the mid-ocean ridge above the Hawaiian mantle plume in the Cretaceous. Collision of this terrain with Kamchatka and jump of the subduction zones to the east took place 6-10 Ma. Late Cenozoic lavas with intra-plate geochemical characteristics (second type) are distributed in the East and West Kamchatka and in the Sredinny Range of Kamchatka above the subduction zones. They are formed by influence of a melt subduction component on the melting substratum of mantle wedge in different from typical island arc lavas formed by influence of fluids from subduction zones. Partial melting of upper part of the subducted slab can be at higher temperatures in the initial stage of subduction (East Kanchatka) and terminated stage one (West Kamchatka and Sredinny Randge) than in the steady state regime of subduction.

INTRODUCTION

Geodynamic conditions of manifestations of volcanic rocks with intra-plate geochemical characteristic within island arc systems are one of the main problems of modern petrology. This problem were discussed in some papers [15, 20, 23, 31]. Two types of intra-plate lavas are known in Kamchatka (Fig. 1). One of them, viz., Cretaceous basalts of Smagin formation located in the Kamchatsky Mys Peninsula, i.e. in the Kamchatka-Aleutian junction [6, 24]. They are a part of the basement of the Kurile-Kamchatka Island Arc System. Late Cenozoic lavas, having intra-plate geochemical characteristics, belong to the second one. They are distributed in the East and West Kamchatka and the Sredinny Range of Kamchatka [31].

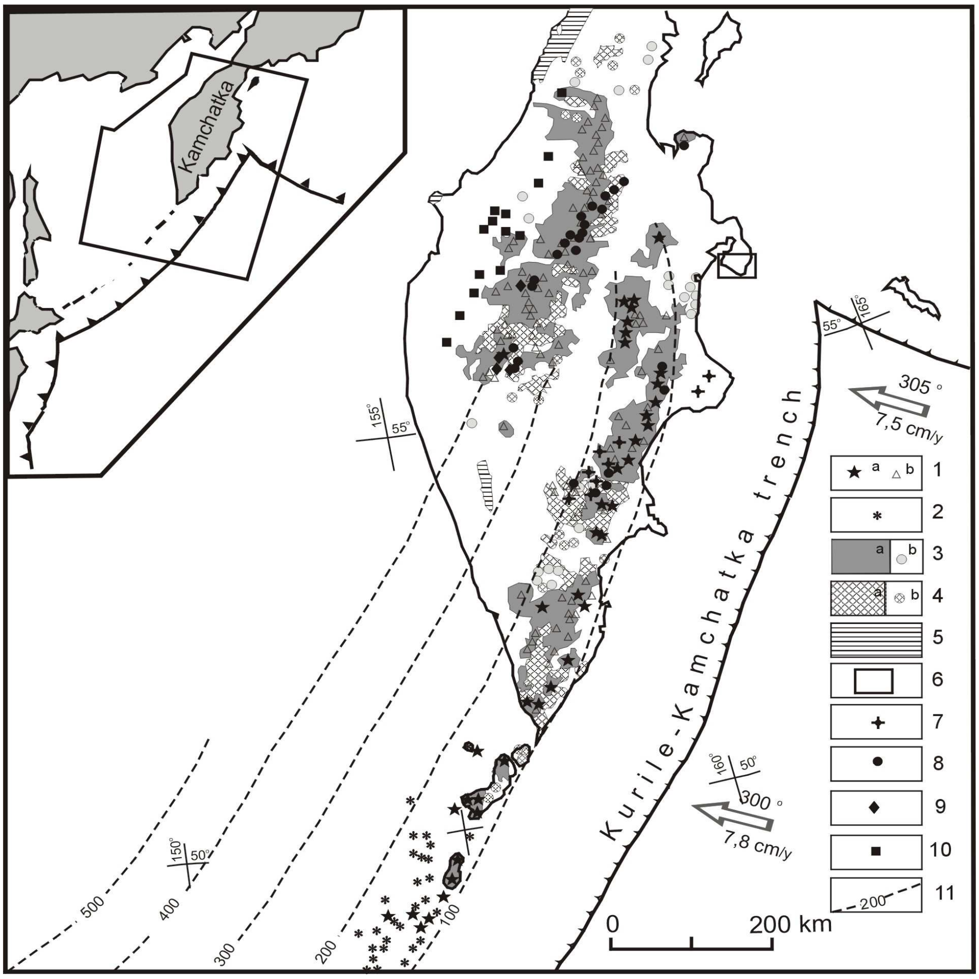

Fig. 1. **Map of distribution of Cenozoic subducted related volcanic formations and Cretaceous mantle plume relates lavas in the Kurile-Kamchatkan Island Arc System.**

1 - Subaerial active (a) and extinct (b) volcanoes; 2 – submarine volcanoes; 3 – areas (a) and local outcrops (b) of Quaternary volcanic formations; 4 – areas (a) and local outcrops (b) of Late Oligocene-Miocene volcanic formations; 5 – Paleogene volcanic formation; 6 – location area of Cretaceous mantle plume related lavas; 7 – 10 – Late Cenozoic formations of the intra-plate geochemical type after O.N.Volynets [31]: 7 – K-Na alkali basalts, 8 – K-Na olivine alkali basalts, 9 – K-Na transitional basalt-comendite, 10 – magnesian K-alkali basalts; 11 – depth isolines of the Benioff zone.

Location of Cretaceous intra-plate lavas in the Kamchatka-Aleutian junction corner near the Obruchev rise, the last link of the Hawaiian-Emperor Seamount Chain, suggest that have some genetic connection. The Obruchev Rise located near the Kamchatka-Aleutian junction consists of the oldest yet known Meiji seamount in the 3000 km Hawaiian-Emperor Seamount Chain. The seamount chain is the trace of the Hawaiian mantle plume on the moving Pacific plate [13, 14, 32]. This hypothesis is well confirmed by the data on ages of the Emperor and Hawaiian guyots (Fig. 2). The idea on possible continuation of the Hawaiian-Emperor Seamount Chain in Kamchatka was proposed on the basis of results of DSDP 19 and 55 Legs and geological features of Kamchatka [1]. Later, fragments of Cretaceous oceanic crust and oceanic island basalts were discovered and studied in the Kamchatsky Mys Peninsula [6, 24, 34].

The great interest to the early stage of the Hawaiian plume evolution has been increased recently after deep sea drilling on Detroit and Meiji Guyots [8, 10, 11, 22,]. We suggest that Cretaceous tholeiitic and alkali basalts having OIB geochemical signatures from the Kamchatsky Mys Peninsula (the Smagin Suite) were formed above the Hawaiian mantle plume and can characterize the earliest stage of its development. The Smagin paleo-guyot representing these rocks had likely positive buoyancy and, therefore, was obducted and accreted to Kamchatka. In this paper we would like to discuss the geological setting, geochemical and mineralogical peculiarities of Cretaceous oceanic crust in the upper part of the Smagin Suite and possible geodynamic conditions of its generation.

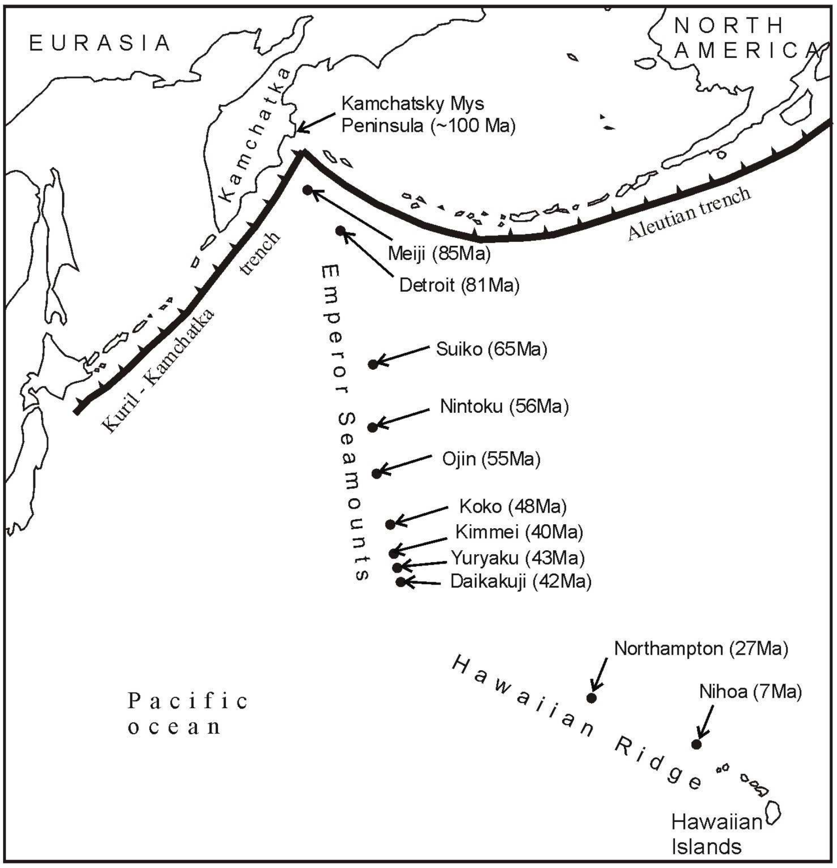

Fig. 2. **Age and location of seamounts in the Hawaiian-Emperor Chain (by M.Regelous et al [22]).**

Besides, Late Cenozoic intra-plate geochemical type lavas are occur in the central part of Kamchatka near the Kamchatka-Aleutian junction from the East to West Kamchatka [31]. Their appearance evidently is related to geodynamics of the Kamchatka-Aleutian and the Hawaiian-Emperor Seamount Chain junction. These lavas were formed above two subduction zones in the initial and terminated stages of their evolution and so they are not typical intra-plate lavas. Generation of these “intra-plate” lavas takes place after the “jump” of subduction zone from Sredinny Range to its present day position at the end of Miocene [3]. Problem of their origin also is to be discussed in this paper.

MANTLE PLUME RELATED CRETACEOUS LAVAS

Geologic setting. Cretaceous lavas with intra-plate geochemical characteristics are located in the south part of the Kamchatsky Mys Peninsula, the northernmost of Eastern Peninsulas of Kamchatka, which occur in fore-arc of the present Kamchatka volcanic arc. The studied area occupies a key position in the Kamchatka-Aleutian junction, directly on a joint of these two island arcs and Hawaiian-Emperor Seamount Chain (Fig. 2). The Kamchatsky Mys terrain consists of different parts of ophiolite complex and associated sediments [4] (Fig. 3). Here the ophiolite assemblage is the most complete in Kamchatka. It includes ultramafic rocks, gabbro, parallel dikes of dolerites, basalts, tuffs, cherts, jaspers and limestones. Relationships within the ophiolite sequence are tectonic, but geochemical and mineralogical data suggest their united genesis. The plutonic series consists of harzburgite, dunite, troctolite and gabbro up to 700-800 m thick. The rocks are strongly deformed and metamorphosed in the greenchist facies.

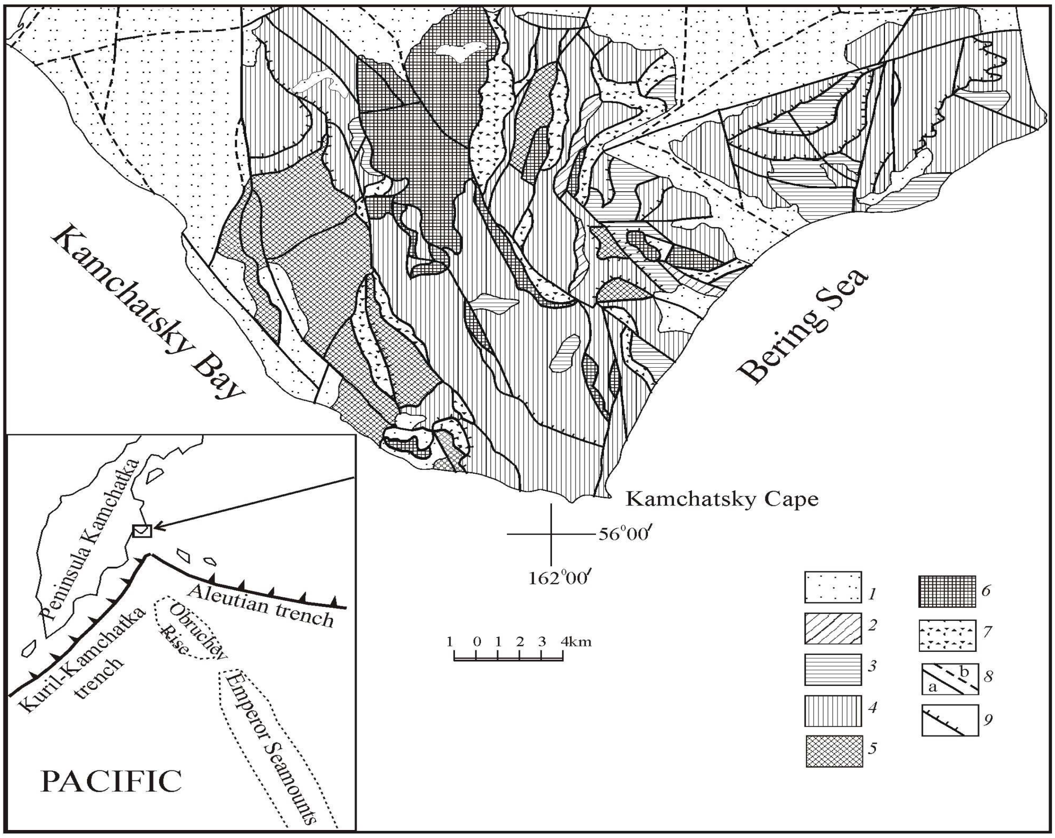

Fig. 3. **Geological map of the southern part of Kamchatsky Mys Peninsula (by M.E. Boyarinova [4])**.

1 – Pliocene-Quaternary deposits; 2 – Miocene deposits; 3 – Turonian-Campanian terrigenous deposits; 4 – Albian-Cenomanian chert-volcanic deposits; 5 – gabbro and dolerites; 6 – ultramafic rocks; 7 – serpentinite melange; 8 – faults (a – proved, b – buried); 9 – thrusts.

Volcanoclastic tuff and chert deposits with the pillow-basalts, jaspers and limestones are united in the Smagin Suite [12, 4]. The age of the sequence was estimated as Albian-Cenomanian by radiolarian assemblage from jaspers among the limestones. Some geologists believe that pillow-basalts, jaspers and limestones

---

----

are olistoliths in the Late Cretaceous chaotic complex [34, 5]. The Smagin Suite is overlaid by the Turonian-Campanian terrigeneous deposits of the Pikezh Suite. Miocene terrigeneous rocks occur in subordinate amounts and were observed in tectonic slices. Late Pliocene and Quaternary marine sediments discordantly cover Cretaceous and Miocene deposits (Fig. 2) [4].

Petrographic, geochemical and mineralogical characteristics of Cretaceous basalts. We carried out petrologic and geochemical investigation of the basalts, studied major and accessory minerals from the basalts and melt inclusions in spinel. The rocks are aphyric, plagioclase and olivine phyric. Groundmass has star-shaped, spherulitic, paniculate (Fig. 4A). The alkali basalts differ from other rocks by presence of Ti-fassaite, K-feldspar, biotite and hornblende (Fig. 4B). In thinsections, Ti-rich clinopyroxene of the alkali basalts has lilac color. Geochemical and petrochemical characteristics of the Cretaceous basalts were reported in publications of A.V.Fedorchuk and D.P.Savelyev [6, 24]. There have been established several geochemical types of basalts in the Kamchatsky Mys Peninsula: normal and depleted tholeiites, enriched and alkali high-K basalts.

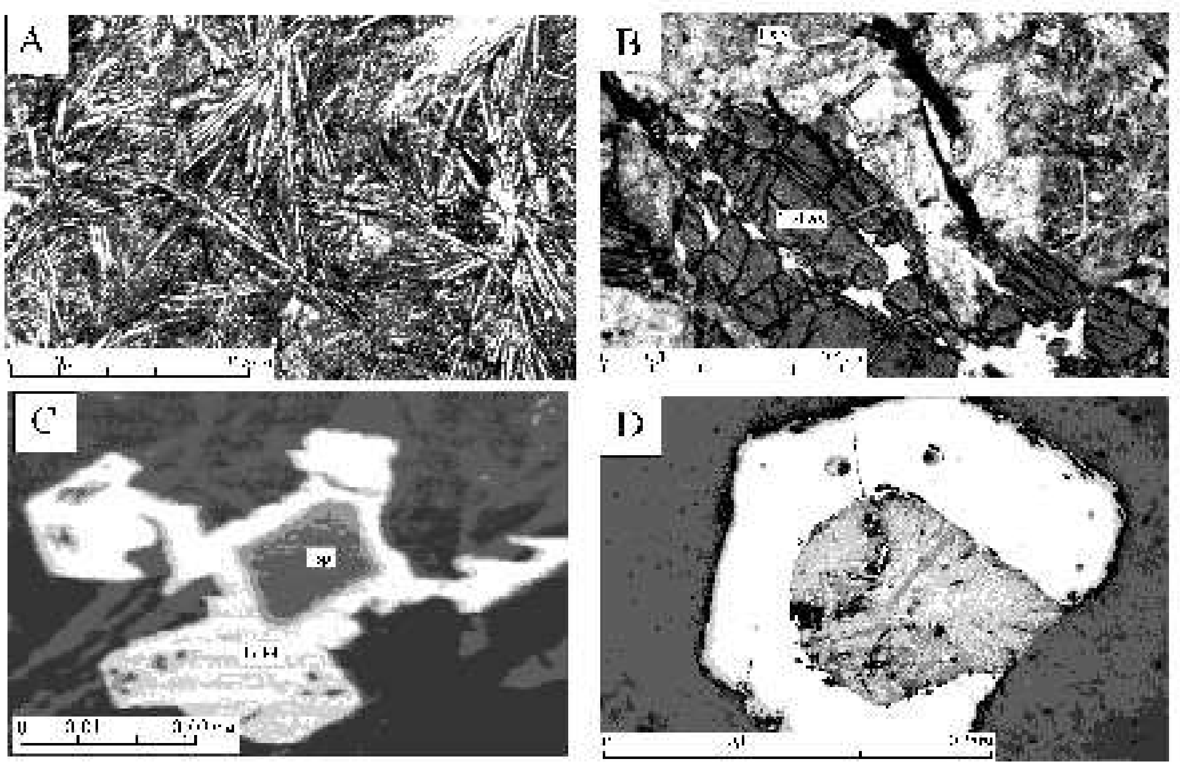

Fig. 4**. Micro photos.**

A - star-shaped texture of the plagioclase microlites in the basalt mesostasis; B - phenocryst of the titan-fassaite in the alkaline basalt (Ti-Fas - titan-fassaite, Fsp – K-feldspar); C – spinel grain (Sp) in the titanomagnetite (Ti-Mt) envelope; D – melt inclusion in the spinel grain.

Alkali basalts account for 5-7% volcanic rocks of the Smagin Suite. Chemical composition of the alkali basalts is very different from other types of basalts. This group of basalts is characterized by high contents of potassium (up to 3.2% K_2O) and phosphorus (P_2O_5=0.49-0.56%). TiO_2/P_2O_5 ratio in the alkali basalts (2.45-4.90) is distinctively high when compared with other types of oceanic basalts. High Zr/Y (7.9–10.0) testifies the basalts as the within plate basalts (WPB) after classification by J.A.Pearce and J.R.Cann [18] (Fig. 5). On the discrimination plots by D.A.Wood [33], these basalts fall within the OIB field. La_N/Sm_N (3.12 – 4.08) and trace element patterns of the alkali basalts normalized to the primitive mantle composition also are similar to ocean island basalts (OIB) [24].

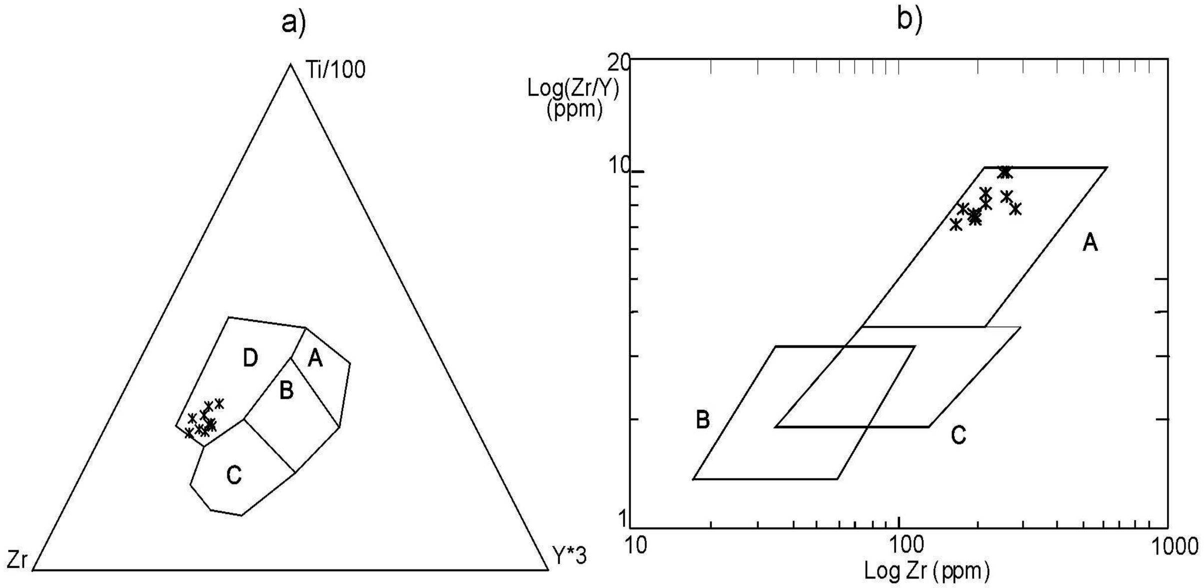

Fig. 5. **Location of Cretaceous alkali basalts of Kamchatsky Mys Peninsula on the geodynamic plots.**

a: Zr-3Y-Ti/100 (D - within plate baslts, B - oceans floor basalts, A and B - low-K tholeiites of island arcs, and C - Calc-alkaline basalts of IA, by J.A. Pearce and J.R. Cann [18]);
b: Log Zr - Log (Zr/Y) (A - within plate baslts, B – island arc basalts, C - MORB, by J.A. Pearce and M.J. Norry [19]).

We studied composition of primary and accessory minerals in different geochemical types of basalts. Mineral analyses were carried out in polished thinsections by electron micro probe “Camebax-244” at the Institute of Volcanology and Seismology, Petropavlovsk-Kamchatsky. Operating conditions were 20 kV accelerating potential and 40 nA beam current. The chemical compositions of clinopyroxene, biotite and hornblende in alkali basalts from Kamchatsky Mys Peninsula are presented in Table 1. Clinopyroxenes have composition of high-Ti and high-Al fassaite (up to 6.44% TiO_2), that is similar to the most Ti-rich pyroxenes yet documented on Earth in alkali basalts from Tahiti Islands [30]. CaO/Al_2O_3 in pyroxenes is 2-3 and evidences high pressure of the pyroxene crystallization. In compliance with the data by G.V.Nesterenko and A.A.Ariskin [16], the pyroxene compositions correspond to the crystallization pressure of 8 kbar. This is similar with conditions of crystallization in the continental rift. Hornblende in the alkali basalts

---

Table 1.

Chemical composition of clinopyroxene, biotite and hornblende in alkali basalts from Kamchatsky Mys Peninsula (weight per cent).

	1	**2**	**3**	**4**	**5**	**6**	**7**	**8**	**9**	**10**	**11**
SiO_2	42.57	42.28	43.35	41.95	41.76	42.20	42.47	47.58	44.86	48.37	48.73
TiO_2	6.15	6.31	5.09	5.98	6.44	6.29	5.61	3.47	4.35	2.45	2.53
Al_2O_3	7.52	7.91	7.04	8.33	8.57	7.84	8.02	4.32	6.60	3.30	3.74
FeO*	9.36	9.52	9.23	9.60	9.99	10.41	9.27	9.03	9.37	9.11	9.88
Cr_2O_3	0.65	0.53	0.55	0.67	0.63	0.74	0.63	0.70	0.73	0.53	0.82
MgO	10.08	9.70	10.66	9.69	9.51	9.62	10.29	12.43	10.90	12.55	11.91
CaO	21.36	21.59	21.37	21.44	21.37	21.40	21.68	21.55	21.25	21.34	21.34
Na_2O	0.65	0.79	0.71	0.59	0.74	0.72	0.54	0.50	0.66	0.62	0.55
K_2O	0.05	0.06	0.03	0.04	0.04	0.03	0.04	0.03	0.04	0.04	0.04
MnO	0.90	0.77	0.76	0.61	0.73	0.66	0.67	0.77	0.83	0.97	0.83
NiO	0.00	0.03	0.04	0.00	0.00	0.02	0.02	0.00	0.00	0.00	0.11
ZnO	0.04	0.08	0.07	0.10	0.07	0.01	0.07	0.04	0.00	0.01	0.01
Total	99.33	99.57	98.90	99.00	99.85	99.94	99.31	100.42	99.59	99.29	100.49
	12	**13**	**14**	**15**	**16**	**17**	**18**	**19**	**20**	**21**	**22**
SiO_2	46.27	45.77	45.96	45.23	45.40	45.47	43.45	43.48	43.17	43.05	45.53
TiO_2	2.59	2.85	2.99	2.78	2.99	3.06	3.80	3.91	4.15	4.40	3.77
Al_2O_3	7.32	7.59	7.80	7.68	7.85	7.84	8.93	8.78	9.13	9.06	6.98
FeO*	7.49	7.07	7.16	7.16	7.20	7.04	7.83	8.16	8.67	9.14	9.65
Cr_2O_3	0.02	0.00	0.00	0.00	0.00	0.00	0.00	0.00	0.00	0.00	0.00
MgO	12.12	12.44	12.11	11.97	12.46	12.09	11.25	11.14	11.12	10.70	10.62
CaO	22.69	22.37	22.55	22.93	22.73	22.80	22.83	22.66	22.45	22.51	22.66
Na_2O	0.44	0.45	0.41	0.39	0.43	0.48	0.42	0.49	0.55	0.44	0.51
K_2O	0.04	0.02	0.03	0.03	0.04	0.05	0.03	0.03	0.03	0.05	0.03
MnO	0.03	0.00	0.03	0.00	0.00	0.00	0.00	0.01	0.05	0.00	0.09
NiO	0.05	0.01	0.06	0.00	0.03	0.00	0.04	0.01	0.01	0.00	0.00
ZnO	0.00	0.00	0.00	0.00	0.00	0.00	0.00	0.00	0.00	0.00	0.00
Total	99.06	98.57	99.10	98.17	99.13	98.83	98.58	98.67	99.33	99.35	99.84
	23	**24**	**25**	**26**	**27**	**28**	**29**	**30**	**31**	**32**	**33**
SiO_2	37.31	37.72	35.96	38.89	38.83	37.92	38.22	36.23	38.45	37.31	37.80
TiO_2	7.15	7.16	4.84	6.41	6.00	6.58	7.13	7.40	6.93	7.33	7.33
Al_2O_3	13.41	13.51	12.08	13.14	13.05	12.89	13.20	16.69	16.04	15.69	15.70
FeO*	14.51	14.86	21.79	14.83	14.52	18.21	14.16	21.61	22.49	18.31	17.67
Cr_2O_3	0.00	0.00	0.00	0.00	0.00	0.00	0.00	0.00	0.00	0.00	0.00
MgO	9.71	9.83	5.08	9.98	10.36	7.54	10.08	7.43	6.30	9.03	8.90
CaO	11.82	11.67	14.62	11.87	11.82	11.48	11.24	1.48	1.01	3.42	3.50
Na_2O	2.32	2.13	2.42	2.21	2.24	1.93	2.18	0.69	0.68	0.74	0.70
K_2O	2.26	2.17	2.06	2.14	2.27	2.43	1.99	7.82	8.03	7.34	7.02
MnO	0.08	0.06	0.25	0.03	0.05	0.23	0.08	0.25	0.17	0.16	0.19
NiO	0.00	0.00	0.02	0.04	0.01	0.02	0.01	0.00	0.01	0.01	0.01
ZnO	0.00	0.00	0.00	0.00	0.00	0.00	0.00	0.00	0.00	0.00	0.00
Total	98.54	99.11	99.12	99.55	99.16	99.24	98.30	99.59	100.11	99.35	98.81

Note. FeO* - total iron. 1- 22 - clinopyroxene; 23-29 – hornblende; 30-33 – biotite. Mineral analyses were carried out in polished thin section on an electron microanalyzer “Camebax-244” at the Institute of Volcanology, Petropavlovsk-Kamchatsky, 2003. Analyses were carried out by Filosofova T.M.

is kaersutite with content of TiO_2 4.84-7.16% (Table 1). This composition is similar to kaersutite composition from the late Miocene teschenites in the Eastern Kamchatka [29]. High content of titanium (to 7.33% TiO_2) is also typical for biotite (Table 1). The chemical composition of the minerals reflects high titanium and high potassium composition of the host alkali basalts.

Spinel. We studied regularity of the changes of spinel composition depending on geochemical type of basalts. The compositions of spinels from alkali and enriched basalts of Kamchatsky Mys Peninsula are presented in Table 2. In large spinel grains, we determined composition of melt inclusions (Fig. 4, C, D). Spinel from normal and depleted tholeiites is similar to spinel of the mid-ocean ridge tholeiites. The composition of the spinels hosting melt inclusions is discussed in detail by M.V. Portnyagin and coauthors [21]. The most Ti-rich spinels were found in the alkali high-potassium basalts. These spinel compositions are similar to spinels from the Hawaiian alkaline rocks (Fig. 6). All spinels from the Kamchatsky Mys ophiolite are different from spinels in Kamchatka arc-type rocks. Very interesting information was obtained from the composition of melt inclusions in spinel. The melt inclusions in spinel from tholeiitic basalts preserved un-altered parental melts for the basalts and extend the basalt compositional field toward compositions, which are extremely depleted in incompatible trace elements. Selective enrichment of these melt inclusions in K, Sr, Ba and LREE compared to elements of similar incompatibility is very similar to melt inclusions from the Hawaiian and Icelandic tholeiites [25].

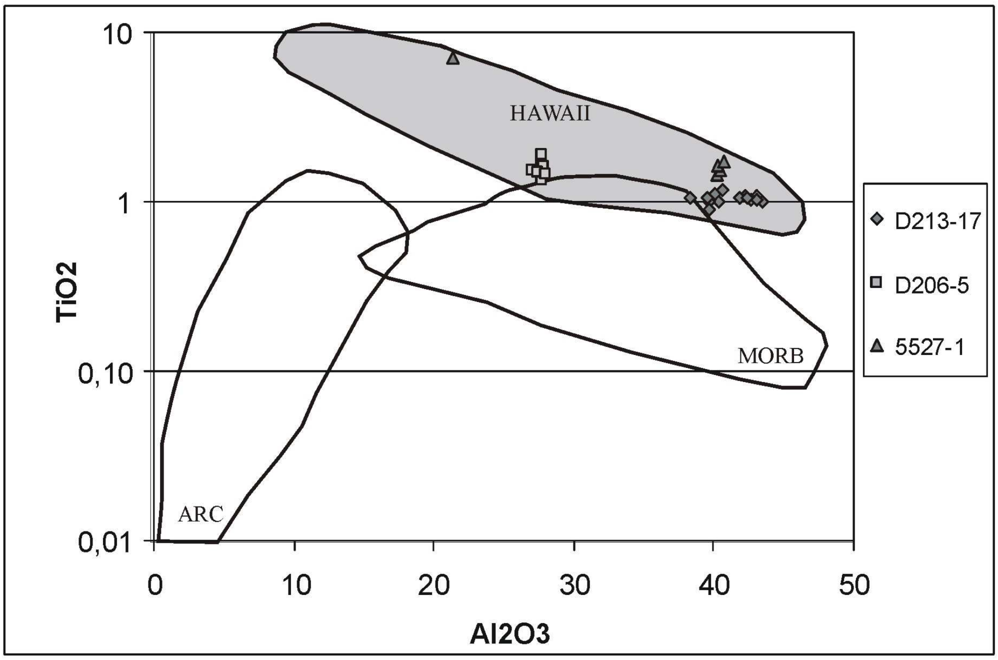

Fig. 6. **Spinel composition of spinels from Kamchatsky Mys Cretaceous basalts.**

Samples D213-17, D206-5 and 5527-1 correspond to number of samples in the table 2. Spinels from basalts of different geodynamic situations: ARC - island arcs, MORB - mid-ocean ridges (by V.S. Kamenetsky et al [9]), Hawaii – from alkali rocks of Hawaii (by A.V.Sobolev and I.K.Nikogosian [25]).

Table 2.

Chemical composition of spinel in alkali and enriched basalts from Kamchatsky Mys Peninsula (in weight per cent).

	1	**2**	**3**	**4**	**5**	**6**	**7**	**8**	**9**	**10**
SiO_2	0.55	0.65	1.15	0.61	1.29	0.34	0.00	0.00	0.00	0.86
TiO_2	1.01	1.08	0.99	1.03	1.09	0.99	0.91	1.06	1.11	1.05
Cr_2O_3	21.04	18.64	18.09	18.23	18.55	20.98	20.28	21.02	21.54	18.59
Al_2O_3	40.32	43.11	43.43	42.60	42.20	39.67	39.74	38.36	40.02	41.78
FeO*	21.41	21.24	20.85	21.26	20.72	21.51	21.42	23.46	22.01	21.36
MnO	0.21	0.15	0.17	0.13	0.14	0.18	0.11	0.16	0.32	0.17
MgO	13.43	14.76	14.14	14.26	13.69	13.59	15.54	15.46	14.37	13.89
NiO	0.19	0.24	0.30	0.28	0.19	0.22	0.23	0.22	0.19	0.23
ZnO	0.13	0.00	0.00	0.00	0.05	0.00	0.00	0.00	0.09	0.09
Total	98.43	99.92	99.19	98.51	98.00	97.54	98.29	99.79	99.71	98.12

	11	**12**	**13**	**14**	**15**	**16**	**17**	**18**	**19**	**20**
SiO_2	0.54	1.27	0.35	0.37	0.08	0.07	0.11	0.10	0.09	0.08
TiO_2	1.06	1.04	1.06	1.18	1.52	1.33	1.50	1.91	1.65	1.62
Cr_2O_3	18.81	17.67	21.15	19.77	32.72	31.71	31.74	33.29	32.79	33.15
Al_2O_3	42.43	43.04	39.50	40.63	26.98	27.69	27.82	27.68	27.68	27.85
FeO*	20.80	20.34	21.64	22.63	22.03	22.32	21.77	22.24	21.64	22.48
MnO	0.14	0.18	0.22	0.27	1.09	0.97	0.98	1.46	1.22	1.22
MgO	13.99	14.05	13.35	14.52	13.92	13.78	14.22	14.00	14.53	13.71
NiO	0.24	0.21	0.30	0.26	0.39	0.24	0.42	0.25	0.30	0.23
ZnO	0.02	0.16	0.04	0.00	0.21	0.15	0.17	0.15	0.23	0.22
Total	98.10	98.02	97.69	99.73	99.10	98.41	98.92	101.49	100.52	101.01

	21	**22**	**23**	**24**	**25**	**26**	**27**	**28**
SiO_2	0.08	0.09	0.00	0.00	0.84	0.00	0.00	0.01
TiO_2	1.50	1.45	1.46	1.65	7.00	1.59	1.58	1.73
Cr_2O_3	32.87	32.53	22.12	21.23	19.13	20.54	19.88	19.07
Al_2O_3	27.49	27.98	40.26	40.71	21.37	40.56	40.78	40.66
FeO*	21.43	21.67	21.07	21.42	41.18	22.12	23.20	23.85
MnO	1.12	1.12	0.18	0.13	0.59	0.19	0.22	0.16
MgO	14.03	14.49	16.80	17.24	8.90	16.58	15.38	15.57
NiO	0.43	0.30	0.01	0.00	0.00	0.09	0.05	0.05
ZnO	0.18	0.23	0.10	0.05	0.29	0.06	0.04	0.06
Total	99.61	100.41	102.00	102.54	99.92	101.89	101.23	101.41

Note. FeO* - total iron. 1 – 14 – spinel in alkali basalt (sample D213-17), 15 – 22 – spinel in enriched basalt (sample D206-5), 23 – 28 – spinel in olivene alkali basalt (sample 5527-1). Mineral analyses were carried out in polished thin section on an electron microanalyzer “Camebax-244” at the Institute of Volcanology and Seismology, Petropavlovsk-Kamchatsky. Analyses were carried out by Filosofova T.M., 2003 and 2005.

Geodynamic conditions of the formation. Geochemical characteristics of the volcanic rocks, spinels from the basalts and melt inclusions allow us relating the formation of the ophiolite assemblage to mantle plume activity. The compositional heterogeneity of the investigated basalts is a consequence of their formation in the middle-oceanic rift above mantle plume. Detroit and Meiji seamounts of the Emperor Chain are the nearest to Kamchatka. The age of these seamounts is 81 and 85 Ma (Fig. 2). The age of jaspers and limestones in association with basalts from the Kamchatsky Mys is about 100 Ma. The Kamchatsky Mys ophiolite can, thus, represent the oldest and presently unknown fragments of the Emperor Seamount Chain accreted to Kamchatka. The formation of the ophiolite assemblage from the Kamchatsky Mys can be related to Cretaceous activity of the Hawaiian mantle plume.

CENOZOIC “INTRA-PLATE” LAVAS

Occurrence of «intra-plate» lavas. Besides Cretaceous intra-plate lavas in the Kamchatsky Mys Peninsula, Late Cenozoic lavas with intra-plate geochemical characteristics were documented in the central part of Kamchatka (Fig. 1). These lavas were first discovered and studied by O.N.Volynets [31]. The «intra-plate» lavas form small cinder cones and outcrops among predominant typical arc-type lavas and have no direct connection to any modern mantle plume. They include both sub-alkaline and alkaline types and classified into four series (Fig. 1). The oldest of them (Late Miocene) are represented by K-Na alkali basalts from the Eastern Kamchatka. Magnesian K-rich alkali basalts and associated shoshonite-latites are found in the Western Kamchatka have nearly the same age (Late Miocene – Pliocene). Pliocene – Early Pleistocene transitional basalts and comendites take place in the Sredinny Range of Kamchatka. K-Na alkali olivine basalts were erupted in Pliocene in the Eastern Kamchatka and in Late Pleistocene – Holocene in the Sredinny Range of Kamchatka [31].

Geological setting of the «intra-plate» lavas is pre-determined by an evolution of the Cenozoic volcanic arcs of Kamchatka and geodynamics of the Kamchatka-Aleutian junction. Three volcanic arcs of different age were formed within the Kurile - Kamchatka Island Arc System: Western Kamchatkan Arc (Eocene); Middle-South Kamchatka – Kurile Arcs (Late Oligocene – Quaternary) and the present-day Kurile - Kamchatkan Arc [3]. The evolution of two young Kamchatkan arcs is shown on (Fig. 7, 8).

Beginning from the end of Oligocene, a system of two subduction-related volcanic arcs (Middle and South Kamchatka – Kurile Arcs) connected with frontal tectonic arcs and deep-sea trenches existed in the Kurile – Kamchatkan region. The formation of this system was caused by the subduction of the Pacific plate to the south from the Kamchatka-Aleutian junction and the subduction of Komandorsky plate in the north. These arcs are marked in the present-day structure by their volcanic rock associations and by gravity anomalies in the frontal tectonic arc [3]. At the end of Miocene, the subduction of the Pacific Plate within the segment between the Kamchatka-Aleutian junction and the Shipunsky Peninsula was blocked by the accretion of the East Kamchatka Peninsulas. This resulted in east-

---

ward «jumping» the subduction zone to its present-day position, and beginning formation of the Eastern Kamchatka volcanic arc.

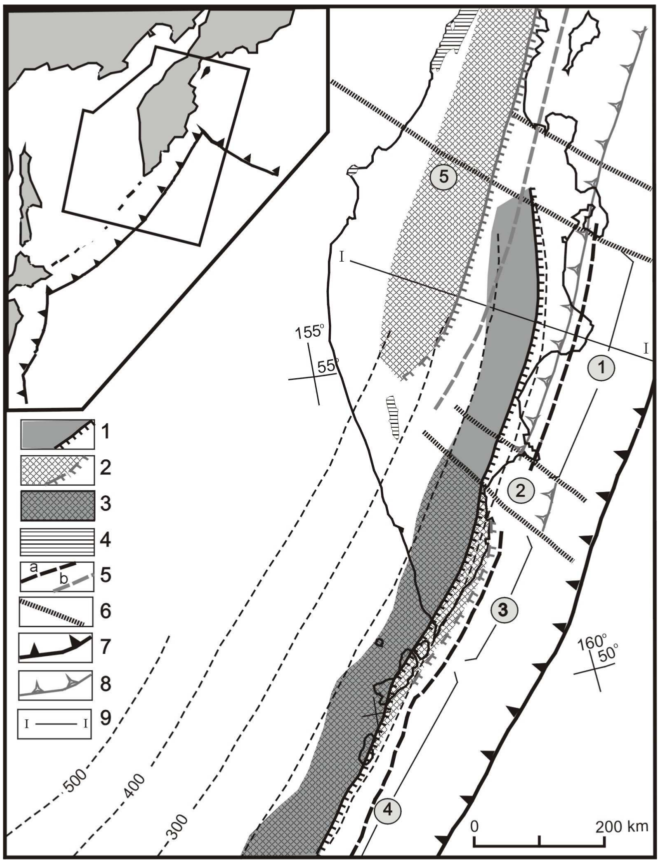

Fig. 7. **Relative location of volcanic arcs of different ages in the Kurile-Kamchatkan Island Arc system (after Avdeiko et al. [3], 2002 with addition).**

1 – East Kamchatka part of the present-day volcanic arc and its volcanic front; 2 – Neogene volcanic arcs of the Sredinny Range, South Kamchatka, and Kuriles and their volcanic fronts; 3 – Kurile – South Kamchatka part of the present-day volcanic arc; 4 – fragments of the Western Kamchatka Paleogene volcanic arcs; 5 – frontal (tectonic) arcs of the present-day (a) and Neogene (b) island arcs; 6 – main transverse zones, which probably were transform faults in the Neogene; 7 – the axes of the present-day Kurile-Kamchatka Trench; 8 – an axes of reconstructed Neogene Mid-Kamchatka trench; 9 – location of the model cross-section in Fig. 7. Numbers in circles indicate segments (arcs) of the system: (1) East Kamchatka, (2) Malka-Petropavlovsk zone of transverse faults, (3) South Kamchatka, (4) North Kuriles, (5) – Mid-Kamchatkan arc.

Some regularity can clearly be recognized in the distribution of lavas of the intra-plate geochemical type. (1) All «intra-plate» lavas occur only within the segment, where the «jump» of subduction zone took place. (2) All «intra-plate» lavas have been formed after the «jump» of subduction zone. (3) The initiation of «intra-plate» volcanism was nearly simultaneous in the East and West Kamchatka. (4) «Intra-plate» lavas are characteristic only for the initial stage of subduction beneath the Eastern Kamchatka. At first, K-Na alkali basalts (Late Miocene) and then K-Na alkali olivine basalts (Pliocene) were erupted. (5) «Intra-plate» lavas were formed during all time of the terminated stage of the Mid-Kamchatkan arc from the end of Miocene until Holocene. We can see a next consecution. At first, Late Miocene – Pliocene magnesian K-alkali basalts were erupted in the West Kamchatka, which was a rear zone of the Mid Kamchatkan volcanic arc. Then, K-Na transitional basalts and comendites (Pliocene – Early Pleistocene) and K-Na alkaline olivine basalts (Late Pleistocene – Holocene) were erupted.

Chemical composition. Chemical composition of Kamchatka arc-type lavas including intra-plate geochemical type lavas was studied by O.N.Volynets [31]. Main peculiar geochemical feature of the intra-plate lavas is high Ti and LILE-concentrations and especially high Ta and Nb concentrations in comparison with arc-type lavas. Arc lavas have distinct Ta-Nb minima in the normalized to the pri

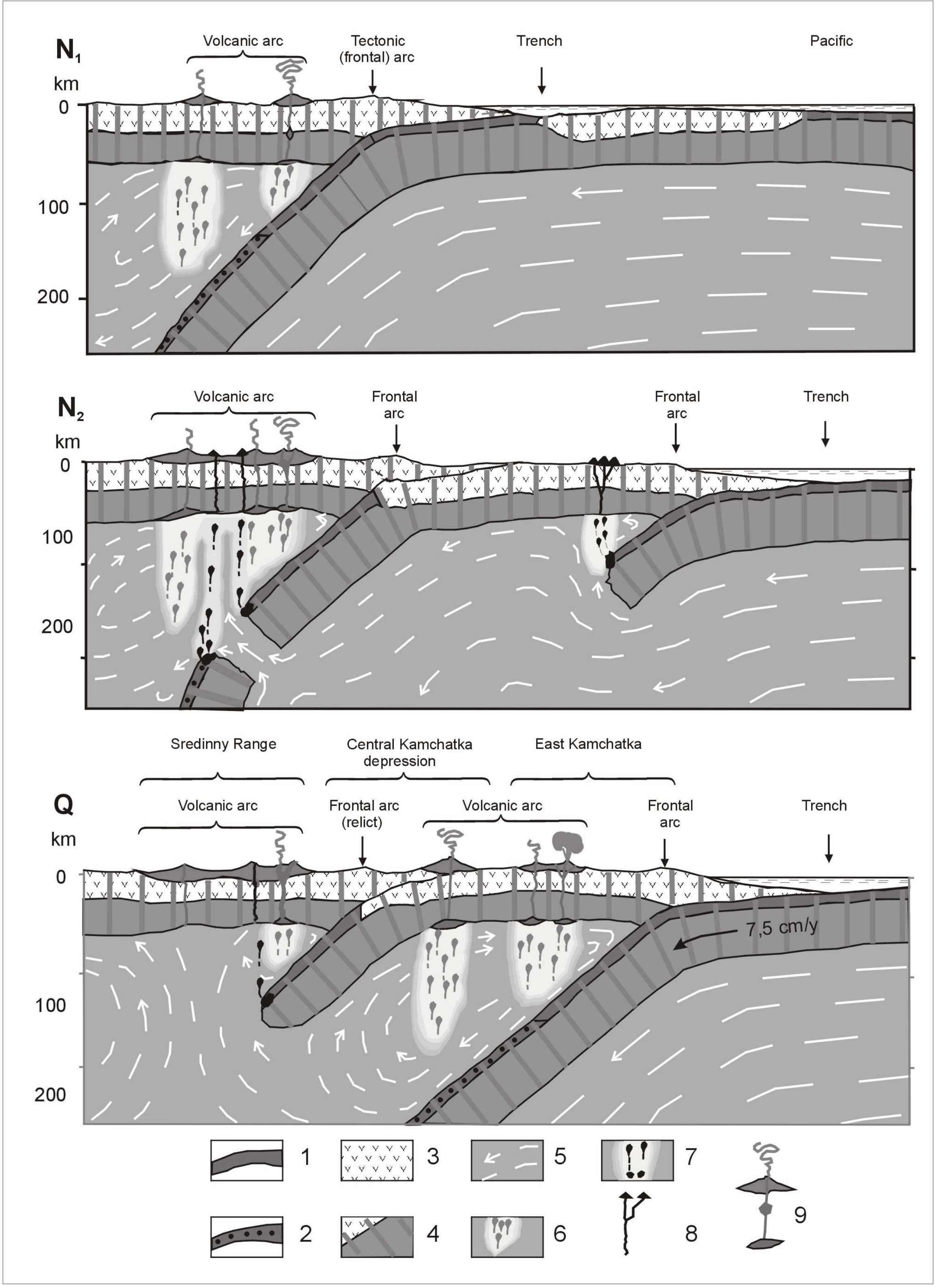

Fig. 8. **Model cross-sections of evolution of the Kurile-Kamchatka island arc system (after Avdeiko et al. [2]. See Fig. 7 for location of cross-sections.**

1 – oceanic crust, 2 – eclogites, 3 – continental crust, 4 – lithosphere, 5 – astenosphere (arrows indicate direction of the convection currents), 6- magma generation zones for typical island arc magmas, 7 – melt and rise zones of the intraplate geochemical type magmas, 8 – channelways of rises

of the “intraplate” magmas, 9 – volcanoes, magma chambers, and channelways of the typical island arc magmas.

mordial mantle trace-element patterns, whereas “intra-plate” lavas have no or very subtle Ta-Nb minima (Fig. 9). Ta and Nb concentrations in Kamchatkan “intra-plate” lavas are 5 to 100 times higher than in typical arc-type lavas. Accordingly, they have low La/Ta, La/Nb, Zr/Nb and Th/Ta ratios and high Ta/Yb ratio, which are typical of intra-plate lavas [Volynets, 1994]. All rocks of the intra-plate type are enriched in Zr, Hf, La, Ce and Th, but there are some differences in geochemical characteristics of rocks of different ages from the Eastern Kamchatka, Sredinny Range and the Western Kamchatka (Fig. 1). The two latter are different zones of the Mid-Kamchatkan arc [3].

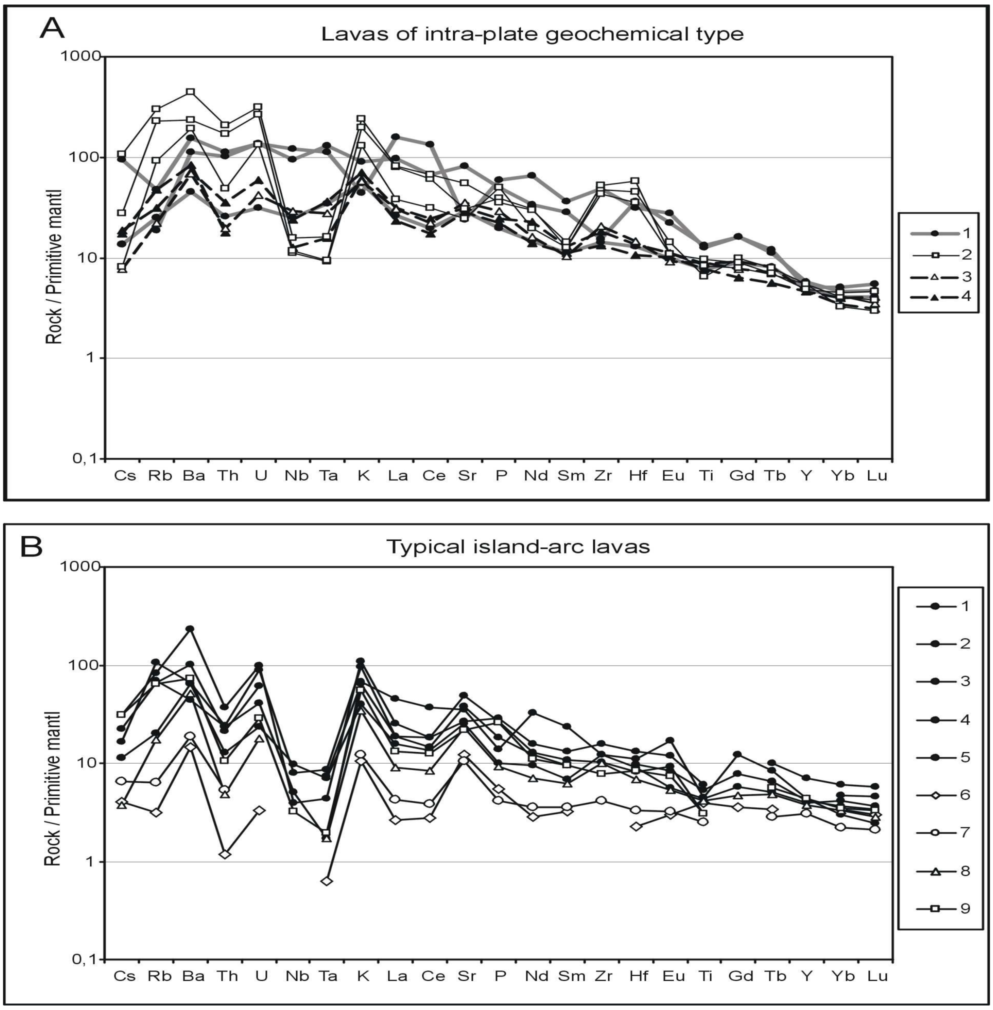

Fig. 9. **Primitive mantle-normalized trace element spidergrams for “intra-plate” (A) and typical (B) island arc lavas of Kamchatka. All analytical data after O.N. Volynets [31, tables 2 and 3].**

A: 1 – Late Miocene K-Na-alkali basalts of Eastern Kamchatka; 2 – Late Miocene K-alkali basalts of Western Kamchatka; 3 – Pliocene K-Na Ol-Pl basalt (basalt-comendite series) of Sredinny Range; 4 – Late Pleistocene-Holocene K-Na alkali basalts.B: 1 – 4 – Sredinny Range Lavas: 1 – Ol-Pl basalt from cinder cone in Ichinskaya zone, 2 – Ol-Cpx-Pl basalt, Kekuknaysky volcano, 3 – plagiophiric basalt, Tekletunup volcano, 4 – Ol-Cpx-Pl basalt, Bolshaya Ketepana volcano; 5 – Ol-Cpx- basalt, Chink cinder cone; 6 – Ol-Pl basalt (avachite), Avachinsky volcano; 8 – Ol-Pl basalt, Kharchinsky volcano, 9 – Phl-Amph-Cpx-Ol basalt, Shiveluch volcano.

Model of "intra-plate" magmas generation. The problem of a generation of the intra-plate geochemical type magmas within island arcs was discussed in some papers [15, 20, 23, 31]. A.E. Ringwood [23] proposed that intra-plate magmas can form in two principal locations within the upper mantle. One of these is located between subducted lithosphere and overlying mantle wedge, and the source of magma enrichment in Nb, Ta, Ti as well as LILE is the subducted slab at depths of about 150-300 km. At shallower depths, typical island-arc magmas are generated. The differences in Ti, Nb and Ta concentrations between typical island-arc and intra-plate magmas result from the pressure-dependent stability of rutile, the main carrier of these elements in subducting slab. The relative depletions in Ti, Nb and Ta in typical island-arc rocks *"are attributed to the retention of these elements by residual rutile during partial melting of the upper layers of the subducted oceanic crust at depths of 80-100 km. At greater depths between 150 and 300 km, when the subducted oceanic crust experiences partial melting, rutile is no longer a residual phase. Therefore, Ti, Nb and Ta become highly incompatible and are effectively transferred from the slab into future source regions of intra-plate magmas"* [23, (p.187)]. A second intra-plate magma source can be formed in case when early subducted "*oceanic crust is buoyantly trapped to form a gravitationally stable layer of garnetite situated on top of the 650-km discontinuity*" [23, (p.187)]. Intra-plate magmas are generated as the result of partial melting of this layer top and reaction the resultant liquid with an overlying pirolite forming ascending mantle diapers (mantle plumes). According to model by E.Nakamura and co-authors [15], the intra-plate magmas in island arcs are formed by reaction of mantle plume melts, rising from great depth, with a mantle wedge material. This model is similar to the second A.E. Ringwood model.

O.N.Volynets [31] believed that origin of the Late Miocene – Pliocene magnesian K-alkali basalts located on the West Kamchatka only can be explained by the first Ringwood model. These rocks are characterized by the highest concentrations of LILE and not much higher Ti, Nb and Ta concentrations in comparison with island-arc lavas. They have Ta-Nb-minima, but not so deep as in island-arc lavas (Fig. 9).The appearance of intra-plate lavas in the Sredinny Range of Kamchatka and in the Eastern Kamchatka, he explained by an influence of mantle plumes. Tracks of any mantle plume, however, is absent beneath Kamchatka, though there are Holocene "intra-plate" lavas in the Sredinny Range.

We believe that the appearance of all Cenozoic "intra-plate" lavas along with typical island-arc lavas in Kamchatka can be explained by two Ringwood´s models with some modifications according to our geodynamic model (Fig. 8). Typical island-arc magmas are generated in the mantle wedge under the influence of fluids derived from the subducted slab [28]. Melting of the upper part of subducted plate is impossible, as its temperature at the depths between 100 and 200 km is low. These magmas have low concentrations of Ti, Nb and Ta, because their principal mineral-concentrator, rutile, is poorly soluble in fluids according to experimental data [27]. Partial melting of the oceanic crust eclogite is possible at higher

---

temperatures exceeding 750°C [17], and these melts contain higher Ti, Nb and Ta concentrations, typical for intra-plate lavas. How can the higher temperatures be reached under Kamchatka arc? Perhaps, the appropriate conditions for slab melting could be achieved beneath the East Kamchatka after the subduction zone jump. The melting of the leading edge of the subducted plate could be possible at the contact with hot mantle during the initial subduction of the Pacific plate beneath the East Kamchatka (Fig. 8, cross-section 2).

The beginning of the Sredinny Range "intra-plate" volcanism is coincided in time with the subduction zone "jump". Geodynamic framework for the volcanism can be determined by break-off of the heavy part of the slab at depths more than 100-150 km after the oceanic crust eclogitization. This resulted in intrusion of a hot mantle material from under subduction zone into the void left by the detached slab. This might have been accompanied by melting of the 1st and 2nd layers of the oceanic crust at the contact with this material. First portions of lavas were erupted in Late Miocene in the West Kamchatka. They generated by higher influence of fluids but at higher temperature and therefore they are magnesian with high concentration of LILE and intermediate between island-arc and intra-plate lavas with regard to concentrations of Nb and Ta (Fig. 9). Following portions of "intra-plate" magmas were formed at depths of about 150 km. They have somewhat lower concentration of Ta and Nb then the first lavas and have no Ta-Nb minimum. The most recent (Holocene) lavas are characterized by the lowest of all "intra-plate" lavas LILE-concentrations and have a very small Ta-Nb though.

The scenario is supported by the P-wave seismic tomography data which shows a gap in the subducting Pacific slab at the 450-600 km depths [7, (Fig. 7, cross-section E-E')]. This cross-section located at the central part of Kamchatka, were the jump of subduction zone took place. We believe that the high velocity body on this cross-section at the depth about 600-1000 km is a fragment of the Pacific plate torn away after termination of subduction beneath the Sredinny Range in Miocene. In comparison, there is no a slab gap in the cross-section D-D' located across the Southern Kamchatka, the segment of the Kamchatka arc operating in steady-state regime over last 50 million years.

Besides, the transition from island-arc characteristics to oceanic ones takes place among the Quaternary volcanic rocks of Kamchatka-Aleutian junction, on the northern end of the Central Kamchatka depression. Conditions of their formation have been discussed in the last time by M. Portnyagin et al. [20] and we will not discuss this problem in the paper.

Conclusion

There are two different intra-plate geochemical type lavas in Kamchatka. One of them, viz., Cretaceous basalts of Smagin formation distributed in the Kamchatsky Mys Peninsula are a prolongation of the Hawaiian Emperor Chain and was formed above the Hawaiian mantle plume. Second one, i.e. Late Cenozoic lavas, having intra-plate geochemical characteristics, are located in the East and

West Kamchatka and the Sredinny Range. They were formed in the terminated (Sredinny Range and West Kamchatka) and initial (East Kamchatka) stages of the Mid-Kamchatkan and East-Kamchatkan volcanic arc above different age subduction zones.

Among oceanic basalts from Kamchatsky Mys we determined several geochemical types – from depleted tholeiites up to enriched alkaline basalts. Melt inclusion in spinels from tholeiitic basalts show an even greater depletion of the initial melt. With respect to their geochemical characteristics one part of the investigated basalts is similar to basalts of the Emperor Seamount Chain, and the other one – to MORB. Spinel compositions are similar to spinels from the Hawaiian alkaline rocks. The chemical composition of the minerals is corroborating a conclusion about the similarity of the alkaline basalts from Kamchatsky Mys Peninsula with rocks of ocean island basalts. The age of jaspers and limestones in association with basalts from Kamchatsky Mys is about 100 Ma, which is in good agreement with the connection between the seamount basalt age and the distance to the Hawaiian “hot spot”. All these facts allow us to connect the formation of the ophiolite assemblage from Kamchatsky Mys with the activity of the Hawaiian mantle plume. This complex was formed in the anomalous fragment of the mid-ocean ridge above the Hawaiian mantle plume at the Cretaceous period. It obviously had positive buoyancy and was obducted and accreted to Kamchatkan edge of the Eurasian plate.

The appearance of Cenozoic lavas with intra-plate geochemical characteristics we expended by a partial melting of the 1-st and 2-nd layers of the subducted oceanic crust at higher temperatures in comparison with ones at the origin of typical island arc magmas. This melt with high concentrations of Nb, Ta, Ti and LILE is raised to the zone of generation of magmas in the mantle wedge. Such high temperature conditions can be at the initial and terminated stages of subduction. At the initial stage the leading edge of the subducted plate has contact with the hotter mantle (more then 1000^0C) than in steady-state regime of subduction (about 650^0C) [2]. At the terminated stage of subduction beneath the Sredinny Range the heavy lower part of the Pacific plate evidently was torn off and sunk into mantle. As a result a hot under-subduction mantle was intruded into the formed gap, melting an upper part of the subducted slab. So, the difference between “intra-plate” and typical island arc lavas can be explained by addition of a subduction component either by melt or by fluid, accordingly.

Thus, intra-plate geochemical type lavas can form not only within plate. They can generat at different geodynamic conditions: (1) above the mantle plume within plate (e.g. present-day Hawaiian one), (2) on the plate edge near spreading rift zone (e.g. Cretaceous Hawaiian and present-day Icelandic plumes), (3) and also above the subduction zones at the high temperatures at the initial and terminated stages of their evolution.

Acknowledgements. The authors are grateful to Dr. M. Portnyagin for helpful comments and constructive criticism. ***This research was funded by FED RAS grant 05-III-08-110 and Russian-German Project KOMEX-II.***

REFERENCES

1. **Avdeiko G.P**., 1980. On possible prolongation of the Hawaiian-Emperor chain in Kamchatka // Jackson E.D., Koisumi I et al. Initial Reports of Deep Sea Drilling Project. Washington D.C., v.55, p.851-854.
2. **Avdeiko G.P., Palueva A.A**., 2003. Geodynamic condition of magma generation of the Kurile-Kamchatkan Island Arc System. In: Volcanism and geodynamics. Proceeding of 2nd Russian sumposium on volcanology and paleovolcanology. Ekaterinburg. P. 164-169 (in Russian)
3. **Avdeiko G.P., Popruzhenko S.V. and Palueva A.A.**, 2002. The Tectonic Evolution and Volcano–Tectonic Zonation of the Kuril–Kamchatka Island-Arc System // *Geotectonics*, v. 36, № 4, p. 312-327.
4. **Boyarinova M.E., Veshnyakov N.A., Korkin A.G., Savelyev D.P**., 1999. Expository report for State geological map, scale 1:200 000, series Estern-Kamchatikan, lists O-58-XXVI, XXXI, XXXII. Sankt-Peterburg, 267 p (in Russian).
5. **Fedorchuk A.V., Vishnevskaya V.S., Izvekov I.N. and Rumiantzeva Yu.S.**, 1989. New data on cherts and volcanics of the Kamchatsky Mys Peninsula // Reports of High School. Geol., v.11, p. 27-33 (in Russian).
6. **Fedorchuk A.V.**, 1992. Oceanic and back-arc basin remnants within accretionary complexes: geological and geochemical evidence from Eastern Kamchatka // Ofioliti, № 17 (2), p. 219–242.
7. **Gorbatov A., Vidiyantoro S., Fukao Y. and Gordeev E.**, 2000. Signature of remnant slabs in the North Pacific from P-wave tomography // Geophys. J. Int., v.142, p.27-36.
8. **Huang S., Regelous M., Thordarson T., Frey F. A**., 2004. Petrogenesis of lavas from Detroit Seamount: Geochemical differences between Emperor Chain and Hawaiian volcanoes // Geochem. Geophys. Geosyst, Q01L06 doi:10.1029/2004 GC000756.
9. **Kamenetsky V.S., Crawford A.J., Meffre S**., 2001. Factors Controlling Chemistry of Magmatic Spinel: an Empirical Study of Associated Olivine, Cr-spinel and Melt Inclusions from Primitive Rocks. // J. Petrology, vol. 42, p. 655-671.
10. **Keller R.A., Fisk M.R., White W.M.**, 2000. Isotopic evidence for Late Cretaceous plume-ridge interaction at the Hawaiian hotspot // Nature, vol. 405, p. 673-676.
11. **Keller R.A., Graham D.W., Farley K.A., Duncan R.A. and Lupton J.E.**, 2004. Cretaceous-to-recent record of elevated 3He/4He along the Hawaiian-Emperor volcanic chain // Geochem. Geophys. Geosyst., Q12L05, doc:10.1029/2004GC 000739.
12. **Khotin M.Yu.**, 1976. Extrusive-tuffaceous-siliceous formation of the Kamchatsky Mys. Moskow: Nauka, 196 p (in Russian).
13. **Morgan W.J**., 1971. Convection plumes in the lower mantle // Nature, v. 230, p. 42-43.
14. **Morgan W.J**., 1972. Deep mantle convection plumes and plate motions // Amer. Assoc. Petrol. Geol. Bull, v. 56(2), p. 203-213.
15. **Nakamura E., McCulloch M.T. and Campbell I.N**., 1990. Chemical geodynamics in the back-arc region of Japan based on the trace element and Sr-Nd isotope component // Tectonophysics, v.174, p. 207-233.
16. **G.V Nesterenko., Ariskin A.A.**, 1993. Depths of crystallization of the basalt magma // Geochemistry, № 1, p. 77-88.

17. **Peacock, S.M., Rushmer, T., Thompson, A.B**., 1994. Partial melting of subducting oceanic crust. *Earth and Planetary Science Letters*, v. 121, p. 227-244.
18. **Pearse J.A., Cann J.R.**, 1973. Tectonic setting of basic volcanic rocks determined using trace element analysis // Ibid., vol. 19, №. 2, p. 290-300.
19. **Pears J.A., Norry M.J**., 1979. Petrogenetic implications of Ti, Zr, Y and Nb variations in volcanic rocks // Contribs Mineral. and Petrol., vol. 69, № 1, p. 33-47.
20. **Portnyagin M.V., Hoernle K., Avdeiko G.P., Hauff F., Werner R., Binderman I., Uspensky V.S., Garbe-Schonberg D.**, 2005. Transition from arc to oceanic magmatism at the Kamchatka-Aleutian junction // Geology, v. 33, № 1, p.25-28.
21. **Portnyagin M.V., Savelyev D.P., Hoernle K.**, 2005. Association of plume-related Cretaceous oceanic basalts from the Eastern Kamchatka: compositional peculiarities of spinel and parental magmas // Petrology (in press).
22. **Regelous M., Hofman A.W., Abouchami W., Galer S.J.G**., 2003. Geochemistry of lavas from the Emperor Seamounts, and the geochemical evolution of Hawaiian Magmatism from 85 to 42 Ma // Journal of Petrology, vol. 44, p. 113-140.
23. **Ringwood A.E.**, 1990. Slab-mantle interactions. 3. Petrogenesis of intraplate magmas and structure of the upper mantle // Chem.Geol., v.82, p.187-207.
24. **Savelyev D.P**. 2003. Intraplate alkali basalts in the Cretaceous Accretionary Complex of the Kamchatkan Peninsula (Eastern Kamchatka) // Volcanology and seismology, N1, p.14-20 (in Russian).
25. **Sobolev A.V., Hofmann A.W., Nikogosian I.K.**, 2000. Recycled oceanic crust observed in 'ghost plagioclase' within the source of Mauna Loa // Nature, v. 404, p. 986-990.
26. **Sobolev A.V., Nikogosian I.K**., 1994. Petrology of long-lived mantle plume magmatism: Hawaii (Pacific) and Reunion Island (Indian Ocean) // Petrology, v. 2, p. 111-144.
27. **Tatsumi Y., Hamilton D.L., Nesbitt R.W.**, 1986. Chemical characteristics of the fluid phase released from a subducted lithosphere and the origin of arc magmas: wevidence from high pressure experiments and natural rocks // J. Volcanol. Geotherm. Res., v. 29, №1-4, p. 293-309.
28. **Tatsumi Y.**, 1989. Migration of fluid phases and genesis of basalt magmas in subduction zones // J. Geophys. Res., vol. 94, № B4, p. 4697-4707.
29. **Tikhomirova S.R**. Late Cenozoic teschenite of Eastern Kamchatka // Reports of Acad. Sci. USSR, 1994. V. 335. № 5. P. 626-629 (in Russian).
30. **Tracy R.J. and Robinson P.**, 1977. Zones titanian augite in alkali olivine basalt from Tahiti and the nature of titanium substitution in augite // Amer. Miner., vol. 62., p. 634-645.
31. **Volynets O.N.**, 1994. Geochemical types, petrology and genesis of Late Cenozoic volcanic rocks from the Kurile-Kamchatka island-arc system. //Intern. Geol. Rev., vol. 36, p. 373-405.
32. **Wilson J.T**., 1963. A possible origin of the Hawaiian Island // Canadian J. Physics, v. 41, p. 863-870.
33. **Wood D.A.**, 1979. A variably veined suboceanic upper mantle – genetic significance for mid-ocean ridge basalts from geochemical evidence // Geology, v. 7, p. 499-503.
34. **Zinkevich V.P., Constantinovskaya E.A., Tsukanov at al**., 1993. Accretion tectonic of Eastern Kamchatka. Moskow: Nauka, 293 p.

UDK 550.42; 552.111

Geochemical diversity in oceanic basalts of the Zasurin Formation, NE Altai, Russia: trace element evidence for mantle plume magmatism

Safonova I.Yu., Buslov M.M.

Institute of Geology, SB RAS, 630090, Koptyuga ave. 3, Novosibirsk, Russia; inna@uiggm.nsc.ru

Diverse types of basalts are present in the 370-350 Ma Charysh-Terekta ophiolitic strike-slip zone of East Kazakhstan as tectonic sheets and fragments. LREE-depleted, transitional and LREE-enriched basalts coexist within this geological structure. LREE-depleted tholeiitic basalts have variably depleted LREE, flat to weakly fractionated HREE patterns (La/Sm_n=0.6-1.0, Gd/Yb_n=1.1-1.3) and negative Nb and Th anomalies (Nb/La_{pm}=0.37-0.8, Th/La_{pm}=0.4-0.85). Transitional basalts have less fractionated REE, positive Nb and negative Th anomalies relative to La (Nb/La_{pm}=1.2-1.4, Th/La_{pm}=0.2-0.9). LREE-enriched basalts are the prevalent volcanic rock type characterized moderately to strongly fractionated HREE patterns (La/Sm_n=1.9-2.8, Gd/Yb_n=1.5-2.5), positive Nb and mostly negative Th anomalies (Nb/La_{pm}=1.04-1.57, Th/La_{pm}=0.6-1.09). Mg# varies from 56 to 20 over a relatively narrow range of SiO_2 (46-52 wt%). Iron, Zr, Nb, Y, LREE Ti, Cr, Ni and Th variably decrease with Mg#. Compositionally, these volcanic rocks are similar to Cenozoic basalts of the Hawaiian hot spot. Mantle melting processes, crust contamination, or fractional crystallization can be ruled out as the main cause of anomalies except for the moderate effect of alteration and metamorphism on the major-element composition of basalts. The anomalies may be rather interpreted as a result of the lithosphere material recycling into the mantle: recycled ocean crust processes through a subduction zone having positive Nb anomalies, and complementary recycled subarc mantle having negative Nb anomalies. Enriched basalts show stronger REE fractionation (La/Yb_n=6-9), higher positive Nb anomalies, like Phanerozoic HIMU ocean island basalts, than transitional counterparts (La/Yb_n=3-4), and also higher Al_2O_3 contents with convex-up trace-element patterns through Th-Nb-La. Both varieties have higher Zr/Hf ratios than depleted basalts. The LREE-depleted basalts are interpreted to have been a mid-oceanic ridge and LREE-enriched basalts – an oceanic island derived from a heterogeneous multi-component plume. The absence of negative Zr (Hf) anomalies suggests rather a spinel-facies depth of melt segregation in the mantle at a depth of < 400 km, whereas the depleted basalts melted at even shallower depths in the entrained upper mantle. The oceanic island was fragmented in a collision-accretion complex and tectonically mixed with underlying MOR tholeiites.

Key words: collision-accretion zone, mantle plume, trace elements, basalts, oceanic plateau/island

INTRODUCTION

In recent years, numerous oceanic crust fragments have been found and identified in accretionary and strike-slip zones of different ages recognized within the Altai-Sayan foldbelt. The fragments of ophiolite, oceanic islands and seamounts are less common in foldbelts than those of island arcs that may be explained by their subduction or poor identification in structures comprising numerous tectonically mixed sedimentary and basaltic-sedimentary terranes (Buslov, Watanabe, 1996; Dobretsov et al., 2004a,b).

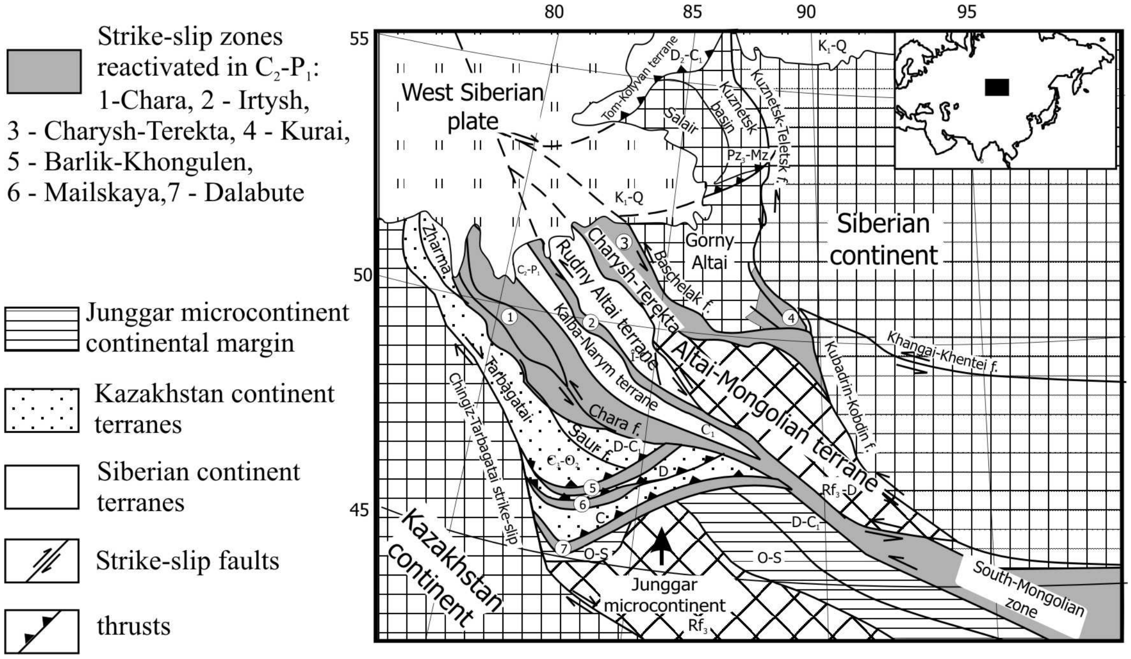

Fig. 1. **The collisional zone between the Siberian and Kazakhstan continents comprising Late Cambrian-Permian terranes and strike-slip zones. Modified from Buslov et al. (2001).**

The paper presents new geochemical data on Late Cambrian-Early Ordovician volcanic rocks occurring within the Charysh-Terekta strike-slip zone of North-West Altai-Sayan. The Charysh-Terekta strike-slip zone was formed as a result of the Late Devonian collision of the Gondwana-derived Altai-Mongolian microcontinent and Siberian continent (Fig. 1). The geological structure of the Charysh-Terekta zone comprising the Zasurin Unit with oceanic crust fragments was discussed in Buslov et al. (1999, 2000, 2001) and Safonova et al. (2004). Biostratigraphy of associated oceanic siliceous sedimentary rocks was reported in Iwata et al. (1997) and Sennikov et al. (2003).

GEOLOGICAL SETTING

The tectonic structure of the Altai-Sayan foldbelt is a collage of terranes of different ages separated by numerous large-scale thrusts, strike-slip faults and nappes (Dobretsov and Zonenshain, 1985; Zonenshain et al., 1990; Buslov et al., 1993, 2003; Berzin and Dobretsov, 1994; Dobretsov et al., 1995). The terranes are classified mainly based on Vendian-Cambrian geodynamic units of the Paleo-Asian Ocean. Fig. 1 shows the major structural units that form part of the Central Asian foldbelt, within the area between the Kazakhstan and Siberian continental blocks – western Altai-Sayan segment. The tectonic pattern of the western Altai-Sayan comprises the Gondwana-derived Altai-Mongolian terrane separated from the margins of the collided continents by systems of strike-slip faults (see Chingiz-Tarbagatai, Chara, Irtysh, and Charysh-Terekta faults in Fig. 1). The northwestern part of Altai belongs to a reactivated suture zone which extends into the Gondwana-derived Altai-Mongolian terrane (Fig. 1).

The Charysh-Terekta strike-slip zone in NW Altai extends over a distance of 120-130 km and consists of five deformed structural units (from west to east): Inya, Kur'ya-Akimov, Charysh, Zasurin, and Talitsa. The structural units which occur as structural sheets and lenses bounded by the late Carboniferous-Permian North-Eastern and Bashchelak faults (Fig. 1). These units are composed of sandstones, cherts, pillow-basalts, volcanoclastics, and gabbro-diabase sills and dikes (Buslov et al., 2000; Safonova et al., 2004).

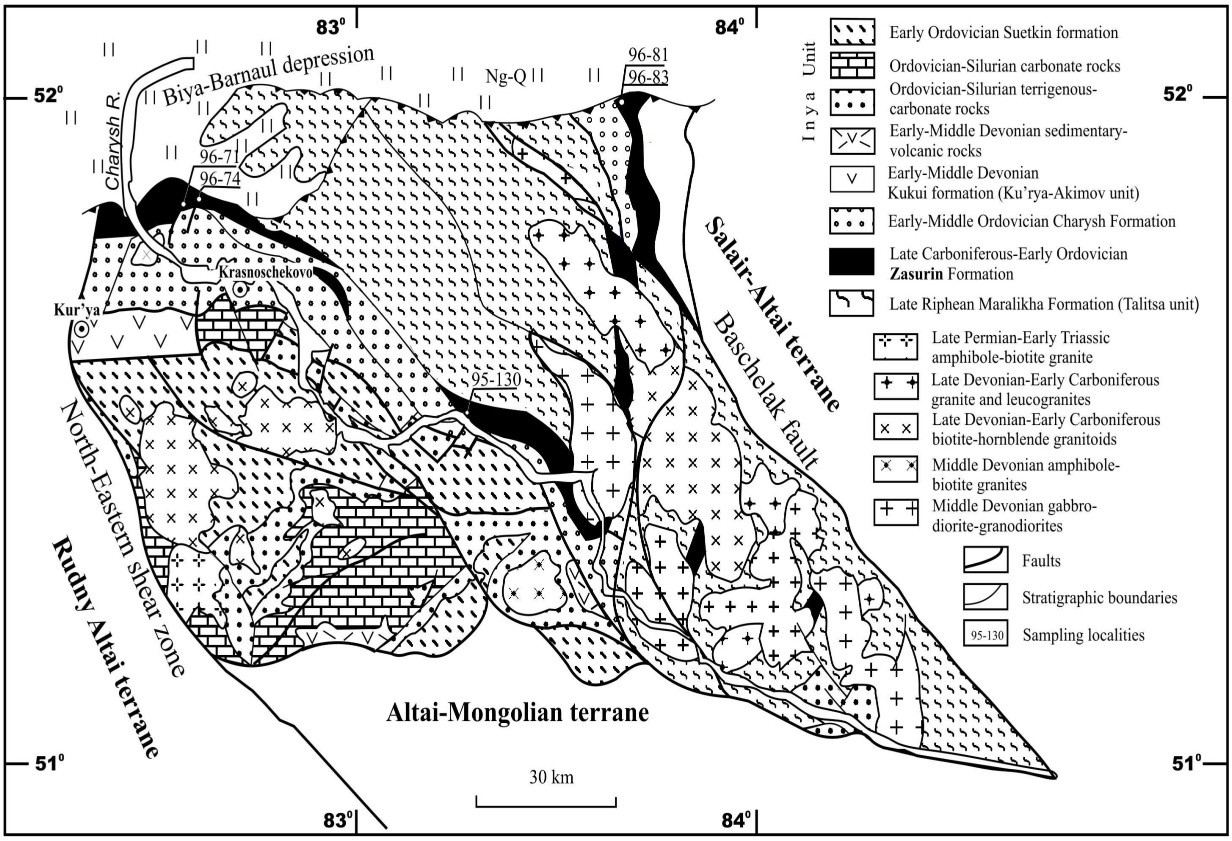

Fig. 2**. Geological map of the Charysh-Terekta strike-slip zone in the north-western Gorny Altai (modified from Buslov et al., 2000).**

The Late Cambrian-Early Ordovician Zasurin Formation is of special interest because it comprises several tectonic lenses consisting of multi-colored sandstones and cherts, variolitic or aphyric pillow-lavas, plagioclase and pyroxene-plagioclase basalts and their volcaniclastic derivatives, gabbro and gabbro-diabase sills and dikes (Fig. 2). The breccia, co-sedimentation and Z-shape folding textural features of the cherts suggest that they represent slope facies of oceanic islands. The Zasurin Formation is characterized by a unique combination of terrigenous, volcanic and siliceous units. The color of the cherts ranges from red and brown to violet, which is typical of present-day seamount slope sedimentation environments. The silica-rich layers are up to several hundred meters thick with individual siliceous beds of 20-30 meters (Sennikov et al., 2003).

The Zasurin Formation consists of three suites: 1) the lower suite of red and gray sandstone-mudstone, cherts, and basalts; 2) the middle suite gray sandstone and siltstone; 3) the upper suite of intercalated red and gray sandstone, chert, tuffs and tuff-sandstone. The stratified cherts of the Zasurin Formation contain Late Cambrian-Early Ordovician pelagic planktonic conodonts, radiolarians with siliceous skeletons and benthonic sponge spicules suggesting the Early Oredovician age of the oceanic basalt-siliceous-terrigenous deposits of the Zasurin Formation (Tremadoc and Arenig stages) (Iwata et al., 1997; Sennikov et al., 2003).

SAMPLING PROCEDURES AND ANALYTICAL METHODS

Samples for geochemical analyses were obtained from the least altered and deformed outcrops of volcanic flows in the Charysh-Terekta zone, along the Charysh and Molchanikha rivers, near Kurya and Krasnoshchekovo villages (Fig. 2). All samples were powdered using a ductile iron mill. Major element oxides were 100±1 wt%.

Except for 5 XRF determinations (performed in the Tokyo Institute of Technology), all analyses were made at the Institute of Geology, SB RAS. Abundances pf the major elements and the trace elements Rb, Sr, Ba, V, Ni, Zn, Ga, Y, Zr, Nb were determined by XRF using a “Nauchpribor” spectrometer (analytical procedure following the Russian state analytical standard OST-41-08-212-82 Mingeo SSSR; analyst – A.D. Kireev). Abundances of Sc, Cr, Co, Hf, Ta, Th and several rare earth elements were determined by instrumental neutron activation at the Institute of Geology SB RAS (analyst V.A. Bobrov) using Ge detectors for Y-rays higher that 30 KeV and below 2000 KeV.

Selected element ratios are normalized to primitive mantle such that zero fractionation represents 1 (e.g. primitive mantle $Nb/Th_{pm}=1$). Hf/Hf* ratios are calculate as for Eu/Eu*, following the method of Taylor and McLennan (1985), but Ti/Ti* was referenced to Sm and Gd.

PETROGRAPHY

Most basalts are relatively fresh containing chloritized clinopyroxene and saussuritized plagioclase and preserved original igneous textures. In their more highly metamorphosed counterparts, chlorite, calcite and epidote are abundant. Oxide minerals, principally magnetite and rarely spinel are present as accessory phases. Carbonatization or silicirication are moderate to sparse, contributing up to three to five modal per cent late carbonates and quartz respectively in some samples. The mafic volcanic rocks range from pillow basalts and massive flows to sills and dikes. In greenschist facies metamorphosed rocks, chlorite and epidote are the dominant minerals. No their amphibolite facies equivalents have been found.

Table 1.

Major (wt%) and trace (ppm) element composition of Zasurin basalts from the Charysh-Terekta strike-slip zone of NE Altai, Russia

	depleted basalts			transitional basalts			enriched basalts						
Sample	**96-81**	*Г-2921*	**97-120-**	**96-83**	**97-120**	**Е-2921**	**96-71**	**96-72**	**Б-292**	**В-292**	**96-74**	**97-120**	**95-13**
SiO_2	48.15	47.93	48.93	46.4	45.91	48.2	49.05	52.37	46.5	47.1	48.10	43.98	46.4
TiO_2	1.96	1.56	1.32	2.04	2.79	1.99	2.73	2.71	3.19	2.71	3.46	4.05	2.39
Al_2O_3	13.78	13.72	13.74	14.3	15.3	16.1	14.08	14.7	19.4	17.7	13.97	16.64	18.7
Fe_2O_3	14.15	13.89	9.68	12.4	13.19	12.14	16.87	15.37	14.1	11.2	11.96	14.71	8.46
MnO	0.26	0.21	0.2	0.22	0.18	0.2	0.08	0.14	0.15	0.17	0.28	0.27	0.11
MgO	6.99	7.45	8.35	8.57	7.72	6.79	2.49	1.97	2.29	7.25	5.90	4.05	5.5
CaO	10.91	9.77	9.66	8.20	8.11	8.08	4.70	4.25	3.18	3.59	6.12	7.24	8.8
Na_2O	2.14	2.27	2.46	2.85	2.5	2.73	4.89	3.15	2.14	3.28	3.79	3.22	2.85
K_2O	0.13	0.24	0.41	0.92	0.36	0.76	2.82	3.25	5.37	2.16	0.08	0.22	0.65
P_2O_5	0.16	0.16	0.18	0.20	0.38	0.27	0.72	0.75	0.57	0.47	0.72	0.48	0.61
L.O.I.	2.7	2.77	5.06	3.44	3.49	2.77	1.94	1.35	2.83	4.15	5.62	5.02	4.92
Total	101.3	99.97	99.99	99.6	99.93	100.0	100.3	100.01	99.9	99.9	100.0	99.88	99.4
Mg	49.71	51.75	63.31	57.9	53.93	52.80	22.79	20.40	24.4	56.3	49.66	35.51	56.5
Cr	100	43	230	93	183	225	78	53	160	87	48		
Co	52	49	44,3	53	43	46,2	26	28	35,7	35,7	30	38	
Ni		56	78		99	99			129	28		29	
Sc	57	48	50	48	42	36	38	35	31	22	29	24	
V		277	224		359	223			386	291		513	
Ta	0.37	0.26	0.07	0.8	1.51	1.12	3	3.2	3.16	2.64	3	1.87	
Nb	5	5	1	19	27	21	54	65	59	50	47	35	
Zr	112	85	84	160	191	124	330	565	259	222	310	239	
Hf	3.2	2.3	2.2	3.5	4.7	3.4	12	12	6.4	5.4	6.2	6	
Th	0.3	0.4	0.3	0.4	1.62	1.4	3.7	4.3	4.5	3.5	3.5	2.5	
Y	40	34	33	32	42	32	54	82	45	34	40	40	
Rb	4	3	10	13	7	18	27	40	124	35	6	11	
Sr	230	144	97	490	425	338	300	360	135	403	408	321	
Ba	30	120	138	500	209	382	320	550	557	905	95	200	
La	6	5.6	2.9	15	18.9	12.7	50	40	33.5	29.8	33	24.9	42
Ce	14.5	14.6	8.9	30	41	27.5	100	76	70	56.5	72	54	77
Nd	10	10	9.5	15	26	16.5	65	44	38	29	44	31	24
Sm	4	3.55	3.2	4.5	7.24	4.8	14	12.5	9.7	6.82	9	8.6	5,6
Eu	1.6	1.29	1.11	1.9	2.34	1.62	4.1	3.8	2.98	2.24	3.1	2.88	2,5
Gd	6	4.6	4.1	4.6	8.1	5.1	14		9.1	7	8.2	8.4	6,3
Tb	1.05	0.834	0.744	0.9	1.29	0.935	2.2	1.8	1.50	1.07	1.7	1.433	1,1
Yb	4.2	3.2	2.61	2.5	3.9	2.66	7.5	6.8	3.39	2.35	3.2	2.8	2,6
Lu	0.64	0.47	0.383	0.38	0.548	0.407	1.1	1.1	0.48	0.31	0.34	0.387	0,40
Ba/Rb	7.50	40.00	13.80	38.4	29.86	21.22	11.85	13.75	4.49	25.8	15.83	18.18	
La/Sm_n	0.97	1.02	0.59	2.15	1.69	1.71	2.31	2.07	2.23	2.82	2.37	1.87	
Gd/Yb_n	1.18	1.18	1.30	1.52	1.70	1.58	1.54		2.22	2.46	2.11	2.48	2.00
La/Yb_n	1.02	1.26	0.80	4.30	3.48	3.42	4.78	4.22	7.09	9.10	7.40	6.38	
$(Eu/Eu^*)_n$	1.03	0.98	0.94	1.19	0.93	0.99	0.88	0.93	0.95	0.98	0.99	1.02	
ΣREE	48	44	33	75	109	72	258	186	169	135	175	134	143
$Al2O_3/TiO_2$	7	9	10	7	5	8	5	5	6	7	4	4	8
Ti/Zr	123	115	95	93	101	108	59	34	90	82	83		
Zr/Y	2.8	2.5	2.5	5.0	4.5	3.9	6.1	6.9	5.8	6.5	7.8	6.0	
Zr/Hf	35	37	38	46	41	36	28	47	40	41	50	40	
Nb/Ta	14	19	14	24	18	19	18	20	19	19	16	19	
Nb/La_{pm}	0.80	0.81	0.37	1.20	1.20	1.40	1.04	1.57	1.48	1.41	1.37	1.19	
Th/La_{pm}	0.40	0.58	0.84	0.22	0.69	0.89	0.60	0.87	1.09	0.95	0.86	0.81	
Nb/Th_{pm}	1.99	1.40	0.44	5.60	1.74	1.57	1.74	1.80	1.36	1.49	1.60	1.47	
Hf/Hf*	0.90	0.69	0.71	0.76	0.61	0.68	0.71	0.91	0.60	0.69	0.56		
Ti/Ti*	1.14	0.96	0.87	1.20	1.00	1.07	0.54	0.62	0.98	1.04	1.06		

Major and trace element compositions

Major element abundances were determined for 20 whole rocks samples and trace element abundances for 12 samples (Table 1). The whole rock analyses of the basaltic rocks of the Zasurin Formation were partly reported by Buslov et al. (1999, 2000, 2001) and Safonova et al. (2004). The analyses in Table 1 are listed as analyzed, with Fe tabulated as Fe_2O_3. On the basis of their Ba/Rb abundance ratios ranging from 5 to 40 compared to the average oceanic basalt ratio of 11.6 (Hofmann and White, 1982) these sample have experiences significant postmagmatic mobility of alkali metals. Most of the analyzed basalts are altered, with phenocrysts and groundmass replaced by saussurite, chlorite, calcite, and magnetite. Most samples contain more than 2 wt% H_2O (based on L.O.I.), and the compositions of these samples may have been slightly modified by late-stage alteration. Basalts have less than 9wt% MgO; they include an Mg- to Fe-tholeiite (thereinafter referred to as "depleted basalts") series, and transitional to alkali (thereinafter referred to as "enriched basalts") basalts.

The whole rock Mg# values were calculated assuming 10%Fe+3, which corresponds to low-pressure crystallization conditions for oxygen fugacity of ~FMQ-1.

Depleted basalts

The depleted basalts are characterized by a relatively large range of Mg# and Fe_2O_3 contents over a restricted range of SiO_2 and by near-flat REE patterns (Table 1). For the Zasurin Formation depleted basalts, SiO_2 spans 48-55 wt%, Mg#=63-50, Fe_2O_3=10-15 wt%, and Ni=56-78 ppm. Concentrations of TiO_2, Fe_2O_3, and P_2O_5 increase as Mg#, Cr and Ni decrease. Similarly, Th, Nb, La, Sm, Zr, and Y increase with decreasing Mg#. These compositional relationships are evident in Fig. 3 and Table 1. In this suite of basalts, La/Sm_n ranges from 0.6 to 1.0, and Gd/Yb_n ranges from 1.1 to 1.3. The most magnesian samples have near-chondritic Ti/Zr ratios, whereas Al_2O_3/TiO_2 ratios are consistently subchondritic value (Table 1).

Thorium-Nb-LREE inter-element relationships are not complex. The Zasurin depleted basalts have negative Nb and Th anomalies with respect to La. Th plots as a negative trend over a range of La/Sm_n, whereas Nb anomalies covary with La/Sm_n (Fig. 4).

Transitional and enriched basalts

These basalts are defined on the basis of their pronounced positively fractionated rare element patterns where La/Yb_n= 3.4-10 (Fig. 5). Relative to the suites of depleted tholeiitic basalts, they have higher contents of incompatible elements at a given MgO value (Fig. 3), and greater incompatible/compatible element ratios (e.g. Zr/Y= 2.4-7.7), but moderately lower Al_2O_3/TiO_2 (6-7 in average) ratios than depleted counterparts (Table 1). Two types are present on the basis of major and trace element compositions: (1) transitional basalts; (2) enriched (alkaline) basalts. Both varieties occur as sheeted fragments within folded structures and it is impossible to identify their original geological relationships. Transitional have similar to enriched basalts Al_2O_3 (15 vs 16 wt%) contents, slightly higher Al_2O_3/TiO_2 (6.5 vs 5.5) ratios, higher Ni (99 vs 62 ppm) contents, and less fractionated REE (La/Yb_n=3.3 vs 6.7 av.) than enriched counterparts (Table 1; Fig. 5). Minor negative to zero Zr and Hf anomalies are present. Both types of basalts show LREE enrichment. Transitional basalts show Th depletion

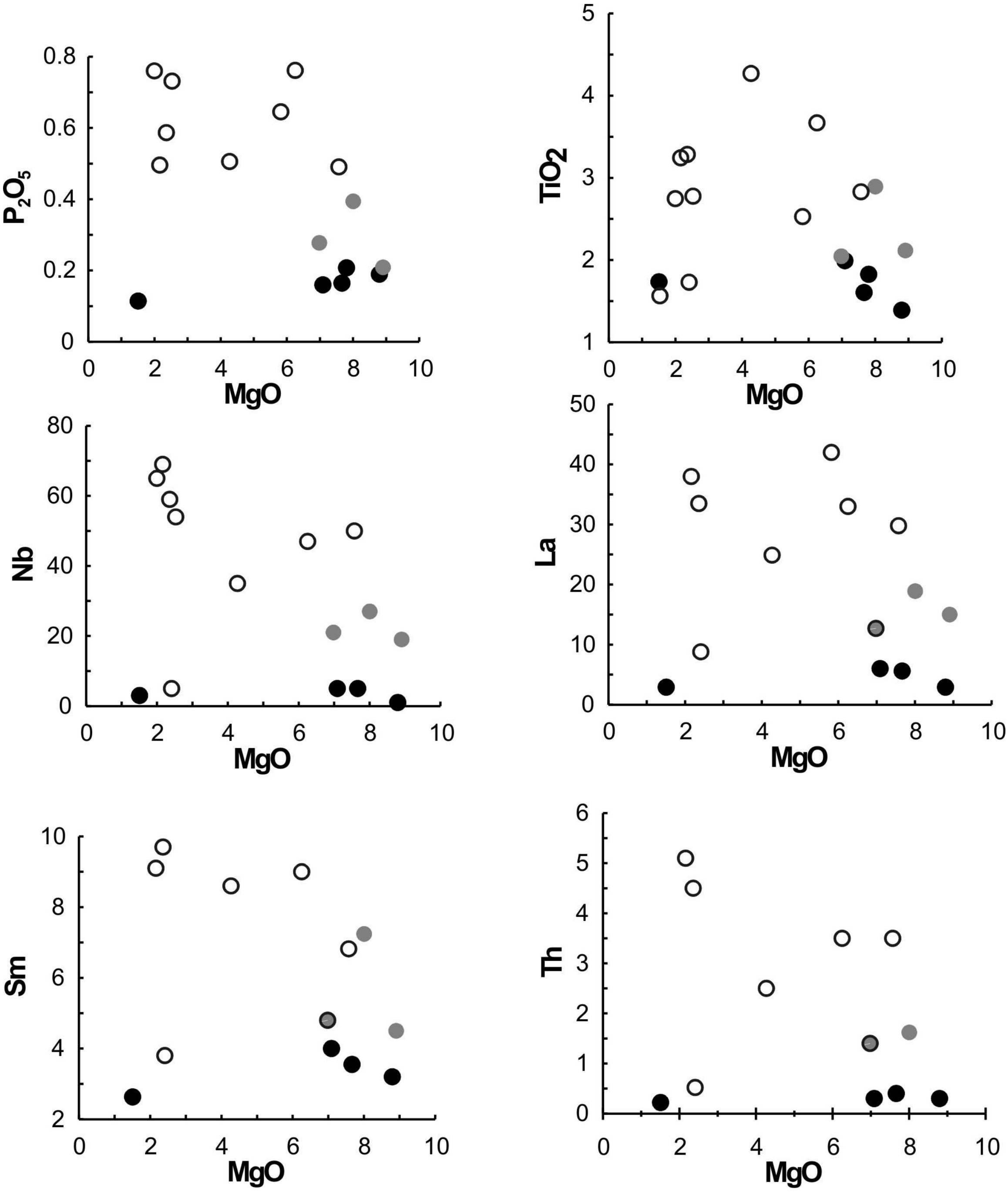

Fig. 3. **Variation diagrams of P_2O_5, TiO_2, Nb, La, Sm and Th vs. MgO for Zasurin basalts: filled circles for depleted varieties; grey circles for transitional varieties; open circles for enriched varieties.**

over La (Th/La_n=0.22-0.89), whereas depleted basalts display less Th depletion (Th/La_n=0.81-1.09). However, enriched basalts have a stronger positive anomaly of Nb with respect to Th and especially La, whereas patterns for transitional basalts weakly peak at La or Ce, and have smoother convex-up patterns through La, Nb and Th (Nb/La_{pm}=1.19-1.57 vs 1.2-1.4).

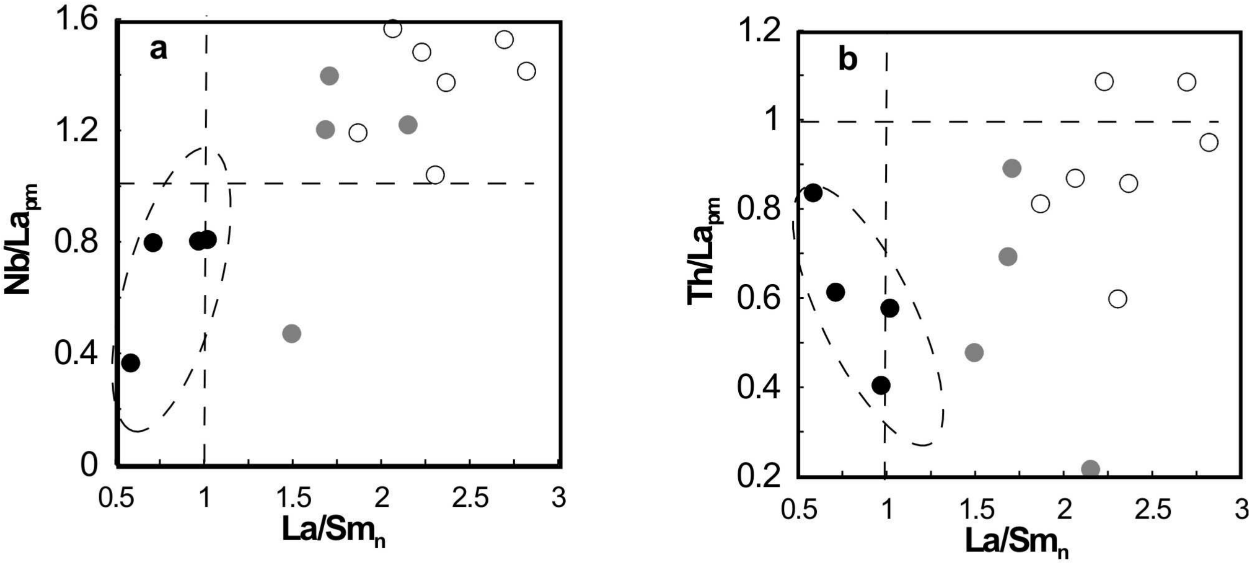

Fig. 4. **Plots of Nb/La_{pm} (a) and Th/La_{pm} (b) vs. La/Sm_n for three basaltic varieties. Symbols as in Fig. 3.**

Similar trace element patterns have been documented for many Phanerozoic transitional to alkaline ocean island basalts and Proterozoic and Archean volcanic rocks interpreted as ocean island basalts (Chen et al., 1991; Weaver, 1991; Stern et al., 1995; Polat et al., 1999).

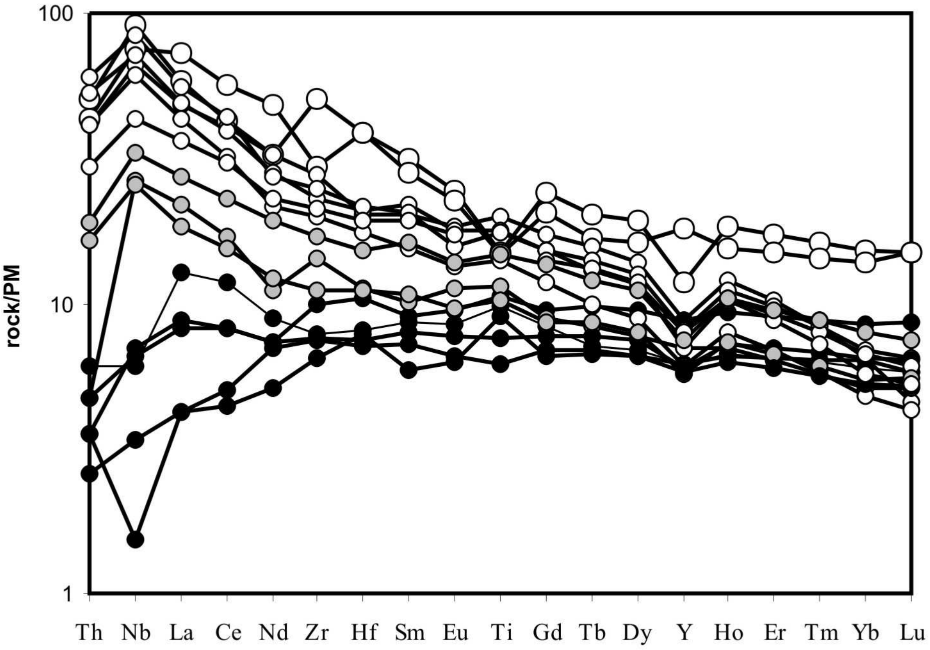

Fig. 5. **Primitive mantle-normalized trace element diagrams for the depleted, transitional and alkaline basalt suites. Normalizing values are from Sun and McDonough (1989). Symbols as in Fig. 3.**

DISCUSSION

In order to address the question of mantle sources components for these basalts, we evaluate in turn questions of possible effects of hydrothermal alteration and metamorphism, crustal contamination, melting processes, and fractional crystallization on composition in general, and Th-Nb-LREE inter-element relationships specifically.

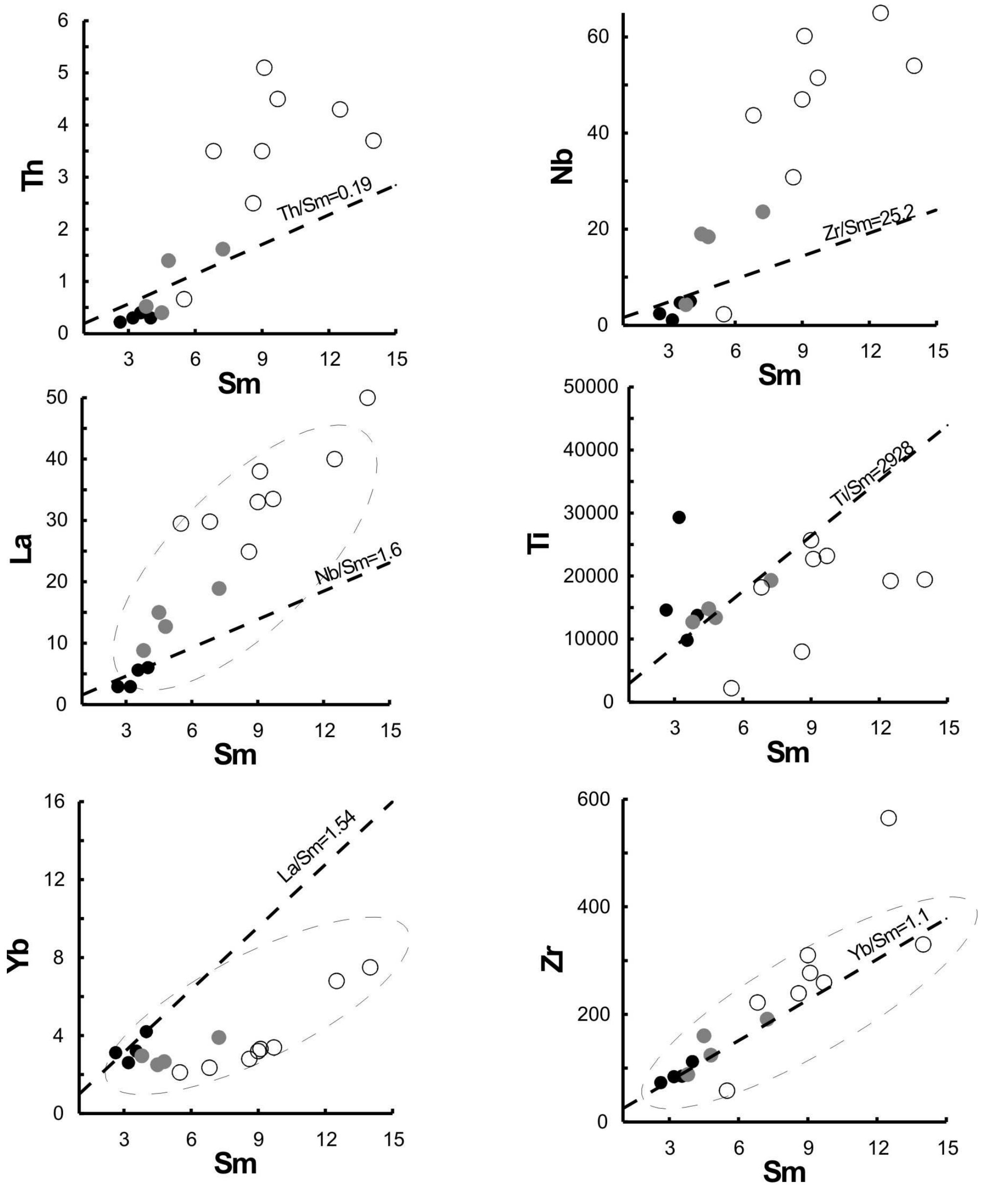

Fig. 6. **Plots of Th, Nb, La, Zr, Ti and Yb vs. Sm. The dashed lines are primitive mantle ratios (from Sun and McDonough, 1989). Symbols as in Fig. 3.**

Post-magmatic alteratio

Variable element mobility is a possibility for Paleozoic volcanic rocks that have undergone seafloor hydrothermal alteration, greenschist to epidote-amphibolite facies metamorphism and polyphase accretion-collision induced tectonic deformation, but there is a general agreements that the REE, HFSE and some transitional metals are least sensitive to mobility (Winchester and Floyd, 1977; Rollinson, 1993 and references cited therein). Those samples with the values of LOI exceeding 4 wt% or large Eu anomalies were not used for petrogenetic interpretation. Primary clinopyroxene is sporadically present in the Zasurin volcanic rocks. However, intense structural transposition which resulted in abrupt lithological changes in many of the Charysh-Terekta sedimentary and volcanic rocks inhibits detailed individual flow scale alteration study.

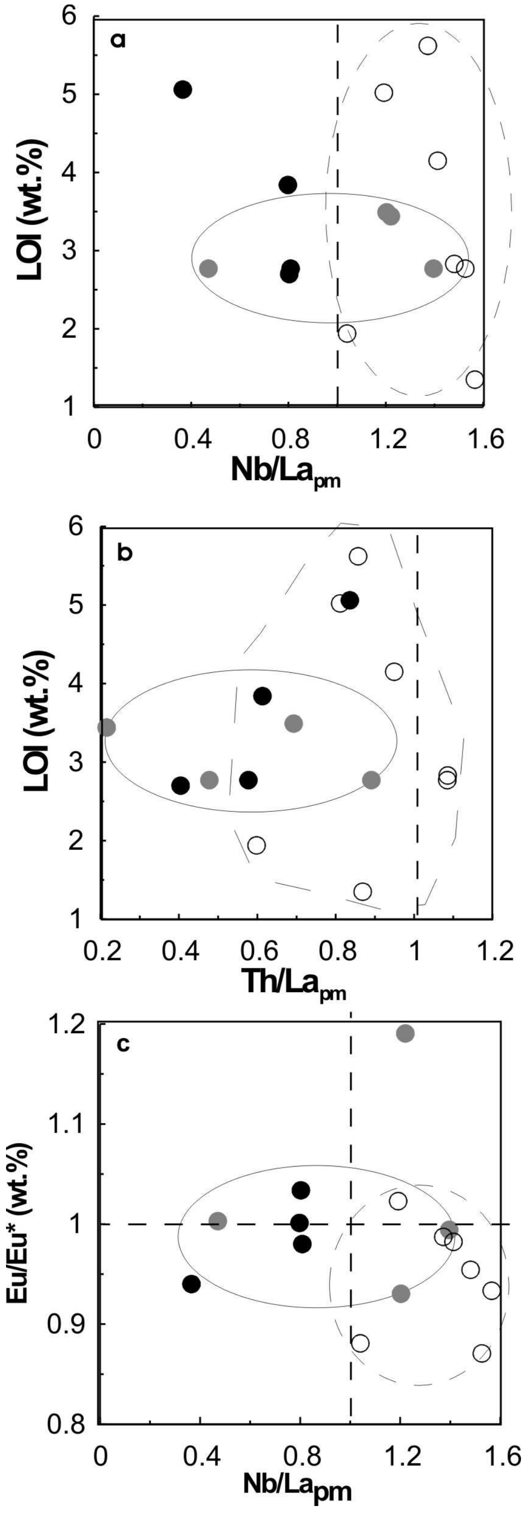

Fig. 7. **Loss on ignition (LOI) vs. Nb/La$_{pm}$ (a) and Th/La$_{pm}$ (b), and Eu/Eu* vs. Nb/La$_{pm}$ (c) for the three basaltic suites, indicating that Th-Nb-La inter-element ratios weakly correlate with alteration and metamorphism. The dashed lines are primitive mantle ratios (from Sun and McDonough, 1989). Symbols as in Fig. 3.**

In the studied set of least altered basaltic rocks, evidence for low to moderate mobility of Th, REE, and HFSE include the following: (1) the depleted and transitional basalts each plot coherently enough on binary diagrams versus Sm (Fig. 6); (2) there is no significant enrichment or depletion of groups of elements (e.g. LREE) in a given rock type over a range of metamorphic grade from greenschist to epidote-amphibolite facies (Table 1, Fig. 3); (3) REE and primitive mantle-normalized trace element diagrams of given suites of basalts associated in the field exhibit coherent patterns for Th, HFSE, and REE (Fig. 5); and (4) Th-Nb-La inter-element relationships do not strictly correlate with the CIA (chemical index of alteration – not shown here), Eu/Eu*, or loss on ignition (Fig. 7).

Similar conclusion concerning the relative immobility of Ti, REE and HFSE in ancient volcanic rocks that have experienced alteration under conditions of low water-rock ratios have been reached by workers in the Altai-Sayan area specifically (Simonov et al., 1994; Safonova and Buslov, 2004a,b), and older, e.g. Archean, terranes in general (e.g. Polat et al., 1999; Jochum et al., 1991; Komiya et al., 2004). Thus, emphasis is placed on HFSE, REE and Th that are relatively immobile during secondary processes.

Crustal contamination

Contamination by continental crust is a possibility, especially for magnesian magmas with high liquidus temperatures (Arndt and Jenner, 1986; Putchel et al., 1997). However, several lines of geological evidence are consistent with an intra-oceanic setting for the basalt sequences. The presence of multi-colored sandstones and cherts with oceanic radiolarian and connodonts interlayered with pillowed basalts and flows suggests an oceanic environment for the eruption of the volcanic rocks (Buslov et al., 2000, 2001; Sennikov et al., 2003; Safonova et al., 2004).

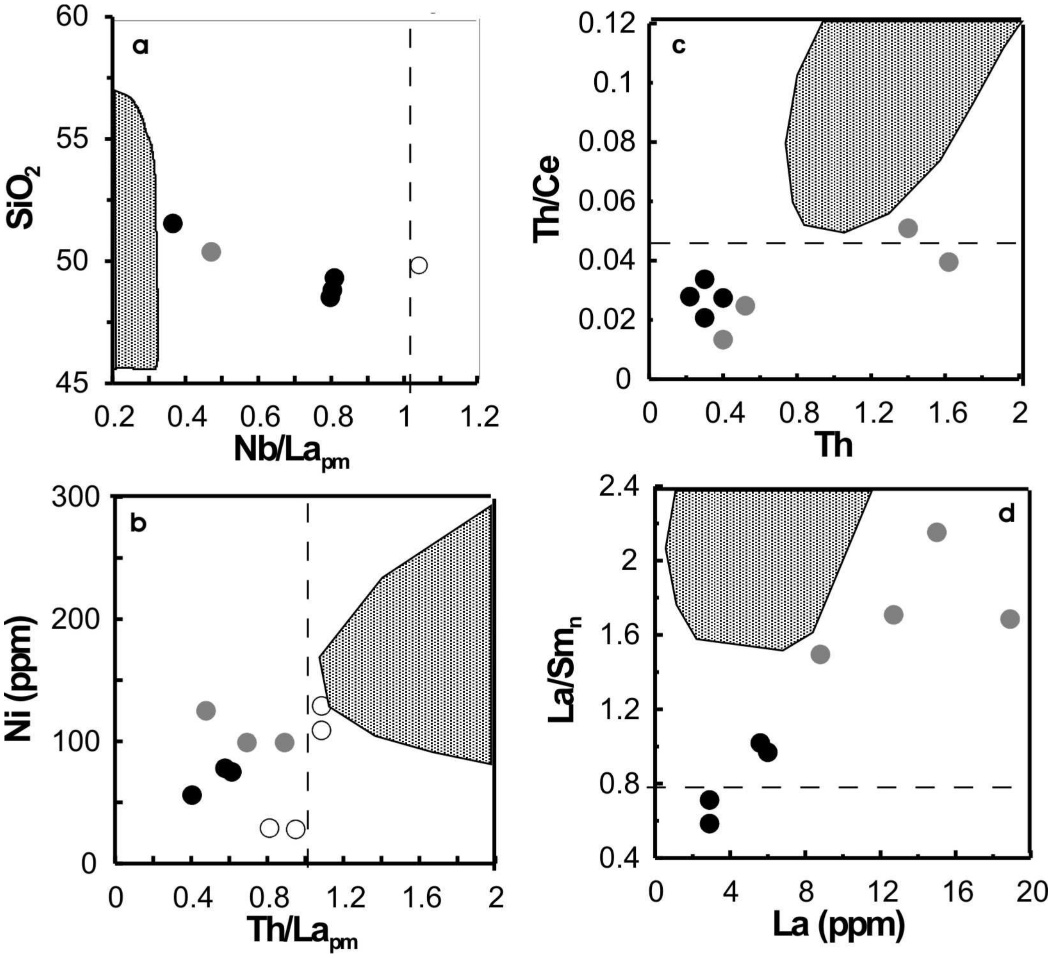

Fig. 8. **Plots of SiO_2 vs. Nb/La_{pm} (a), Ni vs. Th/La_{pm} (b), Th/Ce vs. Th, and La/Sm_n vs. La for the three basaltic suites indicating that crustal contamination did not influence the Th-Nb-La systematics. Shaded areas represent crustally contaminated lavas from the Vetreny belt, Baltic Shield (Puchtel et al., 1997). Symbols as in Fig. 3.**

Negative Nb anomalies in some of the tholeiitic basalts and weak correlations of Nb/La_{pm} and Th/La_{pm} could possibly reflect some crustal contamination (Fig. 4). However, SiO_2, MgO, Ni, Cr and LREE contents in the depleted basalts weakly correlate with the magnitude of negative Nb anomalies as is expected for crustal contamination (Table 1). Those trends are present in crustally contaminated basalts of western Australia and Early Proterozoic basalts of the Baltic shield (Redman and Keys, 1985; Puchtel et al., 1997; Polat et al., 1999). However, the Zasurin data plot separately from those contaminated volcanic rocks (Fig. 8). Additionally, the presence of positive Nb anomalies, low Al_2O_3/TiO_2 and Th/La_{pm} ratios in most of the spatially associated basalts, rules out contamination of these lavas by continental crust (Fig. 5; Table 1).

The geochemical features noted above taken with geological evidence for an intra-oceanic setting in these suites, suggest that the low Nb/La_{pm} values found in some of the Zasurin tholeiites may reflect a subduction-derived component in the mantle rather than crustal contamination. Accordingly, we conclude that the negative covariations of Nb/La_{pm} and Th/La_{pm} with La/Sm_n in some, but not other, basaltic suites does not result from contamination of tholeiitic liquids by continental crust during eruption (exogeneous contamination), but may have resulted from recycling of lithosphere into the mantle (endogeneous contamination with mafic oceanic crust material) (Fig. 4). Collectively, geological and lithological relationships and geochemical characteristics of the Zasurin basalts are inconsistent with continental or flood basalts. More support for the presence or absence of crustal contamination would come from isotopic geochemical study.

Partial melting

The Kurai oceanic plateau basalts (Baratal Formation) and Katun mid-oceanic ridge basalts (Ust-Syoma Formation) of the same western part of the Altai-Sayan foldbelt have deletions of Nb (Ta) relative to LREE generating high La/Nb ratios (Safonova et al., 2004; Safonova and Buslov, 2004). Bach et al. (1996) attributed the Nb depletions to second stage melting of a mantle source that have experienced previous melt extraction under extremely low degrees of partial melting. However, thorium depletion should occur along with Nb depletion during low degrees of partial melting, but this is not consistently seen in the tholeiites. Consequently, there is no evidence that the range of Nb and Th anomalies displayed by the depleted tholeiites can be attributed to partial melting processes. Some of the Zasurin basaltic suites have fractionated HREE, but not as much as regarded a garnet signature and discussed by Hirschmann and Stolper (1996) for mid-oceanic ridge basalts. Although there is no clear correlation of Nb/La_{pm} or Th/La_{pm} with Gd/Yb_n, most transitional and enriched basalt samples with fractionated HREE have positive Nb anomalies. Conclusively, we differentiate the depleted basalts as those formed without partial melting from the transitional and enriched basalts which could have formed at moderate degrees of partial melting (Table 1, Figs. 5, 9a).

Crystallizational differentiation

There is a large variation of Mg# in the depleted and transitional basalt suites and therefore we could test for a fractional crystallization control on Nb anomalies. However, Nb is not compatible in clinopyroxene, but in Fe-Ti oxides which are unlikely to be fractionating phases in ultramafic-mafic liquids.

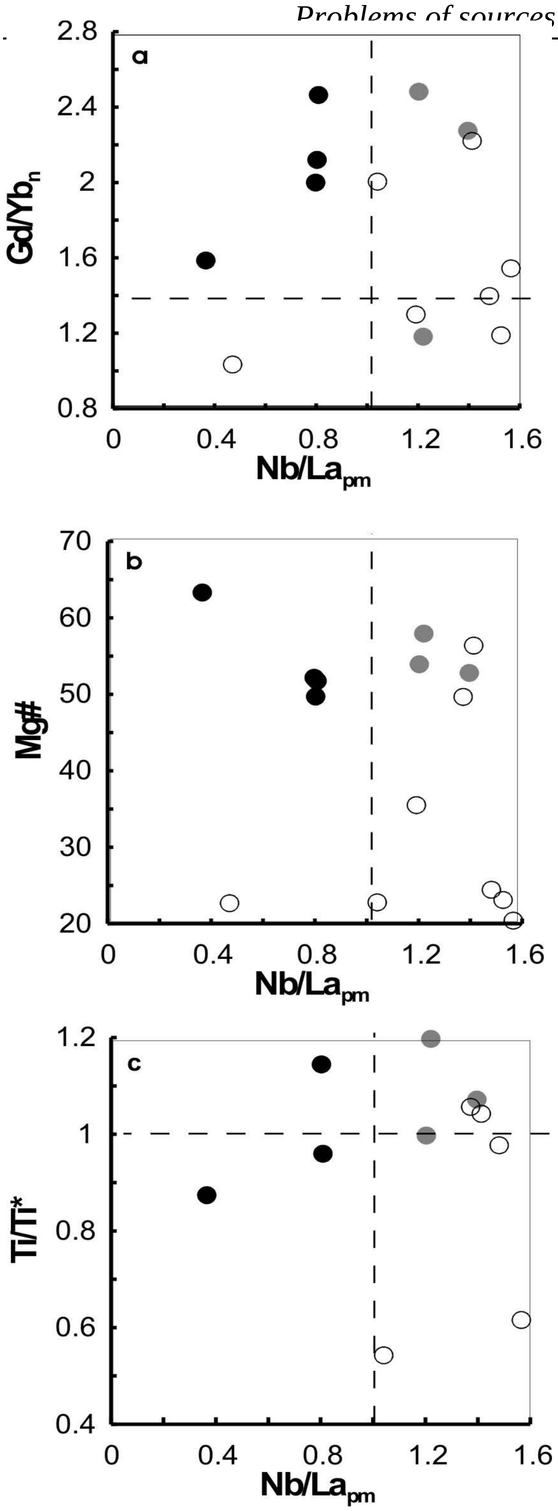

Fig. 9. **Gd/Yb$_n$, Mg#, and Ti/Ti* vs. Nb/La$_{pm}$ variation diagrams for the three basaltic suites, indicating that fractional crystallization weakly influenced the Th-Nb-La systematics. Symbols as in Fig. 3.**

Fowler and Jensen (1989) modeled the evolution of Mg- to Fe-tholeiites in the Kinojevis group of the Abitibi belt: they found that the compositional range could be accounted for by fractional crystallization of olivine, and minor clinopyroxene, plagioclase, and Fe-Ti oxides. The large variation of La/Sm$_n$ ratios over a wide range of MgO contents suggests a more-or-less significant LREE fractionation as a result of fractional crystallization of clinopyroxene, but there is no correlation of Nb anomalies with Mg# (Figs. 5 and 9b). Fe-Ti oxides may accommodate Nb, yet there is no correlation of Nb/La$_{pm}$ with Fe_2O_3 or TiO_2 contents (Fig. 9c). Consequently, Th-Nb-LREE inter-element ratios in the volcanic rocks are independent of clinopyroxene or Fe-Ti oxide fractionation or accumulation.

Mantle sources

If mantle melting processes, fractional crystallization, crustal assimilation, and alteration and metamorphism did not affect the Th-Nb-LREE systematics, then the variations of these elements may be a signature of compositionally heterogeneous mantle, as is observed in Phanerozoic and Cenozoic oceanic plateaus such as Ontong Java (Polat et al., 1999; Mahoney et al., 1993; Neal et al., 1997) and the oceanic islands of Hawaii and Iceland (e.g. Hards et al., 1995; Regelous et al., 2003).

INFERENCES

Tholeiitic basalts

The morphology and basalt composition of oceanic plateaus (OPB) have been compared with those of oceanic islands (OIB) by many investigators (e.g. Floyd et al., 1989; Mahoney et al., 1993; Neal et al., 1997). The OPB are areally extensive tholeiites with relatively uniform morphology, comprising large igneous provinces (LIP) and are the oceanic counterparts of continental flood basalts. In contrast, ocean islands have topographically pronounced volcanic buildings, and generally include tholeiitic, transitional and alkaline basalts.

The Ontong Java plateau is dominated by tholeiitic basalts with flat REE patterns as in the Zasurin tholeiites (Floyd et al., 1989; Mahoney et al., 1993). The basaltic melts erupted through continental lithospheres may have a spectrum of REE abundances from depleted to enriched (Polat et al., 1999). Tholeiitic basalts with incompatible element depletion are known in the western Pacific (Castillo et al., 1994). Given the spatial association of tholeiites with both flat and depleted LREE patterns, and the presence of alkaline basalts, LREE-depleted tholeiites of the Zasurin Formation are unlikely to represent the Early Paleozoic equivalent of MORB. We conclude that some of these tholeiites are oceanic plateau basalts fragmentally accreted during collision.

The Zasurin depleted basalts extend from the field of Ontong Java oceanic plateau basalts at high Ce/Nb and Th/Nb ratios and approach the field of Lau basin (Fig. 10a). They display zero to weakly fractionated REE with La/Yb$_n$ ranging from 0.6 to 1.2 similarly to the Ontong Java tholeiites with La/Yb$_n$ ranging from 0.8 to 1.5 (Table 1; Neal et al., 1997; Simonov et al., 2004).

Transitional to alkaline basalts

Basalts of transitional to enriched composition with strongly fractionated REE are rather abundant in the Zasurin Formation of the Charysh-Terekta strike-slip zone (Sennikov et al., 2003; Safonova et al., 2004). The weak HREE fractionation coupled with small negative Zr and Hf anomalies signify that enriched basaltic liquids segregated in the spinel-facies deep mantle. Transitional basalts are similar to Fe-tholeiites; they have pronounced REE fractionation and zero to positive Zr anomalies. Transitional and enriched basalts have Zr/Hf and Nb/Ta ratios that extend to values a little bit greater in average that the respective mantle values of 36 and 16 in common with many Phanerozoic and Cenozoic within-plate basalts (Kamber and Collerson, 2000; Green et al., 1989, Table 1).

Mantle source components

As far as Nb, La and Th have similar partition coefficients, they are unlikely to be fractionated from one another during the relatively high degrees of partial melting involved in the genesis of ultramafic and mafic oceanic lavas (Polat et al., 1999 and the references cited therein). Saunders et al., (1988) demonstrated that the Th-Nb-Ce systematics of oceanic basalts cab be described in terms of mixing between three mantle components (Fig. 10). Depleted MORB source mantle (DMM) with relatively high Ce/Nb but low Th/Nb; a recycled residual slab component processes through a subduction zone (RSC) having low Ce/Nb and Th/Nb; and a recycled subduction-derived component (SDC) with high Th/Nb and Ce/Nb, complementary to RSC. During subduction Th and LREE are fractionated

---

from Nb: the former elements are preferentially transferred to the subarc mantle from the slab whereas Nb is not, such the residual slab has a positive Nb anomaly relative to Th and LREE (RSC), and the subarc mantle acquires a complementary negative Nb anomaly (SDC). The recycling may occur by subduction and/or delamination.

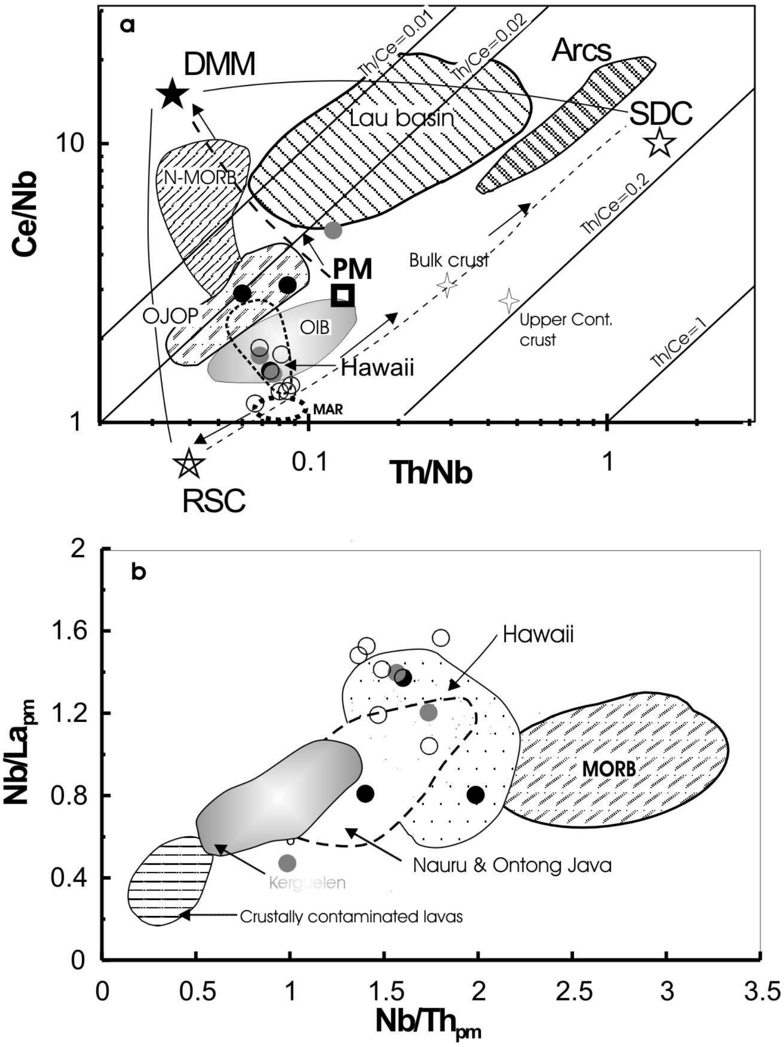

Fig. 10. **(a) Ce/Nb vs. Th/Nb variation diagram after Saunders et al. (1988). Fields for Nauru basin, Ontong Java oceanic plateau (OJOP), Kerguelen plateau, Lau back-arc basin, Mid-Atlantic ridge (MAR) are from Ploat et al. (1999). Data for N-MORB, OIB, MORB, and PM are from Sun and McDonough (1989). Bulk continental crust values after Taylor and McLennan (1985). Field for Hawaii is based on the Geochemical Rock Database (GEOROC) of the Max-Planck-Institute for Chemistry in Mainz, Germany (www.georoc.mpch-mainz.gwdg.de/georoc). (b) Nb/La$_{pm}$ vs. Nb/Th$_{pm}$ variation diagram after Polat et al., (1999).**

Zasurin enriched basalts and most transitional varieties have strong positive Nb anomalies which, based upon analogies with models for present day mantle plumes, are likely formed with participation of recycled oceanic crust material (Sun and McDonough, 1989; Weaver, 1991). As far as we know this is the first time alkaline basalts have been identified in Early Paleozoic basalts of the western Altai-Sayan with a clear positive Nb, HIMU-like trace element signature (Fig. 5).

Least altered depleted and transitional basalts also have Nb and Th anomalies that can be attributed to compositionally heterogenous mantle plumes, incorporating a recycled subduction-derived component ($Nb/La_{pm}<1$) and a residual slab derived component ($Nb/La_{pm}>1$) into the mantle (Polat et al., 1999 and the referenced cited therein). There is no evidence for recycled sediments because there are no samples with negative Nb but positive Th anomalies.

Many investigators have shown that the Cretaceous to Quaternary plume-related oceanic plateau and island basalts, e.g. Ontong Java, Hawaii, Iceland, etc., have diverse geochemical compositions and several mantle components (Neal et al., 1997; Wilson, 1993; Hemond et al., 1993). Like the Zasurin greenstones, other western Altai-Sayan folded structures also have tholeiitic basalts with a wide range of trace element (Th, HFSE, REE) characteristics suggesting that Vendian-Early Paleozoic mantle plumes in general may also have contained several mantle source components (Safonova et al., 2004; Safonova and Buslov, 2004a,b). These different components, partly derived from lithosphere recycling, have note formerly been identified in the Early Paleozoic mantle based on trace element systematics.

Oceanic ridge, plateau and island environments

The Zasurin depleted basalts having the most pronounced Nb depletion may be analogues of Phanerozoic oceanic plateau basalts which are characterized by the Nb/La_{pm} ranging from 0.6 to 1.8 (Lassister and DePaolo, 1997). We suggest that some of them were formed in mid-oceanic ridge environment that is supported by Zr versus Ti/V, Ti/Sc and Ti/Zr diagrams (not shown here; see Table 1; Gamble et al., 1994).

Contacts between the oceanic island, possibly oceanic plateau and ridge series are likely tectonic in the Charysh-Terekta strike-slip zone (Buslov et al., 2000, 2003). However, tectonic strike-slipping destroyed original geological relationships and the tectonic interleaving has not previously been addressed in detail, in part because of the difficulty in distinguishing various basalt subtypes in outcrop.

Buslov et al. (2000, 2001) show that the structural and field relations of imbricated lithotectonic units in the Charysh-Terekta strike-slip zone are comparable with modern collision-accretion complexes (e.g. Naizawa accretionary complex of the Idonappu zone, Hokkaido, Japan; Ueda et al., 2000) over a wide range of scales. The presented geochemical results support this idea and suggest that mid-oceanic ridge tholeiitic sequences, characterized by negative Nb anomalies, may be textonically juxtaposed with accreted ocean plateau and ocean island sequences (small negative to positive Nb and Th anomalies).

Structural complexity of the Charysh-Terekta strike-slip zone in particular, and in Vendian-Early Paleozoic accretionary belts in the western Altai-Sayan in general, creates a major difficulty in identifying all these tectonic entities (Buslov et al., 2000, 2001, Safonova et al., 2004). The spectrum of positive to negative Nb

---

anomalies, and Th/Ce$_{pm}$ ratios mainly <1 in the Zasurin basalts (Fig. 10a), flat REE patterns of OPB-type transitional basalts and the presence of LREE-enriched OIB-type alkaline basalts are compatible with the collision-accretion complex model of Buslov et al. (2000). Another evidence for the oceanic island environment for the alkaline basalts comes from their spatial association with seamount slope-type radiolarian cherts and other siliceous beds (Buslov et al., 2001; Sennikov et al., 2003).

CONCLUSIONS

High precision XRF-SR and INAA trace element data obtained from Early Ordovician basaltic volcanic sequences of the Late Devonian Charysh-Terekta strike-slip zone reveal considerable geochemical diversity. LREE-depleted, LREE-medium and LREE-enriched basalts coexist; the latter two are interpreted as liquids segregated from mantle plumes and erupted in an intra-oceanic environment. Tholeiitic basalts have near-flat REE patterns with dominantly negative Nb and Th anomalies. Many of LREE-medium transitional basalts are compositionally similar to Phanerozoic ocean plateau basalts which have similar Nb and Th anomalies from mixing of different mantle components.

Accordingly, the negative Nb and Th anomalies in the tholeiites and positive Nb and Th anomalies in the transitional basalts are interpreted to stem from a mantle with recycled subduction influenced lithosphere and recycled oceanic crust, respectively, entrained into the plume. Given the structural evidence for a collision-accretion complex setting (Buslov et al., 2000, 2001), the plume from which the transitional and alkaline basalts were derived most probably erupted in an intra-oceanic environment far away from a Late Devonian collision zone.

The enrichment of Nb with respect to La and Th, coupled with positively fractionated LREE patterns, in alkaline basalts is comparable with modern HIMU type OIB involving recycled oceanic crust in the mantle source. Besides, the transitional basalts may have been derived from the mixture of depleted tholeiites and enriched alkaline magmas.

Field relations suggest that all three types of basaltic sequences occur along the same tectonic zone, and have been laterally displaced by strike-slip faults (Buslov et al., 2000). Accordingly, these chemically diverse but tectono-stratographically associated mafic volcanic rocks are likely to be the fragments of an Early Paleozoic (Middle-Late Cambrian) oceanic plateau and oceanic island(s) derived from a heterogeneous mantle plume. The diversity suggest that Late Proterozoic – Early Paleozoic subduction-collision processes may have played an important role in the generation of chemically heterogenous mantle (Silver et al., 1988).

ACKNOWLEDGMENTS

The authors acknowledge financial support for this study from the Russian Foundation for Basic Research *(grant no. 03-05-64668)* and an Interdisciplinary

Research grant of the Siberian Branch of the Russian Academy of Science. Vladislav Bobrov assisted with XRF-SR and INAA analyses. Olga Turkina and Andrei Izokh of the Institute of Geology SB RAS are thanked for constructive discussion of the manuscript.

REFERENCES

1. **Bach W., Erzinger J., Dosso L., Bollinger C., Baugnault H., Etaubleau J., Sauerwein, J.** (1996) Unusually large Nb-Ta depletion in North Chile ridge basalts at 36°-50° to 38°-56° S: major element, trace element and isotopic data. Earth Planet. Sci. Lett, v. 142, pp. 223-240.
2. **Berzin, N.A. and Dobretsov, N.L.** (1994) Geodynamic evolution of Southern Siberia in Late Precambrian – Early Paleozoic time, In: Coleman, R.G. (Ed.) Reconstruction of the Paleo-Asian ocean. Utrecht, The Netherlands, pp. 53-70.
3. **Buslov, M. M. and Watanabe, T.** (1996) Intrasubduction collision and its role in the evolution of an accretionary wedge: the Kurai zone of Gorny Altai, Central Asia. Russian Geol. Geophys., v. 36, pp. 83-94.
4. **Buslov M. M., Berzin N. A., Dobretsov N. L., Simonov V. A.** Geology and Tectonics of Gorny Altai (1993) Guide-book of excursion, IGCP Project 283, United Institute of Geology, Geophysics and Mineralogy Publ., Novosibirsk, 122 p.
5. **Buslov, M.M., Saphonova, I.Yu and Bobrov, V.A.** (1999) An exotic terrane of the Late Cambrian-Early Ordovician oceanic crust in the northwestern Gorny Altai (Zasurin Formation): structural position and geochemistry. Dokl. RAN, v. 368, pp. 650-654.
6. **Buslov, M.M., Fujiwara, Y., Saphonova, I.Yu, Okada, Sh. and Semakov, N.N.** (2000) The junction zone of the Gorny Altai and Rudny Altai terranes: structure and evolution. Russian Geol. Geophys., v. 41, pp. 377-390.
7. **Buslov M. M., Safonova I. Yu., Watanabe T., Obut O., Fujiwara Y., Iwata K., Semakov N. N, Sugai Y., Smirnova L. V., Kazansky A. Yu.** (2001) Evolution of the Paleo-Asian ocean (Altai-Sayan region, Central Asia) and collision of possible Gondwana-derived terranes with the southern marginal part of the Siberian continent. Geosciences Journal, v. 5, pp. 203-224.
8. **Buslov M.M., Watanabe T., Smirnova L.V., Fujiwara Y., Iwata K., J. de Grave, Semakov N.N., Travin A.V., Kiryanova A.P. and Kokh D.A.** (2003) Role of strike-slip faulting in Late Paleozoic-Early Mesozoic tectonics and geodynamics of the Altai-Sayan and East Kazakhstan regions. Russian Geology and Geophysics, v. 44, no. 1-2, p. 47-71.
9. **Chen C.-Y., Frey F.A., Garcia M.O., Dalrymple G.B., Hart S.R.** (1991) The tholeiitic to alkaline basalt transition at Heleakala volcano. Maui, Hawaii. Contrib. Miner. Petrol., v. 106, p. 183-200.
10. **Dobretsov, N.L. and Zonenshain, L.P.** (Eds.) (1985) Riphean-Paleozoic ophiolites of North Eurasia. Nauka, Novosibirsk (in Russian).
11. **Dobretsov, N.L., Berzin, N.A. and Buslov, M.M.** (1995) Opening and tectonic evolution of the Paleo-Asian Ocean. Int. Geol. Rev., v. 35, pp. 335-360.
12. **Dobretsov, N.L., Buslov, M.M. and Uchio,Yu.** (2004a) Fragments of oceanic islands in accretion-collision areas of Gorny Altai and Salair, southern Siberia, Russia: early stages of continental crust growth of the Siberian continent in Vendian-Early Cambrian time. J. Asian Earth Sci., v. 23, 673-690.
13. **Dobretsov, N.L., Buslov, M.M., Saphonova, I.Yu and Kokh D.A.** (2004b) Fragments of oceanic islands in the Kurai and Katun' accretionary wedges of Gorny Altai. Russian Geol. Geophys., v. 45, no. 12, pp. 1381-1403.
14. **Green T.H, Die S.H., Ryan C.G. and Cousens D.R. (1989)** Proton microprobe-

determined partitioning of Nb, Ta, Zr and Y between garnet, clinopyroxene and basaltic magma at high pressure and temperature. Chemical Geology, v. 74, pp. 201-216.

15. **Hemond, C., Arndt, N.T., Lichtenstein, U., Hofmann, A.W., Oskarsson, N., Steinthorsson, S.** (1993) The heterogenous Iceland plume: Nd-Sr-O isotope and trace element constrains. J. Geophys. Res., v. 98, pp. 15833-15850.
16. **Hirschman, M.M. and Stolper, E.M.** (1996) A possible role for garnet pyroxenite in the origin of the “garnet signature” in MORB. Contrib. Miner. Petrol., v. 124, pp. 185-208.
17. **Hofmann, A.W. and White W.M.** (1982) Mantle plumes from ancient oceanic crust. Earth Planet. Sci. Lett, v. 57, pp. 421-436.
18. **Iwata, K., Sennikov, N.V., Buslov, M.M., Obut, O.T., Shokalsky, S.P., Kuznetsov, S.A., and Ermikov, V.D.** (1997) Upper Cambrian-Early Ordovician age of the Zasur'ia basalt-chert-terrigenous formation (northwestern Gorny Altai). Russian Geol. Geophys., v. 38, pp. 1427-1444.
19. **Jochum K.P., Arndt N.T., Hofmann A.W.** (1991) Nb-Th-La in komatiites and basalts: constrains on komatiites petrogenesis and mantle evolution. Earth Planet. Sci. Lett., v. 107, p. 272-289
20. **Kamber B.S. and Collerson K.D. (2000)** Zr-Nb systematics of ocean island basalts reassessed – the case for minary mixing. J. Petrol., v. 41, no. 7, pp. 1007-1021.
21. **Kerrich, R. and Wyman, D.A.** (1997) Reviews of developments in trace-element fingerprinting of geodynamic settings and their implications for mineral exploration. Australian Journal of Earth Sciences, v. 44, pp. 465-487.
22. **Komiya, T., Maruyama Sh., Hirata T., Yurimoto H. and Nohda S.** (2004) Geochemistry of the oldest MORB and OIB in the Isua Supracrustal Belt. Southern West Greenland Implication for the composition and temperature of early Archean upper mantle. The Island Arc, v. 13, pp. 47-72.
23. **Neal C.R., Mahoney J.J., Kroenke L.W., Duncan R.A., Petterson M.G.** (1997) The Ontong Java Plateau. In: Mahoney J.J. and Coffin M.F. (eds.) Large Igneous Provinces: Continental, Oceanic, and Planetary Flood Magmatism. American Geophysical Union Monograph 100, Washington D.C., pp. 183-216.
24. **Polat Al., Kerrich R., Wyman D.** (1999) Geochemical diversity in oceanic komatiites and basalts from the late Archean Wawa greenstone belts, Superior Province, Canada: trace element and Nd isotope evidence for a heterogeneous mant.e, Precambrian Research, v. 94, pp. 139-173.
25. **Putchel, I.S., Hasee, K.M., Hofmann, A.W., Chauvel, C., Kulikov, V.S., Garbe-Schonberg, C.-D., Nemchin, A.A.** (1997) Petrology and geochemistry of crustally contaminated komatiitic basalts from the Vetreny belt, southeastern Baltic shield: evidence for an early Proterozoic mantle plume beneath rifted Archean continental lithosphere. Geochim. Cosmochim. Acta, v. 61, pp. 1205-1222.
26. **Regelous M., Hofmann A.W., Abouchami W. and Galer S.J.G.** (2003) Geochemistry of Lavas from the Emperor Seamounts, and the Geochemical evolution of Hawaiian Magmatism from 85 to 42 Ma. J. Petrol., v. 44, no. 1, pp. 113-140.
27. **Redman, B.A. and Keays, R.R.** (1985) Archean volcanism in the eastern Goldfields Province, Western Australia. Precamb. Res., v. 30, pp. 113-152.
28. **Rollinson, H.R.** (1993) Using Geochemical Data: Evaluation, Presentation, Interpretation. Longman Group UK Ltd., 352 p.
29. **Safonova I.Yu**., **Buslov M.M.** (2004a) Geochemistry of oceanic basalts of the Katun accretionary wedge in northern Gorny Altai: evidence for mantle plume magmatism. In: N.V. Vladykin (Ed.) Deep-seated magmatism: its sources and their relation to plume processes. Irkutsk, Vinogradov Inst. Geochem. Publ., P. 273-292.

30. **Safonova I.Yu., Buslov M.M.** (2004b) Geochemistry of oceanic basalts of the Kurai accretionary prism (Gorny Altai), In: Vladykin N.V. (Ed.) Deep-seated magmatism, its sources and their relation to plume processes, Vinogradov's Inst. Geochem. Publ., Irkutsk, pp.314-332 (in Russian).
31. **Safonova I.Yu., M.M. Buslov, K. Iwata, D.A. Kokh** (2004) Fragments of Vendian-Early Carboniferous oceanic crust of the Paleo-Asian Ocean in foldbelts of the Altai-Sayan region of Central Asia: geochemistry, biostratigraphy and structural setting. Gondwana Research, v. 7, no. 3, pp. 771-790.
32. **Saunders, A.D., Norry, M.J., Tarney, J.** (1988) Origin of MORB and chemically-depleted mantle reservoirs: trace element constrains. J. Petrol. (Special Lithosphere Issue), pp. 415-455.
33. **Saunders, A.D., Norry, M.J., Tarney, J.** (1991) Fluid influence on the trace element compositions of subduction zone magmas, Philos, Trans. Roy. Soc. London, v. A 335, pp. 337-392.
34. **Sennikov, N.V., Iwata, K., Ermikov, V.D., Obut, O.T. and Khlebnikova, T.V.** (2003) Oceanic sedimentation settings and fauna associations in the Paleozoic on the southern framing of the West Siberian Plate. Russian Geol. Geophys., v. 44, pp. 156-171.
35. **Silver P.G., Carlson R.W., Olson P.** (1988) Deep slabs, chemical heterogeneity, and structure of mantle convection: investigation of an enduring paradox. Ann. Rev. Earth. Planet. Sci., v. 16, pp. 477-541.
36. **Simonov, V.A., Dobretsov, N.L. and Buslov, M.M.** (1994) Boninite series in structures of the Paleo-Asian Ocean. Russian Geology and Geophysics, v. 35, pp. 182-199.
37. **Stern R.A., Syme E.C., Lucas S.B.** (1995) Geochemistry of 1.9 Ga MORB and OIB basalts from the Amisk collage, Flin Flon belt, Canada: evidence for an intra-oceanic origin. Geochim. Cosmochim. Acta, v. 59, pp. 3131-3154.
38. **Sun, S. and McDonough, W.F.** (1989) Chemical and isotopic systematics of oceanic basalts: Implications for mantle composition and processes. In: Saunders, A.D. and Norry, M.J. (Eds.) Magmatism in the Ocean Basins. Geol. Soc. London. Spec. Publ., v. 42, pp. 313-345.
39. **Taylor S.T. and McLennan S.M.** (1985) The continental crust: Composition and Evolution. Blackwell, Oxford, p. 312.
40. **Ueda, H., Kawamura, M. and Niida, K.** (2000) Accretion and tectonic erosion processes revealed by the mode of occurrence and geochemistry of greenstones in the Cretaceous accretionary complexes of the Idonappu zone, southern central Hokkaido, Japan. The Island Arc, v. 9, pp. 237-257.
41. **Weaver B.L.** (1991) Thee origin of ocean island basalts and member compositions: trace element and isotopic constrains. Earh Planet. Sci. Lett., v. 104, p. 381-397.
42. **Winchester, J.A. and Floyd, P.A.** (1977) Geochemical discrimination of different magma series and their differentiation products using immobile elements. Chem. Geol., v. 20, pp. 325-343.
43. **Zonenshain, L.P., Kuzmin, M.I. and Natapov, L.M.** (1990) Geology of the USSR: A Plate tectonic synthesis. Geodynamic Monograph, American Geophysical Union, Washington, 242 p.

UDK 550.42; 552.111

Features of the geological structure and Late-Cenozoic volcanism of the East-Asian margin: evidence for mantle rotational geodynamics.

Koloskov A.V.and Anosov G.I.

Institute of Volcanology and Seismology Far East Department of the Russian Academy of Sciences Piip Ave. 9, Petropavlovsk-Kamchatsky 683006, e-mail: kolosav@kcs.iks.ru

The task of this paper is to investigate features of modern structure and volcanism in the East-Pacific transition zone from the position of rotational geodynamics. The considered conception of the “fluid-magmatic tornado” explains tectono-magmatic processes in local rotational structures. The conception isn’t an alternative to plume tectonic, but allows to understand in details mechanisms of the heat-mass transferring of substances and the energy resources of these processes. The Upper Miocene to Quaternary xenolith-bearing volcanites were chosen as display objects to determine rotational structure.

Analyses of the obtained data depend on the age sequence of volcanic evolution and variations in composition and structure of basalts and xenoliths. The results of our research revealed three rotational structures of cyclonic type within the East-Pacific margin. These structures showed common morphological and geological features. We assume that there can be another similar structure of such type arising in the junction of the North-Asia and North-American plates. It is remarkable, that the two rim the adjacent seas (the Japanese and the South China) by characteristic abyssal depressions. The third Kamchatkan structure nests within the boundaries of the Central – Kamchatka depression. Its features apparently were inherited from the Upper Cretaceous-Palaeogene continental margin basin. Generally, intra-plate volcanism (or “sub intra-plate volcanism” for Kamchatka) occurs in the western segment of each structure. This type of volcanism is known for associated xenoliths of spinel – lherzolite type. Island-arc volcanism occurs in the eastern segment of the structures; xenoliths of olivine-plagioclase equilibrium are found in this type of volcanic rocks. Our study revealed gradual changes in major and trace element compositions of volcanic rocks. Thus, the estimates support our view on attenuation of intra-plate and rising of island-arc features.

In respect to geodynamics, these structures have “asthenospheric origin”. Therefore, observed mechanism of rotational evolution is in agreement with the concept of differentially rotated geospheres that have an asthenospheric “lubricating layer” between them [5, 16, 23,]. Hydrodynamics of this layer is well described by the theory of spherical bearing [18]. These models are successfully used in meteorology and oceanology to analyze synoptic whirlwinds and rotor flows.

INTRODUCTION

Existing geological data [25] suggest ancient (Upper Jurassic – Early Cretaceous) origin and relatively stable position of the Western – Pacific transition zone. The evolution of this zone is best studied in Cenozoic. However, a plate tectonic concept can’t answer many questions arising from the study of this zone. Geophysical data and the distribution of the heat flow anomalies [12] are in conflict with to subduction concept. Intraplate volcanism is not typical for the island arc systems. At this point, it will be useful to introduce some terminology

[10] constrained any exotic models as “slab windows” in order to explain the obtained paradoxical phenomena

Recognition and interpretation of the rotational structures are broadly discussed in geological papers [2, 3, 6, 17, 21, 22, 30]. Fig. 1 shows global rotational systems that describe relationships geotectonic and energy of the Earth [6].

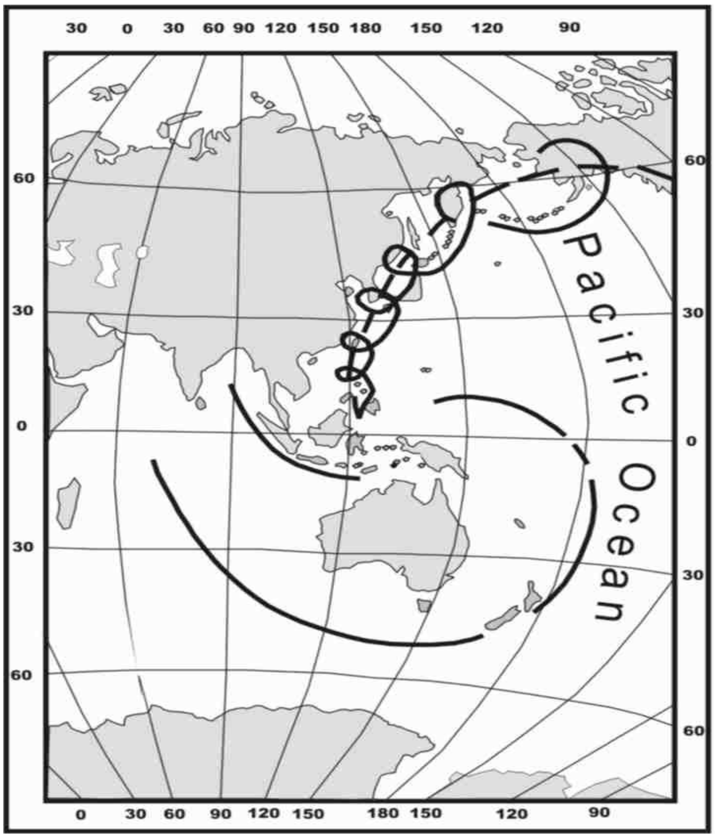

Fig. 1. **The global rotational system of Indo-Pacific Region of the Earth [6].**

In this paper we make an attempt to explain some of characteristic features of the Western – Pacific transition zone based on rotational geodynamics concept. As well known, non-traditional approaches are widely assumed to understand the Earth’s interior processes [7].

XENOLITH-BEARING VOLCANITES AND OTATIONALSTRUCTURES

In our investigation of Upper Miocene to Quaternary xenolith – bearing volcanic rocks were used as indicators to detect rotational geological features. They reflect the deeper processes.

Earlier, G. I. Anosov et al. [2, 3] presented indicative possibilities of the same xenolith – bearing volcanites to display Late – Cenozoic rotational structures within Kamchatkan Peninsula (Fig.2).

Figure 3 shows distribution scheme of the xenolith-bearing volcanites compiled from published papers. A time pattern of volcanic rocks combined with

---

observed spatial patterns of basalt and xenolith compositions could be explained by presence of three rotational structures of cyclonic type. The fourth structure lies around the Bering Sea.

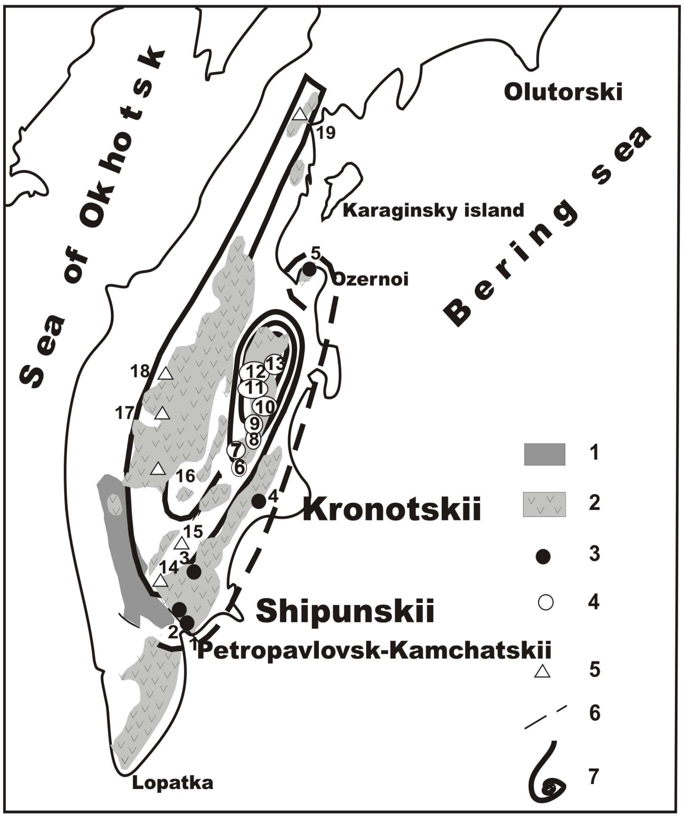

Fig. 2. **Pliocen-Quartery volcanites of Kamchatka, geologic objects hosting the ultramafic xenoliths and attributing the feature outlines of the rotational tectono- magmatic structure.**

1-metamorphic basement outcrops; 2-distribution of the Pliocene-Quartery volcanites; 3-5-xenolit-bearing volcanites: 3-dunite-harzburgite's association (volcanoes: 1-Avachinsky, Koryaksky, 3-Szhupanovsky, 4-Kronotsky, 5-Nachikinsky); 4-dunite-wehrlite-pyroxenite's association (volcanoes: 6-Nikolka, 7-cones of the Great Tolbachik Fissure Eruption, 8- Zimina, 9-Bezymyannyi, 10-Kluchevskoy, 11-Zarechny, 12-Harchinsky, 13-Shiveluch); 5- wehrlite-pyroxenite's association (14-plateau basalts of Backening area, 15-basalt dykes and sills of Stepanova river, 16-Ichinsky volcano, 17-volcanites "Geologist's Doll, 18- Ketepana volcano, 19- Valovaam river); 6-faults; 7-apparent contours of the rotational tectono-magmatic structures.

It is noteworthy that two of them delineate the marginal seas (the Sea of Japan and the South China Sea) where abyssal basins are typical. The third, the Central Kamchatskay depression is part of the Kamchatkan structure and has inherited characteristics of the Upper Cretaceous-Paleogenic continental margin basin (?).

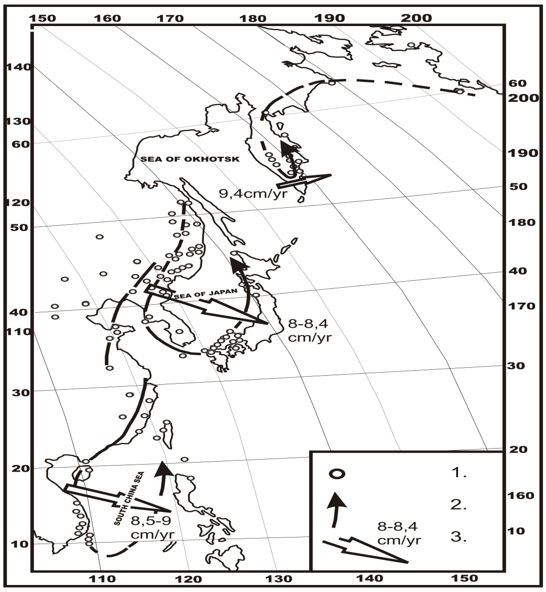

Fig. 3. **Late Cenozoic xenolith-bearing volcanoes in East-Asian margin and rotational structures.**

1-xenolith-bearing volcanoes; 2- rotation structures; direction and velocity of volcanic front. Data from: [11, 13, 26, 28, 29, 34].

These structures have similar morphological and geological compositions.

Intraplate volcanism (or “subintraplate volcanism” for Kamchatka) happens in the western segment of each structure and hosts associated xenoliths of the spinel-lherzolite type.

Island-arc volcanism occurs in the eastern segment of the structures. Xenoliths of olivine-plagioclase equilibrium are found in this type of volcanic rocks. Gradual variations in major- and trace element compositions are observed along each rotational structure. Genetic properties of each structure display a decrease of intraplate features from western to eastern segment of each structure. Age dating allows calculating of average formation time of these structures through displacement of volcanic front. Figure 3 shows directions and velocities of volcanic front. Velocity values exceed slightly that of corresponding to the known velocity of convergent plate in the region [33]. These peculiarities at testifies to autonomy origin of the rotational structures.

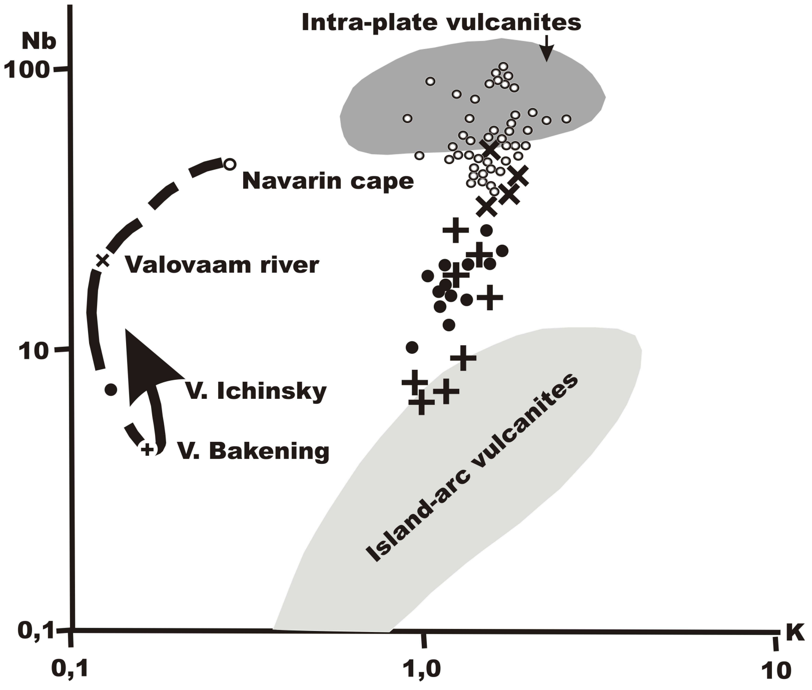

Fig. 4. **Plots of Nb versus K for Late Cenozoic volcanites of Kamchatka’s rotational structure. Different symbols are the same on the rotational curve.**

Figure 4 displays petrologic data used to analyze the deep structure of the studied volcanic centers in respect to those had been resulted in the deep rotational processes. Obviously, the patterns of Kamchatka’s volcanites corresponded well with the changes of these chemical elements along the trend: Navarin cape – the Valovaam river–Ichinsky and Backening volcanoes (fig. 4), which may explain shift in volcanic compositions from intraplate type to island-arc type. Also, Figure 5 confirms the same relationship based on the change trend of Na and Al in clinopyroxene of hyperbasite’s xenoliths: evidence for transition from depth to

---

shallow level. The same regularities may be evident for Japanese rotational structures (Fig. 6 and 7).

Northern American volcanoes have been analyzed by [19, 20]. We examined Precambrian to Early Cretaceous xenolith - bearing kimberlites and Paleogene to Quaternary xenolith – bearing basalts. Figure 8 demonstrates the geodynamic development of Northern America volcanism, where the cyclonic – anti-cyclonic rotational structures are reconstructed on geological and petrologic data. The oldest Precambrian structures of the Eastern – North area.

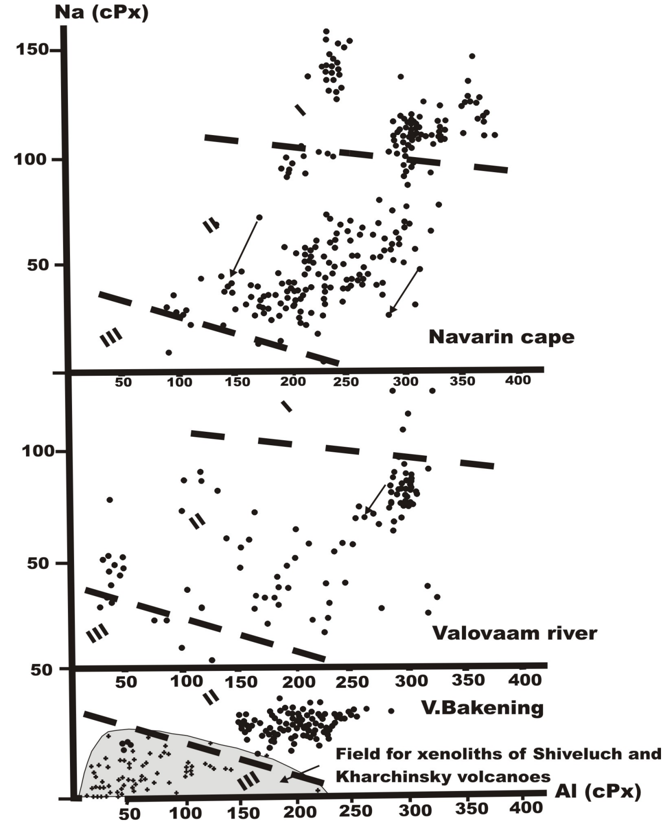

Fig. 5. **Plots of Na (cPx) versus Al (cPx) for clinopyroxene of xenoliths in Late Cenozoic volcanites of Kamchatka's rotational structure.**

I-III – stages of the xenolith's evolution [14]: I- spinel-lherzolite equilibrium, II-intermediary stage, III- olivine-plagioclase equilibrium. Pointer: core-ring of the crystal

The second Devonian-Permian kimberlite western structure restricts the Great basin and Colorado plate. In time, kimberlite magmatism is changed by Pliocene – Quaternary basaltic one and shifts its contours westward.

Earlier, I.V.Melekestcev [21, 22] established this structure based on the morphological data. Notably that Figure 9 displays counters of these structures that agree with locations of the earthquakes ("intra-mountain seismic belt"[31]).

Simultaneously, a pair of rotation structures situated over the central part of California and of the Mexico Gulf is revealed. These structures are well detected on the studied xenolith – bearing basalts.

The North American structures have funnel-like morphology and are similar to those of the Eastern - Asia margin (Fig.3). The average velocities of their formation approach 10 – 11 cm/yr during Pliocene – Quaternary time. These values exceed that of (2.4 cm/yr) the North America plate [31].

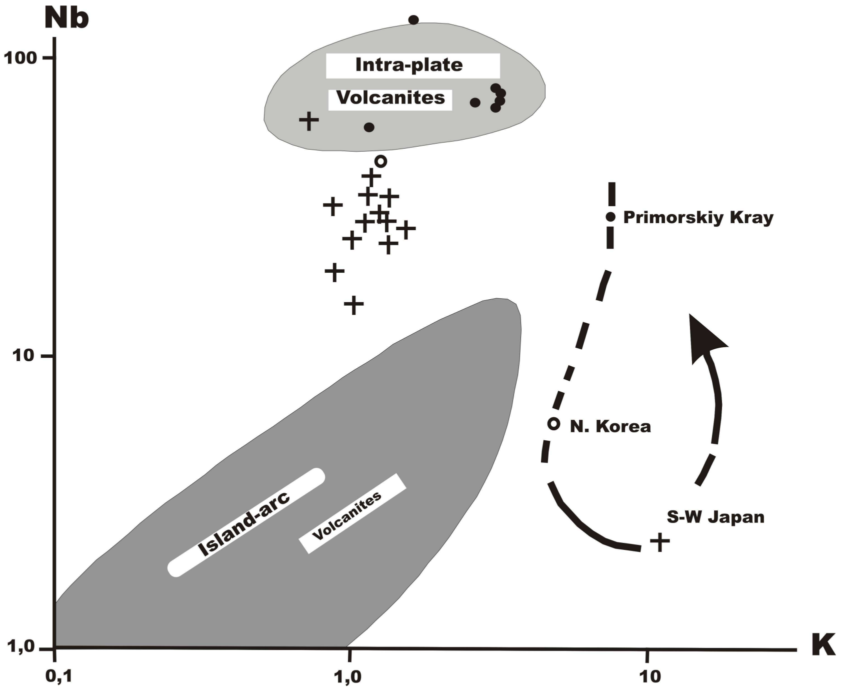

Fig. 6. **Plots of Nb versus K for Late Cenozoic volcanites of Japanese rotational structure. Different symbols are the same on the rotational curve.**

Data from: [8, 9, 15, 24, 32].

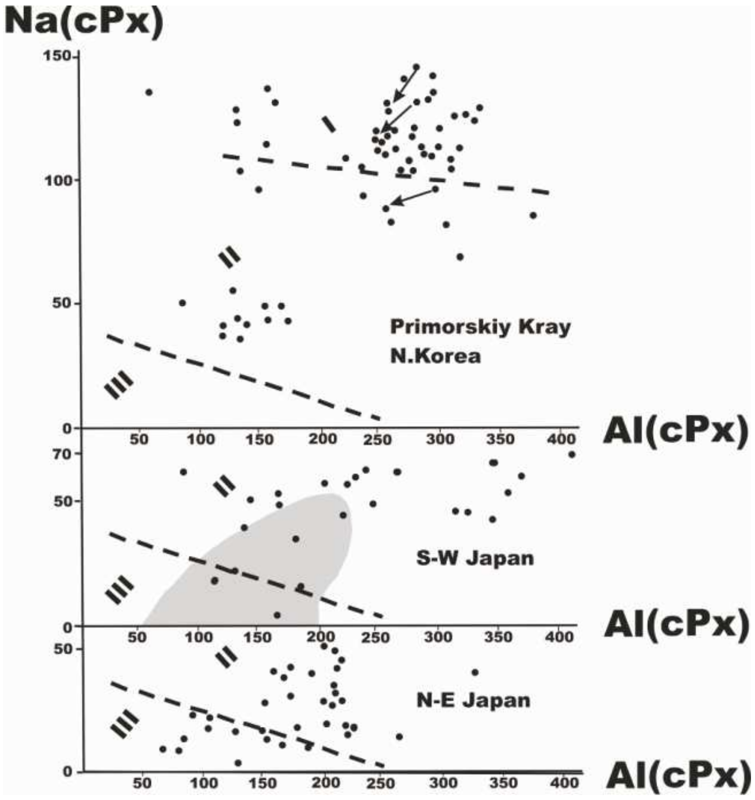

Fig. 7. **Plots of Na (cPx) versus Al (cPx) for clinopyroxene of xenoliths in Late Cenozoic volcanites of Japanese rotational structure.**

I-III – the same on the fig. 5.

CONCLUSION

The existence of the recent tectonic frame in the northwest Pacific has apparently been formed in the middle-upper Cretaceous as suggested by the wide-extended hiatus within the geostratigraphic column of this Pacific province. We assume that this hiatus ended as a result of total crustal uplift, due to a process that was apparently caused by some "asthenospheric dilution" as an outcome of the turbulent processes induced over or nearby the asthenospheric bottom. We consider this process to be reasonable, because our approach deduces from the Earth's radius increasing, rather than a decreasing of mechanical energy, that is apparently released the uppermost levels. We suppose also that both of these processes develop parallel to each other promoting an acceleration of volcanism epochs.

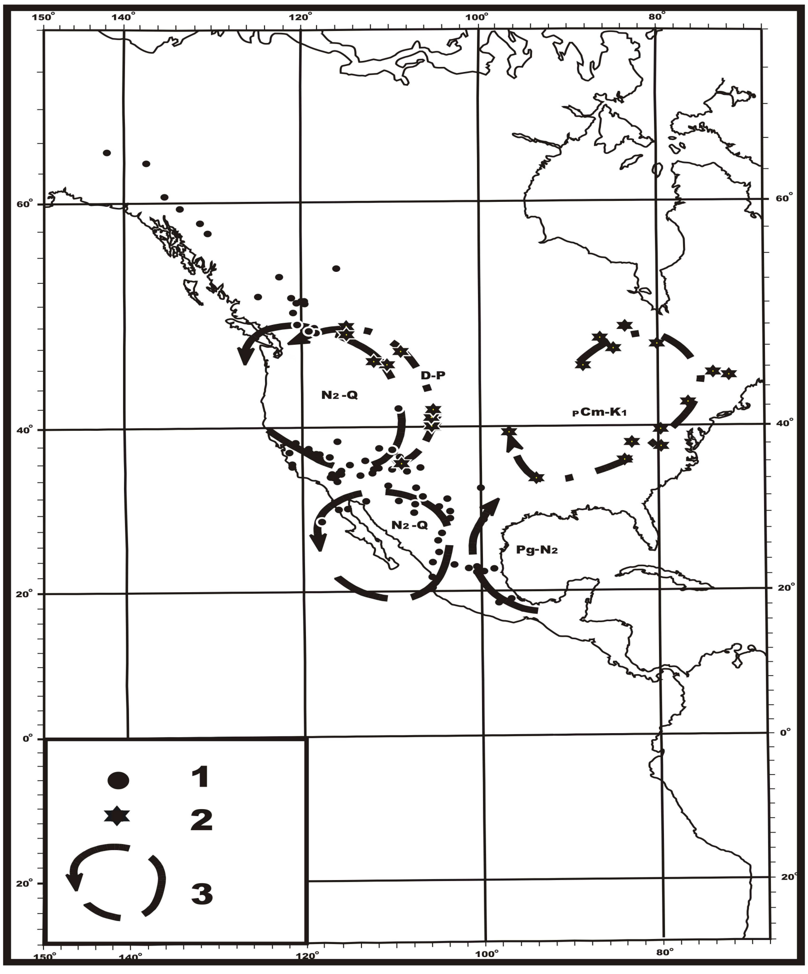

Fig. 8**. The volcanic centers of Northern America (basalts(1) and kimberlites(2)) containing the ultramafic xenoliths and the contours (3) of rotational magmatic structures.**

Data from: [19,20]

We propose also that asthenospheric turbulent mixing is a result of the Earth's radius increasing at the asthenosphere level, due to the reorganization of the Earth's rotation regime prior to this time. Such reorganization is usually accompanied by changes in the Earth's state from contraction to extension.

The same reconstructions are caused by striving of rotational body for an acquisition of body constitution which coincides to active rotation regime because to meet the strong requirements of constant inertia momentum of the Earth's movements.

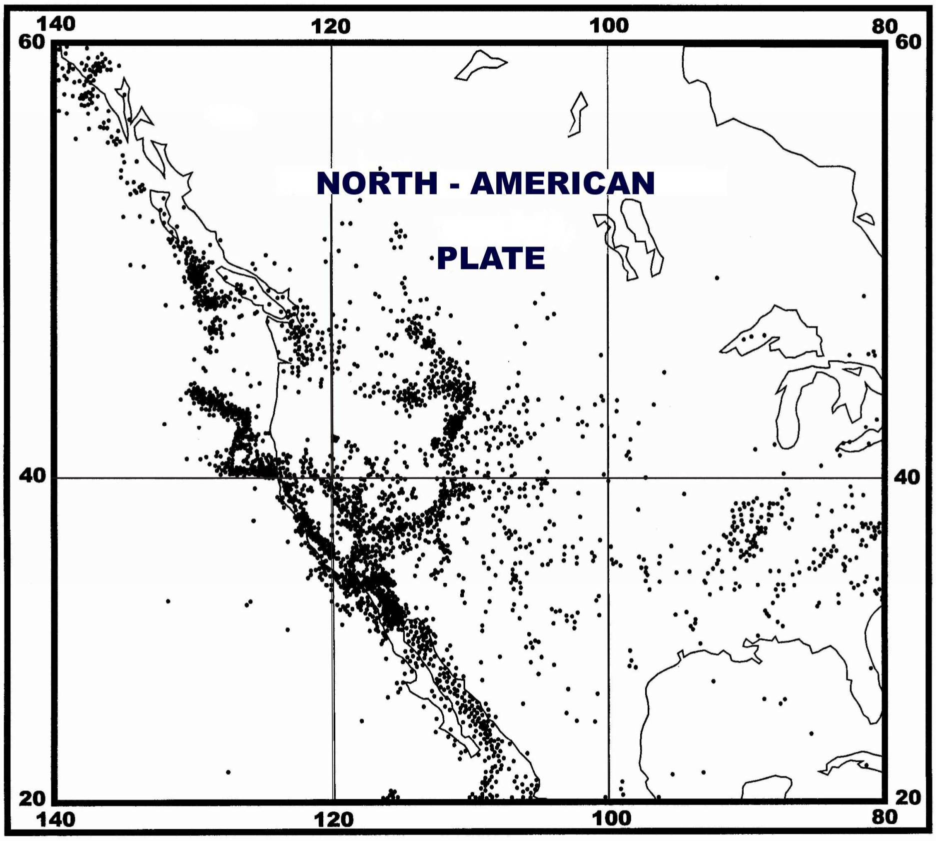

Fig. 9. **Seismic map of Northern America [31]**

As a rule, the same turbulent mixing conditions in the asthenosphere have affected the delimination stage in terms of "lithothermal feathers" or as "asthenospheric injection".

There is hypothesis that most of the major strike-slip faults represent such asthenospheric activities. Therefore we assert that the tectonic evolution due to the changes of the Earth's rotation from a deceleration regime to an acceleration region on epoch about 125 My (between M3 and M4 magnetic anomalies), and the changing from a contraction regime to extension regime (according to the paleomagnetic data about 15-20 My later on due to relaxation constant of the elastic-rigid Earth) are clearly recognized by geological evidence rather than the India-Eurasia collision, because the changes of rotation regimes may cause in and of itself tectonic reorganization.

These objections, as a rule, are based on the entire negations of significant rotation, or the infinitesimal influence onto tectonics. For example, S.K. Runcorn [27], engaging in polemics with Prof. Lyttleton, R.A., assumes that:

"the viscous term in the Navier-Stockes equation of flow in the Earth's mantle is about 10 to power 20 greater than the inertia and acceleration terms", [27, p.521] and,

"... calculated the changes in the moment of inertia (and in the gravitational energy) as the core grew during the Earth's life", ... as "the first order effects of growing core, while the changes in the overall radius of the Earth are a second order effect", and from that ... "took the radius of the Earth to be (nearly) constant" [27, p.522].

Based on these assumptions, the changes in the lithosphere-asthenosphere ranging from several kilometers (not more than 50 km, in general) overturn all of Runcorn's calculations. Furthermore the present astrometric data can monitor the mass replacement on and into the Earth . In our opinion, the changes of Earth's rotation regimes are most of the reliable processes (the first order) as compared to it’s (a second order) convective currents because the latter are also caused by rotational motions of the inner core of the Earth rather than disturbed temperature distributions.

As a result of the Earth's reorganization of it’s rotation and state regimes, the surface geological effects have inertia phase lag relative to rotation changes of approximately 40-60 My. This phase lag is clearly manifested by magnetic data, and is caused by, on the one hand, the delay time (about 15-20 My above) to the beginning of the contraction or extension stages, and on the other hand, the time retardation (about 20-40 My) due to protracted up-promotion of the rotation regime changes cross asthenosphere up to the bottom of the Earth's lithosphere or back turn to mesosphere -asthenosphere boundary, that is to say,- there and back or back and forth directions.

Due to lag of time, the geological events had started after the origin of the delamination stages beneath the lithospheric bottom of the tectonic province in terms of uplifting. The wide extension, caused by a crystal break-up and failure of the Earth's surface which is a break-thrust and strike-slip fault motion, is part of those being demonstrated by Fig.10.

It's necessary to point out that the inertia moment of the Earth, and the changes of its rotation velocity, are very sensitive to the reorganization within the Earth's uppermost shell, so that there adjust enough astrometric data. Therefore, "any tectonic constructions in which the lateral redistributions of the Earth's mass are envisaged the final results of these constructions must be experienced by those data" [4, p 200].

All of the fault dislocations (Fig.10.1) appear to be a reaction of the Earth's shells (in terms of lithosphere) to the changes of the rotation velocities of the Earth. Actually, the longitudinal extension in the high latitudes (from 90° to 34 degree), and the common latitudinal lateral compression of the Earth's shells near equator, are usually revealed for decelerated rotations. And both of them will be backwards if the Earth's rotation is accelerated. In addition, the rotation of the Earth provides tangential displacement (meridian drift), which occurs under pole ward-running forces, forming an ellipsoid of the Earth's. These forces are directed from the poles toward the equator and are especially effective during latitudinal extensions. It is not an exception, that high-speed development of the study area during the last 25-30 My was caused by the transition of the Earth's rotation from a decelerated regime to an accelerated regime after passing the "limiting point" of its orbit.

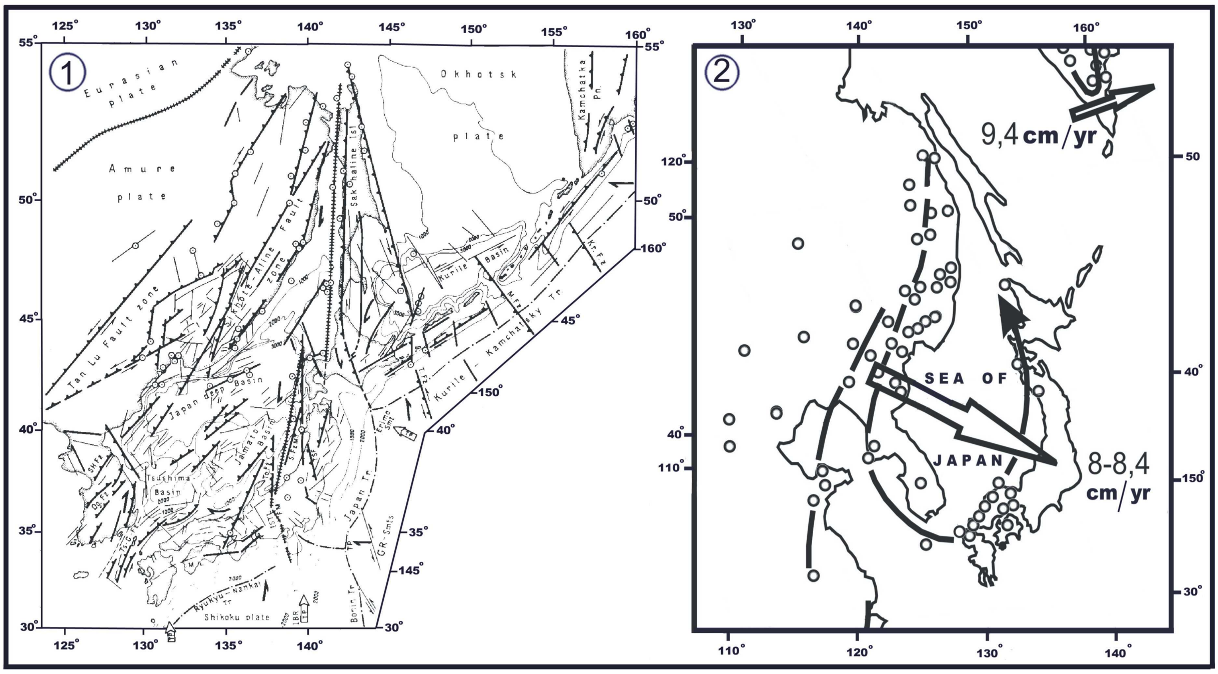

Fig. 10**. The summarizing geodynamic situation in and around the Sea of Japan.**

1. from [1]. Opened circles are the earthquake epicenter locations (M>4), One-sided arrows are the directions of relative dislocations; the wide arrows fix the triple junction points in space. 2. From fig. 3**.**

2.

According to mentioned above, the stage of the global tectonic reconstruction due to such cases is emphasized by the changes in direction of the Pacific plate. These data have been obtained from an analysis of the magnetic lineation of the Japanese and Hawaiian systems at the time boundary between 80-60 My (i.e. 40-60 My later than changes of the Earth's rotation regime or 20-40 My later than the Earth's state alternation from contraction to extension) deduced from termination of Cretaceous magnetic epoch and the beginning of the Cenozoic one.

In line with galactic scale, the Cretaceous "quite zone" may be compared with the time interval when the Earth took passed the point of state change (from contraction to extension). Time interval of these transitions is evaluated at about 30 My and the sign of Earth's rotation was always changed during this time and all of the endogenic processes would run more slowly. Also during this time, the final configuration of the trench-arc systems was formed in North Pacific.

Here at least three triple points (Fig.10.1) had anchored this system in space, and the Ryukyu-Kushu and Izu-Ogasawara - northeast Honshu volcanic belts had fixed this system on the time scale of the evolution of the Japan and Okhotsk back-arc basins began with meridian drift of the lithosphere. This moving is caused by a latitudinal extension accompanied by longitudinal, lateral compression. All of the above resulted the arising stress field and were revealed as a complex system of dextral and synistral strike-slip fault zones and, were formed as some nucleation of future pull-apart basin. The existence of strong inhomogeneties in the lithosphere of the study area produced several independent blocks. Later these blocks cropped up as three separated subbasins of the Sea of Japan.

This suggests tectonic-mechanical modeling which usually describe the origin and evolution of the East Sea area as a whole, may be represented by the effects of a sum of a thin viscous sheet model as latitude components, a drifting model as longitude component, and transcrossing turbulent moving of the thermal-mass – shifting of the asthenosphere matter. Moreover the beginning of the initial stage is similar to that suggested by a pull-apart model as well as a result of the surface effects of the complex rotation of the fluid-magmatic tornado [2].

Nevertheless, the available experimental data may support many other interesting models major features of which would be combined in the sense of the linear accumulation of several independent resolutions with different weight functions. The latter would take into account the scale influence of these models and their phase shifting because of the inertia of the tectonic processes related to a change of the Earth’s rotation. But in these cases the effects of the Earth's rotation regime must be taken into account as first order results because of the multiple, one-directed additive of tidal stresses are cumulative through geological time.

The scale of pull-apart opening is not significant in the sense of sea extension-scale as it was mentioned of the pull-apart model because the strength of the tectonic frame described above does not permit such substantial shifting of the Japanese Islands into south-southeast, relative to latitude.

It seems that tectonic cleavage from southwest to northeast of Honshu Island, which is known at the present time as Itoigawa-Shizuoka Tectonic Line (or Fossa-Magna Transcurrent Zone), as well as obduction along the eastern margin of the Japan Sea, are compensating structures, and not a simple opening as deduced from the pull-apart model.

These movements may be examined as comparative displacements of both the northeastern and southwestern Japan, caused by the interaction of the American and Pacific plates. The excess surface sizes and the crustal volumes resulting have been partly annihilated by thrusting and folding near and along the Median Tectonic Line (MTL), creating here a width of "relict" ancient metamorphic belt. But these tectonic displacements are not observed at the south and southeast side of Honshu.

However, the most significant crustal "over abundances" have been most probably wiped out by south-southeastern bending of the Honshu Island. The results of these movements are represented by a clockwise rotation of southwestern Honshu, caused by slow creep of the triple junction points (the Izu-Bonin-Japan-Nankai trenches) along Nankai the west as well as it follow from the rotation conception related to external their shell [2].

The results of these movements are documented in particularly by a strong thrust zone in the Tsushima trough, and by the fan-shape opening of the Ulleung basin.

All of the above features are presented in Fig.10.1, which shows that the marginal system of strike-slip faults has outlined the rhombic form of the whole East Sea in terms of a dextral and sinistral shear system, the surface images of which have been revealed as the rifting crust beneath marginal areas. Based on the DSS- seismic results (Deep Seismic Sounding), we suggest that the map of crystal types points out the order, or degree, of crystal reconstruction caused by interplating processes that filled in the lowest parts of the crust with dykes and sills. It's difficult to argue that the results of this process have provided the origin of suboceanic crust because the Moho is yet undetermined, and because the uppermost section is continental crust. It's believed that, thinner continental crust exists rather than the new, thick oceanic crust. Presently rift zones along western and eastern sea-boundaries coincide with boundary strike-slip faults are interpreted to be underlain by hot asthenosphere, and would provide the present stage of sea-evolution. It appears that the wide low-velocity zone underlying sea-crust, does not exist, because of the anomalous zone is revealed only under marginal areas where the faults of the strike-slip type are developed.

The beginning of this stage is probably controlled by the age of the northern Ulleung subbasin, called the Kita-Ulleung trough (the latest Miocene-Pleistocene period).

We may demonstrate the interpretations of the four stages as consequent from fig. 10.1 and fig. 10.2 as follows:

1) The stage of the initial stretching due to drifting of the Earth's segments to the south-southeast along strike-slip fault systems, and an appearance of the original magmatic feathers beneath these surface strike-slip fault zones are surmised. This stage resulted in (at 65-42 My) complete reconstruction of the northwestern Pacific due to changes of the Earth's rotation but caused the delay because of the inertia of the Earth’s shell structures. This stage is coincided with primarily clockwise moving being attributed to the external shell of the fluid-magmatic tornado [2].

(2) Future extension caused the strike-slip fault delatancy and the continuation of this process resulted in the rising of the asthenospheric melts to the bottom of the lithosphere at 42-30 My. This is a stage of an origin development of the interior shell of the fluid-magmatic tornado, and of the generation volcanic process, development of which would be directed as counter clock-wise (Fig.10.2), following to internal shell rotation of the fluid-magmatic tornado [2].

---

(3) An origin of the magmatic chamber with just enough sizes could provide the underplating and subsequent interplating processes causing the uplifting specious and local areas. Continued development of the pull-apart strike-slip dislocations accelerated the above processes in time and space. Furthermore, the collapse of the sea margin led to relatively sharp, increased subsidence of this margin. Arial volcanism accompanied and emphasized these movements greatly.

All in all, the rotation conception of the fluid-magmatic tornado presented for an explanation of tectonic development of the Transition Zone from the Asia to Pacific may be applied both of the volcanoes, and of the opening marginal seas. Besides of those the metamorphic or the oldest geologic structures are evidently mapped in central parts of the fluid-magmatic tornado (as Sredinny and Ganal massives, Kamchatka, and so the Sea of Japan), and a rejuvenation of both the structures, and the xenolith – bearing volcanites are resulted along rotational curve.

As to the geodynamic aspect, the studied structures have “asthenospheric origin”. Thus, observed regularities could be explained by the theory of differential rotational geospheres.

Existence has been provided by various geologic and geophysical data [2]. This work provides support to the hypothesis of inferred rotational structure pattern that may be explained regarding the differential rotation spheres of the Earth. In this case, the asthenosphere, as well as “lubricating layer” is situated between lithosphere and mesosphere. The hydrodynamics of this layer and all patterns are fully described by a theory of the spherical bearing. Similar approaches are widely used to analyze synoptic vortex and that of the seabed.

Yr. N. Avsyuk [4] showed that a slowdown of rotation velocity of the Earth is observed in Pliocene – Quaternary time. As a result, a differential shifting of the asthenospheric layer moved eastward. We can see “creeping” of the inferred vortex structure towards the Pacific side in the boundary between Pacific and Indo – Asia lithospheric plates, and to the North – American continent interior along its western boundaries.

As it was mentioned, this cycle was repeated twice for the North – American rotational structures. The first shifting coincides with the slowdown of the Earth rotation in Devonian – Permian time. Westward and south – westward shifting of the rotational structures of the North-American continent reveals in the epoch of relatively accelerating rotation of the Earth (during Permian – early Upper Cretaceous time).

We assume that the most energy advantageous and more realizable in reality the fluid-magmatic tornado would be proposed as it had been based by us elsewhere [2].

ACKNOWLEDGEMENTS

Special thank goes to O. Evdokimova (IVS) and Dr. Tomas P. Miller (AVO, Alaska) for editing this paper.

This paper was supported by the project of FED RAS 04-1-07-004.

REFERENCES

1. **Anosov G.I., Suk B-C., Soynov V.V.** Some geodynamic aspects related to evolution of the Ulleung basin (the East sea of Korea) resulting from integrated geophysical data. Proceedings of the Third International Conference on Asian Marine Geology, 1995, Korean Society of Oceanography, Korea, 1996
2. **Anosov G.I., Koloskov A.V., Flerov G.B.** Non-linear manifestation in petrology and geodynamics of magmatic process in the Kamchatka region //Geodynamics, magmatism and mineralogy of the continental margins of North Pacifica. Magadan: SWKNII DWO RAN, 2003. T. 2. pp. 174-177, (in Russian).
3. **Anosov G.I., Koloskov A.V., Flerov G.B.** 2004, Manifestation of ultramafites of the Kamchatka region resulting from the rotational dynamics, Vortex-related events in the geological processes. Petropavlovsk-Kamchatsky, pp. 129-200, (in Russian).
4. **Avsyuk Yr. N.** Having flown forces and natural processes. M.: OIFZ RAN, 1996. 188 p. (in Russian).
5. **Bobriakov A.P., Revujenko A.F., Shemiakin A.F.** About the possible mechanism of moving of the mass of the Earth. // Dokl. Akad. Nauk SSSR, 1983. v. 272. № 3. pp. 1097-1099, (in Russian).
6. **Dmitrievsky A.N., Volodin I.A., Shipov G.I.** 1993, Energy-Structure of the Earth and Geodinamic. M. Nauka ,154 p. (in Russian).
7. **Dobretcsov N.L., Kirdeashkin A.G., Kirdeashkin A.A.** 2004, The Deyh’s Geodinamic, Novosibirsk. 401 p., (in Russian).
8. **Fedorov P. I., Filatova N.I.** Cenozoic volcanism of the Korean region. //Russian Geochemistry, 2002. № 1. pp. 3-29
9. **Hoang N., Uto K.** Geochemistry of Cenozoic basalts in the Fukuoka district (northern Kyushu, Japan): implications for asthenosphere and lithospheric mantle interaction // Chem. Geology. 2003. V. 198. pp. 249-268
10. **Hole M.J, Rogers G., Saunders A.D.** Storey M. Relation between alkalic volcanism and slab-window formation // Geology, 1991. V. 19. pp. 657-660
11. **Ikeda Y., Nagao K., Kagami H.** Effects of recycled materials involved in mantle source beneath the southwest Japan arc region: evidence from noble gas, Sr, and Nd isotopic systematics //Chem. Geology. 2001. V. 175. pp. 509-522
12. **Ilyichev V.I, and Shevaldin Yr. V.** 1986, About the nature of Western-Pacific transitional zone, DAN, SSSR, v.290, N3, pp.570-573, (in Russian).
13. **Ionov D.A., Prikhod’ko V.S.** O’Reily, 1995, Peridotite xenoliths in alkali basalts from the Sikhote-Alin, southeastern Siberia, Russia: trace-element signatures of mantle beneath a convergent continental margin, Chem. Geology, 120, pp. 275-294
14. **Koloskov A.V.** 1999, Ultramafic inclusion and vulcanites as self-regulation geological system. M. Nauchnii Mir. 223 p. (in Russian).
15. **Kondo H., Tanaka K., Mizuochi Y. et al.** Long-term Changes in distribution and chemistry of middle Miocene to Quaternary volcanism in the Chokai-Kurikoma area across the Northeast Japan arc // The Island Arc. 2004. V.13. pp. 18-46
16. **Kropotkin P.N., Efremov V.N.** Changes of radius of the Earth in the geological past // Geotectonic. 1992. № 4. pp. 3 – 14, (in Russian).
17. **Li-Si-Guan.** Vortex’s structures of northwest China. Moscow: State scientific and technical Izdatel’stvo - in literatures on geology, 1958. 129 p., (in Russian).
18. **Loiizansky L. Gg.** The hydrodynamical theory of the spherical bearing. P.M.M., 1955. V. XIX. T. 5. pp. 531-540, (in Russian).

---

19. Mafic and Ultramafic xenoliths from volcanic rocks of the Western United States. U. S. Geological survey professional paper 1443. (Ed. Wilshire et al.). 1988. Washington. 179
20. Mantle xenoliths, 1987, In: P.H. Nixon (Ed.), JOHN WILEY& SONS, 844 p.
21. **Melekestsev I.V**. 1979.A rotational volcanic hypothesis and some perspective it of application // Problems of the endogenous volcanism. M.Nauka, pp. 125-155, (in Russian).
22. **Melekestsev I.V.** 2004, Significance of vortexes in the origin and existence of the Earth, Vortex-related events in the geological processes. Petropavlovsk-Kamchatsky, pp. 25-70, (in Russian).
23. **Miasnikov V.P., Fadeev V.E.** Hydrodynamical models of evolution of planets of terrestrial group. M. Nauka , 1979. 231 p., (in Russian).
24. **Morris P.A., Itaya T., Iizumi S. et al.** Age relations and petrology of alkalic igneous rocks from Oki Dozen, Southwest Japan //Geochem. Journ. 1997. V. 31. pp. 135-154
25. **Mossakovsky A.A, Pushcharovsky Yu. M.** and Ruzhenstev S.V., 1998, The Earth' Major Structural Asymmetry, Geotectonic, N 5, pp. 3-18 (in Russian).
26. **Qi Qu, Taylor A., Zhou X.** Petrology and Geochemistry of Mantle peridotite xenoliths from SE China // J. Petrology. 1995. V.36. № 1. pp. 55-79
27. **Runcorn S.K.** The geophysical consequences of Professor Lyttleton. //Nature, 1973, V. 241, pp 521-523
28. **Sahno V.G., Denisov E.G.** To a question on an origin of ultramafic inclusions in basalts of the South of Far East. Izv. A.N. USSR, Series. Geol., 1963. № 8. pp. 43-55, (in Russian).
29. **Scheka S.A.** Mafic-ultramafic intrusive rocks and inclusions in extrusive rocks of Far East. M.: Nauka, 1983. 166 p. (in Russian).
30. **Slenzak O.I.** Vortex's systems of Lithosphere and Precambrian structure . Kiev: "Naukova Dumka", 1972. 182 p., (in Russian).
31. The seismic map of America. (Compiled by Tom Simkin, R.I. Tilling, I.N. Taggart et al., 1989 Smithsonian Institution US. Geol. Survey.)
32. **Togashi S., Tanaka T., Yoshida T. et al.** Trace elements and Nd-Sr isotopes of island arc tholeiites from frontal arc of Northeast Japan //Geochem. Journ. 1992. V. 26. pp. 261-277
33. **Uyeda S., and Kanamori H.** Back-Arc opening and the mode of subduction //J.Geophys. Res. 1979. V. 84. N. B3, pp. 1049-1061
34. **Vidal Ph., Dupuy C., Maury R., Richard M.** 1989, Mantle metasomatism above subduction zones: Trace-element and radiogenic isotope characteristics of peridotite xenoliths from Batan Island (Philippines), Geology, v.17, N 12, pp. 1115-1118

UDK 550.42; 552.111

PECULIARITIES OF ALKALINE BASALTOID MINERALOGY IN CENTRAL SIKHOTE-ALIN TERRIGENOUS-VOLCANOGENIC-SILECEOUS COMPLEXES

Petukhova L.L., Voinova I.P., Prikhodko V.S.

Yu.A.Kosygin Institute of Tectonics and Geophysics of Far Eastern Branch of Russian Academy of Sciences, Khabarovsk, vladimir@itig.as.khb.ru

On the example of two geological sections (Anyuisky and Barakhtinsky) the peculiarities of mineralogy of basaltoids from the Central Sikhote Alin terrigenous-volcanogenic-siliceous complexes have been considered. Volcanic rocks refer to alkaline series and are subdivided into sodic and potassic types. Basaltoids are represented by lava, rarely by lava breccia. The rock structure varies from aphyric to magnophyric. The phenocrysts are primarily clinopyroxene, rarely mica, amphibole, olivine, hosted by groundmass, made up by microlites of clinopyroxene, glass, and ore minerals. Clinopyroxene of phenocrysts and groundmass refers to augite and titanaugite. Amphibole, forming megacrysts and phenocrysts, refers to kaersutite. Mica of phenocrysts corresponds to ferruginous phlogopite. Ore minerals are represented by ferro-titanium oxide minerals. The volcanic rocks under consideration, occupying an intermediate position between mafic and ultramafic rocks, represent a rather peculiar group of rocks, which is confirmed by peculiarities of their mineralogy. Plagioclase practically does not occur among the phenocrysts and groundmass; the dominating minerals in these rocks are augite-titanaugite and ferro-titanium oxides. The abundance of amphiboles and mica in these volcanic rocks is suggestive of high water content in parent melts. All this points to the specific conditions of the Mesozoic magmatic activity at the Pacific Ocean intraplate environments.

INTRODUCTION

Nappe-fold structures of the Central Sikhote-Alin formed in the Mesozoic as a result of the processes of accretion and subsequent tectonic transformations. The accretionary system under consideration is made up by lens-shaped packets of terrigenous-volcanogenic-siliceous complexes of Triassic-Jurassic age included into Late Jurassic-Early Cretaceous turbidite matrix. In order to study the evolution of the Mesozoic oceanic magmatism and reconstruct the process of accretion at the Pacific margin of Asia, various aspects of intraplate oceanic basaltoids of the Sikhote-Alin accretionary system have been studied. Mineralogical peculiarities of volcanic rocks of terrigenous-volcanogenic-siliceous complexes from the Central Sikhote-Alin accretionary prisms have been examined in the present paper on the example of two geological sections (Anyuisky and Barakhtinsky).

GEOLOGIC SETTING

Anyuisky section. On the Anyui and Khor rivers' watershed an association of volcanic and siliceous formations makes up a tectonically limited lens among alternating siltstone and sandstone, the southeastern part of which is superimposed on the terrigenous rock mass. The volcanic rock mass is mainly represented by lava flows of picrobasalt (augitite) with the thickness up to tens meters, sometimes with spheroidal jointing. The section is characterized by the layers' northeast trending and steep southeast and northwest dipping. The rock mass is disjunctively dislocated which is manifested in abundant zones of fracture also trending northwest, on which the rocks have been intensively cataclasisised, the basaltoids - silicified and limonitized.

Barakhtinsky section. On the Anyui river midstream, within a terrigenous-volcanogenic-siliceous association there also occur basic rocks with a habit and petrographic characteristics similar to the volcanic rocks from the Anyuisky section. There are observed the volcanic structures which resulted from multiple submarine eruptions. They are composed of flows of alternating diabase, amygdaloidal basalt, hyalobasalt, and hyaloclastite. The thickness of the flows is the first meters to tens meters. Some basaltic flows have a distinct pillow jointing. Volcanic structures are located among variously colored siliceous and siliceous-clayey schist with near-boundary facial alternations of volcanic and siliceous rocks.

METHODOLOGY OF STUDIES

The characteristics of basaltoids from accretionary complexes have been given based on data of petrography, petrochemistry, and geochemistry of rocks and chemical composition of rock-forming and accessory minerals. The chemical composition of the minerals was determined on "Camebax" microanalyzer at the Institute of Volcanology FEB RAS* (analyst Chubarov V.M.).

PETROGEOCHEMICAL AND PETROGRAPHIC CHARACTERISTICS

Basalt and picrobasalt (augitite) from the sections studied are characterized by considerable compositional variations (SiO_2 from 39% to 50%; MgO from 5% to 15%; TiO_2 from 3% to 7%). They refer to alkaline series (sum of alkalis varies from 3 to 9 mass %) and are subdivided into sodic and potassic types with the ratios K_2O/Na_2O equal to 0,3 – 0,55 and 2 – 2,5, respectively. The rocks described refer to ferro-titanium type. The sodic varieties occur in the Anyuisky section, the potassic ones – in the Barakhtinsky. The geological setting of volcanic rocks occurrence, the position of figurative points of their compositions on discrimination geodynamic diagrams (a factor diagram by G. Pearce, TiO_2-K_2O, Zr/4-2Nb-Y, Zr-Ti/100-3Y, Nb-Zr), the character of minor elements distribution testify to their origin under oceanic intraplate setting, and then - accretion in the process of subduction [1].

The volcanic rocks from the terrigenous-volcanogenic-siliceous complex are represented by lava, rarely by lava-breccia of picrobasalt. The rock structure varies with gradual transitions from aphyric fine-grained to coarse-grained. Fine-grained aphyric varieties more frequently make up dikes, porphyritic lava – flows, sometimes with spheroidal and conchoidal jointing. The rock texture is amygdaloidal, rarely dense, and massive. In porphyry varieties phenocrysts make up to 30% of the rock volume.

Phenocrysts of porphyry varieties are primarily clinopyroxene, rarely mica, amphibole, olivine, hosted by groundmass. In potassic varieties of volcanic rocks there sporadically occur large isolated crystals of amphibole [2]. The groundmass is composed of microlites of clinopyroxene, glass, and ore minerals. A ratio between the components and a degree of the groundmass crystallization are not constant, therefore the rock structure changes. Glass is gray-green and brown. In more crystallized varieties in the groundmass there appear spots composed of feldspar, sometimes barium one, penetrated by elongated crystals of amphibole, biotite, “needles” of ore mineral, sphene, sometimes of radial orientation. Aphyric varieties have a habit similar to the groundmass of the porphyry ones.

MINERALOGY

Clinopyroxene forms phenocrysts of several generations. The largest (up to 1 cm) phenocrysts, individual or forming aggregates, are sometimes fractured, along the fractures there occurred the shift of blocks, and their replacement by groundmass. Pyroxene of younger generations makes a series of small phenocrysts substituted by secondary minerals, primarily chlorite. Large grains of clinopyroxene are, as a rule, zoned. Based on the chemical composition, the minerals considered refer to augite, titanaugite, or fassaite. The compositions of pyroxene-phenocrysts and groundmass of sodic volcanic rocks are as follows: f_{16-23} ; Wo_{48-50}; $En_{39,5-43}$;Fs_{8-12} and f_{25-33} ; Wo_{47-50}; $En_{35-39,7}$;$Fs_{12-17,5}$, respectively (Table 1). The pyroxene of picrobasalt of potassic type has the following composition: f_{24-26} ; $Wo_{48,5-49,5}$; $En_{37,5-38,5}$;$Fs_{12,5-13,5}$ and $f_{28-331,5}$; $Wo_{50-51,5}$; En_{33-36};$Fs_{13,5-15}$, respectively (Table 1). The compositions of the external rims of zoned pyroxene correspond to the compositions of clinopyroxene of the groundmass. Pyroxene of the basalt from the Barakhtinsky section is steadily depleted in titanium (Fig. 1). The principal direction in the general evolution of monoclinic pyroxene of picrobasalt from the two sections is manifested in titanium accumulation (+Al, Fe) (Fig. 1). The enrichment in these elements results in Mg, Si, and partly Ca contents depletion. Clinopyroxene compositions in a small group of the Anyuisky section basalt are characterized by titanium intense accumulation, beginning with SiO_2 content in them about 50 weight %, with practically constant aluminum and iron contents.

Olivine in phenocrysts occurs very rarely, and is entirely replaced by calcite, zeolite, serpentinite, iddingsite, chlorite rimmed by opacite. Small phenocrysts of plagioclase are very rare.

Table 1

Composition of clinopyroxene (weight %) in basalt and picrobasalt

	1	**2**	**3**	**4**	**5**	**6**	**7**	**8**	**9**	**10**	**11**
SiO_2	50.61	48.65	51.83	53.27	50.04	45.39	50.71	44.46	47.79	49.69	52.49
TiO_2	2.87	5.27	1.97	1.11	2.77	4.38	1.99	4.32	2.81	2.04	1.44
Al_2O_3	2.36	3.04	1.18	1.51	3.52	6.77	2.67	6.16	5.04	3.15	2.03
Fe_2O_3	5.02	6.37	3.6	4.02	5.33	6.53	6.44	9.20	8.40	5.99	5.20
Cr_2O_3	0.44	0.00	0.72	0.35	0.00	0.00	0.15	0.00	0.00	0.00	0.19
MgO	14.89	13.8	15.65	16.23	14.16	12.26	14.52	11.73	11.92	13.62	14.57
CaO	23.17	22.57	23.03	22.84	24.5	23.97	22.75	22.4	23.33	23.27	23.8
Na_2O	0.23	0.29	0.29	0.27	0.06	0.14	0.18	0.35	0.46	0.28	0.19
K_2O	0.00	0.00	0.00	0.00	0.00	0.00	0.00	0.00	0.00	0.00	0.00
MnO	0.00	0.00	0.00	0.00	0.00	0.00	0.00	0.00	0.00	0.00	0.00
Summa	99.6	100.00	98.26	99.62	100.37	99.44	99.41	98.64	99.75	98.03	99.91
	12	**13**	**14**	**15**	**16**	**17**	**18**	**19**	**20**	**21**	**22**
SiO_2	46.64	48.3	47.53	48.62	47.23	48.91	48.54	48.56	46.77	50.1	51.51
TiO_2	3.40	2.23	2.69	2.06	2.74	1.97	2.31	2.27	2.64	1.73	1.31
Al_2O_3	4.91	4.67	5.88	4.94	6.16	4.42	5.01	4.72	5.83	3.00	2.80
Fe_2O_3	7.72	8.06	8.41	7.31	8.73	7.21	7.88	7.86	8.07	7.89	8.58
Cr_2O_3	0.00	0.00	0.00	0.00	0.00	0.00	0.00	0.00	0.00	0.00	0.00
MgO	12.22	12.64	10.99	12.36	10.71	13.02	12.49	12.2	11.83	13.08	12.54
CaO	23.15	23.29	23.14	21.67	23.19	23.52	23.12	23.34	23	23.12	23.33
Na_2O	0.37	0.73	0.62	0.63	0.76	0.47	0.57	0.63	0.65	0.51	0.34
K_2O	0.00	0.00	0.00	0.00	0.00	0.00	0.00	0.00	0.00	0.00	0.00
MnO	0.00	0.00	0.00	0.00	0.00	0.00	0.00	0.00	0.00	0.00	0.00
Summa	98.41	99.92	99.26	97.58	99.60	99.52	99.92	99.57	98.82	99.42	100.23

Note: 1-12 – Anyuisky section; 13-22- Barakhtinsky section

Amphibole, forming isolated crystals of considerable sizes (megacrysts) in these rocks, has a prismatic habit, perfect cleavage according to (110). Based on the chemical composition, it refers to low-titanium kaersutite. Amphibole-phenocrysts are represented by elongated-prismatic, needle-shaped grains and aggregates of grains, frequently hosted in chrloritized glassy or feldspar groundmass. The content of TiO_2 in amphibole (kaersutite) widely ranges (3,5%-7,5%), the most titaniferous varieties contain the maximum potassium concentrations.

Densely colored brown mica (Table 2) occurs in porphyritic, frequently brecciated varieties, sometimes forming large (up to 1 cm) phenocrysts. Biotite of the groundmass of basalt compositionally corresponds to the most ferruginous varieties of mica (f=60%).

Table 2

Composition of mica (weight %) in basalt and picrobasalt

	1	**2**	**3**	**4**	**5**	**6**	**7**	**8**	**9**	**10**
SiO_2	34.78	36.68	35.38	35.96	35.74	38.44	35.77	34.33	34.51	34.89
MgO	11.27	9.92	9.67	9.25	11.37	12.40	10.9	8.23	4.13	5.36
TiO_2	5.73	5.60	5.81	5.73	5.69	1.05	1.54	6.13	15.79	15.04
Al_2O_3	14.87	15.13	15.02	14.22	14.58	13.23	12.98	14.82	20.6	22.84
FeO	18.65	20.08	20.57	19.32	19.78	19.13	19.55	23.35	0.00	0.00
Cr_2O_3	0.00	0.00	0.00	0.00	0.00	0.00	0.00	0.00	11.69	8.98
CaO	0.26	0.93	0.24	0.51	0.15	0.06	1.53	0.43	0.02	0.02
Na_2O	0.05	0.07	0.02	0.00	0.05	0.00	0.00	0.00	0.26	0.33
K_2O	8.36	8.31	8.50	9.07	9.02	9.43	9.06	9.14	8.57	8.58
MnO	0.11	0.19	0.15	0.21	0.15	0.31	0.40	0.27	0.29	0.45
NiO	0.00	0.00	0.00	0.00	0.00	0.00	0.00	0.00	0.00	0.00
H2O	0.00	0.00	0.00	0.00	3.96	3.89	3.73	3.88	0.00	0.00
Summa	97.97	100.91	99.27	98.14	100.49	97.94	95.46	100.58	95.87	96.49

Note: 1-8- Anyuisky section; 9-10- Barakhtinsky section.

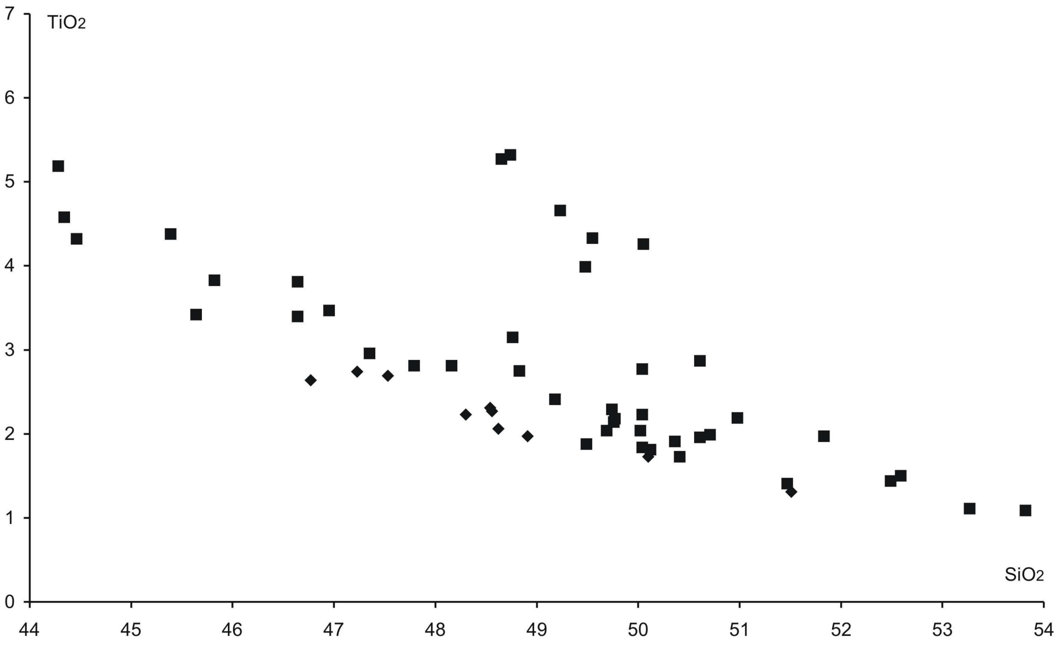

Fig. 1. **TiO_2 (weight %) and SiO_2 contents (weight %) in basalt and picrobasalt.**

■ Anyuisky section ◆ Barakhtinsky section

Ore minerals are represented by iron-titanium oxide minerals. Titanium-magnetite (Table 3) forms large phenocrysts, individual, included into augite, and forming aggregates with them sometimes. Large crystals in the centre are frequently replaced by sphene. Ilmenite is one of the major minerals of the groundmass, forming grains of irregular shape. It practically does not contain MgO with the elevated content of pyrophanite minal (MnO – up to 4 mass %).

CONCLUSIONS

As a rule, the same turbulent mixing conditions in the asthenosphere have affected the delimination stage in terms of "lithothermal feathers" or as "asthenospheric injection".

The volcanic rocks from two spatially separated geological sections in the Central Sikhote Alin nappe-fold structures, occupying an intermediate position between mafic and ultramafic rocks, represent a rather peculiar group of rocks. It is confirmed by the peculiarities of their mineralogy. Plagioclase practically does not occur among the phenocrysts and groundmass; the dominating minerals in these rocks are augite-titanaugite and ferro-titanium oxides. The abundance of amphiboles and mica in these volcanic rocks suggests high water content in parent melts. All this points to the specific conditions of the Mesozoic magmatic activity at the Pacific Ocean intraplate environments.

REFERENCES

1. **Voinova, I.P. and Prikhodko, V.S.** Volcanic rocks in accretionary prisms: geodynamic environment of formation (Central Sikhote Alin)//Tectonics, Geodynamics, and Processes of Magmatism and Metamorphism. Proceedings of XXXII Tectonic Conference. – Moscow, 1999. V.1. P.139-141.
2. **Prikhodko, V.S., Abramova, E.E.**, and Romanenko, I.M. Ultramafic inclusions and megacrysts of amphibole in Jurassic basaltoids of Sikhote Alin//Doklady of USSR Academy of Sciences, 1979, V.249, No 4, P.931-934.